MAGMATIC AND HYDROTHERMAL EVOLUTION OF PERALKALINE GRANITIC ROCKS IN THE HURDAL AREA, OSLO REGION

by

Christopher David Wellings

Thesis submitted for the degree
of Doctor of Philosophy

Imperial College of Science and Technology
University of London

ABSTRACT

The area of study is situated within the northern part of the Oslo Graben, an area of fault-bound rocks formed by a rifting event in the Permian. Felsic rocks of intermediate composition evolving towards more granitic compositions are characteristic of the later stages of igneous activity in the rift.

The felsic rocks exposed in the Hurdal area are compatible with an origin by fractionational crystallisation of intermediate magmas, essentially by separation of clinopyroxene, plagioclase and alkali feldspar. Removal of these minerals has the effect of depleting the melt in elements with high crystal/liquid distribution coefficients for these minerals, at the same time enriching the melt in incompatible trace elements. Thus, the concentrations of V, Co and Sr decrease throughout evolution from monzodiorite to granite. In comparison, Ba, Eu and LREE show moderate early enrichments, followed by gradual depletions. In contrast, the concentratrions of Rb, Nb, Ta, Pb, Th and U increase throughout evolution. The most variable behaviour is shown by Cu, Zn, Li, Cr, Y, Zr, Hf and HREE; these elements showing both enrichments and depletions within individual rock units. The distributions of these elements are believed to have been strongly influenced by late-stage magmatic processes involving complex formation and changes in melt structure. Fluoride complexes, in particular, are believed to have been important. A decline in the importance of ferromagnesian components during evolution from monzodiorite to granite was accompanied by an increase in the volumetric importance of hydrothermal fluids in the system.

Trace element evidence indicates that the intermediate magmas from which the main plutonic series evolved were derived from an alkali basaltic source with a considerable mantle component.

LIST OF CONTENTS

	Page
Abstract	1
List of Contents	2
List of Figures	7
List of Tables	13
Acknowledgements	14
CHAPTER 1: Introduction	
1.1 Outline of the research	15
1.2 Aims of the research	16
1.3 Field studies	17
1.4 Analytical techniques	17
1.4.1 Sample preparation	18
1.4.2 X-ray fluorescence analysis	18
1.4.3 Instrumental methods of neutron activation analysis	18
1.4.4 Inductively coupled plasma spectrometry	19
1.4.5 FeO determinations	19
1.4.6 Fluorine determinations	19
1.4.7 Electron probe microanalysis	20
1.5 Interpretation of the geochemical data	20
1.5.1 Normative mineralogies	22
1.5.2 Magma densities	23
1.5.3 Al-(Na+K)-Ca variation diagrams	23
CHAPTER 2: Regional Geological Setting	
2.1 Introduction	26
2.2 Tectonic setting	29
2.3 Magmatic setting	33
2.3.1 The volcanic rocks	34
2.3.2 The plutonic rocks	39
2.3.2a The Larvik and Skrim massifs	46
2.3.2b The Nordmarka - Hurdalen batholith	47
2.3.2c The Drammen and Finnemarka granite complexes	48

2.4 Tectonomagmatic evolution 48
2.5 Petrogenesis of the Oslo Province 51
2.5.1 Origin of the basaltic rocks 55
2.5.2 Origin of the intermediate rocks 69
2.5.3 Origin of the plutonic igneous rock series 75
2.5.4 Origin of the biotite granites 77
2.5.5 Trace element evidence regarding the origin of the felsic rocks 78
2.5.6 Summary and conclusions 84

CHAPTER 3: Field Relationships and Petrography
3.1 Introduction 87
3.2 Geological structure of the igneous complex 89
3.3 Petrography of the principal rock-types 94
3.3.1 Monzodiorite 94
3.3.2 Biotite syenite 96
3.3.3 Alkali feldspar syenite 97
3.3.4 Quartz syenite 105
3.3.4a Uneven microgranite 108
3.3.4b Feldspar porphyritic microgranite 109
3.3.5 Alkali feldspar granite 109
3.3.5a Aplitic microgranite 112
3.3.6 Extrusive rocks 112
3.3.7 Dyke rocks 114
3.4 Intrusive relationships 114
3.5 Petrogenetic considerations 119
3.5.1 Mineralogical aspects of evolution 123

CHAPTER 4: Mineralisation and Alteration
4.1 Introduction 131
4.2 Metallogenic aspects of rifting 131
4.3 Mineralisation in the Hurdal area 134
4.3.1 The Nordgardshogda - Styggberget area 136
4.3.1.1 Discussion 140
4.3.2 Steinmyrveien 143
4.3.3 The Hegga manganese occurrence 145

4.3.3.1 Discussion 151
4.4 Summary and conclusions 153

CHAPTER 5: Major Element Geochemistry
5.1 Introduction 155
5.2 Major element determinations 155
5.3 Theoretical considerations 167
5.4 Discussion of the results 173
5.5 Magmatic evolution 185
5.5.1 Melt structure 192
5.5.2 Discussion 195
5.5.2.1 Magma viscosities 197
5.5.3 Conclusions 198

CHAPTER 6: Trace Element Geochemistry
6.1 Introduction 199
6.2 Trace element determinations 211
6.3 Theoretical considerations 211
6.4 Discussion of the results 217
6.4.1 Major-plus-trace element distribution patterns 219
6.4.2 Hygromagmatophile element distributions 225
6.4.3 Rare earth element distributions 227
6.4.4 Trace element distributions in the manganogranitoids 235
6.5 Trace element evolution 238
6.5.1 Trace element evidence regarding magma genesis 246
6.5.2 Behaviour of the ore-metals 253

CHAPTER 7: Fluid Inclusion Studies
7.1 Introduction 255
7.2 Fluid inclusion petrography 258
7.2.1 Biotite syenite 258
7.2.2 Quartz syenite 258
7.2.3 Uneven microgranite 260
7.2.4 Feldspar porphyritic microgranite 260

7.2.5 Alkali feldspar granite 260
7.2.6 Quartz vugs 262
7.3 Microthermometry 264
7.3.1 Theoretical considerations 266
7.3.2 Discussion of the results 268
7.4 Chemical analyses of the fluid inclusions 272
7.4.1 Sample preparation 272
7.4.2 Method 273
7.4.3 Calibration 273
7.4.4 Discussion of the results 274
7.5 Hydrothermal evolution 279

CHAPTER 8: Magmatic and Hydrothermal evolution
8.1 Introduction 282
8.2 Magmatic evolution 282
8.2.1 Effects of crystal fractionation upon magma composition 284
8.2.2 Effects of magma composition upon silicate melt structure 289
8.2.3 Effects of phase equilibria upon mineral/liquid evolution 292
8.2.4 Origin of peralkaline magmas in the Hurdal area 293
8.2.4.1 Source rocks 294
8.2.4.2 Mechanisms of fractionation 294
8.2.5.3 Mechanisms of emplacement 297
8.3 Mineralogical aspects of evolution 298
8.4 Hydrothermal evolution 299
8.5 Mineralisation and alteration 302
8.5.1 Origin of Mo - Fe - Zn mineral deposits 303
8.5.2 Origin of the manganogranitoids 305
8.5.2.1 Discussion 308
8.6 Synopsis 311
8.7 Proposals for further work 312

List of Refences 313

Appendix A1: Accuracy and Precision 342
Appendix A2: Calculation of Normative Mineralogies 344
Appendix A3: Chondritic and Primordial Mantle Abundances 349
Appendix A4: Correction of INA Analyses for Variations in Irradiation Flux 351
Appendix A5: D-ICP Determinations 352

LIST OF FIGURES

	Page
2.1 Geological map of the Oslo Region	27
2.2 Simplified geological map of the Oslo Graben	30
2.3 Tectonic map of Scandinavia	32
2.4a Mafic series, Oslo Region	52
2.4b Felsic series, Oslo Region	52
2.5a Al-(Na+K)-Ca variation diagram, equilibrium crystallisation	58
2.5b Al-(Na+K)-Ca variation diagram, fractional crystallisation	59
2.6 Al-(Na+K)-Ca variation diagram, Oahu, Hawaii	61
2.7 Al-(Na+K)-Ca variation diagram, Mull, Kenya, Massif Central, Iceland	62
2.8a REE distribution patterns, Gregory rift, Kenya	64
2.8b REE distribution patterns, Oahu, Hawaii	64
2.9a Al-(Na+K)-Ca variation diagram, volcanic rocks, Oslo Region	66
2.9b Al-(Na+K)-(Mg^{2+}+Fe^{2+}) variation diagram, volcanic rocks, Oslo Region	67
2.10 Al-(Na+K)-Ca variation diagram, volcanic necks, Oslo Region	68
2.11 Al-(Na+K)-Ca variation diagram, Larvik complex, Oslo Region	73
2.12a REE distribution patterns, mafic rocks, Oslo Region	79
2.12b REE distribution patterns, intermediate rocks, Oslo Region	79
2.13 REE ditribution patterns, syenites and granites, Oslo Region	81
2.14 Hygromagmatophile element distribution patterns, Larvik complex, Oslo Region	83
3.1 Geological map of the Hurdal area	88
3.2 Photomicrographs	
3.2a Monzodiorite	95
3.2b Biotite syenite (altered)	95

3.2c Alkali feldspar syenite 103
3.2d Alkali feldspar syenite 103
3.2e Alkali feldspar syenite (sketch) 104
3.2f Quartz syenite 106
3.2g Quartz syenite 106
3.2h Alkali feldspar granite 110
3.2i Alkali feldspar granite 110
3.2j Aplitic microgranite 113
3.2k Trachyte 113
3.3 Geological map of the Nordgardshogda - Styggberget area 116
3.4 Cross-sections accross the Norgardshogda - Styggberget area 117
3.5 Or - Ab - An, feldspar compositions 124
3.6 Scatter plot of Si+Na+K vs. Ca+Al, amphiboles and pyroxenes 127
3.7 biotite analyses 128
3.8 Al-(Na+K)-Ca variation diagram, amphiboles, pyroxenes and biotites 129

4.1 Location of the principal mineral deposits in the Hurdal area 135
4.2 Mineralisation in the Nordgardshogda - Styggberget area 137
4.3 Summary diagram to illustrate the sequence of events in the evolution of the Nordgardshogda - Styggberget area 142
4.4 Geological map of the Hegga manganese occurrence 146
4.5 Photomicrographs
4.5a Manganogranitoid 149
4.5b Contact between alkali feldspar granite and alkali feldspar granite 149
4.5c Rhodonite vein in alkali feldspar granite 150
4.5d Rhodonite vein in manganogranitoid 150

5.1 Sample locality map, Hurdal area 156

5.2a $NaAlSi_3O_8$ - $KAlSi_3O_8$ - SiO_2 - H_2O, P_{H2O} = 1 kbar 169
5.2b $NaAlSiO_4$ - $KAlSiO_4$ - SiO_2 - H_2O, P_{H2O} = 1 kbar 169
5.3a $NaAlSi_3O_8$ - $KAlSI_3O_8$ - SiO_2 - H_2O, P_{H2O} = Ø.5 kbar, 1 kbar, 3 kbar and 5 kbar; P_{H2O} = 1 kbar, 1, 2, and 4 wt % F 171
5.3b $NaAlSi_3O_8$ - $KAlSi_3O_8$ - SiO_2 - H_2O, P_{H2O} = 1 kbar, 4.3 wt % ac + 4.3 wt % ns, 8.3 wt % ac + 8.3 wt % ns 171
5.4 Q - Ab - Or, Hurdal area 175
5.5a Scatter plot of Differentiation Index vs. Si 176
5.5b Scatter plot of Differentiation Index vs. Ti 176
5.5c Scatter plot of Differentiation Index vs. Al 177
5.5d Scatter plot of Differentiation Index vs. $Mg+Fe^{3+}+Fe^{2+}$ 177
5.5e Scatter plot of Differentiation Index vs. Mn 178
5.5f Scatter plot of Differentiation Index vs. Ca 178
5.5g Scatter plot of Differentiation Index vs. Na+K 179
5.5h Scatter plot of Differentiation Index vs. P 179
5.5i Scatter plot of Differentiation Index vs. OH^- 18Ø
5.5j Scatter plot of Differentiation Index vs. F^- 18Ø
5.6a Scatter plot of Differentiation Index vs. Na+K/Al 182
5.6b Scatter plot of Differentiation Index vs. Na/Na+K 182
5.6c Scatter plot of Differentiation Index vs. Na+K/(Al-2Ca) 183
5.7a Scatter plot of Na/Na+K vs. Na+K/Al 184
5.7b Scatter plot of Na/Na+K vs. F^- 184
5.8a Scatter plot of Differentiation Index versus $Mg/Mg+Fe^{3+}+Fe^{2+}$ 186
5.8b Scatter plot of Differentiation Index versus $Mn/Mg+Fe^{3+}+Fe^{2+}$ 186

5.8b Scatter plot of Differentiation Index versus $Fe^{3+}/Fe^{3+}+Fe^{2+}$ 187
5.9 Scatter plot of Mn vs. F^- 187
5.10a Al-(Na+K)-Ca variation diagram, Hurdal area 189
5.10b Al-(Na+K)-Ca variation diagram, Hurdal area, schematic form 189
5.11 Al-(Na+K)-Ca variation diagram, Svartjern 190

6.1a F vs. $C_l/C_\emptyset$, partial melting 214
6.1b F vs. $C_l/C_\emptyset$, fractional crystallisation 214
6.2a Monzodiorite normalised Major-plus-trace element distribution diagram: Biotite syenite 220
6.2b Monzodiorite normalised Major-plus-trace element distribution diagram: Alkali feldspar syenite 220
6.2c Monzodiorite normalised Major-plus-trace element distribution diagram: Quartz syenite 221
6.2d Monzodiorite normalised Major-plus-trace element distribution diagram: Brennhaugen granite 221
6.2e Monzodiorite normalised Major-plus-trace element distribution diagram: Rustadkampen granite 221
6.3a Biotite syenite normalised Major-plus-trace element distribution diagram: Alkali feldspar syenite 222
6.3b Biotite syenite normalised Major-plus-trace element distribution diagram: Trachyte 1 222
6.3c Biotite syenite normalised Major-plus-trace element distribution diagram: Trachyte 2 223
6.3d Quartz syenite normalised Major-plus-trace element distribution diagram: Uneven microgranite 223
6.3e Quartz syenite normalised Major-plus-trace element distribution diagram: Feldspar porphyritic microgranite 223
6.3f Brennhaugen granite normalised Major-plus-trace element distribution diagram: Rustadkampen granite 224
6.3g Brennhaugen granite normalised

Major-plus-trace element distribution diagram: Aplitic microgranite 224
6.4a Primordial mantle normalised Hygromagmatophile element distribution diagram, principal plutonic rock-types, Hurdal area 226
6.4b Monzodiorite normalised Hygromagmatophile element distribution diagram, principal plutonic rock-types, Hurdal area 226
6.5a Chondrite normalised REE distribution patterns, principal plutonic rock-types, Hurdal area 228
6.5b Monzodiorite normalised REE distribution patterns, principal plutonic rock-types, Hurdal area 228
6.6a Chondrite normalised REE distribution patterns, Monzodiorites and related rocks 229
6.6b Chondrite normalised REE distribution patterns, Biotite syenites 230
6.6c Chondrite normalised REE distribution patterns, Alkali feldspar syenites 230
6.6d Chondrite normalised REE distribution patterns, Quartz syenites and related rocks 231
6.6e Chondrite normalised REE distribution patterns, Alkali feldspar granites and related rocks, Brennhaugen area 231
6.6f Chondrite normalised REE distribution patterns, Alkali feldspar granites and related rocks, Rustadkampen area 232
6.6g Chondrite normalised REE distribution patterns, Extrusive rocks 232
6.7a Monzodiorite normalised Major-plus-trace element distribution diagram: Manganogranitoids 236
6.7b Brennhaugen granite normalised Major-plus-trace element distribution diagram: Manganogranitoids 236
6.8a Scatter plot of Differentiation Index vs. V 239
6.8b Scatter plot of Differentiation Index vs. Co 239

6.8c Scatter plot of Differentiation Index vs. Sr 240
6.9 Scatter plot of K vs. Rb 240
6.10a Scatter plot of Mn vs. Li 242
6.10b Scatter plot of Mn vs. Cr 242
6.10c Scatter plot of Mn vs. Zn 243
6.10d Scatter plot of Li vs. F^- 243
6.10e Scatter plot of Cr vs. F^- 244
6.10f Scatter plot of Zn vs. F^- 244
6.11 Scatter plot of Differentiation Index vs. Zr 245
6.12 Primordial mantle normalised Hygromagmatophile element distribution diagram, comparison with Kenya suite 247
6.13a Scatter plot of Y vs. Tb 251
6.13b Scatter plot of Zr vs. Hf 251
6.13c Scatter plot of Nb vs. Ta 252
6.13d Scatter plot of Zr vs. Nb 252

7.1 Sample locality map, Nordgardshogda - Styggberget area 256
7.2 Sample locality map, Brennhaugen area 257
7.3a CO_2 - H_2O - NaCl 267
7.3b CO_2 - H_2O - NaCl 267
7.4 Histograms of salinities 270
7.5 Scatter plot of salinity vs. T_H 271
7.6 Scatter plot of Na vs. K 277
7.7a Scatter plot of Fe+Mn vs. Fe 278
7.7b Scatter plot of Na vs. Mn/Mn+Fe 278

8.1 Summary of fractionation trends, Si_{4+} vs. normative mineralogy 285
8.2a f_v vs. .X, A.G.(B) - W362 310
8.2b f_v vs. .X, A.G.(R) - HC3 310
8.2c f_v vs. .X, A.G.(R) - HC7 310
8.2d f_v vs. .X, A.G.(R) - HC10 310

LIST OF TABLES

	Page
2.1 Representative analyses of the principal volcanic rocks, Oslo Region	36
2.2 Representative analyses of the principal plutonic rocks, Oslo Region	42
3.1 Biotite analyses, Hurdal area	98
3.2 Magnetite plus ilmenite analyses, Hurdal area	100
3.3 Amphibole plus pyroxene analyses, Hurdal area	101
5.1 Major element analyses, Hurdal area (wt % oxide)	157
5.2 Average major element analyses of the principal rock-types, Hurdal area (cation %)	165
6.1 Trace element analyses, Hurdal area ($\mu g\ g^{-1}$)	200
6.2 Average trace element analyses of the principal rock-types, Hurdal area (10^{-8} gram atoms g^{-1})	208
6.3 Trace element ratios, petrogenetic suites	216
6.4 Trace element ratios, Hurdal area	250
7.1 Fluid inclusion petrography	259
7.2 Average chemical compositions of fluid inclusions in granitic quartz	276
A1 Summary of precision and accuracy	343
A2 Chondritic and primordial mantle abundances	350
A3 Sensitivities for the standard solutions	353
A4 Summary of precision for the D-ICP technique	353

ACKNOWLEDGEMENTS

I would like to thank Chris Halls for his support throughout this research project, and for his critical comments on the manuscript. I would also like to thank Professor F.M. Vokes and P.M. Ihlen of the NTH in Trondheim for their guidance in the field; and the prospecting staff of Norsk Hydro A/S for their support.

I would especially like to thank Dr. S. Chryssoulis for his help with the fluid inclusion studies, and for many lenghthy discussions during the course of my work; and Dr. A. Schneider for the encouragement he gave me during the final stages of the research.

I would like to extend my gratitude to Dr. G. Marriner of Bedford college for allowing me to use the XRF facilities there; and to Dr. S. Parry at the University of London Reactor Centre for helping me with the INAA analyses. I acknowledge the help of the technical staff in Mining Geology for their help in preparing samples for the laboratory work.

I would like to thank the NERC for providing the necessary funding for the research, and Norsk Hydro A/S for supporting me in the field.

Last, but not least, I would like to thank Miss G.A. Davies for typing the manuscript.

CHAPTER 1

INTRODUCTION

1.1 Outline of the research

This research project is concerned with the petrological, geochemical and hydrothermal evolution of a suite of alkaline to mildy peralkaline felsic igneous rocks in the Hurdal area, 70 km to the north of Oslo in Southern Norway. The area of study is situated within the northern part of the Oslo Graben, a fault-bound area of rocks formed by a rifting event in the Permian. Felsic rocks of intermediate composition evolving towards more siliceous compositions are characteristic of the later stages of igneous activity in the rift, forming the larger part of the Nordmarka - Hurdalen batholith in the north.

The research has been based on major, trace and rare earth element analyses of a set of 73 rock samples from the Hurdal area. This has been carefully related to detailed field and petrological studies. In addition, a preliminary study of the fluid inclusion populations in granitic quartz has been undertaken, with a view towards unravelling the hydrothermal evolution of the rocks concerned.

Several analytical techniques have been used. These include: X-ray fluorescence analysis (XRF), instrumental methods of neutron activation analysis (INAA), inductively coupled plasma emission spectrometry (ICP), electron probe microanalysis (EPMA), selective ion electrode potentiometry (SIE), and colorimetric methods. In total, forty five elements have been analysed by these methods. A brief description of each of these methods is given in Section 1.4. A summary of the precision and accuracy of each method is given in Appendix A1.

Interpretation of the geochemical data has been aided by the

development of several interactive FORTRAN computer programs. These include routines to tabulate data and to calculate various elemental ratios, together with algorithms to calculate normative mineralogies and magma densities. In addition, several binary and ternary plotting routines have been developed. This approach has enabled a systematic appraisal of the geochemical data to be made. It has resulted in the discovery of at least one valuable new ternary variation diagram, Al-(Na+K)-Ca, which may be used to depict the compositional path along which a crystal/melt system evolves during processes of partial melting and/or fractional crystallisation. It is believed that this diagram is of fundamental importance to petrologists, particularly in the interpretation of mafic rocks, and in alkaline petrogenesis.

The thesis includes a detailed resume of the regional tectonic and magmatic setting, together with a re-appraisal of the petrogenesis of the province. It is believed that a detailed knowledge of the geological background for felsic magmatism is essential, if an unequivocal explanation for the genesis of the felsic rocks is to be found. In particular, emphasis is placed on unravelling the connection between the felsic intrusives and mafic lavas, which together make up a large proportion of the igneous products at the present level of erosion within the rift.

1.2 Aims of the research

The aims of the research have been as follows:

(I) To elucidate the relationship between the felsic intrusives and the mafic lavas;

(II) To explain any major variations or trends in the chemistry of the rocks in terms of their mineralogy, thus revealing any fractionation trends which may have existed;

(III) To explain the nature of any hydrothermal solutions which may have exsolved from the melt during its evolution; and

(IV) To explain the processes responsible for the concentration and precipitation of ore-metals in the Hurdal area.

The overall aim of research has been to deduce a model for the magmatic and hydrothermal evolution of the rocks in question, and to place them in to perspective with the more regional geology of the Oslo Graben.

1.3 Field Studies

Fieldwork has involved regional geological mapping and sampling within an area of approximately 50 km^2 to the west of Hurdalssjoen, together with more detailed mapping of smaller areas within the complex (Figure 3.1). These include the Brennhaugen, Rustadkampen and Nordgardshogda - Styggberget areas (Chapters 3 and 4). The fieldwork was done under the supervision of Dr. C. Halls of Imperial College, together with Professor F.M. Vokes of Trondheim University. Additional help was provided by P.M. Ihlen of Trondheim University, and by the prospecting staff of Norsk Hydro A/S, who have coordinated a large part of the exploration program in the area.

Regional mapping was mainly on the scale of 1 to 10,000. More detailed mapping was usually on the scale of 1 to 5000. However, locally mapping was undertaken on a much smaller scale, for instance 1 to 2000 in the Steinmyrveien area and 1 to 200 at the Hegga river locality (Section 4.3.3). Base maps for the regional study were provided by Norsk Hydro A/S.

1.4 Analytical techniques

1.4.1 Sample preparation

Representative samples of rock from the Hurdal area were prepared for analysis by the following procedure. Approximately 1 kg of sample was ground to the size fraction of less than 4 mm using a jaw crusher. The gravel obtained was then split several times in order to obtain a uniform sample of approximately 50 g. This was then ground to a fine powder (<60 µm) using an agate TEMA mill. The apparatus was cleaned thoroughly between each preparation in order to minimise the effects of contamination.

1.4.2 X-ray fluorescence analysis

A total of ten majcr elements and nine trace elements were analysed using the Philips PW1400 automatic spectrometer at Bedford College, London. The sample preparation and analytical procedure were similar to that described by Marsh et al. (1980). Major element determinations were made on fusion beads using a Ag-anode X-ray tube. Trace element abundances were determined on 46 mm briquettes using the Ag-anode (Rb, Sr, Y, Zr, Nb and Th) and W-anode (V, Ni and Ba) X-ray tubes. All elements have been corrected for mass absorption, and for interference effects where necessary. Several internal reference standards were also run. The precision of the method for all elements was extremely good (Appendix A1, Table A1). Loss on ignition was determined separately.

1.4.3 Instrumental methods of neutron activation analysis

A total of eleven rare earth elements, together with Hf, Ta, W, Th and U were analysed by this method. The samples and standards were irradiated for a duration of seven days in the University of London nuclear reactor at Silwood Park, near Ascot. They were then allowed to cool for five days prior to

analysis at the reactor centre. All elements were analysed using a high energy Ge detector. The principles of this technique are described by Goles (1977). All elements have been corrected for variations in irradiation flux according to the procedure outlined in Appendix A4. Gadolinium and Tantalum were recounted at a later date, after certain shortlived isotopes had decayed. No corrections for irradiation flux were applied in this case. The precision and accuracy of this technique are summarised in Appendix A1 (Table A1).

1.4.4 Inductively coupled plasma emission spectrometry

A total of twenty five elements were analysed on the ARL 34000c emission spectrophotometer at Imperial College. Of these elements, the ten major elements have been analysed by other techniques and will not be considered here. The samples were decomposed using a combination of hydrofluoric, nitric and perchloric acid as described by Thompson and Walsh (1983). The samples were then allowed to evaporate to dryness on a hotplate prior to being dissolved in hydrochloric acid. The samples were analysed following the procedure outlined by Thompson and Walsh (1983). Standard solutions were run at regular intervals. The precision and accuracy of this technique are summarised in Appendix A1 (Table A1).

1.4.5 FeO determinations

Ferrous iron determinations were made using the standard colorimetric method, following the procedure of Whipple (1974). This procedure utilises pentavalent vanadium to oxidise divalent Fe as it is released from the silicate by hydrofluoric acid. Sodium diphenylamine p-sulfonic acid was used as the indicator.

1.4.6 Fluorine analyses

Fluorine determinations were made by selective ion electrode potentiometry, following a procedure similar to that of Bodkin (1977). The rock powders were fused with a lithium metaborate flux, $LiBO_2$, and then dissolved in 2N nitric acid. The concentration of fluoride in the sample solution was determined with the fluoride ion electrode by the method of standard addition. This method utilises the changes in potential resulting from the addition of a known volume of standard fluoride solution to the sample solution in order to determine the fluoride concentration in the sample.

1.4.7 Electron probe micro-analysis

Electron probe analyses of the principal rock-forming minerals in granitic rocks from the Hurdal area were obtained from polished thin sections by analysing in the energy dispersive mode (EDS, Long 1977). The accelerating voltage was set at 15 KeV and the specimen current on the cobalt standard at 4.ØØ nA. Standard reference samples were analysed at regular intervals. The average compositions of biotites, Fe-Ti oxides, amphiboles and pyroxenes are listed in Tables 3.1, 3.2 and 3.3. Feldspar analyses are not presented, due to the problems of obtaining representative analyses caused by the extensive exsolution of albite and orthoclase domains.

1.5 Interpretation of the geochemical data

Major, trace and rare earth element analyses of the principal plutonic and volcanic rock-types from the Hurdal area are presented in Chapters 5 and 6. In total 73 rock samples have been analysed for 1Ø major and 35 trace elements. Several of the elements have been determined by more than one analytical technique. Where this is the case, the determination with the better analytical precision has been chosen. In particular, the thorium analyses from INAA have proved to be very erratic, varying by as much as 22 percent (Table A1). The Th analyses from XRF have therefore been chosen. Caution should

be taken when considering the distributions of Ni, Mo, Ag, Cd, W and Tm, since these elements are often present in levels close to detection limits.

The major element analyses in Table 5.1 are presented in the form of weight percent oxide. In comparison, the trace element analyses in Table 6.1 are presented in the form of micrograms per gram of sample. For purposes of interpretation, however, the major and trace element analyses have been recalculated in terms of ionic proportions. The average major element compositions in Table 5.2 are therefore presented in the form of cation percent and anion equivalent. In comparison, the average trace element analyses in Table 6.2 are presented in the form of 10^{-8} gram atoms per gram of sample.

Recalculation of the major element analyses in terms of cation % poses certain problems, in a statistical sense, due to the effects of closure (all the analyses add up to 100%). These effects are most prominent when a major element expressed in cation % is plotted against a trace element expressed in gram atoms g^{-1}. The reason for this is simple. In calculating the proportion of an element in cation %, the number of cations present in one gram of sample is divided through by the total number of cations present in one gram of that sample. This varies from sample to sample, thus causing distortion of the data points. In order to overcome this problem in plots of this type, the major element analyses have been converted back into gram atoms g^{-1}. Expressing the major and trace element analyses respectively in terms of 10^{-4} and 10^{-8} gram atoms g^{-1} may seem a somewhat artificial division. It does, however, allow a direct comparison to be made between the concentrations of an element expressed in mass proportions and those expressed in atomic proportions, since they are of the same order of magnitude. Similarly, expressing the major element concentrations in terms of cation % produces a similar range of values to those

expressed in terms of Wt % oxide (compare Tables 5.1 and 5.2).

The benefits of recalculating the chemical analyses in terms of atomic proportions, however, far exceed their disadvantages. Barth (1944) and Eskola came to the same conclusion. A rock consists of a limited number of minerals in certain proportions. Each mineral in turn consists of a very large, but finite number of atoms arranged in an ordered structural state and in specific proportions defined by the chemical formula for that mineral. Expressing the major element analyses in terms of atomic proportions therefore allows a direct comparison to be made between the composition of a rock or liquid and the arrangement of the atoms in terms of its principal mineral constituents. The geochemical evolution of a mineral/liquid system may therefore be modelled in terms of poly-dimensional compositional space in which the composition of a mineral is defined by a point in space. This can be related to the bulk composition of the system by a vector. Removal of that mineral from the system will result in a change in the composition of the liquid along a path opposite to that defined by the mineral vector, the length and magnitude of which are proportional to the amount of the mineral phase being removed.

The trace element ratios presented in Tables 6.3 and 6.4 have also been calculated in terms of atomic porportions. The discussion of crystal/liquid distribution coefficients in Section 6.3, however, considers the distribution of the elements in terms of mass proportions, following the precedence in the literature. The principles, however, are exactly the same, since the factor of mass divides out.

1.5.1 Normative mineralogy

A new norm calculation has been devised based on progressive silicification of the minerals. The results produced from

this calculation are essentially the same as those obtained from the conventional CIPW calculation, only the sequence of the steps is different. The exact procedure is outlined in Appendix A2. The new norm does, however, differ from the CIPW norm in that the pyroxene components are calculated in terms of their principal end-members, and in that the Mn-bearing components are calculated separately. Diopside, hedenbergite, johannsenite, enstatite, ferrosilite, pyrophanite, and jacobsite are therefore included within the norm. again, for the purposes of this thesis, the normative mineralogies have been calculated in terms of cation percent.

1.5.2 Magma densities

Anhydrous magma densities have been calculated from partial molar volumes of oxide components according to the procedure of Bottinga and Weill (1970). Corrections have been applied for pressure and temperature as suggested by Bottinga and Weill. Calculated anhydrous magmas densities of the principal igneous rock-types are listed in Table 5.2.

1.5.3 Al-(Na+K)-Ca variation diagrams

The interpretation of the geochemical data has been aided by the development of several interactive FORTRAN computer programs. These include a program for the rapid production at a line-printer of binary and ternary scatter plots. As a result, several thousand plots have been generated. This empirical approach has lead to the discovery, more or less accidentally, of one new ternary variation diagram, Al-(Na+K)-Ca (Figures 2.5a and 2.5b). The significance of this diagram is easily recognised when it is observed that trends in composition involving alkali feldspar, plagioclase, clinopyroxene, sodic pyroxene, sodic amphibole, common hornblende, garnet, melilite and mica may all be shown by variations in one or more of these components. Among the major rock forming minerals, only olivine, orthopyroxene and

quartz contain none of these components. In addition, the importance of this diagram in the interpretation of peralkaline fractionation trends is easily understood when it is observed that the diagram may be divided into two halves, a sub-alkaline to peraluminous field and a peralkaline field (Na+K/Al > 1).

During crystallisation of a silicate melt, the composition of a mineral in equilibrium with the melt can be related to the bulk composition of the system by a vector (dashed tie-lines in Figure 2.5a). Crystallisation of that mineral will cause the composition of the liquid to migrate along a path in Al-(Na+K)-Ca compositional space opposite to that defined by the mineral vector, the length and magnitude of which are controlled by the proportion of the mineral phase crystallising. Thus, during equilibrium crystallisation of a peridotitic composition corresponding to that of pyrolite (Ringwood 1975), crystallisation of garnet will cause the liquid composition to migrate along a path Ia in Figure 2.5a. Similarly, crystallisation of moderately aluminous clinopyroxene will cause the liquid composition to migrate along a path Ib. In comparison, simultaneous crystallisation of garnet and clinopyroxene in equal proportions will result in migration of the liquid composition along a path defined by the sum of the two vectors, path III in Figure 2.5a.

The proportion of mineral phases crystallising will not, however, always remain constant. The proportion of mineral phases crystallising at any one point, x, is defined by the tangent to the curve at that point (Figure 2.5a). In comparison, the proportion of mineral phases in the residue is defined by a line extrapolated back through the bulk composition to the Al-Ca join.

Providing equilibrium is maintained, the bulk composition of the mineral/melt system will remain constant throughout crystallisation. If, however, full equilibrium is not

achieved, then the composition of the liquid will begin to evolve away from the initial composition of the system. The direction of evolution will depend upon the composition of the mineral phases being crystallised. Thus crystallisation of clinopyroxene from a melt of initial composition Ø will cause the composition of the melt to evolve along path Ø to 1 in Figure 2.5b. At this point, clinopyroxene may be joined on the liquidus by plagioclase. Combined crystallisation of clinopyroxene, and plagioclase in increasing proportions, will cause the composition of the melt to migrate along paths 1 to 4. Further separation of plagioclase will drive the composition of the residual melt into the peralkaline field. This is the "plagioclase effect" of Bowen (1945). Removal of hornblende or garnet may have a similar effect.

CHAPTER 2

REGIONAL GEOLOGICAL SETTING

2.1 Introduction

The Oslo Region is geographically defined as an area of approximately 10,000 km^2 in Southern Norway in which the rocks are younger than the surrounding Precambrian terrain and in which the city of Oslo has a central situation (Figure 2.1; Dons 1978). It extends for approximately 200 km in a north-south direction from the coast of the Skagerrak in the south to the Lake Mjosa district in the north, although its northern limits are poorly defined (Dons 1978). It varies in width between 35 and 65 kilometres.

In contrast, the Oslo Graben is a genetic term used to define an area of fault bound rocks which have subsided into the Precambrian basement. As such its boundaries more or less coincide with those of the Oslo Region (Figure 2.1), except that rocks of Precambrian age are also included within the subsided area. The Oslo Graben is interpreted as a palaeorift of Permian age and is believed to have formed the northern part of a more extensive fracture system, the Oslo Rift. The Oslo Graben shows many similarites to both modern and ancient rift systems, although structurally and morphologically it only partly fulfills the requirements (Section 2.2; Ramberg 1976, Girdler 1977).

The Oslo Region contains a sedimentary succession of Cambrian, Ordovician and Silurian rocks together with minor sediments, volcanic and intrusive rocks of Permian age. Rocks from the Devonian and Carboniferous periods are not represented, although a possible late Carboniferous age has been hinted at for some of the earliest sediments associated with the rifting episode (Henningsmoen 1978). A possible Triassic age has been inferred for some of the latest dykes

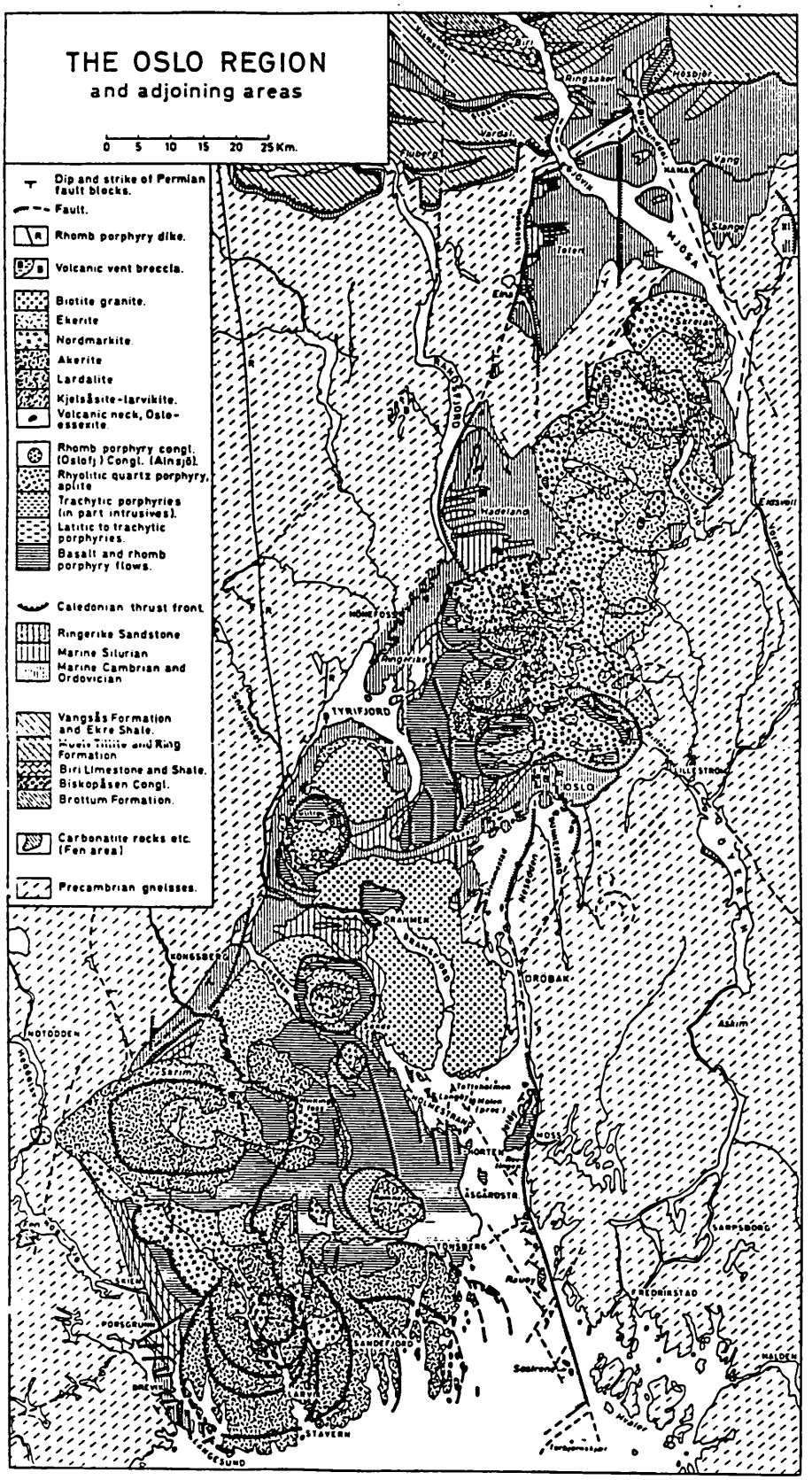

FIGURE 2.1. Geological map of the Oslo Region (after Oftedahl 1960, Ramberg 1976, Petersen 1977, and Segalstad 1975).

(Dons 1977; Larsen 1975) and sediments (Spjeldnaes 1972).

The Precambrian rocks immediately adjacent to the Oslo Region, and partially included within the graben, consist of a variety of gneisses and migmatites together with quartzites, amphibolites, syn- and post-orogenic granitic and gabbroic rocks belonging to the Sveco-Norwegian zone of the Fennoscandian craton (Ramberg 1976). These rocks give isotopic ages of around 1000 Ma and younger (Grenvillian), although relict ages of rocks dating back to 1600-1700 Ma have been recorded (Ramberg 1976, ref. cit. Neumann 1960, Broch 1964, O'nions et al., 1969, Priem et al. 1970, O'nions and Heier 1972).

The Oslo Region has been the subject of a vast geological literature dating back to the beginning of the last century (see Dons 1978 for history of investigations). Perhaps the most significant contribution towards the understanding of the Oslo petrogenetic province was made by Professor W.C. Brogger (1851-1940) whose series of monographs "Eruptivegesteine des Kristiana (Oslo) Gebietes" remains one of the major works on the Oslo Region. Among the other early contributors, J. Schetelig (1875-1935), J.H.L. Vogt (1858-1932), V.M. Goldschmidt (1888-1947) and O. Holtedahl (1885-1975) are significant. The monograph series "Studies on the Igneous rock complex of the Oslo Region" was introduced by Holtedahl in 1943 and includes such works as Barth (1944, 1954), Barth and Bruun (1945), Oftedahl (1946, 1948, 1952, 1953, 1957 a and b), Saether (1946, 1947, 1962), Dietrich et al. (1965), and more recently Nystuen (1975a), and Weigand (1975).

Some of the latest views on the development of the Oslo palaeorift are to be found in a series of publications originating from the proceedings of the NATO Advanced Study Institute held at Sundvollen near Oslo in 1977 (Dons and Larsen 1978; Neumann and Ramberg 1977; Ramberg and Neumann

1977). Whilst metallogenic aspects of the Oslo rifting and igneous activity have been reviewed by Vokes (1973), Vokes and Gale (1976), Ihlen and Vokes (1978 a and b) and Vokes and Ihlen (198Ø), as outlined in Ihlen et al. (1982).

2.2 Tectonic setting

The Oslo Graben is composed of two north-south trending graben segments, arranged en echelon (Figure 2.2): The Vestfold - Ringerike graben in the south-west and the Akershus graben in the north-east; more or less separated by a northward wedging block, the Ostfold horst (Ramberg and Larsen 1978; Ramberg and Spjeldnaes 1977). Both graben segments are asymmetrically tilted towards the central north-south trending Oslofjord fault and its northward extrapolation, the Randsfjord - Hundselv fault. The two faults show vertical displacements of the order of 1 km (Ramberg 1976), and together have the characteristics of a scissor fault. Both graben segments are transected by a series of normal or antithetic step faults, giving the subsided area a basin-and-range type structure (Ramberg 1976). The segments show maximum subsidence in their southern parts, which also correspond to the areas of major felsic batholith emplacement (Section 2.3.2; Ramberg and Larsen 1978).

The main fault trends in the Oslo Graben are NNW to N and NNE to NE, although NW-SE and NE-SW trends are also apparent. In comparison, the Precambrian Telemark area to the west of the Oslo Region shows mainly NW-SE and NE-SW fracture patterns (Ramberg and Larsen 1978). It is therefore evident that rejuvenation of pre-existing fracture systems was only partly responsible for the present pattern within the rift. However, the occurrence of late Precambrian mafic intrusions near Kongsberg and Tyrifjorden and the Early Cambrian Fen carbonatite complex along a line parallel to the main rift axis and coinciding with the incipient western border of the

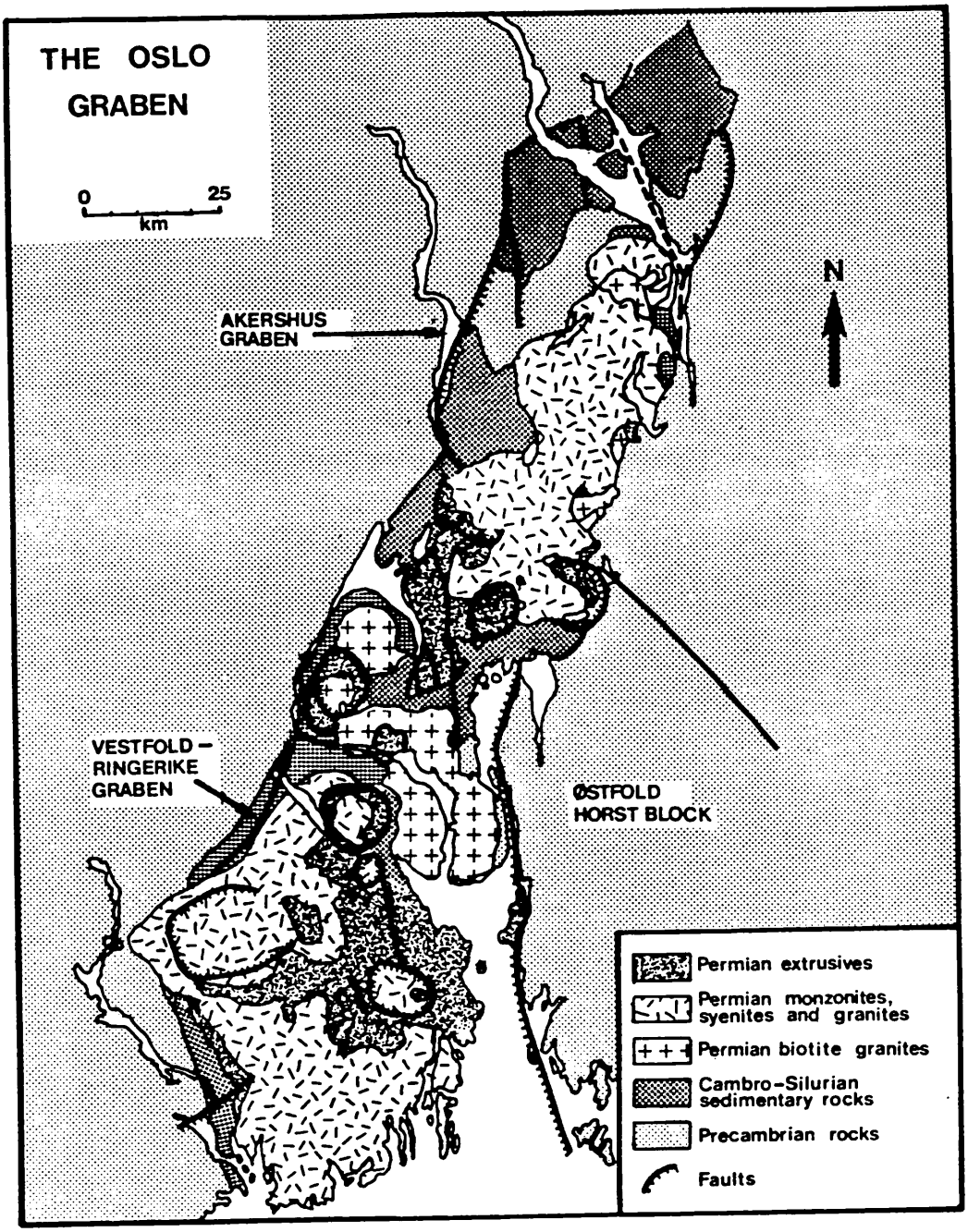

FIGURE 2.2. Simplified geological map of the Oslo Graben, showing the main tectonic and lithological units.

Oslo rift indicates the existence of a significant crustal weakness in the area, dating back to Late Precambrian times (Ramberg and Larsen 1978). In addition, the presence of the Eocambrian fault-bound Sparagmite basin to the north of the Oslo Region and the narrow Cambro-Silurian sedimentary troughs (aulacogens) in the area of the palaeorift, suggests that rift-related subsidence had commenced by the beginning of the Cambrian.

Structurally and morphologically the Oslo Graben is very similar to many modern and ancient rift systems. The en echelon displacement of the two rift segments with respect to each other is typical of many intracontinental rift zones (e.g. The Gregory Rift, Kenya; Baker and Wohlenberg 1971). The average graben width of 40 km is also similar to that of many continental and oceanic rifts (Ramberg 1976, Table 1). The Oslo Graben differs, however, from a "typical" rift in two important respects: (1) The absence of major boundary faults in the southwestern and northeastern parts; and (2) the lack of any evidence of crustal doming preceding rift development (2 to 3 km in the case of the East African Rift Systems; Baker et al. 1972). The absence of major boundary faults in the above areas is presumably due to the fact that they have been obscurred or obliterated by the intrusion of the major felsic batholiths, which occurred after the main period of fault activity (Section 2.4; Ramberg and Larsen 1978). The lack of evidence of crustal doming may be partly due to the Permian age of the rift and subsequent re-attainment of thermal and isostatic equilibrium (Ramberg 1976), and partly due to the present level of erosion. The absence of rocks of Devonian and Carboniferous age could be evidence of relative uplift during these periods.

The formation of continental rift zones is interpreted as the response of the structurally anisotropic continental crust to tensional stress and to sub-lithospheric mantle processes, the degree of interdependence of these two factors being a

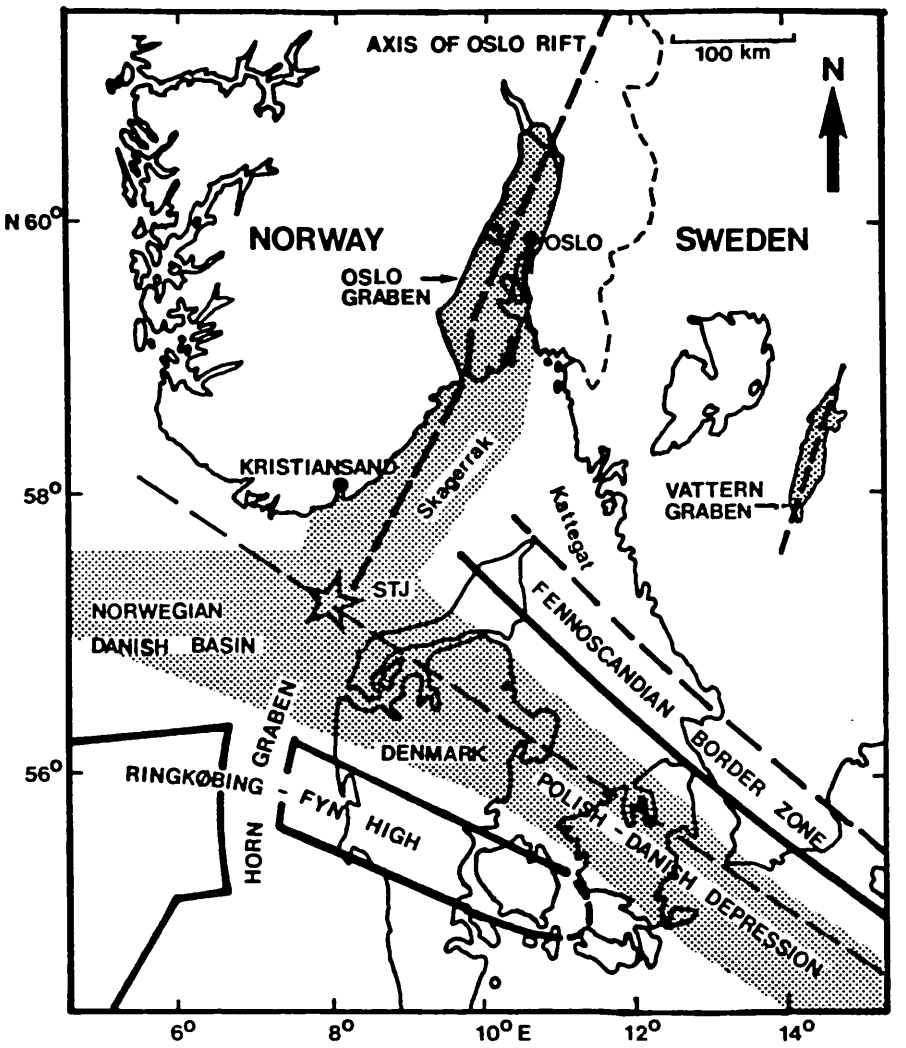

FIGURE 2.3. Tectonic map of Scandinavia, showing the presumed location of the Skagerrak triple junction, STJ (after Husebye and Ramberg 1978).

matter of considerable debate (Neumann and Ramberg 1977a). In plate tectonic theory, intracontinental rifting is believed to mark the initial stages in an evolutionary process leading to oceanic rifting and "sea-floor" spreading (Burke and Dewey 1973, Falvey 1974, Kinsman 1976, Ramberg and Larsen 1978). The fact that palaeorifts exist, however, attests to the fact that this process is sometimes aborted.

The Oslo Rift is interpreted as a "failed-arm" of a Permian triple junction, the other arms being located in the Norwegian - Danish Basin to the southwest, and the Polish - Danish Depression to the southeast (Figure 2.3; Husebye and Ramberg 1978). The Oslo Rift System forms but part of a larger, worldwide network of rift systems which were active during upper palaeozoic and mesozoic times (Illies 1970, Burke and Dewey 1973) indicating that this period was a major period of crustal break-up in Earth's history.

2.3 Magmatic Setting

The Oslo Region is a so-called "mixed" petrographic province consisting of a variety of silica-saturated and undersaturated alkaline and peralkaline igneous rocks, together with subalkaline granites (Neumann 1978). Plutonic and volcanic rocks in this compositional range form between 75 and 80 percent of the present graben surface (Figure 2.1; Ramberg 1976). The volcanic rocks (Section 2.3.1) show a distinctly bi-modal population with mafic rocks of alkali olivine basalt affinity and intermediate "rhomb porphyries" predominating. In contrast, the exposed plutonic rocks (Section 2.3.2) show a bias towards more intermediate and granitic compositions with only minor representation from more mafic compositions.

The volcanic and plutonic products show a number of silimarities to those described from other anorogenic continental magmatic settings, notably the East African Rift

System (Williams 1970, 1972; King 1970, King and Chapman 1972; Baker et al. 1972, Baker et al. 1977; Norry et al. 1980), the Midland Valley of Scotland (Tomkeieff 1937, MacDonald 1975, 1980), and the Nigerian Granite complex (Black and Girod 1970, Bowden 1966, 1982, Bowden and Jones 1974, Bowden and Turner 1974, Bowden and Whitley 1974, Bowden et al. 1977, Turner and Bowden 1979). Similar magmatic products have also been described from within certain palaeozoic fold belts, such as the Topsails igneous complex of western Newfoundland (Taylor et al. 1980, Taylor et al. 1981), and the Lachlan Fold Belt of Southeastern Australia (Wyborn et al. 1981; Collins et al. 1982).

2.3.1 The volcanic rocks

Volcanic rocks in the Oslo Region presently cover a total of roughly 1500 km^2, and occur in five principal areas (Figure 2.1; Ramberg and Larsen 1978, Ramberg and Spjeldnaes 1977):

(1) The Skien basalt area in the southwest, consisting of a thick (circa 2 km) succession of (B_1) basaltic flows;
(2) The Jeloya volcanics in the southeast, consisting of a 1.2 km thick sequence of (B_1) basalts and rhomb-porphyry flows.
(3) The Vestfold lava plateau consisting of a thick (circa 3 km) sequence of rhomb porphyry lavas with intercalated basalts (B_1 to B_6), trachytes and rhyolites;
(4) The Krokskogen lava plateau consisting of a 1.6 km thick sequence of rhomb porphyry flows with occasional basalts (B_1 to B_4), and trachytes; and
(5) The cauldron complexes comprising basaltic lavas of the central volcano stage and alkaline trachytes and rhyolites of the subsidence and cauldera-filling stages.

Weigand (1975) classified the Oslo basalts into four groups on the basis of phenocryst mineralogy: Pyroxene basalt, plagioclase - pyroxene basalt, plagioclase basalt and aphyric

basalt. These rocks differ from "typical" basalts in that they have somewhat lower Ca and higher K contents (Table 2.1). However, the presence of only one pyroxene (essentially a titaniferous augite) in all but the most evolved basalts indicates alkali olivine basalt affinities. Broadly speaking the least evolved basaltic rocks (pyroxene and plagioclase-pyroxene basalts) may be compared with the basanites and alkali basalts of the oceanic island (Hawaii-type) and continental magmatic settings. More mafic magmas are poorly represented, although Segalstad (1979) has reported the presence of nephelinites among the B_1 basalts in the Skien area. The more evolved basaltic rocks exposed in the Oslo Region show more tholeiitic affinities, containing normative hypersthene and/or quartz (Weigand 1975, Segalstad 1977, 1979).

The rhomb porphyry lavas are of more intermediate composition, and may be referred to as trachyandesites or latites (Oftedahl 1977). Mineralogically and chemically they are similar to the plutonic monzonites (kjelsasites and larvikites; Section 2.3.2) and are therefore interpreted as their volcanic equivalents (Ramberg and Larsen 1978). Although it is debatable whether they are all strictly comagmatic in origin (Section 2.5.2).

Felsic volcanic rocks, alkaline trachytes and trachytes predominate towards the higher levels of the volcanic sequence, and make up approximately 10 percent by volume of the extrusive products in the rift (Ramberg and Larsen 1978). Felsic magmas were probably derived from subvolcanic chambers now represented at the surface by the major plutons, thus suggesting a comagmatic origin for these rocks.

Table 2.1 lists average chemical analyses of the principal volcanic rock-types, after Weigand (1975), Ramberg and Larsen (1978), Segalstad (1979) and Rasmussen (1982). The analyses have been recalculated in terms of cation percent as outlined

TABLE 2.1 REPRESENTATIVE GEOCHEMICAL ANALYSES OF THE VOLCANIC ROCKS

AREA	SKIEN		KROKSKOGEN				VESTFOLD			
ROCK TYPE:	BX-BAS	PL-PX BAS	NEPH	PX-BAS	PL-BAS	Aph-BAS	PX-BAS	PLPX-BAS	PL-BAS	Aph-BAS
NUMBER OF SAMPLES:	15	6	1	2	2	12	2	7	1	1
CATION PERCENT:										
Si^{4+}	41.98	42.98	35.65	41.92	46.92	47.69	43.43	45.34	44.96	45.39
Ti^{4+}	2.30	2.08	2.41	2.98	2.57	1.93	1.95	2.02	2.20	2.15
Al^{3+}	12.51	16.08	12.07	14.58	16.62	15.76	12.78	15.85	16.67	16.54
Fe^{3+}	4.94	5.21	6.11	5.59	6.33	5.01	4.22	5.09	4.86	5.24
Fe^{2+}	4.79	3.95	3.31	4.61	3.94	5.26	5.04	3.98	4.39	4.96
Mn^{2+}	.16	.15	.22	.19	.12	.16	.16	.17	.12	.19
Mg^{2+}	13.33	10.88	11.09	10.87	7.73	8.28	14.18	8.73	8.30	7.61
Ca^{2+}	12.63	9.73	19.71	10.67	6.57	8.79	10.07	9.02	7.23	9.14
Na^{+}	4.68	5.56	6.33	6.12	6.86	5.69	4.53	6.73	8.05	6.15
K^{+}	2.31	2.96	1.63	1.81	2.02	1.12	3.22	2.71	2.93	2.26
P^{5+}	.37	.42	1.48	.66	.30	.31	.41	.36	.29	.36
Total	100.00	100.00	100.00	100.00	100.00	100.00	100.00	100.00	100.00	100.00
ANION EQUIVALENT:										
O^{2-}	150.06	152.08	145.39	152.01	156.98	157.07	150.63	153.65	152.89	154.76
OH^{-}	0	0	0	0	0	0	0	0	0	0
F^{-}	0	0	0	0	0	0	0	0	0	0
MOLAR RATIOS (CATIONS):										
$Fe^{3+}:Fe^{2+}$	1.03	1.32	1.84	1.21	1.60	.95	.84	1.28	1.11	1.06
$Mg:Mg^{+}Fe$	.58	.54	.54	.52	.43	.45	.60	.49	.47	.43
Ca:Na+K	1.81	1.14	2.48	1.35	.74	1.29	1.30	.96	.66	1.09
Na:Na+K	.67	.65	.80	.77	.77	.84	.58	.71	.73	.73
Na+K:Al	.56	.53	.66	.54	.53	.43	.61	.60	.66	.51
MODIFIED C.I.P.W. NORMS (CAT. PC):										
Q	0	0	-2.70	0	2.60	5.25	0	0	0	0
Or	11.57	14.80	0	9.05	10.11	5.61	16.10	13.56	14.64	11.29
Ab	10.51	19.17	0	22.31	34.31	28.47	15.62	29.68	31.14	30.77
An	13.78	18.91	10.28	16.63	19.33	22.35	12.58	16.01	14.24	20.32
Ks	0	0	4.88	0	0	0	0	0	0	0
Ne	7.73	5.17	18.99	4.97	0	0	4.23	2.39	5.45	0
Wo	0	0	8.19	0	0	0	0	0	0	0
Di	36.54	20.98	44.36	24.97	8.80	13.59	25.42	20.90	15.56	17.06
Hd	.48	0	0	0	0	1.56	1.99	0	0	.83
Js	.02	0	0	0	0	.05	.06	0	0	.03
En	0	0	0	0	11.05	9.77	0	0	0	4.99
Fs	0	0	0	0	0	1.15	0	0	0	.25
Fo	6.29	8.45	0	6.94	0	0	11.73	5.25	6.61	1.27
Fa	.09	0	0	0	0	0	.95	0	0	.06
Mt	7.17	5.85	3.15	5.24	4.34	7.30	6.14	6.14	6.72	7.57
Jc	.24	.22	.21	.22	.14	.22	.19	.26	.18	.29
He	0	1.16	3.86	1.95	3.34	0	0	.83	.26	0
Ilm	4.45	4.01	4.52	5.72	4.99	3.75	3.78	3.87	4.29	4.13
Pn	.15	.15	.30	.24	.16	.11	.12	.16	.12	.16
Ap	.99	1.13	3.95	1.77	.81	.83	1.10	.96	.78	.96
D.I.	29.81	39.15	21.18	36.33	47.03	39.32	35.95	45.63	51.23	42.06
CALCULATED ANHYDROUS MAGMA DENSITIES (G CM-3):										
PRESSURE: 1 BAR										
1200°C	2.72	2.66	2.75	2.69	2.61	2.64	2.69	2.63	2.62	2.65
1000°C	2.76	2.69	2.80	2.73	2.64	2.67	2.73	2.66	2.65	2.68
800°C	2.80	2.73	2.85	2.77	2.68	2.70	2.77	2.69	2.69	2.71
PRESSURE: 1 KBAR										
1200°C	2.72	2.66	2.76	2.70	2.62	2.65	2.69	2.63	2.62	2.65
1000°C	2.76	2.70	2.80	2.74	2.65	2.68	2.73	2.66	2.66	2.68
800°C	2.80	2.73	2.85	2.78	2.68	2.71	2.77	2.70	2.69	2.72

AREA:	JELOYA	BAERUM		AINSJO	NITTEDAL	DRAMMEN	GLITRVNN			
ROCK TYPE:	PLPX-BAS	PL-BAS	Aph-BAS	PL-BAS	PL-BAS	PL-BAS	PL-BAS	RH-PY	TRACHYTE	RHYOLITE
NUMBER OF SAMPLES:	3	5	1	1	1	1	5	4	2	1
CATION PERCENT:										
Si^{4+}	47.71	47.21	44.72	50.82	46.55	45.33	46.43	51.69	59.97	71.29
Ti^{4+}	2.13	2.14	2.20	1.62	2.26	2.32	1.97	1.22	.60	.05
Al^{3+}	16.69	17.99	19.76	18.90	16.49	18.59	19.19	19.20	17.79	13.73
Fe^{3+}	4.76	5.96	4.57	5.56	4.87	5.97	5.03	5.39	2.93	.35
Fe^{2+}	3.97	2.94	4.59	2.60	3.74	3.16	3.70	1.21	1.19	.79
Mn^{2+}	.15	.18	.16	.15	.17	.18	.14	.22	.06	.09
Mg^{2+}	5.85	6.53	6.61	4.33	7.48	7.69	6.10	2.51	1.72	.73
Ca^{2+}	6.50	7.80	8.76	6.78	8.84	8.14	8.08	5.17	1.86	.01
Na^{+}	7.53	6.37	5.77	5.88	7.51	7.05	7.52	8.19	5.48	4.36
K^{+}	4.36	2.47	2.41	3.09	1.76	1.27	1.54	4.43	8.17	8.60
P^{5+}	.35	.40	.45	.28	.31	.32	.30	.76	.22	.01
TOTAL	100.00	100.00	100.00	100.00	100.00	100.00	100.00	100.00	100.00	100.00
ANION EQUIVALENT:										
O^{2-}	155.14	157.51	155.67	160.61	155.33	156.25	156.43	160.04	164.43	171.91
O^{2-}	0	0	0	0	0	0	0	0	0	0
F^{-}	0	0	0	0	0	0	0	0	0	0
MOLAR RATIOS (CATIONS):										
$Fe^{3+}:Fe^{2+}$	1.20	2.03	.99	2.14	1.30	1.89	1.36	4.45	2.45	.44
Mg:Mg+Fe	.40	.42	.42	.35	.46	.46	.41	.28	.29	.39
Ca:Na+K	.55	.88	1.07	.76	.95	.98	.89	.41	.14	.00
Na:Na+K	.63	.72	.71	.66	.81	.85	.83	.65	.40	.34
Na+K:Al	.71	.49	.41	.47	.56	.45	.47	.66	.77	.94
MODIFIED C.I.P.W. NORMS (CAT. PC):										
Q	0	2.44	0	8.32	0	0	.51	4.12	14.29	31.03
Or	21.80	12.37	12.05	15.43	8.81	6.33	7.69	22.17	40.84	42.98
Ab	35.24	31.87	28.87	29.39	37.56	35.25	37.60	40.94	27.42	21.80
An	11.98	22.85	28.95	24.83	18.05	25.68	25.34	16.43	7.52	0
Ne	1.46	0	0	0	0	0	0	0	0	0
Di	14.08	10.24	8.54	5.38	18.84	9.86	10.02	2.47	0	0
Hd	0	0	.33	0	0	0	0	0	0	0
Js	0	0	.01	0	0	0	0	0	0	0
En	0	7.94	7.02	5.97	2.83	10.29	7.20	3.79	3.44	1.47
Fs	0	0	.28	0	0	0	0	0	0	1.31
Fo	3.49	0	1.45	0	2.03	.12	0	0	0	0
Fa	0	0	.06	0	0	0	0	0	0	0
Mt	5.75	2.76	6.63	3.20	4.73	2.90	5.41	.52	1.88	.47
Jc	.22	.17	.22	.18	.21	.16	.20	.09	.10	.05
He	.78	4.02	0	3.30	1.57	3.93	1.29	4.98	1.60	0
Ilm	4.11	4.04	4.26	3.07	4.33	4.39	3.80	2.08	1.13	.09
Pn	.16	.24	.14	.17	.20	.24	.14	.37	.06	.01
Ap	.93	1.07	1.20	.75	.84	.85	.81	2.03	.58	.02
C	0	0	0	0	0	0	0	0	1.13	.78
D.I.	58.50	46.68	40.92	53.14	46.37	41.58	45.80	67.23	82.55	95.81
CALCULATED ANHYDROUS MAGMA DENSITIES (G CM-3):										
PRESSURE: 1 BAR										
1200°C	2.57	2.59	2.63	2.54	2.61	2.62	2.60	2.47	2.39	2.31
1000°C	2.61	2.62	2.66	2.57	2.64	2.65	2.63	2.50	2.42	2.33
800°C	2.64	2.65	2.70	2.59	2.68	2.68	2.66	2.53	2.44	2.35
PRESSURE: 1 KBAR										
1200°C	2.58	2.59	2.64	2.54	2.62	2.62	2.60	2.48	2.40	2.32
1000°C	2.61	2.62	2.67	2.57	2.65	2.65	2.63	2.50	2.42	2.34
800°C	2.64	2.65	2.70	2.60	2.68	2.68	2.66	2.53	2.44	2.36

AREA:	SVARTJERN				
ROCK TYPE:	SKAU	STOR	BEKK	IGN	TUFF
NUMBER OF SAMPLES:	10	7	9	9	4
CATION PERCENT:					
Si^{4+}	53.97	52.11	52.06	62.80	60.02
Ti^{4+}	1.10	1.36	1.40	.41	.68
Al^{3+}	20.85	20.98	19.22	17.81	18.89
Fe^{3+}	4.19	4.19	3.04	2.37	3.24
Fe^{2+}	.70	1.38	2.87	.40	.24
Mn^{2+}	.07	.11	.14	.12	.10
Mg^{2+}	2.02	3.23	3.89	1.04	1.16
Ca^{2+}	4.04	4.73	4.66	1.15	1.08
Na^{+}	7.47	6.23	7.67	7.78	7.91
K^{+}	5.22	5.15	4.60	6.05	6.52
P^{5+}	.38	.54	.44	.09	.15
TOTAL	100.00	100.00	100.00	100.00	100.00
ANION EQUIVALENT:					
O^{2-}	160.56	158.81	157.06	164.07	162.42
OH^{-}	2.53	4.73	4.11	4.89	4.70
F^{-}	0	0	0	0	0
MOLAR RATIOS (CATIONS):					
$Fe^{3+}:Fe^{2+}$	6.02	3.03	1.06	5.99	13.24
Mg:Mg+Fe	.29	.37	.40	.27	.25
Ca:Na+K	.32	.42	.38	.08	.08
Na:Na+K	.59	.55	.63	.56	.55
Na+K:Al	.61	.54	.64	.78	.76
MODIFIED C.I.P.W. NORMS (CAT. PC):					
Q	7.11	7.08	3.86	18.29	13.90
Or	26.08	25.75	23.00	30.23	32.61
Ab	37.34	31.15	38.36	38.89	39.57
An	16.97	19.17	17.38	4.99	4.15
Di	0	0	1.73	0	0
Hd	0	0	.04	0	0
Js	0	0	.00	0	0
En	4.04	6.46	6.91	2.09	2.31
Fs	0	0	.17	0	0
Mt	0	.34	4.34	.25	0
Jc	0	.03	.22	.08	0
He	4.19	3.94	0	2.15	3.24
Ilm	1.39	2.53	2.66	.62	.49
Pn	.14	.19	.13	.19	.21
Ap	1.03	1.43	1.18	.23	.41
Rt	.33	0	0	0	.33
C	1.37	1.93	0	1.99	2.79
D.I.	70.53	63.98	65.22	87.41	86.08
CALCULATED ANHYDROUS MAGMA DENSITIES (G CM-3):					
PRESSURE: 1 BAR					
1200°C	2.44	2.47	2.50	2.36	2.37
1000°C	2.46	2.50	2.52	2.38	2.40
800°C	2.49	2.53	2.55	2.40	2.42
PRESSURE: 1 KBAR					
1200°C	2.44	2.48	2.50	2.36	2.38
1000°C	2.47	2.50	2.53	2.39	2.40
800°C	2.49	2.53	2.55	2.41	2.42

in Chapter 1, as it is believed that this provides a more informative framework for the comparison and interpretation of rock compositions. Table 2.1 also lists various atomic ratios and normative mineralogies, calculated on the basis of the procedure outlined in Appendix A2. Estimates of anhydrous magma densities have been calculated on the basis of partial molar volumes of oxide components using the method of Bottinga and Weill (1970), as outlined in Section 1.5.2.

2.3.2 The plutonic rocks

The plutonic rocks in the Oslo Region may be divided into two distinct groups (Neumann 1978):

(1) A series of mafic volcanic necks consisting of a variety of mafic to ultramafic rocks collectively grouped under the heading of Oslo Essexite; and

(2) A number of large batholiths comprising intrusive rocks in the compositional range monzodiorite to granite, but also including silica undersaturated varieties (plagifoyaites and nepheline syenites); altogether forming 60 percent of the present graben surface (Ramberg 1976). Rocks in this compositional range are exposed in three principal regions (Figure 2.1):

(a) The Larvik, Skrim and Eikeren massifs in the south;
(b) The Nordmarka - Hurdalen Batholith in the north; and
(c) The Drammen and Finnemarka granite complexes in the centre.

The plutonic rocks have been described by a number of authors including Barth (1944), Dietrich (1965, 1967), Czamanske (1965, 1972, 1973), Nystuen (1975b), Neumann (1976, 1978 and 1980), Gaut (1981) and Ihlen et al. (1982). The principal rock-types fall into the following categories (Ramberg 1976, Appendix; Neumann 1978, classification after Streckeisen 1976

in parenthesis):

OSLO ESSEXITE: Gabbroic rocks of alkaline affinity (Neumann 1978), showing considerable diversity in mineralogy and chemistry, and including the rock-types: Pyroxenite, olivine gabbro, bojite, kauaiite, mafraite and akerite (Ramberg 1976). The volcanic necks with which these rocks are associated have been shown to have limited vertical extent (Ø.5 to 1.5 km; Ramberg 1976) and are interpreted as subvolcanic magma chambers, probably representing feeder zones to the more volumetrically important subaerial lava flows.

KJELSASITE (monzodiorite - syenite): Generally coarse-grained rocks containing plagioclase (An > 3Ø) and alkali feldspar in variable proportions, with sporadic quartz and about 2Ø percent dark minerals. For practical purposes this rock-type is often considered together with the larvikites (Neumann 1978).

LARVIKITE (monzonite - monzosyenite): Medium to coarse-grained rocks containing plagioclase (An < 30) and alkali feldspar, usually in roughly equal proportions. The kjelsasites and larvikites generally contain a Ti-poor augite as the main ferromagnesian mineral, sometimes accompanied by kaesuritic hornblende or olivine. Quartz or nepheline may be present.

LARDALITE (nepheline monzonite to nepheline syenite): Fine to coarse-grained silica undersaturated rocks containing nepheline, antiperthite, Ti-poor augite, and possibly biotite.

FOYAITE/HEDRUMITE (nepheline syenite): Nepheline-free to nepheline-rich rocks containing mesoperthite and aegirine augite or aegirine.

NORDMARKITE (alkali feldspar syenite): Peralkaline rocks containing aegirine-augite and/or riebeckitic amphibole, both of which may be zoned, with mesoperthite and occasionally minor quartz.

GREFSEN SYENITE (alkali syenite): Alkaline rocks containing zoned plagioclase rimmed by mesoperthite, Na-rich alkali feldspar, common hornblende, biotite and possibly Ti-poor augite, with minor amounts of quartz.

EKERITE (alkali feldspar granite): Peralkaline rocks consisting of quartz, mesoperthite, aegirine, riebeckitic arfvedsonite and/or biotite. Dietrich et al. (1965) have reported the presence of astrophyllite and elpidite within some of the ekerites, particularly in their contact zones.

BIOTITE GRANITE (granite to alkali granite): Medium to coarse-grained rocks containing plagioclase and alkali feldspar in variable proportions, quartz biotite, and sometimes hornblende. Gaut (1981) distinguishes two groups of biotite granite, mainly on the basis of age relationships: Biotite Granite I which occurs in the Drammen and Finnemarka granite complexes; and Biotite Granite II which occurs as small bodies in close association with syenites and ekerites, particularly in the northern batholith.

Magnetite, ilmenite, apatite and zircon are important accessory minerals in all the above named rock-types. In addition, sphene and rutile may be present.

Table 2.2 lists average chemical analyses of the principal plutonic rock-types, after Neumann (1976, 1980), Ihlen et al. (1982), Rasmussen (1982) and Spangsberg Jensen (1982), expressed in cation percent. Table 2.2 also lists various atomic ratios including agpaitic index, normative mineralogies and calculated anhydrous magma densities. Trace element data are not included.

TABLE 2.2 REPRESENTATIVE GEOCHEMICAL ANALYSES OF THE PLUTONIC ROCKS

AREA:									LARVIK	
ROCK TYPE:	H-7	J-9	E-11	E-10	KJELS	GREF SY	NDMKT	EKERITE	LARV	LARD
NUMBER OF SAMPLES:	1	1	1	1	4	1	5	5	24	8
CATION PERCENT:										
Si^{4+}	43.65	45.35	37.62	47.49	52.29	57.41	58.07	68.58	53.36	48.83
Ti^{4+}	1.66	2.74	3.97	2.17	1.15	.73	.63	.25	.90	.91
Al^{3+}	4.56	15.72	5.15	17.94	19.19	18.89	17.31	13.52	20.04	21.40
Fe^{3+}	4.11	1.66	8.97	3.08	1.47	1.34	1.49	1.45	1.84	1.52
Fe^{2+}	6.89	10.55	10.01	6.34	3.61	1.34	1.02	.47	2.18	2.36
Mn^{2+}	.16	.24	.34	.31	.10	.11	.14	.13	.13	.14
Mg^{2+}	20.56	9.40	16.79	5.05	3.57	1.67	1.06	.52	1.90	2.28
Ca^{2+}	17.47	8.79	16.11	5.58	5.66	2.00	1.17	.31	3.68	2.70
Na^{+}	.92	4.75	.91	7.85	8.69	10.52	12.65	9.24	10.59	13.79
K^{+}	.02	.81	.13	4.19	3.79	5.77	6.25	5.50	4.95	5.41
P^{5+}	0	0	0	0	.48	.20	.21	.03	.45	.65
TOTAL	100.00	100.00	100.00	100.00	100.00	100.00	100.00	100.00	100.00	100.00
ANION EQUIVALENT:										
O^{2-}	149.17	154.00	148.14	154.15	157.28	160.41	158.97	168.00	156.28	150.55
OH^{-}	0	0	0	0	1.28	0	0	1.32	2.40	2.69
F^{-}	0	0	0	0	0	0	0	0	0	0
S^{2-}	0	0	0	0	0	0	0	0	0	0
MOLAR RATIOS (CATIONS):										
$Fe^{3+}:Fe^{2+}$	.60	.16	.90	.49	.41	1.00	1.46	3.08	.85	.65
Mg:Mg+Fe	.65	.43	.47	.35	.41	.38	.30	.21	.32	.37
Ca:Na+K	18.58	1.58	15.60	.46	.45	.12	.06	.02	.24	.14
Na:Na+K	.97	.85	.88	.65	.70	.65	.67	.63	.68	.72
Na+K:Al	.21	.35	.20	.67	.65	.86	1.09	1.09	.78	.90
MODIFIED C.I.P.W. NORMS (CAT. PC):										
Q	0	0	0	0	1.23	3.84	.70	24.58	0	0
Or	.12	4.05	.63	20.93	18.97	28.87	31.23	27.50	24.77	27.07
Ab	4.58	23.75	4.51	33.08	43.43	52.62	55.33	40.09	52.94	35.69
An	9.04	25.40	10.30	14.76	16.77	6.49	0	0	11.24	5.50
Ne	0	0	.01	3.71	0	0	0	0	0	19.95
Ac	0	0	0	0	0	0	5.95	4.87	0	0
Ns	0	0	0	0	0	0	.15	0	0	0
Di	53.90	8.40	50.49	6.65	4.01	1.44	2.18	.70	2.20	1.51
Hd	8.56	6.31	5.52	3.69	1.99	.04	.96	.25	.52	.51
Js	.20	.14	.19	.18	.06	.00	.13	.07	.03	.03
En	6.06	10.49	0	0	5.13	2.61	1.04	.69	.04	0
Fs	.98	8.06	0	0	2.63	.08	.52	.32	.01	0
Fo	6.09	3.08	6.24	5.08	0	0	0	0	1.99	2.86
Fa	.99	2.37	.71	2.96	0	0	0	0	.50	1.03
Mt	6.03	2.43	13.02	4.41	2.15	1.86	0	.27	2.61	2.16
Jc	.14	.05	.44	.22	.06	.16	0	.08	.15	.13
Ilm	3.24	5.36	7.68	4.13	2.24	1.35	1.10	.39	1.71	1.73
Pn	.08	.12	.26	.20	.06	.12	.15	.11	.10	.10
Ap	0	0	0	0	1.27	.53	.56	.08	1.19	1.74
D.I.	4.70	27.80	5.15	57.72	63.62	85.32	87.26	92.17	77.72	82.71
CALCULATED ANHYDROUS MAGMA DENSITIES (G CM-3):										
PRESSURE: 1 BAR										
1200°C	2.83	2.76	2.96	2.61	2.50	2.39	2.37	2.32	2.44	2.44
1000°C	2.88	2.80	3.01	2.64	2.53	2.42	2.40	2.34	2.47	2.47
800°C	2.92	2.83	3.06	2.67	2.55	2.44	2.42	2.36	2.49	2.51
PRESSURE: 1 KBAR										
1200°C	2.84	2.77	2.96	2.61	2.50	2.40	2.37	2.33	2.45	2.45
1000°C	2.88	2.80	3.01	2.64	2.53	2.42	2.40	2.35	2.47	2.48
800°C	2.93	2.84	3.06	2.68	2.56	2.45	2.43	2.37	2.50	2.51

AREA:	LARVIK		DRAMMEN	GLITRVNN	SVARJERN					
ROCK TYPE	FOY/HED	DITROITE	GRANITE	GRANITE	GANG	GABB	BISY	NORD	KVPO	KVSY
NUMBER OF SAMPLES:	6	2	4	41	2	7	13	4	4	3
CATION PERCENT:										
Si^{4+}	51.56	50.77	70.62	70.51	45.72	48.54	61.11	60.60	68.78	67.13
Ti^{4+}	.67	.59	.23	.18	2.71	1.97	.47	.47	.25	.22
Al^{3+}	21.68	21.47	14.51	14.09	16.29	17.90	18.12	17.96	14.78	15.34
Fe^{3+}	1.16	1.01	.84	.71	3.48	2.67	1.33	1.43	1.01	.91
Fe^{2+}	1.21	2.70	.17	.31	5.92	4.86	.77	.68	.62	.46
Mn^{2+}	.13	.15	.03	.02	.19	.20	.12	.14	.11	.10
Mg^{2+}	1.09	.90	.14	.13	7.37	5.71	.82	.51	.52	.27
Ca^{2+}	1.27	1.66	.58	.39	8.42	6.59	1.32	.77	.47	.49
Na^{+}	14.41	13.65	7.08	7.96	6.77	7.72	8.96	10.09	7.77	8.26
K^{+}	6.62	6.94	5.76	5.69	2.28	3.24	6.84	7.27	5.75	6.78
P^{5+}	.19	.15	.02	.01	.83	.60	.13	.08	.05	.04
TOTAL	100.00	100.00	100.00	100.00	100.00	100.00	100.00	100.00	100.00	100.00
ANION EQUIVALENT										
O^{2-}	150.83	150.50	170.44	170.26	149.00	152.29	160.90	162.20	170.13	168.02
OH^{-}	3.44	2.70	1.95	1.35	8.01	5.19	3.59	0	0	0
F^{-}	0	0	.21	0	0	0	0	0	0	0
S^{2-}	0		.12	0	0	0	0	0	0	0
MOLAR RATIOS (CATIONS):										
$Fe^{3+}:Fe^{2+}$	.96	.37	4.87	2.27	.59	.55	1.72	2.11	1.63	1.97
Mg:Mg+Fe	.32	.19	.12	.11	.44	.43	.28	.20	.24	.16
Ca:Na+K	.06	.08	.05	.03	.93	.60	.08	.04	.03	.03
Na:Na	.69	.66	.55	.58	.75	.70	.57	.58	.57	.55
Na+k:Al	.97	.96	.89	.97	.56	.61	.87	.97	.91	.98
MODIFIED C.I.P.W. NORMS (CAT. PC):										
Q	0	0	30.82	28.85	0	0	10.70	7.07	26.81	21.18
Or	33.09	34.72	28.82	28.45	11.42	16.20	34.19	36.35	28.76	33.90
Ab	37.78	31.58	35.41	39.78	33.86	38.61	44.79	50.45	38.84	41.29
An	1.63	2.18	2.79	1.10	18.09	17.34	5.49	1.50	1.94	.75
Ne	20.57	22.01	0	0	0	0	0	0	0	0
Wo	0	0	0	.06	0	0	0	0	0	.02
Di	2.31	1.31	0	.50	11.16	6.50	0	1.35	0	1.07
Hd	.17	2.42	0	0	2.43	1.92	0	0	0	0
Js	.02	.14	0	0	.08	.08	0	0	0	0
En	0	0	.28	0	5.50	5.47	1.65	.35	1.05	0
Fs	0	0	0	0	1.24	1.69	0	0	0	0
Fc	.77	.86	0	0	2.74	2.02	0	0	0	0
Fa	.06	1.68	0	0	.62	.62	0	0	0	0
Mt	1.57	1.43	0	.45	5.06	3.85	1.10	.87	1.22	.85
Jc	.17	.08	0	.03	.16	.16	.17	.18	.22	.17
He	0	0	.84	.39	0	0	.49	.73	.04	.23
Ilm	1.22	1.13	.35	.33	5.26	3.78	.82	.78	.42	.36
Pn	.13	.06	.06	.02	.17	.16	.13	.16	.08	.08
Ap	.51	.41	.04	.02	2.22	1.60	.36	.21	.13	.11
Rt	0	0	.03	0	0	0	0	0	0	0
C	0	0	.55	0	0	0	.13	0	.48	0
D.I.	91.44	88.32	95.05	97.08	45.27	54.81	89.68	93.86	94.41	96.36
CALCULATED ANHYDROUS MAGMA DENSITIES (G CM-3):										
PRESSURE: 1 BAR										
1200°C	2.39	2.42	2.31	2.31	2.65	2.58	2.36	2.35	2.33	2.32
1000°C	2.42	2.45	2.33	2.33	2.68	2.61	2.38	2.38	2.35	2.34
800°C	2.45	2.48	2.35	2.35	2.71	2.64	2.41	2.40	2.37	2.36
PRESSURE: 1 KBAR										
1200°C	2.40	2.43	2.32	2.32	2.65	2.58	2.36	2.36	2.33	2.33
1000°C	2.43	2.46	2.34	2.33	2.68	2.61	2.39	2.38	2.35	2.35
800°C	2.45	2.49	2.35	2.35	2.72	2.64	2.41	2.41	2.37	2.37

AREA:	SVARJIERN
ROCK TYPE:	GRAN
NUMBER OF SAMPLES:	6
CATION PERCENT:	
Si^{4+}	72.19
Ti^{4+}	.13
Al^{3+}	13.31
Fe^{3+}	.70
Fe^{2+}	.40
Mn^{2+}	.09
Mg^{2+}	.18
Ca^{2+}	.28
Na^{+}	6.96
K^{+}	5.74
P^{5+}	.02
TOTAL	100.00
ANION EQUIVALENT:	
O^{2-}	173.00
O^{-}	0
F^{-}	0
S^{2-}	0
MOLAR RATIOS (CATIONS):	
$Fe^{3+}:Fe^{2+}$	1.73
Mg:Mg+Fe	.14
Ca:Na+K	.02
Na:Na+K	.55
Na+K:Al	.95
MODIFIED C.I.P.W. NORMS (CAT. PC):	
Q	33.38
Or	28.70
Ab	34.78
An	1.29
En	.37
Fs	.03
Mt	.86
Jc	.19
Ilm	.21
Pn	.05
Ap	.04
	.10
D.I.	96.86
CALCULATED ANHYDROUS MAGMA DENSITIES (G CM-3):	
PRESSURE: 1 BAR	
1200°C	2.31
1000°C	2.33
800°C	2.34
PRESSURE : 1 KBAR	
1200°C	2.31
1000°C	2.33
800°C	2.35

Rocks belonging to the kjelsasite and larvikite rock groups are exposed mainly in the southern part of the Oslo Region, in the Larvik and Skrim massifs where they occur in close association with the undersaturated rock-types lardalite and foyaite/hedrumite (Figure 2.1). However, they also occur in isolated areas and as "stoped" blocks within the northern batholith. In comparison, the alkaline to peralkaline syenitic and granitic rocks occur in both the southern and northern plutons, comprising the Eikeren massif in the south and a large part of the Nordmarka-Hurdalen batholith in the north.

Estimates of the areal frequency of the Oslo Region plutonic rocks (Barth 1944, 1954; Ramberg 1976) indicate a bi-modal population with rocks in the compositional range larvikite - nordmarkite and granite predominating at the surface. This is in marked contrast to the volcanic rocks which fall into two compositional groups, mafic rocks of alkali olivine basalt affinity on the one hand, and intermedite trachyandesites and trachytes on the other (cf. the Kenya rift; Williams 1972, Baker et al. 1977); and to the volcanic rocks exposed in the Midland Valley of Scotland (Tomkeieff 1937), where rocks of alkali olivine basalt affinity predominate. Clearly, the surface expression of magmatic products in the rift is not necessarily a good indication of their true volumetric proportions.

Gravity studies by Ramberg (1976) have located the presence of a large positive gravity anomaly (of the order of 45 mgal) parallel to the main rift axis and extending out into the Skagerrak. The existence of this gravity anomaly is believed to imply both the occurrence of a significant mantle upwarp in the vicinity of the rift, and the presence of large volumes of dense rock immediately underlying the graben. On the basis of their calculated densities, these rocks are interpreted to be of mafic to ultra-mafic composition,

although the possibility can not be precluded that they include crustal rocks in a high metamorphic (? granulite) facies . Volume estimates by Ramberg (1976) suggest that the felsic rocks exposed at the surface (circa 1.4 x $1Ø^4$ km^3) are accompanied by considerably greater volumes (circa 1.2 x $1Ø^5$ km^3) of mafic rocks at depth.

Gravity modelling by Ramberg has also provided significant information about the spatial configurations of the major felsic batholiths which, when combined with petrological and structural criteria, provides a useful framework for unravelling the petrogenesis of the Oslo province.

A. The Larvik and Skrim massifs are located at the southern end of the Vestfold - Ringerike graben (Section 2.2; Figure 2.2), and comprise the largest areas of exposed monzonitic rocks in the Oslo Region. Structurally, both massifs are composed of a number of ring-segments (Figure 2.1).

The Larvik ring-complex, in the extreme south, consists of at least ten semi-circular ring-segments showing a systematic decrease in age and size towards the west, and forms an important profile across the rift (Petersen 1977a). The ring-segments show a progressive trend towards silica-undersaturation, the outermost segments (RS1 and RS2) being composed of quartz-bearing larvikite (Tonsbergite); the intermediate segments (RS3 to RS8) being composed of nepheline-bearing larvikite; and the innermost segments (RS9 and RS1Ø), consisting of the extremely undersaturated rock-types lardalite and foyaite/hedrumite (Petersen 1977 a and b; Neumann 1977, 198Ø).

The Skrim massif and adjoining area of nordmarkitic rocks to the south are composed of at least three ring-structures: The Mykle ring-structure, and the Skrehelle and Vealos cauldrons (Segalstad 1975). In both massifs, contact relationships are generally sharp, although transitions between larvikite and

nordmarkite have been reported (Neumann 1978, ref. cit. Raade 1973).

Gravity measurements in the Larvik and Skrim areas are unable to provide much information about the configurations of these plutons with depth, due to similarities in density between the monzonites (2.71 g cm^{-3}) and surrounding gneisses, (2.74 g cm^{-3}; Ramberg 1976). However, several lines of evidence, especially the preponderance of compositionally similar extrusive rocks (rhomb porphyries) at the surface, suggest that these bodies extend downwards to depth (Ramberg 1976).

B. The Nordmarka - Hurdalen Batholith is located in the south-eastern part of the Akershus graben, just to the north of Oslo (Figure 2.2). It is a large composite batholith consisting of numerous, essentially high level intrusions of alkaline to peralkaline syenites and granites. The latter show both transitional and sharp, cross-cutting intrusive relationships indicating several closely related stages of evolution. Locally, large areas of monzonitic rocks are included within the batholith, reflecting an earlier intrusive episode. Monzonitic rocks are particularly common in some of the cauldron complexes within the southern part of the batholith. Several lines of evidence suggest that the present level of erosion is close to the original roof of the batholith. In particular, the presence of roof pendants, the widespread development of porphyritic textures and the occurrence of miarolitic cavities and druses within the intrusives, are believed to be diagnostic (Section 3.2; Nystuen 1975b, Ramberg 1976).

On the basis of a negative residual gravity anomaly and an assumed constant density contrast between the felsic rocks and surrounding gneisses of -.12 g cm^{-3}, the Nordmarka - Hurdalen batholith is interpreted as a wedge- or funnel-shaped body extending downwards to depths of 10 or 12 kilometres, with a total volume of approximately 9809 km^3

(Ramberg 1976). Although, a postulated reduced density contrast towards the walls of the intrusion, due to the presence of stoped blocks of country rock, would widen the dimensions of this model somewhat. The felsic body is probably underlain by rocks of intermediate density, either intrusive rocks of monzonitic composition or basement gneisses, or a combination of the two.

C. The Drammen and Finnemarka Granite complexes are located in the central part of the Oslo Region (Figure 2.2), and constitute the main areas of biotite granite in the palaeorift (Gaut 1981). For these reasons they would appear to show a somewhat different provenance from the main plutonic series (Section 2.5.4).

The Drammen Granite complex consists of several intrusive phases of essentially granitic composition, with only minor representation from less siliceous rocks (only the Lindum breccia; Ihlen et al. 1982). It is a subcircular body and is interpreted as a shallow (2 to 4 km), tabular batholith, either grading downwards into a mixture of stoped blocks and intrusives, or floored by Precambrian gneisses (Ramberg 1976).

In comparison, the Finnemarka complex (Czamanske 1965, Czamanske and Mihalik 1972, Czamanske and Wones 1973) comprises a central granite stock with peripheral intrusions of granodiorite and monzonite. The granite stock probably extends downwards to 7 or 8 kilometres, tapering with depth, and is believed to be floored by intrusive rocks of intermediate composition (on the basis of multiple intrusion; Ramberg 1976).

2.4 Tectonomagmatic evolution

The Tectonomagmatic evolution of the Oslo Graben has been described in detail by Ramberg and Larsen (1978), and Ramberg

and Spjeldnaes (1977). Only the main details will be summarised here.

Rift-related tectonism and magmatism in the Oslo Region almost certainly began in late Precambrian times with the emplacement of major gabbroic intrusions in the Kongsberg and Tyrifjorden areas, and the Fen carbonatite complex (Section 2.2). The formation of the Eocambrian fault-bound Sparagmite basin, and the Cambro-Silurian sedimentary troughs in the area of the incipient rift, suggests that rift-related subsidence was active throughout most of this period. Subsidence was presumably in response to deep crustal and/or mantle processes, resulting in an increased density contrast in the lower crust (above the level of isostatic compensation). Such processes may have involved mantle upwarping and intrusion of mafic material into the lower crust (underplating) and/or an upward migration of the granulite/amphibolite facies boundary within the crust (cf. Falvey 1974), in either case implying the presence of a significant thermal anomaly in the vicinity of the rift dating back to late Precambrian times.

The Devonian and Carboniferous periods may have represented a relatively quiet period in pre-rift development. However late Caledonian deformation in the Devonian presumably preceded a renewed erosional cycle. The lack of sediments from this period may reflect subaerial conditions, or subsequent removal during the Permian event. Whilst there is no unequivocal evidence for crustal doming at this time (Section 2.2), it is unlikely that none took place, in view of the likely existence of a thermal anomaly beneath the rift. Renewed subsidence and sedimentary deposition in late Carboniferous or early Permian times immediately preceded rift development.

The main rifting episode began in early Permian times with the extrusion of huge volumes of basaltic lavas of alkali

olvine basalt affinity, mainly from fissures, and possibly in an interdome basin (Ramberg and Larsen 1978). Volcanism began in the south and migrated northwards and eastwards with time (see Segalstad 1977, Figure 2), incorporating the eruption of more evolved magmas. Basaltic volcanism was later accompanied by the eruption of rhomb porphyry lavas throughout the Oslo Region. Rhomb porphyries were also intruded as axial dykes. This stage of evolution (Stage 3; Ramberg and Larsen 1978) also involved the formation of the major boundary faults and general "rift valley" attainment. The Drammen and Finnemarka granite complexes may have been emplaced at this time. Although intrusive relationships suggest that the Drammen Granite may be younger than the Glitrevann Cauldron (Oftedahl 1953, Geyti and Schonwandt 1979).

A reduction in tensional stress in the Oslo Graben was marked by the formation of central volcanoes at the intersection of the major tectonic lineaments (NNW and NE) with an average volcano spacing of 28 km $\pm$ 10 km (16). A drop in magmatic pressure beneath these central volcanoes was presumably responsible for the formation of major caulderas which were subsequently infilled by lavas and ignimbrites of trachytic to rhyolitic composition. The volcanic necks (Oslo-Essexites) may have been formed during this stage, possibly representing a late, violent phase in the central volcano stage.

The final stage in the evolution of the Oslo Rift involved the emplacement and consolidation of the major felsic batholiths (Section 2.3.2), and marked a change towards more stable tectonic conditions. To some extent this stage overlapped with preceding stages in that intermediate to granitic magmas provided the reservoirs for extensive subaerial eruption. Following the same trend as rift development in general, the southern batholith was probably emplaced somewhat earlier. Ring structures in the Larvik area indicate the importance of circular tectonic structures in rift development and the general migration of intrusive

centres from east to west and towards the centre of the rift. The Nordmarka - Hurdalen batholith in the north may represent a somewhat higher crustal level being close to its original roof, but is probably underlain by rocks of more intermediate and mafic compositions at depth.

Emplacement of the felsic batholiths is believed to have taken place essentially by a mechanism of stoping, in which the magmas literally traded place with the country rocks. However, there is evidence to suggest that some of the more highly evolved granitic magmas may have been emplaced by more forcefull mechanisms (Nystuen 1975b, Section 3.5).

2.5 Petrogenesis of the Oslo Province

Theories concerning the origin and evolution of volcanic and plutonic rocks in the Olso Region have covered a whole spectrum of possibilities ranging from fractional crystallisation of basaltic magma to anatexis of continental crust. Brogger in the 1890's believed that all the igneous rocks of the Region had the same origin, as a result of fractional crystallisation of basaltic magma corresponding to "essexite" in composition (Dons 1978). In contrast, Barth (1944, 1954) postulated two sources of magma, one giving rise to the alkali olivine basalt lavas and volcanic necks; and the other giving birth to the felsic rocks, probably at shallow depths within the crust (Dons 1978).

Barth recognised four principal rock series within the Oslo Region:

(1) A basic series (Oslo-essexites) responsible for the basaltic lavas and volcanic necks (Figure 2.4a);
(2) An intermediate to acid series responsible for the observed evolutionary sequence: Kjelsasite, larvikite, nordmarkite, ekerite (Figure 2.4b);
(3) An intermediate peralkaline series responsible for the

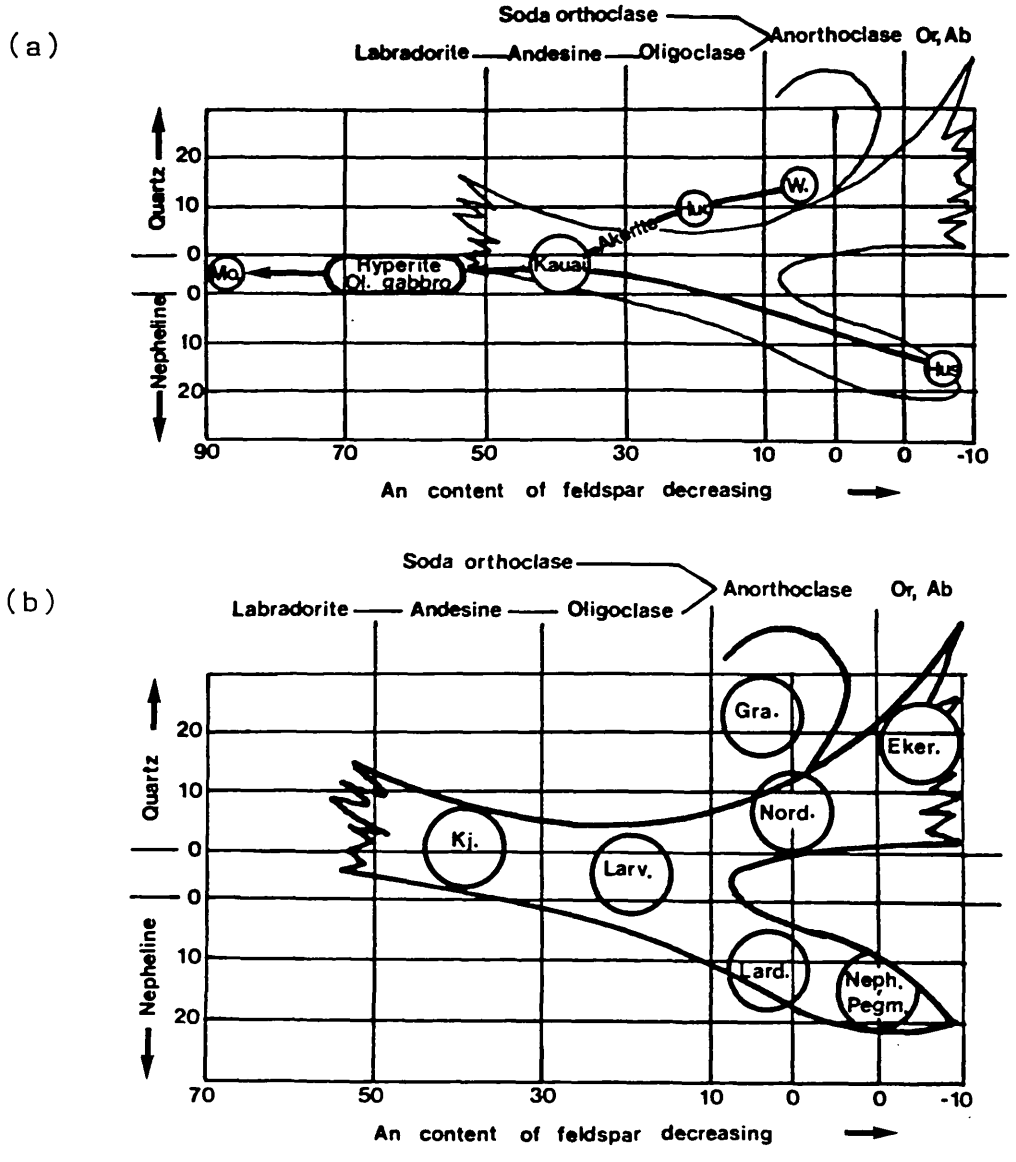

FIGURE 2.4. Barth's "Family Trees", showing the systematic position and mutual relationship of the principal rock-types in the Oslo Region: (a) Oslo essexite series; and (b) Main kjelsasite - granite series (slightly modified after Barth 1944). Mod = Modumite, Kauai = Kauiite, Hur = Hurumite, W = Windsorite, Hus = Husbyite, Kj = Kjelsasite, Larv = Larvikite, Nord = Nordmarkite, Eker = Ekerite, Gra = Granite, Lard = Lardalite.

undersaturated rock-types lardalite and foyaite/hedrumite; and
(4) An acid series responsible for paraluminous granites such as the Drammen and Finnemarka granites.

Barth (1944, 1954) demonstrated that the principal members of the kjelsasite to ekerite series could be explained in terms of differentiation of a syenitic magma, essentially by fractionation of feldspar. Barth proposed a mineral reaction series in which separation of plagioclase of increasingly more sodic composition was accompanied and later superceded by anorthoclase fractionation. The role of mafic minerals in this process was assumed to be of secondary importance, early pyroxenes being replaced by common hornblende and sodic amphiboles.

Barth (1954) postulated that the syenitic magma from which the main plutonic series evolved was formed as a result of wholesale differentiation of the Precambrian crust, involving introduction to higher levels of "eminations" from depth. These eminations were conceived as incorporating Si, Al, Na and K, together with volatile phases such as H_2O, CO_2, HF and HCl. They were believed to have been produced as a result of heating and degassing of the deep crust, resulting in a depleted lower crust which may have provided the source for some of the more mafic magmas. Barth's model was highly dependent upon the observed proportions of magmatic products at the graben surface, and now seems to be untenable in the light of recent geophysical evidence (Section 2.3.2, Ramberg 1976).

Gravity surveys by Ramberg (1976) have revealed that the intermediate to granitic rocks exposed at the graben surface are underlain at depth by considerably greater volumes of dense rock, of presumed mafic to ultramafic composition (Section 2.3.2). There is therefore no objection on volumetric grounds to the hypothesis that the felsic rocks of

the Oslo Region originated by differentiation from a basaltic parent magma ultimately of upper mantle provenance. By analogy with many active rift systems (e.g. Fairhead 1976; Banks and Beamish 1979), it has been suggested that uprise of a partially molten mantle diapir into the lower crust was accompanied by plastic deformation of this region and tensile faulting and fracturing of the upper crust, leading to the intrusion of large volumes of hot magma into deep and intermediate crustal levels (Ramberg 1976). Subsequent differentiation and uprise of these evolved magmas would have lead to the extreme diversity of magmatic products now observed at the graben surface.

An important consequence of this hypothesis is that partial melting of lower crustal material is obligatory. The width of the aureole of partial melting and the proportion of minimum melt produced depend on a number of factors including composition, availability of volatiles, and the geothermal gradient (Ramberg 1976; Brown and Hennessy 1978). Significant volumes of anatectic melt may be produced, providing an ample reservoir of potentially fusible lower crust is present. Constraints on the composition of the source regions of the various magmatic derivatives may be obtained from isotopic studies. Initial $^{87}Sr/^{86}Sr$ ratios (Heier and Compston 1969; Sundvoll 1977) range between Ø.7Ø34 and Ø.7Ø54 for the basaltic rocks and Ø.7Ø38 and Ø.7Ø73 for the felsic rocks, supporting an origin by partial melting of upper mantle or lower crustal material with only minor contributions from crustal contaminants with more evolved isotopic compositions. This precludes the possibility that the source regions of any of these rocks contained significant volumes of pelitic sediments or granitic material. On the basis of the geophysical and isotopic evidence, it therefore seems likely that the source regions of even the most evolved granitic magmas contained substantial proportions of mafic or ultramafic rocks, or intermediate rocks in a high metamorphic facies. The likelyhood of a prolonged thermal history dating

back to late Precambrian times in the vicinity of the rift (Section 2.4) allows for the possibility that considerable underplating may have occurred, producing a lower crustal layer (or zone) of similar isotopic composition to the underlying mantle.

2.5.1 Origin of the basaltic rocks

The composition of an uncontaminated basaltic magma at the earth's surface is principally the result of the interplay of two processes (Ringwood 1975): Partial melting in the mantle to generate the primary magma; and partial crystallisation of the magma during its journey to the surface, which leads to modification of the primary composition. The degree to which either of these processes dominates during basalt genesis has been a matter of considerable controversy (Ringwood 1975; ref. cit. O'Hara 1965, 1968).

The nature and composition of residual mineral phases in equilibrium with a partial melt, or phenocrysts in equilibrium with a magma during fractional crystallisation, may be determined experimentally from the composition of phases which occur on or near the liquidus. Thus Ringwood (1975) and coworkers have been able to show that the crystallisation of alkali basalts under anhydrous conditions is dominated by clinopyroxene and olivine at pressures up to 30 kbars. Separation of these phases has the effect of driving the residual liquid towards more undersaturated and aluminous compositions, but cannot account for the generation of highly undersaturated magmas such as basanites, nephelinites and nepheline melilitites. In order to produce more undersaturated magma compositions it is necessary to enlarge the primary field of orthopyroxene crystallisation, since removal of this phase has the effect of driving the residual liquid directly towards silica undersaturation. This may only be achieved at high pressures and in the presence of H_2O and/or CO_2 (Ringwood 1975, ref. cit. Bultitude and Green

1968, 1971, Green 1973 a and b; Wyllie 1979). In particular, an increasing CO_2/H_2O ratio in the source region is likely to have this effect, since olivine and clinopyroxene participate in sub-solidis carbonation reactions in the presence of CO_2 to produce orthopyroxene and dolomite (Wyllie 1979).

The presence of as little as Ø.1 wt % H_2O in the upper mantle has been shown to have significant effects upon the phase relationships of mantle peridotite, lowering the position of the solidus by as much as 4ØØ°C at pressures greater than 27 kbars (Ringwood 1975, Figure 4-6), thereby considerably extending the temperature range over which partial melting may occur. CO_2 is likely to have a similar effect (Wyllie 1979). The fact that partial melting of the mantle in moderately hydrous conditions is likely to occur at lower temperatures (11ØØ to 12ØØ°C; Ringwood 1975) has an important effect upon the composition of residual mineral phases involving a decrease in the degree of solid solution between orthopyroxene and clinopyroxene, and a corresponding decrease in Al_2O_3 solubility in both pyroxenes, thereby favouring garnet as a near-solidus phase (Ringwood 1975).

A natural consequence of the very large increase in melting interval of mantle peridotite in the presence of volatile phases is that a large increase in temperature will only be accompanied by a small increase in the degree of partial melting. It is true therefore that complete melting of mantle peridotite is unlikely to occur. Also, if one assumes a moderately hydrous mantle (Ø.1 wt % H_2O; Ringwood 1975), a small amount of partial melting should be ubiquitous at depths greater than about 75 km, since hornblende (and dolomite) breaks down at this point to provide a free volatile phase. This effect may account for the presence of a low-velocity zone for s-waves in this depth interval.

Gravitational instability within the low-velocity zone may lead to diapiric uprise of mantle peridotite in the incipient

stages of melting (circa 1 % by volume; Ringwood 1975). Assuming the diapir rises adiabatically, with only minor heat loss to the surrounding mantle, the degree of partial melting will increase as the diapir rises, so that at higher levels it will consist of a mush of crystals and interstitial liquid. Assuming chemical equilibrium is maintained, the composition of the partial melt and residual mineral phases will change continually until a stage is reached where the melt is segregated within the source region. From this point onwards any changes in magma composition are independent of the source.

The compositional path along which a rising mantle diapir evolves during progressive partial melting may be illustrated with reference to a ternary variation diagram in which Al, (Na + K), and Ca or (Mg + Fe) are the components (Section 1.5.3; Figure 2.5a). The composition of successive melt fractions produced during progressive partial melting defines a path evolving back towards the bulk mantle peridotite composition. This assumes the simple case for equilibrium partial melting of a homogeneous mantle source. In contrast, the compositional path followed by a mafic magma during fractional crystallisation (Figure 2.5b) is dependent only on the composition and relative proportions of the crystallising phases and is independent of the bulk source composition. Only in the unique case where the proportion of phases removed during crystallisation remains constant may the defined path be extrapolated back to the source composition.

In nature an infinite number of compositional paths exist, each one being unique to a particular starting composition and prevailing conditions of temperature, pressure and volatile activity. The application of this diagram to the petrogenesis of alkaline rocks is easily understood when it is observed that fractionation involving any combination of garnet, plagioclase and hornblende leads to the generation of more alkaline magma compositions, irrespective of whether

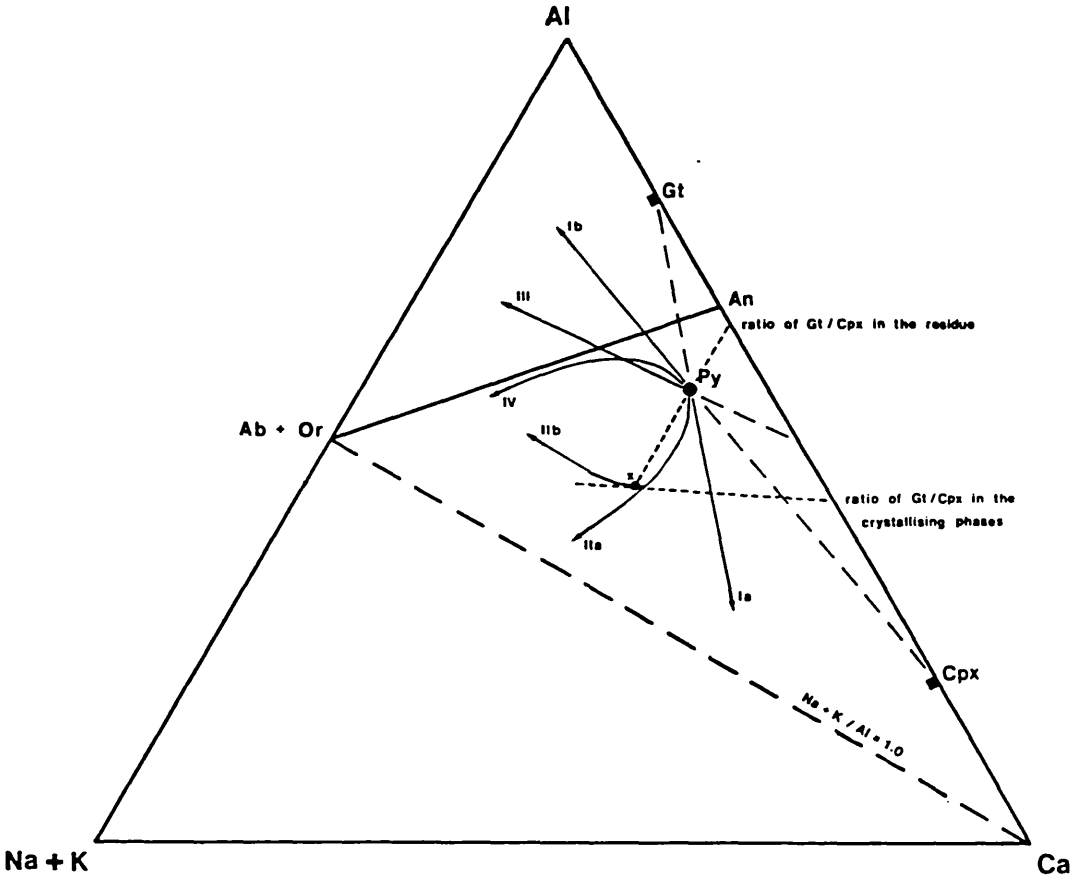

FIGURE 2.5a Paths followed by equilibrium crystallisation of mantle peridotite; Pyrolite composition of Ringwood (1975), Py, used as an example (cation %). Arrows depict direction of evolution of liquid composition during increasing crystallisation (decreasing partial melting).

I. Extreme case: (a) Crystallisation of Garnet ($Py_{69}Al_{17}Gr_{14}$; Ringwood 1975, page 153); (b) crystallisation of subcalcic aluminous clinopyroxene.

IIa. Early crystallisation of garnet (near total melting), joined by clinopyroxene.

IIb. Early crystallisation of garnet, joined by clinopyroxene, followed by crystallisation of clinopyroxene only. Ratio of phases crystallising at point x is given by tangent to curve. Ratio of phases in the residue is given by a line extrapolated back from compositional point x through the bulk composition, Py, to the Al - Ca join.

III. Simultaneous crystallisation of garnet and clinopyroxene in equal proportions.

IV. Early crystallisation of clinopyroxene, joined by garnet or anorthite in increasing proportions.

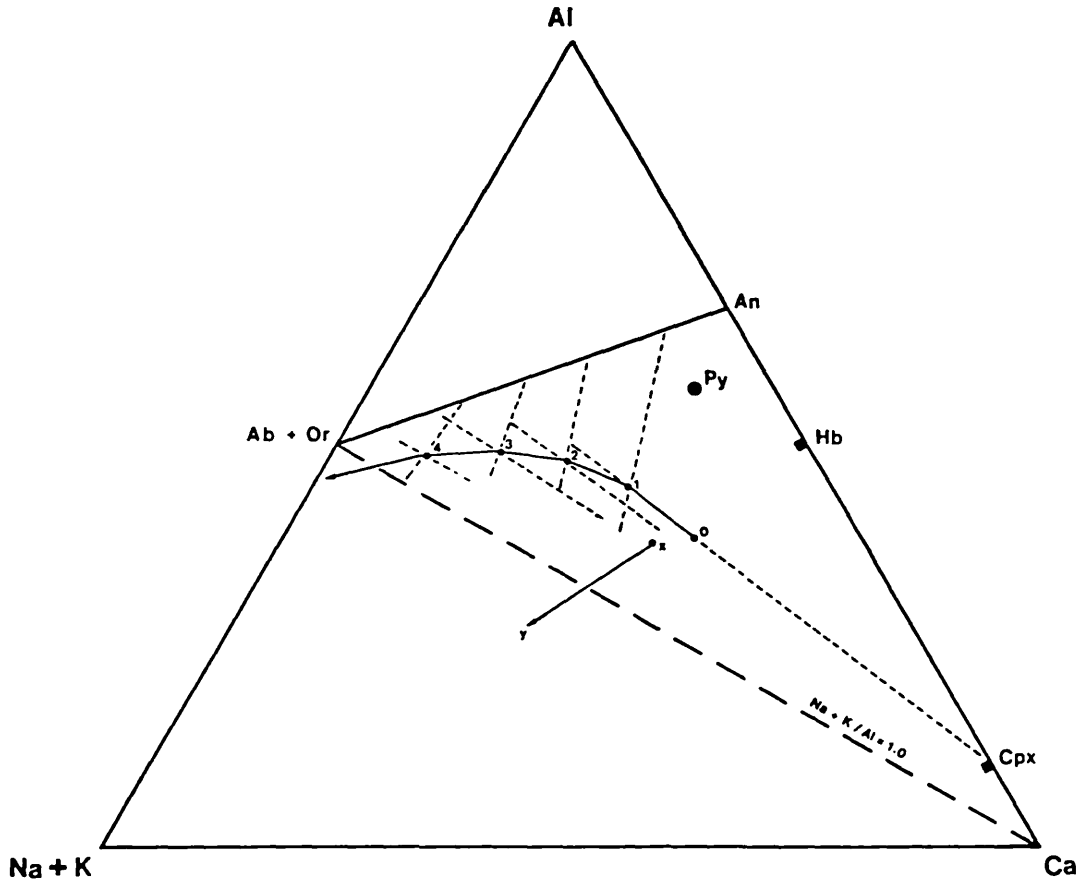

FIGURE 2.5b. Paths followed by fractional crystallisation of mafic magma, demonstrating the "plagioclase effect" of Bowen (1945; cation %). Early crystallisation and removal of moderately aluminous clinopyroxene results in the migration of the liquid composition along path 0 to 1. Continued removal of clinopyroxene, and plagioclase in increasing proportions, causes the composition of the liquid to migrate along paths 1 to 4, and into the peralkaline field. Crystallisation of hornblende might also produce peralkaline liquid compositions, path x - y.

partial melting or fractional crystallisation is the predominant process.

Figure 2.6 illustrates the compositional paths followed by a suite of alkali olivine basalts, basanites, nephelinites and nepheline melilititesfrom the Honolulu volcanics, Oahu, Hawaii, believed to have been produced by different degrees of partial melting of a mantle source (Claque and Frey 1982). Under the conditions of the smallest amounts of partial melting, retention of garnet and clinopyroxene in the residue has lead to the generation of extremely undersaturated alkaline magmas (nepheline melilititesr Na+K/Al ~ .86). Successive melt fractions removed from the source region during progressive partial melting define a path projecting back towards the bulk composition of the mantle source. Subsequent separation of melilite $\pm$ clinopyroxene ($\pm$ olivine) at different stages in the evolution of the crystal/melt system has lead to the development of three subsidiary evolutionary trends. A general decrease in Mg/Mg+Fe ratio and absolute contents of Ni and Cr away from the predicted mantle partial melting trend support the interpretation of these divergent trends as the product of fractional crystallisation processes.

Figure 2.7 illustrates the compositional paths followed by a number of other alkaline suites and indicates the importance of garnet and clinopyroxene in controlling the fractionation of alkaline magmas. In general these suites may be divided into two categories: Those in which clinopyroxene is the dominant phase controlling fractionation, as for instance in Mull and Kenya (tholeiitic trend); and those in which garnet is the dominant phase controlling fractionation, as for instance in Oahu, and possibly the Massif Central (alkali basaltic trend). Separation from the melt of clinopyroxene, often accompanied by olivine, leads to the generation of more saturated magma compositions, moving into the Q-normative field of the basalt tetrahedron of Yoder and Tilley (1962).

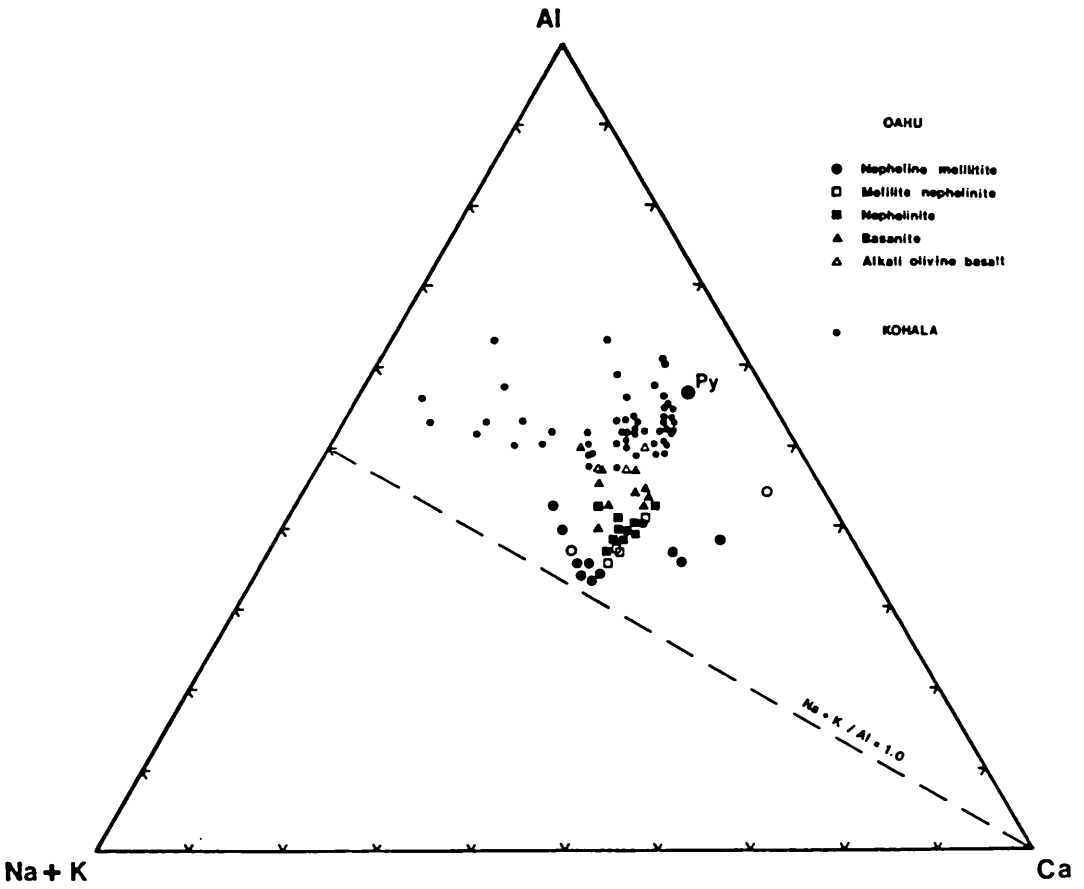

FIGURE 2.6. Al-(Na+K)-Ca variation diagram (cation %), illustrating the compositional paths followed by a suite of alkali olivine basalts, basanites, nephelinites and melilitites from Oahu, Hawaii (Claque and Frey 1982). Open circles are of uncertain affinity. A suite of tholeiitic basalts transitional to alkali basalts from Kohala volcano, Hawaii, is shown for comparison (Feigenson et al. 1983).

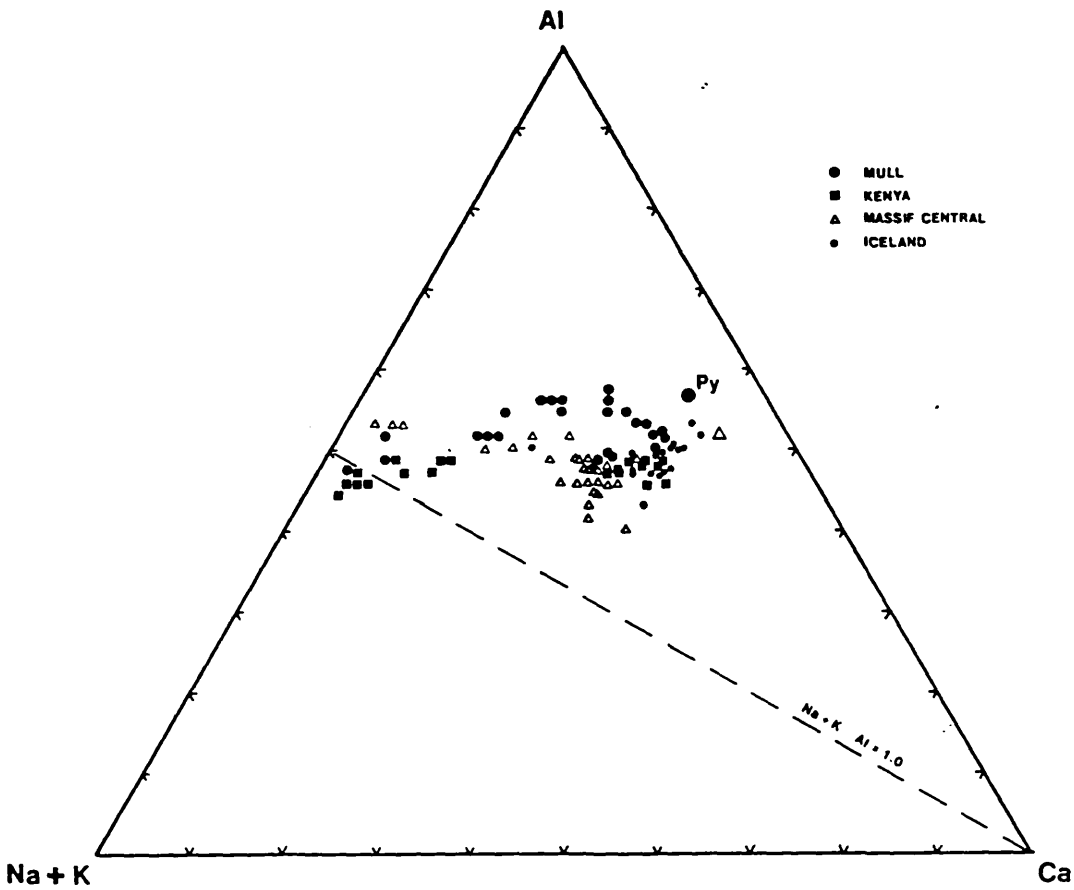

FIGURE 2.7. Al-(Na+K)-Ca variation diagram (cation %), illustrating the compositional paths followed by a suite of basalts, hawaiites, mugearites and trachytes from the Isle of Mull, Scotland (Beckinsale et al. 1978); a suite of basalts, benmoreites and trachytes from the Gregory Rift, Kenya (Baker et al. 1977); a suite of nephelinites, basanites, alkali basalts, mugearites, phonolites and trachytes from the Massif Central (Chauvel and Jahn 1984); and a suite of mafic lavas from Iceland (Wood et al. 1979b). The large open triangle is a spinel luerzolite nodule from the massif central.

In contrast, separation from the melt of garnet, often accompanied by orthopyroxene, leads to the generation of more undersaturated magma compositions, moving directly toward the Ne-apex of the basalt tetrahedron. Clearly, the compositional paths followed by these suites reflect different conditions of pressure (depth), temperature and volatile activity. Fractionation involving separation of garnet and clinopyroxene occurs under conditions of higher pressure, in the presence of a free volatile phase (H_2O, CO_2).

Retention of garnet in the residue during partial melting is likely to have a significant effect upon the behaviour of the rare earth elements (Shimzu and Arculus 1975). Preferential partitioning of the heavy rare earths into garnet may cause systematic enrichments in LREE relative to HREE, and depletions in HREE relative to chondritic abundances, during the process of fractionation (Kay and Gast 1973). In contrast, both light and heavy rare earth elements are in general strongly excluded from olivine and pyroxenes. Increasing fractionation when garnet is absent as a significant residual phase should, therefore, result in relative enrichment in the melt of both light and heavy REE. This relationship is illustrated with reference to the Oahu and Kenya suites in Figure 2.8.

The absence of significant europium anomalies for the basaltic members of these suites either means that plagioclase was not a major mineral phase controlling fractionation or, where considerations of mineralogy and major element geochemistry suggest otherwise, that Eu was mainly in the trivalent form. This would imply conditions of high oxygen fugacity during their formation ($-\log_{10} fO_2 < 10$; Irving 1978, Drake and Weill 1975).

The basaltic rocks in the Oslo Region broadly speaking fall into the compositional range basanite - alkali basalt (Section 2.3.1). They differ, however, from typical alkali

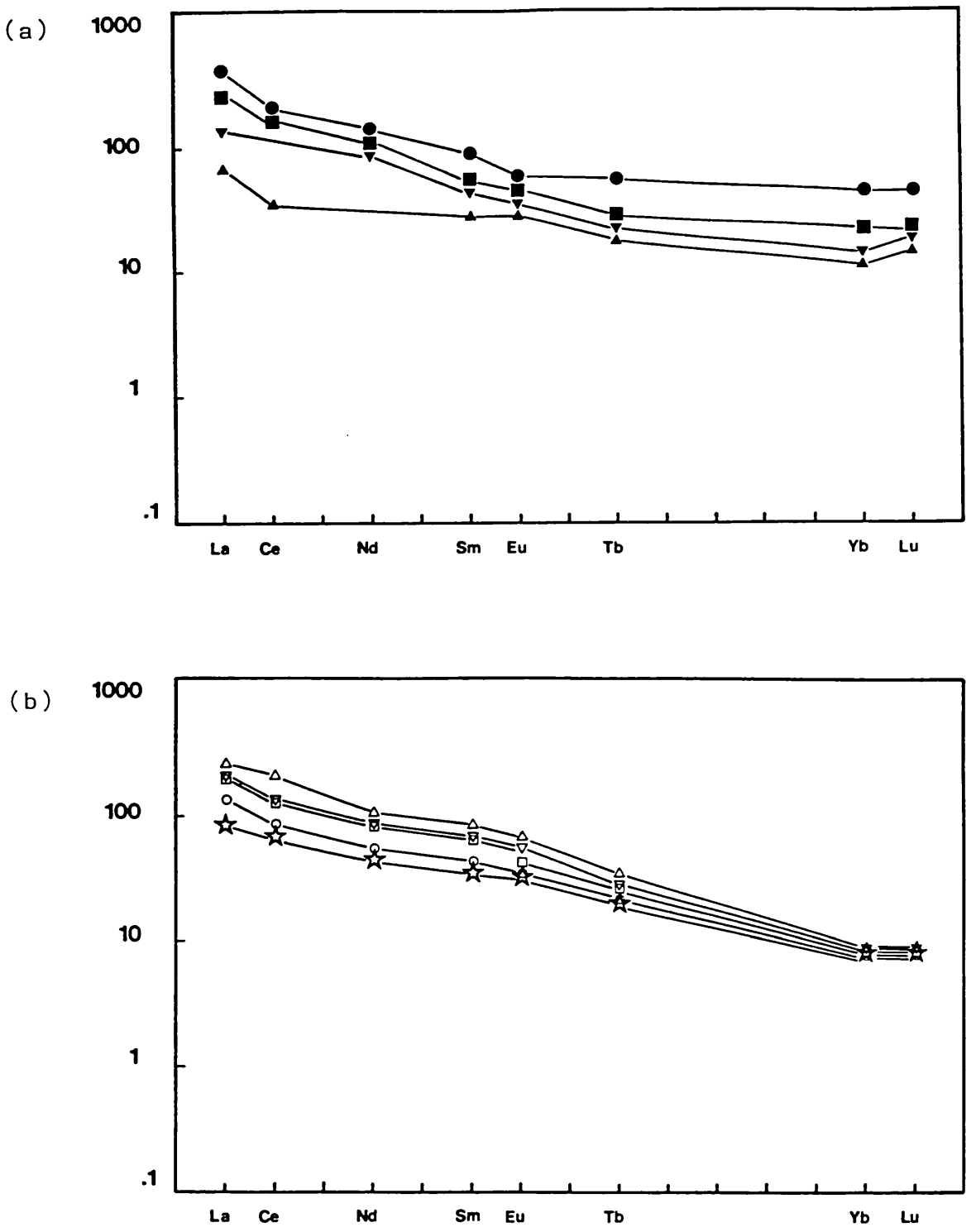

FIGURE 2.8. Chondrite normalised Rare earth element distribution patterns: (a) The Gregory Rift, Kenya (Baker et al. 1977); (b) Oahu, Hawaii (Claque and Frey 1982). Symbols: ▲ = basalt, ▼ = ferrobasalt, ■ = benmoreite, ● = trachyte, Kenya; △ = nepheline melilitite, ▽ = melilite nephelinite, □ = nephelinite, ○ = basanite, ☆ = alkali olivine basalt, Oahu.

olivine basalts in that olivine is often only a subordinate phase, and in that they may contain melanite (andradite garnet) as a groundmass phase (Segalstad 1979). When plotted on an Al-(Na+K)-Ca variation diagram (Figure 2.9a), these rocks show considerable scatter. This might be attributed to varying degrees of alteration. The fact, however, that many of these rocks are porphyritic suggests that they may not be representative of the melt from which they crystallised.

The basaltic rocks define two distinct compositional trends: A "calcic" trend (pyroxene basalts, plagioclase - pyroxene basalts and some aphyric basalts) controlled by separation of moderately aluminous clinopyroxene; and an "alkaline" trend (plagioclase basalts and aphyric basalts) controlled by separation of clinopyroxene, and garnet or plagioclase. This latter trend includes several aphyric (B_1) basalts from the Kolsas area, within the Krokskogen lava plateau, which Weigand (1975) identified as typical quartz tholeiites. Both trends are also apparent on plots of Al-(Na+K)-($Mg+Fe^{2+}$) (Figure 2.9b). Absolute contents of Ni and Cr (29 - 174 $\mu g\ g^{-1}$ Ni and 25 - 392 $\mu g\ g^{-1}$ Cr in the pyroxene basalts and plagioclase - pyroxene basalts; 18 - 67 $\mu g\ g^{-1}$ Ni and 14-122 $\mu g\ g^{-1}$ Cr in the aphyric basalts and plagioclase basalts; Weigand 1975) suggest that significant fractional crystallisation of olivine has occurred.

The pyroxene basalts (ankaramites; Segalstad 1979) and plagioclase - pyroxene basalts (basanites) were derived by fractionation involving clinopyroxene and olivine $\pm$ orthopyroxene of an extremely calcic starting composition (Figure 2.9a). The latter either reflects an amomalously calcic, and alkaline, mantle source composition, or derivation by partial melting of mantle peridotite in which garnet was an important residual phase. The limited trace element evidence available (above; see also Section 2.5.5) suggests that the latter possibility is most likely. Prolonged residence at the base of the crust, and/ or in high

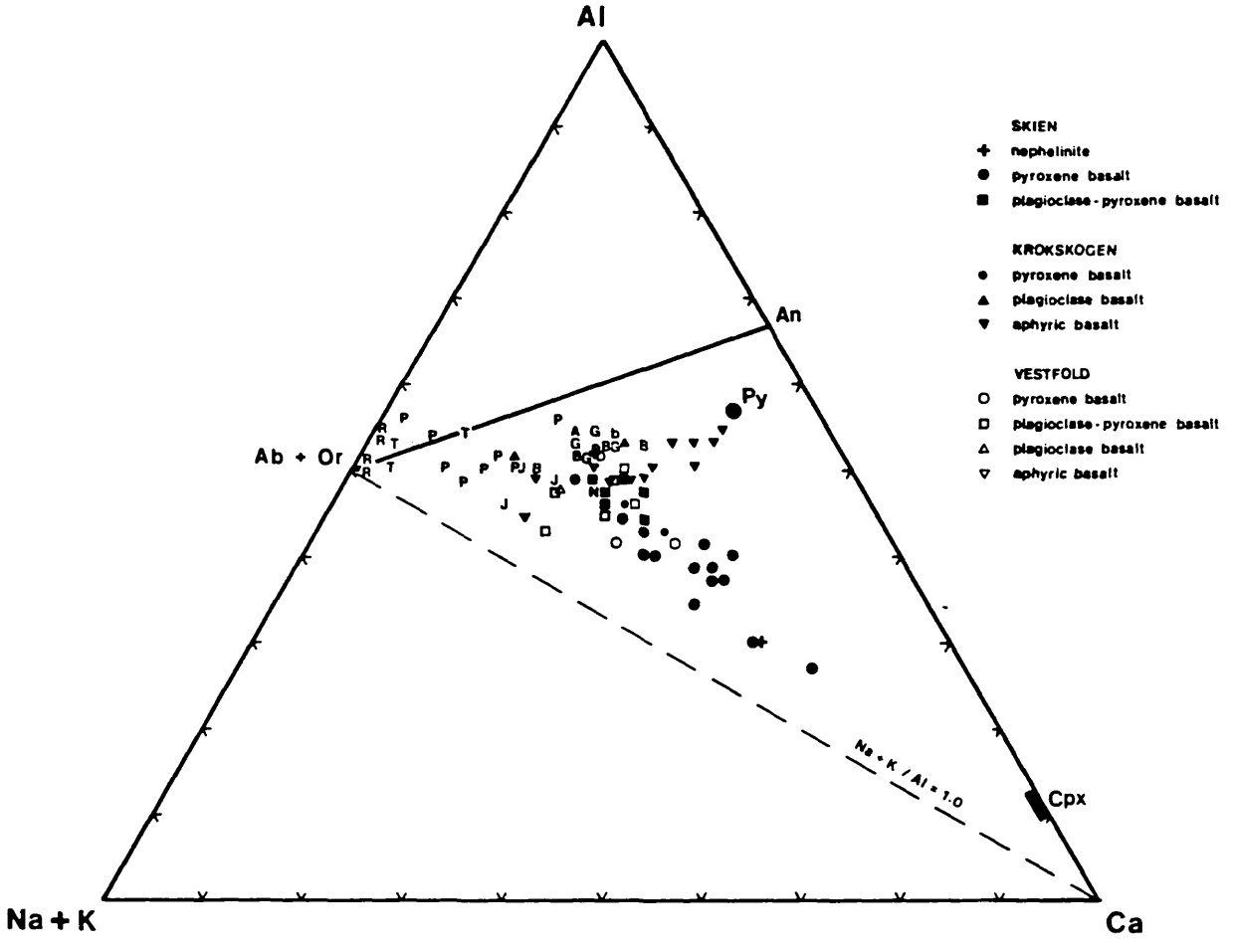

FIGURE 2.9a. Al-(Na+K)-Ca variation diagram (cation %), volcanic rocks, Oslo Region. Data from Weigand (1975), Ramberg and Larsen (1978), Oftedahl and Petersen (1978), Segalstad (1979), and Rasmussen (1982). Composition of clinopyroxene after Weigand (1975).

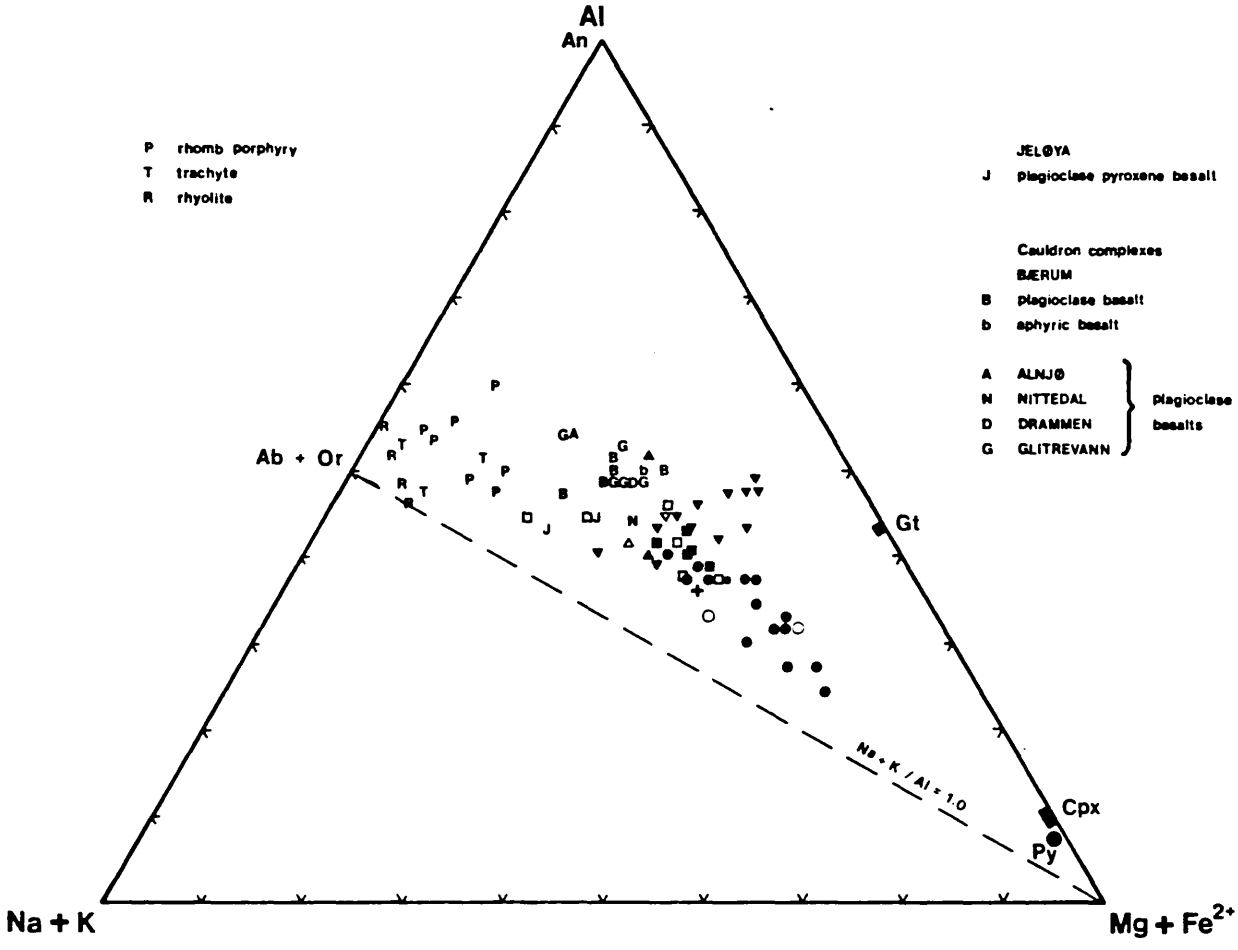

FIGURE 2.9b. Al-(Na+K)-($Mg+Fe^{2+}$) variation diagram (cation %), volcanic rocks, Oslo Region.

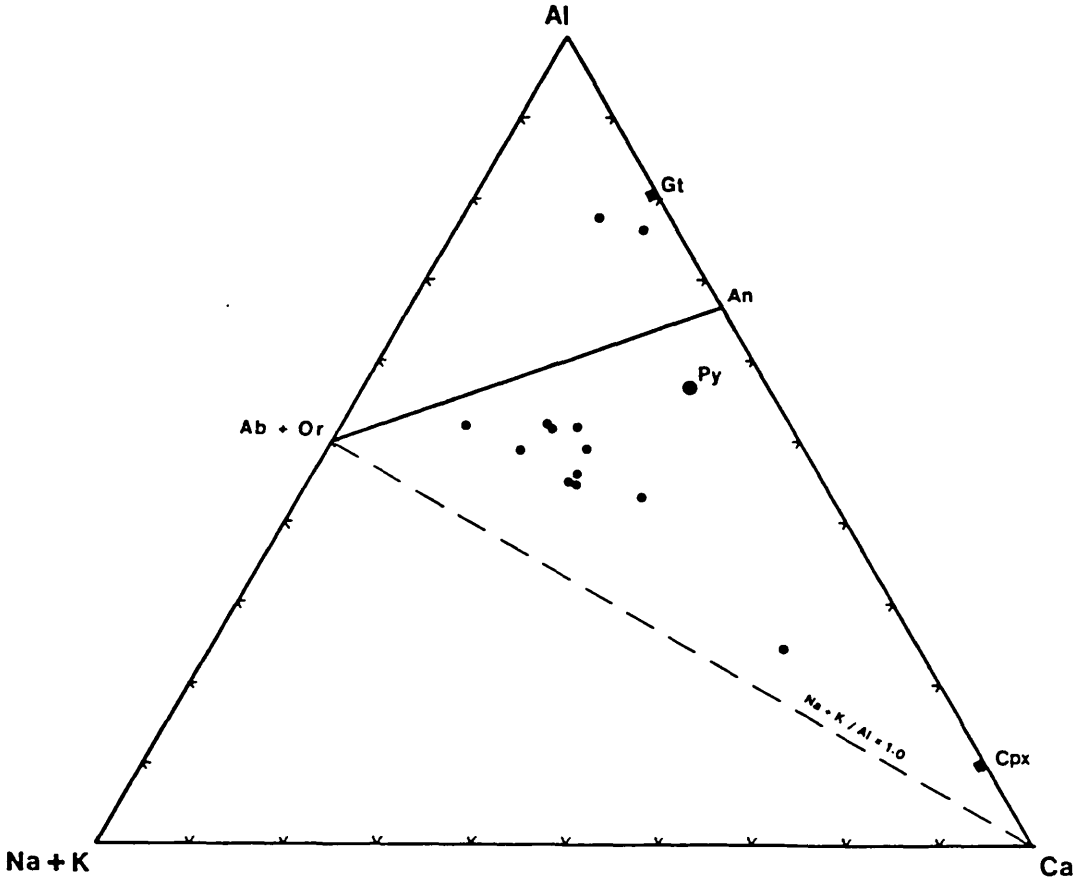

FIGURE 2.10. Al-(Na+K)-Ca variation diagram (cation %), volcanic necks, Oslo Region (from Brogger 1933). Composition of clinopyroxene as in Figure 2.9a.

level magma chambers now represented by the volcanic necks (Figure 2.1Ø) has presumably obscured the "mantle" inheritance. This is in agreement with Segalstad (1979) who concluded that the basaltic rocks in the Skien area were derived essentially by fractional crystallisation of clinopyroxene at moderate pressures from a parent magma of postulated olivine nephelinite composition, itself derived from great depths within the mantle.

The plagioclase basalts and aphyric basalts, which make up a large part of the Krokskogen lava plateau as well as some of the cauldron complexes, appear to have a different provenance (Figure 2.9), fractionation being controlled by clinopyroxene, and garnet or plagioclase, at shallower depths within the mantle. When compared with the pyroxene basalts and plagioclase - pyroxene basalts, these rocks show systematically lower contents of incompatible trace elements (Rb, Sr, Th and U, Weigand 1975; and LREE, Sundvoll 1978) reflecting derivation by larger degrees of partial melting in the mantle source region. Nevertheless, absolute contents of Ni and Cr (above) again suggest that significant fractional crystallisation (of olivine) has occurred.

2.5.2 Origin of the intermediate rocks

Intermediate rocks in the Oslo Region include the extrusive rhomb porphyries, together with the intrusive kjelsasites, larvikites and associated feldspathoidal rocks (lardalites and foyaite/hedrumites; Section 2.3). Genetically these rocks are closely related to the more evolved syenites and granites, transitions between kjelsasite/larvikite and nordmarkite, and between nordmarkite and ekerite, commonly being observed in the field (Section 2.3.2). A clear genetic link between the monzonites and more mafic rocks is, however, harder to define. Evidently an understanding of the origin of the intermediate rocks is crucial if an unequivocal explanation of the petrogenesis of the more felsic rocks is

to be found.

Three possible sources for the intermediate rocks should be considered:

I. Fractional crystallisation of an alkali basaltic parent magma (calcic trend; Figure 2.9a); II. Fractional crystallisation of a tholeiitic parent magma (alkaline trend); and III. Direct derivation of intermediate magmas by partial melting of upper mantle or lower crustal material. In nature, several combinations of these processes may be capable of explaining the variety of intermediate rocks exposed at the graben surface.

I. Continued removal of clinopyroxene from an alkali basaltic magma will lead to the generation of intermediate magmas which are approximately silica saturated (cf. Neumann 1980). Further separation of clinopyroxene will modify the melt composition, but will not produce more silica-saturated magma compositions. This is because the silica contents of the clinopyroxene and the melt from which it is being removed are the same (at approximately 56 Wt % SiO_2). At this stage, separation of feldspar will drive the composition of the residual liquid away from the plane of silica saturation. The critical control on the direction of evolution of magma composition is the bulk composition of the feldspar. In the case of an intermediate magma, containing approximately 56 Wt % SiO_2 (above), the critical composition is An_{30}. Separation of feldspar more calcic than An_{30} will drive the residual liquid towards more siliceous compositions. In contrast, separation of more sodic feldspar, An < 30, will drive the residual liquid back into the undersaturated field.

It would appear that the composition of feldspar crystallising at any one point is a function of the clinopyroxene/plagioclase ratio in the crystallising phases, which itself is a function of the P-T-X-P(H_2O, CO_2) path

along which the magma has evolved. This is clearly demonstrated by phase relationships in the synthetic system diopside - forsterite - anorthite (Presnall et al. 1978, Figure 5) which indicate that the primary field of crystallisation of clinopyroxene expands at the expense of the anorthite field with increasing pressure. The composition of plagioclase phenocrysts in the plagioclase - pyroxene basalts (An_{20} - An_{30}; Segalstad 1979) suggests that continued separation of plagioclase from magmas of this composition would lead to the generation of a series of undersaturated rocks similar to those observed in the Larvik ring complex (Figure 2.11; Section 2.3.2a).

II. Continued separation of calcic plagioclase (An > 30) $\pm$ clinopyroxene $\pm$ olivine from a tholeiitic magma will lead to the generation of intermediate magmas. Further separation of plagioclase of increasingly less calcic composition will drive the the melt directly towards more siliceous compositions. A tendency to evolve back towards more undersaturated magma compositions will not be developed, providing the bulk composition of the mineral phases being removed remains less siliceous than the magma. The more evolved end-members of the basalt-trachyte lavas of Mull (Beckinsale et al. 1978) and the basalt-benmoreite-trachyte lavas of the southern part of the Gregory rift, Kenya (Baker et al. 1977) may have evolved in this way (Figure 2.7). The composition of plagioclase phenocrysts in the plagioclase basalts (An_{50} - An_{60}; Weigand 1975) suggests that continued separation of plagioclase from magmas of this composition would lead to the generation of more siliceous magma compositions (trachytes and rhyolites).

III. Experimental partial melting of materials of assumed mantle composition (see Wyllie et al. 1976) indicates that direct derivation of the intermediate rocks by partial melting in the mantle is an unlikely mechanism (Neumann 1980). Partial melting of gabbroic or intermediate material

in the lower crust could, however, lead to the formation of intermediate to granitic magmas, depending on the degree of partial melting involved. The postulated intrusion of huge volumes of mafic magma into the lower crust (above) requires that a certain amount of crustal anatexis should take place. However, the likelyhood that the source rocks for anatexis should be of mafic or intermediate composition (on the basis of geophysical and isotopic evidence; above) means that the importance of this phenomenon is difficult to assess.

From the above discussion, it appears that the intermediate to granitic rocks exposed in the Oslo Region may have evolved along a number of compositional paths from several different sources. The problem is to assess the relative contributions of the different sources.

Mineralogically and chemically the intermediate monzonites and related feldspathoidal rocks in the Larvik area (Section 2.3.2a) are compatible with a derivation by fractionation of sub-calcic plagioclase (An < 30) $\pm$ clinopyroxene $\pm$ olivine (+ Fe-Ti oxides + apatite; Neumann 1980) from an alkali basaltic parent corresponding in composition to the plagioclase - pyroxene basalts (Figure 2.11). Consideration of phase relationships in synthetic systems (for instance diopside - forsterite - anorthite; Presnall et al. 1978) has lead Neumann (1980) to suggest that the approximately silica-saturated intermediate magmas which invaded the upper crust were formed by fractional crystallisation of basaltic melts at pressures between about 7 and 10 kbars, corresponding to the lower part of the crust. However, a tendency towards successively more undersaturated magma compositions might be explained equally well by fractional melting of a progressively depleted source region in the same pressure interval (see trace element evidence below; Section 2.5.5). Subsequent emplacement and fractional crystallisation in situ would lead to the range of undersaturated felsic rocks exposed at the graben surface.

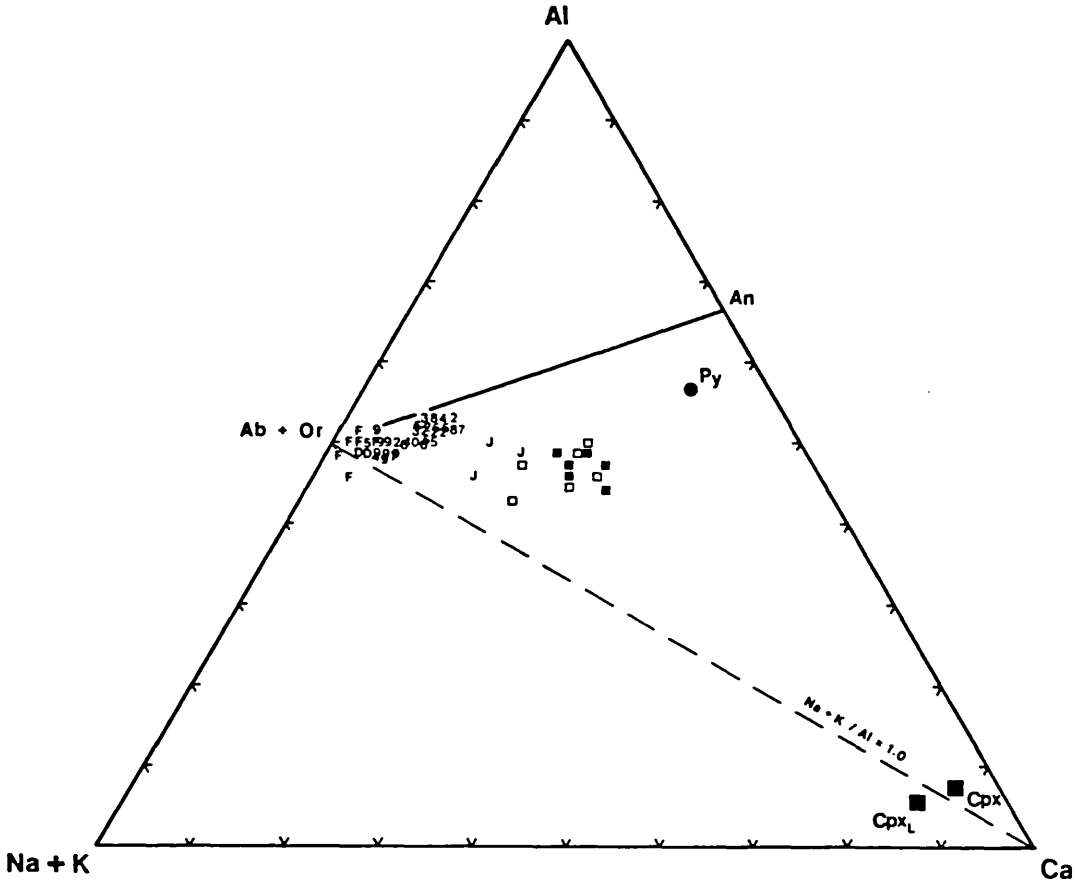

FIGURE 2.11. Al-(Na+K)-Ca variation diagram (cation %), Larvik complex, Oslo Region (from Neumann 1980). Numbers refer to the ring segments, RS2 to RS8 are larvikites, RS9 and RS10 (0) are lardalites; D = Ditroite, F = Foyaite/Hedrumite; Cpx = composition of clinopyroxene in the Larvikites, Cpx_L = composition of clinopyroxene in the Lardalites (from Neumann 1980). Plagioclase - pyroxene basalts shown for comparison (symbols as in Figure 2.9).

Evidence indicating that alkali basaltic magmas evolved towards both silica-saturated and silica-undersaturated compositions is provided by the volcanic necks (Oslo essexites; Figure 2.4a). The most evolved end-members of these evolutionary trends consist of quartz monzonite (akerite) and nepheline syenite (husebyite) respectively. In contrast, the variation in average chemical composition of feldspar phenocrysts in the rhomb porphyry lavas from the Krokskogen lava plateau and adjacent Oyangen Cauldron fall in the range An_{50} to An_{10} (Larsen 1978, Figure 4), suggesting that these rocks were derived by fractional crystallisation of a tholeiitic parent corresponding in composition to the plagioclase basalts. This conclusion is supported by Oftedahl (1952) who noted that the so-called "rectangular porphyries" (RP13) in the Krokskogen and Vestfold areas were intermediary in terms of chemistry and texture between the least evolved rhomb porphyry lavas and most evolved plagioclase basalts.

The large variation in plagioclase to alkali feldspar ratio in the kjelsasites, which varies between 10:1 and 1:2 (Barth 1944), may reflect both alkali basaltic and tholeiitic lines of evolution. In comparison, the more stable distributions of these mineral phases within the rhomb porphyry lavas, when combined with the considerable lateral extent and homogeneiity of individual rhomb porphyry flows (for instance RP1, RP2, RP4, RP5, and RP6; Oftedahl 1952) suggests that these rocks were derived mainly from a tholeiitic source.

Transitions between quartz-bearing larvikite and rhomb porphyry lavas in the Tonsberg area (Oftedahl 1952) indicate a comagmatic relationship for some of these rocks. However, the fact that the intermediate larvikites are associated with both silica-saturated and undersaturated lines of evolution (Section 2.5.3) means a comagmatic relationship cannot necessarily be assumed.

2.5.3 Origin of the plutonic igneous rock series

Barth (1944,1954) demonstrated that the principal members of the plutonic igneous rock series could be explained in terms of fractionation of a syenitic parent magma, essentially by separation of feldspar (above, Figure 2.4b). Intermediate magmas evolving towards more siliceous compositions may have been derived from a variety of possible sources including fractional crystallisation of an alkali basaltic or tholeiitic parent magma, or partial melting of crustal material of gabbroic or intermediate composition. Low pressure fractionation in which feldspar is the dominant liquidus phase would lead to a convergence of melt compositions, regardless of the initial affiliation of the magma. As stated above, the critical control on the direction of evolution of melt composition is the bulk composition of mineral phases being removed. In the case of an intermediate magma, in which feldspar is the dominant liquidus phase, this is approximately An_{30}.

The composition of plagioclase in the kjelsasites falls in the range An_{50} to An_{30} (Barth 1944), indicating that continued fractionation of magmas of this composition would lead to the generation of more silica-saturated felsic derivatives. Such derivatives might include quartz-bearing larvikite, nordmarkite and ekerite. Fractionation of a kjelsasitic magma is incapable of producing more undersaturated derivatives such as those observed in the Larvik area. This is in agreement with Barth (1944) who concluded that the nepheline-bearing larvikites and lardalites could not have been derived from a kjelsasitic parent, thus underlining a fundamental difference, in general, between the nepheline-bearing and quartz-bearing larvikites.

Whilst an origin for the felsic rocks of the Oslo Region is satisfactorily explained in terms of fractional

crystallisation of a combination of alkali basaltic and tholeiitic parent magmas, a possible origin by partial melting of crustal material should not be excluded altogether. In theory, the intermediate to silica-saturated felsic rocks which make up the plutonic igneous rock series may be explained in terms of a "restite" model similar to that proposed by Chappell and White (1974), and White and Chappell (1977), reflecting different degrees of partial melting of a common crustal source. Progressive separation of the partial melt from restite mineral phases such as pyroxenes, hydrated silicates and zoned feldspars, together with apatite and Fe-Ti oxides, would lead to the generation of progressively more silica-saturated crystal/liquid compositions, culminating at the low pressure minimum melting composition for granite. The high viscosity inferred for such a mineral/melt system suggests that the partial melt would not rise far from its source region. Large areas of kjelsasitic rocks and so-called "stoped-blocks" of country rock concentrated towards the walls of the northern batholith (Section 2.3.2.b; Ramberg 1976) might therefore be interpreted as relict source rocks.

The isotopic and geophysical evidence discussed above suggests that the most likely source rocks for partial melting should be of gabbroic or intermediate composition, with isotopic compositions similar to the upper mantle (initial $^{87}Sr/^{86}Sr$ ratios of .7Ø4). Wholesale anatexis of the Precambrian craton (cf. Barth 1954) is therefore an unlikely mechanism. Age relationships in the Oslo Region indicate that basaltic to trachyandesitic volcanism began much earlier than the main period of felsic plutonism, at 29Ø Ma as opposed to 27Ø Ma (Sundvoll 1978). Consolidation of the plutonic equivalents of these early lavas may therefore have provided the source rocks for later felsic plutonism. Kjelsasitic and related rocks exposed at the present graben surface might, therefore, represent the source rocks for partial melting.

The restite model discussed above is essentially one of equilibrium (batch) partial melting. In comparison, fractional melting of gabbroic or intermediate rocks would have a strikingly different effect. Successive melt fractions generated by partial melting of a source region progressively depleted in Si, Na, K, Al, and volatile elements would produce a series of silica-saturated magmas, moving towards more intermediate compositions with time (Helz 1976). This predicted sequence is contrary to the intrusive sequence of kjelsasite to ekerite observed within the Region. It may, therefore, be concluded that fractional melting of lower crustal material was not an important mechanism in the generation of the plutonic igneous rock series.

2.5.4 Origin of the biotite granites

Biotite granites in the Oslo Region form the larger parts of the Drammen and Finnemarka granite complexes. Compositionally similar rocks also occur within the Glitrevann Cauldron and in association with peralkaline syenites and granites in the northern part of the Region. The biotite granites in the Drammen and Finnemarka areas (BGI; Gaut 1981) are distinct from other granitic rocks in the Region, not only in a geographical sense, but in that they are not associated with large volumes of intermediate rocks at the surface, and in that they were emplaced at an earlier stage in the evolution of the rift (Section 2.4; Ramberg and Larsen 1978). For these reasons they are generally regarded to have a somewhat different origin.

Mineralogically and chemically, however, the biotite granites are not so distinct from other granitic rocks in the Region, with the exception that biotite is the principal ferromagnesian phase. They consist of perthitic alkali feldspar, plagioclase and quartz, accompanied by biotite, apatite, Fe-Ti oxides, zircon and sphene. These rocks have an agpaitic index, Na+K/Al, of .89 $\pm$.Ø4 and an Mg/Mg + Fe

ratio of approximately .12 (Table 2.2). The principal differences between these rocks and the other granites are marginally higher contents of Ca and Al, balanced by a somewhat lower Si content. This is reflected in the mineralogy by larger and more variable amounts of plagioclase, so that both hypersolvus and subsolvus varieties exist within this group of rocks (Gaut 1981). The initial $^{87}Sr/^{86}Sr$ ratios for these rocks (.7044 - .7067; Sundvoll 1977) are also similiar to other granitic rocks in the Region (.7048 - .7073).

The biotite granites in the Oslo Region, in common with the other felsic rocks, may therefore be explained either in terms of fractional crystallisation of mafic magmas derived directly from the mantle, or by partial melting of lower crustal material of gabbroic or intermediate composition, itself recently derived from the mantle (on the basis of initial $^{87}Sr/^{86}Sr$ ratios). The scarcity of intermediate rocks associated with the biotite granites (BGI) might suggest that the latter explanation is more probable.

2.5.5 Trace element evidence regarding the origin of the felsic rocks

A study of rare-earth element distributions within the principal plutonic rock-types has lead Neumann et al. (1977) to conclude that the intermediate kjelsasites and larvikites were derived from a source or sources fairly homogeneous with respect to REE. Uniform enrichment in LREE relative to HREE is a characteristic of these rocks (Figure 2.12). The limited REE data available for the volcanic rocks (Sundvoll 1978; ref.cit. Finstad 1972) suggest that the rhomb porphyry lavas have similar distributions.

When compared with the more mafic rocks in the Oslo Region the intermediate rocks show systematic enrichments in both light and middle REE (Figure 2.12). The heavy REE, however,

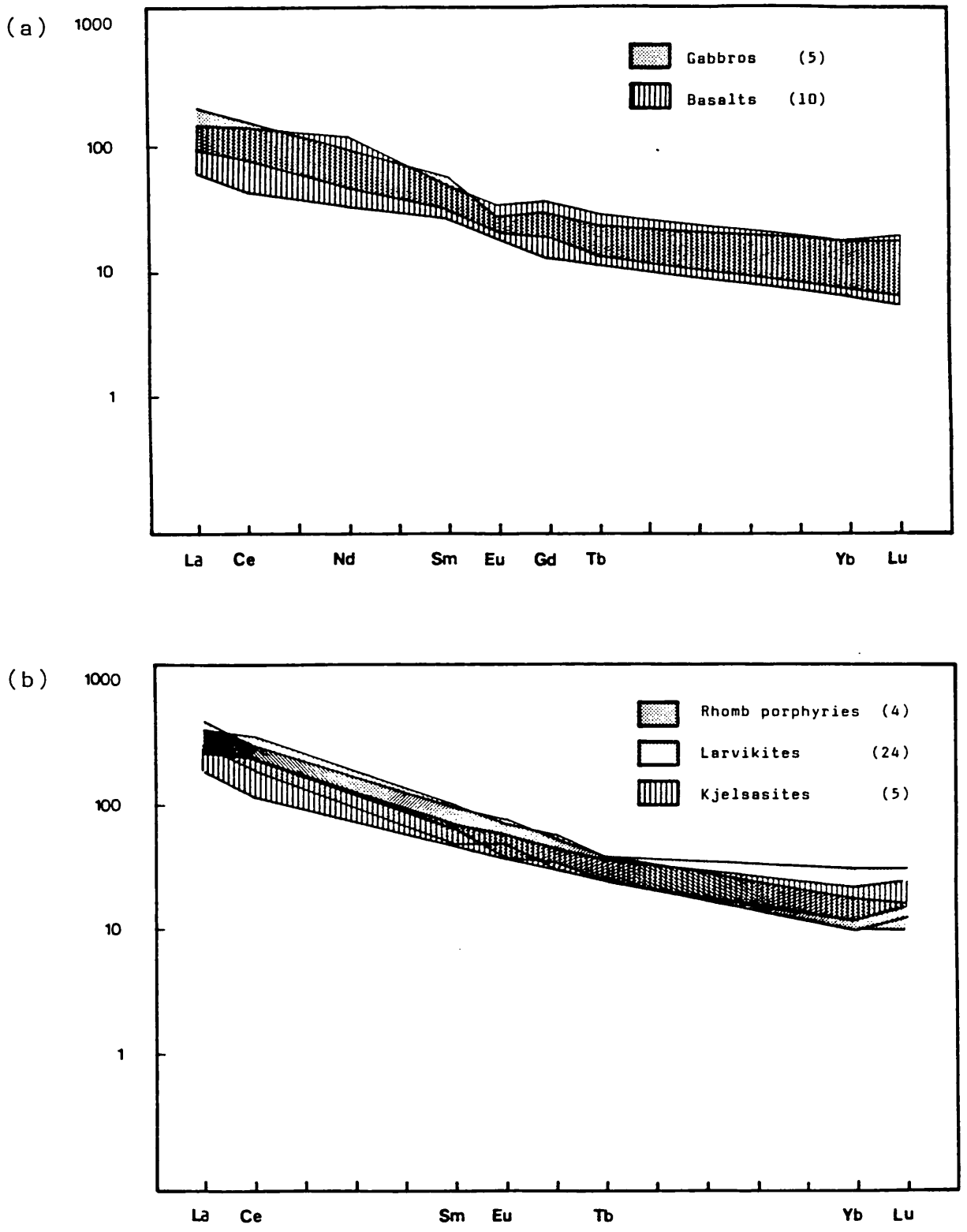

FIGURE 2.12. Chondrite normalised Rare earth element distribution patterns for (a) the mafic rocks; and (b) the intermediate rocks, Oslo Region (after Neumann et al. 1977, Neumann 1980). Number of samples in parenthesis.

remain relatively unfractionated, indicating bulk distribution coefficients for these elements, D_{Yb} and D_{Lu}, of near unity (Section 6.3). It is therefore safe to conclude that the REE evolution of these rocks has been controlled by separation of a mineral phase which preferentially retains HREE. The most likely candidates for this are garnet or clinopyroxene, or possibly amphibole (Irving 1978); or a combination of these minerals. The fact that HREE remain relatively unfractionated in rocks from both alkali basaltic and tholeiitic sources suggests similar processes operating in both cases. In particular, fractionation involving separation of clinopyroxene would appear to be important.

The presence of weak positive or negative Eu anomalies in the REE distributions of the intermediate rocks presumably reflects minor amounts of plagioclase accumulation or separation (Neumann et al. 1977). The absence, however, of large negative Eu anomalies in some of these rocks suggests that they were formed under conditions of high f_{O2} (a low Eu^{2+}/Eu^{3+} ratio; Section 2.5.1). This is because considerations of mineralogy and major element geochemistry indicate that significant plagioclase fractionation has occurred (Section 2.5.2).

In comparison, the more evolved syenites and granites tend to show far more variable REE distributions, displaying progressive depletions in LREE and Eu, and enrichments in HREE during evolution (Figure 2.13). Development of large negative Eu anomalies within the nordmarkites and ekerites indicates that significant fractionation of plagioclase $\pm$ anorthoclase has occurred. Progressive depletions in LREE and enrichments in HREE, however, are difficult to explain in terms of fractionation of the principal rock-forming minerals, since olivine, orthopyroxene and garnet usually exclude LREE to a greater exent than HREE, and feldspar excludes both light and heavy REE, but not Eu^{2+}, equally. This has lead to the suggestion (Neumann et al. 1977) that

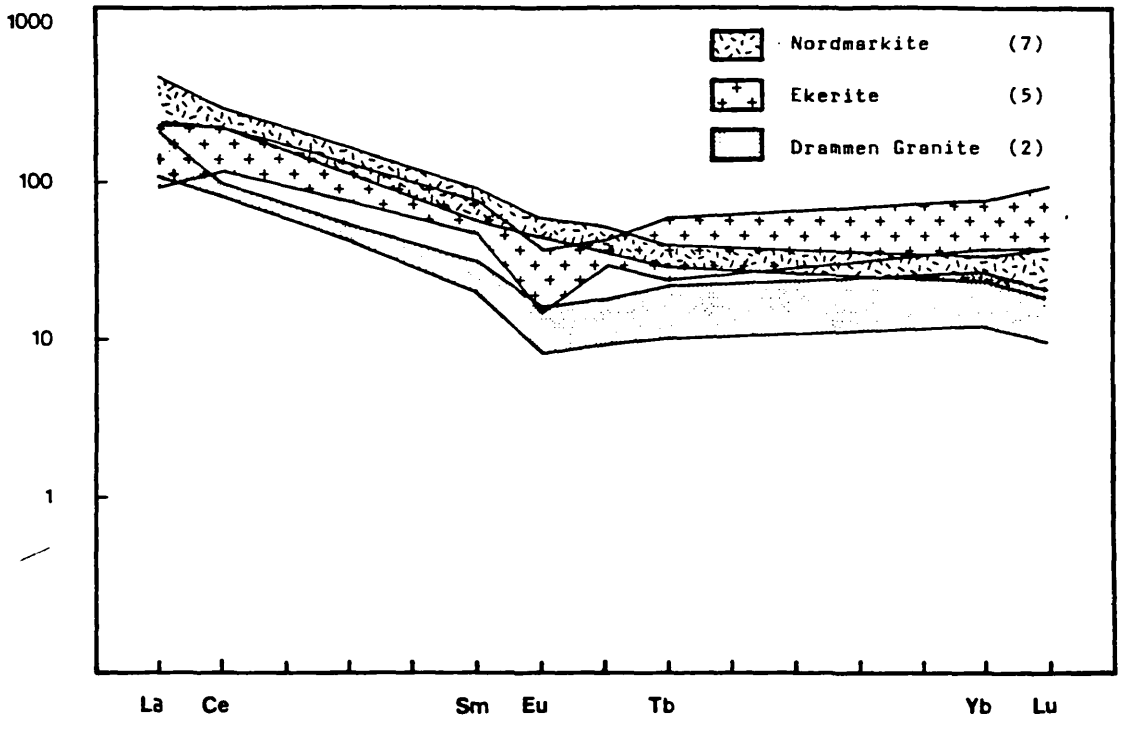

FIGURE 2.13. Chondrite normalised Rare earth element distribution patterns for the syenites and granites, Oslo Region (after Neumann et al. 1977). Number of samples in parenthesis

the rare earth element evolution of these rocks may have been controlled by the presence of accessory mineral phases which preferentially retain LREE, such as apatite, zircon and sphene. This problem will be considered again in a later section (6.4.3).

When compared with the other granitic rocks in the Oslo Region, the biotite granites (BGI from the Drammen area; Figure 2.13) show much lower contents of HREE. Similarity in REE distributions between these rocks and certain Precambrian granites and palaeozoic shales has lead Neumann et al. (1977) to suggest that the biotite granites may have been formed by partial melting of Precambrian crust. However, the fact that HREE remain relatively unfractionated in these rocks supports the hypothesis (Section 2.5.4) that they were formed by partial melting of gabbroic rocks in the lower crust, with clinopyroxene, or garnet, in the residue.

Consideration of the distributions of HREE and elements such as Th, U, Ta and Hf, within the intermediate rocks from the Larvik area leads to some important conclusions concerning the origin of these rocks (Figure 2.14). The larvikites from the younger ring segments (RS4, RS7 and RS8) tend to be depleted in these elements relative to their older counterparts. This is contrary to what might be expected from a simple fractionation process, indicating that these rocks do not belong to a single cogenetic series, but to several parallel evolutionary series. Neumann (198Ø) also reached the same conclusion on the basis of major element geochemistry.

Relative depletion in incompatible trace elements ($D < 1$; Section 6.3) in the later formed melt fractions might be explained in terms of a fractional melting model in which these elements are concentrated in the first formed melt fractions. However, the fact that volatiles (H_2O, CO_2) would also tend to be concentrated in the first formed melt fractions poses problems for subsequent melting, raising the

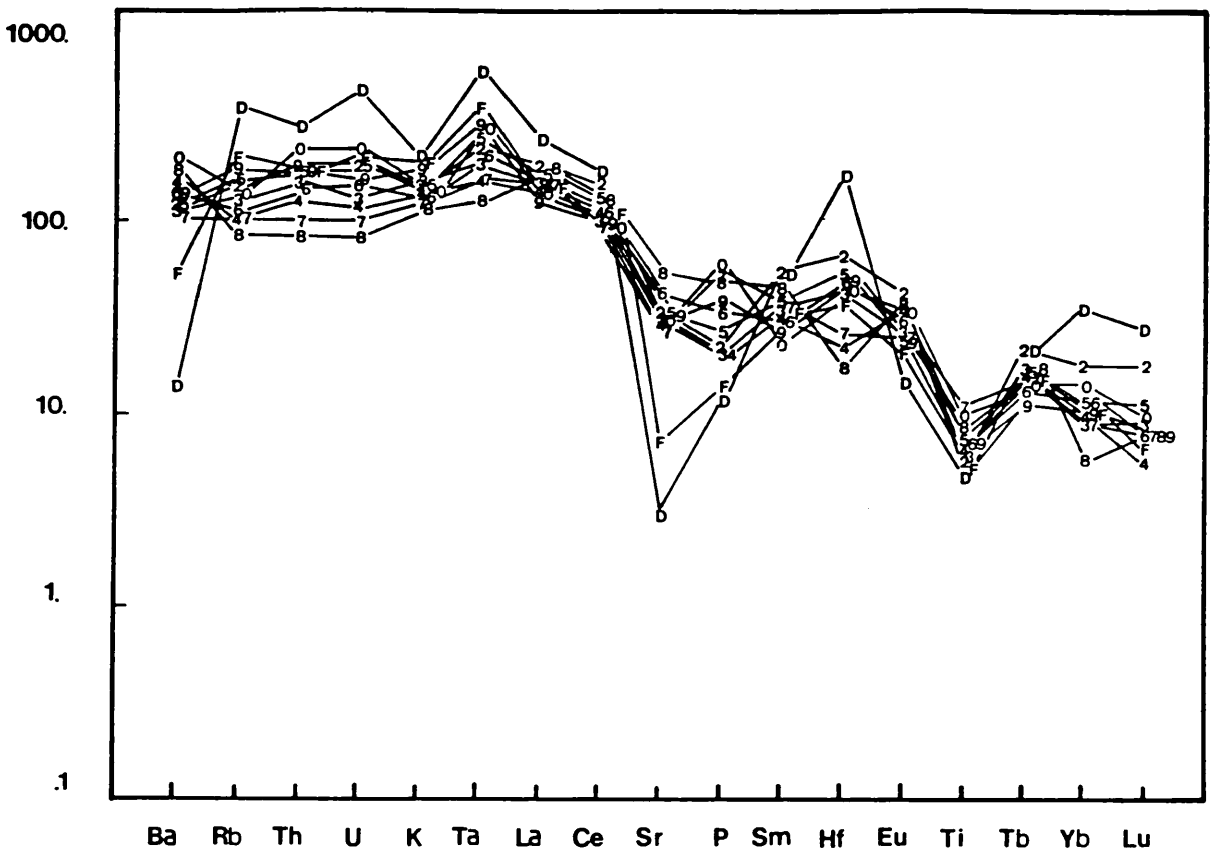

FIGURE 2.14. Primordial mantle normalised Hygromagmatophile element plot for the intermediate rocks from the Larvik complex, Oslo Region (from Neumann 1980). Symbols as in Figure 2.11.

solidus considerably (Helz 1976; Hanson 1978). Fractional melting of lower crustal material, therefore, is only a likely mechanism if H_2O and/or CO_2 are being introduced from an external source (ie. the mantle). The distributions of incompatible trace elements within the larvikites may also be explained in terms of a model in which these elements are concentrated into the inter-cumulous liquid of large stratified magma chambers at the base of the crust. Successive melt fractions removed from the magma chambers during tectonic disturbances would tend to be progressively depleted in these elements .

Finally, consideration of the ratios of certain incompatible trace elements, such as Zr/Nb (Oftedahl 1977) and Th/U (Raade 1977), may provide important information concerning the nature of the source rocks for partial melting and/or fractional crystallisation processes (Section 6.3). On the basis of Zr/Nb ratios, Oftedahl (1977) has demonstrated that the basaltic rocks, which are mainly pyroxene basalts and plagioclase - pyroxene basalts (Weigand 1975), and rhomb porphyry lavas from the Vestfold lava plateau could not have been derived from the same source. These rocks have Zr/Nb atomic ratios of 3.8 and 5.85 respectively. This is in agreement with the mineralogical and geochemical evidence (Sections 2.5.1 and 2.5.2) which indicate alkali basaltic and tholeiitic sources respectively, for these rocks. Ratios of Th to U, however, are not so useful in this respect, since rocks from both alkali basaltic and tholeiitic sources tend to have similar values (Table 6.3).

2.5.6 Summary and Conclusions

The petrogenesis of the Oslo province may be summarised as follows:

I. Basaltic rocks in the Oslo Region define two distinct compositional trends, reflecting derivation by partial

melting at different depths within the mantle:

A. An alkali basaltic trend (calcic trend, Figure 2.9a; pyroxene basalts and plagioclase-pyroxene basalts) controlled by fractional crystallisation of moderately aluminous clinopyroxene + olivine from an extremely calcic, and alkaline, starting composition. The latter indicates either an anomalously calcic mantle source composition, or derivation by partial melting of mantle peridodite in which garnet was an important residual phase, at great depths and in the presence of a free volatile phase (CO_2, H_2O). Prolonged residence at the base of the crust and/or in high level magma chambers has obscured the "mantle" inheritance.

B. A tholeiitic trend (alkaline trend, Figure 2.9a; aphyric basalts and plagioclase basalts) controlled by fractionation of clinopyroxene + plagioclase or garnet $\pm$ olivine at moderate pressures. This group of rocks is characterised by systematically lower contents of incompatible trace elements (Rb, Sr, Th, U and LREE), reflecting derivation by larger degrees of partial melting at shallower depths within the mantle.

II. Felsic rocks in the Oslo Region were derived from a variety of sources:

A. The intermediate monzosyenites and related feldspathoidal rocks in the Larvik area were derived by fractional crystallisation of subcalcic plagioclase (An < 30) $\pm$ clinopyroxene $\pm$ olivine from an alkali basaltic parent. Progressive depletion in incompatible trace elements (D < 1) in the later formed melt fractions may reflect fractional melting processes in the source region, but more probably is the result of concentration of these elements into the intercumulous liquid of large stratified magma chambers at the base of the crust. According to this model, successive melt fractions removed from the magma chambers during

tectonic disturbances would tend to be progressively depleted in incompatible elements.

B. The intermediate kjelsasites and quartz-bearing larvikites were derived from a combination of alkali basaltic and tholeiitic sources by fractionation of calcic plagioclase (An_{50} - An_{30}) $\pm$ clinopyroxene. In comparison, the intermediate rhomb porphyry lavas were derived mainly from a tholeiitic source, corresponding in composition to the plagioclase basalts.

C. The more evolved nordmarkites and ekerites were either derived directly by fractional crystallisation of kjelsasitic parent magmas, or by partial melting of compositionally similar rocks in the crust. As proposed by Barth (1944, 1954), the principal mechanism of fractionation was by separation of feldspar, under conditions of low pressure (shallow depth).

D. The biotite granites (BGI; Gaut 1981) have compositions compatible with a derivation by partial melting of lower crustal material of gabbroic composition, essentially by fractionation of clinopyroxene.

CHAPTER 3

FIELD RELATIONSHIPS AND PETROGRAPHY

3.1 Introduction

The area of study is situated within the igneous complex to the west of Hurdalssjoen in the northern part of the Oslo Region (Figure 3.1). The igneous complex comprises part of the Nordmarka - Hurdalen batholith which dominates the geology of the northern part of the Region (Figure 2.1; Section 2.3.2). The batholith is composite in nature, consisting of a variety of intrusive rocks ranging between monzonitic and granitic in composition, and including the rock-types: Kjelsasite (monzodiorite - syenite), larvikite (monzonite - monzosyenite), nordmarkite (alkali feldspar syenite) and ekerite (alkali feldspar granite), which together make up the plutonic igneous rock series as defined by Barth (1944; Section 2.5).

An area of approximately 50 km^2 was mapped during the summers of 1980 and 1981 (Section 1.3). Fieldwork was more concerned with deducing the spatial and temporal relationships of the various intrusive (and extrusive) phases than verifying the actual positions of intrusive contacts. The latter has been done adequately by Martinsen et al. (1979), Tronnes (1980), Ihlen and Rasmussen (1981), and Tronnes (1982); upon whose work the geological map in Figure 3.1 is based. The areas to the north and west of the studied area have been described in detail by Nystuen (1975b) and Rasmussen (1982), respectively. In addition, a general description of the petrography and intrusive relationships of plutonic rocks in the Hurdal area, including the area to the east of Hurdalssjoen, has been given by Ihlen and Rasmussen (1981).

The nomenclature used to describe this suite of rocks has traditionally incorporated such terms as kjelsasite, larvikite, nordmarkite, grefsen syenite, ekerite and biotite

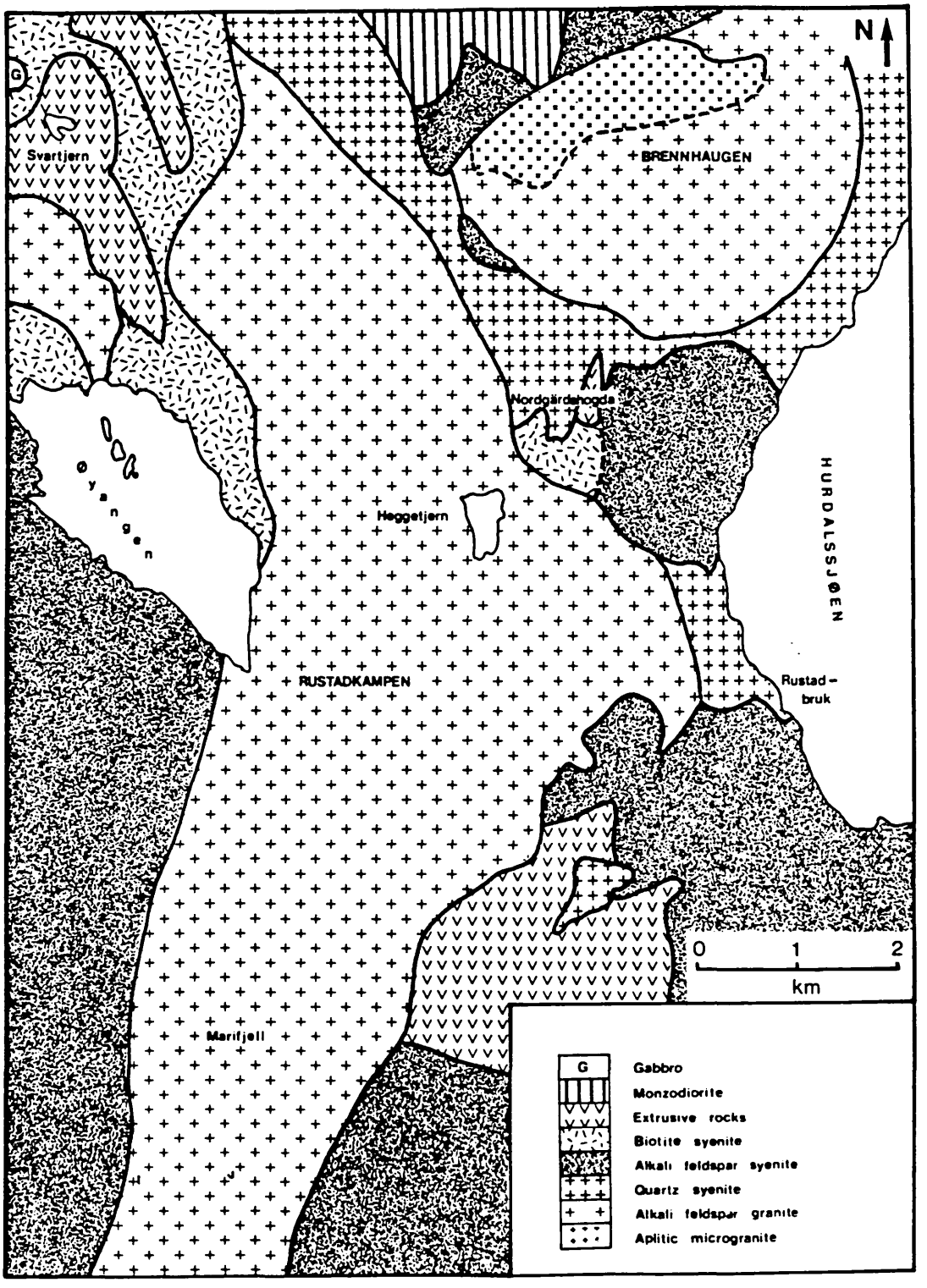

FIGURE 3.1. Geological map of the Hurdal area (modified after Tronnes 1980).

granite (Section 2.3.2). These are named mostly after type localities within the Region and have fairly strict definitions in terms of mineralogy, and sometimes texture. However, detailed observations of the plutonic rocks indicate that several parallel evolutionary series exist, and that many rocks do not fall conveniently into any of the above named categories. For this reason it has been decided to adopt the classification system of Streckeisen (1976), but to retain the traditional terms for purposes of cross-reference.

3.2 Geological structure of the igneous complex

The igneous complex in the Hurdal area consists of numerous, irregularly shaped intrusions of intermediate to granitic rocks displaying both transitional and sharp, cross-cutting intrusive relationships. The complex is largely composed of alkaline to peralkaline syenites and granites, although locally areas of monzonitic rock (kjelsasite) are also present. The occurrence of several enclosed areas of volcanic rocks, for instance in the Svartjern, Styggberget and Rustad areas, and also of several diatremes in the area to the north of Hurdal (Nystuen 1975a) suggests a subvolcanic level of emplacement for the complex. This is supported by the widespread development of porphyritic texture, local transitions between coarse-grained, equigranular rocks and fine-grained, porphyritic rocks sometimes being observed, as for instance in the Nordgardshogda area (below). In addition, the presence of miarolytic cavities and druses within many of the plutonic rocks, particularly in their contact zones, is believed to be indicative of shallow depths of emplacement (Ramberg 1976). The volcanic rocks probably represent foundered roof pendants.

On the basis of mineralogy and texture, the igneous rocks in the Hurdal area may be divided into the following categories:

MONZODIORITE - MONZOSYENITE (kjelsasite): Dark grey to

reddish rocks containing fairly calcic plagioclase (An_{30} - An_{50}), alkali feldspar, clinopyroxene, hornblende and biotite, and showing variable grain size.

BIOTITE SYENITE (Grefsen syenite): Essentially coarse-grained (Ø.5 to 4 mm), inequigranular rocks containing zoned phenocrysts of alkali feldspar often with plagioclase cores, accompanied by alkali feldspar, biotite (<5%) and quartz (circa 2%).

ALKALI FELDSPAR SYENITE (nordmarkite): Coarse-grained (1 to 4 mm), fairly inequigranular rocks containing alkali feldspar, minor plagioclase, amphibole, biotite, quartz (circa 5%) and sphene.

QUARTZ SYENITE (transitional between nordmarkite and ekerite): Medium to coarse-grained (2 to 3 mm average), equigranular, leucocratic rocks containing a hypidiomorphic granular intergrowth of alkali feldspar with interstitial quartz (<5% to > 20%), biotite and possibly amphibole. Two textural variants of the quartz syenite may also be distinguished: UNEVEN MICROGRANITE and FELDSPAR PORPHYRITIC MICROGRANITE.

ALKALI-FELDSPAR GRANITE (ekerite): Coarse-grained (Ø.5 to 5 mm), fairly equigranular, leucocratic rocks containing a xenomorphic granular intergrowth of alkali feldspar and quartz (15 to 30%) with minor amphibole, biotite and zircon. A fine-grained textural variety of this rock is also distinguished: APLITIC MICROGRANITE.

EXTRUSIVE ROCKS (Alkali trachytes and rhomb porphyries): fine grained, aphyric or weakly porphyritic rocks often showing compositional layering, consisting essentially of alkali trachytes (comenditic trachytes; MacDonald 1974), with minor representation from trachyandesites (rhomb porphyries).

DYKE ROCKS: fine grained, aphyric or weakly porphyritic rocks of gabbroic to granitic composition.

Ihlen and Rasmussen (1981) distinguish an additional rock-type: QUARTZ-BIOTITE SYENITE, which lacks the blue-zoned feldspars. This rock-type has not been observed in the area of study.

Rocks of monzonitic affinity represent the oldest intrusive rocks in the complex. Dark grey monzodiorites and reddish monzosyenites are only exposed in the northern part of the area, where they are seen to grade into biotite syenites (Figure 3.1; Ihlen and Rasmussen 1981). The biotite syenites also show a close intrusive relationship to the volcanic rocks, transitions between porphyritic varieties of biotite syenite and fine grained trachytic rocks sometimes being observed, as for instance in the Nordgardshogda area.

Mineralogically and texturally the biotite syenites are similar to the alkali feldspar syenites, but may be distinguished from the latter in that they lack amphibole. Zoned phenocrysts of alkali feldspar with plagioclase cores may be observed within both rock-types. The alkali feldspar in the alkali feldspar syenite, however, is much redder in colour. Transitions between biotite syenite and alkali feldspar syenite probably occur, but have not been observed in the area of study; although a possible transitional nature is inferred in the area to the south-east of Nordgardshogda where poor exposure obscures the contact. The alkali feldspar syenite in this area cannot be equated with typical nordmarkite (Section 2.3.2), since biotite takes the place of amphibole as the principal ferromagnesian mineral. However, this rock-type does grade into more typical nordmarkite to the east of Hurdalssjoen (Ihlen and Rasmussen 1981).

The quartz syenite in the area of study has a distinctive outcrop pattern, occurring in a narrow NW-SE trending zone

between the Brennhaugen and Rustadkampen granite massifs; but also occurs in a small intrusion in the Kongen area. Texturally, the quartz syenite is easily recognised by its hypidiomorphic granular intergrowth of alkali feldspar grains, a feature which might equate this rock-type with ekerite (Dietrich et al. 1965). However, the quartz syenite shows considerable variation in quartz content, on the scale of the hand specimen and at outcrop, suggesting that this rock-type is in fact transitional between nordmarkite and ekerite. The quartz syenite in the Kongen area is a peralkaline variety containing sodic amphibole, and with its high quartz content (15 - 20%; Section 3.3.4) may be regarded as a typical ekerite.

Particularly towards its contact zones, the quartz syenite shows considerable variation in grain size, and a tendency to become slightly inequigranular is sometimes observed (Section 3.3.4). Locally, variations in grain size, and quartz content, are so large as to warrant the use of a separate name, uneven microgranite, for the contact facies in these areas. The presence within this rock-type of "pegmatitic" segregations of quartz, 10 to 20 cm in diametre, is believed to indicate the importance of volatile exsolution in the contact zone (Chapter 7).

In addition, a porphyritic variety of quartz syenite has been identified, feldspar porphyritic microgranite. This rock-type is found in association with extrusive rocks in the Styggberget area, and as xenoliths within the quartz syenite and uneven microgranite to the east of this area. As such it would appear to represent a porphyritic precursor of the quartz syenite. A similar rock-type is found as dykes intruding alkali feldspar syenite along Vekensbekken.

Alkali feldspar granite occurs in two principal areas, forming the fairly extensive Brennhaugen and Rustadkampen granite massifs. This rock-type is easily distinguished from

the quartz syenite on the basis of its higher quartz content and xenomorphic granular texture, tending to be very homogeneous over considerable distances. Extensive exsolution of alkali feldspar and local redistribution of alkalies within the granite has lead to widespread autometasomatism, imparting a bleached appearance to these rocks. Locally, however, leaching of the Na from these rocks and oxidation of Fe has resulted in more reddened varieties, particularly along joint surfaces. In addition, redistribution of Mn has resulted in widespread manganese oxide staining.

The alkali feldspar granite in the Brennhaugen area contains sodic amphibole, and may therefore be referred to as ekerite, although texturally it is not a typical ekerite (see Dietrich et al. 1965). Amphibole also occurs in miarolytic cavities within the granite. However, particularly towards its contact zones with the quartz syenite, along Rudsetraveien, biotite takes the place of amphibole as the principal ferromagnesian mineral. Also in the contact zones, quartz filled miarolytic cavities similar to those observed within the margins of the quartz syenite, are common.

The north-western face of the Brennhaugen massif is occupied by a fine-grained, aplitic microgranite. The latter is mineralogically and chemically very similar to the alkali feldspar granite and is therefore regarded as a quenched facies of the granite. Transitions between the two rock-types have been observed. A similar rock-type has also been observed on a much smaller scale in the contact zones of the Rustadkampen granite and is seen in the Hegga River (Section 4.3.3).

Mineralogically and texturally the Rustadkampen granite is identical to the Brennhaugan granite, biotite being the principal ferromagnesian mineral. It is therefore likely that these intrusions join up at depth to form one large homogeneous pluton. Emplacement of this pluton is believed to

have been one of the latest magmatic events in the igneous complex.

A number of late dykes have been observed to cut the granite in several places. For instance at Steinbratebekken within the Brennhaugen Granite, several monzonitic and syenitic dykes are observed within a short distance of each other. The presence of these dykes implies the existence of residual pockets of intermediate magma throughout the period of felsic magmatism.

3.3 Petrography of the principal rock-types

3.3.1 Monzodiorite

Only two samples of monzonitic rocks have been studied (M1 and M2; Figure 5.1).

The monzodiorite is a coarse-grained (1 to 4 mm), equigranular, mesotype igneous rock consisting of aggregates (2 to 4 mm) of clinopyroxene, biotite, hornblende, apatite and magnetite in a groundmass of plagioclase and alkali feldspar (Figure 3.2a). The ferromagnesian mineral aggregates tend to be totally surrounded by feldspar and are randomly distributed throughout the rock which has a blue-grey colour. No quartz or nepheline has been observed.

The ferromagnesian mineral aggregates make up between 20 and 40 percent of the rock. They consist largely of blue-grey to mauve titanaugite, showing varying degrees of uralitic alteration, and dark brown biotite. Apatite and magnetite tend to be poikilitically enclosed within these minerals. Apatite also occurs as inclusions within magnetite, suggesting that it was the first mineral to crystallise. Magnetite probably belongs to two generations, occuring as early euhedral crystals and later irregular masses associated with biotite. Biotite occurs largely around the margins of

FIGURE 3.2a. Photomicrograph of the Monzodiorite (sample M1), showing the relationship between ferromagnesian mineral aggregates and antiperthite.

FIGURE 3.2b. Photomicrograph of the biotite syenite (sample N9ØA7 from the Nordgardshogda area), partially altered to an assemblage of alkali feldspar + muscovite.

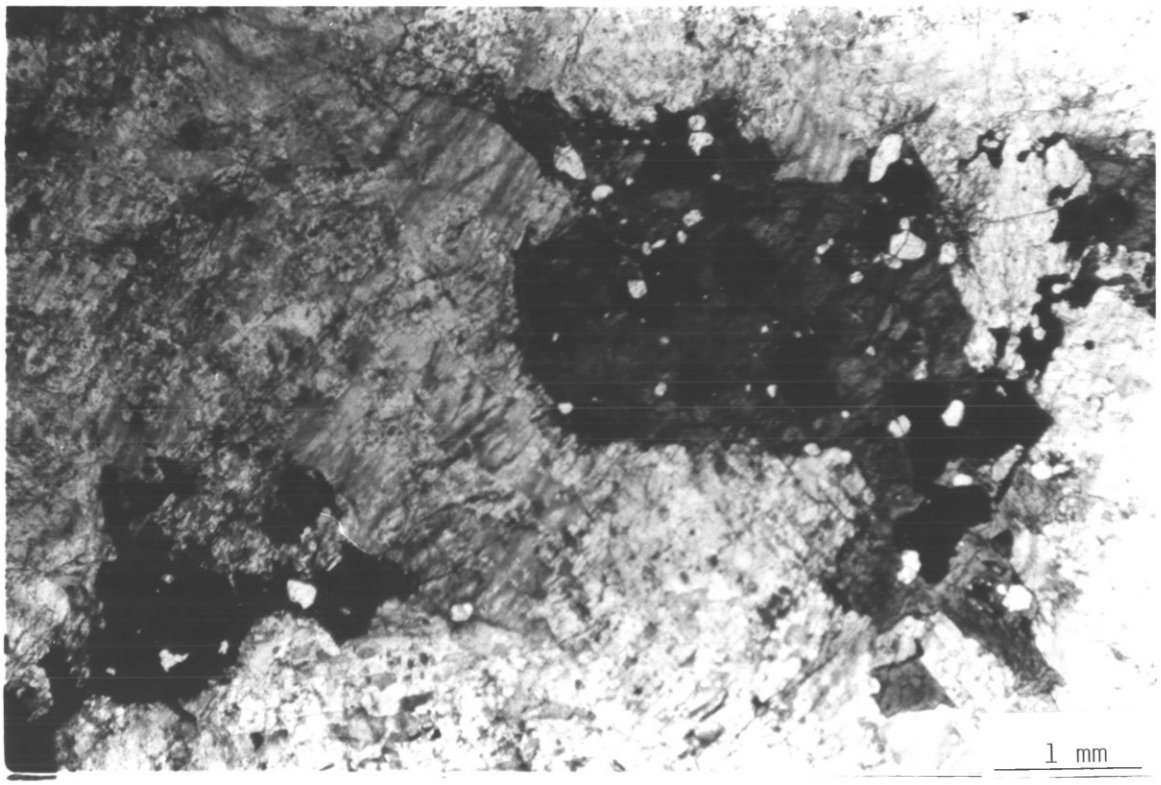
1 mm

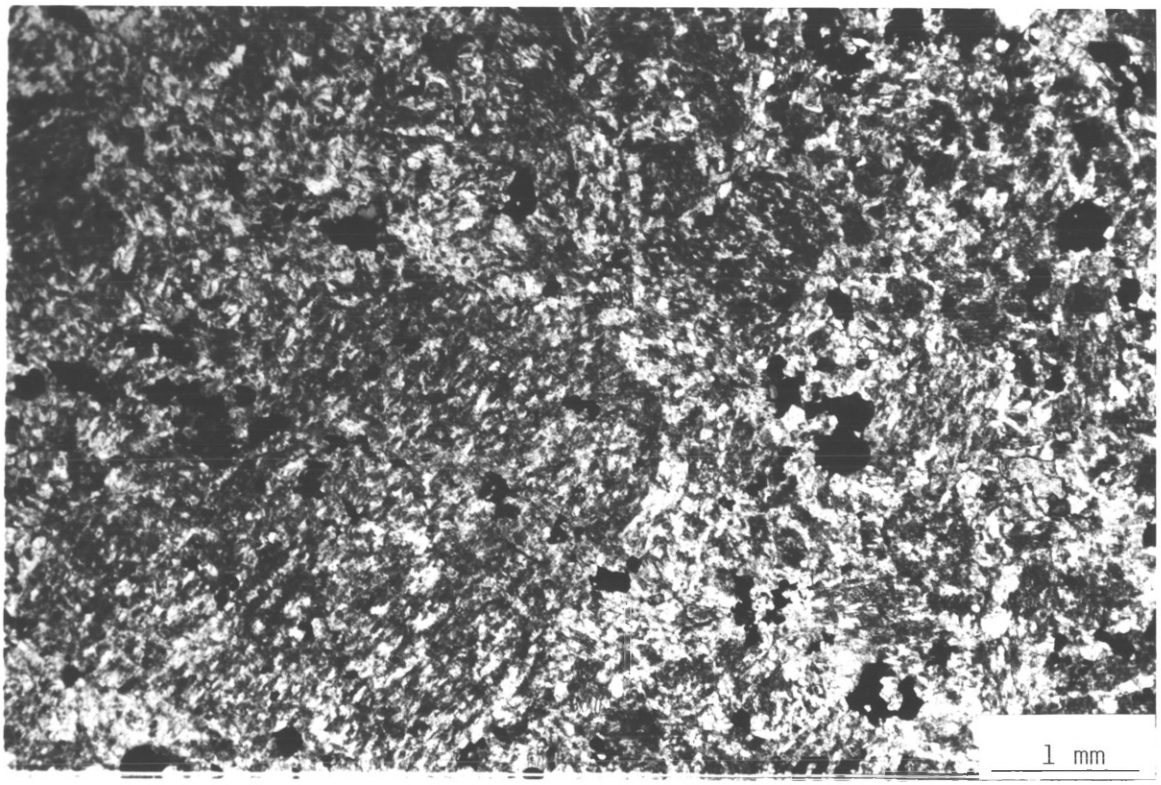
1 mm

pyroxene grains and would appear to have formed from it by reaction, presumably with K-feldspar.

The remainder of the rock is composed of an intergrowth of plagioclase and alkali feldspar in the approximate ratio of 3 to 1. The plagioclase is essentially an andesine but may be zoned. It tends to show antiperthitic exsolution of orthoclase. Small euhedral inclusions of magnetite are common.

3.3.2 Biotite syenite

The biotite syenite described here is confined to the southern part of the Nordgardshogda area, where it forms a separate intrusion (Figure 3.1). A similar rock-type is observed in the Buraskollen area (Ihlen and Rasmussen 1981).

The biotite syenite is an inequigranular, but tending towards distinctly porphyritic, leucocratic igneous rock consisting of euhedral to subhedral phenocrysts of alkali feldspar, and to a lesser extent plagioclase, in a fine to medium grained (<Ø.1 to Ø.5 mm) groundmass of quartz (2 %), alkali feldspar, plagioclase, biotite, magnetite, ilmenite and minor apatite (Figure 3.2b). Phenocrysts range in size between 1 mm and 1 cm (2 to 3 mm average) and constitute between 1Ø and 2Ø percent of the rock by volume. The ratio of alkali feldspar to plagioclase phenocrysts is variable, ranging between 1Ø to 1 and 2 to 1. Both plagioclase and alkali feldspar phenocrysts may be zoned, and plagioclase sometimes forms the cores to alkali feldspar grains. Ferromagnesian minerals constitute up to 5 percent of the rock by volume.

Alkali feldspar phenocrysts range in size up to 1 cm. They tend to be euhedral to subhedral with somewhat corroded grain boundaries. Patchy to braided microperthitic texture is ubiquitous. Inclusions of magnetite and occasionally ilmenite, are common. In contrast, plagioclase grains range

in size from groundmass grains up to 3 mm. They tend to be subhedral, often with resorbed grain boundaries. The plagioclase ranges in composition between albite and oligoclase and shows characteristic lamellar twinning, according to the albite law. Combined carlsbad-albite twinning is also common. The plagioclase tends to be relatively inclusion free.

Biotite ocurs mainly as a groundmass phase but also occurs as small poikilitic phenocrysts, up to 2 mm in size, with inclusions of quartz and magnetite and occasionally plagioclase as well. It is not certain whether these represent true phenocrysts or poikiloblasts. Biotite is a common alteration product of the biotite syenite (Section 4.3.1).

The biotite is magnesium rich containing between 60 and 70 percent of the phlogopite end-member (Table 3.1). Manganese forms up to 0.2 atoms per formula unit. The biotite tends to be fairly constant in composition and shows no signs of zoning.

Opaque minerals occur both as discrete grains in the groundmass as well as inclusions in feldspar grains. Aggregates of magnetite and ilmenite ranging up to 1 mm in dimension may also be observed. These are intepreted as early phases. Magnetite often contains exsolved lamellae of ilmenite. The ilmenite is manganoan, containing up to 1.3 Mn ions per formula unit, on the basis of twelve oxygen atoms. Magnetite and ilmenite compositions are listed in Table 3.2.

3.3.3 Alkali feldspar syenite

Samples of alkali feldpsar syenite from the Rundhaugen area, from the wall-rocks of the Brennhaugen granite along Rudsetraveien, from along Vekensbekken, and from the Rustad area, have been studied.

TABLE 3.1: BIOTITE ANALYSES

SAMPLE:	N164	N253,1	W74	N7	N10	N60A
ROCK TYPE:	B.S.	B.S.	A.S.	Q.S.	Q.S.	Q.S.
NUMBER OF ANALYSES:	9	12	13	7	4	13
ELEMENTS (Wt % Oxide):						
SiO_2	39.81	38.95	39.68	41.55	42.46	40.76
TiO_2	1.66	3.02	1.22	1.66	1.24	1.33
Al_2O_3	11.92	11.89	10.48	8.85	8.78	10.16
FeO	13.95	14.10	13.64	14.73	11.11	13.09
MnO	1.23	1.63	3.04	2.01	2.53	2.92
MgO	15.93	16.06	16.11	14.48	16.14	15.67
CaO	.01	.22	.09	.03	.14	.01
Na_2O	.37	.23	.84	.20	.40	.33
K_2O	10.27	10.04	9.65	9.99	9.43	10.25
TOTAL	95.15	96.14	94.75	93.50	92.23	94.52
NUMBER OF CATIONS ON THE BASIS OF 22 OXYGEN ATOMS:						
Si	5.98	5.81	6.03	6.37	6.47	6.18
Al	2.02 } 8.00	2.09 } 7.90	1.88 } 7.91	1.60 } 7.97	1.53 } 8.00	1.81 } 7.99
Al	.08	0.	0.	0.	.05	0.
Ti	.19	.34	.14	.19	.14	.15
Fe	1.75 } 5.74	1.76 } 5.88	1.73 } 5.91	1.89 } 5.65	1.42 } 5.60	1.66 } 5.73
Mn	.16	.21	.39	.26	.33	.38
Mg	3.56	3.57	3.65	3.31	3.67	3.54
Ca	.00	.04	.02	.01	.02	.00
Na	.11 } 2.08	.07 } 2.01	.25 } 2.13	.06 } 2.02	.12 } 1.97	.10 } 2.08
K	1.97	1.91	1.87	1.95	1.83	1.98
PERCENTAGE OF END-MEMBERS:						
Phlogopite	65.14	64.50	63.20	60.62	67.78	63.51
Annite	34.86	35.50	36.80	39.38	32.22	36.49

SAMPLE:	N63		W412		W52		W58		WW16	
ROCK TYPE:	Q.S.		A.G.		A.G.		A.G.		A.G.	
NUMBER OF ANALYSES:	6		7		7		16		5	
ELEMENTS (Wt % Oxide):										
SiO_2	41.92		38.84		39.43		37.56		40.70	
TiO_2	1.03		1.61		1.40		1.26		1.33	
Al_2O_3	9.62		7.77		7.02		7.43		6.84	
FeO	10.94		24.44		23.47		24.67		20.15	
MnO	2.63		8.50		9.88		11.42		9.14	
MgO	16.75		4.44		4.20		3.22		3.33	
CaO	0.		.10		0.		.01		0.	
Na_2O	.27		.88		.71		.46		.25	
K_2O	10.13		9.13		9.42		9.24		9.32	
TOTAL	93.99		95.71		95.53		95.27		91.06	
NUMBER OF CATIONS ON THE BASIS OF 22 OXYGEN ATOMS:										
Si	6.34	8.00	6.34	7.83	6.46	7.81	6.30	7.74	6.82	8.00
Al	1.66		1.49		1.35		1.46		1.18	
Al	.05	5.67	0.	5.79	0.	5.78	0.	6.03	.17	5.30
Ti	.12		.20		.17		.16		.17	
Fe	1.38		3.33		3.21		3.45		2.83	
Mn	.34		1.17		1.37		1.62		1.30	
Mg	3.78		1.08		1.03		.80		.83	
Ca	0.	2.03	.02	2.20	0.	2.19	.00	2.12	0.	2.07
Na	.08		.28		.23		.15		.08	
K	1.95		1.90		1.97		1.97		1.99	
PERCENTAGE OF END-MEMBERS:										
Phlogopite	68.70		19.32		18.27		13.67		16.79	
Annite	31.30		80.68		81.73		86.33		83.21	

TABLE 3.2: MAGNETITE AND ILMENITE ANALYSES

SAMPLE:	N164	N164	N253,1	N253,1	W74
ROCK TYPE:	B.S.	B.S.	B.S.	B.S.	A.S.
NUMBER OF ANALYSES:	6	5	1	2	1
COMPOSITION:	ilmenite	magnetite	ilmenite	magnetite	magnetite
ELEMENTS (Wt % Oxide):					
TiO_2	47.23	.48	50.14	.86	2.70
Fe_2O_3	0.	67.09	0.	66.94	66.99
FeO	36.39	30.17	32.57	30.10	30.12
MnO	13.58	.36	16.21	1.02	2.88
TOTAL	97.20	98.10	98.92	98.92	102.69
NUMBER OF CATIONS ON THE BASIS OF 12 OXYGEN ATOMS:					
Ti	3.77	.04	3.89	.08	.23
Fe^{3+}	0.	5.94	0.	5.87	5.64
Fe^{2+}	3.23	2.97	2.81	2.94	2.82
Mn	1.22	.04	1.42	.10	.27

SAMPLE:	K13	K13	N7	N60A	N63
ROCK TYPE:	Q.S.	Q.S.	Q.S.	Q.S.	Q.S.
NUMBER OF ANALYSES:	9	4	9	8	6
COMPOSITION:	ilmenite	magnetite	magnetite	magnetite	magnetite
ELEMENTS (Wt % Oxide):					
TiO_2	50.05	3.71	2.39	.96	1.22
Fe_2O_3	0.	64.31	65.59	66.87	66.12
FeO	30.72	28.92	29.29	30.07	29.73
MnO	17.28	2.40	.54	1.82	1.74
TOTAL	98.05	99.34	97.81	99.72	98.81
NUMBER OF CATIONS ON THE BASIS OF 12 OXYGEN ATOMS:					
Ti	3.91	.32	.21	.08	.11
Fe^{3+}	0.	5.56	5.77	5.83	5.81
Fe^{2+}	2.67	2.78	2.87	2.91	2.90
Mn	1.52	.23	.05	.18	.17

SAMPLE:	W52	W58
ROCK TYPE:	A.G.	A.G.
NUMBER OF ANALYSES:	1	1
ELEMENTS (Wt % Oxide):		
TiO_2	1.91	1.68
Fe_2O_3	67.56	67.45
FeO	30.38	30.33
MnO	4.49	3.85
TOTAL	104.34	103.31
NUMBER OF CATIONS ON THE BASIS OF 12 OXYGEN ATOMS:		
Ti	.16	.14
Fe^{3+}	5.63	5.68
Fe^{2+}	2.81	2.84
Mn	.42	.36

TABLE 3.3: AMPHIBOLE AND PYROXENE ANALYSES

SAMPLE:	W74	N63	K13	WW14	WW16
ROCK TYPE:	A.S.	Q.S.	Q.S.	A.G.	A.G.
NUMBER OF ANALYSES:	11	15	20	1	2
COMPOSITION:	edenite	silicic edenite	arfvedsonite	arfvedsonite	arfvedsonite
ELEMENTS (Wt % Oxide):					
SiO_2	46.72	50.38	52.52	49.38	49.10
TiO_2	.61	.46	.56	.39	.41
Al_2O_3	4.92	2.72	1.43	.40	.65
FeO	15.65	14.22	21.66	23.68	25.23
MnO	5.24	4.53	3.64	6.66	6.98
MgO	11.43	12.15	7.24	2.10	1.65
CaO	9.37	8.18	.90	.31	0.
Na_2O	3.24	3.53	9.42	8.68	9.13
K_2O	.79	.84	1.25	1.08	1.16
TOTAL	97.97	97.01	98.62	92.68	94.51
NUMBER OF CATIONS ON THE BASIS OF 23 OXYGEN ATOMS:					
Si	7.10	7.58	7.98	8.23	8.12
Al	.88 → 7.98	.42 → 8.00	.02 → 8.00	- → 8.23	- → 8.12
Al	0.	.07	.24	.08	.13
Ti	.07	.05	.06	.05	.05
Fe	1.99 → 5.32	1.79 → 5.21	2.75 → 5.17	3.30 → 4.89	3.49 → 5.05
Mn	.68	.58	.47	.94	.98
Mg	2.59	2.73	1.64	.52	.41
Ca	1.53	1.32	.15	.06	0.
Na	.96 → 2.63	1.03 → 2.51	2.78 → 3.17	2.80 → 3.09	2.93 → 3.17
K	.15	.16	.24	.23	.25

SAMPLE:	K13
ROCK TYPE:	Q.S.
NUMBER OF ANALYSES:	9
COMPOSITION:	aegerine
ELEMENTS (Wt % Oxide):	
SiO_2	52.95
TiO_2	.44
Al_2O_3	.44
FeO	28.18
MnO	1.38
MgO	1.10
CaO	3.57
Na_2O	12.19
K_2O	.01
TOTAL	100.26
NUMBER OF CATIONS ON THE BASIS OF 6 OXYGEN ATOMS:	
Si	2.13
Al	0. → 2.13
Al	.02
Ti	.01
Fe	.95
Mn	.05 → 2.20
Mg	.07
Ca	.15
Na	.95
K	.00

The alkali feldspar syenite is a coarse-grained (1 to 4 mm), inequigranular (2 to 3 mm average), leucocratic igneous rock consisting of quartz (less than 5 %), perthitic alkali feldspar, minor plagioclase, amphibole, biotite, sphene, apatite, magnetite and ilmenite (Figure 3.2 c and d). In many respects this rock-type is similar to the biotite syenite described above, with the exception that it contains amphibole and sphene, and generally has a somewhat higher quartz content. Dark minerals constitute approximately 5 percent of the rock by volume.

Alkali feldspar occurs as large subhedral to anhedral grains showing patchy to braided microperthitic texture. Inter-feldspar grain boundaries tend to be irregular, often with minor amounts of exsolved albite. Alkali feldspar grains are occasionally zoned and carlsbad twinning is common. Solid inclusions are moderately rare, although trails of biotite grains may be present, aligned along healed fractures. Magnetite inclusions may also be present.

Plagioclase occasionally occurs as the cores to alkali feldspar phenocrysts, but in general is restricted to the groundmass. The plagioclase is a sodic oligoclase, or albite ($An_{1Ø}$ to $An_{2Ø}$). Discrete patches of albite are occasionally observed towards the margins of alkali feldspar grains. Quartz only occurs interstitially, small grains (Ø.25 mm) of quartz often being observed along inter-feldspar grain boundaries.

Amphibole is essentially a groundmass phase, occurring in the interstices between alkali feldspar grains, usually in conjunction with magnetite and quartz, but often with biotite and sphene as well. The amphibole is a green pleochroic variety and is essentially edenite (Leake 1978, Hawthorne 1981), showing little variation in composition (Table 3.3). Brown to yellow pleochroic biotite also occurs

FIGURE 3.2c. Photomicrograph of the alkali feldspar syenite (sample W7 from Rudsetraveien), showing a zoned phenocryst of alkali feldspar.

FIGURE 3.2d. Photomicrograph of the alkali feldspar syenite (sample V51 from Vekensbekken), containing biotite.

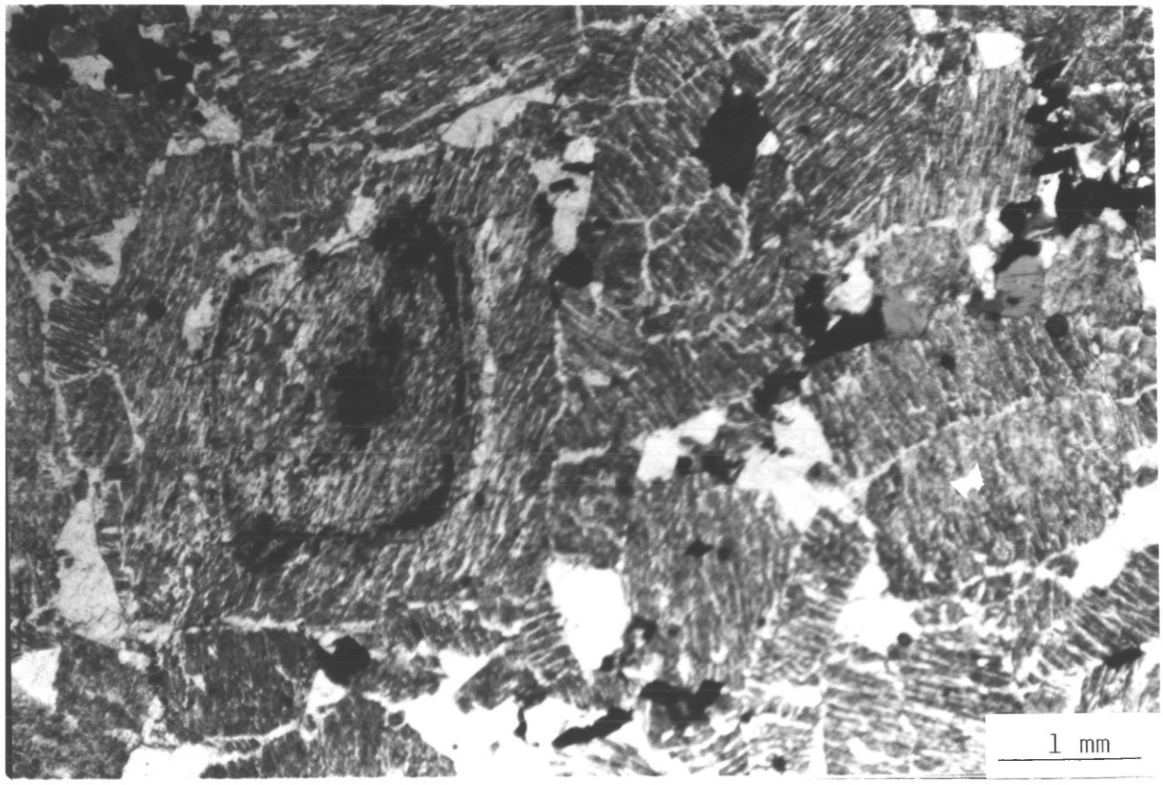
1 mm

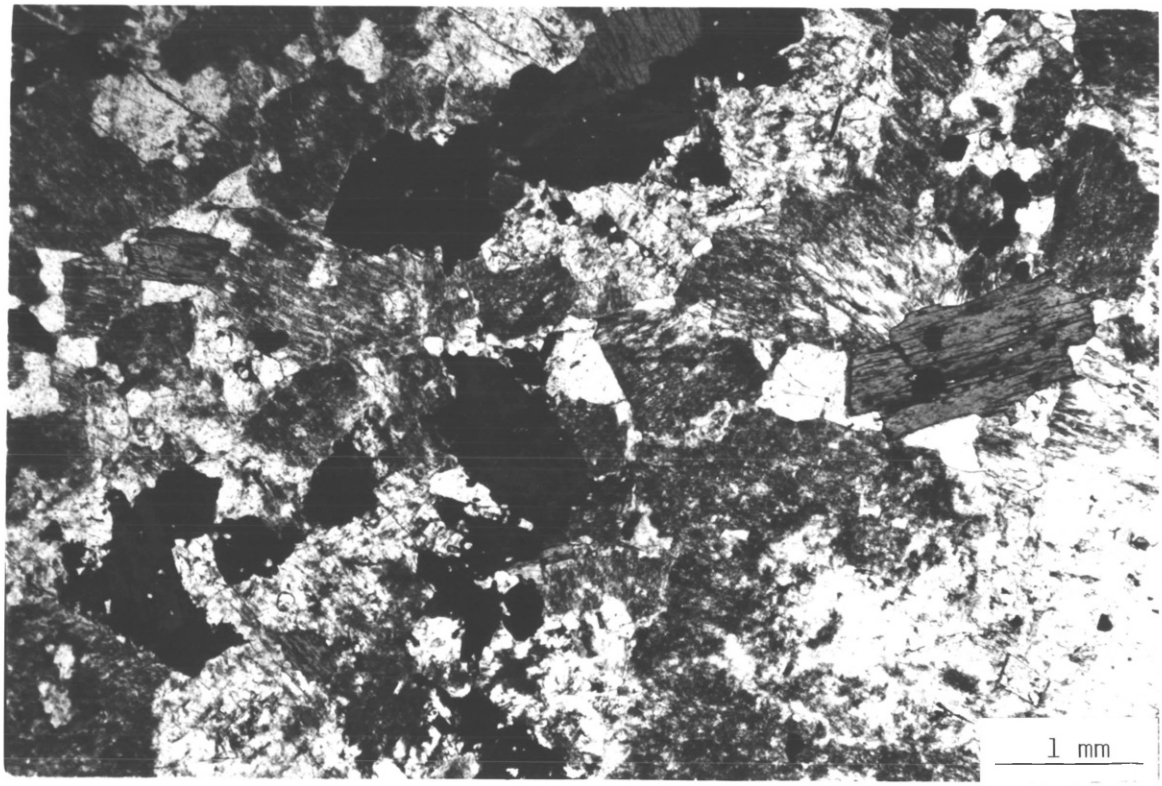
1 mm

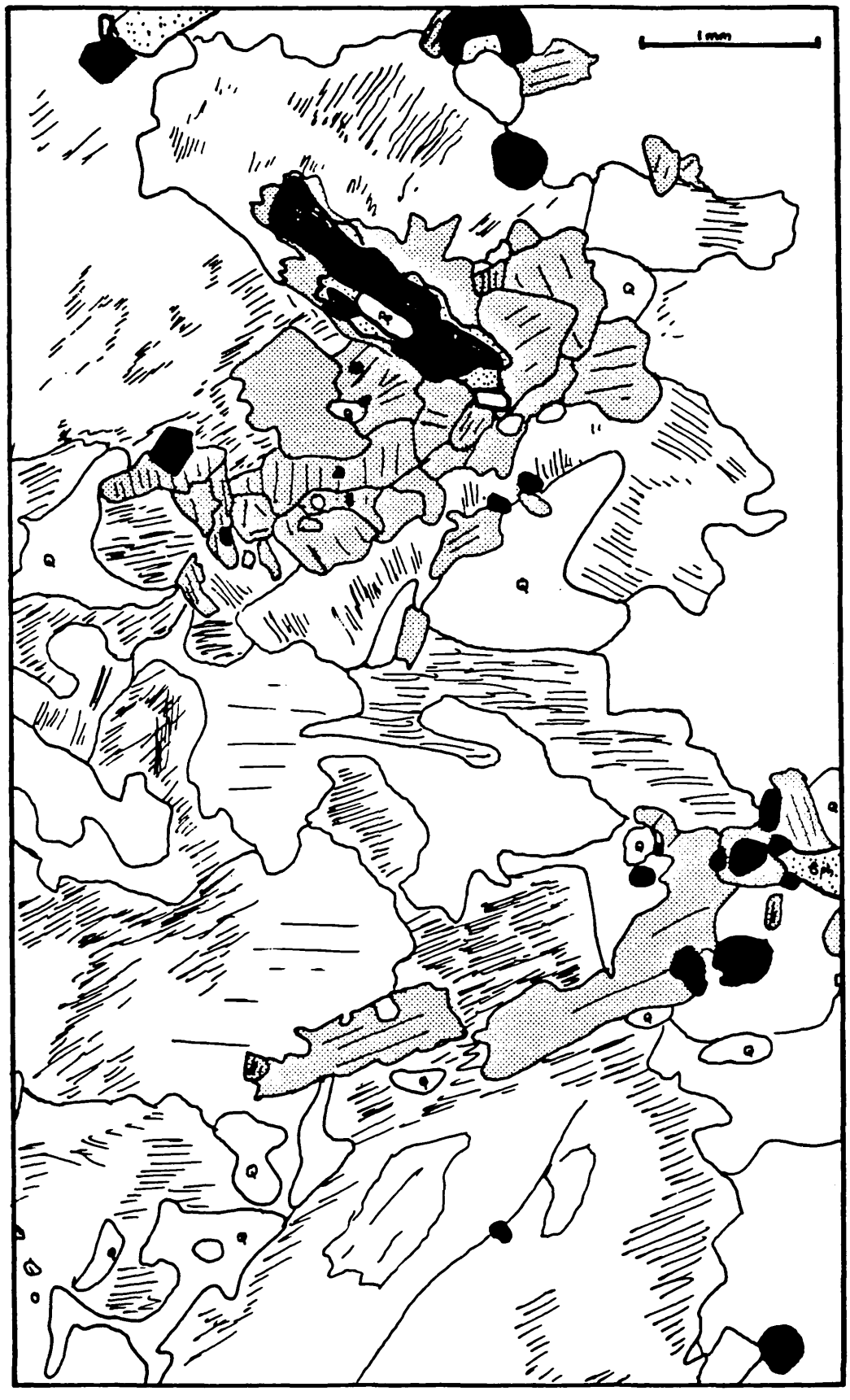

FIGURE 3.2e. Sketch of sample W74, showing the relationship between ilmenite (speckled grey), sphene (dotted), and biotite (shaded) in the alkali feldspar syenite. Magnetite (black), apatite (high relief), quartz (Q), and alkali feldspar showing varying degrees of exsolution.

interstitially, either on its own or in conjunction with virtually any combination of magnetite, ilmenite, quartz, amphibole and sphene. The biotite is magnesium rich and similar in composition to that observed within the biotite syenite (Table 3.1). Intergrowths between amphibole and biotite are common, but evidence of a replacement relationship, for instance alteration of amphibole to biotite along cleavages, is rare. Biotite does, however, show a very clear reaction relationship with ilmenite and sphene, ilmenite grains often being mantled by a layer of sphene, surrounded by biotite (Figure 3.2e). The ilmenite contains up to 1.4 Mn ions per formula unit (Table 3.2).

The alkali feldspar syenite in the Hurdal area shows considerable variation in mineralogy, particularly with regard to its ferromagnesian mineral content. In most areas amphibole is usually the predominant ferromagnesian mineral, being accompanied by biotite. However, in the vicinity of Vekenksbekken biotite plays a more important role, amphibole sometimes being absent (for instance sample V51, Figure 3.2d).

3.3.4 Quartz syenite

The quartz syenite is a coarse-grained (2 to 4 mm), equigranular, leucocratic igneous rock consisting of a hypidiomorphic granular intergrowth of alkali feldspar grains with interstitial quartz, biotite and/or amphibole, magnetite, ilmenite and occasionally sphene (Figure 3.2f). The quartz content of this rock is extremely variable, ranging from less than 5 percent to greater than 20 percent, thus crossing the divisions between syenite, quartz syenite and granite in Streckeisen's (1976) classification system. Tronnes (1980) quite correctly refers to this rock-type as "even-grained quartz syenite to granite". However, the term "quartz syenite" is used here for convenience, since rocks with quartz in the range 5 to 15 percent are most common. The

FIGURE 3.2f. Photomicrograph of the quartz syenite (sample N7 from the Nordgardshogda area), showing the typical hypidiomorphic, granular texture.

FIGURE 3.2g. Photomicrograph of the quartz syenite (sample N63 from the Nordgardshogda area), showing a slightly inequigranular texture.

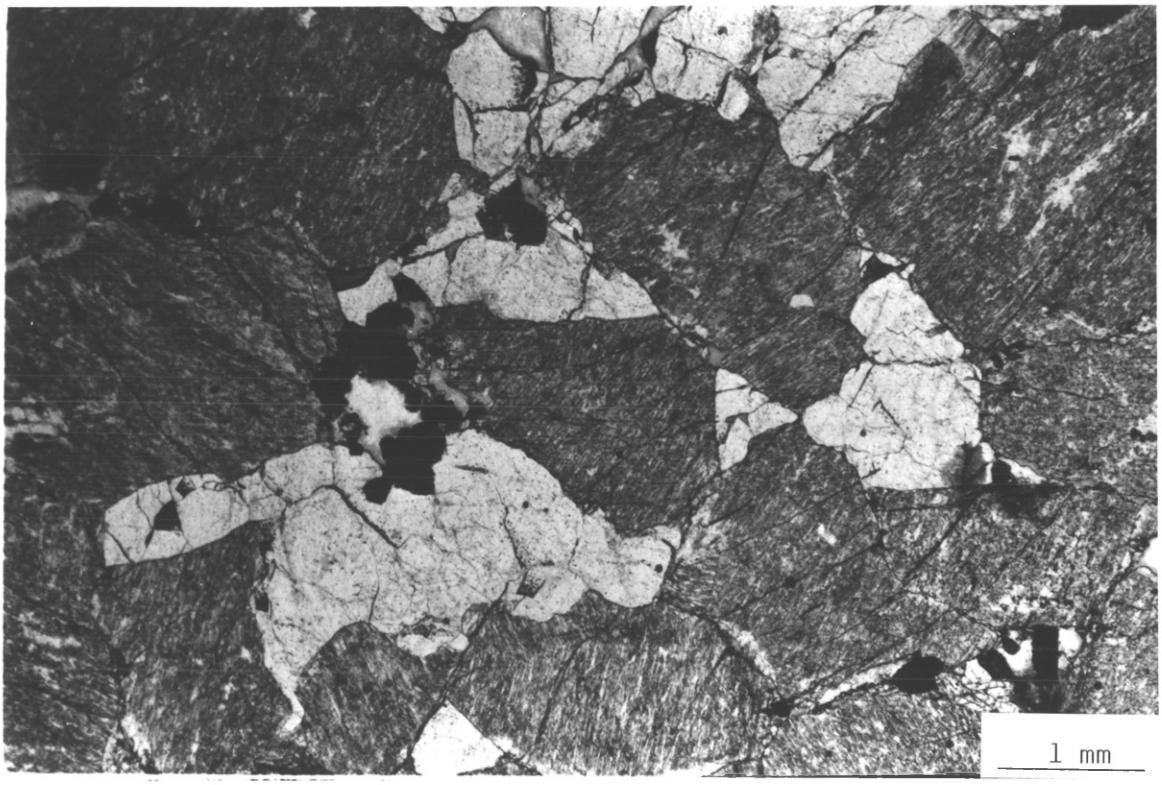
1 mm

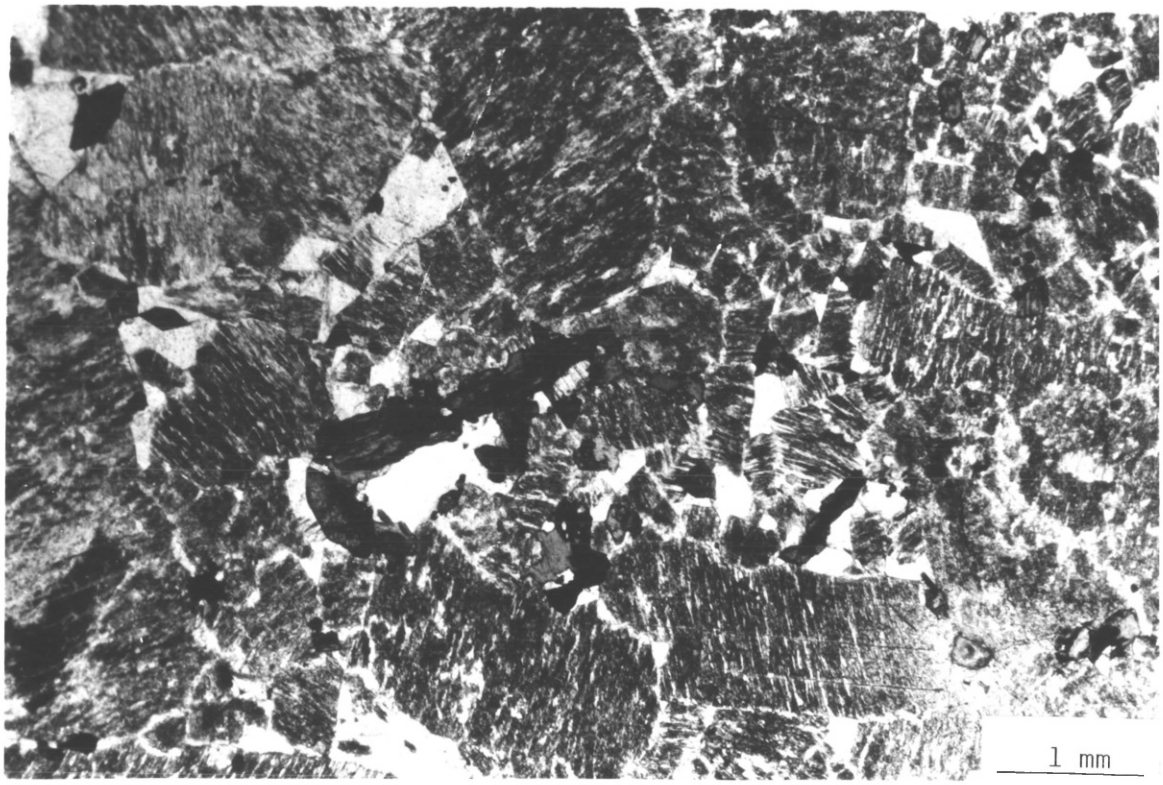
1 mm

quartz syenite lacks significant plagioclase and the ferromagnesian mineral content is low (<2%).

Alkali feldspar grains vary in size between 1 and 4 mm. They tend to be euhedral to subhedral and show typical patchy to braided microperthitic texture. Simple carlsbad twinning is common. Zoning is rare. Alkali feldspar-quartz grain boundaries tend to be sharp, whereas inter-alkali feldspar grain boundaries tend to be slightly less well-defined, often with small amounts of exsolved albite. Inclusions of magnetite or biotite may be present.

Light brown to yellowey-brown pleochroic biotite is the principal ferromagnesian mineral. Although occasionally dark green to light green pleochroic amphibole may also be present. Biotite occurs interstitially, either on its own or in conjunction with quartz, sphene and Fe-Ti oxides. The biotite is again magnesium-rich, containing up to 68 percent of the phlogopite end-member (Table 3.1). When compared with the biotite in the alkali syenites, the biotite is appreciably depleted in aluminium, containing between 1.5 and 1.8 ions per formula unit. Amphibole, where present (for instance sample N63; Table 3.3) is also subaluminous, corresponding to silicic edenite in composition (Hawthorne 1981).

Magnetite is the dominant opaque mineral, but may be accompanied by ilmenite or columbite. The magnetite often contains exsolved lamellae of ilmenite. Magnetite analyses are presented in Table 3.2.

The quartz syenite in the area of study shows considerable variation in terms of grainsize and texture, and several textural variants may be distinguished. A tendency to become slightly inequigranular, particularly in those rocks with a low quartz content (<5%), is marked by the occurrence of alkali feldspar in addition to quartz and ferromagnesian

minerals in the interstices between alkali feldspar grains (Figure 3.2g). In addition, a porphyritic variety of quartz syenite (feldspar porphyritic microgranite) and a fine grained aplitic variety (uneven microgranite) may be identified (below).

The quartz syenite in the Kongen area differs from the typical quartz syenite described above in that it contains both sodic amphibole and pyroxene, and has a somewhat higher quartz content (15 to 20 %). Strictly speaking it is a granite, but is grouped together with the quartz syenite on textural grounds. Dark green to yellowey green, moderately pleochroic aegirine appears to be early in the crystallisation sequence, occurring as large grains (1 to 3 mm) intergrown with alkali feldspar. In contrast, green to lavender blue, strongly pleochroic arfvedsonite is late in the crystallisation sequence, occurring in the interstices between alkali feldspar grains, often in association with albite. The degree of exsolution of the alkali feldspars is more advanced, indicating strong mobility of Na in these rocks at sub-solidus temperatures. The ilmenite is extremely manganoan, containing up to 1.9 Mn ions per formula unit (Table 3.2).

3.3.4a Uneven microgranite

The uneven microgranite is observed in several places in the contact zones of the quartz syenite, most notably in the Nordgardshogda area. This rock-type differs from the quartz syenite in that its grainsize is extremely variable over very short distances, on the scale of the outcrop, ranging from less than 0.25 mm to greater than 2 mm; although it is fairly constant on the scale of the hand specimen. However, the hypidiomorphic granular texture so characteristic of the quartz syenite is retained, indicating that this rock is almost certainly a contact facies of it. The quartz content of this rock is also highly variable, ranging up to as much

as 50 percent.

Mineralogically, the uneven microgranite is very similar to the quartz syenite consisting of perthitic alkali feldspar, quartz, minor biotite and magnetite. However, ferromagnesian minerals are of minor importance, constituting much less than 1 percent of the rock by volume.

3.3.4b Feldspar porphyritic microgranite

The feldspar porphyritic microgranite is a porphyritic, leucocratic igneous rock consisting of phenocrysts of alkali feldspar (3 to 6 mm in dimension), and occasionally quartz, in a medium to coarse-grained (0.25 to 1.5 mm) groundmass of alkali feldspar, quartz (10 to 15 percent), amphibole and opaque minerals. The ferromagnesian mineral content is low (much less than 1 percent).

Texturally, the feldspar porphyritic microgranite shows a number of similarities to the quartz syenite. The fact that it tends to be restricted to the contact zones of the quartz syenite suggests that it is a porphyritic precursor of the latter. However, critical contacts between the feldspar porphyritic microgranite and quartz syenite have not been observed. The true position of this rock-type in the petrogenetic sequence is therefore uncertain.

3.3.5 Alkali feldspar granite

The alkali feldspar granite is a coarse-grained (0.5 to 5 mm), inequigranular (2 to 3 mm average), leucocratic igneous rock consisting of a xenomorphic granular intergrowth of perthitic alkali feldspar and quartz (15 to 30 percent), with minor biotite or amphibole, zircon, magnetite, ilmenite, columbite and occasionally sphene (Figure 3.2 h and i). The ferromagnesian mineral content is low, usually forming less than 1 percent of the rock by volume.

FIGURE 3.2h. Photomicrograph of the alkali feldspar granite (sample W24 from the Brennhaugen area), showing the typical xenomorphic, granular texture with interstitial manganoan biotite.

FIGURE 3.2i. Photomicrograph of the alkali feldspar granite (sample W52 from the Brennhaugen area), showing the typical xenomorphic, granular texture.

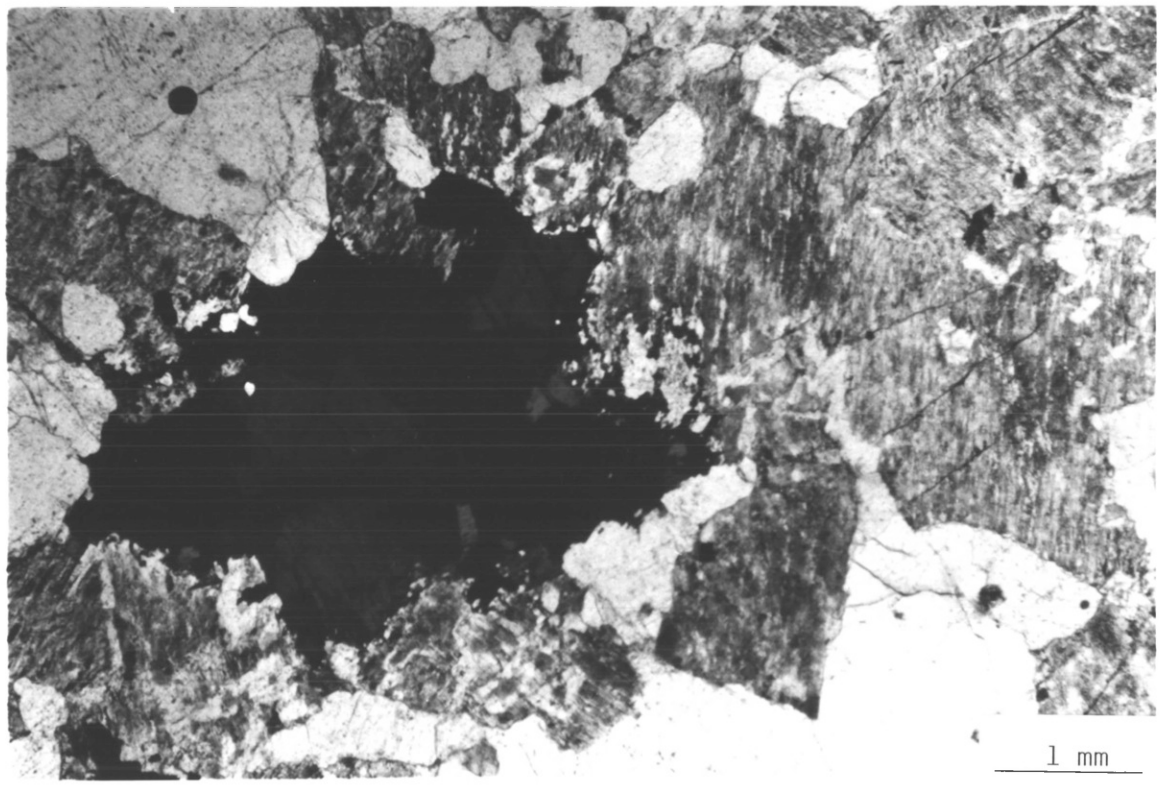
1 mm

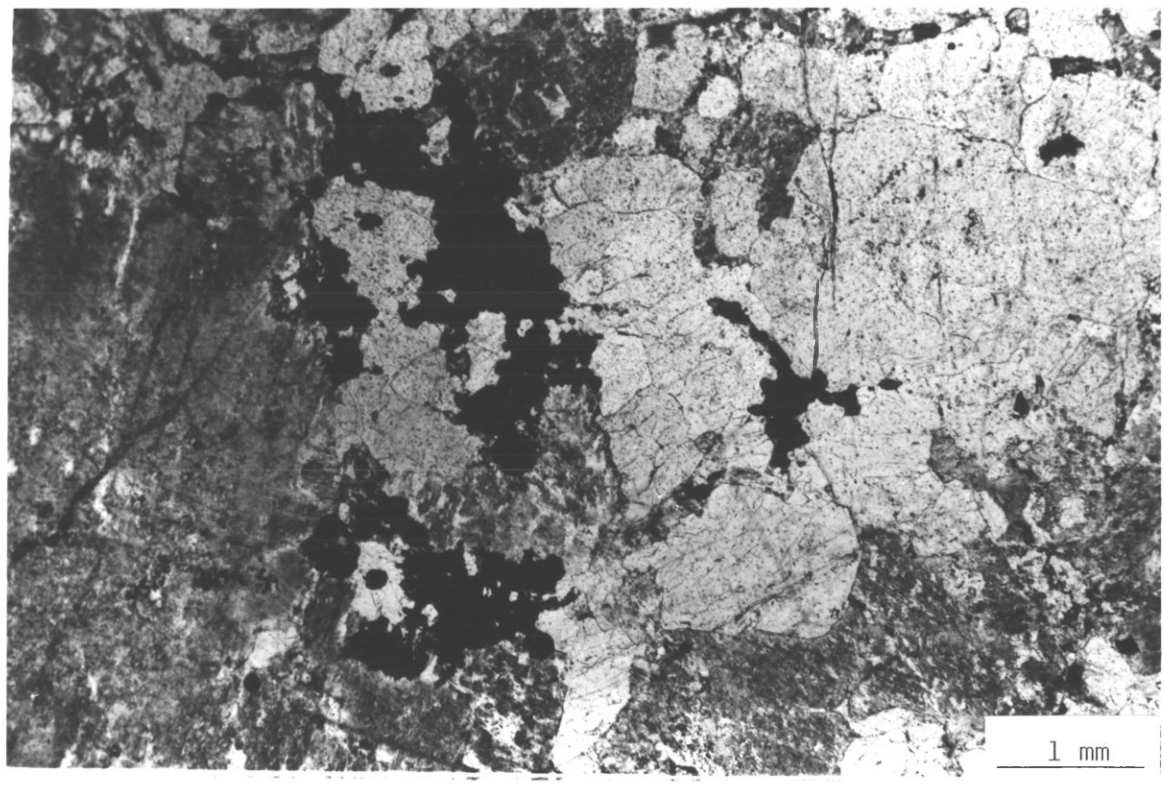
1 mm

Quartz occurs in two modes, either as subhedral to anhedral grains ranging in size up to 5 mm, or as aggregates of euhedral grains up to 1 cm across. Small grains of quartz may also be observed along inter-feldspar grain boundaries. Quartz grain boundaries are usually embayed and triple junctions are often asymmetrical (90 to 180°).

Alkali feldspar occurs as anhedral grains ranging in size up to 5 mm. The alkali fedlspar displays characteristic patchy to braided microperthitic texture with alternating domains of albite and orthoclase. Orthoclase domains tend to be clouded due to numerous microscopic fluid inclusions. Albite domains, in contrast, tend to be clear. Discrete areas of albite displaying typical lamellar twinning are found towards the margins of alkali feldspar grains. Small amounts of exsolved albite are also found along inter-feldspar grain boundaries. The latter tend to be irregular and are often sinusoidal. Microscopic inclusions of hematite are sometimes observed within the feldspar. These are believed to have formed as a result of a reduction in Fe solubility in the feldspars at sub-solidus temperatures (Deer et al. 1977).

Amphibole, where present, occurs as large grains up to 3 mm in dimension. The amphibole is a blue-green to mauve pleochroic variety approximating to arfvedsonite in composition (Table 3.3). Locally, fine-grained clusters of hydrated silicates and iron oxides appear to be pseudomorphs after amphibole.

Biotite occurs interstitially, either as individual grains of variable size, or in aggregates; usually in association with magnetite and to a lesser extent ilmenite. The biotite is an orange to green, pleochroic variety of unusual composition, containing up to 1.5 Mn ions per formula unit (Table 3.1). It might therefore be referred to as a subaluminous manganoan biotite, or as manganophyllite (Deer et al. 1977). Leaching

of manganese from the biotites is presumably partially responsible for the widespread Mn oxide staining associated with the granite.

Magnetite is the predominant opaque mineral phase, usually accompanied by minor amounts of ilmenite and columbite. The magnetite typically contains exsolved lamellae of ilmenite, and may be partially altered to hematite. Zircon is an important accessory phase. Small amounts of fluorite are occasionally observed.

3.3.5a Aplitic microgranite

The Aplitic microgranite is a fine-grained (less than Ø.25 mm), equigranular, leucocratic igneous rock consisting of a graphic intergrowth of perthitic alkali feldspar and quartz (2Ø to 3Ø %; Figure 3.2j). The ferromagnesian mineral content is low, although hematite spotting may be common. This rock-type is confined to the contact zones of the alkali feldspar granite and would appear to be a contact facies of it. Transitions between aplitic microgranite and alkali feldspar granite are common, involving a gradual increase in grainsize (over several tens of metres in the Brennhaugen area).

3.3.6 Extrusive rocks

Extrusive rocks are exposed in several localities within the igneous complex, for instance in the Svartjern, Styggberget and Rustad areas. They include aphyric or weakly porphyritic trachytes, usually showing compositional layering (Figure 3.2k), together with rhomb porphyry lavas. Rhyolites are poorly represented in the Hurdal area. Trachytic lavas and ignimbrites in the Styggberget area are totally recrystallised, essentially due to contact metamorphism in the aureole of the biotite syenite. Breakdown of feldspar phenocrysts and recrystallisation of quartz in these rocks is

FIGURE 3.2j. Photomicrograph of the aplitic microgranite (sample H1 from the Hegga river locality), showing a fine-grained intergrowth of quartz and alkali feldspar.

FIGURE 3.2k. Photomicrograph of the trachyte (sample N342 from the Styggberget area), showing typical compositional layering.

what are these ?

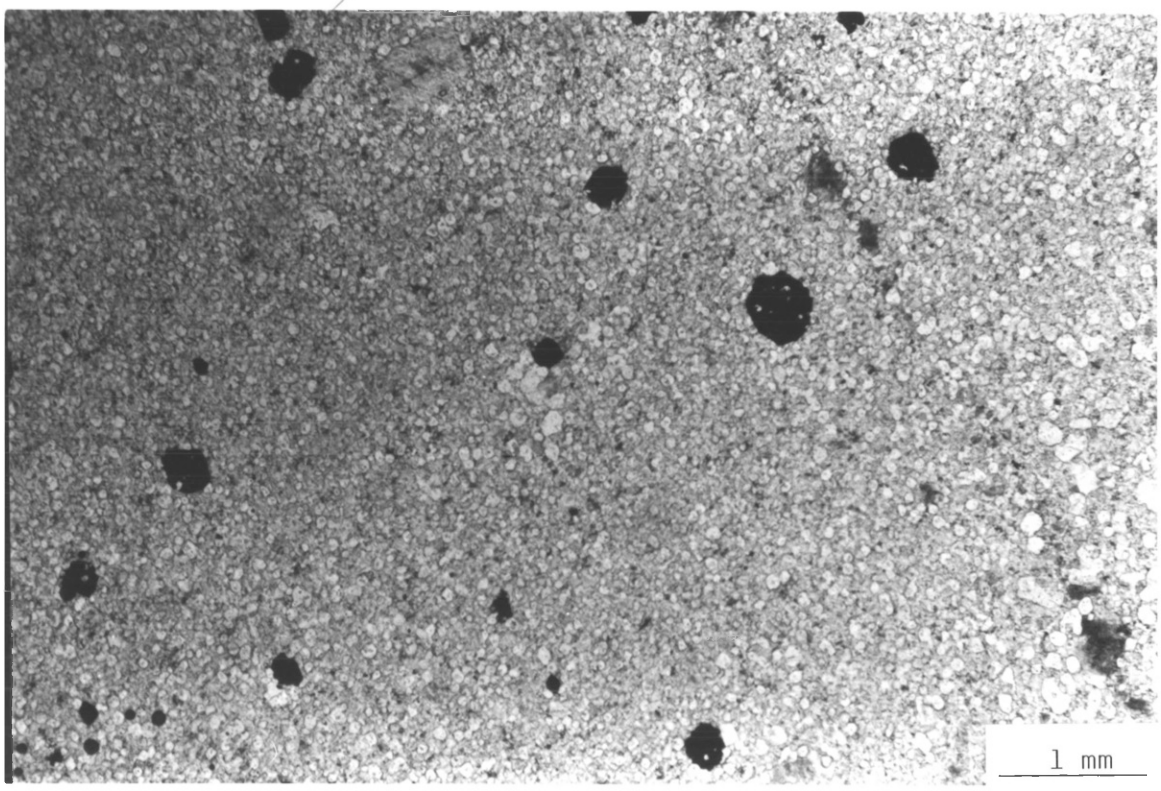

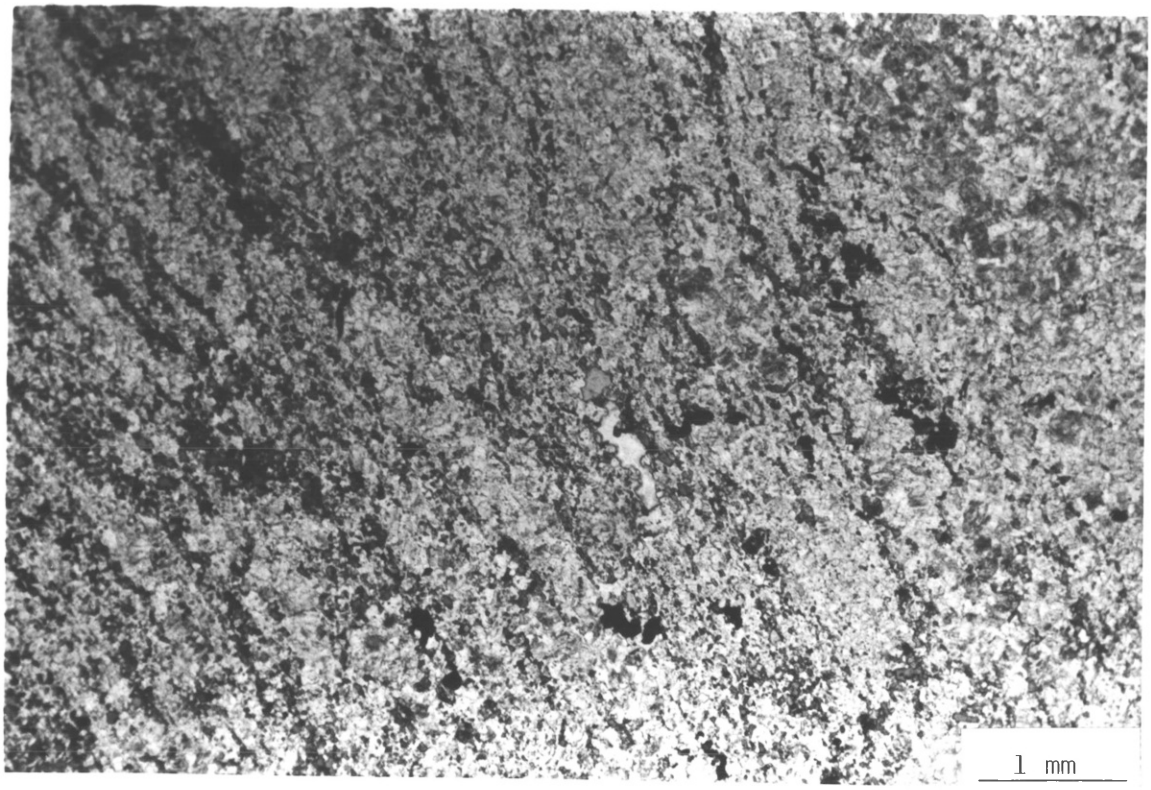

accompanied by secondary biotite.

3.3.7 Dyke rocks

Several contrasting types of dyke rock have been sampled from the Hurdal area. These include a dolerite dyke to the south of Nordgardshogda (sample N400; Figure 5.1), a monzodioritic dyke and a trachytic dyke from Steinbratebekken, intruding the Brennhaugen granite (samples W18A and W36A respectively), and a granitic dyke from the Hegga river locality (sample HA4D). The latter is of particular interest because it intrudes manganese deposits in the area (Section 4.3.3).

3.4 Intrusive relationships

Monzonitic rocks belonging to the kjelsasite rock group appear to be the oldest intrusive rocks in the igneous complex. Volcanic rocks in the Svartjern, Styggberget and Rustad areas are probably of a similar age. It is not certain whether the monzonites are genetically related to the younger syenites and granites in the area, or whether they represent the products of an earlier intrusive episode. Ihlen and Rasmussen (1981) have reported a transitional nature for the contact between the biotite syenite and the monzonites in this part of the Region.

Biotite syenite intrudes compositionally similar volcanic rocks in the Nordgardshogda - Styggberget area. However, an exact contact has not been observed due to convergence of lithological facies. The biotite syenite becomes increasingly finer grained and more porphyritic towards the contact. In contrast, the trachytes become, if anything, coarser grained due to thermal metamorphism in the aureole of the biotite syenite.

The contact between the alkali feldspar syenite and biotite syenite has not been observed, but is believed to be of a

transitional nature. A possible transitional contact is also conjectured for the alkali feldspar syenite and quartz syenite along Vekensbekken.

The quartz syenite shows sharp, cross-cutting intrusive relationships with both biotite syenite and extrusive rocks in the Nordgardshogda - Styggberget area (Figure 3.3), and with alkali feldspar syenite and extrusive rocks in the Rustad and Kongen areas. The biotite syenite and extrusive rocks in the Nordgardshogda - Styggberget area are intruded by the quartz syenite in an irregular, three-dimensional network of dykes and veins. In the case of the biotite syenite, the intensity of quartz syenite veining decreases in a south-easterly direction, away from the contact. In the case of the extrusive rocks, however, the relationships are more complicated, the intensity of quartz syenite veining increasing outwards from a central, relatively unaffected zone, through a zone in which the intensity of veining is high, into an outer zone in which "blocks" and "lenses" of extrusive rocks exist as xenoliths "within a sea of quartz syenite". Small xenoliths of extrusive rocks and biotite syenite also occur as roof pendants enclosed within the main area of quartz syenite. These relationships are illustrated with reference to a series of schematic cross-sections in Figure 3.4.

The thickness of quartz syenite apophyses is highly variable, ranging from less than 1 cm up to several metres. The quartz syenite seldom shows any signs of quenching towards these contacts and the typical hypidiomorphic granular texture is retained. The quartz content, however, is extremely variable ranging up to as much as 50 percent. An increase in ferromagnesian mineral content towards the walls of the quartz syenite may also be observed, implying contamination in the wall-rock zone.

Alkali feldspar granite is observed to intrude quartz syenite

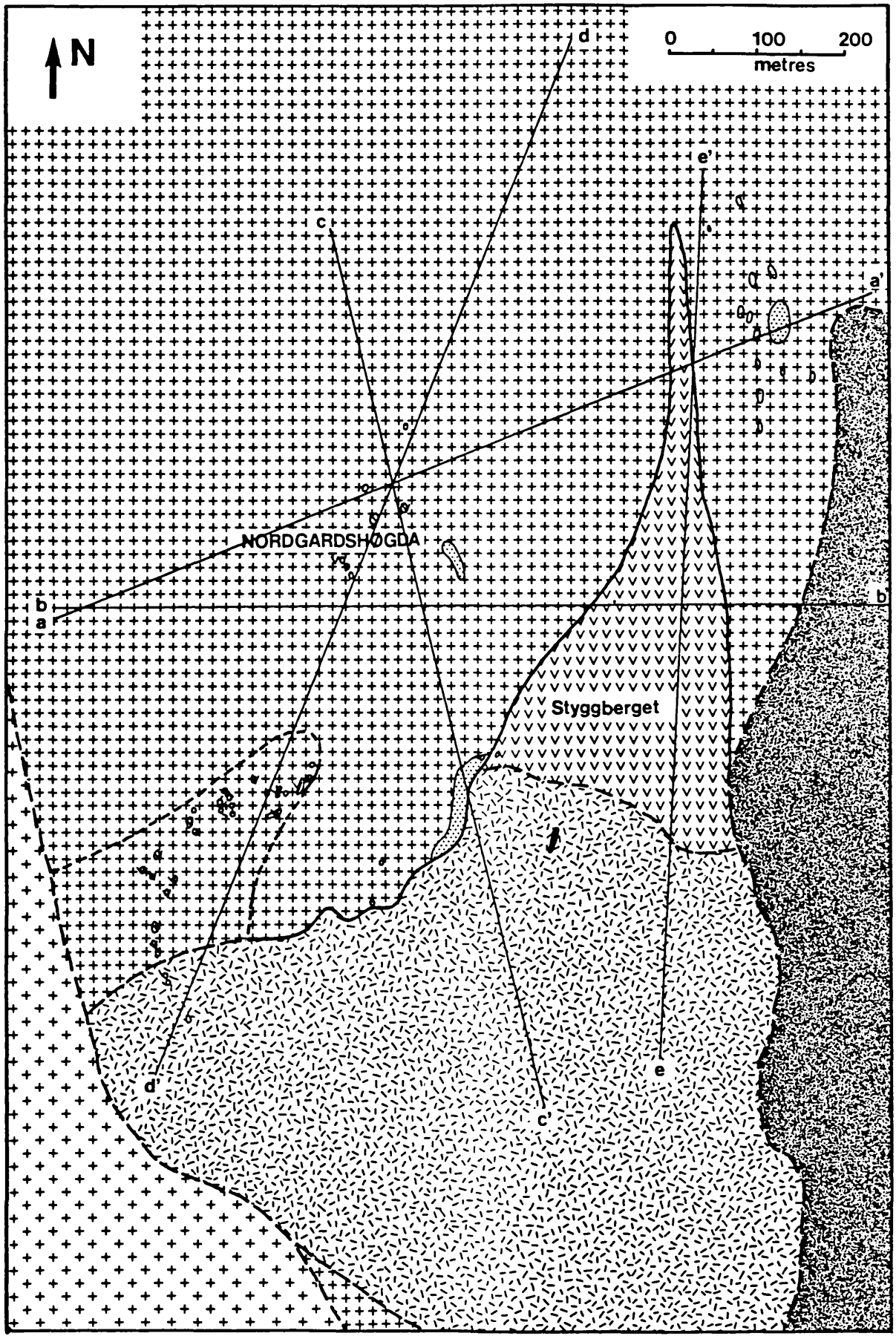

FIGURE 3.3. Geological map of the Nordgarshogda - Styggberget area. Symbols as in Figure 3.4.

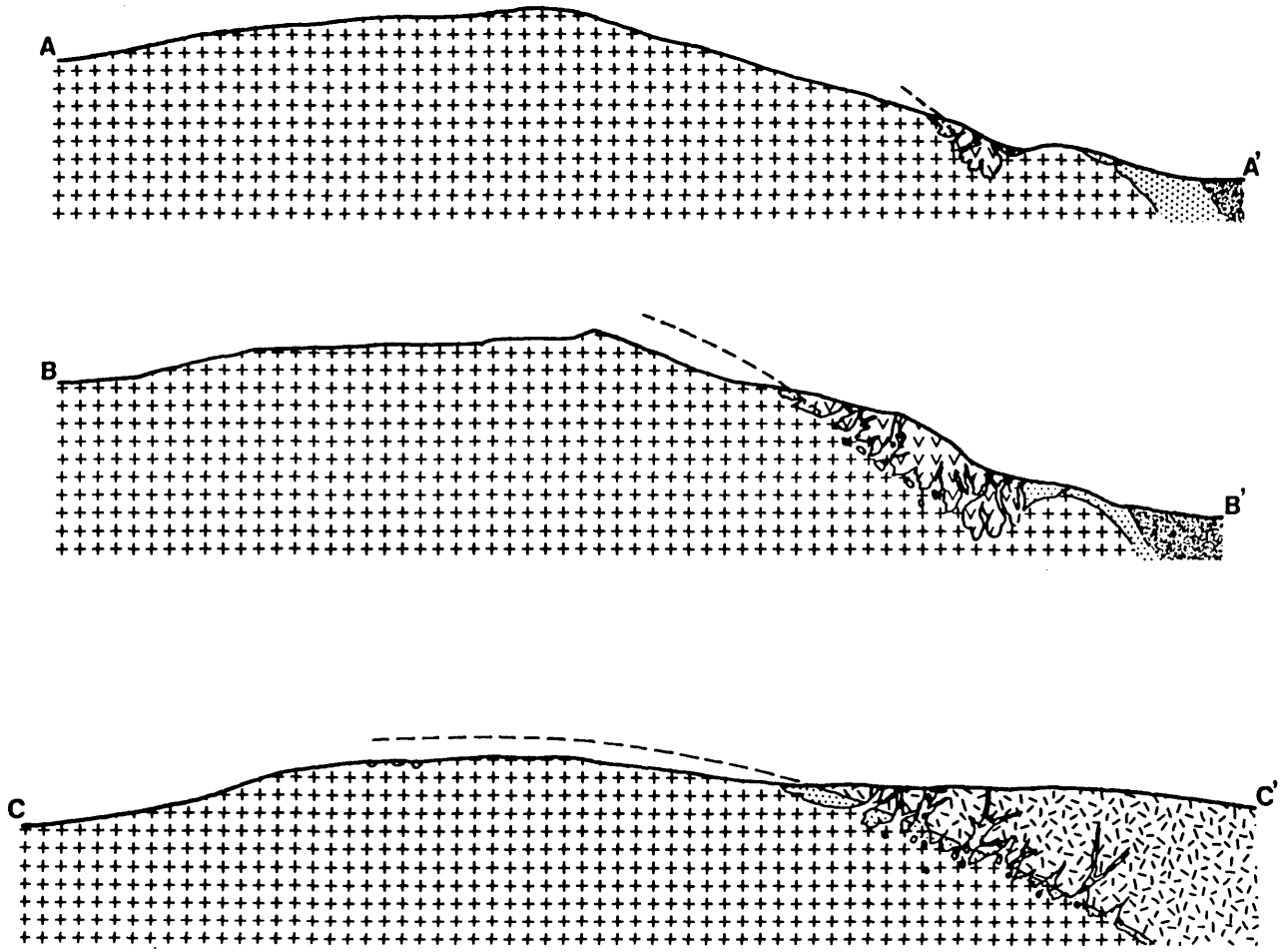

FIGURE 3.4. A series of schematic cross-sections across the Nordgardshogda - Styggberget area. Cross-sections A to E are marked on the geological map in Figure 3.3.

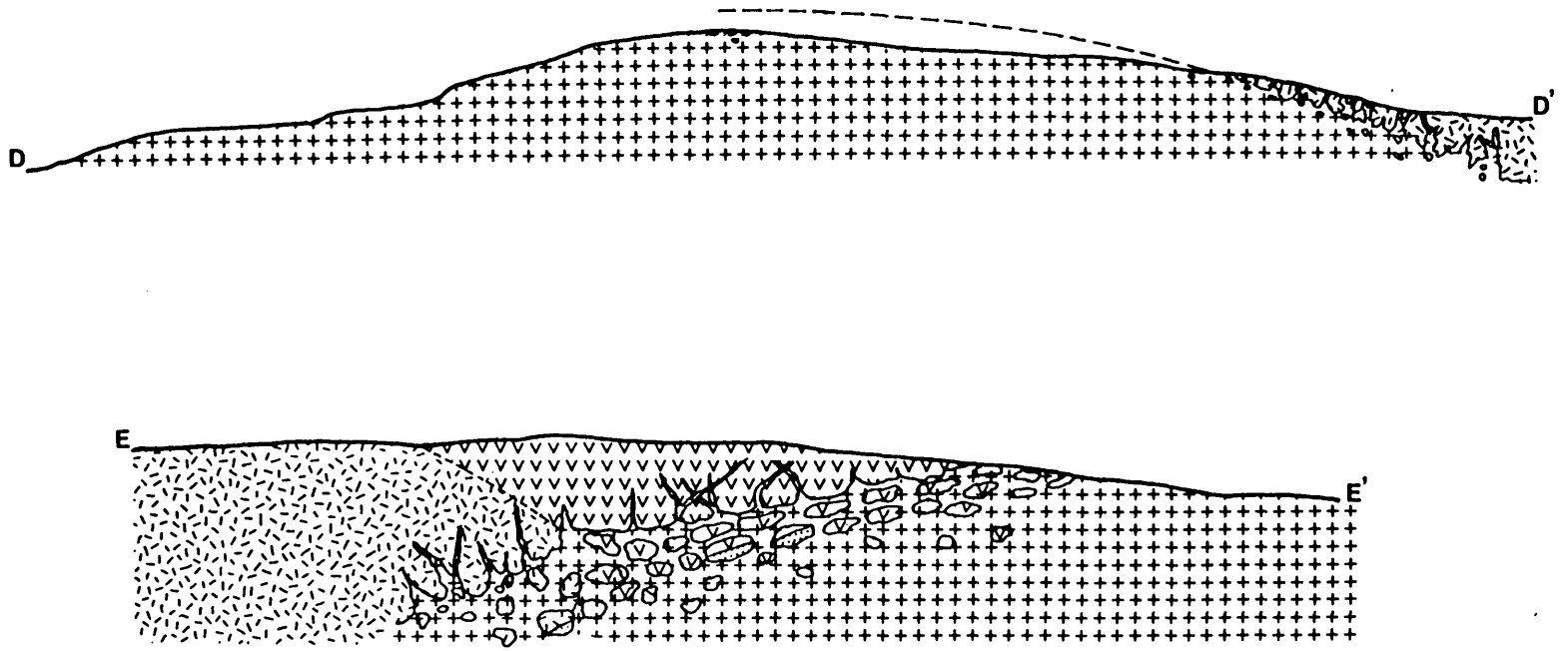

KEY:

- EXTRUSIVES
- BIOTITE SYENITE
- ALKALI FELDSPAR SYENITE
- UNEVEN MICROGRANITE
- QUARTZ SYENITE
- ALKALI FELDSPAR GRANITE

along Rudsetraveien, and both quartz syenite and alkali feldspar syenite at the Hegga river locality. The contact between the Brennhaugen granite and the quartz syenite may be observed over several hundred metres in the vicinity of Rudsetraveien. The contact is sharp and irregular, the quartz syenite appearing to have been brecciated by the granite (see Figure 7.2). No quenching of the granite has been observed. At the Hegga river locality, however, small pockets of quenched granite, up to several metres in diametre, are common.

Dyke rocks, where present, generally show sharp, cross-cutting intrusive relationships with clear signs of quenching. Their lateral extent, however, is usually fairly limited (20 to 30 metres maximum).

3.5 Petrogenetic considerations

The plutonic igneous rocks and associated volcanic rocks in the Hurdal area evidently belong to a single cogenetic series in which late stage granitic intrusions show a close spatial and temporal relationship to earlier formed intrusions of intermediate composition. The principal plutonic rock-types: Biotite syenite, alkali feldspar syenite, quartz syenite and alkali feldspar granite define a single differentiation series in which separation of plagioclase was accompanied and later superceded by fractionation of alkali feldspar. As such it would appear to belong to, or closely parallel, the main plutonic igneous rock series, kjelsasite - larvikite - nordmarkite - ekerite, as defined by Barth (1944; 1954; Section 2.5). The extrusive rocks (mainly trachytes; Section 3.3.6) would also appear to belong to the same differentiation series, being comagmatic with their compositionally similar plutonic equivalents.

The mechanism by which fractionation has occurred is however subject to considerable doubt. Intermediate to granitic

magmas such as those exposed in the Hurdal area may have evolved directly from more mafic precursors by processes of fractional crystallisation, either in large crustal magma chambers or by incremental crystallisation on rising buoyantly through the crust. Alternatively, they may have been derived by progressive partial melting of compositionally similar rocks already emplaced in the crust (Section 2.5.3). The last possibility of course implies considerable temperature gradients (>2 HFU; Ramberg 1976).

Crucial to this problem is the position in the genetic sequence of the monzodiorites and related rocks which, as stated previously (Section 3.4), is uncertain. The monzodiorites (kjelsasites) provide the logical connection between the more mafic rocks, alkali basaltic and tholeiitic lines of evolution (Section 2.5.1), and the main plutonic series. The question is whether they represent the parental magmas for fractional crystallisation, or the source rocks within which partial melting took place.

Mineralogically and texturally the monzodiorites are very distinct, consisting of discrete aggregates of clinopyroxene, biotite, hornblende, apatite and magnetite randomly distributed within a groundmass of plagioclase and alkali feldspar (Section 3.3.1). The occurrence of biotite around the margins of clinopyroxene grains is unusual, probably resulting from interaction between the pyroxene grains and adjacent K-feldspar. This may have occurred at sub-solidus temperatures, during exsolution of alkali feldspar. The possibility also exists, however, that the ferromagnesian mineral aggregates represent xenocrysts (cf. Hatch et al. 1975, page 275). Such xenocrysts may be the relicts (restite) of partial melting processes (Section 2.5.3). Transitions from monzodiorite, through monzosyenite, into biotite syenite (Ihlen and Rasmussen 1981) might therefore reflect progressive separation of partial melt from refractory mineral phases in the source.

There are two main objections to the partial melting hypothesis: Firstly, the absence of migmatitic textures; and secondly the occurrence of late monzonitic dykes (Section 3.2). If separation of partial melt from restite mineral phases such as clinopyroxenes, amphiboles and biotites was the principal mechanism by which fractionation occurred, one might reasonably expect to see migmatitic textures similar to those described from other terrains (Mehnert 1968). The absence of preferred orientations of ferrogmanesian mineral aggregates within the monzodiorites is a major objection to the restite model. Secondly, the occurrence of late monzonitic dykes implies the prolonged presence of reservoirs of intermediate magma throughout the period of felsic magmatism. This strongly supports the liquid line of descent, namely through fractional crystallisation.

Fractional crystallisation of intermediate magmas is therefore the most likely mechanism by which fractionation occurred. Likewise, the intermediate magmas were probably derived from more mafic precursors by similar processes, albeit under different conditions of pressure (depth), temperature and volatile activity. This contradicts one of the major conclusions drawn by Barth (1944), namely that the felsic rocks of the Oslo Region could not have been consanguineous with the mafic rocks.

Additional evidence which supports the liquid line of descent is provided by the extensive quartz syenite veining in the Nordgardshogda - Styggberget and Kongen areas. The widespread occurrence of extremely narrow quartz syenite veins (<1 cm; Section 3.4) implies a low viscosity for the quartz syenite in these areas. This suggests that the quartz syenite crystallised from a magma which was more or less entirely molten, probably with a high content of dissolved volatiles.

The form of the quartz syenite intrusion in the

Nordgardshogda - Styggberget area also provides important information concerning the mechanisms of emplacement. The main quartz syenite intrusion may be interpreted as a dome-shaped pluton, dipping away radially at a shallow angle (15 to 20°) beneath both the extrusive rocks to the east, and the biotite syenite to the south (cross-sections A to E, Figure 3.4). Apophyses of quartz syenite arise from this main pluton, cutting the extrusive rocks and biotite syenite in an irregular, three-dimensional network of dykes and veins (as described in Section 3.4).

Arching and subsequent fracturing and dilation of the wall-rocks probably occurred largely in response to magmatic pressures. Whilst initial failure may have been caused by a combination of magmatic and fluid pressures in the apical zone of the intrusion, the absence of significant hydrothermal alteration halos to the quartz syenite veins suggests that magmatic pressures were dominant. Magmatic updoming may have arisen as a result of one or several processes (see for comparison the discussion on resurgent doming in Smith and Bailey 1968). These include: (i) Continuous uprise of magma and build-up of magma pressure, if the magma chamber was being fed directly from below; (ii) convective overturn within the magma chamber; and (iii) re-attainment of isostatic equilibrium between the magma and the wall-rocks subsequent to removal of magma from the chamber, either to a higher level within the crust, or to the surface. Of these processes, (i) is most likely to have been responsible for magmatic updoming in the Nordgardshogda - Styggberget area. The effects of convection within a magma chamber are subject to conjecture; and there is no evidence that the quartz syenite has vented to the surface in the Hurdal area.

Intrusive relationships in the Brennhaugen area also indicate a forceful mechanism of emplacement, the alkali feldspar granite having brecciated the quartz syenite in a very

dynamic manner (Section 3.4). The existence, however, of several large areas of volcanic rock without any apparent basement indicates that the predominant mechanism of emplacement had to be by piecemeal stoping.

3.5.1 Mineralogical aspects of evolution

All the igneous rocks in the Hurdal area are composed essentially of alkali feldspar and quartz in variable proportions, with subordinate amounts of plagioclase and ferromagnesian minerals (Section 3.3). Alkali feldspar is always perthitic, showing well developed exsolution textures. Braided to patchy microperthitic textures, consisting of alternating domains of albite and orthoclase, are characteristic of all the plutonic rocks, the degree of coarsening of perthite texture and irregularity of grain boundaries increasing from syenite to granite.

Average feldspar compositions lie in the range Ab_{63} to Ab_{50} (Figure 3.5), clustering to the potassium rich side of the minimum in the pseudobinary system $NaAlSi_3O_8$ - $KAlSi_3O_8$ (Tuttle and Bowen 1958). They also have similar Na/Na+K ratios to their parent rocks (Table 5.1, Figure 5.7a). Whilst the average composition of alkali feldspar remains relatively constant during evolution, the compositions of albite and orthoclase domains become progressively more sodic and potassic respectively, and the calcium content decreases to a minimum. These changes partly reflect exsolution at lower temperatures on the alkali feldspar solvus, but are also the result of increased mobility of magmatic fluids at sub-solidus temperatures (see Parsons 1978). Increased mobility of magmatic fluids would also appear to be responsible for the increasing degree of heterogeneity of perthite textures described previously. The presence of numerous microscopic fluid inclusions within the orthoclase domains of the alkali feldspar granite (Section 3.3.5) supports this contention.

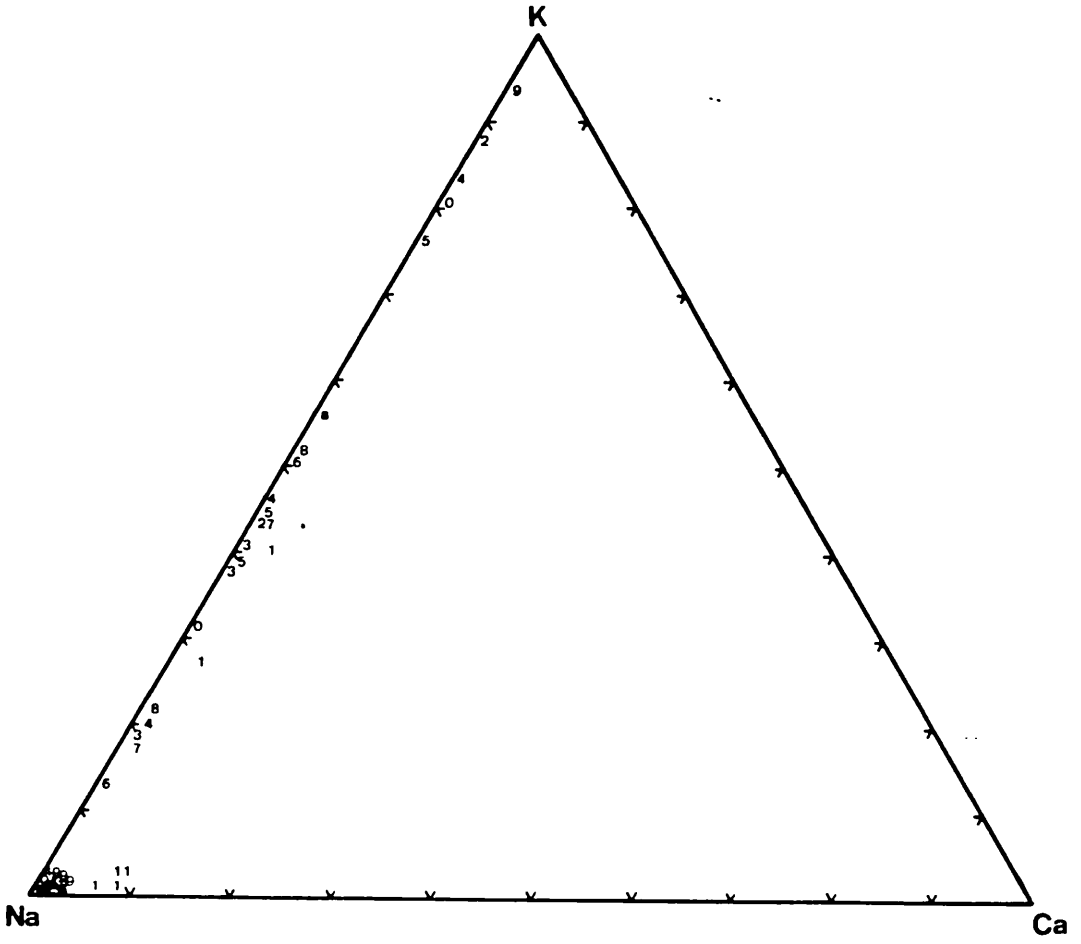

FIGURE 3.5. Compositions of feldspars, determined by EPMA (cation %). Symbols: 1 = N164, Biotite syenite; 2 = W74, Alkali feldspar syenite; 3 = N7, 4 = N1Ø, 5 = N6ØA, 6 = N63, 7 = K13, Quartz syenite; 8 = WW14, 9 = W412, Ø = W52, a = W58, Alkali feldspar granite.

One of the most striking features in the Hurdal area is the difference in texture between the quartz syenite and the alkali feldspar granite (Sections 3.3.4 and 3.3.5, respectively). One possible reason for this is that crystallisation of quartz in the quartz syenite was restricted to late stage, interstitial positions. This would enable unimpeded growth of alkali feldspar grains and the development of euhedral crystal forms. In contrast, crystallisation of quartz in the alkali feldspar granite commenced on or close to the liquidus, resulting in impeded crystal growth and the development of xenomorphic crystal intergrowths. The growth rates and nucleation densities of alkali feldspar and quartz in this latter case must have been fairly similar (Swanson 1977).

The position of quartz in the crystallisation sequence is not, however, the only factor responsible for the difference in textures. This is indicated by the fact that apophyses of quartz syenite, containing up to 50 % quartz (Section 3.4), retain the hypidiomorphic granular texture. Following the argument presented above, such rocks should crystallise quartz at liquidus temperatures (Figure 5.2a), resulting in impeded growth of alkali feldspar and the development of xenomorphic textures. The fact that the textures do not show this indicates that the growth rates and/or nucleation densities of alkali feldspar and quartz must have been different. A factor of 10 difference between the growth rates of alkali feldspar and quartz, as predicted by Swanson (1977), would result in hypidiomorphic intergrowths. Growth rates tend to be greater in systems which are saturated with respect to H_2O. Thus, the presence in the alkali feldspar granite of CO_2-bearing, aqueous fluids of magmatic origin (as indicated by fluid inclusion studies; Chapter 7) may have been responsible for increased growth rates of quartz, leading to the the development of xenomorphic granular intergrowths.

The plutonic rocks in the Hurdal area also show progressive changes in the nature and composition of ferromagnesian mineral phases, reflecting modifications to bulk-rock geochemistry and the fluid regime. Amphibole, where present, is always moderately sodic containing greater than approximately one Na^+ ion per formula unit (Table 3.3), and is usually zoned. The alkali feldspar syenite and quartz syenite contain edenite and silicic edenite respectively, showing progressive substitution of Si+Na+K for Ca+Al (Figure 3.6). In contrast, the quartz syenite from the Kongen area and the Brennhaugen granite contain arfvedsonite, with up to 3 Na+ ions per formula unit. It is no coincidence that these rocks also show greater degrees of alkali feldspar exsolution, reflecting increased mobility of Na at sub-solidus temperatures. The Kongen syenite, however, contains sodic pyroxene as well, indicating that it must have crystallised under different conditions of PH_2O and fO_2. Aegerine also tends to be zoned.

Two contrasting types of biotite are observed in the Hurdal area (Figure 3.7). The biotite syenite, alkali feldspar syenite and quartz syenite contain biotite of an unusually magnesium-rich composition, with up to 68 percent of the phlogopite end-member (Tabel 3.1). In comparison, the biotite in the alkali feldspar granite is extremely manganiferous, containing up to 1.6 Mn ions per formula unit. These differences partly reflect changes in composition of the parent rock, in particular a decrease in the total contents of Fe and Mg, but also build up of Mn in the residual fluids. In addition, a decline in the importance of ilmenite as an accessory phase permits Mn to be incorporated into the biotite structures.

The compositional variations of amphiboles, pyroxenes and biotites from the Hurdal area are illustrated with reference to an Al-(Na+K)-Ca variation diagram in Figure 3.8. This

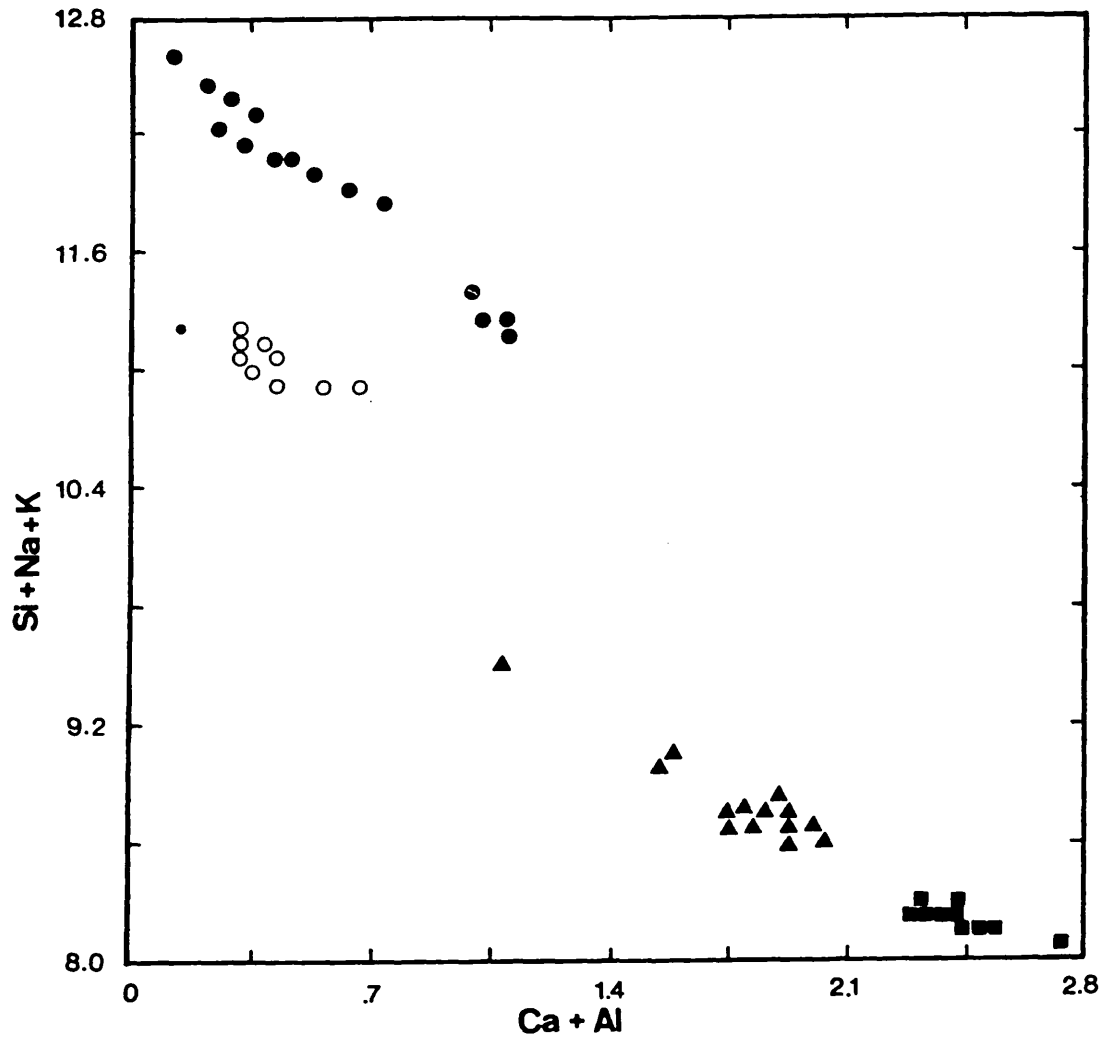

FIGURE 3.6. Compositions of amphiboles, determined by EPMA (on the basis of 23 oxygens per formula unit). Symbols: ■ = W74, Alkali feldspar syenite; ▲ = N63, ● = K13, Quartz syenite; . = WW14, . = WW16, Alkali feldspar granite. Pyroxene analyses, o , from sample K13 are shown for comparison.

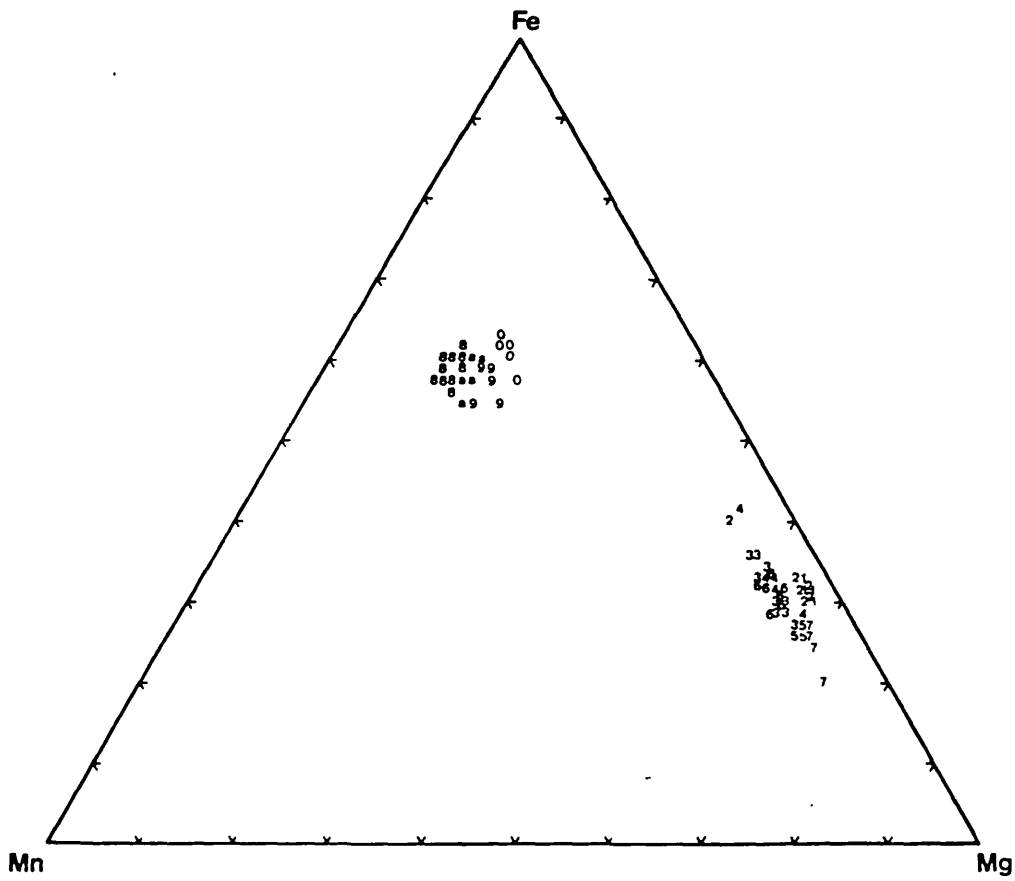

FIGURE 3.7. Compositions of biotites, determined by EPMA (cation %). Symbols: 1 = N164, 2 = N253,1, Biotite syenite; 3 = W74, Alkali feldspar syenite; 4 = N7, 5 = N1Ø, 6 = N6ØA, 7 = N63, Quartz syenite; 8 = W58, 9 = W52, Ø = W412, a = WW16, Alkali feldspar granite.

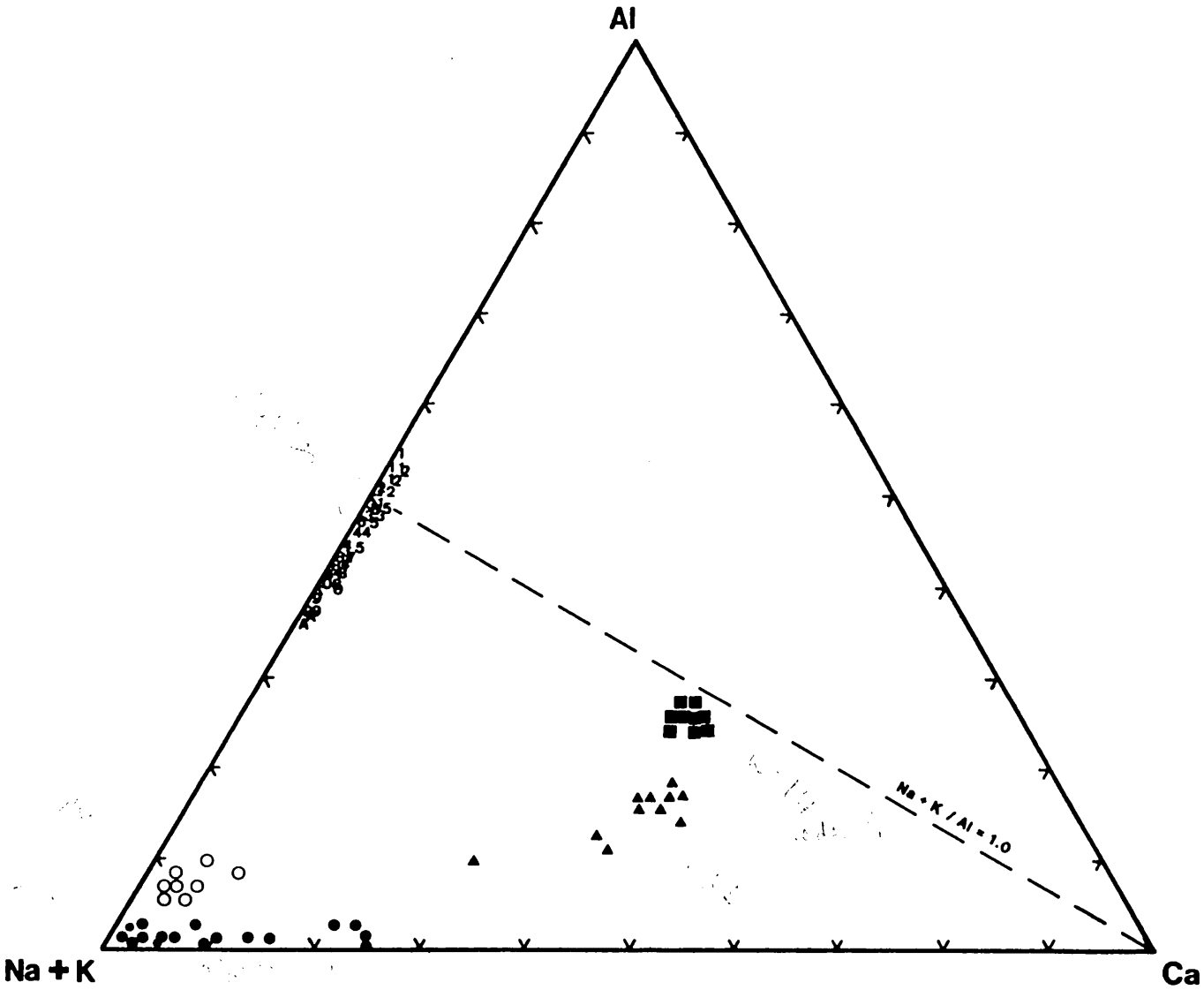

FIGURE 3.8. Al-(Na+K)-Ca variation diagram (cation %), amphiboles, pyroxenes, and biotites, Hurdal area. Symbols as in Figures 3.6 and 3.7.

diagram illustrates the influence of whole-rock geochemistry upon the compositions of ferromagnesian minerals (see for comparison Figure 5.1Ø). Presence of alkalies, in particular Na, in excess of aluminium in the parent rock is reflected by the increasing ratio of Na+K/Al in the amphibole compositions. Comparison with Figure 5.1Ø indicates that the Na+K/Al ratios of the biotites are also very strongly influenced by bulk rock geochemistry, in spite of the fact that the Na/Na+K ratios are quite different. This suggests that the agpaitic index is a very sensitive indicator of peralkalinity in these rocks.

Finally, chemical analyses of amphiboles and biotites carried out by Tronnes (1982) indicate that these minerals contain significant amounts of fluorine (up to 1.3 F ions and 2.4 F ions per respective formula units). This is reflected in the whole-rock geochemistry by a decrease in the ratio of OH^- to F, which is at a minimum in the biotite syenite and alkali feldspar granite (Table 5.1), indicating the importance of the role played by F in the magmatic evolution of these rocks. Presence of F in the magma increases the activity of SiO_2 in the melt, and is reflected in the subsequent mineralogy by a trend towards progressively more siliceous compositions of amphiboles and biotites (Section 5.5.1; Kogarko and Krigman 1973).

CHAPTER4

MINERALISATION AND ALTERATION

4.1 Introduction

Mineral deposits of both vein and disseminated type are observed in close association with several of the plutonic igneous rock-types in the Hurdal area, most notably within the biotite syenite, quartz syenite and alkali feldspar granite. These deposits consist of sulphides of Fe, Zn, Mo and to a lesser extent Pb, together with certain rare Mn-silicate phases, locally in high concentrations. In addition, quartz and fluorite are important gangue minerals. The ore-deposits are of limited lateral and vertical extent and are of sub-economic importance. Their close spatial and temporal relationship to observed igneous rocks in the area is indicative of a close genetic relationship between mineralisation and magmatic evolution within the rift.

4.2 Metallogenic aspects of rifting

Mineral deposits in the Oslo Graben may be divided into two categories (Ihlen and Vokes 1978a): Those occurring within or closely associated with the magmatic products in the rift; and those occurring within the surrounding lower palaeozoic and Precambrian rocks. Only deposits belonging to the first category will be considered here. These include oxide deposits of Fe, Mn, Ti and W and sulphide deposits of Fe, Zn, Pb, Cu and Mo. They are usually of sub-economic importance.

Mineral deposits related to the magmatic products in the rift include (Ihlen and Vokes 1978a): I. Orthomagmatic segregation deposits; II. Intra- and peri-magmatic vein and disseminated deposits; III. Porphyry-type stockwork deposits; and IV. Contact metasomatic deposits.

I. Deposits originating through processes of differentiation

and segregation within magmas are not all that common within the rift (Ihlen and Vokes 1978a). They include a P - Ti - Fe bearing "jacupirangitic" body within the larvikite massif as Kodal; and magnetite - ilmenite bearing pyroxenite bodies within the volcanic necks. Disseminated molybdenite occurring within some of the more evolved syenitic and granitic rocks would also appear to be closely linked to the magmatic stage of crystallisation. This is indicated by its mode of dissemination in the igneous fabric, and by the lack of any appreciable hydrothermal alteration (Geyti and Schonwandt 1979; this study).

II. Vein deposits including sulphides of Mo, Fe, Cu, Pb and Zn have been observed in association with most of the plutonic rock-types in the Region (Ihlen and Vokes 1978a). They are particularly common, however, in association with the more granitic end-members, the biotite granites and alkali feldspar granites.

Molybdenite mineralisation in the Oslo Region is commonly found inside the apical contact zones of granitic plutons, for instance within the Drammen Granite complex (Ihlen et al. 1982). Molybdenite mineralisation is often associated with the later, finer-grained and most highly evolved granitic facies. Quartz veins containing molybdenite $\pm$ pyrite $\pm$ fluorite and "dry" (quartz free) molybdenite $\pm$ K-feldspar veins tend to show a strong dependence upon tectonic lineaments and are associated with only minor wall-rock alteration, mainly silicification. Early quartz + pyrite $\pm$ sphalerite $\pm$ topaz veins in the Drammen area, however, tend to have well developed sericite + chlorite alteration envelopes. Molybdenite may also occur in disseminated form, but this is not ubiquitous.

III. Stockwork molybdenum deposits with a number of similarities to the Climax-type porphyry molybdenum deposit (Wallace et al. 1968, Clark 1972, Woodcock and Hollister

1978, Mutschler et al. 1981) have been reported from several localities within the Region. Most notable amongst these occurrences are the Bordvika deposit within the Glitrevann Cauldron (Geyti and Schonwandt 1979; Ihlen and Vokes 1978b), the Skrukkeli deposit on the north-western margin of the Graben (Olerud and Sandstad 1984), and the Nordli deposit to the north of Hurdal.

As in the case of the vein systems discussed above, molybdenite mineralisation is more or less confined to the later, finer grained, and often porphyritic, facies of granitic stocks, of which there are usually several. Stockwork vein systems containing molybdenite $\pm$ quartz $\pm$ K-feldspar $\pm$ pyrite typify these deposits, and are often associated with alteration-mineralisation zonation patterns comparable to those observed within "typical" porphyry deposits (Lowell and Guilbert 1970). An inner zone of weakly developed potassic alteration passes out into a zone of more pervasive quartz-sericite alteration. The latter is generally surrounded by an outer zone of propylitic alteration (chlorite $\pm$ calcite $\pm$ epidote $\pm$ fluorite).

IV. Contact metasomatic deposits in the Oslo Region include both endo- and exo- contact varieties. Examples of endo-contact metasomatic deposits are not that common, but probably include certain Mn $\pm$ Zn $\pm$ (Pb) deposits found in association with alkaline granitic rocks in the Hurdal and Drammen areas (Section 4.3; Ihlen and Vokes 1978a). Among the exo-contact metasomatic deposits, the skarn-hosted Fe + Cu + Zn + Pb + Bi $\pm$ W $\pm$ Mo deposits are most common. These are located within the contact aureoles of granitic bodies intruding into sedimentary rocks (usually limestones), for instance in the Drammen area (Ihlen et al. 1982) and along the north-eastern margin of the Oslo Region (Skreia area; Ihlen 1977, 1985). The predominant skarn minerals are grossular - andradite, diopside - hedenbergite, epidote - clinozoisite, amphibole and chlorite, associated with varying

amounts of vesuvianite and wollastonite (Ihlen and Vokes 1978a). The ore-minerals include magnetite, hematite, scheelite, sphalerite, galena, chalcopyrite, pyrite, bismuthinite and pyrrhotine, and occasionally molybdenite.

The formation of mineral deposits in the Oslo Graben was evidently very closely related to magmatic evolution within the rift. Thus, the majority of mineral deposits are found in association with the most highly evolved, silicic rocks; either in a vein-hosted, plutonic environment (types II and IV above) or in a stockwork-hosted subvolcanic environment (type III; cf. Geyti and Schonwandt 1979, Sillitoe 1973). The presence of orthomagmatic segregation deposits (type I above) indicates that in certain circumstances, magmatic processes alone may have been responsible for the concentration and precipitation of ore-metals. More commonly, however, preferential partitioning of ore-metals into a coexisting hydrothermal phase, in the presence of certain halide (Cl, F), carbonate and sulphate ions, is likely to have been responsible for ore-formation. The fact, however, that many of the ore-deposits are associated with only minor wall-rock alteration suggests that the volumes of fluid involved may have been relatively small. Only in the contact metasomatic deposits and the porphyry-type stockwork deposits are the volumes of fluid likely to have been large, due to influx of waters of connate or meteoric origin.

4.3 Mineralisation in the Hurdal area

Two distinct types of mineralisation have been observed in the Hurdal area, more or less restricted to specific stages of the magmatic evolution:

(I) Molybdenite $\pm$ pyrite $\pm$ sphalerite mineralisation with associated quartz $\pm$ muscovite $\pm$ fluorite alteration, related to the biotite syenite (trachyte) - quartz syenite stage of evolution. The most notable occurrence of this mineralisation

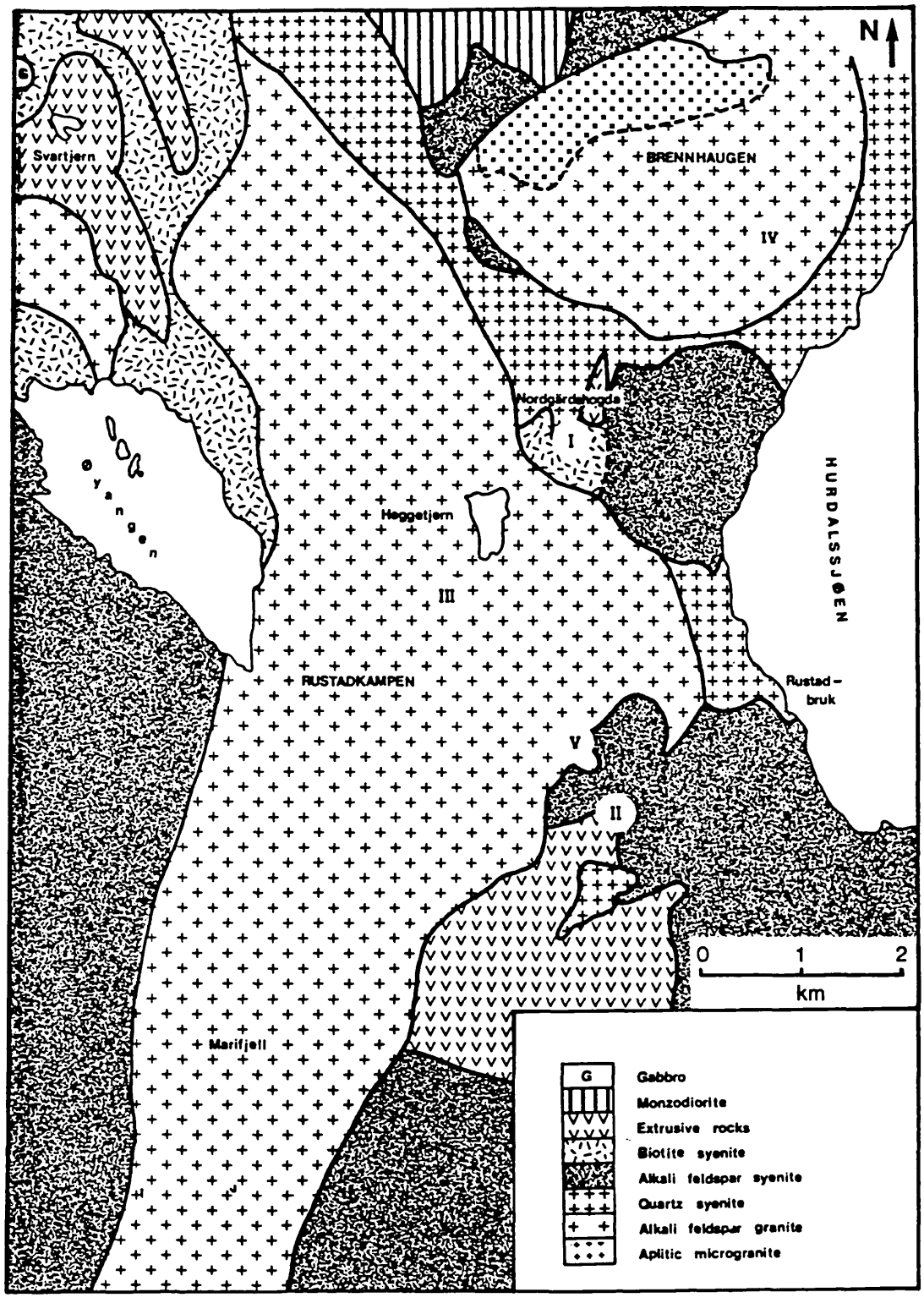

FIGURE 4.1. Geological map of the Hurdal area, showing the location of the main mineral deposits. I. Mo - Fe - Zn mineralisation in the Nordgardshogda - Styggberget area; II. Mo - Fe - Zn mineralisation in the Rustad area; III. Albite + Fe + Zn ± pyroxmangite mineralisation at Steinmyrveien; IV. Rhodonite + albite ± Zn mineralisation at Steinbratebekken; and V. Rhodonite + albite ± Zn mineralisation at the Hegga river locality.

- alteration assemblage is in the Nordgardshogda - Styggberget area (Section 4.3.1), although a minor occurrence has also been observed in the Rustad area (along Kongeliveien; Figure 4.1).

(II) Mn-silicate ± sphalerite ± pyrite ± galena mineralisation associated with albitised facies of alkali feldspar granite in the Brehnhaugen and Rustadkampen granite massifs. Manganese - Zn - (Fe) - (Pb) mineral deposits may be divided into two categories: (a) Disseminated pyrite ± galena ± sphalerite mineralisation associated with small pods, Ø.2 to 1.Ø m in dimension, of albitised alkali feldspar granite along Rudsetraveien (sample locality W58; Figure 7.2), and at Steinmyrveien (Section 4.3.2); and (b) Manganese - silicate + albite ± sphalerite mineralisation, occurring as large pods, 2 to 1Ø m in dimension, within the alkali feldspar granite, particularly in its contact zones; most notably at the intersection between Steinbratebekken and Rudsetraveien, and at the Hegga river locality (Figure 4.1; Section 4.3.3).

4.3.1 The Nordgardshogda - Styggberget area

Mineralisation and alteration in the Nordgardshogda - Styggberget area affect both the biotite syenite and extrusive rocks in the southern and eastern parts of the area, together with xenoliths of these rock-types within the quartz syenite (Figure 4.2). The quartz syenite itself shows little or no signs of mineralisation or alteration, except within its contact zones where apophyses of the quartz syenite may contain minor amounts of pyrite and/or molybdenite.

Mineralisation consists of pyrite and molybdenite in both vein and disseminated form, together with local concentrations of black sphalerite. The relationship between pyrite and molybdenite mineralisation is not certain. However, it is likely that a simple zonation exists. Whereas

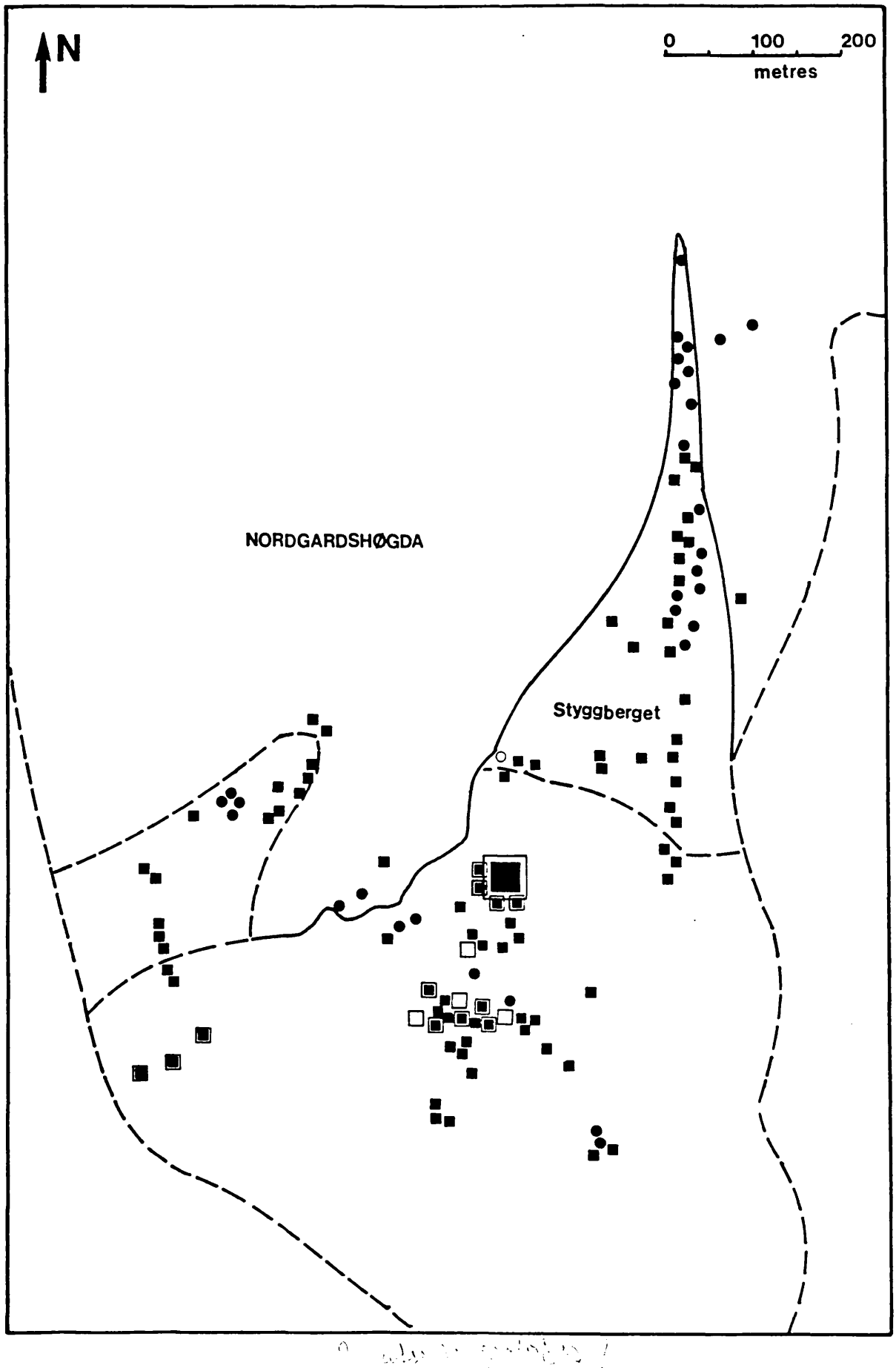

FIGURE 4.2. Geological map of the Nordgardshogda - Styggberget area, showing the distribution of pyrite, molybdenite and sphalerite. Symbols: ■ = pyrite veins; ● = disseminated pyrite; □ = molybdenite veins; ○ = disseminated molybdenite; ■ = sphalerite.

pyrite veining is apparent throughout most of the area, with the exception of the main body of quartz syenite, molybdenite has only been observed within the biotite syenite in the southern part of the area, and within apophyses of the quartz syenite to the south-west of Nordgardshogda. Pyrite and molybdenite may occur together within the same vein or separately. Pyrite is generally accompanied by quartz ± sericite. In comparison, molybdenite usually occurs along very fine veinlets, often accompanied by secondary biotite, and less commonly by quartz. No chalcopyrite has been observed within the mineralised area.

Sphalerite occurs together with both molybdenite and pyrite in association with the most pervasive quartz-sericite alteration in the southern part of the Nordgardshogda area (Figure 4.2). Located within the apical part of the biotite syenite intrusion, sphalerite mineralisation would appear to form the inner zone to mineral zonation in the area. Coarse-grained sphalerite (1 to 3 mm) may form as much as 60 to 80 percent of the rock, the remainder being made up mainly by quartz + fluorite ± muscovite ± biotite ± pyrite ± molybdenite.

Alteration is marked by a patchy development of the mineral assemblage: quartz ± muscovite ± fluorite (± pyrite). Fine- to medium-grained quartz-sericite alteration affects both the biotite syenite to the south of Nordgardshogda and the extrusive rocks in the highest levels of Styggberget. In addition, thin discontinuous veinlets, of 2 to 3 cm in width, consisting of coarse-grained (1 to 2 mm average) fluorite + quartz ± sericite ± pyrite have been observed within both rock-types, both in association with the strongest quartz-sericite alteration and within relatively unaltered rocks. These veinlets are believed to represent fissure - infills as opposed to alteration of the country rocks. There is no obvious zonation of alteration products.

The most extensive alteration is observed within the biotite syenite to the south of Nordgardshogda. This rock-type displays an extremely uneven development of the alteration assemblage, affecting both groundmass minerals and phenocrysts to variable extents. Progressive alteration is marked by the development of a fine- to medium-grained (<Ø.2 to Ø.6 mm) assemblage of quartz + muscovite + pyrite + fluorite ± biotite ± chlorite ± plagioclase. Replacement of the groundmass is followed by, and to a certain extent accompanied by, corrosion and breakdown of the feldspar phenocrysts. Alkali feldspar is first broken down in to aggregates of smaller grains (Ø.2 to Ø.4 mm) and then replaced by an intergrowth of quartz + muscovite. The aggregates of smaller feldspar grains are often clouded in appearance, either due to an extremely fine-grained sericitic alteration or due to numerous microscopic fluid inclusions (as in the case of the alkali feldspar granite; Section 3.3.5). Plagioclase phenocrysts, where present, are usually sericitised. The most intense alteration, however, is marked by a conspicuous absence of phenocrysts.

In contrast, the extrusive rocks in the Styggberget area show only local development of this alteration assemblage, with silicification predominating over sericitic alteration. Whilst the extrusive rocks have been subjected to extensive modifications, involving recrystallisation of groundmass minerals and corrosion of phenocrysts, the primary igneous foliation and compositional layering are retained (Figure 3.2k). It is therefore likely that recrystallisation of quartz and the generation of secondary biotite within these rocks were the result of essentially isochemical processes, due to breakdown of K-feldspar and magnetite during contact metamorphism. The widespread presence of disseminated pyrite within these rocks, in many places replacing magnetite, is attributed to a separate (? later) sulphidation event.

Finally, a number of thin, microcrystalline quartz veins have

been observed within the quartz syenite on top of Nordgardshogda, and to a lesser extent within the extrusive rocks to the east of this area (Figure 4.2). These veins have a prominent east-west trend (100°) and, particularly on the top of Nordgardshogda, occur in sets of sub-parallel veins (from less than 1 mm up to 1 cm in thickness) with an average spacing between veins of 1 to 1.5 metres. A red colour is often imparted to these veins, presumably by hematite. However, no ore-minerals have been observed.

4.3.1.1 Discussion

Intrusive relationships in the Nordgardshogda - Styggberget area (Section 3.4, Figure 4.2) indicate very clearly that the bulk of mineralisation and alteration occurred prior to the intrusion of the quartz syenite, since the latter cuts right across the observed mineralisation - alteration pattern. The fact, however, that apophyses of the quartz syenite may contain minor amounts of pyrite and/or molybdenite (above) indicates that a weak mineralisation event may be attributed to the intrusion of the quartz syenite. Thermal metamorphism of extrusive rocks in the Styggberget area is directly attributable to the intrusion of the biotite syenite, although subsequent intrusion of the quartz syenite may have provided a metamorphic overprint. Gradual variations in grain-size and texture across the contact between the biotite syenite and extrusive rocks (Section 3.4) are believed to be indicative of uniformly high temperatures across the contact.

The main mineralisation event in the Nordgardshogda area may therefore be attributed to the period immediately post-dating biotite syenite intrusion and preceding quartz syenite intrusion. Sulphidation of extrusive rocks in the Styggberget area probably occurred during the same period. It is not certain, however, whether mineralisation was related directly to the intrusion of the biotite syenite or to some later, hydrothermal event. In theory, development of a hydrothermal

convection cell in the period immediately preceding quartz syenite intrusion might have been responsible for the observed zonation of mineral deposits in the area. However, the absence of a similar zonation of hydrothermal alteration products (there is no evidence of potassic or propylitic alteration), and the preference for silicification and simple recrystallisation over sericitic alteration suggest that this was not the case. The observed mineral zonation and the apical position of mineral deposits with respect to the biotite syenite intrusion are, however, compatible with an origin by closed-system fractionation of the biotite syenite magma. Migration of volatile components and complexes incorporating metallic elements to the apical zone of the intrusion may have lead to the formation of a Zn-Mo-Fe-S enriched residual melt fraction. Deposition of ore-minerals from the residual melt fraction or from a coexisting fluid phase may therefore have lead to the observed sequence of ore-deposits in the area. The widespread presence of fluorite within these rocks suggests that F-rich fluids may have been responsible.

In conclusion, the geological history of the rocks at present exposed within the Nordgardshogda - Styggberget area may be summarised as follows (Figure 4.3):

(I) Extrusion of a series of trachytes and minor trachyandesites, presumably as a succesion of lavas and/or pyroclastic flows upon a sub-surface which is nowhere exposed.

(II) Intrusion of the biotite syenite into the extrusive rocks.

(III) Thermal metamorphism of the extrusive rocks combined with closed-system fractionation of the biotite syenite magma leading to the formation of a Zn-Mo-Fe-S and F enriched residual melt fraction leading to ore-deposition.

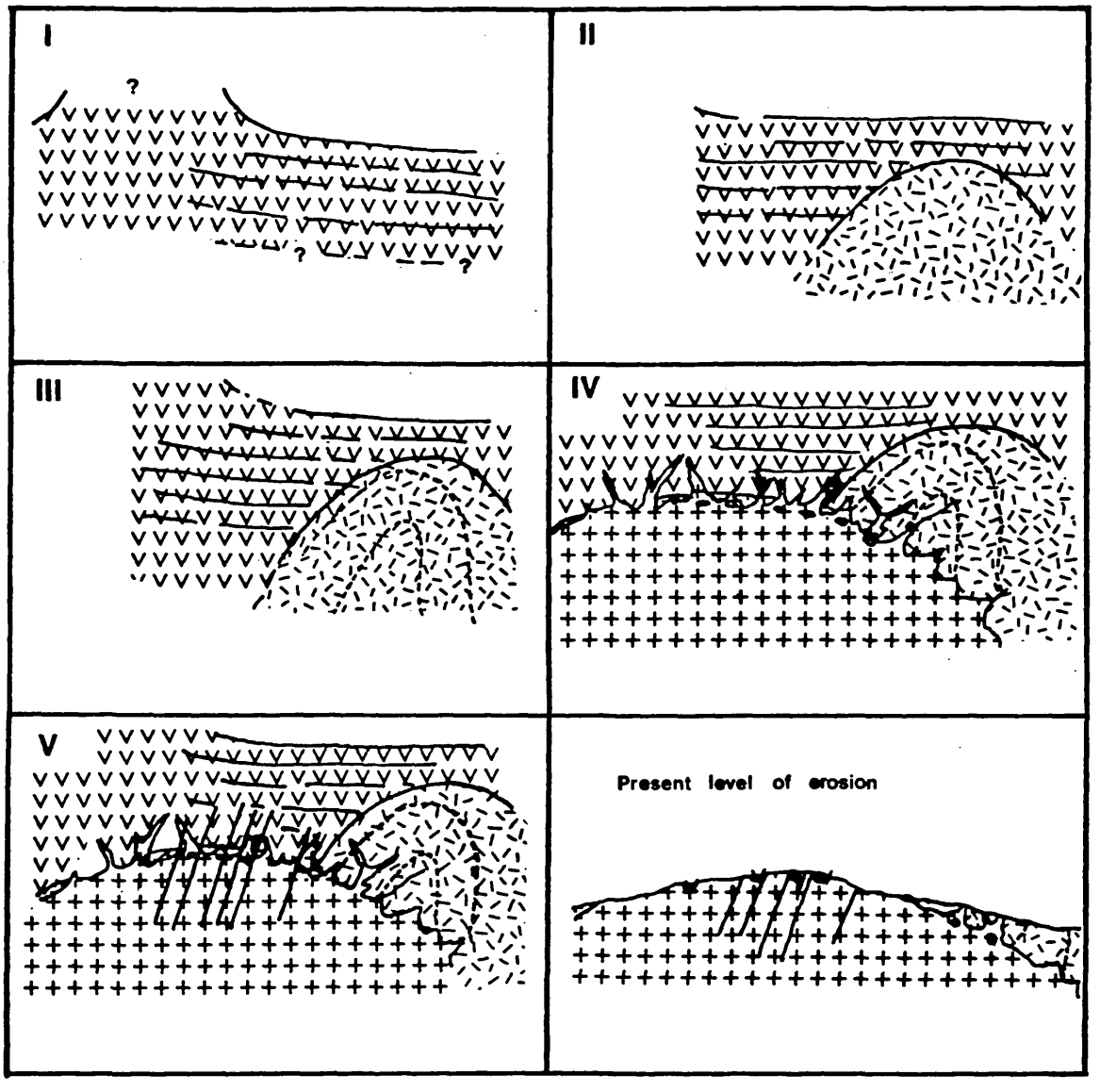

FIGURE 4.3. Series of schematic cross-sections to illustrate the sequence of events in the evolution of the Nordgardshogda - Styggberget area: I. Extrusion of a series of trachytes; II. Intrusion of the biotite syenite; III. Closed system differentiation of the biotite syenite magma + thermal metamorphism of the wall-rocks; IV. Intrusion of the quartz syenite; and V. Development of a series of roughly parallel, E-W trending, barren quartz veins (see text for discussion).

(IV) Intrusion of the quartz syenite pluton, accompanied by fracturing and brecciation of the wall-rocks (biotite syenite and extrusives) and development of a network of quartz syenite dykes and veins (Section 3.5). A weak mineralising episode was related to this event.

(V) Development of a series of sub-parallel, roughly east-west trending, microcrystalline, barren quartz veins mainly within the quartz syenite intrusion, but also within the extrusive rocks to the east of Nordgardshogda.

Finally, a dolerite dyke is observed to cut the biotite syenite to the south of Nordgardshogda (sample locality N4ØØ, Figure 5.1). This is believed to belong to a series of late dykes in the area.

4.3.2 Steinmyrveien

The Steinmyrveien area is situated immediately to the south-west of Heggetjern in the central part of the Rustadkampen granite massif (Figure 4.1). It therefore comprises rocks in the compositional field of alkali feldspar granite. However, poor exposure in the area restricts the outcrop to a number of small exposures along a 5ØØ m section of the road and to one outcrop on the adjacent Jeppedalsveien.

The alkali feldspar granite in the vicinity of Steinmyrveien displays considerable variation in terms of both grainsize and texture, superimposed upon which are the affects of minor mineralisation and alteration. Medium to coarse-grained (Ø.5 to 3 mm), moderately inequigranular varieties of alkali feldspar granite, displaying the typical xenomorphic granular texture (Section 3.3.5), are accompanied by finer-grained (Ø.5 mm), aphyric to weakly porphyritic varieties of granite. Phenocrysts, where present are of quartz, and the

ferromagnesian mineral content is low (much less than 1% by volume).

Extensive exsolution of alkali feldspar within the granite has lead to the widespread development of bleaching (Section 3.2). In addition, two distinct types of alteration are observed; (i) Fine-grained (< Ø.2 mm) silicification with associated pyrite ± molybdenite mineralisation; and (ii) Albitisation of the granite, occurring as small pods (Ø.2 to 1.Ø m) of albite ± quartz ± pyroxmangite, with associated pyrite ± galena ± sphalerite mineralisation.

Development of the mineral assemblage quartz + pyrite ± muscovite is probably associated with the finer-grained facies of the granite. However, the discontinuous nature of the outcrop makes this assumption difficult to confirm. Fine-grained aggregates of quartz and alkali feldspar, with only minor associated muscovite, impart a blue-grey colour to these rocks. Pyrite occurs in disseminated form. In addition, fine molybdenite veinlets (<Ø.3 mm in width) are observed to cut this alteration type at several localities within the area.

In comparison, albitisation is exclusively associated with the coarser-grained facies of the granite. Elongate pods of coarse-grained (2 to 3 mm) albite ± quartz (<1%) ± pyrite ± galena ± sphalerite are observed at two localities within the Steinmyrveien area. In addition loose blocks of albitised granite containing Mn-silicates are observed at the road side. The albite-rich pods may be surrounded either by reddened, orthoclase-rich granite or by apparently unaltered granite. Pyrite is the predominant sulphide mineral. However, galena and yellow sphalerite may be present. The Mn-silicate mineral has been identified as pyroxmangite (Tronnes 1982). Pyroxmangite is a pyroxenoid mineral with a structure similar to wollastonite (Deer et al. 1977). Its chemical formula is $(MnFe)SiO_3$.

4.3.3 The Hegga manganese occurrence

The Hegga Mn occurrence is situated in the Hegga river, approximately 2 km to the west of Rustad (Figure 4.1). It is located within the eastern border of the Rustadkampen granite, close to its contacts with the alkali feldspar syenite. The geology in this area comprises rocks in the compositional field of alkali feldspar granite, but also includes rocks belonging to the alkali feldspar syenite and quartz syenite stages of evolution. The complicated spatial relationships shown by these rocks along a 70 m section of the river are illustrated in Figure 4.4.

The alkali feldspar granite in the vicinity of the Hegga river displays considerable variation in grainsize and texture. Medium to coarse-grained (0.5 to 2 mm), moderately equigranular varieties of alkali feldspar granite are accompanied by fine-grained (<0.4 mm), aplitic varieties of granite. The latter are similar in terms of mineralogy and texture to the aplitic microgranite which forms the north-western face of the Brennhaugen granite massif (Section 3.3.5a). They are therefore interpreted as a contact facies of the granite. In addition, several late, fine-grained micro-dykes, varying in width between 5 cm and 15 cm, are observed to cut both facies of the granite and Mn-rich rocks in the area.

The alkali feldspar granite is intruded into alkali feldspar syenite to the west. The contact with the alkali feldspar syenite continues further to the south and then swings round to the north-east (Figure 4.1). The studied area therefore exists as an embayment within its wall-rocks of alkali feldspar syenite. The intrusive relationships are further complicated by the presence of quartz syenite in the contact zones (Figure 4.4). However, it is not certain whether the exposed areas of quartz syenite are older or younger than the

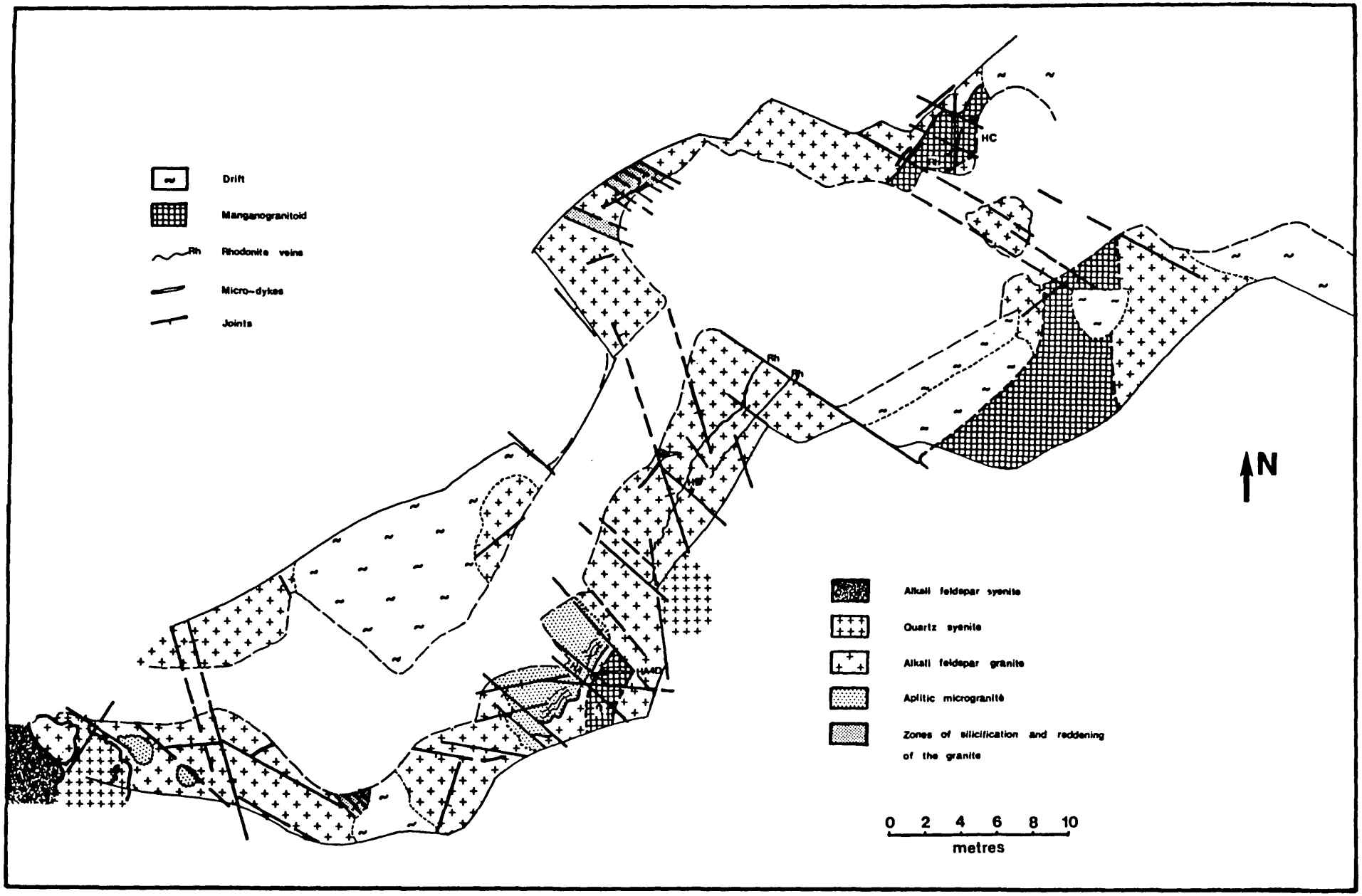

FIGURE 4.4. Geological map of the Hegga manganese occurrence.

alkali feldspar granite. The possibility that they are younger can not be excluded.

The granite is transected by a series of steeply dipping joints (Figure 4.4). The Most prominent trends are NW-SE and NNW-SSE, although sub-horizontal jointing is also apparent. Horizontal displacements of the order of 1 m are observed in several places. The presence of quartz-fill within joint fractures suggests that the formation of the joints was closely connected to the cooling history of the granite.

Two types of alteration are observed in the Hegga river area: (i) Reddening of the granite; and (ii) albitisation of the granite, occurring as large pods (2 m to 10 m) of albite + Mn-silicates ± sphalerite ± fluorite. In addition, thin veins (1 to 2 mm) of Mn-silicate are observed to cut both albitised rocks and unaltered granite in the area (Figure 4.4). The Mn-silicate has been identified as rhodonite (Tronnes 1982). The principal difference between the latter and pyroxmangite is that rhodonite has a higher Ca content (Deer et al. 1977).

Reddening of the granite occurs along narrow zones, oriented parallel to NW-SE trending joint surfaces (Figure 4.4). The altered granite consists of a medium-grained (<0.5 mm) intergrowth of K-feldspar and quartz. Reddening of the granite might therefore be attributed to potassic alteration. However, studies of major element geochemistry (Chapter 5) indicate that the altered rocks have been silicified, at the expense of Na. The red colour imparted to these rocks is presumably the result of oxidation of Fe impurities within the feldspar, since discrete grains of hematite are not observed.

Albite-rich rocks containing rhodonite are observed in three localities within the area (Figure 4.4). The largest of these is located up the slope from the river and is associated with appreciable Mn oxide staining, imparting a thick, black crust

to the surface of the rocks. The other two areas of rhodonite-bearing rock are located in the river bed itself, and are not associated with any appreciable Mn oxide staining. Coarse-grained (Ø.5 to 2 mm) albite, accompanied by minor orthoclase, forms between 8Ø and 9Ø percent of the rock, the remainder being composed largely of rhodonite (Figure 4.5a). However, yellow sphalerite, fluorite and minor quartz (<2%) may be present. Rhodonite occurs interstitially, either in the form of large (Ø.5 to 2 mm), anhedral grains or, more commonly, as aggregates of smaller grains (Ø.1 to Ø.3 mm). Inter-feldspar grain boundaries are highly irregular, indicating strong mobility of Na in these rocks at sub-solidus temperatures.

Texturally, the Mn-rich rocks are very similar to the alkali feldspar granite with which they are associated, except that rhodonite takes the place of quartz in the interstices between feldspar grains (Figure 4.5a). In order to describe this relationship, the Mn-rich rocks are therefore defined as manganogranitoids (manganese-rich rocks with a granitic texture).

Abrupt contacts between rhodonite-bearing, albite-rich rocks and quartz-bearing granite are observed in all three localities in the Hegga river, and in places may be traced for several metres (Figures 4.4 and 4.5b). The outlines of the manganogranitoids are irregular and show no obvious relationship to the orientation of joints in the area. It is therefore not certain whether these bodies represent part of a single deposit, or three separate entities. However, the presence of several thin veins of rhodonite along a line between two of the bodies suggests that they may be connected at depth.

Finally, the aplitic microgranite in the vicinity of the smallest of the manganogranitoid bodies exhibits a distinct vertical foliation (Figure 4.4). This might be attributed to

FIGURE 4.5a. Photomicrograph of the manganogranitoid (sample HC7 from the Hegga river locality), showing the relationship between rhodonite and albite.

FIGURE 4.5b. Photomicrograph of the contact between the manganogranitoid and alkali feldspar granite (sample HA11 from the Hegga river locality).

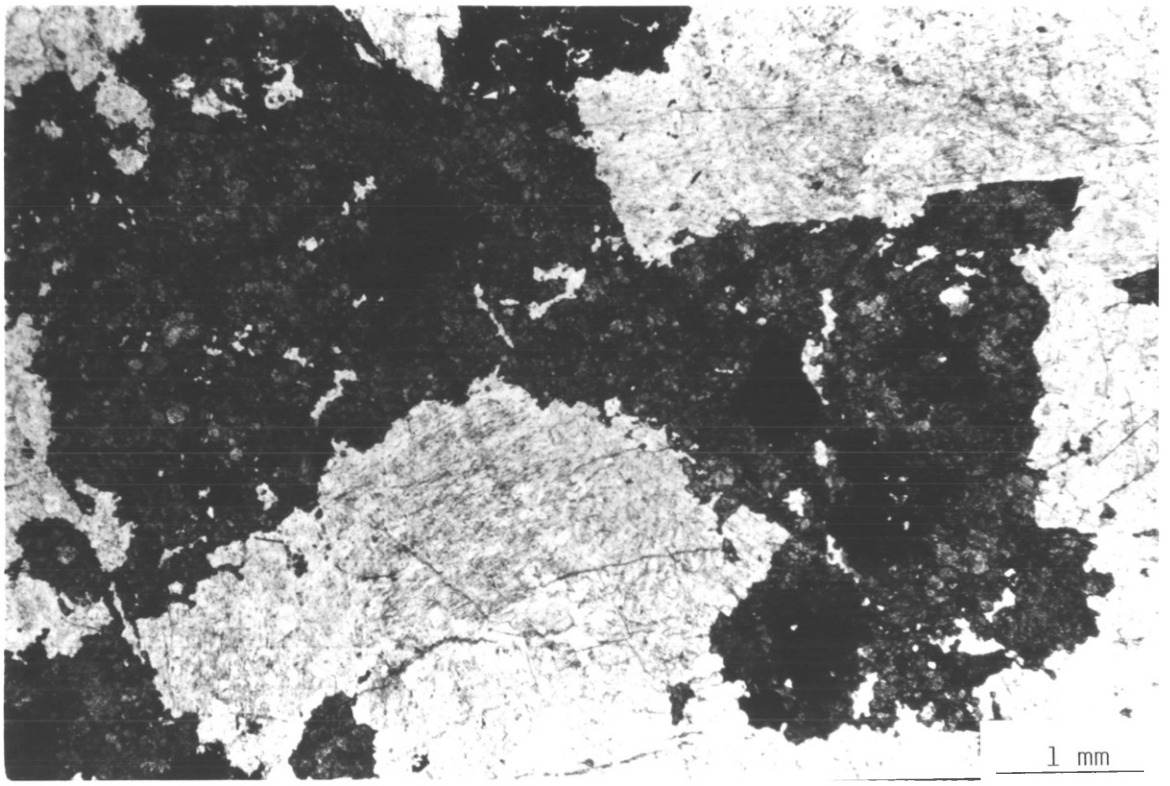
1 mm

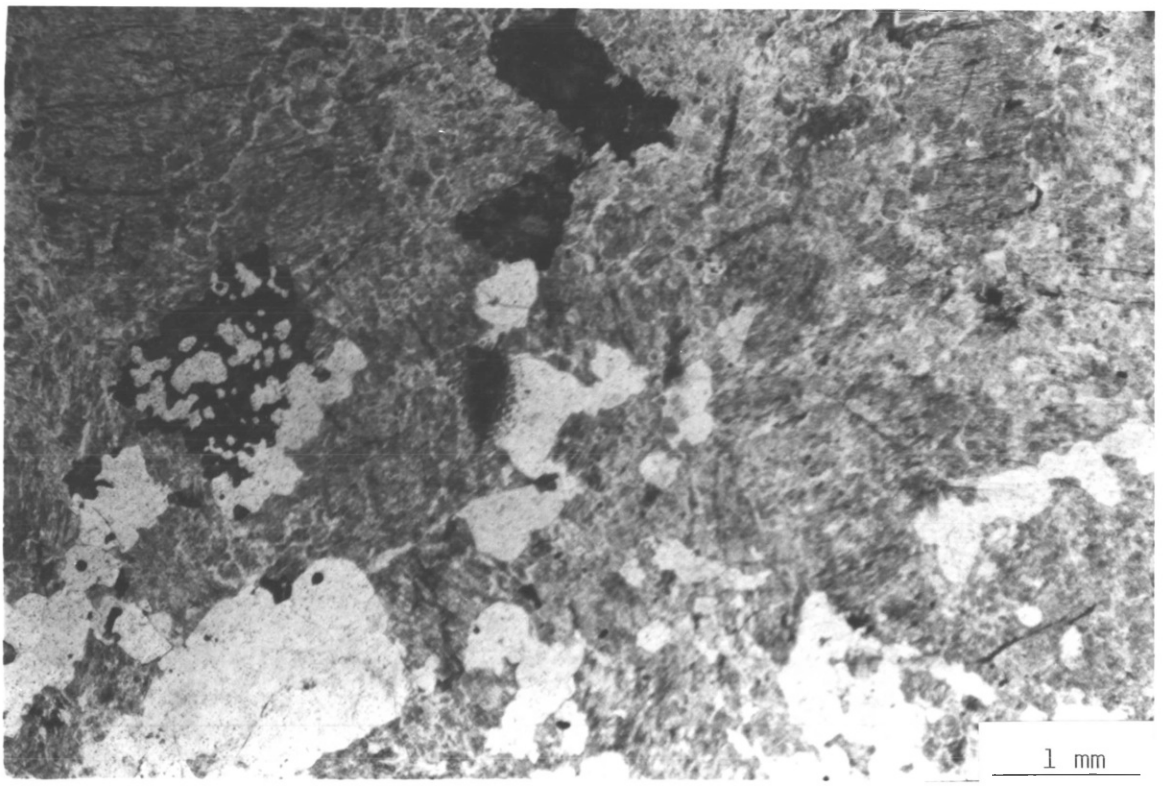
1 mm

FIGURE 4.5c. Photomicrograph of a rhodonite vein cutting the alkali feldspar granite (sample HAB from the Hegga river locality).

FIGURE 4.5d. Photomicrograph of a rhodonite vein cutting the manganogranitoid (sample HC6 from the Hegga river locality).

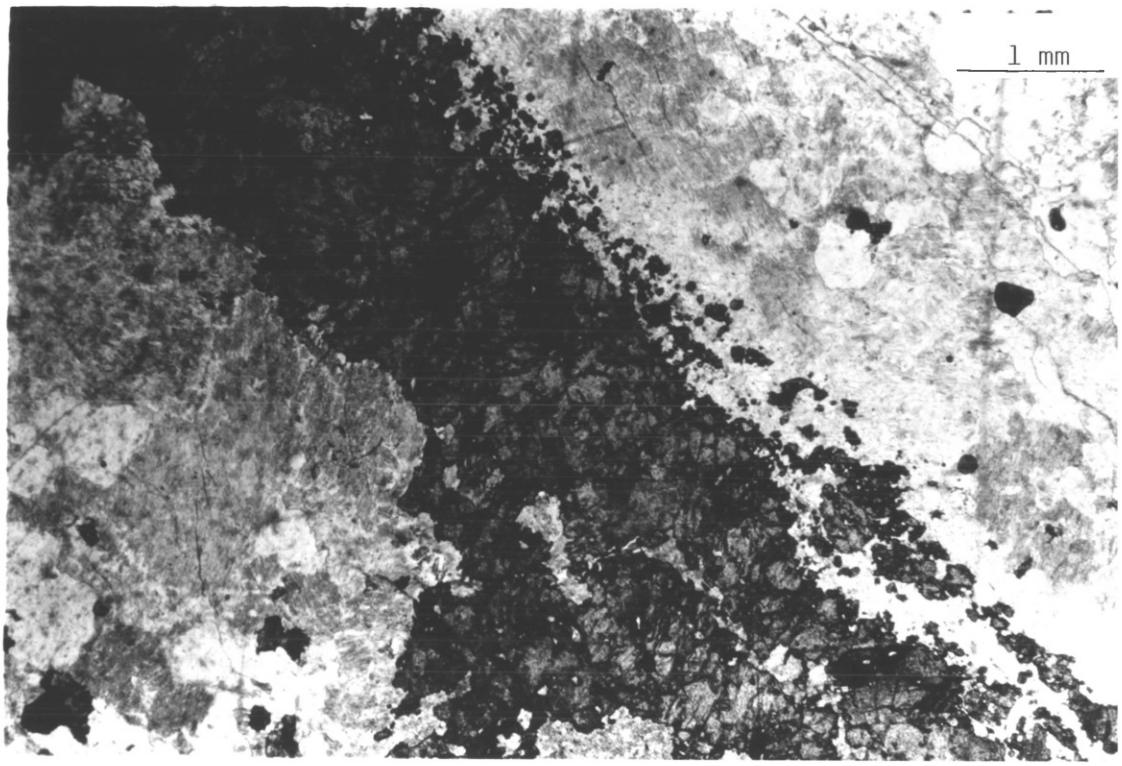
1 mm

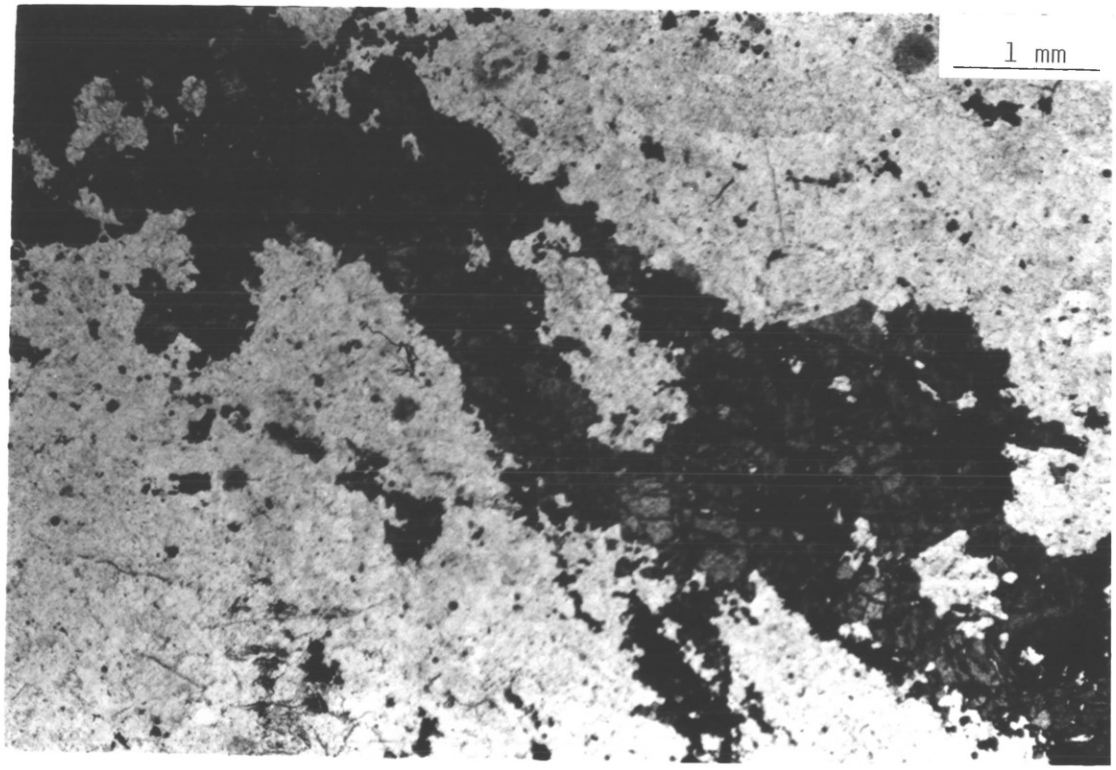
1 mm

the presence of a rotated xenolith of pyroclastic material. However, the absence of compositionally similar extrusive rocks in the area, most of which are trachytic, suggests that this is unlikely. More probably, the vertical foliation is the result of plastic deformation, caused by the sinking of a dense body of Mn enriched rock through the partially consolidated granite. The measured densities of 2.8 and 2.61 g cm^{-3} respectively for these rocks give support to this hypothesis.

4.3.3.1 Discussion

The complicated spatial and temporal relationships exhibited by the granitic rocks in the Hegga river suggest that Mn enriched rocks displaying a distinct granitic texture were formed as a result of magmatic processes. Furthermore, the close proximity of rocks belonging to both the alkali feldspar syenite and quartz syenite stages of evolution, together with the large variations in texture observed within the granite, suggest that these processes were operative in the contact zones of the granite. The presence within the adjacent microgranite of textures believed to be indicative of plastic deformation, suggests that the Mn enriched rocks were formed prior to the complete consolidation of the granite, while the latter was still in a hot, viscous state. Indeed, the continuity in granitic texture observed between the rhodonite-bearing rocks and adjoining alkali feldspar granite suggests that the manganogranitoids were formed as a direct result of changes occurring within the granite during its consolidation. The subsequent injection of a series of granitic micro-dykes into both the manganogranitoids and contiguous granitic rocks indicates that residual pockets of granitic magma were available throughout this process. The observed dependence of zones of silicified granite upon the orientation of joint surfaces, however, indicates that silicification occurred at a later stage, under sub-solidus conditions.

Three possible sources for the manganogranitoids should be considered: I. Direct precipitation of albite, followed by rhodonite from a residual granitic melt of unusual composition; II. Metasomatism of granitic material by a Na and Mn enriched fluid of magmatic origin; and III. Contamination of a granitic magma by material of extraneous origin.

Direct precipitation of albite and rhodonite from a residual melt fraction enriched in these components would explain both the well defined geometry of the Mn-rich phase and the continuity of granitic texture across the boundary between the manganogranitoids and the alkali feldspar granite. The formation of a residual liquid of such unusual composition, however, can not occur by processes of crystal fractionation alone. The coexistence of the Mn-rich rocks and the alkali feldspar granite, with such contrasting silica contents, implies that processes of silicate liquid immiscibility should have been responsible.

Metasomatism of granitic material by a Na and Mn enriched fluid of magmatic origin is perhaps a more favourable mechanism. The tendency for rhodonite to occur in the form of fine-grained aggregates in the interstices between albite grains is consistent with an origin by replacement, suggesting that rhodonite may have replaced quartz in the granitic texture (see Figure 4.5b). At the same time, alkali exchange reactions between a Na enriched fluid and alkali feldspar may have lead to replacement of orthoclase by albite. The interstitial position of rhodonite with respect to albite grains and the occurrence of thin veins of rhodonite both within the manganogranitoids themselves and within the unaltered granite (Figure 4.5 c and d), however, indicate that albitisation and Mn enrichment were not entirely synchronous. Manganese enrichment is at least in part attributable to a separate, probably later, event. The

occurrence within the alkali feldspar granite at Steinmyrveien of discrete segregations of albite without significant Mn enrichment supports this contention.

Contamination of a granitic magma by foreign material would require the presence of xenoliths of country rock containing extremely high concentrations of manganese. Rocks of this type are very unusual in igneous environments, but are occasionally found within sedimentary successions, particularly those from deep marine environments. It is very unlikely that rocks of this type exist within the Oslo Region. It may therefore be concluded that Mn enrichment was not the result of contamination.

The origin of the manganogranitoids will be discussed in greater detail in Chapter 8, following the discussions on major and trace element geochemistry (Chapters 5 and 6).

4.4 Summary and Conclusions

Two distinct types of mineralisation are recognised in the Hurdal area, related to specific stages in the magmatic evolution:

I. Molybdenite ± pyrite ± sphalerite mineralisation with associated quartz ± muscovite ± fluorite alteration, related to the biotite syenite stage of evolution; for instance in the Nordgardshogda - Styggberget and Rustad areas.

II. Rhodonite and/or pyroxmangite ± sphalerite ± pyrite ± galena mineralisation, associated with discrete segregations of albite ± quartz ± fluorite within the alkali feldspar granite; for instance at the Hegga river locality, at Steinmyrveien, and at Steinbratebekken.

Molybdenum - Fe - Zn mineralisation in the Nordgardshogda - Styggberget area is located in the apical, endo-contact

position of the biotite syenite intrusion. Mineralisation involves a zonal arrangement of sphalerite, molybdenite and pyrite, distributed around a central intrusion of biotite syenite. Mineralisation is associated with only minor wall-rock alteration. Silicification and sulphidation are predominant. Sericitic alteration is only of minor importance. The biotite syenite itself, however, is extensively altered. Mineralisation is believed to be the product of late stage magmatic processes involving closed system fractionation of the biotite syenite magma, leading to the generation of a Zn-Mo-Fe-S and F enriched residual melt fraction. Deposition of ore-minerals from this residual melt fraction or from a coexisting hydrothermal phase is believed to have lead to the observed zonation of ore deposits in the area.

Mn - Zn - (Fe) - (Pb) mineralisation is exclusively associated with albitised facies of the alkali feldspar granite in the contact zones of the Brennhaugen and Rustadkampen granites. Manganese enrichment is believed to be the product of late stage magmatic and/or metasomatic processes. An origin by contamination of granitic magma is not favoured by the geological evidence.

CHAPTER 5

MAJOR ELEMENT GEOCHEMISTRY

5.1 Introduction

Intermediate to granitic igneous rocks such as those observed in the Hurdal area, and in other anorogenic continental magmatic settings (Section 2.3), are largely composed of the following elements: Si, Al, Fe, Na and K, with variable amounts of Mg, Ca, Ti, Mn and P. In the Hurdal area, these elements constitute greater than 99.7 percent of the analysed cations (Table 5.2) and are therefore justifyably referred to as major elements. The major anion is overwhelmingly oxygen (O^{2-}), with subordinate amounts (usually less than 5 percent equivalent) of hydroxyl (OH^{-}), fluoride (F^{-}), chloride (Cl^{-}), and carbonate (CO_3^{2-}) ions.

In addition to the major elements listed above, felsic rocks in anorogenic magmatic settings may also contain significant amounts (seldom greater than $1Ø^3$ $\mu g\ g^{-1}$, or approximately $1Ø^{-5}$ gram atoms g^{-1}) of the following elements (in order of increasing atomic number): Li, Be, (Sc), V, Cr, Co, Ni, Cu, Zn, (Ga), Rb, Sr, Y, Zr, Nb, Mo, Ag, (Sn), (Cs), Ba, rare earth elements (REE; La to Lu), Hf, Ta, W, Pb, Th and U (the elements in parenthesis have not been analysed during this study). In the Hurdal area these elements seldom constitute greater than a total of .25 percent of the analysed cations and are therefore designated as trace elements. For reasons of simplicity these elements are discussed in a separate chapter (6, below).

5.2 Major element determinations

Major element determinations on a representative set of 73 rock samples from the Hurdal area have been carried out by X-ray fluorescence analysis as outlined in Chapter 1. The

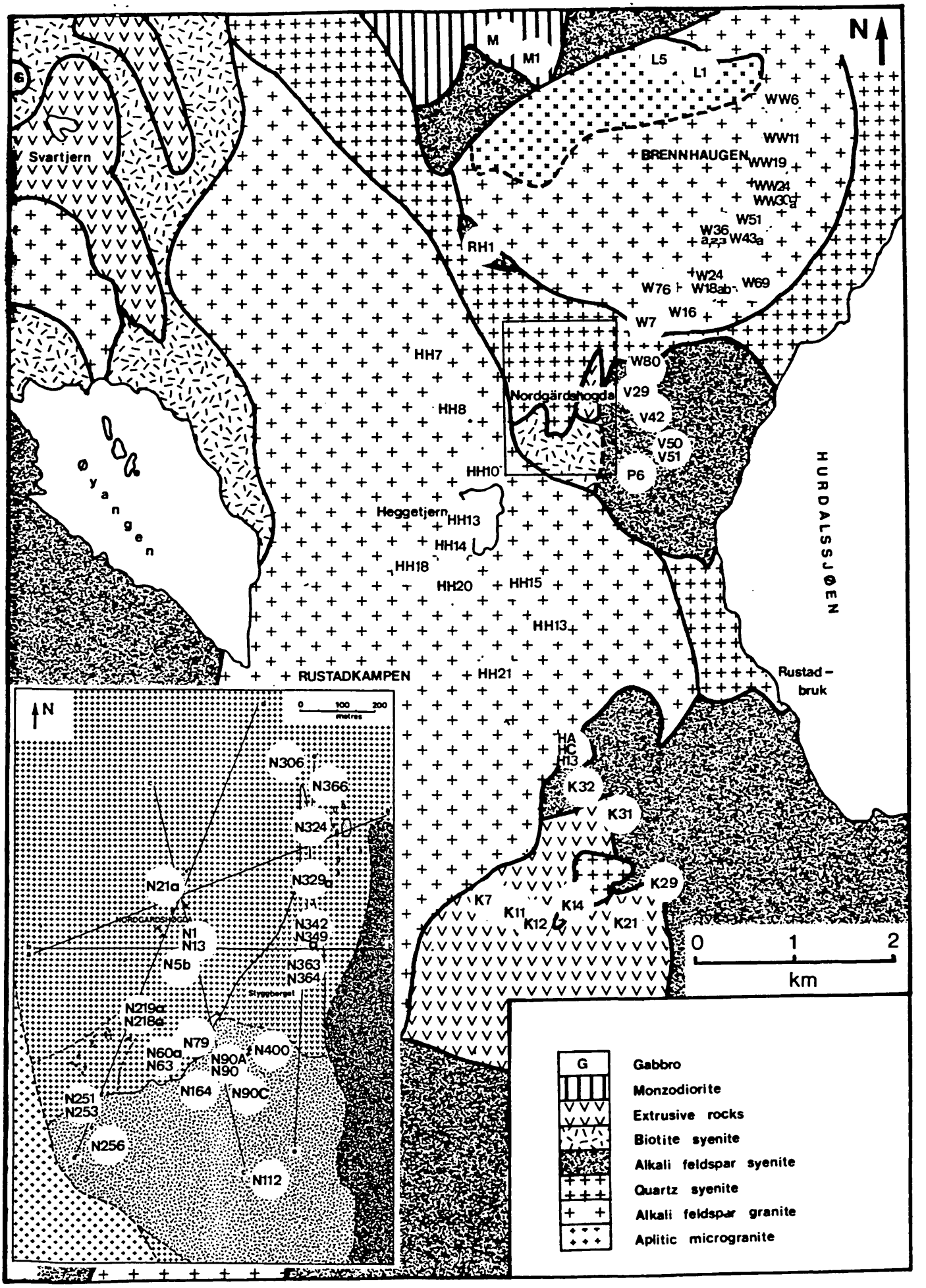

FIGURE 5.1. Sample locality map, Hurdal area.

TABLE 5.1 MAJOR ELEMENT GEOCHEMISTRY

	1	2	3	4	5	6	7	8	9	10
SAMPLE NO:	M1	M2	N112	N164	N253,1	N9OB3	N9OC6	W7	W8O	V29
ROCK TYPE:	MONZDRT	MONZDRT	B.S.	B.S.	B.S.	B.S.	B.S.	A.S.	A.S.	A.S.
MAJOR ELEMENTS (WT % OXIDES):										
SiO_2	52.81	54.36	62.80	62.70	62.47	62.26	62.93	66.21	69.00	67.95
TiO_2	2.32	2.08	.85	1.10	.96	1.03	.91	.48	.53	.60
Al_2O_3	17.50	16.54	17.31	17.10	17.61	17.12	16.77	15.96	15.70	16.09
Fe_2O_3	2.44	2.29	1.83	.38	1.81	.75	0	1.55	1.54	1.65
FeO	5.68	5.63	1.50	3.30	1.80	2.77	2.78	.52	.87	.71
MnO	.23	.20	.14	.35	.27	.51	.30	.23	.15	.14
MgO	2.99	2.72	.65	1.25	1.00	1.06	1.12	.20	.51	.40
CaO	6.44	5.37	.93	1.50	1.91	1.48	1.79	.58	1.08	.87
Na_2O	4.67	4.44	6.04	6.57	5.52	6.17	6.58	5.70	5.25	5.43
K_2O	3.01	3.95	5.96	3.81	5.31	4.58	4.00	6.13	4.92	5.63
P_2O	.67	.39	.15	.27	.20	.23	.22	.03	.11	.09
H_2O+	.79	.82	.72	.63	.45	.46	.89	.58	.37	.36
F	-.00	-.00	-.00	.31	-.00	-.00	.52	.14	-.00	-.00
TOTAL (O=F)	99.55	98.79	98.88	99.14	99.31	98.42	98.59	98.25	100.03	99.92
MOLAR RATIOS (CATIONS):										
$Fe^{3+}:Fe^{2+}$	.39	.37	1.10	.10	.90	.24	0	2.68	1.59	2.09
Mg:Mg+Fe	.40	.39	.27	.38	.34	.35	.42	.16	.29	.25
Ca:Na+K	.54	.42	.05	.09	.12	.09	.11	.03	.07	.05
Na:Na+K	.70	.63	.61	.72	.61	.67	.71	.59	.62	.59
Na+K:Al	.63	.70	.95	.87	.84	.88	.90	1.00	.89	.93
OH-:F	-.00	-.00	-.00	2.13	-.00	-.00	1.80	4.35	-.00	-.00
MODIFIED C.I.P.W. NORMS (CAT. PC):										
Q	0	0	2.32	3.23	4.44	2.89	2.99	8.19	15.54	11.76
OR	17.94	23.77	35.13	22.40	31.23	27.07	23.66	36.48	28.91	33.01
AB	42.06	40.61	54.10	58.69	49.34	55.43	59.14	51.27	46.89	48.39
AN	18.06	13.79	2.51	5.65	7.56	5.49	4.41	0	4.62	2.88
NE	.15	0	0	0	0	0	0	0	0	0
AC	0	0	0	0	0	0	0	.23	0	0
WO	0	0	0	0	0	0	0	.52	0	0
DI	5.17	5.36	.85	0	.38	.14	1.14	1.11	0	.66
HD	2.54	3.13	.04	0	.07	.12	1.16	0	0	0
JS	.10	.11	.00	0	.01	.02	.13	0	0	0
EN	0	2.11	1.36	3.43	2.56	2.86	2.53	0	1.40	.77
FS	0	1.28	.06	3.84	.57	3.06	2.87	0	0	0
FO	4.31	2.15	0	0	0	0	0	0	0	0
FA	2.21	1.30	0	0	0	0	0	0	0	0
MT	2.47	2.35	1.74	.36	1.64	.66	0	.52	1.07	.60
JC	.10	.08	.16	.04	.25	.12	0	.23	.19	.12
HE	0	0	0	0	0	0	0	.53	.23	.66
ILM	3.13	2.85	1.08	1.38	1.16	1.21	1.14	.47	.63	.69
PN	.13	.10	.10	.15	.18	.23	.13	.21	.11	.14
AP	1.41	.83	.31	.56	.42	.48	.46	.06	.23	.19
C	0	0	0	.09	0	0	0	0	.04	0
D.I.	60.15	64.39	91.55	84.31	85.02	85.40	85.79	95.94	91.34	93.16
Q'	24.00	26.60	38.37	37.48	37.45	37.38	37.46	43.29	46.21	44.51
KS'	10.77	14.26	21.08	13.44	18.74	16.24	14.19	21.89	17.35	19.81
NE'	25.39	24.37	32.46	35.22	29.61	33.26	35.49	30.76	28.13	29.03
OL'	6.52	5.98	1.07	5.46	2.35	4.44	4.05	0	1.05	.58

	11	12	13	14	15	16	17	18	19	20
SAMPLE NO:	V42	V50	V51	P6	K32	RH1	H13	W16	N1	N5B
ROCKTYPE:	A.S.	A.S.	A.S.	A.S.	A.S.	A.S.	A.S.	Q.S.	Q.S.	Q.S.
MAJOR ELEMENTS (WT% OXIDES):										
SiO_2	65.13	62.03	63.00	63.96	67.25	63.67	64.99	73.72	69.70	69.68
TiO_2	.68	.81	1.04	.78	.66	.83	.83	.27	.41	.45
Al_2O_3	16.91	17.13	16.88	16.92	15.72	17.18	16.56	13.05	16.09	15.76
Fe_2O_3	1.63	1.53	1.90	1.73	1.57	1.37	1.80	1.29	2.13	1.98
FeO	1.30	1.84	1.59	1.19	1.12	1.66	1.39	0.74	0	0
MnO	.16	.16	.18	.14	.16	.14	.18	.26	.16	.12
MgO	.62	.86	1.02	.58	.57	.81	.73	.13	.07	.05
CaO	1.35	1.93	2.06	1.36	.98	1.74	.81	.42	.11	.12
Na_2O	5.38	5.46	5.12	5.59	5.87	5.81	6.09	4.73	5.43	5.66
K_2O	5.92	5.37	5.48	5.90	5.47	5.56	5.69	4.95	5.91	5.84
P_2O_5	.13	.18	.22	.13	.13	.18	.18	.02	.05	.03
H_2O+	.46	.66	.55	.92	.24	.40	.48	.54	.66	.45
F	-.00	-.00	.13	-.00	-.00	-.00	-.00	-.00	.04	-.00
TOTAL	99.67	97.96	99.11	99.20	99.74	99.35	99.73	100.12	100.74	100.14
(O=F)										
MOLAR RATIOS (CATIONS):										
$Fe^{3+}:Fe^{2+}$	1.13	.75	1.08	1.31	1.26	.74	1.17	1.57	-.00	-.00
Mg:Mg+Fe	.29	.32	.36	.27	.29	.33	.30	.11	.06	.05
Ca:Na+K	.08	.12	.13	.08	.06	.10	.05	.03	.01	.01
Na:Na+K	.58	.61	.59	.59	.62	.61	.62	.59	.58	.60
Na+K:Al	.90	.86	.85	.92	.99	.91	.98	1.01	.95	.99
OH-:F	-.00	-.00	4.44	-.00	-.00	-.00	-.00	-.00	17.40	-.00
MODIFIED C.I.P.W. NORMS (CAT. PC):										
Q	7.29	4.46	6.82	5.50	9.51	4.10	5.36	24.72	14.01	13.01
OR	34.75	32.08	32.48	34.89	32.00	32.58	33.26	29.40	34.53	34.19
AB	48.00	49.57	46.12	50.24	52.19	51.74	54.09	42.20	48.22	50.37
An	4.48	6.44	6.91	3.65	.38	4.34	1.03	0	.22	.34
Ac	0	0	0	0	0	0	0	.39	0	0
Wo	0	0	0	0	0	0	0	.05	0	0
Di	.97	1.19	1.52	1.80	2.87	1.87	1.41	.72	0	0
Hd	.09	.42	0	0	0	.53	.02	.56	0	0
Js	.01	.04	0	0	0	.04	.00	.20	0	0
En	1.22	1.81	2.07	.70	.12	1.28	1.29	0	.19	.14
Fs	.13	.69	0	0	0	.39	.02	0	0	0
Mt	1.51	1.49	1.75	1.31	1.38	1.31	1.65	.89	0	0
Jc	.19	.13	.20	.16	.20	.11	.22	.32	0	0
He	0	0	.03	.23	.03	0	0	0	1.47	1.37
Ilm	.84	1.05	1.30	.97	.80	1.06	1.01	.28	0	0
Pn	.10	.09	.15	.12	.12	.09	.13	.10	.25	.19
Ap	.27	.38	.46	.27	.27	.37	.37	.04	.10	.06
Sph	0	0	0	0	0	0	0	0	0	.03
Rt	0	0	0	0	0	0	0	0	.16	.21
C	0	0	0	0	0	0	0	0	.73	0
D.I.	90.04	86.11	85.41	90.63	93.69	88.43	92.71	96.31	96.77	97.57
Q'	40.73	37.74	38.77	39.73	43.21	38.25	40.63	53.36	47.16	46.88
KS'	20.85	19.25	19.49	20.93	19.20	19.55	19.95	17.64	20.72	20.52
Ne'	28.80	29.74	27.67	30.14	31.31	31.05	32.46	25.32	28.93	30.22
OL'	1.01	1.87	1.55	.53	.09	1.25	.98	0	.14	.10

	21	22	23	24	25	26	27	28	29	30
SAMPLE NO:	N13	N60A	N63	N306	N363	K14	K29	N79	N218A	N251,6
ROCK TYPE:	Q.S.	Q.S.	Q.S.	Q.S.	Q.S.	Q.S.	Q.S.	U.M.	U.M.	U.M.
MAJOR ELEMENTS (WT% OXIDES):										
SiO_2	69.48	68.47	68.04	70.09	74.91	71.03	68.00	73.41	78.08	75.71
TiO_2	.41	.45	.50	.46	.11	.35	.48	.32	.17	.32
Al_2O_3	15.78	16.34	16.19	15.47	11.78	14.37	16.13	14.34	11.22	12.55
Fe_2O_3	2.01	1.31	1.45	2.03	1.17	1.46	1.86	1.31	1.97	1.45
FeO	0	.61	.68	0	.30	.52	.36	.35	0	.71
MnO	.16	.14	.14	.20	.03	.16	.17	.05	.15	.15
MgO	.02	.23	.24	.07	.07	.15	.20	.05	.03	.11
CaO	.09	.53	.51	.23	.09	.40	.28	.12	.09	.18
Na_2O	5.57	6.01	5.91	5.25	3.80	5.59	6.21	4.94	3.90	4.40
K_2O	5.75	5.79	6.05	5.83	4.65	5.29	5.83	5.60	4.47	4.83
P_2O_5	.03	.04	.03	.03	.01	.02	.03	.02	.01	.02
H_2O+	.58	.20	.26	.53	.54	.59	.26	.30	.25	.20
F	-.00	-.00	-.00	-.00	.03	-.00	-.00	-.00	-.00	.07
TOTAL (O=F)	99.88	100.12	100.00	100.19	97.48	99.93	99.81	100.81	100.34	100.67
MOLAR RATIOS (CATIONS):										
$Fe^{3+}:Fe^{2+}$	-.00	1.93	1.92	-.00	3.51	2.53	4.65	3.37	-.00	1.84
Mg:Mg+Fe	.02	.19	.18	.06	.08	.13	.15	.06	.03	.09
Ca:Na+K	.01	.03	.03	.01	.01	.02	.02	.01	.01	.01
Na:Na+K	.60	.61	.60	.58	.55	.62	.62	.57	.57	.58
Na+K:Al	.98	.99	1.01	.97	.96	1.04	1.02	.99	1.00	.99
OH-:F	-.00	-.00	-.00	-.00	19.10	.-00	-.00	-.00	-.00	3.00
MODIFIED C.I.P.W. NORMS (CAT. PC):										
Q	13.77	9.46	8.90	15.42	33.53	16.82	8.66	21.10	35.86	29.02
Or	33.82	33.64	35.24	34.28	28.62	31.16	33.98	32.80	26.77	28.61
Ab	49.79	53.07	51.89	46.91	35.55	47.04	52.87	43.98	35.30	39.60
An	.25	.50	0	.94	.40	0	0	0.41	0	.23
Ac	0	0	.35	0	0	2.40	1.71	0	.15	0
Wo	0	.11	.27	0	0	.17	0	0	.07	0
Di	0	1.25	1.31	0	0	.83	.94	.04	.17	.43
Hd	0	0	0	0	0	.23	0	0	0	0
Js	0	0	0	0	0	.07	0	0	0	0
En	.05	0	0	.19	.20	0	.07	.12	0	.09
Mt	0	.64	.71	0	.51	.47	.16	.23	0	1.10
Jc	0	.15	.15	0	.05	.15	.07	.03	0	.24
He	1.39	.37	.34	1.41	.48	0	.70	.73	1.35	.12
Ilm	0	.50	.57	0	.14	.37	.45	.39	0	.37
Pn	.25	.12	.12	.31	.01	.12	.21	.06	.24	.08
Ap	.06	.08	.06	.06	.02	.04	.06	.04	.02	.04
Sph	0	0	0	0	0	0	0	0	..00	0
Rt	.16	0	0	.16	0	0	0	0	0	0
C	..33	0	0	.19	.40	0	0	0	0	0
D.I.	97.39	96.17	96.03	96.61	97.70	95.02	95.50	97.88	97.93	97.23
Q'	47.23	44.15	43.75	47.94	59.25	48.10	43.42	51.84	60.69	56.33
KS'	20.29	20.18	21.15	20.57	17.17	18.70	20.39	19.68	16.06	17.16
Ne'	29.88	31.84	31.13	28.15	21.33	28.22	31.72	26.39	21.18	23.76
Ol'	.04	0	0	.14	.15	0	.06	.09	0	.07

	31	32	33	34	35	36	37	38	39	40
SAMPLE NO:	N329A	N366	W24	W43A	W511	W69	W76	WW6	WW11	WW19
ROCK TYPE:	F.P.MG	F.P.MG	A.G.(B)	A.G.(B)	A.G.(B)	A.G.(B)	A.G.(B)	A.G.(B)	A.G.(B)	A.G.(B)
MAJOR ELEMENTS (WT% OXIDES):										
SiO_2	75.25	75.43	77.16	77.26	77.06	77.95	77.23	76.29	78.20	77.24
TiO_2	.24	.26	.17	.16	.16	.10	.14	.15	.15	.13
Al_2O_3	13.06	12.69	11.33	11.55	11.79	11.81	11.95	11.94	11.89	11.62
Fe_2O_3	.98	1.27	.83	1.24	1.10	.40	.86	.95	1.92	.96
FeO	.71	.36	.72	.25	.43	.11	.19	.57	0	.45
MnO	.08	.11	.24	.20	.16	.03	.08	.32	.13	.18
MgO	.12	.12	.09	.04	.06	.02	.03	.03	.04	.09
CaO	.14	.39	.36	.13	.07	.09	.53	.23	.43	.51
Na_2O	4.34	4.42	4.14	4.06	4.08	3.83	4.05	4.00	.14	3.64
K2O	4.83	4.78	4.29	4.45	4.74	5.03	4.77	4.77	4.63	4.40
P_2O_5	.02	.02	.01	.01	.01	.01	.01	.01	.01	0
H_2O^+	.47	.34	.51	.28	.30	.31	.35	.70	2.67	.92
F	.05	-.00	.21	-.00	-.00	-.00	-.00	-.00	-.00	-.00
TOTAL (O=F)	100.27	100.19	99.97	99.63	99.96	99.69	100.19	99.96	100.21	100.14
MOLAR RATIOS (CATIONS):										
Fe^{3+}:Fe^{2+}	1.24	3.17	1.04	4.46	2.30	3.27	4.07	1.50	-.00	1.92
Mg:Mg+Fe	.12	.12	.10	.05	.07	.07	.05	.04	.04	.11
Ca:Na+K	.01	.03	.03	.01	.01	.01	.04	.02	.07	.04
Na:Na+K	.58	.58	.59	.58	.57	.54	.56	.56	.04	.56
Na+K:Al	.95	.98	1.01	1.00	1.00	.99	.99	.98	.44	.93
OH-:F	9.89	-.00	2.56	-.00	-.00	-.00	-.00	-.00	-.00	-.00
MODIFIED C.I.P.W. NORMS (CAT. PC):										
Q	28.89	28.62	33.75	34.27	32.89	34.09	32.49	32.10	58.30	35.90
Or	28.73	28.41	25.75	26.73	28.33	30.15	28.45	28.64	29.32	26.54
Ab	39.23	39.93	37.08	37.06	36.77	34.89	36.71	36.51	1.35	33.37
An	.57	.67	0	.15	0	.18	.34	.54	2.22	2.42
Ac	0	0	.55	0	.23	0	0	0	0	0
Wo	0	.12	0	.06	0	.03	.82	0	0	0
Di	0	.67	.33	.22	.23	.11	.17	.06	0	.09
Hd	0	0	.80	0	0	0	0	.24	0	.03
Js	0	0	.27	0	0	0	0	.14	0	.01
En	.33	0	.09	0	.05	0	0	.05	.12	.21
Fs	.21	0	.29	0	0	0	0	.33	0	.11
Mt	.93	.42	.50	.40	.77	.09	.24	.64	0	.73
Jc	.11	.13	.17	.33	.29	.03	.10	.37	0	.30
He	0	.52	0	.39	.01	.20	.38	0	1.43	0
Ilm	.30	.28	.18	.13	.16	.11	.14	.14	0	.13
Pn	.03	.09	.06	.10	.06	.03	.06	.08	.22	.05
Ap	.04	.04	.02	.02	.02	.02	.02	.02	.02	0
Rt	0	0	0	0	0	0	0	0	.00	0
C	.53	0	0	0	0	0	0	0	6.89	0
D.I.	96.85	96.95	96.57	98.06	96.00	99.13	97.66	97.25	88.97	95.81
Q'	56.21	55.95	58.97	59.79	58.95	60.11	58.56	58.26	70.59	59.95
Ks'	17.24	17.05	15.45	16.04	17.00	18.09	17.07	17.19	17.59	15.92
Ne'	23.54	23.96	22.25	22.24	22.06	20.94	22.03	21.90	.81	20.02
Ol'	.41	0	.28	0	.04	0	0	.29	.09	.24

	41	42	43	44	45	46	47	48	49	50
SAMPLE NO:	WW24	WW30A	HH3	HH7	HH8	HH10	HH13	HH15	HH18	HH20
ROCK TYPE:	A.G.(B)	A.G.(B)	A.G.(R)	A.G.(R)	A.G.(R)	A.G.(R)	A.G.(R)	A.G.(R)	A.G.(R)	A.G.(R)
MAJOR ELEMENTS (WT % OXIDES)										
SiO_2	76.76	78.18	77.41	74.47	74.74	76.69	76.90	76.89	77.41	76.20
TiO_2	.14	.12	.16	.23	.21	.18	.14	.13	.12	.12
Al_2O_3	11.51	11.55	11.79	13.11	13.05	13.05	11.56	11.71	11.58	12.00
Fe_2O_3	.95	1.33	.69	1.06	1.02	.73	1.03	.85	1.22	.71
FeO	.40	0	.69	.43	.43	0	.45	.36	.13	.74
MnO	.14	.08	.12	.17	.11	.03	.17	.25	.06	.38
MgO	.07	.03	.03	.14	.11	.05	.05	.06	.02	.05
CaO	.78	.08	.17	.44	.35	.09	.48	.28	.48	.26
Na_2O	3.81	4.01	4.32	4.41	4.82	4.37	4.16	4.22	4.08	4.40
K_2O	4.43	4.35	4.37	4.95	4.82	5.05	4.43	4.40	4.42	4.36
P_2O_5	.01	.01	.01	.02	.02	.02	.01	.01	.01	.01
H_2O+	.81	.32	.42	.51	.16	.27	.41	.42	.37	.32
F	.38	-.00	.07	-.00	-.00	-.00	-.00	-.00	-.00	.14
TOTAL (O=F)	100.03	100.06	100.22	99.94	99.84	100.53	99.79	99.58	99.90	99.63
MOLAR RATIOS (CATIONS):										
$Fe^{3+}:Fe^{2+}$	2.14	-.00	.90	2.22	2.13	-.00	2.06	2.12	8.44	.86
Mg:Mg+Fe	.09	.04	.04	.15	.13	.12	.06	.09	.03	.06
Ca:Na+K	.06	.01	.01	.03	.02	.01	.04	.02	.04	.02
Na:Na+K	.57	.58	.60	.58	.60	.57	.59	.59	.58	.61
Na+K:Al	.96	.98	1.00	.96	1.01	.97	1.01	1.00	.99	1.00
OH-:F	2.26	-.00	6.28	-.00	-.00	-.00	-.00	-.00	-.00	2.43
MODIFIED C.I.P.W. NORMS (CAT.PC):										
Q	34.48	35.70	32.80	27.02	25.88	29.39	33.07	32.96	34.00	30.95
Or	26.73	26.05	26.07	29.49	28.56	29.83	26.56	26.41	26.49	26.10
Ab	34.94	36.50	38.91	39.93	42.87	39.24	37.46	38.49	37.17	40.04
An	1.25	.34	0	1.37	0	.32	0	.01	.23	.12
Ac	0	0	.21	0	.42	0	.35	0	0	0
Wo	.86	0	0	0	.34	0	.66	1.19	.79	0
Di	.39	0	.08	.56	.61	0	.28	.34	.11	.10
Hd	0	0	.47	0	0	0	.20	.21	0	.52
Js	0	0	.08	0	0	0	.08	.15	0	.27
En	0	.08	.05	.11	0	.14	0	0	0	.09
Fs	0	0	.33	0	0	0	0	0	0	.70
Mt	.73	0	.55	.66	.65	0	.70	.53	.13	.49
Jc	.26	0	.10	.26	.17	0	.27	.37	.06	.26
He	.02	.94	0	.13	.06	.51	0	0	.73	0
Ilm	.15	0	.19	.23	.23	0	.14	.11	.12	.11
Pn	.05	.13	.03	.09	.06	.05	.05	.08	.05	.06
Ap	.02	.02	.02	.04	.04	.04	.02	.02	.02	.02
Rt	0	.02	0	0	0	.10	0	0	0	0
C	0	.14	0	0	0	.30	0	0	0	0
D.I.	96.15	98.25	97.77	96.44	97.31	98.46	97.09	97.87	97.66	97.09
Q'	59.15	60.74	58.89	54.82	54.45	57.05	58.68	58.92	59.46	57.60
KS'	16.04	15.63	15.64	17.69	17.13	17.90	15.93	15.85	15.90	15.66
Ne'	20.96	21.90	23.34	23.96	25.72	23.54	22.48	23.10	22.30	24.02
Ol'	0	.06	.29	.08	0	.10	0	0	0	.59

	51	52	53	54	55	56	57	58	59	60
SAMPLE NO:	HH21	HH14	W362	HC3	HC7	HC10	L1	L5	W18AB	W36A
ROCK TYPE	A.G.(R)	A.G.(R)	MN.R	MN.R	MN.R	MN.R	AP.MG	AP.MG	DYKE	DYKE
MAJOR ELEMENTS (WT% OXIDES):										
SiO_2	76.56	76.97	61.67	62.85	59.57	60.35	77.14	76.85	53.51	67.76
TiO_2	.12	.15	.23	.13	.13	.35	.10	.14	2.12	.55
Al_2O_3	11.97	12.12	15.42	16.02	14.43	14.74	11.54	11.54	16.29	16.23
Fe_2O_3	1.03	.32	1.75	0	0	1.75	1.82	0	4.29	0
FeO	.32	.97	.43	2.15	2.17	2.81	.12	1.59	3.96	2.30
MnO	.10	.10	9.06	8.25	13.31	10.44	.28	.24	.14	.10
MgO	.04	.04	.31	.21	.28	.24	.05	.05	3.24	.25
CaO	.63	.22	1.32	.55	.92	.93	.20	.29	4.08	.44
Na_2O	4.02	3.67	9.17	9.36	8.37	8.50	4.19	4.15	5.10	5.02
K_2O	4.55	5.11	.14	.53	.85	.68	4.15	4.38	3.22	5.35
P_2O_5	.01	.01	.01	.01	.01	.01	.01	.01	1.17	.10
H_2O+	.59	.43	1.91	1.43	1.99	1.31	.48	.42	1.74	1.83
F	-.00	-.00	.49	-.00	-.00	-.00	-.00	.14	-.00	.06
TOTAL	99.94	100.11	101.70	101.49	102.03	102.11	100.08	99.74	98.86	99.96
MOLAR RATIOS (CATIONS):										
$Fe^{3+}Fe^{2+}$	2.90	.30	3.66	0	0	.56	13.65	0	.97	0
Mg:Mg+Fe	.05	.05	.22	.15	.19	.09	.05	.05	.42	.16
Ca:Na+K	.05	.02	.08	.03	.06	.06	.02	.02	.31	.03
Na:Na+K	.57	.52	.99	.96	.94	.95	.61	.59	.71	.59
Na+K:Al	.96	.95	.99	1.00	1.02	1.00	.99	1.00	.73	.87
OH-:F	-.00	-.00	4.11	-.00	-.00	-.00	-.00	3.14	-.00	32.10
MODIFIED C.I.P.W. NORMS (CAT. PC):										
Q	32.69	32.74	0	0	0	0	34.34	32.23	1.09	14.45
Or	27.28	30.58	.81	3.04	4.97	3.89	24.89	26.30	19.48	31.90
Ab	36.63	33.38	81.09	81.65	72.92	73.89	38.20	37.72	46.90	45.49
An	1.19	1.04	.49	.13	0	.05	.43	0	12.34	1.54
Ns	0	0	0	0	.42	0	0	.05	0	0
Wo	.65	0	0	0	0	0	.06	0	0	0
Di	.22	0	.28	.07	.11	.12	.28	.06	.43	0
Hd	0	0	.20	.39	.48	.71	0	.92	.02	0
Js	0	0	4.23	1.51	2.97	2.66	0	.14	.00	0
En	0	.11	.40	.13	.03	.18	0	.11	8.95	.70
Fs	0	1.24	6.20	3.47	.83	5.24	0	2.16	.41	2.98
Fo	0	0	.23	.30	.51	.30	0	0	0	0
Fa	0	0	3.54	8.41	15.93	8.62	0	0	0	0
Mt	.56	.31	.08	0	0	.37	.22	0	4.43	0
Jc	.18	.03	1.72	0	0	1.40	.52	0	.16	0
He	.24	0	0	0	0	0	.79	0	0	0
Ilm	.13	.19	.01	.04	.02	.10	.04	.17	2.92	.74
Pn	.04	.02	.30	.14	.15	.37	.10	.03	.10	.03
Ap	.02	.02	.02	.02	.02	.02	.02	.02	2.51	.21
C	0	.19	0	0	0	0	0	0	0	1.78
D.I.	96.60	96.71	81.91	84.69	77.89	77.78	97.43	96.26	67.47	91.84
Q'	58.26	58.67	34.41	34.78	31.37	32.47	59.58	58.41	29.98	46.32
KS'	16.37	18.35	.49	1.83	2.98	2.33	14.94	15.78	11.69	19.14
Ne'	21.98	20.03	48.65	48.99	43.75	44.33	22.92	22.63	28.14	27.29
Ol'	0	1.02	8.72	11.41	17.09	12.99	0	1.70	7.02	2.76

	61	62	63	64	65	66	67	68	69	70
SAMPLE NO:	W363	HA4D	N400	N219A	N342	N349A	N364	N324	K7A	K11
ROCK TYPE:	alt.Dyke	DYKE	DYKE	TRACH-AND	TRACH-1	TRACH-1	TRACH-1	RHYOLITE	TRACH-2	TRACH-2
MAJOR ELEMENTS (WT % OXIDES):										
SiO_2	70.91	77.57	44.96	59.80	67.18	67.39	67.54	78.57	63.54	65.60
TiO_2	.65	.16	2.65	.79	.61	.61	.61	.16	.92	.96
Al_2O_3	15.87	10.77	15.71	17.20	16.19	16.33	16.50	11.01	17.16	15.96
Fe_2O_3	3.21	1.91	5.34	0	.62	1.89	0	0	1.73	2.27
FeO	0	.83	5.58	5.41	1.75	.62	2.35	1.18	1.93	1.53
MnO	.27	.28	.21	.37	.15	.18	.29	.03	.15	.16
MgO	.09	.04	4.47	.51	.26	.31	.38	.03	.91	.78
CaO	.08	.16	6.25	1.28	.55	.57	.48	.11	2.27	2.03
Na_2O	.07	4.08	3.91	6.12	5.23	5.78	5.91	2.47	5.30	5.84
K_2O	4.91	4.17	3.05	5.91	5.96	5.31	5.69	5.50	4.94	3.92
P_2O_5	.03	.02	2.57	.13	.05	.06	.05	.02	.21	.32
H_2O+	4.28	.14	4.40	1.59	.62	.74	.43	.95	.50	.52
F	-.00	-.00	.19	.42	-.00	-.00	.20	-.00	-.00	.14
TOTAL	100.37	100.13	99.21	99.36	99.17	99.79	100.35	100.03	99.56	99.97
MOLAR RATIOS (CATIONS):										
$Fe^{3+}:Fe^{2+}$	-.00	2.07	.86	0	.32	2.74	0	0	.81	1.34
Mg:Mg+Fe	.05	.03	.43	.14	.17	.19	.22	.04	.32	.28
Ca:Na+K	.01	.01	.58	.07	.03	.03	.03	.01	.15	.13
Na:Na+K	.02	.60	.66	.61	.57	.62	.61	.41	.62	.69
Na+K:Al	.34	1.04	.62	.96	.93	.93	.96	.91	.82	.87
OH-:F	-.00	-.00	24.43	4.00	-.00	-.00	2.28	-.00	-.00	3.92
MODIFIED C.I.P.W. NORMS (CAT. PC):										
Q	51.72	35.61	0	0	10.79	11.00	7.53	40.12	7.48	11.53
Qr	31.46	25.02	19.15	35.12	35.30	31.23	33.09	33.49	29.11	23.07
Ab	.68	34.68	37.31	48.48	47.07	51.67	52.24	22.86	47.47	52.24
An	.22	0	15.11	2.02	2.41	2.43	1.66	.43	8.42	5.73
Ne	0	0	0	4.08	0	0	0	0	0	0
Ac	0	2.02	0	0	0	0	0	0	0	0
Di	0	.08	0	.43	0	0	.07	0	.89	1.77
Hd	0	.34	0	2.23	0	0	.19	0	.24	0
Js	0	.12	0	.15	0	0	.02	0	.02	0
En	.27	.07	2.27	0	.72	.85	1.00	.09	2.06	1.26
Fs	0	.45	.29	0	1.67	0	3.09	1.70	.60	0
Fo	0	0	8.13	.90	0	0	0	0	0	0
Fa	0	0	1.03	5.04	0	0	0	0	0	0
Mt	0	.95	5.72	0	.60	.45	0	0	1.67	1.73
Jc	0	.32	.22	0	.05	.13	0	0	.13	.18
He	2.43	0	0	0	0	.92	0	0	0	.30
Ilm	0	.17	3.78	1.04	.78	.65	.74	.22	1.19	1.20
Pn	.46	.06	.14	.07	.07	.19	.09	.01	.09	.13
Ap	.07	.04	5.71	.27	.10	.12	.10	.04	.44	.67
Rt	.26	0	0	0	0	0	0	0	0	0
C	12.27	0	.89	0	.28	.20	0	.95	0	0
D.I.	83.86	95.30	56.46	87.67	93.16	93.90	92.87	96.47	84.06	86.84
Q'	64.64	59.62	23.22	33.44	44.34	44.38	42.69	63.11	38.77	41.97
Ks'	18.87	15.01	11.49	21.07	21.18	18.74	19.86	20.09	17.47	13.84
Ne'	.41	20.81	22.39	33.16	28.24	31.00	31.34	13.71	28.48	31.34
Ol'	.20	.39	11.08	5.94	1.79	.64	3.06	1.34	2.00	.94

	71	72	73
SAMPLE NO:	K12A	K21	K31
ROCK TYPE:	TRACH-2	TRACH-2	TRACH-2
MAJOR ELEMENTS (WT% OXIDES):			
SiO_2	65.79	63.60	62.96
TiO_2	.62	.75	.88
Al_2O_3	16.38	17.43	17.37
Fe_2O_3	2.04	1.82	2.52
FeO	.84	.99	1.30
MnO	.23	.16	.35
MgO	.53	.42	1.02
CaO	1.05	1.28	1.55
Na_2O	6.40	6.27	7.13
K_2O	5.19	6.24	4.72
P_2O_5	.10	.10	.20
H_2O+	.31	.91	.33
F	-.00	-.00	.22
TOTAL	99.48	99.97	100.46
(O=F)			
MOLAR RATIOS (CATIONS):			
$Fe^{3+}.Fe^{2+}$	2.19	1.65	1.74
Mg:MG+Fe^{+}	.26	.22	.34
Ca:Na+K	.06	.07	.08
Na:Na+K	.65	.60	.70
Na+K:Al	.99	.98	.97
Oh-:F	-.00	-.00	1.60
MODIFIED C.I.P.W. NORMS (CAT. PC):			
Q	6.22	1.08	.19
Or	30.32	36.38	27.16
Ab	56.82	55.56	62.35
An	.63	.97	1.41
Wo	.10	.72	0
Di	2.89	2.29	3.84
En	0	0	.82
Mt	.93	.94	1.53
Jc	.26	.15	.42
He	.62	.52	.41
Ilm	.67	.89	.94
Pn	.19	.15	.26
Ap	.21	.21	.41
D.I.	93.35	93.02	89.69
Q'	41.07	37.85	36.20
KS'	18.19	21.83	16.29
Ne'	34.09	33.33	37.41
OL'	0	0	.62

TABLE 5.2: AVERAGE MAJOR ELEMENT ANALYSES

ROCK TYPE:	Monzdrt		B.S.		A.S.		Q.S.		U.M.	
NUMBER OF SAMPLES:	2		5		10		10		3	
	$\bar{x}$	σ_{n-1}	$\bar{x}$	σ_{n-1}	$\bar{x}$	σ_{n-1}	$\bar{x}$	σ_{n-1}	$\bar{x}$	σ_{n-1}
MAJOR ELEMENTS (cation %):										
Si^{4+}	50.32	1.37	57.89	.30	60.34	1.90	64.96	3.22	70.34	2.94
Ti^{4+}	1.55	.11	.67	.07	.50	.12	.27	.08	.19	.06
Al^{3+}	18.83	.62	18.72	.30	17.97	.69	16.41	1.46	13.89	1.56
Fe^{3+}	1.67	.06	.66	.58	1.13	.11	1.16	.25	1.10	.26
Fe^{2+}	4.44	0.	1.88	.58	.94	.33	.25	.24	.27	.28
Mn^{2+}	.17	.02	.25	.11	.13	.02	.12	.05	.09	.05
Mg^{2+}	4.00	.24	1.40	.31	.87	.33	.17	.11	.09	.06
Ca^{2+}	5.94	.72	1.51	.38	1.26	.50	.27	.17	.13	.05
Na^{+}	8.29	.24	11.07	.79	9.98	.51	9.68	1.13	7.94	.85
K^{+}	4.17	.82	5.58	1.06	6.61	.41	6.58	.46	5.88	.62
P^{5+}	.42	.15	.17	.03	.11	.04	.02	.01	.01	0.
TOTAL	99.80	.03	99.80	.03	99.84	.02	99.89	.02	99.93	.01
ANION EQUIVALENT:										
O^{2-}	155.32	.36	159.02	.73	161.50	1.75	165.25	2.98	170.74	2.99
OH^{-}	2.52	.07	1.94	.57	1.55	.60	1.42	.51	.77	.15
F^{-}	-.00	-.00	1.21	.44	.40	.02	.10	.02	.21	0.
CALCULATED ANHYDROUS MAGMA DENSITIES (g cm^{-3}):										
PRESSURE: 1 bar										
1200 °C	2.53	0.	2.39	.02	2.36	.01	2.33	.01	2.31	.01
1000 °C	2.56	0.	2.42	.02	2.39	.01	2.35	.01	2.33	.01
800 °C	2.59	0.	2.44	.02	2.41	.01	2.37	.01	2.35	.01
PRESSURE: 1 kbar										
1200 °C	2.54	0.	2.40	.02	2.37	.01	2.33	.01	2.32	.01
1000 °C	2.57	0.	2.42	.02	2.39	.01	2.35	.01	2.33	.01
800 °C	2.60	0.	2.45	.02	2.41	.01	2.37	.01	2.35	.01

ROCK TYPE:	Fp.mG		A.G.(B)		A.G.(R)		Ap.mG		Mn.R	
NUMBER OF SAMPLES:	2		9		10		2		4	
	$\bar{x}$	σ_{n-1}	$\bar{x}$	σ_{n-1}	$\bar{x}$	σ_{n-1}	$\bar{x}$	σ_{n-1}	$\bar{x}$	σ_{n-1}
MAJOR ELEMENTS (cation %):										
Si^{4+}	70.23	.08	72.66	.52	71.54	1.19	72.45	.13	55.37	1.21
Ti^{4+}	.18	.01	.10	.02	.11	.03	.08	.02	.14	.07
Al^{3+}	14.14	.29	12.94	.21	13.45	.63	12.80	.01	16.18	.72
Fe^{3+}	.79	.14	.68	.19	.61	.18	.64	.91	.60	.69
Fe^{2+}	.42	.19	.27	.18	.35	.23	.67	.82	1.43	.77
Mn^{2+}	.07	.02	.13	.07	.12	.08	.21	.02	7.89	1.76
Mg^{2+}	.17	0.	.07	.04	.08	.05	.07	0.	.35	.06
Ca^{2+}	.26	.18	.31	.26	.34	.17	.25	.06	.90	.31
Na^{+}	7.92	.10	7.22	.28	7.71	.52	7.61	.04	15.55	.84
K^{+}	5.71	.04	5.50	.29	5.55	.34	5.12	.20	.64	.35
P^{5+}	.02	0.	.01	0.	.01	0.	.01	0.	.01	0.
TOTAL	99.91	.01	99.89	.04	99.87	.03	99.91	.01	99.06	.77
ANION EQUIVALENT:										
O^{2-}	170.45	.18	172.37	.75	171.47	1.06	172.15	.72	153.21	1.27
OH^{-}	1.26	.28	1.57	.79	1.22	.38	1.41	.15	5.03	1.08
F^{-}	.15	0.	.88	.36	.31	.15	.42	0.	1.41	0.
CALCULATED ANHYDROUS MAGMA DENSITIES (g cm^{-3}):										
PRESSURE: 1 bar										
1200 °C	2.31	.01	2.31	.01	2.31	.01	2.31	.02	2.51	.05
1000 °C	2.33	.01	2.32	.01	2.33	.01	2.33	.02	2.53	.05
800 °C	2.35	.01	2.34	.01	2.34	.01	2.35	.02	2.56	.05
PRESSURE: 1 kbar										
1200 °C	2.32	.01	2.31	.01	2.31	.01	2.32	.02	2.51	.05
1000 °C	2.34	.01	2.33	.01	2.33	.01	2.33	.02	2.54	.05
800 °C	2.35	.01	2.34	.01	2.35	.01	2.35	.02	2.56	.05

ROCK TYPE:	Trach-1		Trach-2		Trachand	Rhy.	Dol.	W18AB	W36A	HA4D
NUMBER OF SAMPLES:	3		5		1	1	1	1	1	1
	$\bar{x}$	σ_{n-1}	$\bar{x}$	σ_{n-1}						
MAJOR ELEMENTS (cation %):										
Si^{4+}	62.03	.40	58.88	1.54	55.71	75.00	44.26	50.75	63.34	72.97
Ti^{4+}	.42	0.	.57	.10	.55	.11	1.96	1.51	.39	.11
Al^{3+}	17.73	.02	18.19	.64	18.88	12.39	18.23	18.21	17.88	11.94
Fe^{3+}	.58	.67	1.43	.21	0.	0.	3.96	3.06	0.	1.35
Fe^{2+}	1.21	.67	1.01	.34	4.21	.94	4.59	3.14	1.80	.65
Mn^{2+}	.16	.06	.16	.06	.29	.02	.18	.11	.08	.22
Mg^{2+}	.43	.08	1.00	.34	.71	.04	6.56	4.58	.35	.06
Ca^{2+}	.53	.05	1.61	.51	1.28	.11	6.59	4.15	.44	.16
Na^{+}	10.07	.57	10.98	1.10	11.05	4.57	7.46	9.38	9.10	7.44
K^{+}	6.64	.41	5.84	.97	7.02	6.70	3.83	3.90	6.38	5.00
P^{5+}	.04	0.	.14	.07	.10	.02	2.14	.94	.08	.02
TOTAL	99.84	.01	99.81	.05	99.80	99.90	99.76	99.73	99.84	99.92
ANION EQUIVALENT:										
O^{2-}	162.37	.75	160.22	2.02	153.78	174.23	147.39	154.96	162.17	173.30
OH^{-}	1.84	.49	1.58	.73	4.95	3.03	14.45	5.51	5.69	.45
F^{-}	.58	0.	.52	.15	1.24	-.00	.59	-.00	.18	-.00
CALCULATED ANHYDROUS MAGMA DENSITIES (g cm^{-3}):										
PRESSURE: 1 bar										
1200 °C	2.35	.02	2.38	.01	2.43	2.30	2.59	2.50	2.35	2.32
1000 °C	2.37	.02	2.40	.01	2.45	2.32	2.62	2.53	2.38	2.33
800 °C	2.40	.02	2.42	.02	2.48	2.34	2.65	2.56	2.40	2.35
PRESSURE: 1 kbar										
1200 °C	2.36	.02	2.38	.01	2.43	2.31	2.59	2.50	2.36	2.32
1000 °C	2.38	.02	2.40	.01	2.46	2.33	2.62	2.53	2.38	2.34
800 °C	2.40	.02	2.43	.02	2.49	2.34	2.66	2.56	2.40	2.35

results, expressed in weight percent oxide, together with various ionic ratios and normative mineralogies, are listed in Table 5.1. Estimates of precision and accuracy are given in Appendix A1. Sample localities are marked on the map in Figure 5.1.

All the principal rock-types in the Hurdal area have been investigated. These include monzodiorite, biotite syenite, alkali feldspar syenite, quartz syenite, uneven microgranite, feldspar porphyritic microgranite, alkali feldspar granite (from both the Brennhaugen and Rustadkampen areas), aplitic microgranite, and various extrusive and dyke rocks. In addition, four samples of manganogranitoid, from the Steinbratebekken and Hegga river localities (Section 4.3), have been analysed. Average major element analyses of all the principal rock-types, together with calculated anhydrous magma densities, are listed in Table 5.2. The major element analyses have been recalculated in terms of cation percent for comparative purposes (see Section 1.5).

5.3 Theoretical considerations

The felsic rocks in the Hurdal area are largely composed of quartz and alkali feldspar with subordinate, but variable, amounts of plagioclase (Section 3.3). Ferromagnesian minerals such as amphibole, biotite and Fe-Ti oxides are generally formed late in the crystallisation sequence, occurring interstitially, and seldom constitute greater than 5 percent of the rock by volume. As such they would appear only to be of secondary importance as influences upon magma composition. This is reflected in the major element geochemistry by the fact that between 94 and 99 percent of the analysed cations are represented by Si, Al, Ca, Na and K (Table 5.2). The only exceptions are the monzodiorites (88 percent) and the manganogranitoids (89 percent). In addition, Ca constitutes less than 1.5 percent of the analysed cations in all but the least evolved rocks (monzodiorites; Table 5.2). The magmatic

evolution of the rocks in question may therefore be satisfactorily modelled by consideration of phase relationships in synthetic systems containing SiO_2, Al_2O_3, Na_2O and K_2O as the principal components. These are the components of the system: $NaAlSi_3O_8$ (albite) - $KAlSi_3O_8$ (orthoclase) - SiO_2 (quartz) - H_2O (Tuttle and Bowen 1958), which constitutes the silica-saturated part of the system: $NaAlSiO_4$ (nepheline) - $KAlSiO_4$ (kalsilite) - SiO_2 - H_2O (Hamilton and MacKenzie 1965).

Liquidus phase relationships for the water-saturated parts of these systems are illustrated in Figures 5.2a and 5.2b respectively. Figure 5.2a indicates that under conditions of constant pressure ($P_{TOTAL} = P_{H2O} = 1$ kbar), the liquidus surface dips down steeply from the SiO_2 apex to intersect the alkali feldspar liquidus surface at the field boundary. The latter separates the field in which quartz is the initial phase to crystallise from that in which a solid solution of alkali feldspar crystallises first (Carmichael et al. 1974). The minimum temperature on the boundary curve is the isobaric minimum, m. The composition of alkali feldspar in equilibrium with quartz and liquid at m is given by m'. The latter does not coincide with M, the minimum in the pseudobinary system $NaAlSi_3O_8$ - $KAlSi_3O_8$.

The curve M-q in Figure 5.2a is the unique fractionation curve. This is the locus of liquid compositions which cannot be crossed by any fractionating liquid developing out of the anorthoclase or sanidine fields and corresponds to a thermal valley (low temperature zone) in the system. In theory, fractionation of alkali feldspar from a liquid with an initial composition close to M will drive the residual liquid along a curved path, in T - X space, towards the liquidus at q, slightly displaced from the isobaric minimum, m.

Figure 5.2b indicates that liquids originating to the silica-undersaturated side of the feldspar join cannot evolve

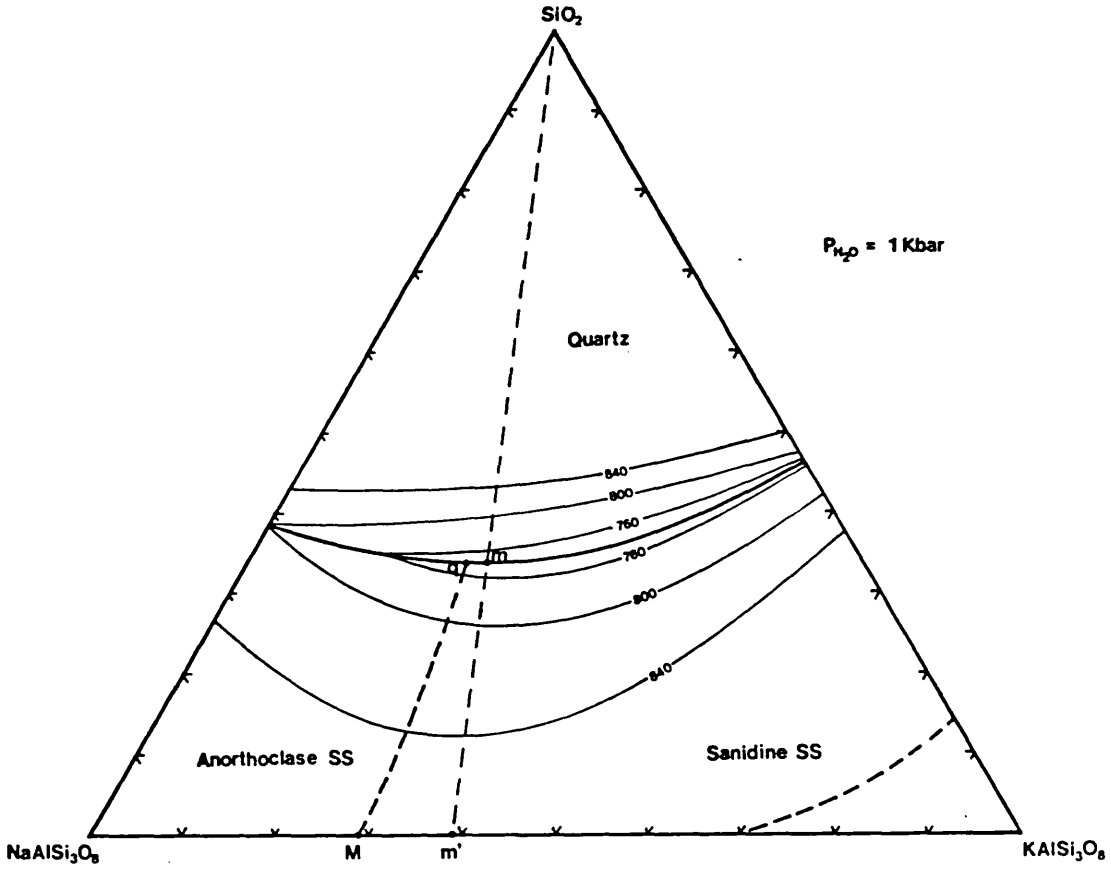

FIGURE 5.2a. The system: $NaAlSi_3O_8$ - $KAlSi_3O_8$ - SiO_2 - H_2O, P_{H2O} = 1 kbar (after Tuttle and Bowen 1958, Carmichael et al. 1974; cation %).

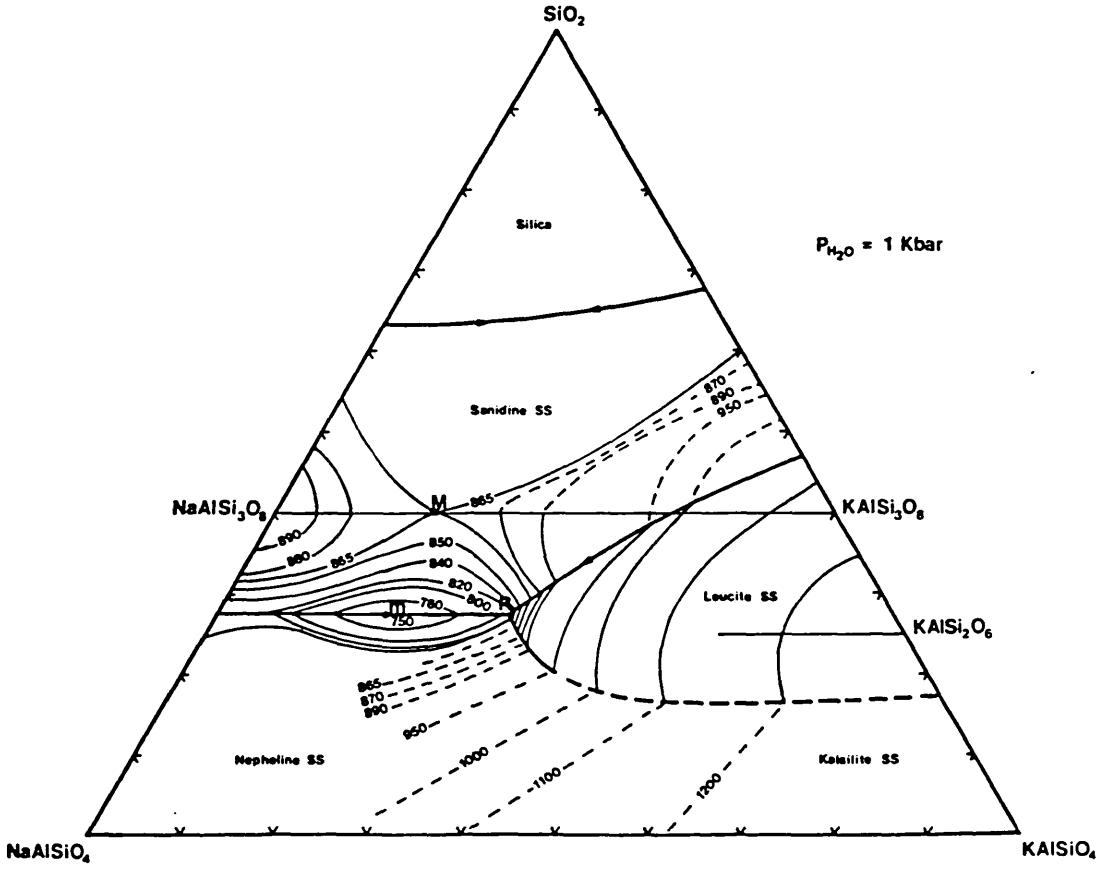

FIGURE 5.2b. The system: $NaAlSiO_4$ - $KAlSiO_4$ - SiO_2 - H_2O, P_{H2O} = 1 kbar (after Hamilton and MacKenzie 1965; cation %).

into the saturated field of syenites and granites, since the feldspar join represents an effective thermal divide at low pressures, under water saturated conditions.

Figure 5.3a indicates that under conditions of increasing confining pressure ($P_{TOTAL} = P_{H2O}$), the ternary minimum in the system $NaAlSi_3O_8$ - $KAlSi_3O_8$ - SiO_2 - H_2O migrates towards the albite apex. The unique fractionation curve, M-q in Figure 5.2a, migrates in a similar direction. At a pressure of 5 kbars, the liquidus surface intersects the alkali feldspar solvus, thereby promoting the simultaneous precipitation of two feldspars. Under these conditions, the minimum on the liquidus surface may be regarded as a ternary eutectic.

Whilst a general outline of magmatic evolution may be obtained by consideration of phase relationships in these systems, the exact positions in compositional space (SiO_2 - Al_2O_3 - Na_2O - K_2O - X) of isobaric minima, liquidus surfaces and "unique" fractionation curves may only be determined by examining the effects of additional components present in the magma (X, above). These include in particular H_2O, F and CO_2, but also CaO, Fe_2O_3 and FeO (together with any other major oxides present in the melt). Addition or subtraction of one or more of these components to or from the system may have considerable effects upon subsequent magmatic evolution. Similarly, the presence of alkalies in excess of aluminium may have significant effects upon liquidus phase relationships in these systems.

The principal effect of adding Ca to a granitic melt is to increase the temperature of the alkali feldspar solvus, thereby promoting the co-precipitation of two feldspars (Parsons 1978). Addition of anorthite to the systems described above is the basis of the granite tetrahedron (Carmichael et al. 1974, Winkler 1976). It is significant that the plutonic rocks in the Hurdal area are in general low

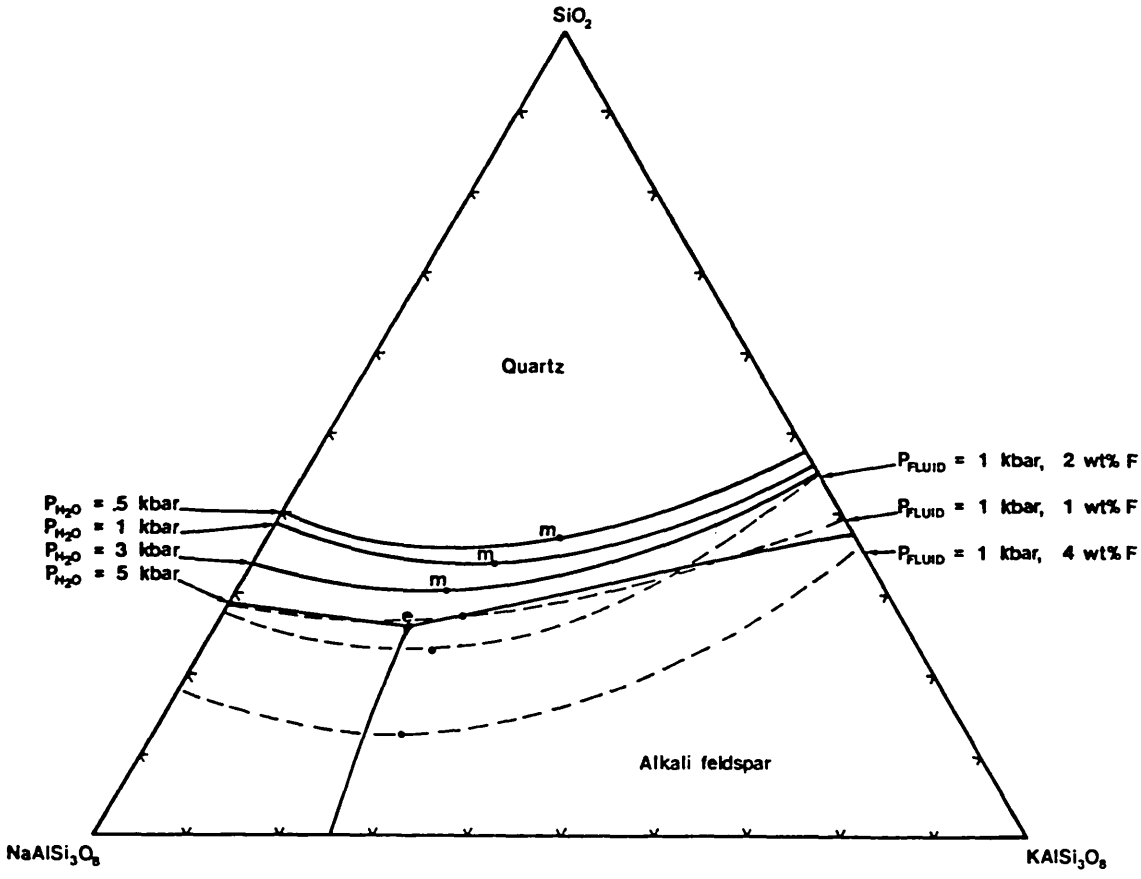

FIGURE 5.3a. The system: $NaAlSi_3O_8$ - $KAlSi_3O_8$ - SiO_2 - H_2O, P_{H2O} = 0.5 kbar, 1 kbar, 3 kbar and 5 kbar (after Tuttle and Bowen 1958, Carmichael et al. 1974); and P_{Fluid} = 1kbar, 1, 2 and 4 wt % F (Manning 1981; cation %).

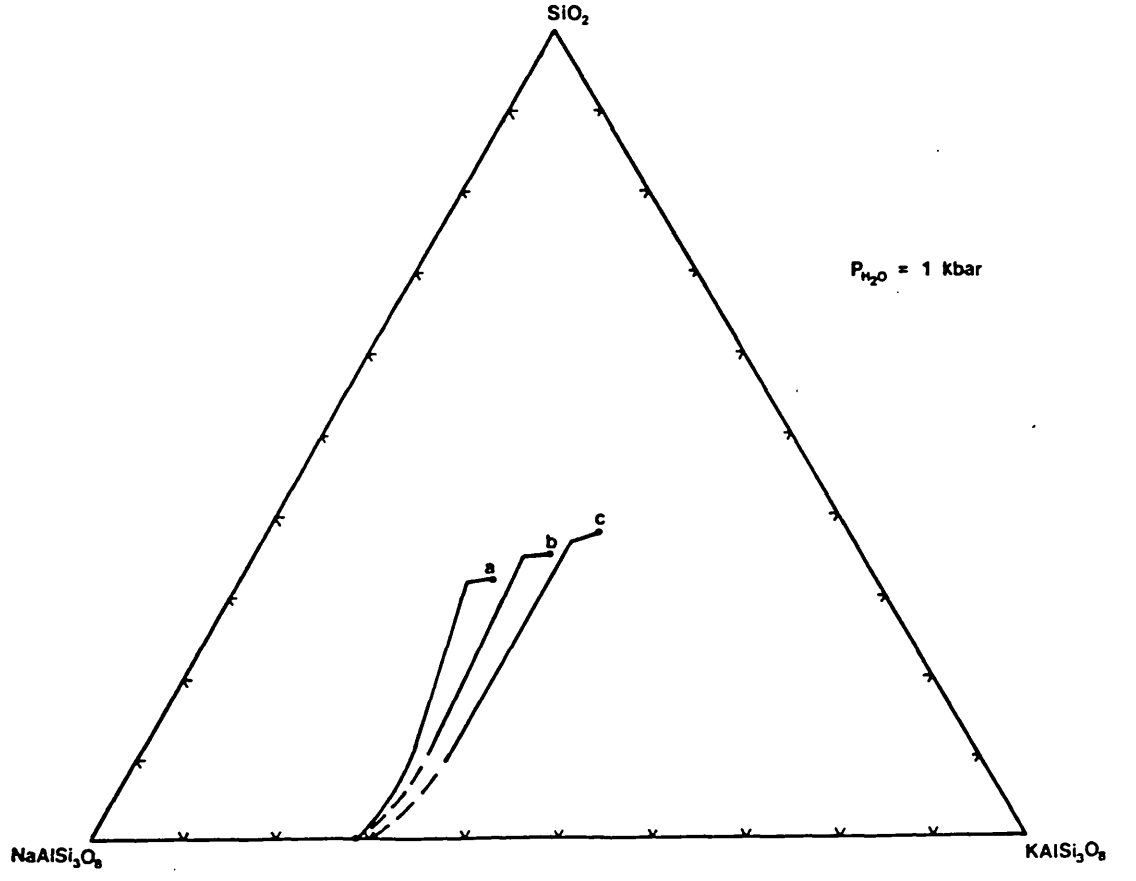

FIGURE 5.3b. The system: $NaAlSi_3O_8$ - $KAlSi_3O_8$ - SiO_2 - H_2O: (a) P_{H2O} = 1 kbar; (b) 4.3 wt % ac + 4.3 wt % ns; and (c) 8.3 wt % ac + 8.3 wt % ns (after Carmichael and MacKenzie 1963; cation %).

Ca rocks. They therefore contain only one feldpsar, having crystallised at temperatures above the solvus.

Manning (1981) has demonstrated that the effect of adding increasing amounts of fluorine to compositions in the system $NaAlSi_3O_8$ - $KAlSi_3O_8$ - SiO_2 - H_2O at constant pressure ($P_{TOTAL} = P_{H2O}$ = 1 kbar) is to drive the isobaric minimum towards the albite apex and to increase the field of primary quartz crystallisation (Figure 5.3a). It thereby has a similar effect to that of increasing pressure ($P_{H2O} = P_{TOTAL}$). One of the petrogenetic implications of this is that late stage enrichments in magmatic F may result in extremely Na-rich fluids. Albitisation is a common phenomenon in peralkaline granitic terrains (see for instance Bowden and Whitley 1974). Late stage enrichments in CO_2, in comparison, are likely to have a much less pronounced effect since carbon dioxide is strongly partitioned into the vapour phase, having a low solubility in silicate melts (Holloway 1976, Wyllie 1979).

Carmichael and MacKenzie (1963) have examined the effects of adding equal amounts of acmite ($NaFeSi_2O_6$) and sodium metasilicate (Na_2SiO_3) to compositions in the system $NaAlSi_3O_8$ - $KALSi_3O_8$ - SiO_2 - H_2O at constant pressure ($P_{TOTAL} = P_{H2O}$ = 1 kbar; Figure 5.3b). In addition, Thompson and Mackenzie (1967) have determined separately the effects of adding Na_2SiO_3, $NaFeSi_2O_6$, K_2SiO_3 and $NaKSiO_3$ to compositions in the same system under similar pressure conditions. One of the principal conclusions to be drawn from these experiments is that plotting the results in Q - Ab - Or compositional space provides ambiguous results due to the convention of calculating crystal/liquid composotions in terms of normative mineralogy (Bailey and Schairer 1964, Bailey 1974). This ignores the Ac and Ns components on the one hand, and calculates all K as orthoclase, disregarding biotite, on the other (see Appendix A2). Nevertheless the principal effect of adding Na in excess of aluminium to

compositions in this system is to drive the isobaric minimum towards the $KAlSi_3O_8$ - SiO_2 join, thereby favouring the crystallisation of albite over a wider range of compositions. Removal of K, the orthoclase effect of Bailey and Schairer (1964), has the same effect. Addition of K, on the otherhand, has the opposite effect.

Finally, attempts to model the magmatic evolution of a suite of granitic rocks such as those in the Hurdal area have to bear in mind that the so-called "isobaric" minima within these systems are not invariant points, but univariant curves or polyvariant surfaces, since P_{TOTAL} and P_{H2O} are also variables. It is therefore only conceivable to obtain a generalised picture of the P - T - X - P_{Fluid} path along which a magma has evolved.

5.4 Discussion of the results

The plutonic rock-types in the Hurdal area are mostly coarse-grained, phaneritic rocks and would appear to have consolidated directly from the magma. Whilst they have been subjected to considerable sub-solidus reorganisation, involving in particular exsolution of alkali feldspar, these effects would appear largely to have involved redistribution of Na and K as opposed to wholesale introduction of these elements from an external source. It is therefore reasonable to assume that the chemical analyses of the plutonic rocks listed in Tables 5.1 and 5.2 are representative of the original magma composition. Similarly, the analyses of the extrusive rocks may be regarded as approximate magma compositions, possibly allowing a small correction for phenocryst content. Extensive recrystallisation of extrusive rocks in the Styggberget area is believed to have been essentially isochemical, induced by thermal metamorphism in the aureole of the biotite syenite (Section 4.3.1).

All the plutonic rocks in the Hurdal area are quartz

normative with the exception of the monzodiorites (M1 and M2; Table 5.1) which contain minor amounts of normative olivine ± nepheline, and the manganogranitoids which contain normative olivine. In addition, a dolerite dyke from the Nordgardshogda area (N4ØØ) contains normative olivine. Among the extrusive rocks, only the trachyandesite (N219A) is undersaturated with respect to silica, containing normative nepheline.

The quartz content of the plutonic rocks increases from 2 to 4 cation % in the biotite syenite, through 4 to 15 % in the alkali feldspar syenite, 9 to 35 % in the quartz syenite and related rocks, up to 25 to 36 % in the alkali feldspar granite (Table 5.1). There is therefore a certain amount of overlap between the principal rock-types. These relationships are illustrated with reference to Q - Ab - Or compositional space in Figure 5.4, and will be discussed in greater detail in Section 5.5. Samples WW11 and W63 have been silicified (at the expense of Na).

The major elements all show fairly simple relationships with differentiation index (D.I. = normative Q + Or + Ab + Ne + Ks, expressed in cation %; Figure 5.5 a to j). Silicon and oxygen (not illustrated) both increase with differentiation index, showing rapid increases at the felsic end. In contrast Ti, Al, Fe^{3+} + Fe^{2+} + Mg, Ca and P all decrease during fractionation. Total alkalies, Na + K, increase until the quartz syenite stage of evolution, but then show a rapid reversal, marking the changeover from plagioclase to alkali feldspar fractionation. Among the major cations, only Mn behaves irregularly, being at a maximum in the biotite syenite and showing large variations in the alkali feldspar granite (Figure 5.5e; the manganogranitoids have been excluded from this plot, containing on average 7.89 cation percent Mn). Among the major anions, structurally bound hydroxyl (estimated from loss on ignition) and F show no clear relationships with differentiation index. Fluorine, however, is at a maximum in the biotite syenite and

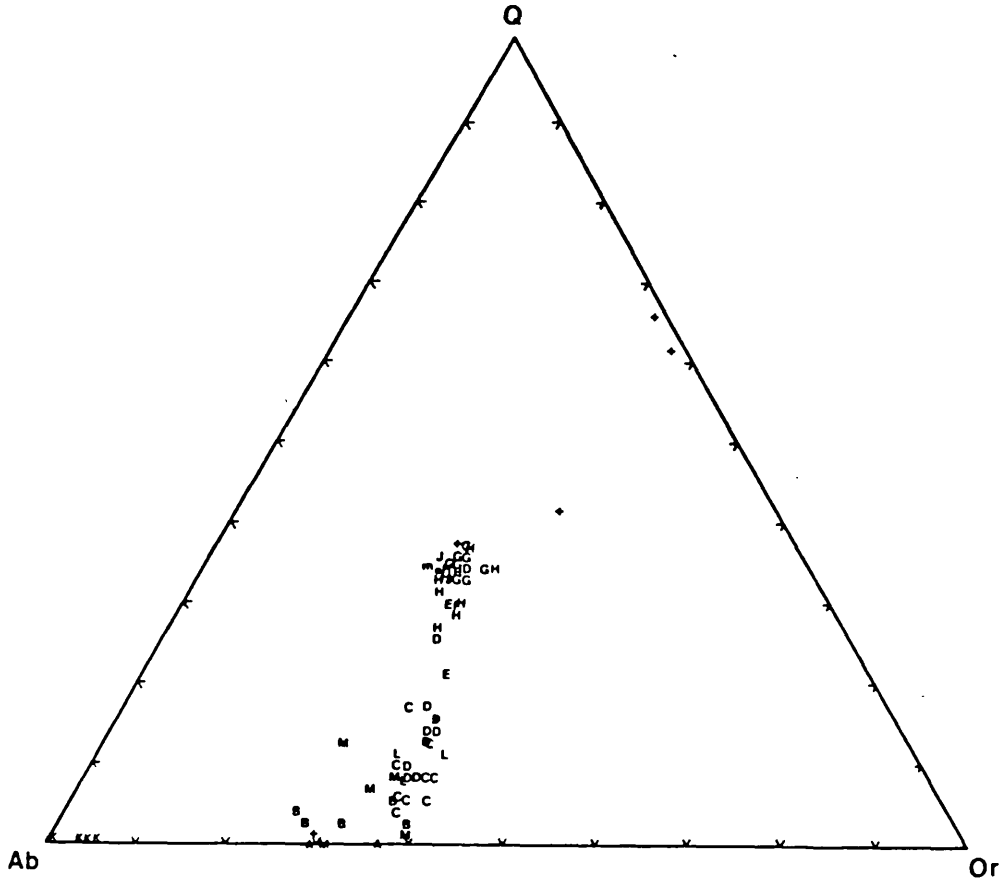

FIGURE 5.4. Normative Ab - Or - Q (cation %), Hurdal area. Symbols: A = Monzodiorite; B = Biotite syenite; C = Alkali feldspar syenite; D = Quartz syenite; E = Uneven microgranite; F = Feldspar porphyrititic microgranite; G = Alkali feldspar granite (Brennhaugen); H = Alkali feldspar granite (Rustadkampen); J = Aplitic microgranite; K = Manganogranitoid; L = Trachyte 1 (Nordgardshogda - Styggberget area); M = Trachyte 2 (Kongeliveien area).

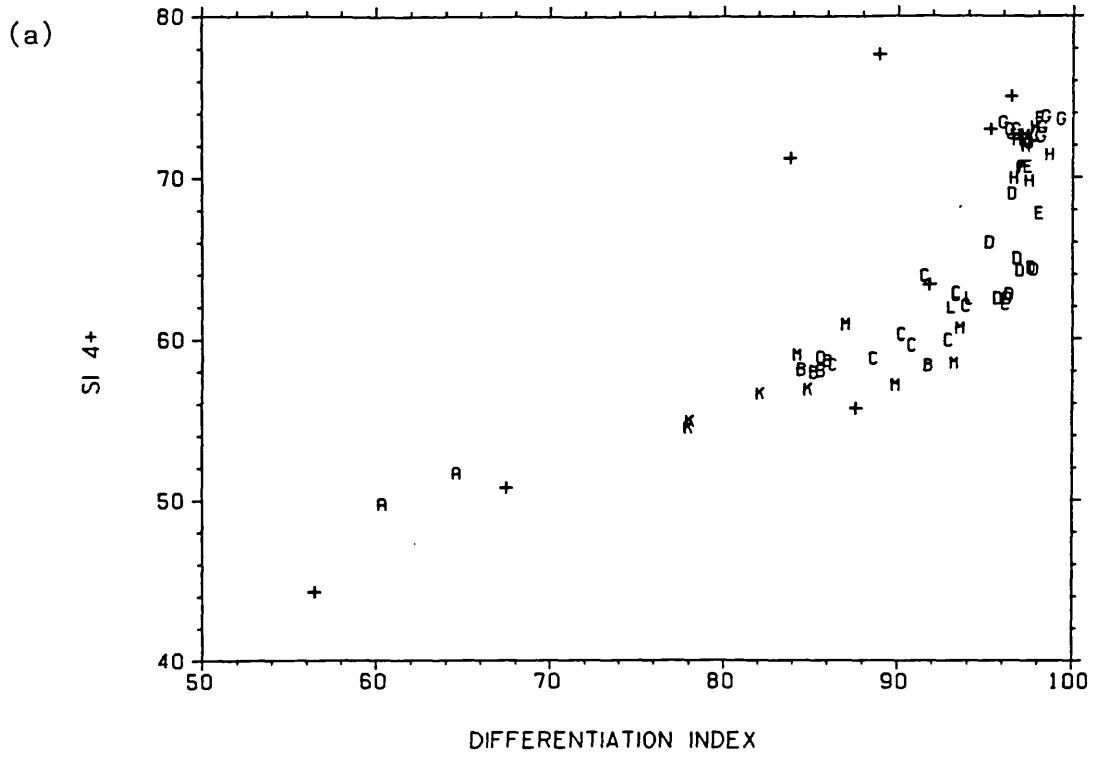

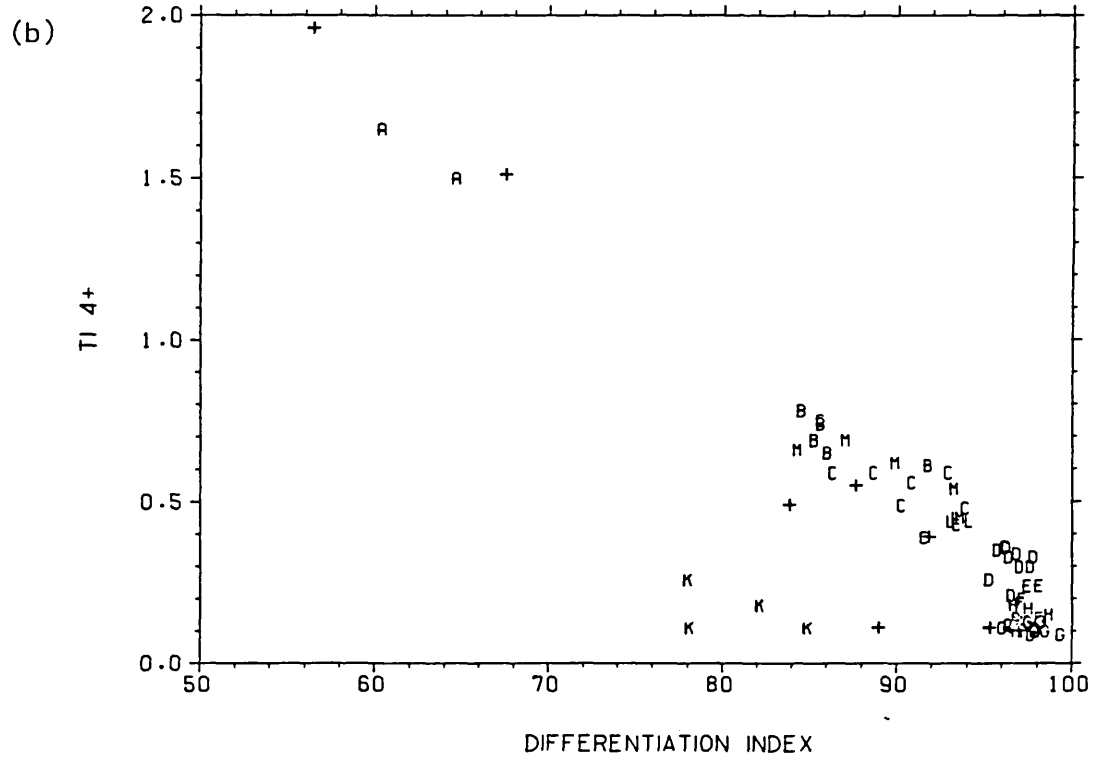

FIGURE 5.5. Scatter plots (cation %) of Differentiation Index (D.I. = normative Q + Or + Ab + Ne + Ks) versus: (a) Si^{4+}; (b) Ti^{4+}; (c) Al^{3+}; (d) $Mg+Fe^{3+}+Fe^{2+}$; (e) Mn^{2+}; (f) Ca^{2+}; (g) $Na^{+}+K^{+}$; (h) P^{5+}; (i) OH^{-}; and (j) F^{-}. Symbols as in Figure 5.4.

(c)

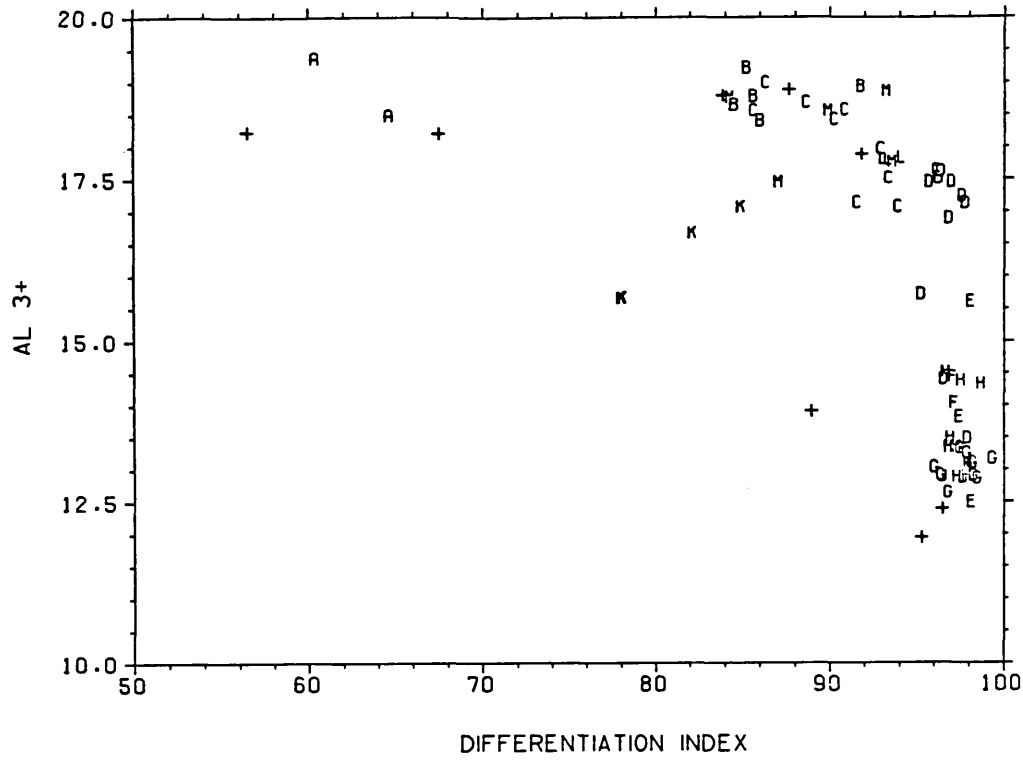
20.0
17.5
15.0
12.5
10.0
AL 3+
50
60
70
80
90
100
DIFFERENTIATION INDEX

(d)

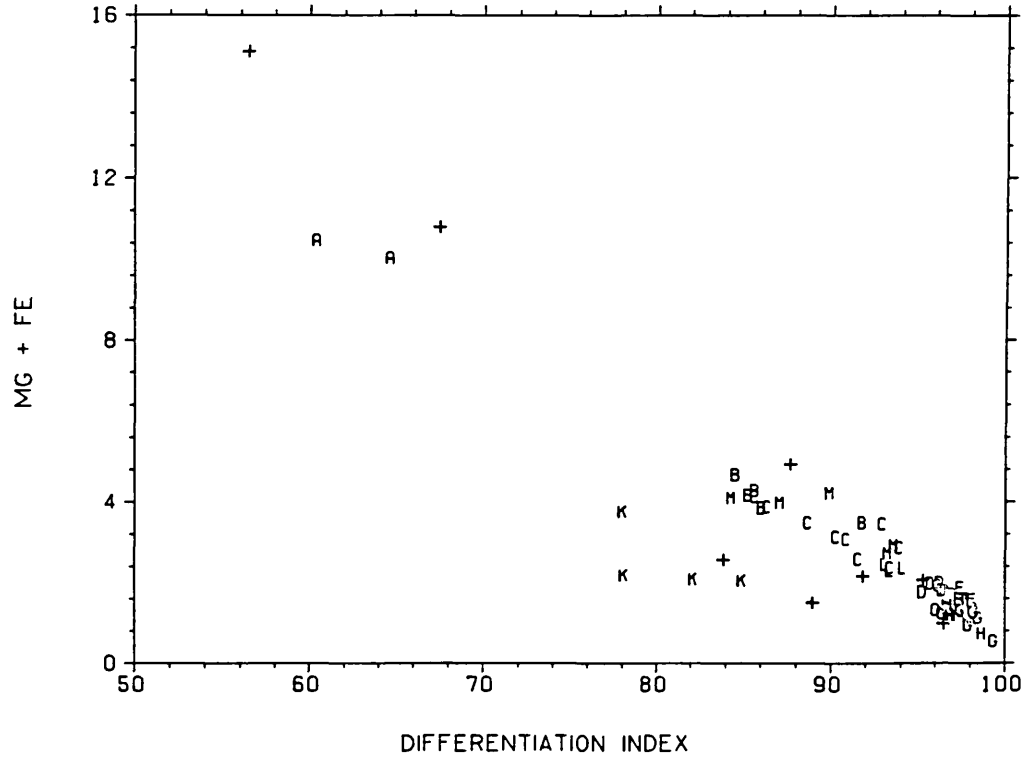
16
12
8
4
0
MG + FE
50
60
70
80
90
100
DIFFERENTIATION INDEX

(e)

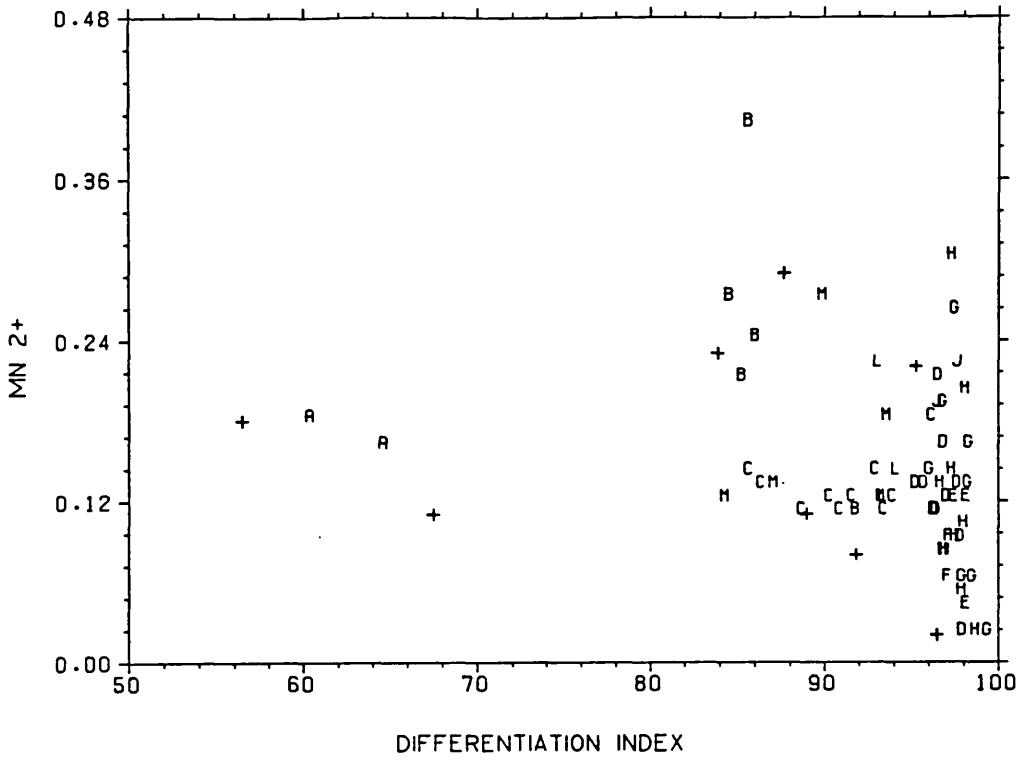
0.48
0.36
0.24
0.12
0.00
MN 2+
50
60
70
80
90
100
DIFFERENTIATION INDEX

(f)

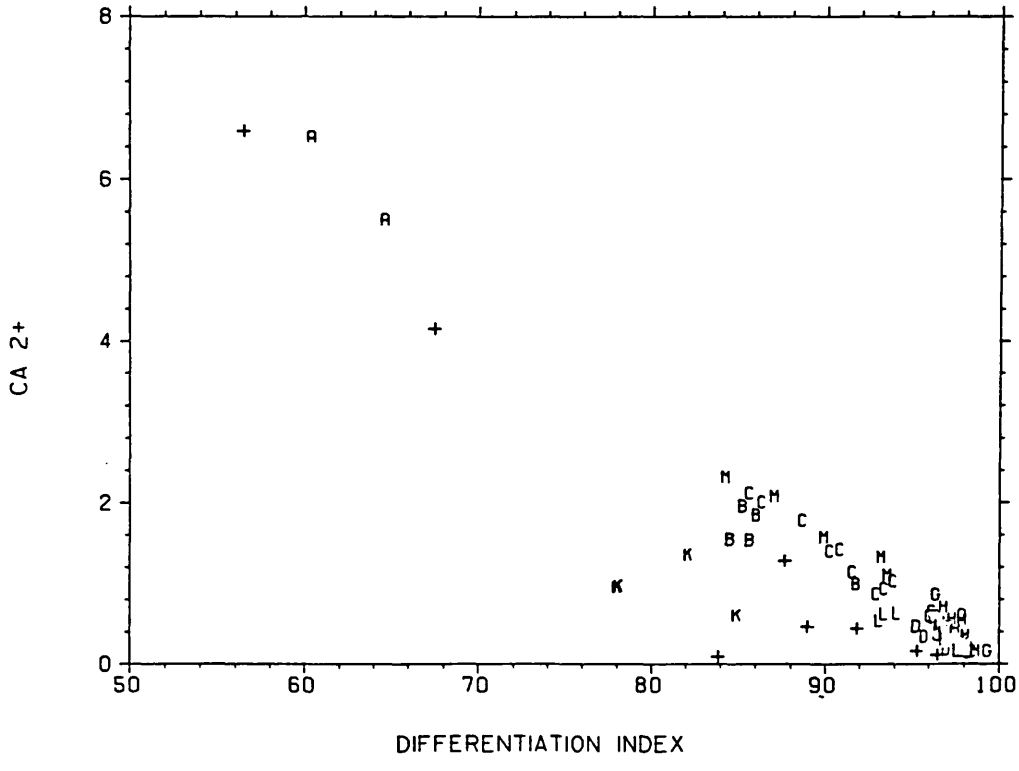
8
6
4
2
0
CA 2+
50
60
70
80
90
100
DIFFERENTIATION INDEX

(g)

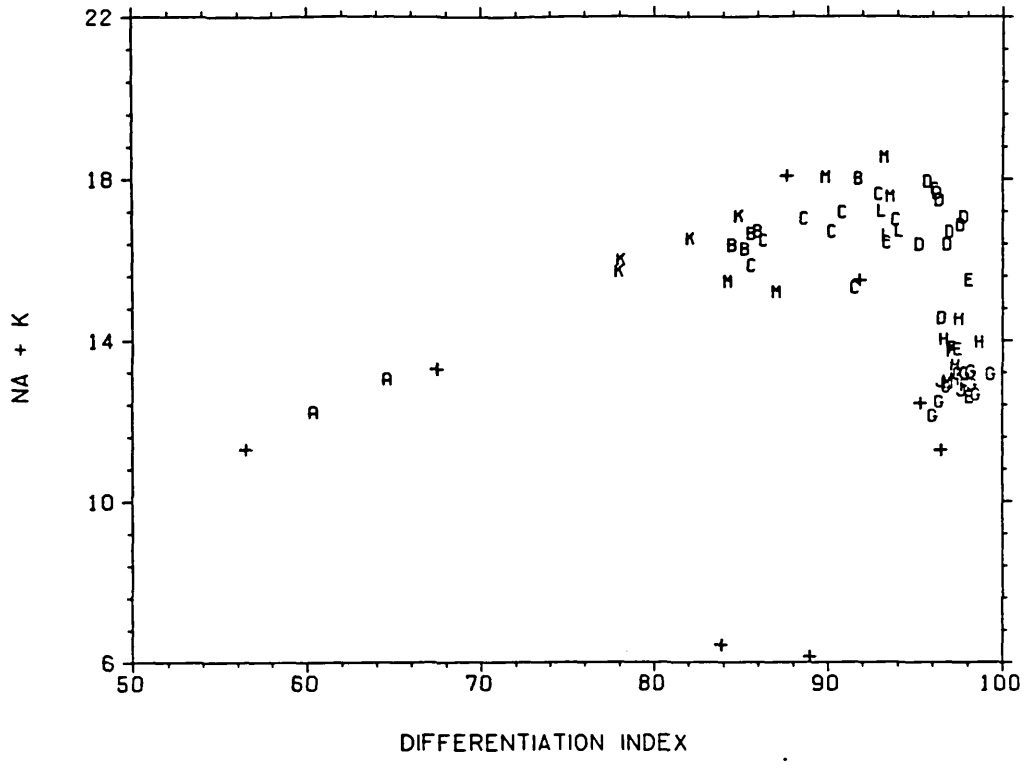
22
18
14
10
6
NA + K
50
60
70
80
90
100
DIFFERENTIATION INDEX

(h)

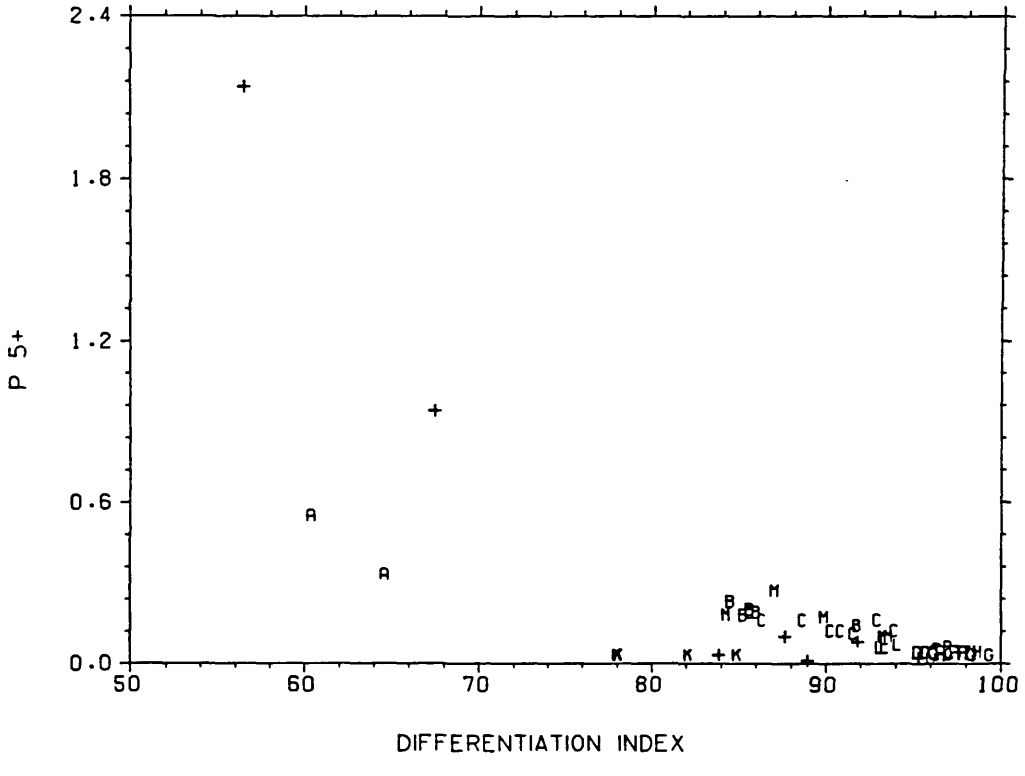
2.4
1.8
1.2
0.6
0.0
P 5+
50
60
70
80
90
100
DIFFERENTIATION INDEX

(i)

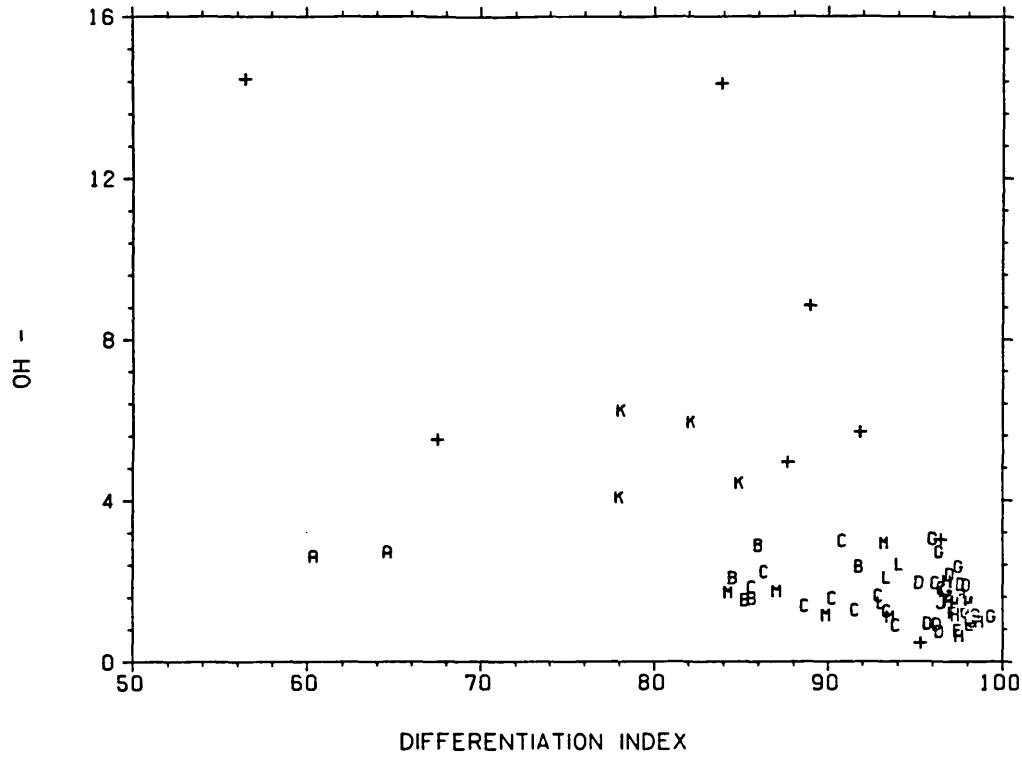
16
12
8
4
0
OH -
50
60
70
80
90
100
DIFFERENTIATION INDEX

(j)

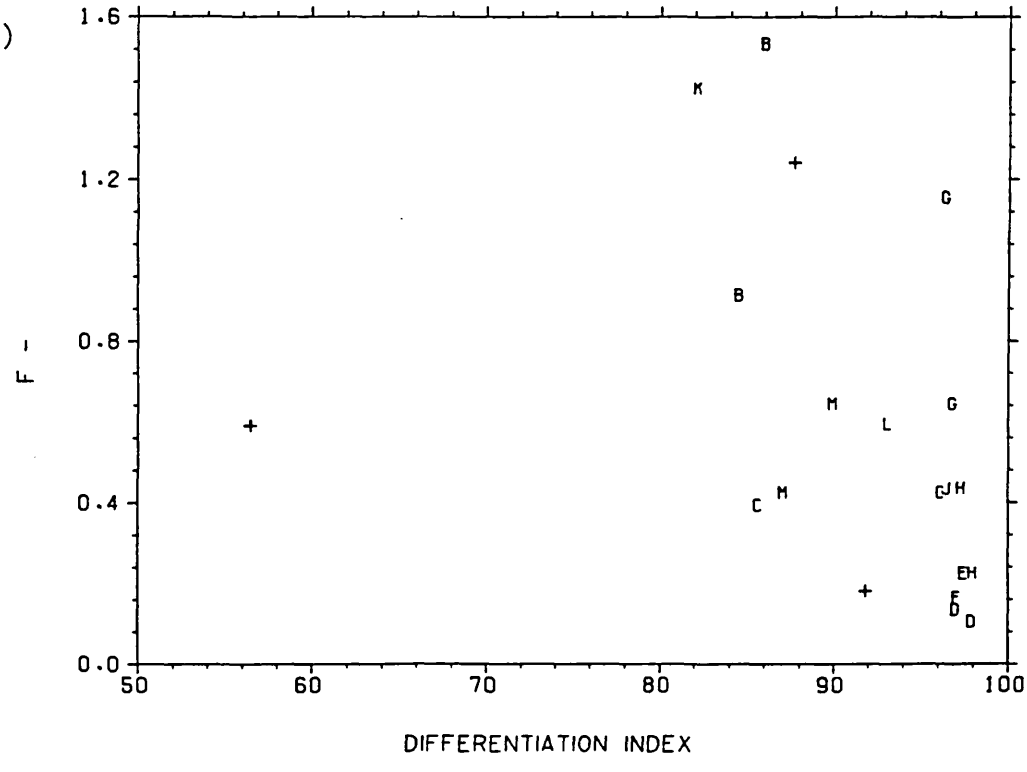
1.6
1.2
0.8
0.4
0.0
F -
50
60
70
80
90
100
DIFFERENTIATION INDEX

manganese-rich rocks (manganogranitoids; Section 4.3.3).

The agpaitic index, Na+K/Al, shows a fairly linear relationship with differentiation index (Figure 5.6a), increasing from a minimum (Ø.63) in the monzodiorites to level off at approximately 1.ØØ (± .Ø2) in the quartz syenites and alkali feldspar granites, these rocks being exactly peralkaline. At the same time, the ratio of Na to total alkalies, Na/Na+K, decreases from a maximum (Ø.7Ø) to level off at approximately Ø.6Ø (± .Ø2) (Figure 5.6b). Only the biotite syenites and manganogranitoids behave differently, showing enrichment in Na relative to K (up to .72 and .99 respectively; Table 5.1). These rocks also tend to have the highest F contents (Figure 5.5j) and lowest OH/F ratios (Table 5.1). In comparison, the (Na+K)/(Al-2Ca) ratios of these rocks (agpaitic index corrected for the amount of aluminium in plagioclase, making the assumption that all Ca is incorporated in plagioclase) decrease from a maximum in the monzodiorites and related rocks to level off at approximately 1.Ø (Figure 5.6c).

The relationship between Na/Na+K and agpaitic index is illustrated in Figure 5.7a. The main conclusion which may be obtained from this diagram is that magmatic evolution was controlled by early fractionation of plagioclase, followed by separation of alkali feldspar of more or less constant composition ($Ab_{6Ø}$). A similar conclusion was reached on the basis of mineralogical evidence in Section 3.5.1. Separation of alkali feldspar has no effect upon agpaitic index. Consideration of Figure 5.6c, however, indicates that early magmatic evolution was also controlled by a Ca-bearing phase other than plagioclase (Na+K/(Al-2Ca) . 1). On the basis of mineralogical evidence (Section 3.3.1), this is identified as clinopyroxene. The relationship between Na/Na+K and F content is illustrated in Figure 5.7b.

The ratio of Mg to Mg plus total Fe, $Mg/Mg+Fe^{3+}+Fe^{2+}$,

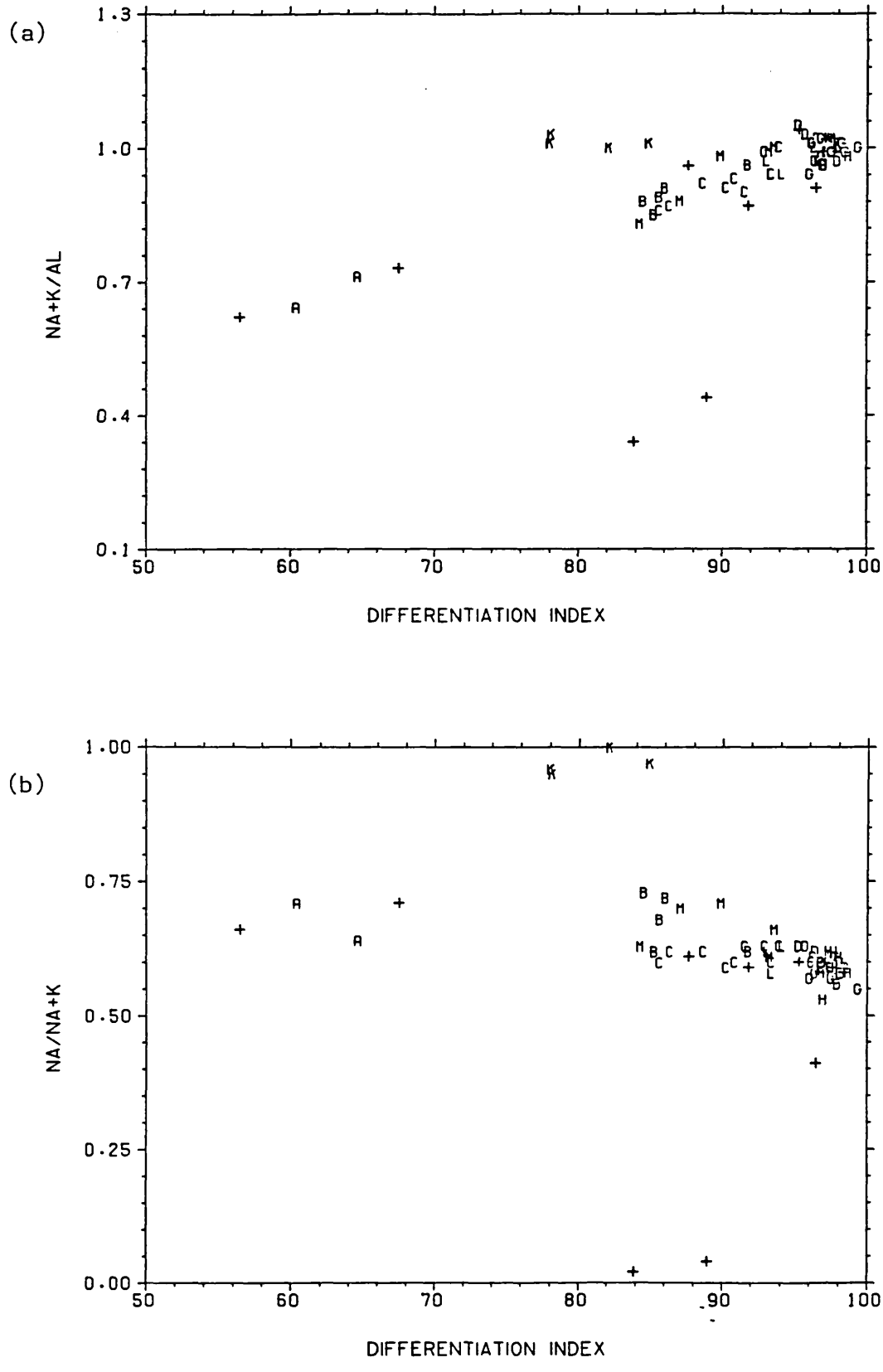

FIGURE 5.6. Scatter plots (cation %) of Differentiation Index versus: (a) Na+K/Al; (b) Na/Na+K; and (c) Na+K/(Al-2Ca). Symbols as in Figure 5.4.

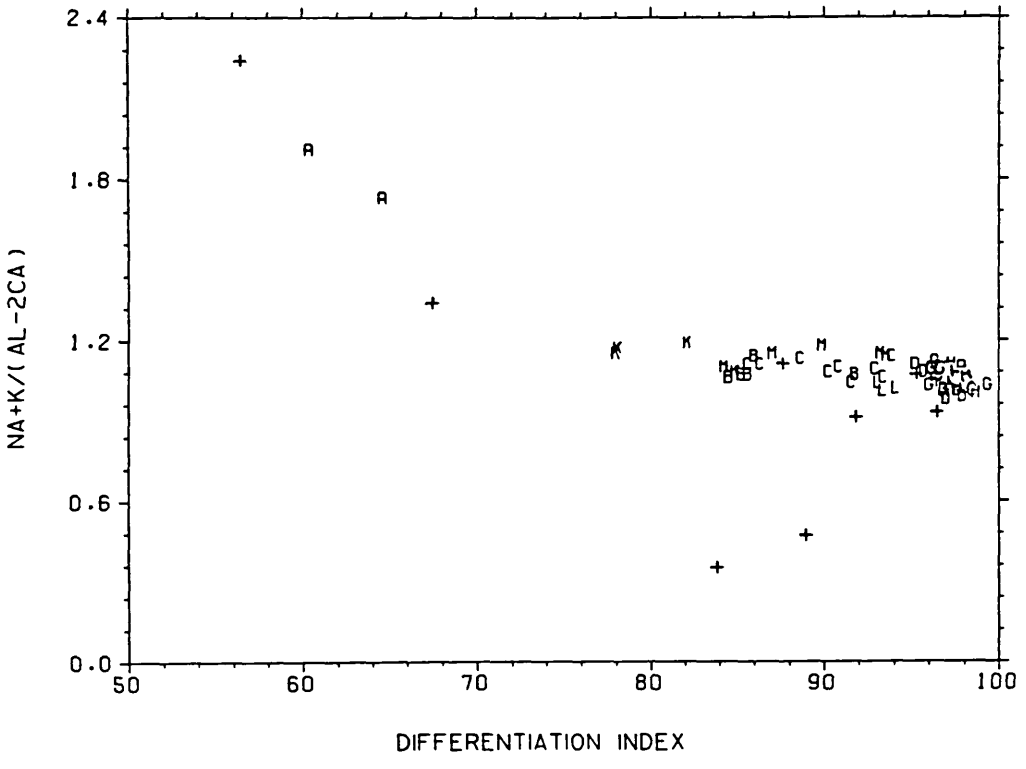
2.4
1.8
1.2
0.6
0.0
NA+K/(AL-2CA)
50
60
70
80
90
100
DIFFERENTIATION INDEX

FIGURE 5.6c.

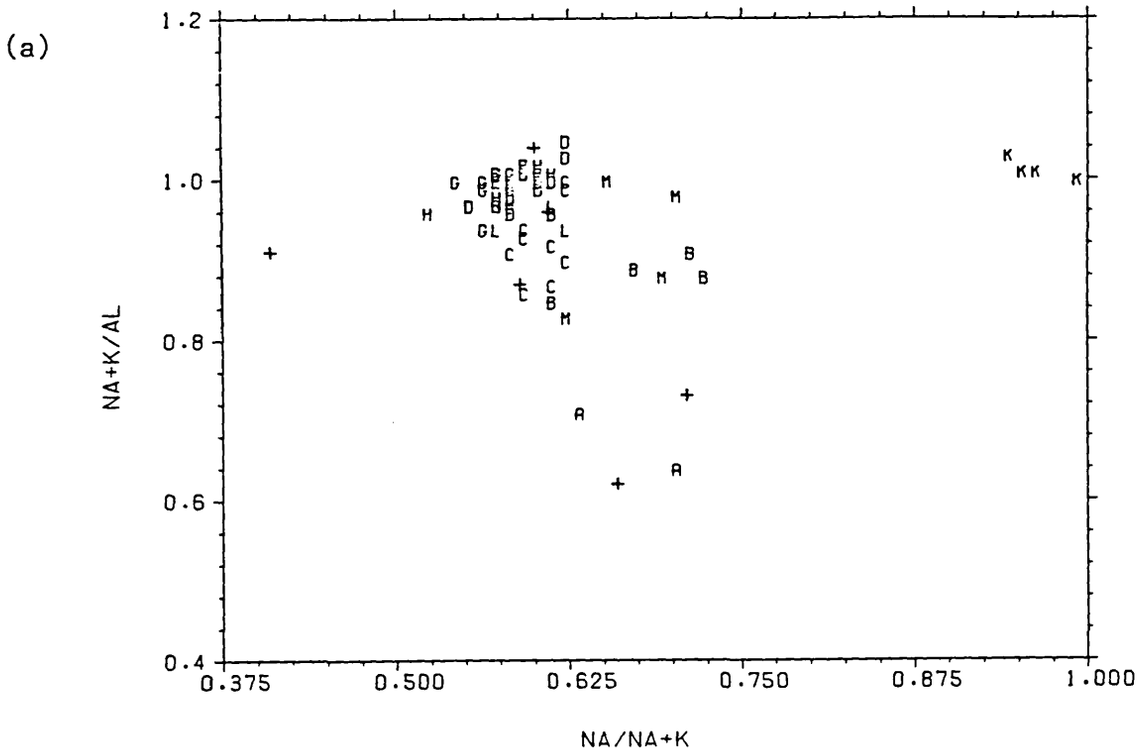

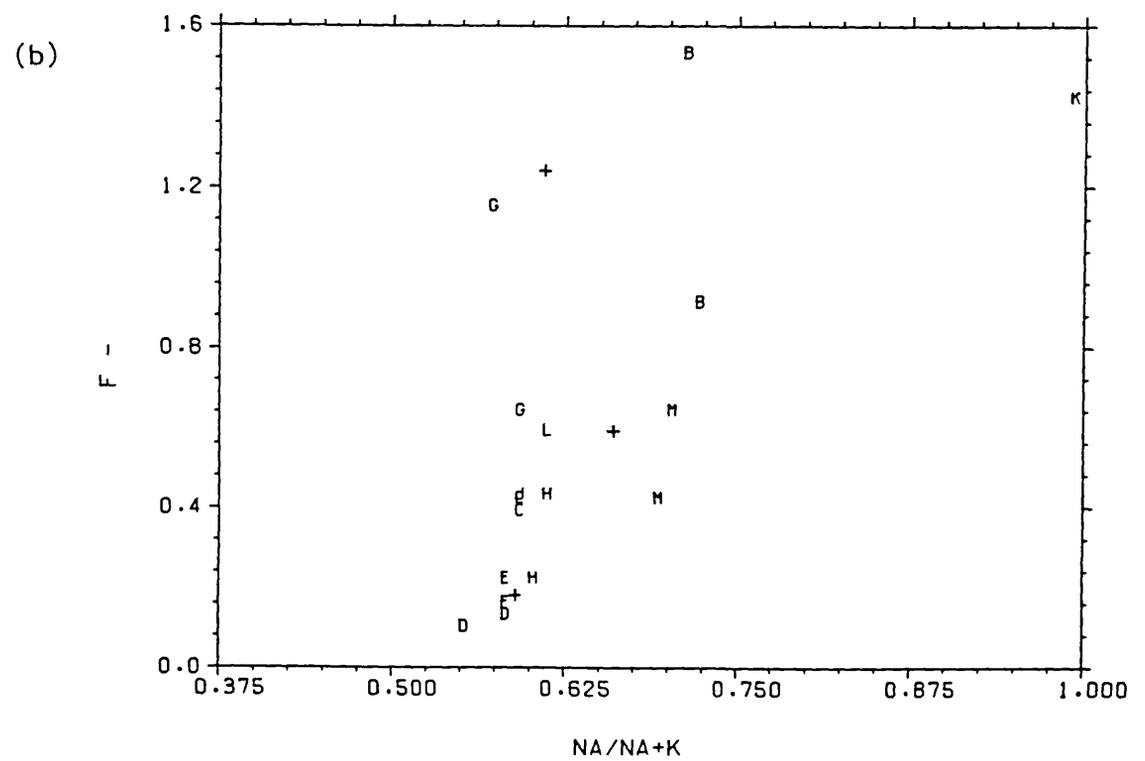

FIGURE 5.7. Scatter plots (cation %) of Na/Na+K versus: (a) Na+K/Al; and (b) F^-. Symbols as in Figure 5.4.

decreases from a maximum in the monzodiorites and related rocks (.43 in the dolerite dyke N4ØØ) to as low as .Ø2 in the quartz syenites and alkali feldspar granites (Figure 5.8a). This is matched by a corresponding decrease in the absolute amount of these elements ($Mg+Fe^{3+}+Fe^{2+}$; Figure 5.5d), and indicates a decline in the importance of ferromagnesian minerals in these rocks. In contrast, the ratio of Mn to Mg plus total Fe, $Mn/Mg+Fe^{3+}+Fe^{2+}$, increases by a factor of two to three times in the more granitic end-members (Figure 5.8b). This is reflected in the mineralogy by strong partitioning of Mn into biotite (Section 3.5.1).

The ratio of Fe^{3+} to total Fe, $Fe^{3+}/Fe^{2+}+Fe^{2+}$, increases from approximately .25 in the monzodiorites to approximately 1.ØØ in the quartz syenites, indicating a change towards more oxidising conditions (Figure 5.8c). The more evolved granitic rocks, in comparison, appear to show a trend towards more reducing conditions. The oxidation state of Fe must, however, be treated with caution, since all these rocks have been subjected to subaerial weathering.

The extremely variable behaviour of Mn in the alkali feldspar granite (Figure 5.5e) is presumably the result of late stage magmatic and/or metasomatic processes, inducing redistribution of this element. A strong correlation between Mn and F contents (Figure 5.9) suggests that fluorine-rich liquids were responsible. Build-up of magmatic fluorine in the biotite syenite and alkali feldspar granite stages of evolution is indicated by low OH/F ratios for these rocks (Table 5.1), and by the high F contents of hydrous mineral phases (Section 3.5.1). The quartz syenite stage of evolution, on the other hand, is characterised by high OH/F ratios, indicating much lower fluorine activity.

5.5 Magmatic evolution

Comparison between Tables 2.2 and 5.2 indicates that the

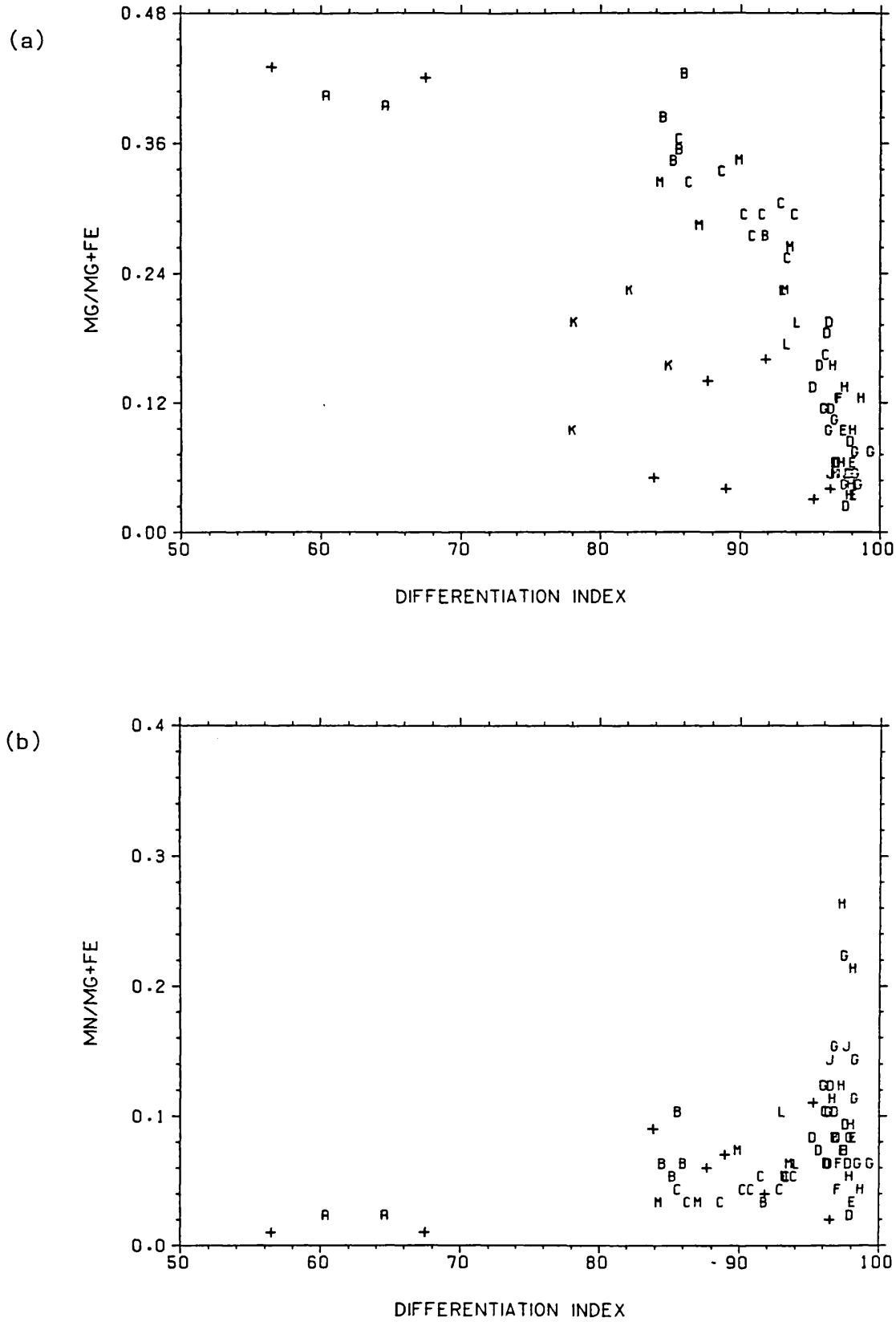

FIGURE 5.8. Scatter plots (cation %) of Differentiation Index versus: (a) $Mg/Mg+Fe^{3+}+Fe^{2+}$; (b) $Mn/Mg+Fe^{3+}+Fe^{2+}$; and (c) $Fe^{3+}/Fe^{3+}+Fe^{2+}$. Symbols as in Figure 5.4.

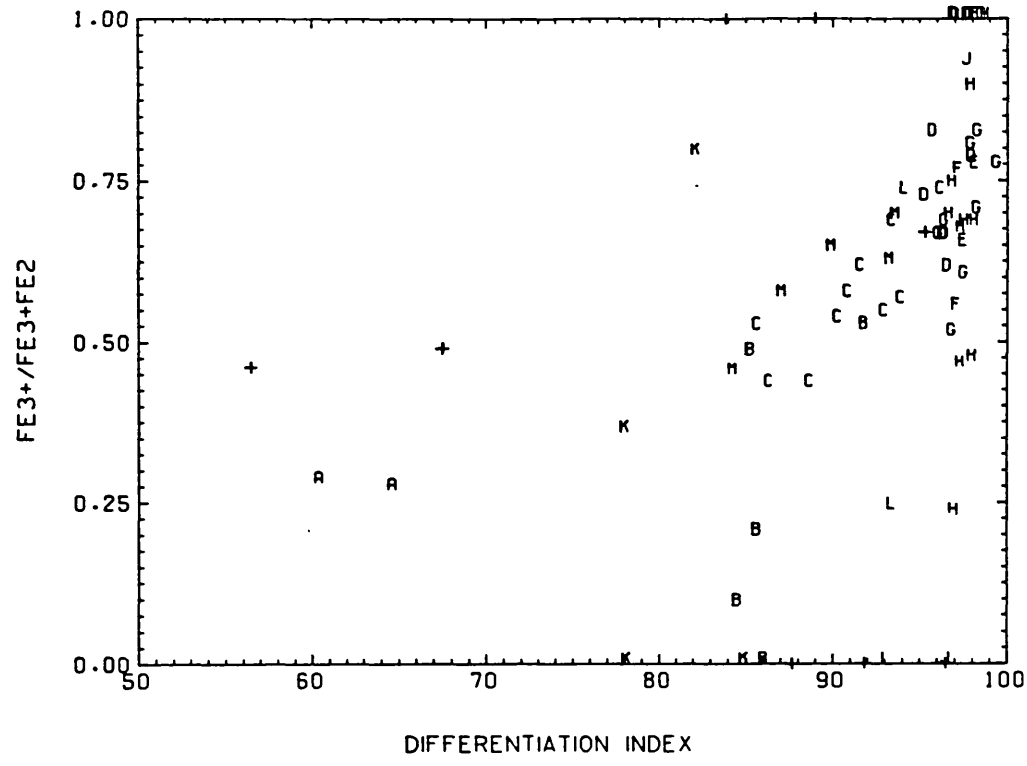

FIGURE 5.8c.

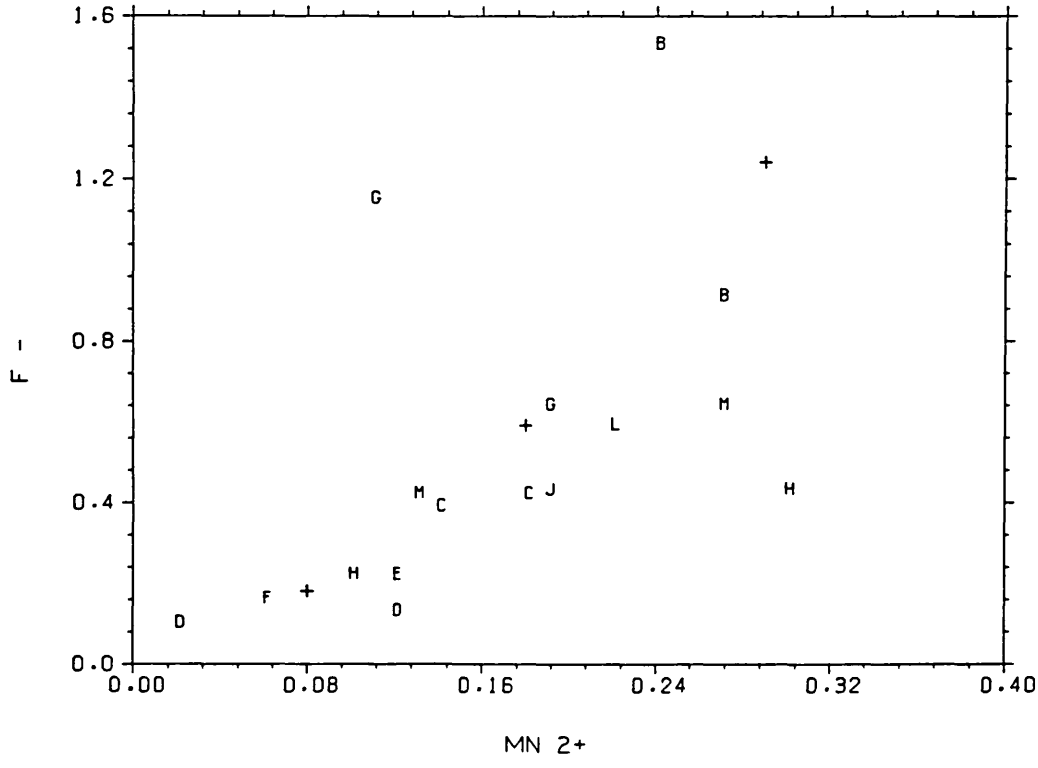

FIGURE 5.9. Scatter plot (cation %) of Mn^{2+} vs. F^-. Symbols as in Figure 5.4.

principal plutonic rock-types in the Hurdal area are similar in terms of major element geochemistry to other plutonic rocks observed within the Region (including the Drammen Granite). They are not however identical, differing in absolute amounts of Na + K, Ca, Si and Al. These differences partly reflect differences in analytical accuracy, but are mainly the result of separate paths of crystal/liquid evolution, reflecting different P - T - P_{Fluid} - fO_2 paths on ascent through the crust.

The magmatic evolution of intermediate to granitic rocks in the Hurdal area may be summarised as follows. Early magmatic evolution, corresponding to the compositional interval between monzodiorite and biotite syenite, was controlled by fractionation of clinopyroxene and plagioclase of initial composition An_{30} - An_{50} (Sections 2.5.3 and 3.3.1). Subsequent evolution, corresponding to compositions in the range biotite syenite - quartz syenite, was predominantly controlled by fractionation of plagioclase of increasingly sodic composition, accompanied by separation of alkali feldspar of constant composition (Ab_{60}; Sections 3.5.1 and 5.4). The final stages of evolution, responsible for compositions in the range quartz syenite - alkali feldspar granite, were controlled by separation of alkali feldspar alone, early fractionation of plagioclase having removed the magma from the compositional field in which two feldspars crystallise.

These relationships are illustrated with reference to an Al-(Na+K)-Ca variation diagram in Figure 5.10a, and in schematic form in Figure 5.10b. Development of the peralkaline condition in these rocks (Na+K/Al > 1) is largely the result of plagioclase fractionation (the plagioclase effect of Bowen 1945). Separation of clinopyroxene, plotting close to the Ca apex, has had little effect on agpaitic index. In contrast, the orthoclase effect of Bailey and Schairer (1964) has not been operative in this system.

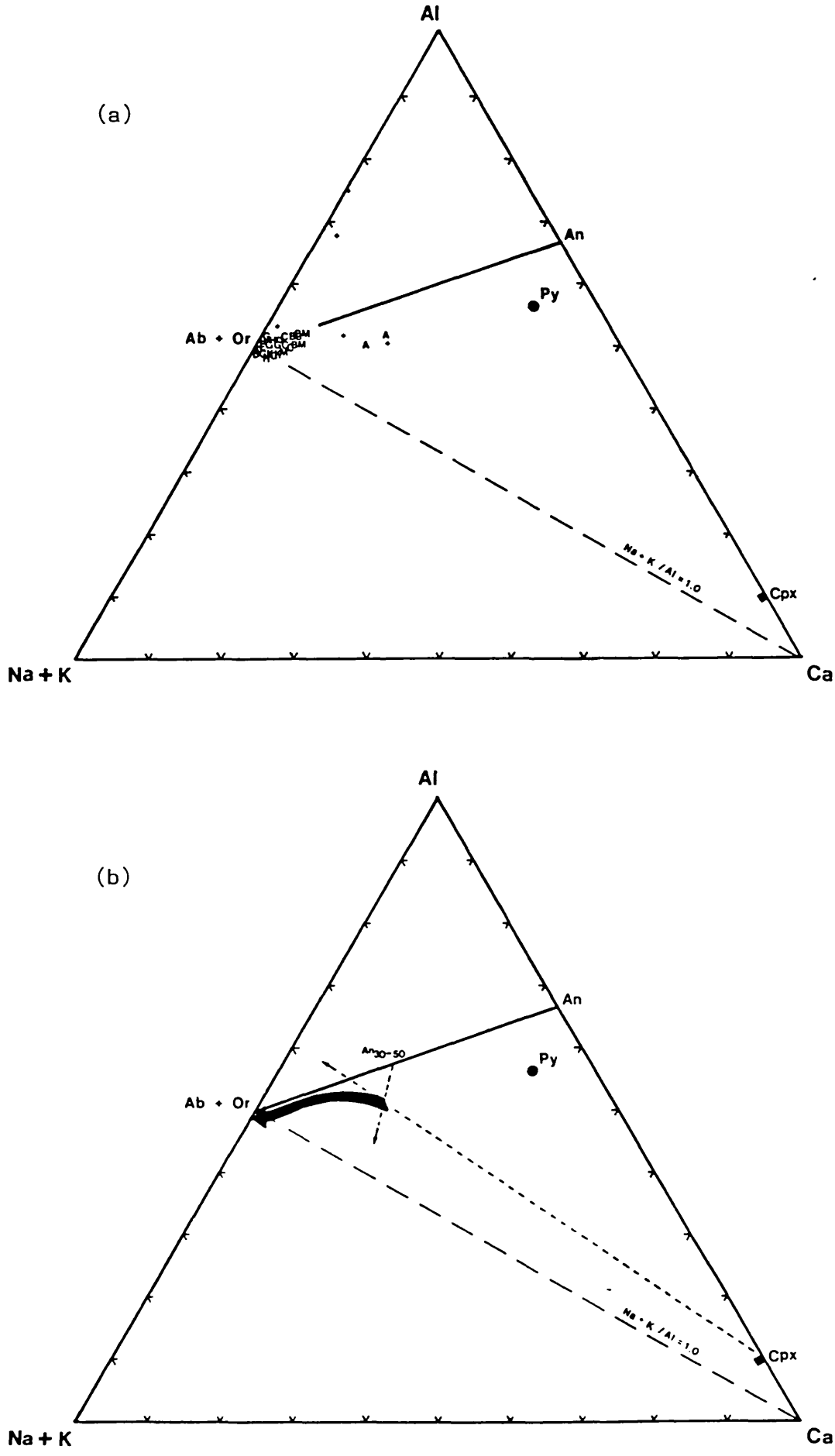

FIGURE 5.1Ø. Al-(Na+K)-Ca variation diagram (cation %), Hurdal area: (a) Data points; and (b) schematic form. Symbols as in Figure 5.4.

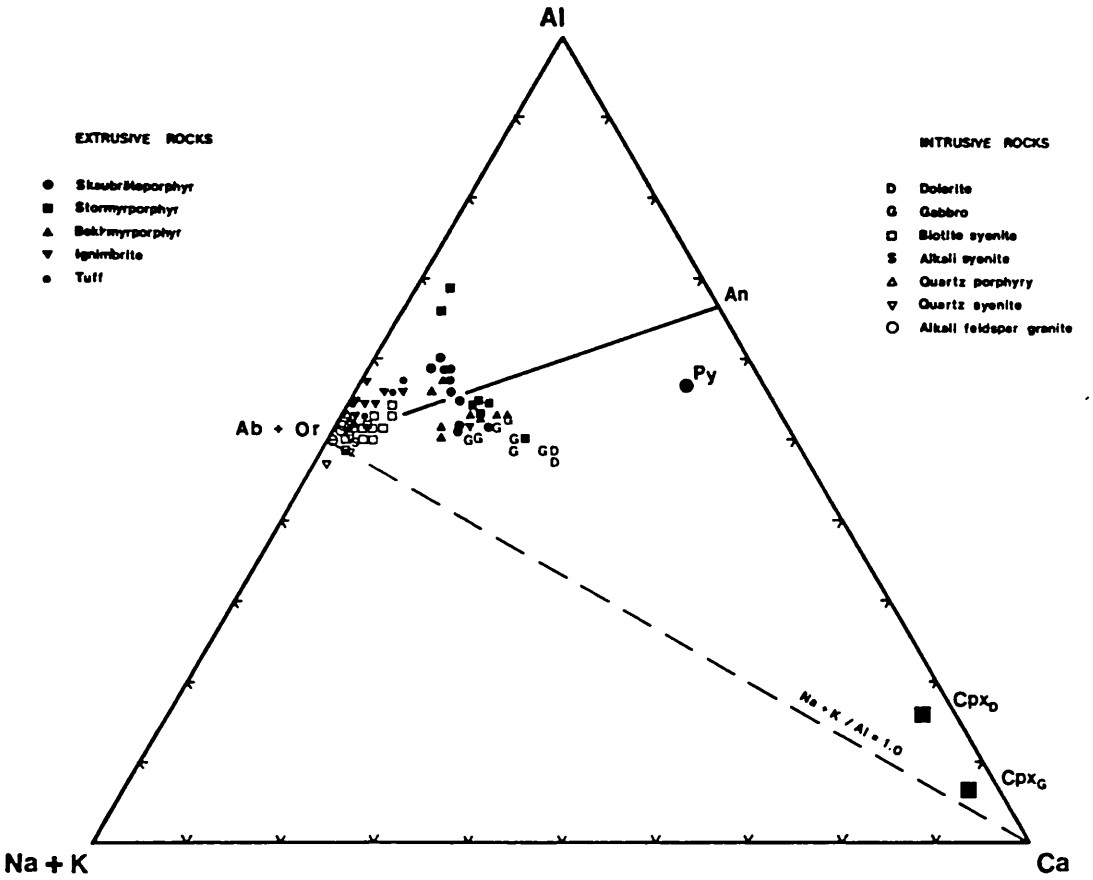

FIGURE 5.11. Al-(Na+K)-Ca variation diagram (cation %), Svartjern (from Rasmussen 1982).

Late-stage enrichments in Na/Na+K in the biotite syenite and manganogranitoids (Figure 5.7a) are attributed to increased fluorine activity in the melt (Figure 5.7b).

The felsic rocks in the Hurdal area were therefore derived from more mafic precursors essentially by fractionation of clinopyroxene, plagioclase and alkali feldspar. Compositionally similar intrusive rocks in the Svartjern area (Rasmussen 1982) would appear to have been derived by similar processes (Figure 5.11). Gabbroic rocks in the Svartjern area could provide the logical parent to felsic rocks in this part of the Region. The fact that these gabbroic rocks contain both normative clinopyroxene and orthopyroxene (Table 2.2), might suggest tholeiitic lines of descent. However, the predominance of clinopyroxene fractionation in the early stages of evolution in the Hurdal area is more compatible with a derivation by differentiation of alkali basaltic magmas. But this requires confirmation from trace element geochemistry (Chapter 6).

The later stages of evolution in the Hurdal area may be modelled with reference to phase relationships in the synthetic system $NaAlSi_3O_8$ - $KAlSi_3O_8$ - SiO_2 - X, where X equals other components present in minor amounts in the system (in particular H_2O, CO_2, and F; Section 5.3). Compositions of plutonic and associated extrusive rocks plot along a curved path developing out of the Ab-Or join at Ab_{70} and culminating close to the minimum at 1 kbar water-saturated conditions (Figure 5.4). The position of the fractionation curve does not, however, coincide with the thermal valley in the system under the same pressure conditions, but lies to the K-rich side of this curve. The reasons for this are likely to be complex. Firstly, the prerequisite in the synthetic system that pressure is constant does not necessarily hold for the natural system. P_{TOTAL} and P_{FLUID} are both variables, P_{FLUID} representing some finite fraction of the total pressure at liquidus

temperatures ($P_{FLUID} \leq P_{TOTAL}$). Secondly, liquidus phase relationships in the natural system are modified by the presence of additional components such as CaO, FeO, MgO, CO_2 and F.

In order to assess the influence of these additional components, it is necessary to turn to a discussion of melt structure (below).

5.5.1 Melt Structure

The structure of a silicate melt is a function of bulk composition, pressure and temperature, consisting essentially of an infinite network of linked SiO_4 tetrahedra in which some of the bridging bonds, Si-O-Si, are replaced by non-bridging bonds, 2Si-O-M; where M represents a cation other than Si4+ (Hess 1980). Addition of free oxygen ions to the system, M-O-M, has the effect of modifying the silicate network, so that melts containing high proportions of modifier cations such as Ca^{2+}, Fe^{2+} and Mg^{2+} tend to be less polymerised, and consequently less viscous, than more siliceous melts. Depending on the number of non-bridging oxygens per silicon atom, NBO/Si = 1,2 or 4 (Mysen et al. 1980c), the melt will be broken down to a series of sheets, chains or monomers.

The role of aluminium in silicate melts is complex, occurring in both four- and six-fold coordination with oxygen, depending on whether Al is outnumbered by or in excess of potential charge-balancing cations such as K^+, Na^+ and Ca^{2+} (Hess 1980, Mysen et al. 1981). In alkaline to peralkaline granitic melts such as those in the Hurdal area, in which the ratio of potential charge-balancing cations to aluminium, i.e. 2Ca+Na+K/Al, is greater than one, Al is likely to be confined more or less to the tetrahedral position, thereby acting in a network-forming role. Magmas consisting of alkalies and aluminium in roughly equal proportions should

therefore be highly polymerised, and consequently viscous. Presence of potential charge-balancing cations in excess of aluminium, however, provides free oxygen ions to the system, thereby performing in a network-modifying role. The strength of bridging bonds between charge-balancing cations and Al is likely to decrease with increasing ionization potential ($I_K < I_{Na} < I_{Ca} < I_{Mg} < I_{Mn} < I_{Fe}$; Hess 1980, Hess and Wood 1982). A tendency towards increasing peralkalinity of magma compositions (Na+K/Al > 1) should therefore be accompanied by a reduction in silicate polymerisation, with a preference towards Na as opposed to K in the network-modifying role.

Presence of free alkali ions in the melt is also known to have significant effects upon redox equilibria, in particular favouring the stability of Fe^{3+} over Fe^{2+}, and Eu^{3+} over Eu^{2+} (Hess 1980, Mysen et al. 1980a, Moller and Muecke 1984). A preference towards trivalent Fe in peralkaline melts is reflected in the resultant mineralogy by incorporation of Fe^{3+} into Na-bearing pyroxenes and amphiboles. Europium on the otherhand has already been depleted in the melt by the peralkaline stage of evolution in the Hurdal area. The redox ratios of Fe^{2+}/Fe^{3+} and Eu^{2+}/Eu^{3+} and the oxygen fugacity of a system are clearly interrelated variables, being a function of temperature, melt structure and ultimatley bulk composition (Hildreth 1981, ref. cit. Lauer 1977).

Perhaps the most significant influence on melt structure, and liquidus phase relationships, is provided by the presence of volatile phases such as H_2O, CO_2 and F (Section 5.3). Disruption of the strong Si-O-Si bonds through reaction in particular with H_2O results in a reduction in silicate polymerisation, and a decrease in magma viscosity. In addition, the formation of complexes incorporating hydroxyl, carbonate, fluoride, phosphate, and to a lesser extent sulphate ligands is likely to have significant effects upon network ordering and trace element partitioning (Section 6.5). Under extreme conditions, an increase in the degree of

ordering of oxygen species in the melt may lead to the formation of two coexisting silicate liquids, one rich in non-bridging oxygens and metal cations, a hydrous or fluorine rich silicate melt; the other in silicon and bridging oxygens (liquid immiscibility; Hess 1980).

The solubility of H_2O in silicate melts is believed to be controlled by two distinct mechanisms (Mysen et al. 1980b). Firstly, water reacts with bridging oxygens to form two OH^- groups per broken oxygen bond. This has the effect of breaking down the three-dimensional network and is believed to be accompanied by an expulsion of Al^{3+} from tetrahedral coordination. Secondly, water reacts with both non-bridging oxygens and network modifers, such as Na^+, to form Si-OH bonds and M(OH) and $M(OH)_2$ complexes. Hydroxyl does not, however, appear to form bonds with aluminium.

In contrast, fluorine (and carbon dioxide; below) would appear only to react with modifier cations and not with silicon (Kogarko and Krigman 1973). This has the effect of increasing the concentration of bridging oxygens in the melt, and thereby the activity of SiO_2 and the degree of polymerisation. Contrary to popular belief (Bailey 1977, Burnham 1979a), there is no evidence that fluorine forms bonds with silicon (Kogarko and Krigman 1973). This is supported by a general decrease in fluorine solubility in the melt with increasing SiO_2 content (Kovalenko 1973), and by the fact that F seldom forms bonds with Si in the resultant mineral phases (Kogarko and Krigman 1973).

Fluorine is most likely to form complexes with monovalent cations such as Na^+. However, release of Al^{3+} into six-fold coordination during hydrolysis (above) may lead to the formation of AlF_6^{3-} complexes (Manning et al. 1980, Manning 1981). The large expansion of the quartz field and contraction of the albite field with increasing fluorine content observed in the granite system under water-saturated

conditions (Section 5.3) may be the result of the formation of such complexes, with Na^+ in the charge-balancing role (Na^3AlF^6 complexes; Manning 1981). However, expansion of the quartz field, on its own, may simply be the result of increased SiO_2 activity (Kogarko and Krigman 1973).

Carbon dioxide dissolves in silicate melts predominantly in the form of CO_3^{2-}, the ratio of $CO_3^{2-}/(CO_3^{2-} + CO_2)$ being a function of the availability of network modifying cations, such as Ca^{2+}, in the melt (Mysen 1976, Mysen and Virgo 1980a). Reaction between CO_2 and network modifying cations leads to the formation of MCO_3 and M_2CO_3 complexes, at the same time increasing the concentration of bridging oxygens in the melt. A general decrease in the solubility of CO_2 with decreasing pressure and increasing SiO_2 content is believed to ensure the possibility of a coexisting CO_2 vapour phase throughout magmatic evolution, providing CO_2 is present in the source (Holloway 1976). This is likely to have considerable influence not only on the physicochemical properties (heat transfer, mass transfer and viscosity) of the melt, but also on the activity of H_2O, since water is also partitioned into the vapour phase (Holloway 1976).

5.5.2 Discussion

Discrepencies between the actual behaviour of magmas of granitic composition and the behaviour predicted from phase relationships in synthetic systems (Section 5.3) leads to some important inferences concerning melt structure, and in particular the roles of Na and F in the evolution of peralkaline magmas in the Hurdal area. Comparison between Figures 5.2, 5.3, and 5.4 indicates that the net effect of additional components, such as TiO_2, Fe_2O_3, FeO, MgO, CaO, P_2O_5, CO_2 and F, present in the natural system is similar to that of adding excess Na to the system. It is not at all like that of adding increasing amounts of F to the system, determined experimentally under water-saturated conditions.

Only in the biotite syenite and manganogranitoids do the compositions move over significantly towards the albite apex, the Na/Na+K ratios of these rocks increasing with increasing F content (Figure 7.7b).

These relationships indicate that an important control upon the magmatic evolution is likely to have been the complexing behaviour of F, and the structural position of Na in the melt. Two types of reaction would appear to have been important. Firstly, fluorine reacts with modifier cations in the melt to form MF and MF_2 complexes. Secondly, fluorine, in the presence of hydroxyl, combines with alkalies and Al^{3+} to form M_3AlF_6 complexes, thereby releasing Al^{3+} into six-fold coordination. The first type of reaction leads to an increase in the concentration of bridging oxygens in the melt, and therefore the degree of silicate polymerisation. In contrast, release of Al^{3+} into a network modifying role results in a significant reduction in silicate polymerisation, and consequently melt viscosity (Hess 1980).

Reaction between F and network modifying cations in the melt results in the formation of complexes of the type NaF, KF and CaF_2. Strong correlations in the whole-rock compositions between Mn and F (Figure 5.8), however, indicate that fluorine also forms complexes with manganese. Saturation of the melt with respect to F, at approximately 0.5 Wt% F in melts of alkali feldspar granite composition (Kovalenko 1973), leads to the precipitation of fluorite (CaF_2). The latter is occasionally observed as a minor mineral phase in the alkali feldspar granite, for instance in the Brennhaugen area (Section 3.3.5). This type of reaction is not accompanied by any significant enrichment in Na relative to K, suggesting that these elements are incorporated into MF complexes equally (Figure 5.7b).

Reaction between F and alkalies in their role of stabilising Al^{3+} in tetrahedral coordination results in the formation of

complexes of the type AlF_6^{3-}, with a combination of monovalent and divalent cations in the charge-balancing role. Consideration of the distribution of major elements in the manganogranitoids (Section 5.4) indicates that, in addition to Na, Mn is strongly enriched in these rocks. Potassium, on the other hand, is strongly depleted. It is therefore reasonable to assume that Mn is readily incorporated into alumino-fluoride complexes (e.g. $NaMnAlF_6$). The low ionization potentials and large ionic radii of K, however, would appear to preclude the possibility of complex formation with this element. Reactions of this type are therefore accompanied by considerable enrichment in Na relative to K (Figure 5.7b).

5.5.2.1 Magma viscosities

Evolution from monzodiorite to alkali feldspar granite involves both a considerable increase in the concentration of SiO_2 in the melt, and significant reductions in the proportions of potential modifier cations such as Fe^{2+}, Mg and Ca. In addition, the ratio of potential charge-balancing cations such as Na, K and Ca, to aluminium increases to approximately unity. Magmatic evolution is therefore accompanied by a substantial decrease in the ratio of non-bridging oxygens to tetrahedrally coordinated cations in the melt (NBO/T; Mysen et al. 1980c) and, as a consequence, by an increase in the degree of silicate polymerisation. In the absence of dissolved volatiles, the most evolved magmas (quartz syenite and alkali feldspar granite) should be highly polymerised and therefore viscous; with viscosities in the range 10^8 to 10^{10} poise (Shaw 1965, Burnham 1979a).

Build-up of dissolved volatiles, particularly in the apical zones of granitic intrusions, leads to disruption of the three-dimensional network (increase in NBO/T; Mysen et al. 1980c), and a consequent reduction in both silicate polymerisation and melt viscosity. However, the degree to

which this occurs depends on the types and relative proportions of volatiles concerned (H_2O, CO_2 and F; Section 5.5.1). The greatest effect is provided by H_2O, since water reacts with both bridging and non-bridging oxygens in the melt. The effects of CO_2 and F, on the otherhand, are much less pronounced and under certain circumstances may infact lead to increases in silicate polymerisation.

5.5.2.2 Conclusions

In conclusion, the intermediate to granitic rocks in the Hurdal area are compatible with an origin by fractionation of intermediate magmas, essentially by separation of clinopyroxene, plagioclase and alkali feldspar. The magmatic evolution was strongly influenced by the presence within the melt of volatile constituents such as H_2O, CO_2 and F. In particular, the formation of fluoride complexes is believed to have been important.

CHAPTER 6
TRACE ELEMENT GEOCHEMISTRY

6.1 Introduction

A combination of petrological studies (Chapter 3) and major element geochemistry (Chapter 5) has lead to the conclusion that the magmatic evolution of intermediate to granitic rocks in the Hurdal area may be explained essentially in terms of feldspar fractionation. Whilst it is possible to place some constraints on the likely compositions of source rocks and mineralogical controls on magma composition from a study of major element geochemistry, it is not possible, or at least it is very difficult, to distinguish the mechanism(s) by which fractionation has occurred. Thus, from the point of view of major element geochemistry, the felsic rocks in the Oslo Region may be explained equally well in terms of continued fractional crystallisation of basaltic parent magmas, as by partial melting of a variety of possible source rocks in the crust. In an earlier section (2.5.1), trace element evidence, concerning in particular Ni and Cr, has been shown to have some bearing on this problem for the more mafic rocks. In this chapter, an attempt will be made to apply trace element evidence to the petrogenesis of the felsic rocks.

A study of the major element geochemistry of the basaltic rocks (Section 2.5.1) has enabled two distinct lines of evolution to be identified, alkali basaltic and tholeiitic lines of descent. This is reflected in the trace element geochemistry by systematically lower concentrations of incompatible trace elements in the tholeiitic rocks. A similar study of the intermediate rocks (Section 2.5.2) and felsic rocks (Sections 2.5.3 and 2.5.4), however, has provided inconclusive evidence. The question is whether a study of the trace element distributions among the felsic rocks in the Hurdal area can provide any information

TABLE 6.1: TRACE ELEMENT GEOCHEMISTRY

	1	2	3	4	5	6	7	8	9	10
SAMPLE NO:	M1	M2	N112	N164	N253,1	N90B3	N90C6	W7	W80	V29
ROCK TYPE:	MONZDRT	MONZDRT	B.S.	B.S.	B.S.	B.S.	B.S.	A.S.	A.S.	A.S.
TRACE ELEMENTS (μg/g):										
Li	16.65	13.15	40.00	28.00	20.00	13.40	20.00	16.50	21.00	16.40
Be	2.65	3.80	10.10	10.30	4.10	9.30	5.80	9.90	7.40	5.60
V	89.00	124.00	23.00	66.00	36.00	45.00	39.00	5.00	12.00	11.00
Cr	1.55	2.30	3.50	5.50	7.40	5.00	6.00	3.60	3.90	3.20
Co	28.45	35.45	9.50	12.00	11.90	11.80	12.40	5.50	6.90	7.10
	2.00	3.00	1.50	2.00	2.00	2.00	1.00	2.00	1.00	1.00
Cu	26.15	21.45	3.80	5.20	3.80	3.50	5.00	5.30	4.50	2.00
Zn	39.95	90.70	95.00	93.00	108.00	320.00	630.00	94.00	70.00	84.00
Rb	100.00	134.00	309.00	173.00	147.00	142.00	138.00	281.00	241.00	185.00
Sr	1215.00	620.00	198.00	409.00	488.00	429.00	528.00	51.00	291.00	184.00
Y	44.00	51.00	72.00	66.00	48.00	56.00	47.00	137.00	50.00	64.00
Zr	387.00	413.00	676.00	481.00	481.00	525.00	527.00	995.00	431.00	512.00
Nb	99.00	106.00	193.00	142.00	110.00	116.00	111.00	250.00	174.00	171.00
Mo	7.20	6.85	30.00	19.20	15.50	19.20	24.00	24.00	14.00	13.80
Ag	2.35	2.95	-.00	-.00	-.00	-.00	1.35	1.06	-.00	-.00
Cd	3.45	3.70	.66	.59	.81	2.20	1.74	-.00	-.00	-.00
Ba	918.00	610.00	839.50	864.00	1530.00	1121.00	1345.00	163.00	665.00	558.00
Hf	9.66	11.64	21.95	11.94	16.40	13.93	14.79	29.76	14.85	16.25
Ta	11.13	11.77	25.54	17.69	13.06	14.45	12.19	31.87	19.44	20.33
W	0	0	178.42	14.10	137.16	0	9.15	1.59	4.83	0
Pb	15.60	38.70	59.00	59.00	54.00	133.00	95.00	86.00	80.00	57.00
Th	11.00	21.00	40.00	20.00	13.00	22.00	22.00	42.00	35.00	34.00
U	3.07	3.69	3.09	1.67	4.45	3.61	3.89	3.72	5.05	9.12
RARE EARTH ELEMENTS:										
La	87.12	102.57	157.35	108.56	139.66	129.93	132.44	124 .97	83.26	110.52
Ce	183.82	207.64	367.01	225.07	288.87	252.33	259.08	279.00	167.49	261.98
Nd	71.89	81.19	107.61	82.43	96.32	92.84	91.26	114.80	57.36	89.08
Sm	13.06	14.26	17.44	14.23	15.98	14.03	15.18	25.60	10.14	16.10
Eu	3.60	3.10	2.45	2.58	4.23	2.72	3.78	1.64	1.92	2.47
Gd	10.23	12.64	13.23	13.20	12.06	15.89	11.60	28.06	8.86	18.12
Tb	1.22	1.35	1.98	1.77	1.67	1.53	1.30	4.02	.87	2.11
Ho	.82	2.62	3.13	2.31	2.94	2.18	2.89	5.30	2.43	3.30
Tm	0	0	0	0	0	0	0	0	0	0
Yb	2.59	3.59	6.64	3.50	3.47	3.25	2.95	8.25	4.56	4.21
Lu	.36	.43	3.05	.47	2.18	.51	.46	1.25	.69	.71

	11	12	13	14	15	16	17	18	19	20
SAMPLE NO:	V42	V50	V51	P6	K32	RH1	H13	W16	N1	N5B
ROCK TYPE:	A.S.	A.S.	A.S.	A.S.	A.S.	A.S.	A.S.	Q.S.	Q.S.	Q.S.
TRACE ELEMENTS (µg/g):										
	12.00	8.90	14.20	6.70	11.40	10.70	14.00	22.00	11.00	10.00
Be	4.40	2.80	5.90	4.60	3.00	4.60	5.70	4.30	12.80	4.30
V	16.00	20.00	25.00	17.00	20.00	26.00	26.00	1.00	5.00	3.00
Cr	3.70	3.70	4.10	3.80	3.70	3.20	4.60	3.90	3.40	3.10
Co	8.10	9.50	11.40	8.20	6.60	9.00	9.20	3.10	5.00	5.20
Ni	1.00	1.00	2.00	1.00	0	1.00	1.00	1.00	0	0
Cu	2.30	2.80	4.10	2.50	2.20	2.70	2.90	4.40	3.70	3.40
Zn	103.00	82.00	166.00	59.00	84.00	64.00	91.00	186.00	97.00	55.00
Rb	148.00	127.00	149.00	151.00	103.00	148.00	115.00	307.00	188.00	176.00
Sr	287.00	504.00	492.00	311.00	175.00	301.00	139.00	25.00	19.00	8.00
Y	68.00	53.00	72.00	68.00	49.00	71.00	49.00	84.00	67.00	47.00
Zr	663.00	505.00	549.00	649.00	292.00	616.00	300.00	541.00	567.00	538.00
Nb	134.00	116.00	153.00	155.00	95.00	149.00	97.00	335.00	185.00	183.00
Mo	14.00	16.50	20.00	14.90	11.10	14.70	16.00	14.90	15.70	11.10
Ag	-.00	-.00	-.00	-.00	1.35	-.00	-.00	-.00	1.06	1.16
Cd	-.00	-.00	1.14	-.00	.63	-.00	-.00	.00	.94	.74
Ba	770.00	1067.00	1137.00	827.00	1277.00	1243.00	1418.00	78.00	94.00	96.00
Hf	15.60	14.80	15.95	18.19	7.85	14.25	8.62	22.68	16.52	15.59
Ta	16.46	13.67	17.98	20.33	12.66	18.25	10.03	31.68	19.45	19.98
W	60.50	0	2.72	0	37.18	81.96	7.30	3.42	1.72	0
Pb	57.00	51.00	68.00	44.00	46.00	53.00	42.00	63.00	68.00	65.00
Th	22.00	15.00	22.00	24.00	19.00	21.00	16.00	58.00	31.00	31.00
U	1.44	2.54	4.47	2.37	2.63	2.64	2.79	8.78	4.42	3.48
RARE EARTH ELEMENTS:										
La	113.92	123.43	144.26	125.07	102.02	112.86	130.73	89.38	72.29	59.48
Ce	249.93	253.15	293.37	271.43	219.92	247.34	258.26	157.63	250.20	197.35
Nd	85.85	88.42	109.29	90.68	81.90	99.06	95.02	37.91	45.76	39.58
Sm	14.80	14.24	18.65	16.87	13.96	16.71	15.95	8.73	9.34	7.54
Eu	2.24	3.23	3.94	2.98	3.41	3.64	4.29	.67	.46	.34
Gd	17.81	12.47	15.35	18.28	16.63	12.85	13.49	11.81	4.90	45.93
Tb	1.68	1.50	1.93	1.87	1.46	2.11	1.52	.70	1.29	.78
Ho	3.21	2.31	3.31	3.02	1.73	2.43	2.39	3.10	2.49	2.03
Tm	0	0	.29	0	0	0	0	0	0	0
Yb	3.89	3.67	4.84	4.18	2.52	4.16	2.48	6.82	4.81	4.50
Lu	.56	.53	.75	.63	.40	.64	.35	1.21	.71	.62

	21	22	23	24	25	26	27	28	29	30
SAMPLE NO:	N13	N60A	N63	N306	N363	K14	K29	N79	N218A	N251,6
ROCK TYPE:	Q.S.	Q.S.	Q.S.	Q.S.	Q.S.	Q.S.	Q.S.	U.M.	U.M.	U.M.
TRACE ELEMENTS (µg/g):										
Li	12.30	15.50	16.40	4.30	3.40	14.20	21.00	6.40	4.00	11.40
Be	7.80	3.90	3.60	8.30	5.30	5.50	4.10	3.80	3.60	7.60
V	4.00	6.00	4.00	7.00	0	7.00	11.00	2.00	1.00	2.00
Cr	3.00	2.90	3.20	3.20	4.50	3.10	3.00	2.40	3.40	3.90
Co	5.00	5.10	5.20	5.20	1.09	3.40	5.20	3.40	2.60	3.50
Ni	1.00	1.00	1.00	2.00	1.00	1.00	2.00	1.00	0	1.00
Cu	3.40	1.32	2.80	4.70	2.70	2.00	2.60	1.80	2.40	1.47
Zn	72.00	42.00	34.00	134.00	18.90	116.00	99.00	37.00	16.20	19.00
Rb	202.00	174.00	163.00	283.00	242.00	182.00	151.00	160.00	150.00	203.00
Sr	14.00	27.00	13.00	21.00	9.00	7.00	44.00	10.00	16.00	13.00
Y	77.00	82.00	82.00	66.00	27.00	84.00	107.00	42.00	14.00	50.00
Zr	573.00	587.00	548.00	595.00	315.00	676.00	550.00	421.00	395.00	273.00
Nb	216.00	174.00	179.00	228.00	272.00	180.00	136.00	192.00	113.00	120.00
Mo	-.00	10.60	10.00	11.50	-.00	-.00	10.40	-.00	-.00	-.00
Ag	-.00	1.43	1.45	1.08	-.00	1.56	-.00	-.00	-.00	-.00
Cd	-.00	-.00	-.00	1.02	-.00	-.00	-.00	-.00	-.00	-.00
Ba	80.00	148.00	94.00	123.00	62.00	68.00	79.00	85.00	174.00	115.00
Hf	16.78	16.10	16.40	18.10	14.13	18.35	14.57	12.72	17.17	8.44
Ta	23.90	21.47	17.46	26.06	20.26	17.65	15.39	20.15	11.46	19.35
W	130.74	0	6.08	0	9.24	2.92	97.65	4.76	0	4.02
Pb	60.00	55.00	53.00	83.00	48.00	62.00	50.00	54.00	55.00	51.00
Th	36.00	21.00	25.00	40.00	59.00	25.00	16.00	24.00	22.00	18.00
U	4.32	5.00	3.23	4.71	4.01	5.02	1.53	7.22	1.99	5.80
RARE EARTH ELEMENTS:										
La	47.97	83.70	90.72	90.38	31.75	82.19	118.33	40.69	12.31	62.37
Ce	203.41	230.38	255.73	224.12	47.15	181.87	277.20	93.44	18.26	151.14
Nd	34.26	102.71	95.23	54.04	10.53	71.01	120.47	28.73	4.32	42.66
Sm	6.99	19.26	19.25	9.33	1.22	13.98	24.43	5.47	.63	9.38
Eu	.39	1.02	.96	.65	.14	1.39	2.20	.32	.08	.56
Gd	6.30	16.12	13.49	7.33	4.76	13.85	18.52	5.72	1.34	6.94
Tb	1.54	2.65	2.63	.64	.19	1.72	3.50	.70	0	1.52
Ho	2.91	4.51	4.22	2.62	1.09	3.74	3.19	2.19	.57	2.37
Tm	0	0	.88	0	0	.44	0	0	0	0
Yb	5.38	5.19	5.50	5.32	3.22	4.94	5.06	3.52	2.06	3.23
Lu	.87	.80	.84	.92	.58	.80	.72	.49	.35	.48

	31	32	33	34	35	36	37	38	39	40
SAMPLE NO:	N329A	N366	W24	W43A	W511	W69	W76	WW6	WW11	WW19
ROCK TYPE :	F.P.MG	F.P.MG	A.G.(B)	A.G.(B)	A.G.(B)	A.G.(B)	A.G.(B)	A.G.(B)	A.G.(B)	A.G.(B)
TRACE ELEMENTS (µg/g):										
Li	9.30	15.40	45.00	23.00	65.00	2.10	3.90	28.00	10.60	8.70
Be	8.50	5.70	1.83	3.70	5.50	2.80	3.00	4.30	6.00	6.10
V	1.00	2.00	0	0	0	0	0	0	0	0
Cr	3.20	2.80	3.50	4.00	3.80	2.50	2.90	3.90	3.20	3.50
Co	3.30	2.90	2.80	2.80	2.20	1.39	2.20	2.10	2.00	1.75
Ni	0	1.00	2.00	1.00	1.00	0	1.00	2.00	2.00	1.00
Cu	1.73	3.00	4.60	6.20	5.90	2.70	3.60	6.50	7.10	5.00
Zn	35.00	50.00	76.00	135.00	127.00	13.70	37.00	160.00	73.00	119.00
Rb	212.00	263.00	393.00	387.00	473.00	362.00	304.00	458.00	409.00	397.00
Sr	21.00	24.00	12.00	12.00	1.00	5.00	8.00	21.00	25.00	39.00
Y	41.00	44.00	73.00	33.00	13.00	15.00	72.00	83.00	44.00	59.00
Zr	395.00	394.00	129.00	469.00	530.00	283.00	339.00	368.00	481.00	430.00
Nb	204.00	235.00	179.00	333.00	344.00	131.00	209.00	352.00	405.00	218.00
Mo	25.00	-.00	750.00	16.70	12.30	11.00	11.60	15.80	-.00	-.00
Ag	-.00	-.00	-.00	-.00	-.00	-.00	-.00	-.00	-.00	-.00
Cd	-.00	-.00	-.00	-.00	-.00	-.00	-.00	-.00	-.00	-.00
Ba	114.50	102.00	60.00	69.00	66.00	69.00	72.00	36.00	59.00	45.00
Hf	16.77	14.75	6.71	31.34	32.20	13.75	20.41	18.70	23.80	23.25
Ta	20.06	21.35	18.75	34.65	37.22	28.79	30.49	34.28	48.84	24.08
W	6.21	0	0	0	6.89	4.38	4.06	4.67	7.25	0
Pb	61.00	70.00	62.00	102.00	119.00	55.00	63.00	97.00	94.00	63.00
Th	41.00	52.00	25.00	54.00	56.00	9.00	13.00	61.00	48.00	37.00
U	5.59	7.12	7.77	10.21	10.44	14.50	19.85	8.14	16.14	11.94
RARE EARTH ELEMENTS:										
La	76.32	84.91	159.07	50.12	53.26	5.18	26.78	48.74	40.62	29.88
Ce	161.13	137.35	238.24	68.95	82.33	10.31	72.80	77.73	59.92	50.32
Nd	39.08	33.36	40.55	18.05	8.75	5.05	18.90	21.95	13.12	14.40
Sm	6.17	5.20	4.98	2.30	.66	.47	4.10	3.85	1.74	2.33
Eu	.50	.40	.53	.09	.11	.22	.63	.31	.33	.31
Gd	4.86	15.82	3.65	12.50	1.43	0	4.45	6.32	2.00	3.00
Tb	.78	.23	.56	.21	.08	0	.62	.37	0	.28
Ho	1.93	2.20	2.08	1.68	1.23	1.65	3.74	2.70	2.41	2.68
Tm	0	0	0	0	0	0	0	0	0	0
Yb	3.57	3.81	5.98	3.29	2.04	1.03	6.06	6.23	5.19	4.79
Lu	.61	.63	1.02	.56	.43	.18	2.61	1.16	.96	.85

	41	42	43	44	45	46	47	48	49	50
SAMPLE NO:	WW24	WW30A	HH3	HH7	HH8	HH10	HH13	HH15	HH18	HH20
ROCK TYPE:	A.G. (B)	A.G. (B)	A.G. (R)	A.G. (R)	A.G. (R)	A.G. (R)	A.R. (R)	A.G. (R)	A.G. (R)	A.G. (R)
TRACE ELEMENTS (µg/g):										
Li	6.90	9.10	4.30	26.00	30.00	9.80	67.00	33.00	12.60	28.00
Be	5.60	5.10	27.00	8.10	7.50	4.30	5.20	5.40	3.90	13.00
V	0	0	0	0	0	0	0	0	0	0
Cr	3.10	2.90	3.50	5.60	3.40	2.10	4.20	4.00	3.40	3.60
Co	3.00	1.77	2.20	4.00	3.60	2.50	-.00	1.98	2.50	-.00
Ni	2.00	1.00	1.00	1.00	1.00	0	2.00	2.00	1.00	2.00
Cu	4.60	5.70	4.80	5.20	5.30	4.70	4.40	6.00	4.60	6.40
Zn	171.00	47.00	70.00	98.00	24.00	112.00	114.00	122.00	53.00	260.00
Rb	486.00	404.00	445.00	264.00	250.00	261.00	499.00	440.00	275.00	489.00
Sr	70.00	3.00	9.00	18.00	13.00	9.00	7.00	6.00	9.00	8.00
Y	66.00	36.00	47.00	63.00	53.00	30.00	78.00	63.00	44.00	67.00
Zr	331.00	219.00	320.00	333.00	352.00	266.00	225.00	328.00	315.00	334.00
Nb	277.00	234.00	321.00	245.00	228.00	200.00	352.00	373.00	217.00	310.00
Mo	29.00	-.00	-.00	-.00	-.00	-.00	-.00	-.00	-.00	270.00
Ag	-.00	-.00	1.48	2.40	2.30	-.00	-.00	1.51	2.40	1.49
Cd	-.00	-.00	-.00	-.00	-.00	-.00	-.00	-.00	-.00	-.00
Ba	49.00	81.00	59.00	89.00	77.00	74.00	38.00	37.00	43.00	42.00
Hf	18.19	10.44	15.74	-.00	11.95	10.24	12.25	14.33	15.12	18.81
Ta	28.43	23.04	33.93	-.00	26.14	21.90	32.19	38.84	25.76	34.69
W	3.05	0	4.64	-.00	49.03	44.50	6.72	2.65	26.04	10.52
Pb	98.00	69.00	78.00	63.00	57.00	71.00	67.00	88.00	56.00	310.00
Th	55.00	37.00	16.00	47.00	46.00	41.00	52.00	43.00	56.00	78.00
U	19.66	4.01	11.35	-.00	10.94	10.83	26.05	23.09	31.87	20.06
RARE EARTH ELEMENTS:										
La	51.82	24.23	41.64	-.00	60.85	41.26	67.44	54.53	107.38	53.95
Ce	84.94	35.05	78.56	-.00	107.71	75.46	102.01	84.89	67.82	86.85
Nd	22.00	9.37	17.42	-.00	31.03	16.75	25.64	20.17	15.44	10.54
Sm	3.37	1.48	2.74	-.00	5.85	2.47	4.22	2.78	8.15	2.92
Eu	.37	.17	.33	-.00	.60	.31	.28	.57	.32	.45
Gd	6.58	1.73	2.49	-.00	11.81	1.98	12.42	5.36	16.62	2.47
Tb	.34	0	.41	-.00	0	.27	.45	.22	3.78	.09
Ho	3.54	.85	1.78	-.00	2.36	1.85	4.52	3.17	14.13	3.03
Tm	0	0	0	-.00	0	0	0	0	5.89	0
Yb	6.24	2.90	3.79	-.00	3.59	2.73	7.14	5.26	3.73	6.82
Lu	1.10	.47	.67	-.00	.60	.49	1.24	.98	.90	1.30

	51	52	53	54	55	56	57	58	59	60
SAMPLE NO:	HH21	HH14	W362	HC3	HC7	HC10	L1	L5	W18AB	W36A
ROCK TYPE:	A.G.(R)	A.G.(R)	MN.R	MN.R	MN.R	MN.R	AP.MG	AP.MG	DYKE	DYKE
TRACE ELEMENTS (µg/g):										
Li	45.00	5.00	6.30	5.60	7.30	7.50	-.00	-.00	42.00	3.60
Be	21.00	9.30	12.10	360.00	290.00	1880.00	-.00	-.00	2.50	4.70
V	0	0	2.00	2.00	4.00	9.00	0	0	103.00	11.00
Cr	3.00	3.40	11.80	10.90	11.90	10.80	0	0	1.50	5.30
Co	-.00	2.70	2.40	1.60	4.50	3.10	0	0	15.40	7.00
Ni	2.00	1.00	0	0	1.00	1.00	2.00	1.00	2.00	1.00
Cu	4.30	6.70	8.00	6.30	12.40	8.10	-0.00	-.00	3.80	4.40
Zn	133.00	100.00	3100.00	4700.00	4000.00	9999.99	-0.00	-.00	230.00	79.00
Rb	494.00	553.00	6.00	33.00	58.00	47.00	386.00	411.00	82.00	189.00
Sr	13.00	8.00	67.00	200.00	280.00	273.00	24.00	14.00	1085.00	281.00
Y	61.00	60.00	58.00	59.00	91.00	101.00	75.00	61.00	54.00	49.00
Zr	466.00	503.00	473.00	450.00	422.00	385.00	423.00	379.00	399.00	653.00
Nb	341.00	361.00	360.00	324.00	416.00	803.00	443.00	329.00	75.00	108.00
Mo	-.00	31.00	26.00	26.00	30.00	-.00	-.00	-.00	14.10	22.00
Ag	1.13	1.99	4.10	2.70	1.90	1.58	-.00	-.00	1.09	3.60
Cd	-.00	-.00	7.30	15.90	12.50	9.80	-.00	-.00	-.00	-.00
Ba	31.00	56.00	16.00	273.00	239.00	239.00	36.00	39.00	1585.00	1378.00
Hf	27.75	24.55	16.95	24.65	28.60	21.15	23.66	19.65	8.89	14.55
Ta	31.11	35.77	44.39	51.57	47.09	73.92	52.01	34.07	6.80	10.51
W	11.68	16.27	106.13	18.49	22.21	24.12	7.12	11.83	63.11	0
Pb	77.00	105.00	860.00	142.00	240.00	151.00	-.00	-.00	34.00	80.00
Th	88.00	86.00	466.00	59.00	81.00	56.00	78.00	73.00	9.00	20.00
U	19.21	15.57	29.62	27.21	32.94	39.15	19.84	25.20	2.43	4.69
RARE EARTH ELEMENTS:										
La	63.77	62.47	33.23	48.16	60.72	57.43	52.69	54.56	89.34	74.41
Ce	84.14	91.99	1.66	76.56	91.65	8.91	89.00	90.97	195.55	140.11
Nd	19.91	21.66	17.43	19.61	26.60	32.06	20.90	21.96	81.35	50.60
Sm	2.84	3.78	3.76	3.92	5.62	5.96	3.42	2.88	15.25	8.46
Eu	.48	.56	.47	.64	.08	1.06	.33	.54	4.42	2.10
Gd	22.26	5.21	98.88	3.78	0	12.65	6.99	0	13.15	7.22
Tb	0	0	0	.34	.50	.71	.25	.38	1.53	.90
Ho	3.05	2.87	4.30	4.54	6.71	7.27	3.10	4.19	1.71	1.98
Tm	0	0	0	0	0	0	0	.72	0	0
Yb	6.62	6.87	8.91	11.15	16.73	15.73	7.45	6.13	2.74	3.09
Lu	1.19	1.15	2.57	3.07	17.35	2.67	1.38	1.14	.39	.51

	61	62	63	64	65	66	67	68	69	70
SAMPLE NO:	W363	HA4D	N400	N219A	N342	N349A	N364	N324	K7A	K11
ROCK TYPE:	alt.DYKE	DYKE	DYKE	TRACH-AND	TRACH-1	TRACH-1	TRACH-1	RYHOLITE	TRACH-2	TRACH-2
TRACE ELEMENTS (µg/g):										
Li	33.00	8.70	-.00	18.90	13.00	13.50	30.00	1.18	13.00	8.00
Be	9.90	3.00	-.00	3.40	5.60	5.80	11.80	4.40	3.20	3.70
V	21.00	1.00	112.00	25.00	14.00	11.00	11.00	0	32.00	18.00
Cr	4.90	4.70	0	5.30	3.90	3.80	3.70	2.10	4.10	4.90
Co	6.80	2.20	0	10.80	7.40	6.50	6.50	1.62	11.30	10.70
Ni	2.00	1.00	3.00	1.00	1.00	3.00	1.00	0	0	1.00
Cu	5.50	5.20	-.00	4.50	4.20	3.50	4.30	3.80	6.80	7.40
Zn	156.00	280.00	-.00	151.00	128.00	100.00	56.00	94.00	75.00	85.00
Rb	188.00	382.00	123.00	169.00	217.00	180.00	284.00	274.00	138.00	121.00
Sr	85.00	14.00	1878.00	175.00	79.00	72.00	88.00	68.00	647.00	795.00
Y	80.00	32.00	38.00	43.00	72.00	64.00	60.00	22.00	53.00	46.00
Zr	720.00	70.00	172.00	548.00	765.00	750.00	749.00	397.00	600.00	520.00
Nb	236.00	49.00	56.00	116.00	187.00	179.00	172.00	277.00	124.00	114.00
Mo	14.80	-.00	-.00	42.00	9.70	21.00	14.50	52.00	12.00	-.00
Ag	3.70	-.00	-.00	2.30	1.53	1.75	2.20	1.62	2.30	1.72
Cd	-.00	-.00	-.00	-.00	.64	.62	-.00	-.00	-.00	-.00
Ba	94.00	48.00	1568.00	1283.00	396.00	429.00	404.00	183.00	936.00	1015.00
Hf	17.83	2.42	3.00	17.09	18.02	21.02	20.35	20.01	12.85	12.25
Ta	22.31	4.99	4.63	52.48	21.37	19.17	16.55	27.18	15.32	10.85
W	5.58	0	0	22.67	82.94	0	10.22	9.68	51.28	0
Pb	88.00	41.00	-.00	74.00	87.00	64.00	77.00	99.00	51.00	48.00
Th	21.00	9.00	5.00	15.00	33.00	34.00	38.00	17.00	24.00	19.00
U	6.02	3.92	.51	9.35	4.91	5.81	5.13	19.89	3.98	3.29
RARE EARTH ELEMENTS:										
La	47.38	9.89	56.54	107.75	161.93	132.32	124.02	15.10	100.33	98.36
Ce	309.51	19.04	158.08	217.33	298.93	305.66	229.83	24.60	198.46	202.06
Nd	41.38	6.09	67.71	72.31	100.89	93.17	77.69	10.03	71.76	73.89
Sm	9.59	1.21	13.68	11.74	15.96	14.51	12.38	1.94	12.06	12.57
Eu	1.47	.17	4.54	3.33	2.19	2.22	1.88	.53	2.03	3.16
Gd	14.50	1.30	8.95	8.42	18.57	8.36	10.17	0	17.81	10.63
Tb	1.89	.20	1.23	1.18	1.27	1.35	1.10	.24	.95	1.15
Ho	3.31	1.17	1.53	2.75	3.02	3.56	2.57	2.79	2.31	1.54
Tm	0	0	39.60	9.86	0	0	.38	0	0	0
Yb	4.96	1.17	1.52	3.72	4.60	5.24	4.14	3.40	3.05	2.80
Lu	.76	.21	.17	5.35	.65	.84	.70	.55	.49	.46

	71	72	73
SAMPLE NO:	K12A	K21	K31
ROCK TYPE:	TRACH-2	TRACH-2	TRACH-2
TRACE ELEMENTS (µg/g):			
Li	17.40	8.60	127.00
Be	5.00	2.90	4.10
V	15.00	20.00	28.00
Cr	4.30	4.00	4.60
Co	6.60	8.40	11.30
Ni	1.00	1.00	1.00
Cu	4.70	4.30	5.40
Zn	163.00	79.00	139.00
Rb	162.00	122.00	202.00
Sr	180.00	258.00	312.00
Y	56.00	48.00	53.00
Zr	518.00	634.00	422.00
Nb	162.00	123.00	111.00
Mo	13.00	11.90	11.80
Ag	1.13	-.00	1.80
Cd	-.00	-.00	.74
Ba	968.00	981.00	1241.00
Hf	12.49	15.39	12.55
Ta	16.42	12.57	12.42
W	79.22	0	85.96
Pb	59.00	78.00	139.00
Th	23.00	13.00	18.00
U	4.49	2.79	.40
RARE EARTH ELEMENTS:			
La	89.73	113.07	143.76
Ce	158.39	222.88	310.42
Nd	52.81	79.68	107.23
Sm	9.82	12.96	17.83
Eu	2.51	3.24	3.53
Gd	12.97	12.65	12.58
Tb	1.06	1.35	1.79
Ho	2.04	2.22	2.34
Tm	0	0	32.37
Yb	3.54	2.99	3.27
Lu	.51	.44	.56

TABLE 6.2: AVERAGE TRACE ELEMENT ANALYSES

ROCK TYPE:	Monzdrt		B.S.		A.S.		Q.S.		U.M.	
NUMBER OF SAMPLES:	2		5		10		10		3	
	$\bar{x}$	σ_{n-1}	$\bar{x}$	σ_{n-1}	$\bar{x}$	σ_{n-1}	$\bar{x}$	σ_{n-1}	$\bar{x}$	σ_{n-1}
TRACE ELEMENTS (10^{-8} gram atoms g^{-1}):										
Li	214.67	35.66	349.81	146.92	189.89	59.84	187.44	89.28	104.69	54.39
Be	35.78	9.02	87.88	31.09	59.81	23.23	66.47	32.05	55.48	25.01
V	209.06	48.58	82.05	30.90	34.94	13.78	9.42	6.26	3.27	1.13
Cr	3.70	1.02	10.54	2.74	7.21	.79	6.40	.96	6.22	1.47
Co	54.21	8.40	19.55	1.95	13.83	2.90	7.38	2.36	5.37	.84
Ni	4.26	1.20	2.90	.76	1.87	.97	1.70	1.14	1.14	.98
Cu	37.45	5.23	6.70	1.23	4.93	1.75	4.88	1.63	2.97	.74
Zn	99.84	55.00	381.16	357.18	137.20	45.98	130.61	78.64	36.81	17.26
Rb	136.89	28.13	212.71	84.72	192.82	65.78	241.96	61.83	200.08	32.95
Sr	1047.14	480.17	468.39	145.84	312.14	165.32	21.34	12.92	14.84	3.42
Y	53.43	5.57	65.01	12.38	76.60	29.22	81.32	25.01	39.74	21.26
Zr	438.50	20.15	589.78	88.10	604.25	222.76	601.84	100.43	397.94	86.62
Nb	110.33	5.33	144.66	37.95	160.81	48.53	224.74	61.94	152.48	47.07
Mo	7.32	.26	22.49	5.83	16.57	3.80	12.54	2.39	-.00	0.
Ag	2.46	.39	1.25	0.	1.12	.19	1.20	.20	-.00	0.
Cd	3.18	.16	1.07	.65	.79	.32	.80	.13	-.00	0.
Ba	556.32	158.59	830.04	218.74	664.46	281.83	67.14	18.97	90.78	32.97
Hf	5.97	.78	8.85	2.13	8.75	3.34	9.48	1.36	7.16	2.45
Ta	6.33	.25	9.17	3.00	10.00	3.29	11.79	2.65	9.39	2.65
W	0.	0.	38.86	45.48	10.67	16.22	13.69	25.92	1.59	1.39
Pb	13.10	7.88	38.61	16.35	28.19	7.26	29.30	4.94	25.74	1.00
Th	6.90	3.05	10.08	4.31	10.77	3.86	14.74	6.28	9.19	1.32
U	1.42	.18	1.40	.44	1.54	.92	1.87	.77	2.10	1.14
RARE EARTH ELEMENTS:										
La	68.28	7.86	96.17	12.69	84.30	12.08	55.16	17.83	27.69	18.07
Ce	139.69	12.02	198.74	38.86	178.05	25.61	144.52	46.70	62.53	47.55
Nd	53.06	4.56	63.85	7.26	63.19	10.92	42.39	24.33	17.50	13.45
Sm	9.08	.56	10.22	.93	10.84	2.65	7.98	4.70	3.43	2.91
Eu	2.20	.23	2.07	.53	1.96	.58	.54	.40	.21	.26
Gd	7.27	1.08	8.39	1.06	10.30	3.27	9.09	7.70	2.97	1.87
Tb	.81	.06	1.04	.16	1.20	.52	.98	.67	.47	.48
Ho	1.04	.77	1.63	.25	1.78	.59	1.81	.62	1.04	.60
Tm	0.	0.	0.	0.	.05	.10	.08	.18	0.	0.
Yb	1.79	.41	2.29	.87	2.47	.92	2.93	.52	1.70	.45
Lu	.23	.03	.76	.69	.37	.14	.46	.10	.25	.04

ROCK TYPE:	F.p.mG		A.G.(B)		A.G.(R)		Ap.mG		Mn.R	
NUMBER OF SAMPLES:	2		9		10		2		4	
	$\bar{x}$	σ_{n-1}	$\bar{x}$	σ_{n-1}	$\bar{x}$	σ_{n-1}	$\bar{x}$	σ_{n-1}	$\bar{x}$	σ_{n-1}
TRACE ELEMENTS (10^{-8} gram atoms g^{-1}):										
Li	177.93	62.14	306.87	310.07	375.59	282.68	-.00	0.	96.17	12.80
Be	78.78	21.97	46.76	16.34	116.18	86.03	-.00	0.	7051.83	9355.59
V	2.94	1.39	0.	0.	0.	0.	0.	0.	8.34	6.49
Cr	5.77	.54	6.43	1.00	6.96	1.73	0.	0.	21.83	1.12
Co	5.26	.48	3.77	.93	4.72	1.26	0.	0.	4.92	2.09
Ni	.85	1.20	2.08	1.14	2.21	1.15	2.55	1.20	.85	.98
Cu	3.72	1.41	7.83	1.97	8.25	1.34	-.00	0.	13.69	4.09
Zn	65.00	16.22	150.52	86.75	166.11	96.28	-.00	0.	8335.88	4746.44
Rb	277.88	42.19	476.33	67.39	464.50	140.32	466.26	20.68	42.12	26.28
Sr	25.68	2.42	21.68	25.52	11.41	4.13	21.68	8.07	233.96	112.82
Y	47.80	2.39	56.24	29.54	63.66	15.23	76.49	11.13	86.89	24.79
Zr	432.47	.78	377.35	136.46	377.33	91.26	439.60	34.11	474.13	41.57
Nb	236.26	23.59	272.32	84.19	317.31	70.68	415.47	86.76	512.07	238.33
Mo	26.06	0.	126.03	289.21	156.87	176.15	-.00	0.	28.49	2.41
Ag	-.00	0.	-.00	0.	1.70	.46	-.00	0.	2.38	1.04
Cd	-.00	0.	-.00	0.	-.00	0.	-.00	0.	10.12	3.28
Ba	78.82	6.44	44.26	10.61	39.76	14.40	27.31	1.54	134.89	84.09
Hf	8.83	.80	10.89	4.84	9.38	3.32	12.13	1.59	12.79	2.78
Ta	11.44	.50	15.95	3.35	17.21	3.04	23.79	7.01	29.98	7.43
W	1.69	2.39	1.39	1.43	10.40	9.34	5.15	1.81	23.25	23.02
Pb	31.61	3.07	39.04	11.14	46.91	36.79	-.00	0.	168.07	166.03
Th	20.04	3.35	16.62	8.39	23.83	9.74	32.54	1.52	71.32	86.47
U	2.67	.45	4.97	2.25	7.89	3.10	9.46	1.59	13.54	2.17
RARE EARTH ELEMENTS:										
La	58.04	4.37	35.92	31.72	44.26	14.07	38.61	.95	35.91	8.86
Ce	106.51	12.00	57.15	45.84	61.81	8.97	64.22	.99	31.90	32.84
Nd	25.11	2.80	12.25	7.27	13.75	4.13	14.86	.52	16.59	4.64
Sm	3.78	.46	1.74	1.05	2.64	1.26	2.09	.25	3.20	.76
Eu	.30	.05	.20	.12	.29	.08	.29	.10	.37	.27
Gd	6.58	4.93	2.80	2.38	5.70	4.58	2.22	3.14	18.33	29.89
Tb	.32	.24	.17	.14	.36	.76	.20	.06	.24	.19
Ho	1.25	.12	1.36	.61	2.48	2.34	2.21	.47	3.46	.91
Tm	0.	0.	0.	0.	.39	1.16	.21	.30	0.	0.
Yb	2.13	.10	2.48	1.16	2.99	1.00	3.92	.54	7.59	2.15
Lu	.35	.01	.53	.41	.54	.17	.72	.10	3.67	4.17

ROCK TYPE:	Trach-1		Trach-2		Trachand	Rhy.	Dol.	W18AB	W36A	HA4D
NUMBER OF SAMPLES:	3		5		1	1	1	1	1	1
	$\bar{x}$	σ_{n-1}	$\bar{x}$	σ_{n-1}						
TRACE ELEMENTS (10^{-8} gram atoms g^{-1}):										
Li	271.33	139.37	501.37	744.57	272.30	17.00	-.00	605.10	51.87	125.34
Be	85.81	39.09	41.94	9.13	37.73	48.82	-.00	27.74	52.15	33.29
V	23.56	3.40	44.36	13.99	49.08	0.	219.86	202.19	21.59	1.96
Cr	7.31	.19	8.42	.71	10.19	4.04	0.	2.88	10.19	9.04
Co	11.54	.88	16.39	3.54	18.33	2.75	0.	26.13	11.88	3.73
Ni	2.84	1.97	1.36	.76	1.70	0.	5.11	3.41	1.70	1.70
Cu	6.29	.69	9.00	2.10	7.08	5.98	-.00	5.98	6.92	8.18
Zn	144.79	55.51	165.49	61.39	230.96	143.77	-.00	351.79	120.83	428.27
Rb	265.60	61.68	174.33	39.73	197.74	320.59	143.91	95.94	221.14	446.95
Sr	90.92	9.15	500.34	305.16	199.73	77.61	2143.35	1238.30	320.70	15.98
Y	73.49	6.87	57.59	4.60	48.37	24.75	42.74	60.74	55.11	35.99
Zr	827.30	9.83	590.66	90.46	600.75	435.21	188.56	437.40	715.85	76.74
Nb	193.03	8.08	136.48	22.02	124.86	298.15	60.28	80.73	116.25	52.74
Mo	15.70	5.91	12.69	.58	43.78	54.20	-.00	14.70	22.93	-.00
Ag	1.69	.32	1.61	.44	2.13	1.50	-.00	1.01	3.34	-.00
Cd	.56	.01	.66	0.	-.00	-.00	-.00	-.00	-.00	-.00
Ba	298.31	12.54	748.71	89.04	934.25	133.26	1141.78	1154.15	1003.42	34.95
Hf	11.09	.88	7.34	.73	9.57	11.21	1.68	4.98	8.15	1.36
Ta	10.52	1.33	7.47	1.26	29.00	15.02	2.56	3.76	5.81	2.76
W	16.89	24.60	23.55	22.63	12.33	5.27	0.	34.33	0.	0.
Pb	36.68	5.57	36.20	18.16	35.71	47.78	-.00	16.41	38.61	19.79
Th	15.08	1.14	8.36	1.89	6.46	7.33	2.15	3.88	8.62	3.88
U	2.22	.20	1.26	.67	3.93	8.36	.21	1.02	1.97	1.65
RARE EARTH ELEMENTS:										
La	100.37	14.35	78.51	15.21	77.57	10.87	40.70	64.32	53.57	7.12
Ce	198.50	29.95	155.90	40.30	155.10	17.56	112.82	139.56	99.99	13.59
Nd	62.80	8.19	53.43	13.62	50.13	6.95	49.94	56.40	35.08	4.22
Sm	9.50	1.20	8.68	1.95	7.81	1.29	9.10	10.14	5.62	.80
Eu	1.38	.12	1.90	.40	2.19	.35	2.99	2.91	1.38	.11
Gd	7.86	3.46	8.48	1.70	5.35	0.	5.69	8.36	4.59	.83
Tb	.78	.08	.79	.21	.74	.15	.77	.96	.57	.13
Ho	1.85	.30	1.27	.20	1.67	1.69	.93	1.04	1.20	.71
Tm	.07	.13	3.83	8.57	5.84	0.	23.44	0.	0.	0.
Yb	2.69	.32	1.81	.16	2.15	1.96	.88	1.58	1.79	.68
Lu	.42	.06	.28	.03	3.06	.31	.10	.22	.29	.12

concerning the possible alkali basaltic or tholeiitic nature of the source.

6.2 Trace element determinations

Trace element determinations on the same set of 73 samples as was analysed for major elements have been carried out using a variety of analytical techniques. Vanadium, Ni, Rb, Sr, Y, Zr, Nb, Ba and Th were analysed by X-ray fluorescence spectrometry. Rare earth elements (La, Ce, Nd, Sm, Eu, Gd, Tb, Ho, Tm, Yb and Lu), together with Hf, Ta, W and U were analysed by instrumental methods of neutron activation analysis. Lithium, Be, Cr, Co, Cu, Zn, Mo, Cd and Pb were analysed by inductively coupled plasma spectrometry. The methods used are outlined in Section 1.4. Estimates of precision and accuracy are given in Appendix A1. The results, expressed in $\mu g\ g^{-1}$ are listed in Table 6.1. Average trace element analyses for all the principal rock-types are listed in Table 6.2, recalculated in terms of 10^{-8} gram atoms g^{-1}.

6.3 Theoretical Considerations

The concentration of a trace element in a particular mineral relative to its concentration in the liquid with which the mineral is in equilibrium is given by the crystal/liquid distribution coefficient, K_D, for that element (Cox et al. 1979):

K_D = concentration in mineral/concentration in liquid.

The weighted sum of crystal/liquid distribution coefficients for all the minerals in a particular rock gives the bulk distribution coefficient:

$$D = \Sigma_{i=1}^{n} X_i K_{Di}$$

Where X_i is the mass fraction of a given mineral, i, in the

assemblage; and n is the number of mineral phases.

Trace elements for which the bulk distribution coefficient, D, is considerably less than 1 tend to be excluded from the constituent mineral phases during crystallisation, and are therefore concentrated in the liquid during progressive fractionation, whether by partial melting or fractional crystallisation processes. Included within this category are elements with large ionic radii (Large ion lithofile or LIL elements; Cox et al. 1979) such as K, Cs, Rb, Sr, Ba and light rare earth elements (LREE); and highly charged cations such as Zr, Nb, Mo, Hf, Ta, W, Th and U, and possibly Ti and P as well, which have a strong affinity for the melt (High field strength or HFS elements; Brown et al. 1984). In the literature, these elements have been referred to as incompatible trace elements since, particulary in the more mafic rocks, they show a strong tendency to be excluded from the crystalline phases. However, at the felsic end of the spectrum, many of these elements are far from incompatible, forming important constituents of the principal rock forming minerals. For instance K is partioned into K-feldspar and biotite; Sr and Eu into plagioclase; Ba into K-feldspar; and Zr and Hf into Zircon. For this reason the terms large ion lithophile and high field strength are sometimes preferred. However, the term incompatible trace element is retained here for specific cases in which the bulk distribution coefficient, D, is less than 1. Similarly, the term compatible trace element is used for specific cases in which the bulk distribution coefficient is greater than one. In addition, the term hygromagmatophile (cf. Ferrara and Treuil 1974, Cox et al. 1979, Wood et al. 1979a) is used as a general term to encompass all these elements, which in general show an affinity towards the melt.

From the above discussion, it is clear that the bulk distribution coefficients for particular trace elements may be strongly influenced by the presence of minor mineral

phases with high distribution coefficients, K_D, for those elements. This has important implications for the interpretation of REE distributions in felsic rocks, since the presence of accessory mineral phases such as apatite, zircon and sphene, which preferentially retain REE, may effectively control the rare earth evolution of these rocks (Henderson 1980, Fourcade and Allegre 1981, Gromet and Silver 1983).

Knowledge of the crystal/liquid distribution coefficients, whether determined experimentally or from phenocryst-matrix relationships, permits the trace element evolution of a crystal-liquid system to be modelled. The simplest models for partial melting are those for equilibrium (batch) partial melting and fractional melting respectively. However, only the model for equilibrium partial melting will be considered here, since fractional melting involving separation of successive melt fractions from a source region progressively depleted in elements such as Si, Na, K, Al and volatiles, is believed to be an unlikely mechanism (Section 2.5.3; Hanson 1978). The simplest model for fractional crystallisation is for the ideal case of Rayleigh fractionation in which only surface equilibrium is attained between the crystals and the melt, and the crystals are removed as fast as they are formed. More "realistic" models have been defined, for instance that for incremental equilibrium crystallisation (McCarthy and Hasty 1976), but will not be discussed here.

Under conditions of equilibrium partial melting, the concentration of an element in the liquid, C_l, is related to that in the original unmelted source, $C_\emptyset$, by the expression (Hanson 1978; Cox et al. 1979):

$$C_l/C_\emptyset = 1/(D(1-F)+F);$$

where F is the mass fraction of melt formed and D is the bulk distribution coefficient for the residual solids at the

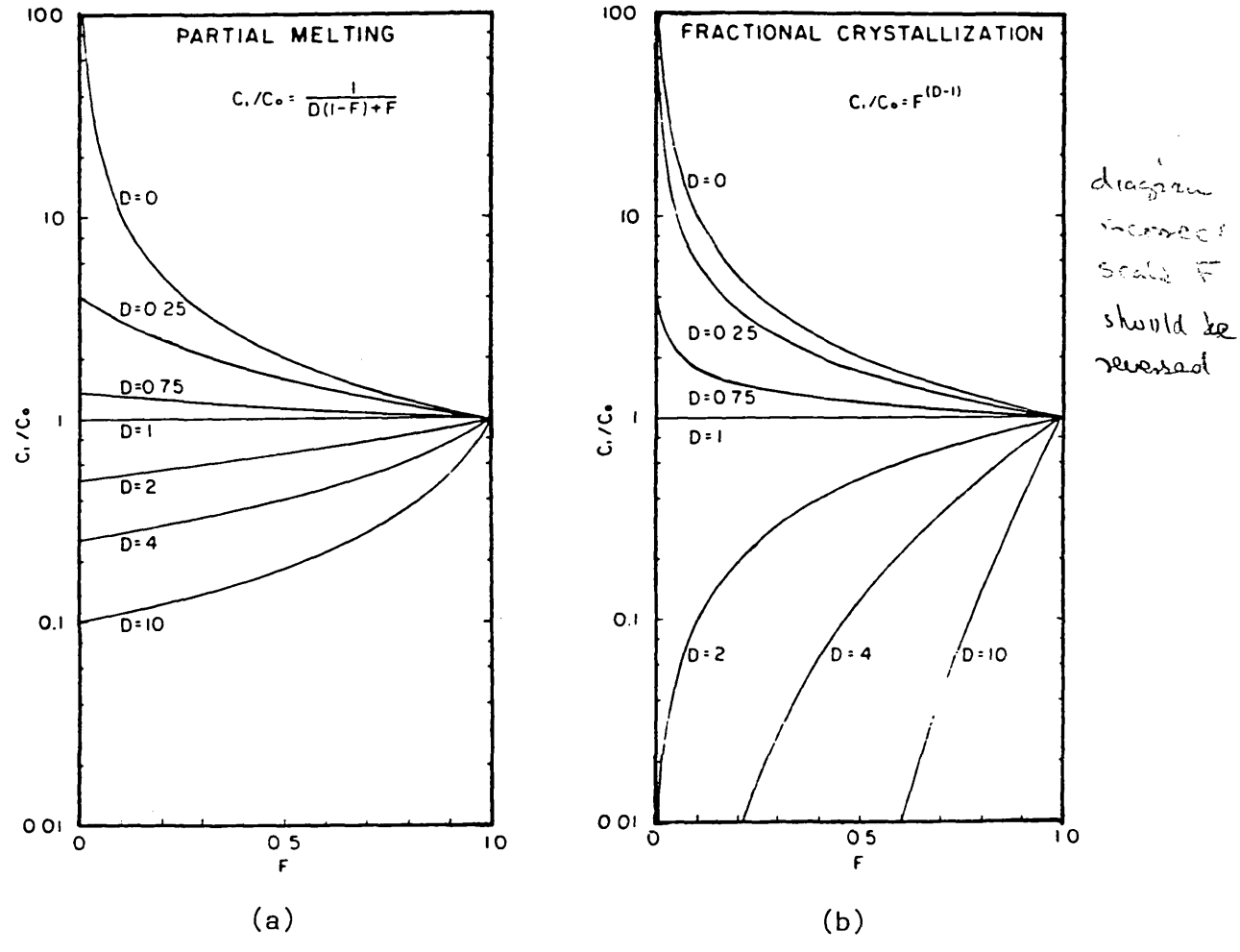

FIGURE 6.1. F vs. $C_1/C_\emptyset$: (a) Partial melting; and (b) Fractional crystallisation. D is the bulk mineral/melt distribution coefficient (after Hanson 1978).

delete F in each case

moment when the melt is removed from the system. The relative enrichment factors, $C_l/C_\emptyset$, predicted by this model for different degrees of partial melting, F, are illustrated in Figure 6.1a for different values of D.

In comparison, the case for closed system fractional crystallisation is given by the expression:

$$C_l/C_\emptyset = F^{(D-1)}.$$

$C_\emptyset$ in this case refers to the concentration of the element in the original liquid. The predicted enrichment factors for different degrees of fractional crystallisation, 1-F, are depicted in Figure 6.1b.

Comparison between Figures 6.1a and 6.1b leads to two important conclusions. Firstly, as the bulk distribution coefficient, D, tends towards zero, the enrichment factors in the melt approach 1/F, irrespective of whether partial melting or fractional crystallisation is the predominant mechanism. Secondly, fractional crystallisation causes a more rapid decrease in the concentration of compatible trace elements ($D > 1$) than would be the case for partial melting. A knowledge of the distribution of incompatible trace elements ($D < 1$) is therefore unlikely to provide any information about whether partial melting or fractional crystallisation is the predominant mechanism, whereas a study of compatible elements may have some bearing on the problem (Hanson 1978). However, the presence of an incompatible element for which D is close to zero may be used to estimate the mass fraction of melt removed during evolution from parent to daughter, since when $D = \emptyset$, $F = C_\emptyset/C_l$.

Elements with bulk distribution coefficients considerably less than one may also provide important information concerning the nature of the source rocks for partial melting or fractional crystallisation processes, since pairs of trace

TABLE 6.3: TRACE ELEMENT RATIOS, PETROGENETIC SUITES

	Y/Tb	Zr/Hf	Nb/Ta	Zr/Nb	Zr/Y	Th/U
Chondritic Abundances[1]	74.5	58.7-78.3	29.2-33.1	-	-	-
Oceanic basalts[1]	75.1 ± 8.9	76.3 ± 9.8	31.2 ± 3.9	-	-	-
ICELAND:[2]						
Krafla	76.0 ± 8.1	74.2 ±10.6	31.4 ± 2.6	8.9 ± 1.3	3.3 ± .7	4.9 ± .6
Askja	63.2 ± 4.8	79.4 ± 3.4	27.5 ± 4.1	9.6 ± 2.5	4.6 ± .3	3.7 ± .2
Vadalda	72.1 ±10.5	79.3 ± 8.4	30.3 ± 2.2	13.0 ± 3.4	4.0 ±1.6	3.5 ± 0.
Kverkfjöll	58.0 ± 4.0	74.8 ± 1.5	25.9 ± 8.3	11.1 ± 4.8	5.3 ± .9	4.8 ± .5
KENYA:[3]						
Alkali basalt	65.3 ±14.0	81.7 ± 8.0	50.5 ± 8.5	3.5 ± .3	3.9 ± .6	-
Ferrobasalt	70.1 ± 5.0	79.0 ± 3.2	43.7 ± 4.0	3.3 ± .1	4.4 ± .4	-
Benmoreite	69.5 ±10.5	72.7 ±16.3	39.5 ± 3.2	3.4 ± 1.1	6.4 ± .7	-
Trachyte	65.7 ± 3.2	79.5 ± 4.7	35.2 ± .9	3.7 ± .3	7.8 ± .4	-
OAHU:[4]						
Nepheline melilitite	35.3 ± 2.8	106.3 ±14.2	34.4 ± 1.3	3.4 ± 0.	5.6 ± .1	-
Melilite nephelinite	33.0 ± 0.	98.6 ±11.3	-	3.5 ± 0.	7.8 ± 0.	-
Nephelinite	31.7 ± 3.4	94.0 ± 8.9	32.8 ± 4.5	3.6 ± .3	5.3 ± .6	-
Basanite	38.3 ± 0.	90.2 ± 7.2	28.0 ± 0.	4.4 ± 0.	6.6 ± 0.	-
Alkali olivine basalt	38.9 ± 0.	83.9 ± 5.6	26.0 ± 0.	4.7 ± 0.	5.4 ± 0.	-
MASSIF CENTRAL:[5]						
Nephelinite	-	-	-	3.1 ± .2	9.8 ±1.1	-
Basanite	-	-	-	3.4 ± .3	9.6 ±2.2	-
Alkali basalt	-	-	-	3.2 ± .3	8.7 ±1.9	-
Mugearite	-	-	-	3.6 ± 0.	15.2 ± 0.	-
Phonolite	-	-	-	5.3 ± .6	35.5 ± .6	-
Trachyte	-	-	-	3.4 ± 0.	14.7 ± 0.	-
Spinel peridotite nod.	-	-	-	32.6	5.2	-
MULL:[6]						
Basalt	-	-	-	61.9 ±25.0	4.7 ± .1	-
Hawaiite	-	-	-	60.3 ± 7.2	8.7 ± 0.	-
Basalt-Hawaiite	-	-	-	39.8 ± 6.4	4.4 ± .6	-
Mugearite	-	-	-	25.1 ± .9	23.9 ± 0.	-
Trachyte	-	-	-	18.6 ± 3.0	14.5 ± 0.	-
OSLO REGION:						
Vestfold lava plateau[7]						
Basalts	-	-	-	3.8	-	-
Rhomb porphyries	-	-	-	5.85	-	-
Ekerite[8]	-	-	-	3.9 ± 1.1	6.3 ±1.9	-

References: 1 = Bougault et al. 1980, 2 = Wood et al. 1979b, 3 = Baker et al. 1977, 4 = Claque and Frey 1982, 5 = Chauvel and Jahn 1984, 6 = Beckinsale et al. 1978, 7 = Oftedahl 1977, 8 = Dietrich et al. 1965.

elements with comparably low D's should show linear relationships (Ferrara and Treuil 1974). Thus the ratios of these elements should remain constant during evolution. Bougault et al. (1980) have used this relationship to infer that Y/Tb, Zr/Hf and Nb/Ta ratios in oceanic basalts from the Atlantic and Pacific oceans should reflect similar ratios in their mantle source regions (Table 6.3). Whereas, Baker et al. (1977) have used Zr/Hf and Nb/Ta ratios for a basalt - benmoreite - trachyte suite from the Gregory rift, Kenya, to infer a cogenetic relationship for these rocks.

Other ratios which might be used include Th/U (Raade 1977), Zr/Nb and Y/Zr (Oftedahl 1977; Section 2.5.5). In theory, any combination of the elements Y, Tb, Zr, Hf, Nb and Ta might be used, since the bulk distribution coefficients for these elements tend to be similar (Bougault et al. 1980):

$$D_Y \approx D_{Tb} > D_{Zr} \approx D_{Hf} > D_{Nb} \approx D_{Ta}.$$

However, Zr should be used with caution, since the Zr contents of the more felsic rocks may be buffered by a high alkalinity (Watson 1979). Various trace element ratios for different petrogenetic suites are listed in Table 6.3.

6.4 Discussion of the results

Trace elements in the Hurdal area may be divided into four groups: (I) Those which increase in concentration during evolution from monzodiorite to granite; (II) those which decrease in concentration during evolution; (III) those which show both late stage enrichments and depletions in concentration; and (IV) those which show no clear relationship with differentiation index.

Included within Group I are elements with bulk distribution coefficients which are generally considerably less than one: Rb, Nb, Ta, Pb, Th and U. These elements tend to be excluded

from the principal mineral phases and are therefore concentrated in the residual liquid during fractionation. Their behaviour is in general independent of major element geochemistry.

Included within Group II are elements with bulk distribution coefficients which are generally greater than one: V, Co, Sr, Ba, light REE and Eu. These elements tend to be partitioned into ferromagnesian minerals and feldspars and are therefore depleted in the residual liquid during fractionation. Group II elements may be subdivided into two categories: (a) Elements which show progressive depletions throughout evolution from monzodiorite to granite (V, Co and Sr); and (b) elements which show moderate early enrichments, during the monzodiorite - biotite syenite stage of evolution, followed by progressive depletions during the later stages of development (Ba, Eu and LREE). Elements belonging to group IIa tend to show strong correlations with the major elements Mg, Fe, Ca, Ti and P, and particularly in the early stages of evolution are partitioned into clinopyroxene, plagioclase, Fe-Ti oxides and apatite. In comparison, elements belonging to group IIb show only moderate correlations with the same major elements, and are concentrated more into alkali feldspars and accessory mineral phases. Overlap between the members of group IIa and IIb provides a continuum in their behavioural patterns (Figures 6.2 a to e).

Group III contains the ore-metals Cu and Zn, together with Li, Cr, Y, Zr, Hf and heavy REE. These elements tend to show only moderate enrichments in the early stages of evolution, followed by both enrichments and depletions in the later stages. This group may also be divided into two categories: (a) Elements which show strong to moderate correlations with Mn and F (Cu, Zn, Li and Cr); and (b) elements which show moderate to weak correlations with these elements (Y, HREE, Zr and Hf). The evolution of group III elements is likely to have been complex, particularly in the later stages when the

influence of alkalies and F is likely to have been greatest.

The remainder of the elements analysed during this study are grouped together in Group IV: Be, Ni, Mo, Ag, Cd and W. These elements show no clear relationships with differentiation index, or each other, and are grouped together for convenience. Beryllium is at a maximum in the Mn-rich rocks, Mo in the alkali feldspar granite. Nickel and Cd are usually close to detection limits, and W is analytically unreliable (Section 1.5). Silver apparently shows no relationship with any other element analysed.

6.4.1 Major-plus-trace element distribution patterns

The geochemical evolution of intermediate to granitic rocks in the Hurdal area may be summarised with reference to a series of enrichment factor diagrams (Figures 6.2 and 6.3). The order of the elements in these diagrams is one of increasing enrichment in the alkali feldspar granite (Brennhaugen) when normalised by the average monzodiorite composition. The latter is regarded as the least evolved rock-type in the Hurdal area (disregarding the dyke N4ØØ). When plotted in this manner, the elements fall naturally into the groups I to III defined above. Elements from group IV and the ore-metals Cu and Zn have been excluded from these diagrams in order to facilitate inter-element comparisons.

Evolution from monzodiorite to biotite syenite and alkali feldspar syenite is reflected in the trace element geochemistry by moderate enrichments in LREE and all Group I and group III elements (Figures 6.2a and 6.2b). Only elements belonging to group IIa show strong depletions, reflecting fractionation in particular of clinopyroxene and plagioclase. Subsequent evolution from alkali feldspar syenite through to alkali feldspar granite (Figure 6.2 c to e) is marked by progressive depletions in all group II elements, accompanied by moderate enrichments in group I and group III elements.

(a)

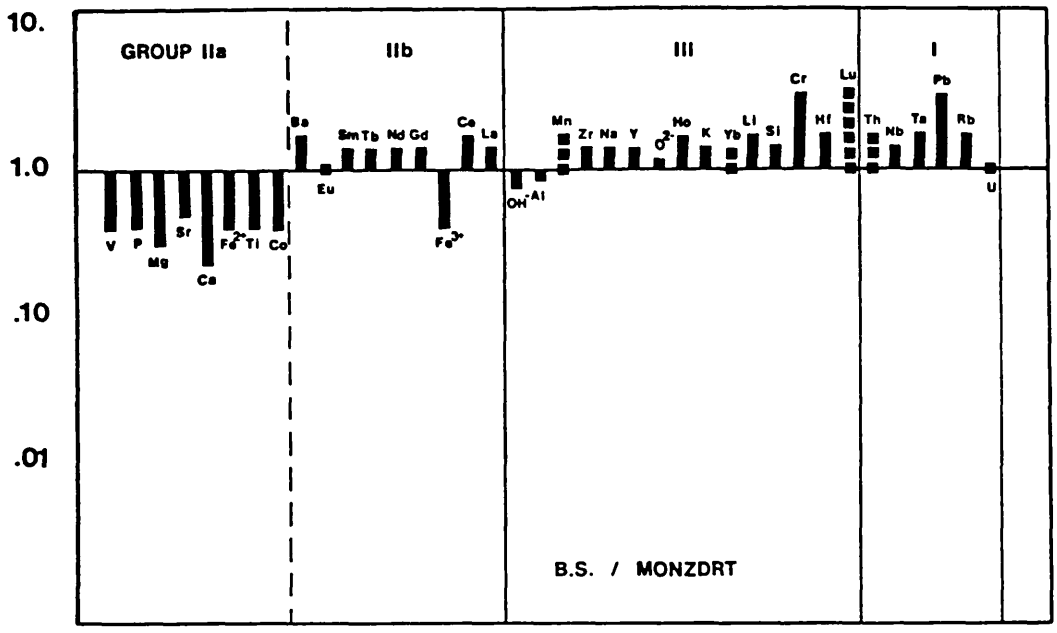

(b)

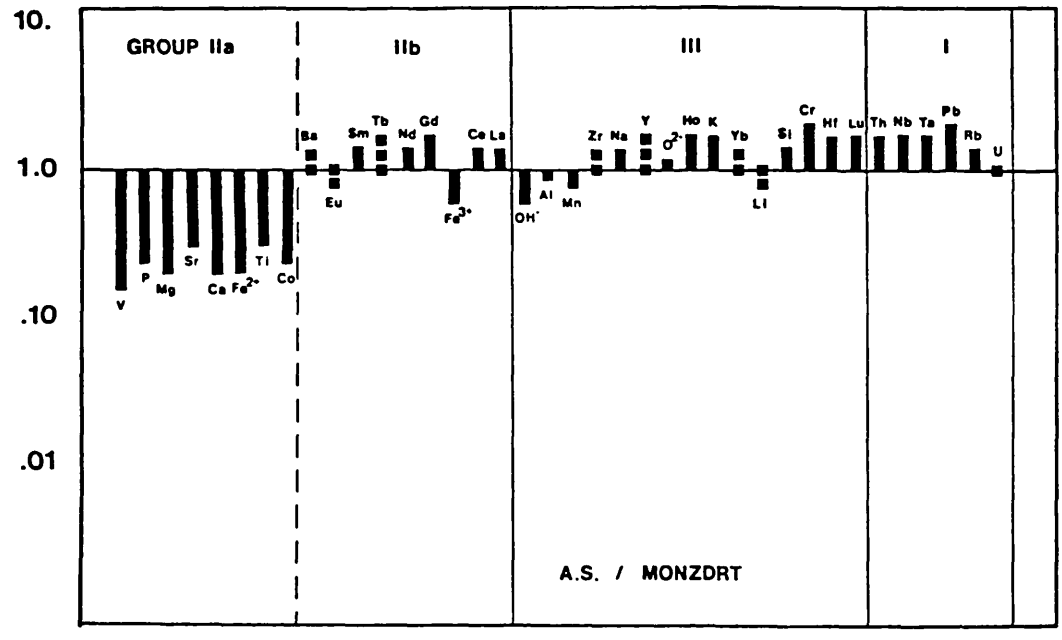

FIGURE 6.2. Monzodiorite (Monzdrt) normalised major-plus-trace element enrichment factor diagrams: (a) Biotite syenite (B.S.); (b) Alkali feldspar syenite (A.S.); (c) Quartz syenite (Q.S.); (d) Alkali feldspar granite (Brennhaugen; A.G.(B)); and (e) Alkali feldspar granite (Rustadkampen; A.G.(R)). The order of the elements is one of increasing enrichment in the Brennhaugen granite.

(c)

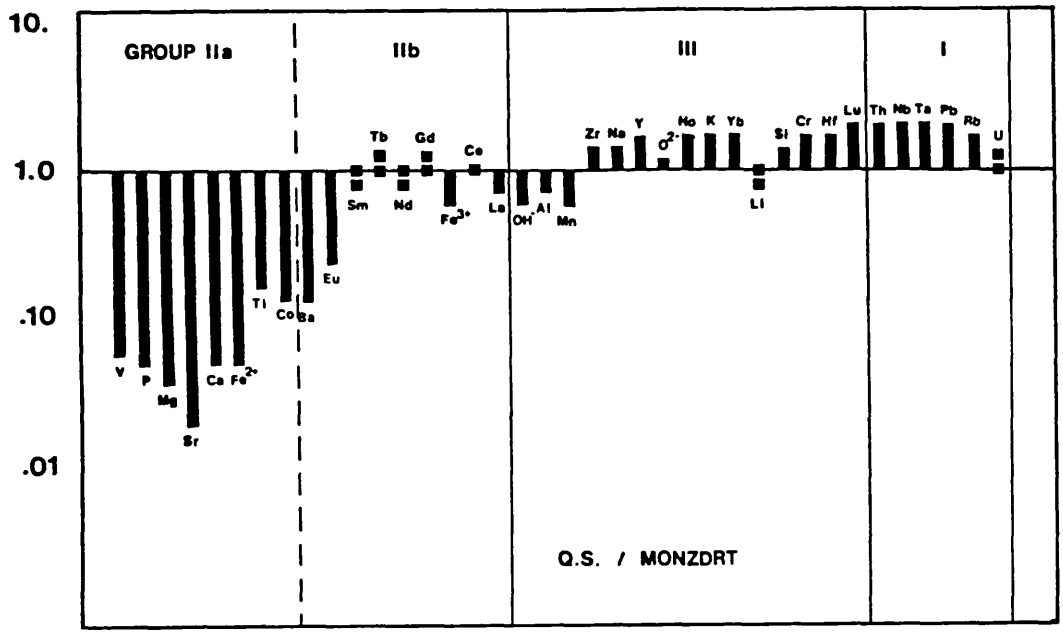
10.
1.0
.10
.01
GROUP IIa
IIb
III
I
V P Mg Sr Ca Fe2+ Ti Co Ba Eu Sm Tb Nd Gd Fe3+ Ce La OH- Al Mn Zr Na Y O2- Ho K Yb Li Si Cr Hf Lu Th Nb Ta Pb Rb U
Q.S. / MONZDRT

(d)

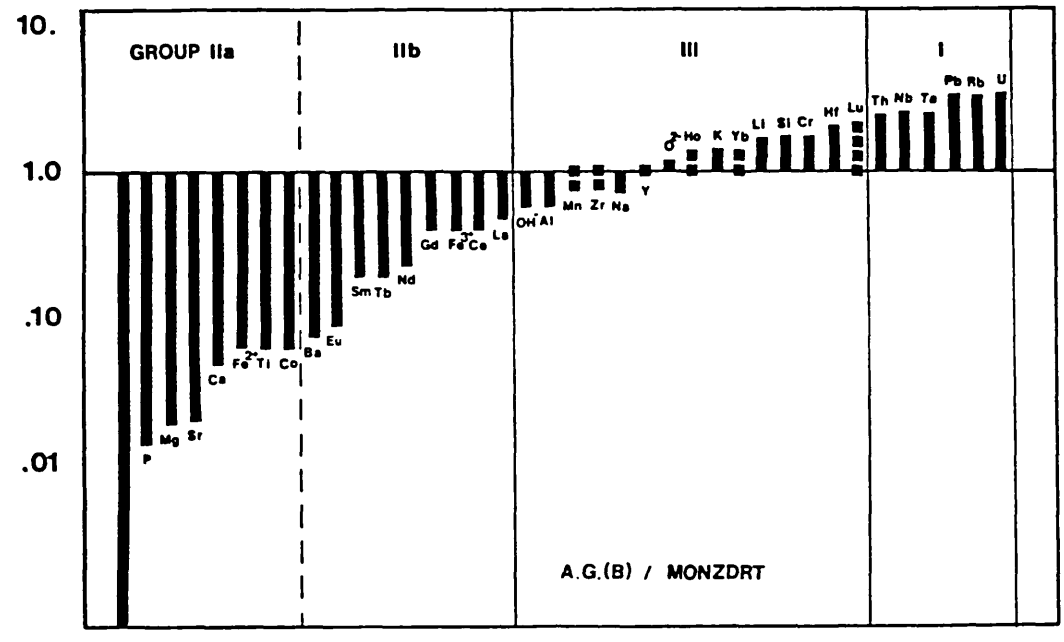
10.
1.0
.10
.01
GROUP IIa
IIb
III
I
P Mg Sr Ca Fe2+ Ti Co Ba Eu Sm Tb Nd Gd Fe3+ Ce La OH- Al Mn Zr Na Y O2- Ho K Yb Li Si Cr Hf Lu Th Nb Ta Pb Rb U
A.G.(B) / MONZDRT

(e)

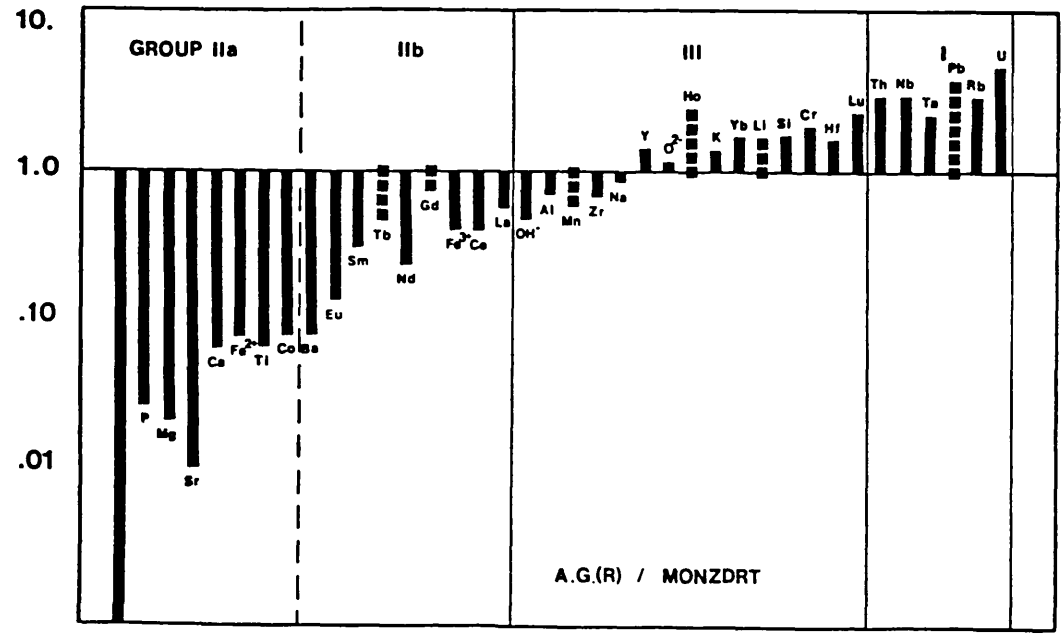
10.
1.0
.10
.01
GROUP IIa
IIb
III
I
P Mg Sr Ca Fe2+ Ti Co Ba Eu Sm Tb Nd Gd Fe3+ Ce La OH- Al Mn Zr Na Y O2- Ho K Yb Li Si Cr Hf Lu Th Nb Ta Pb Rb U
A.G.(R) / MONZDRT

(a)

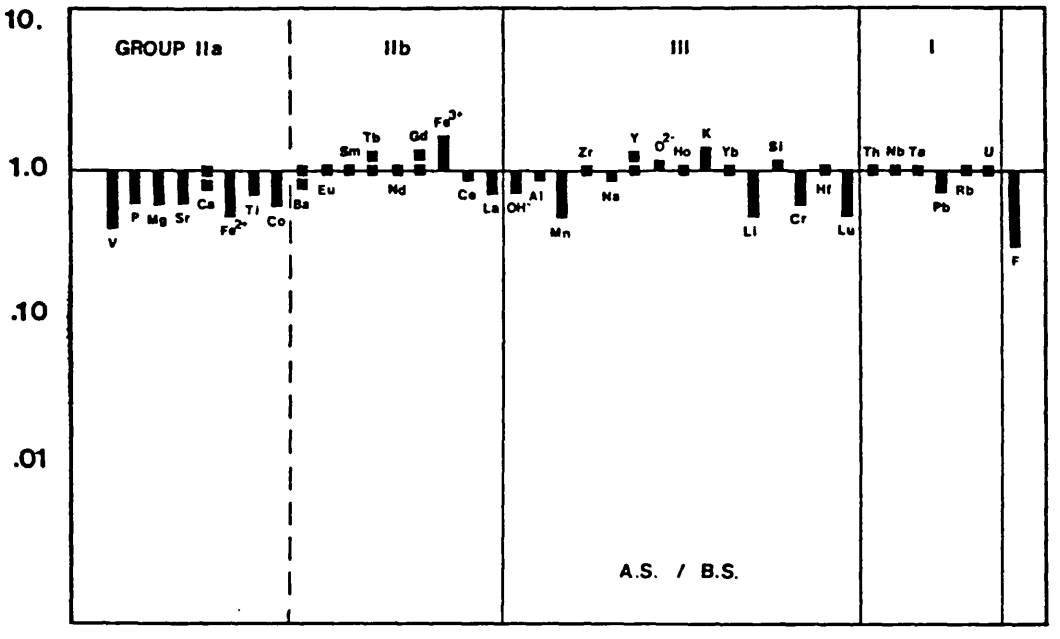

(b)

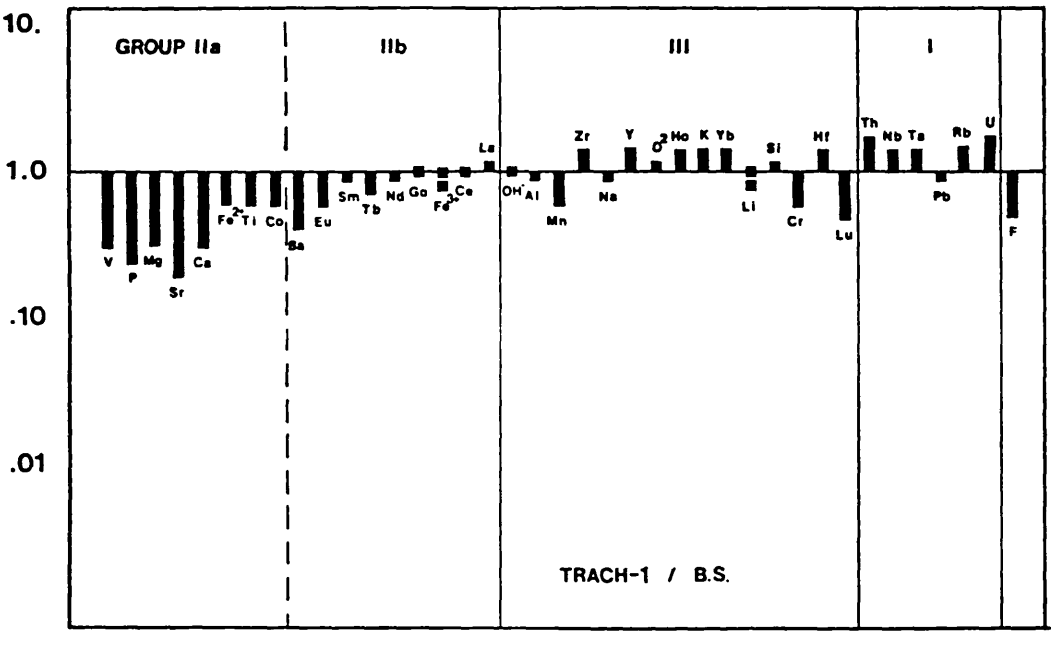

FIGURE 6.3. Comparison between some of the principal rock-types: (a) Biotite syenite normalised Alkali feldspar syenite; (b) Biotite syenite normalised Trachyte (Trach-1 from the Nordgardshogda - Styggberget area); (c) Biotite syenite normalised Trachyte (Trach-2 from the Kongeliveien area); (d) Quartz syenite normalised uneven microgranite (U.M.); (e) Quartz syenite normalised Feldspar porphyritic microgranite (F.P.mG); (f) Brennhaugen granite normalised Rustadkampen granite, and (g) Brennhaugen granite normalised Aplitic microgranite (Ap.mG).

(c)

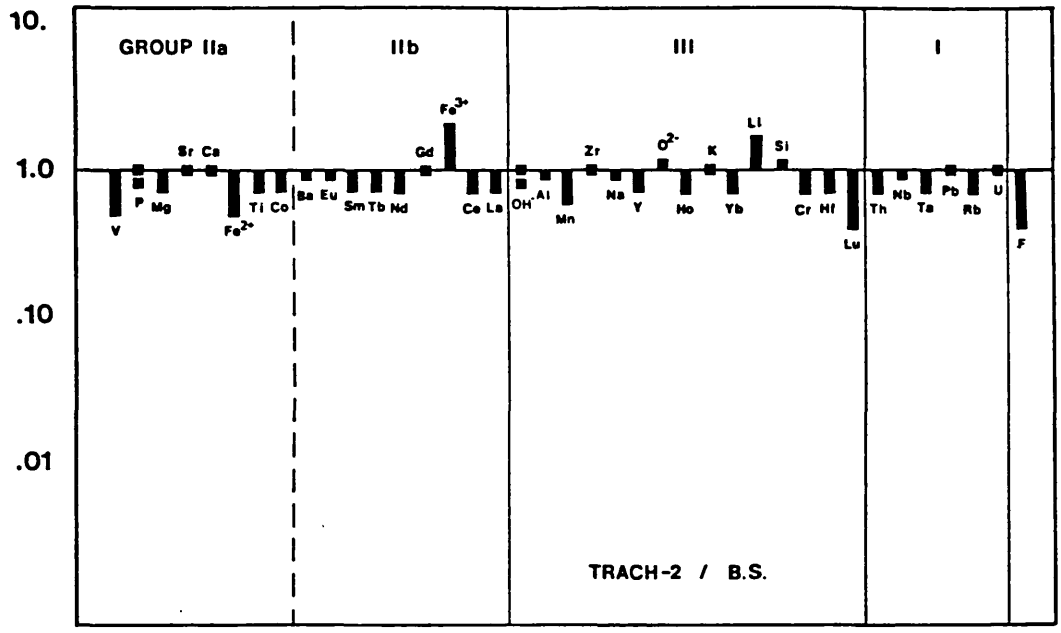
10.
1.0
.10
.01
GROUP IIa
IIb
III
I
V
P
Mg
Sr
Ca
Fe2+
Ti
Co
Ba
Eu
Sm
Tb
Nd
Gd
Fe3+
Ce
La
OH-
Al
Mn
Zr
Na
Y
O2-
Ho
K
Yb
Li
Si
Cr
Hf
Lu
Th
Nb
Ta
Pb
Rb
U
F
TRACH-2 / B.S.

(d)

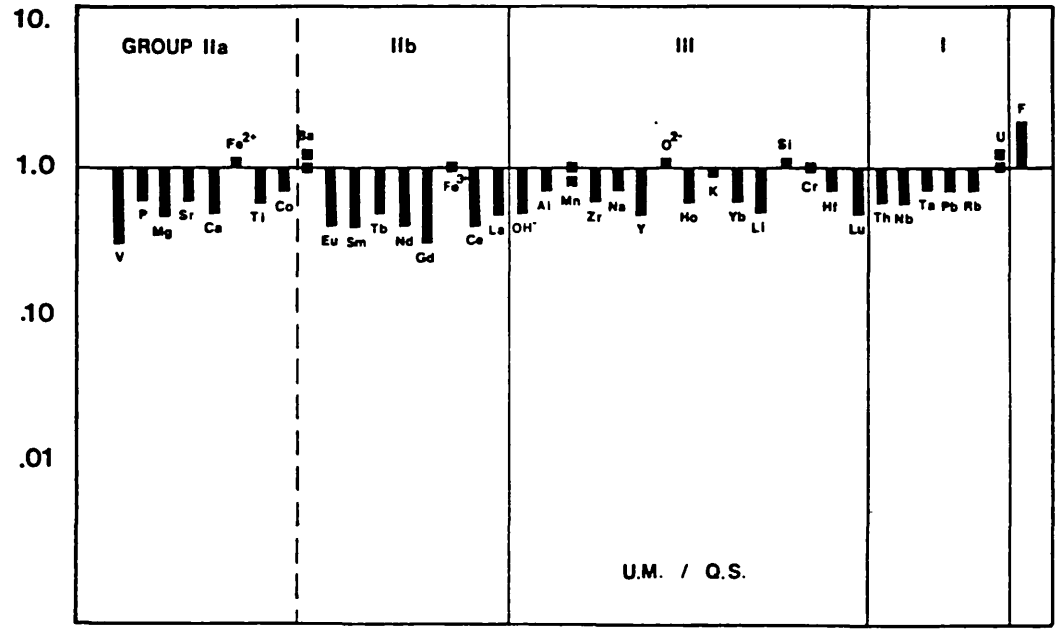
10.
1.0
.10
.01
GROUP IIa
IIb
III
I
V
P
Mg
Sr
Ca
Fe2+
Ti
Co
Ba
Eu
Sm
Tb
Nd
Gd
Fe3+
Ce
La
OH-
Al
Mn
Zr
Na
Y
O2-
Ho
K
Yb
Li
Si
Cr
Hf
Lu
Th
Nb
Ta
Pb
Rb
U
F
U.M. / Q.S.

(e)

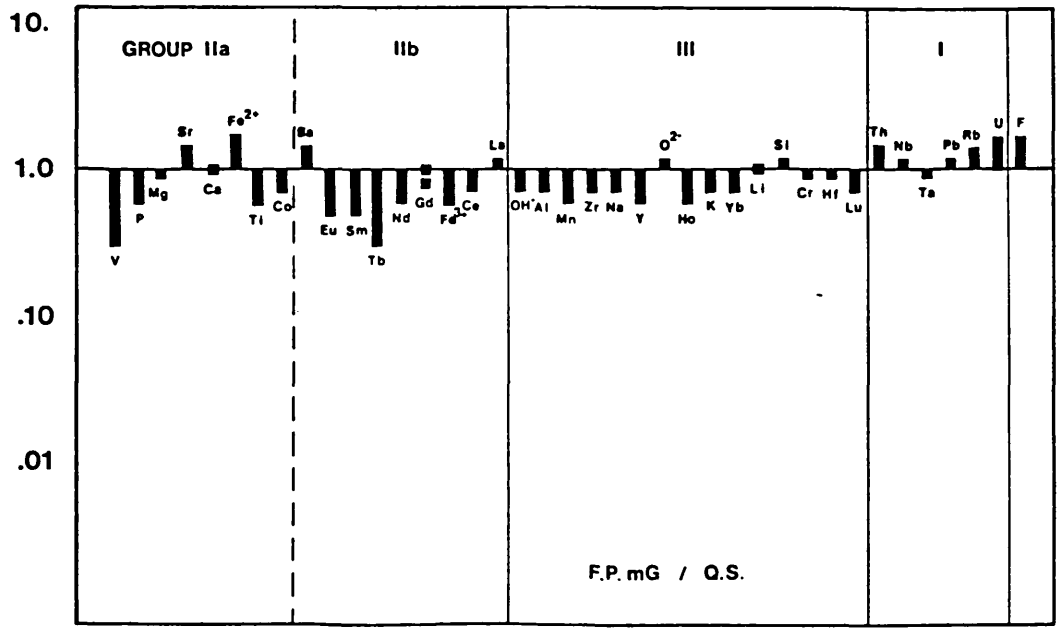
10.
1.0
.10
.01
GROUP IIa
IIb
III
I
V
P
Mg
Sr
Ca
Fe2+
Ti
Co
Ba
Eu
Sm
Tb
Nd
Gd
Fe3+
Ce
La
OH-
Al
Mn
Zr
Na
Y
O2-
Ho
K
Yb
Li
Si
Cr
Hf
Lu
Th
Nb
Ta
Pb
Rb
U
F
F.P. mG / Q.S.

(f)

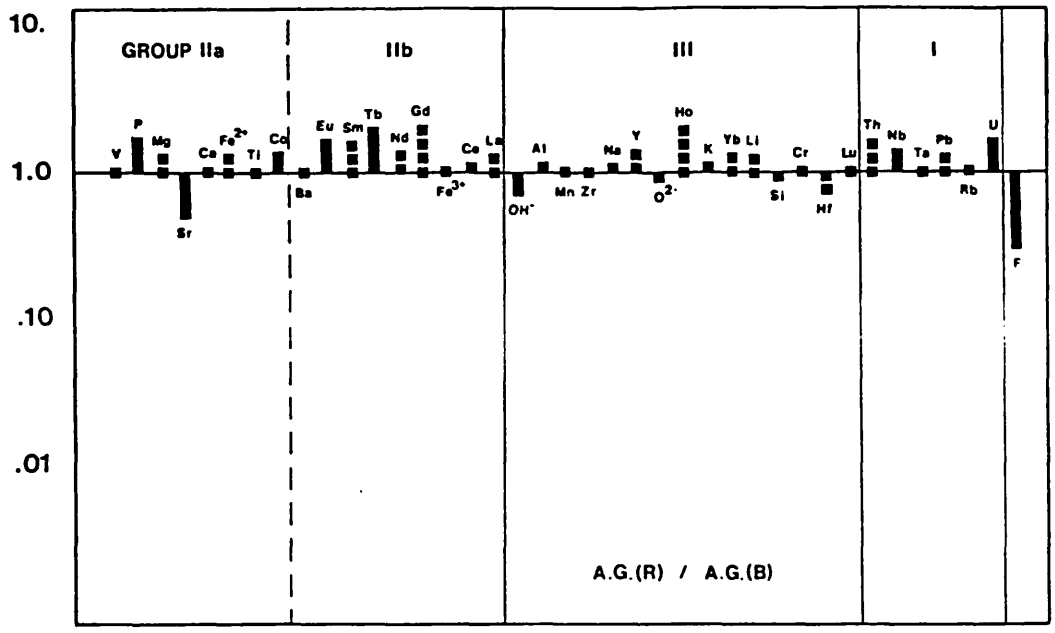
10.
1.0
.10
.01
GROUP IIa
IIb
III
I
V
P
Mg
Sr
Ca
Fe2+
Ti
Co
Ba
Eu
Sm
Tb
Nd
Gd
Fe3+
Ce
La
Al
Mn
Zr
Na
Y
OH-
O2-
Ho
K
Yb
Li
Si
Cr
Hf
Lu
Th
Nb
Ta
Pb
Rb
U
F
A.G.(R) / A.G.(B)

(g)

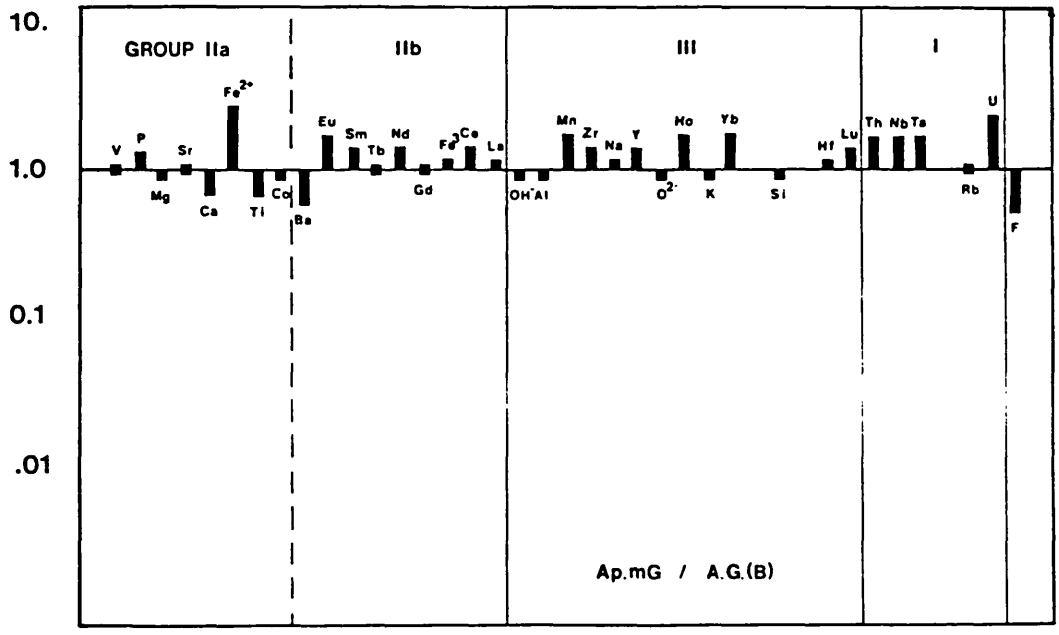
10.
1.0
0.1
.01
GROUP IIa
IIb
III
I
V
P
Sr
Mg
Ca
Fe2+
Ti
Co
Ba
Eu
Sm
Tb
Nd
Gd
Fe3+
Ce
La
Mn
Zr
Na
Y
OH-
Al
O2-
Ho
K
Yb
Si
Hf
Lu
Th
Nb
Ta
U
Rb
F
Ap.mG / A.G.(B)

The reversal in the behaviour of LREE reflects the decrease in importance of clinopyroxene and plagioclase as the dominant phases controlling fractionation and the introduction of a phase which preferentially incorporates LREE (see Section 6.4.3). This stage of evolution is strongly influenced by fractionation of alkali feldspar, reflected in the major element geochemistry by reductions in the total amounts of alkalies and aluminium.

Comparisons between some of the principal rock-types are illustrated in Figure 6.3. The main conclusions which may be obtained from these diagrams are as follows:

(i) Relative to the biotite syenite, the alkali feldspar syenite (Figure 6.3a), and trachytes (TRACH-1 from the Nordgardshogda area, Figure 6.3b; TRACH-2 from the Rustad area, Figure 6.3c) show moderate depletions in all group II elements, together with Na, Mn, group IIIa elements and fluorine.

(ii) Relative to the quartz syenite, the uneven microgranite (Figure 6.3d) and feldspar porphyritic microgranite (Figure 6.3e) are depleted in all group II and group III elements. However, the feldspar porphyritic microgranite is enriched in elements belonging to group I.

(iii) The Brennhaugen and Rustadkamgen granites are more or less identical in terms of major and trace element geochemistry (Figure 6.3f), supporting the hypothesis (Section 3.2) that they belong to a single intrusive phase.

(iv) Relative to the Brennhaugen granite, the aplitic microgranite (Figure 6.3g) is enriched in all elements with the exception of Ca, Ti, Ba and F.

6.4.2 Hygromagmatophile element distributions

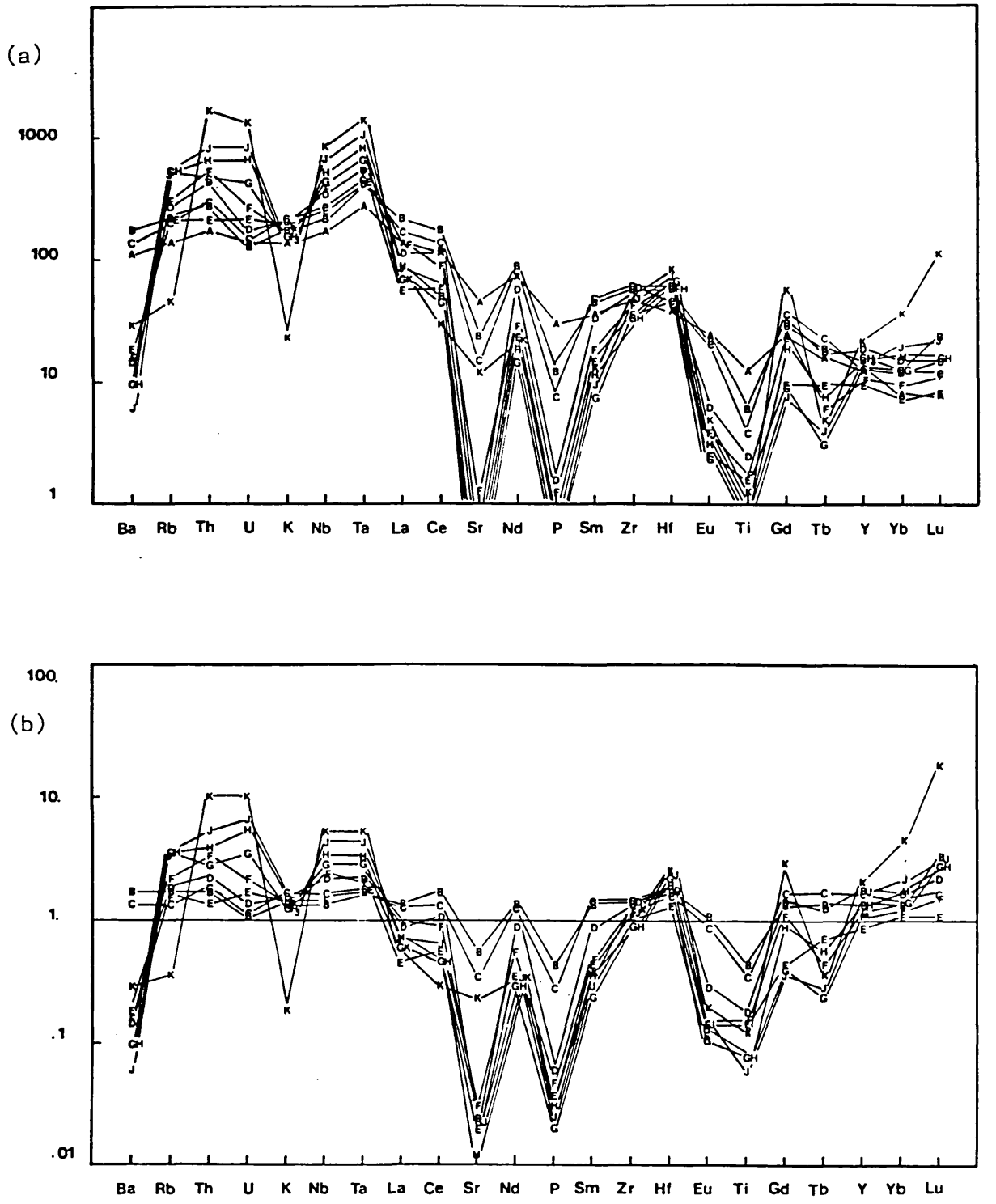

FIGURE 6.4. Hygromagmatophile element distributions for the principal plutonic rock-types in the Hurdal area, normalised to: (a) The primordial mantle (Sun 1982, Wood et al. 1979); and (b) The average monzodiorite composition. Symbols: A = Monzodiorite; B = Biotite syenite; C = Alkali feldspar syenite; D = Quartz syenite; E = Uneven microgranite; F = Feldspar porphyritic microgranite; G = Alkali feldspar granite (Brennhaugen); H = Alkali feldspar granite (Rustadkampen); J = Aplitic microgranite; K = Manganogranitoid; L = Trachyte 1 (Nordgardshogda - Styggberget area); M = Trachyte 2 (Kongeliveien).

The average hygromagmatophile element compositions of the principal rock-types from the Hurdal area are compared with estimated primordial mantle abundances (Wood et al. 1979b, Sun 1982; Appendix A3) in Figure 6.4a, and with the average monzodiorite composition in Figure 6.4b. The order of the elements chosen is that used by Thompson (1982) with minor additions.

Comparison between Figure 6.4a and Figure 2.14 indicates that the average monzodiorite (kjelsasite) from the Hurdal area has hygromagmatophile element distributions similar to those within the larvikites from the southern part of the Region, showing systematic enrichments in the more incompatible trace elements (D much less than one). Figure 6.4a also indicates that the monzodiorite has the largest enrichments in group II elements and the lowest enrichments in elements belonging to groups I and III, relative to the primordial mantle. This supports the contention made in the previous section that the monzodiorite represents the least evolved rock-type in the Hurdal area.

Comparison between Figures 6.4a and 6.4b indicates very clearly the importance of group I and group II elements in alkali granite genesis. Progressive enrichments in Rb, Th, U, Nb and Ta reflect low bulk distribution coefficients for these elements. In contrast, extreme depletions in Ba, Sr, P, Ti and Eu reflect preferential partitioning of these elements into discrete mineral phases such as feldspars, apatite and ilmenite. Group III elements, on the other hand, show far more variable behaviour, late-stage enrichments and/or depletions in Zr, Hf, HREE and Y possibly reflecting magmatic and/or metasomatic processes (Section 6.5).

6.4.3 Rare earth element distributions

The average rare earth element compositions of the principal plutonic rock-types from the Hurdal area are compared with

(a)

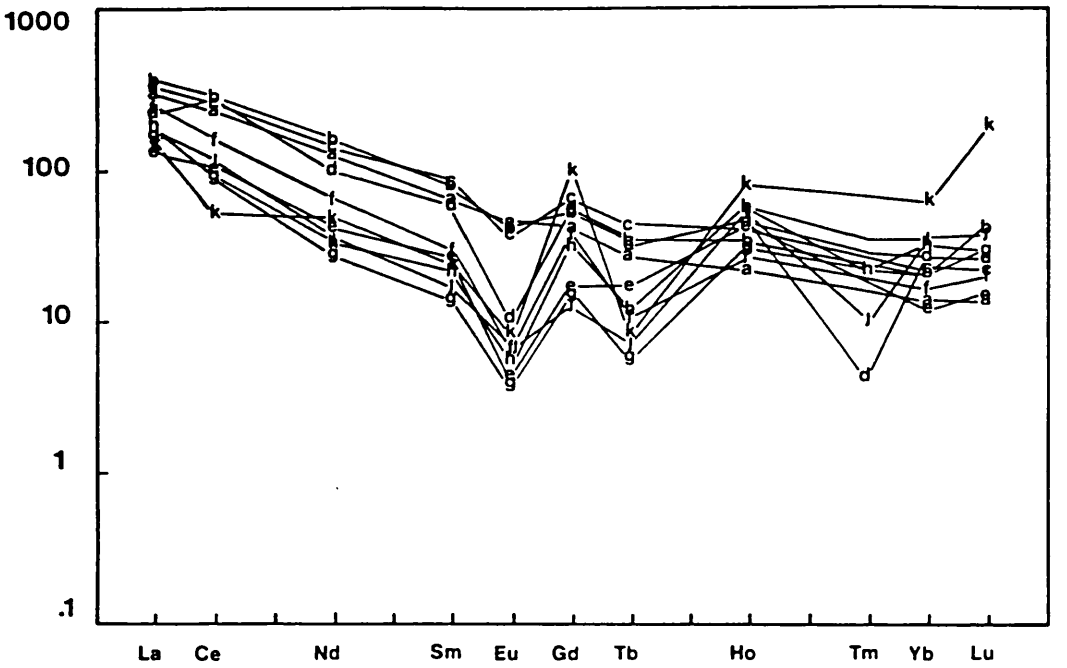

(b)

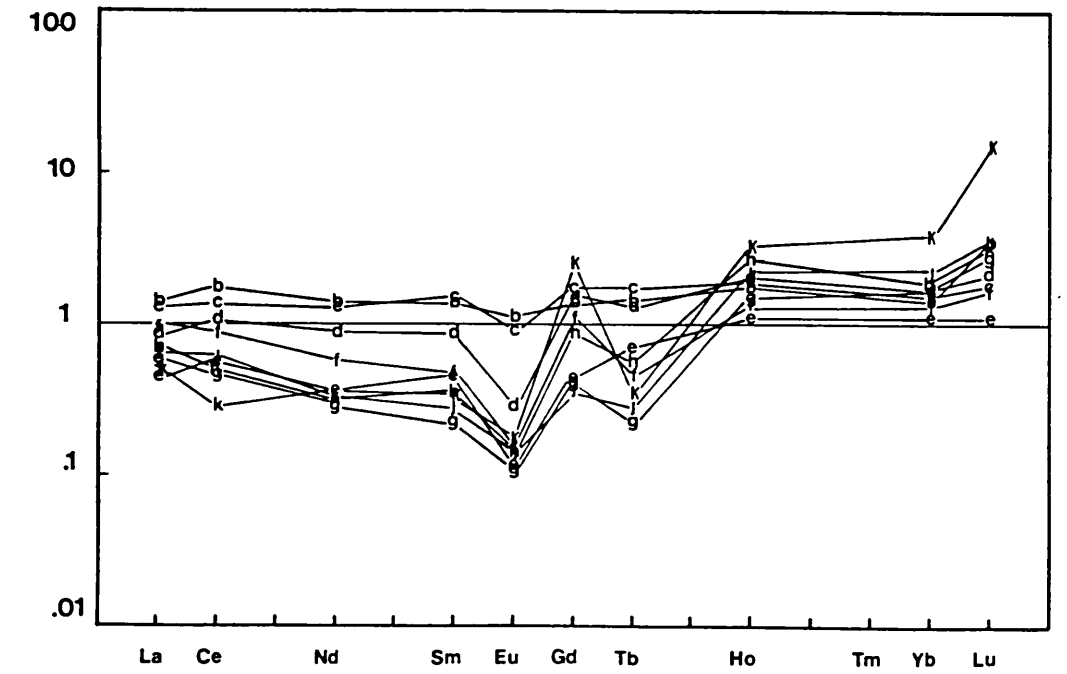

FIGURE 6.5. Rare earth element distributions for the principal plutonic rock-types in the Hurdal area, normalised to: (a) The average of ten ordinary chondrites (Nakamura 1974); and (b) The average monzodiorite composition. Symbols as in Figure 6.4.

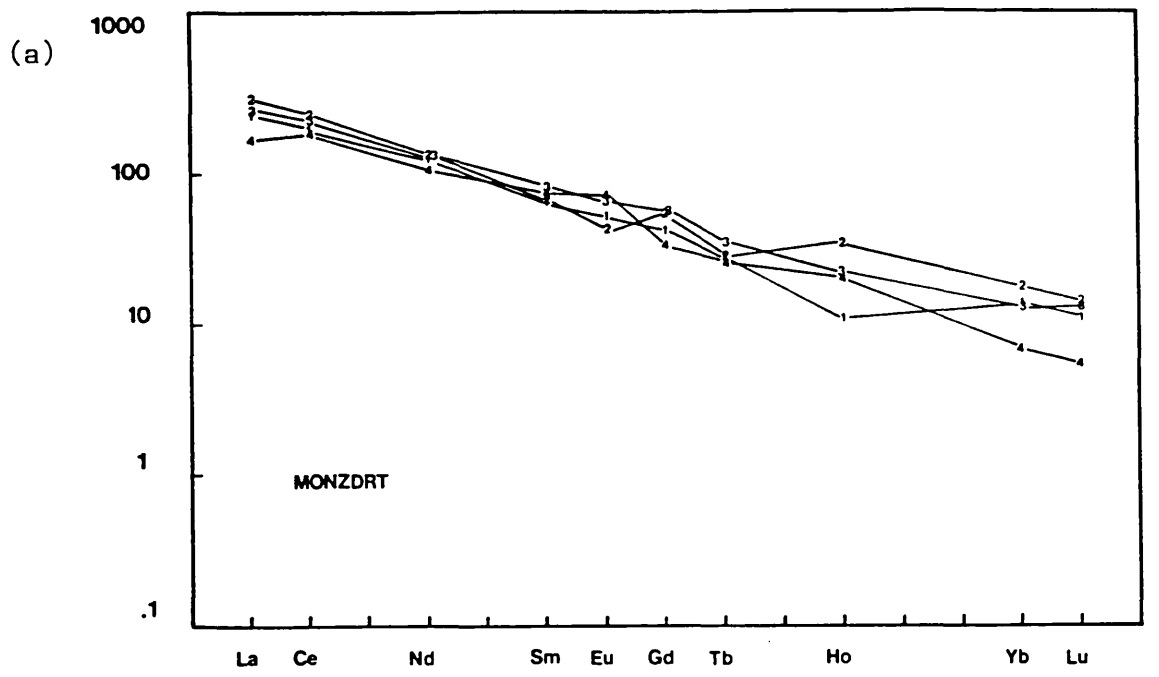

FIGURE 6.6. Chondrite normalised rare earth element distribution patterns for the individual rock-types: (a) Monzodiorites and related rocks (1 = M1, 2 = M2, 3 = W18AB, 4 = N400); (b) Biotite syenite (1 = N112, 2 = N164, 3 = N253,1, 4 = N90B3, 5 = N90C6); (c) Alkali feldspar syenite (1 = W7, 2 = W80, 3 = V29, 4 = V42, 5 = V50, 6 = V51, 7 = P6, 8 = K32, 9 =RH1, 0 = H13, a = W36A); (d) Quartz syenite and related rocks (1 = W16, 2 = N1, 3 = N5B, 4 = N13, 5 = N60A, 6 = N63, 7 = N306, 8 = N363, 9 = K14, 0 = K29, a = N79, b = N218A, c = N251,6, e = N329A, f = N366); (e) The Brennhaugen granite and related rocks (1 = W24, 2 = W43A, 3 = W511, 4 = W69, 5 = W76, 6 = WW6, 7 = WW11, 8 = WW19, 9 = WW24, 0 = WW30A, a = L1, b = L2, M = W362); (f) The Rustadkampen granite and related rocks (1= HH3, 3 = HH8, 4 = HH10, 5 = HH13, 6 = HH15, 7 = HH18, 8 = HH20, 9 = HH21, 0 = HH14, H = HA4D, a = HC3, b = HC7, c = HC10); and (g) The extrusive rocks (1 = N219A, 2 = N342, 3 = N349A, 4 = N364, 5 = N324, 6 = K7A, 7 = K11, 8 = K12A, 9 = K21, 0 = K31).

(b)

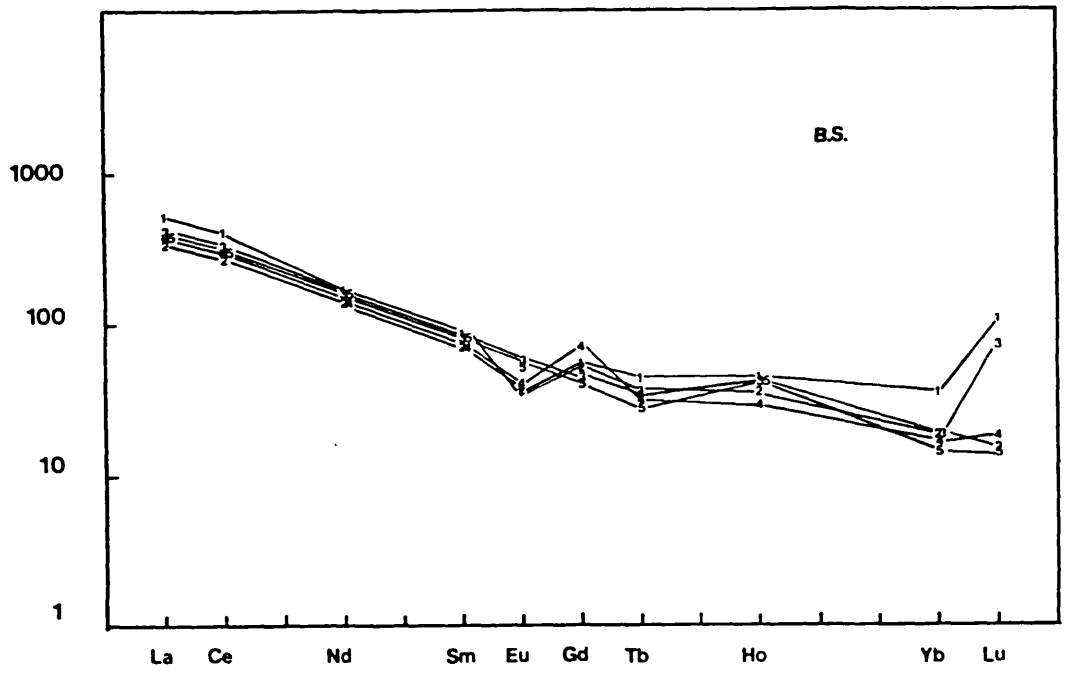
B.S.
1000
100
10
1
La
Ce
Nd
Sm
Eu
Gd
Tb
Ho
Yb
Lu

(c)

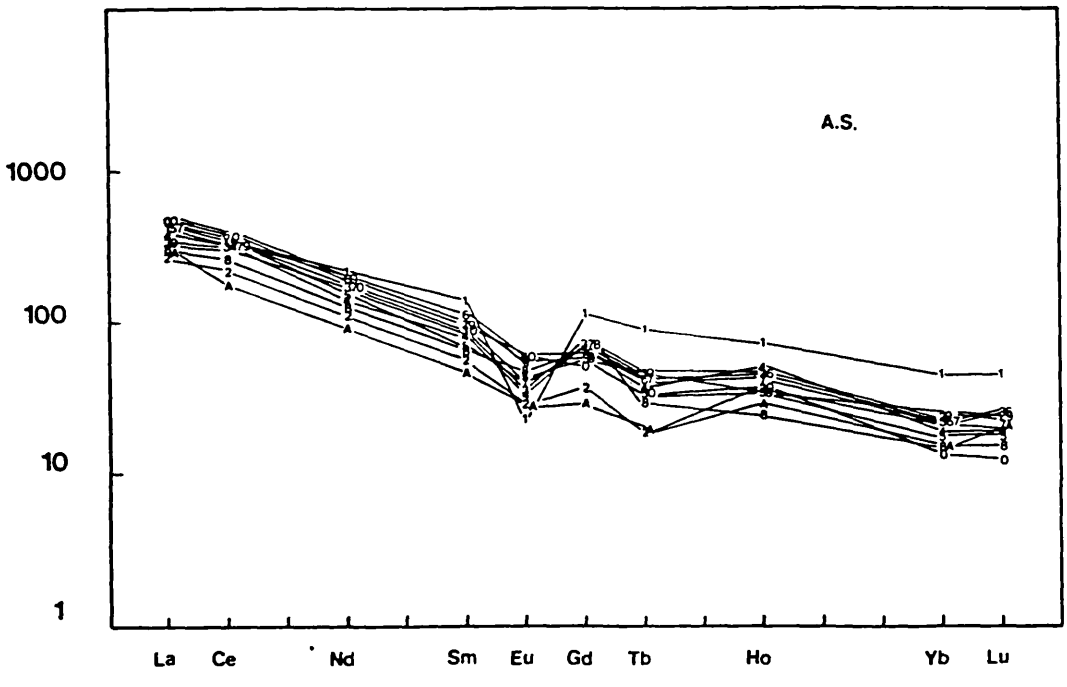
A.S.
1000
100
10
1
La
Ce
Nd
Sm
Eu
Gd
Tb
Ho
Yb
Lu

(d)

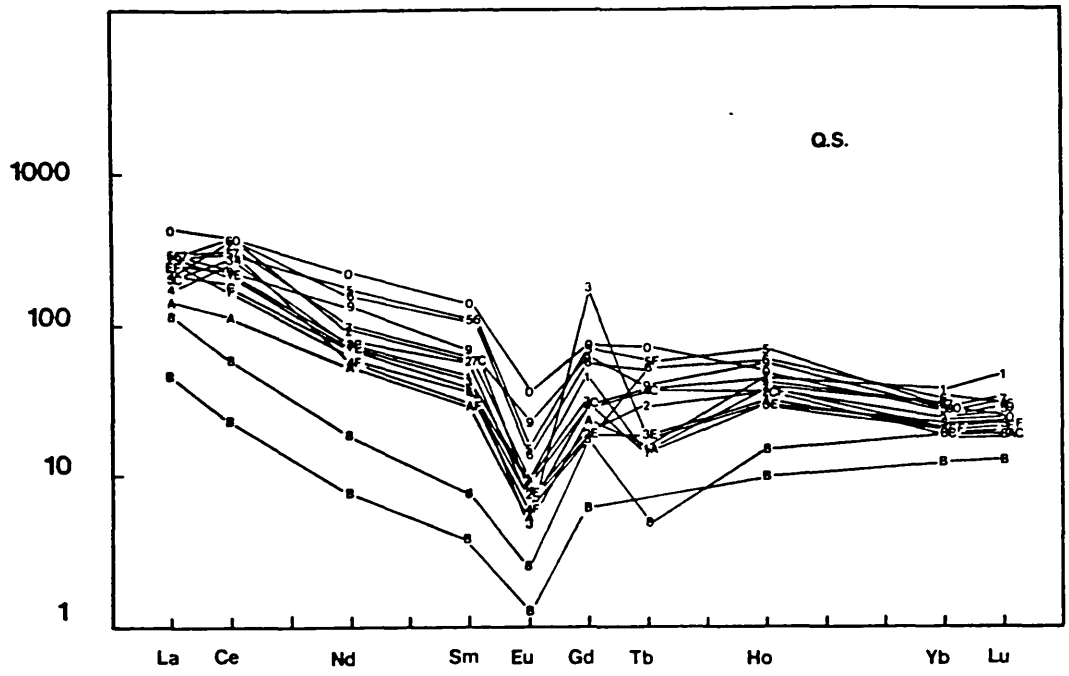
Q.S.
1000
100
10
1
La
Ce
Nd
Sm
Eu
Gd
Tb
Ho
Yb
Lu

(e)

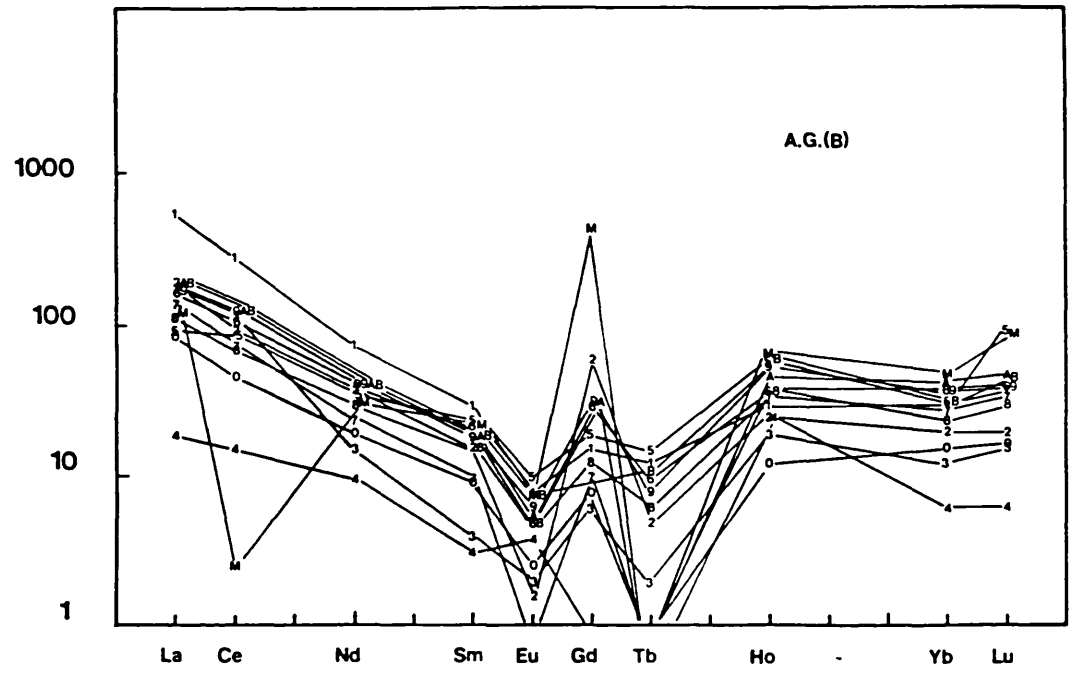
A.G.(B)
1000
100
10
1
La
Ce
Nd
Sm
Eu
Gd
Tb
Ho
Yb
Lu

(f)

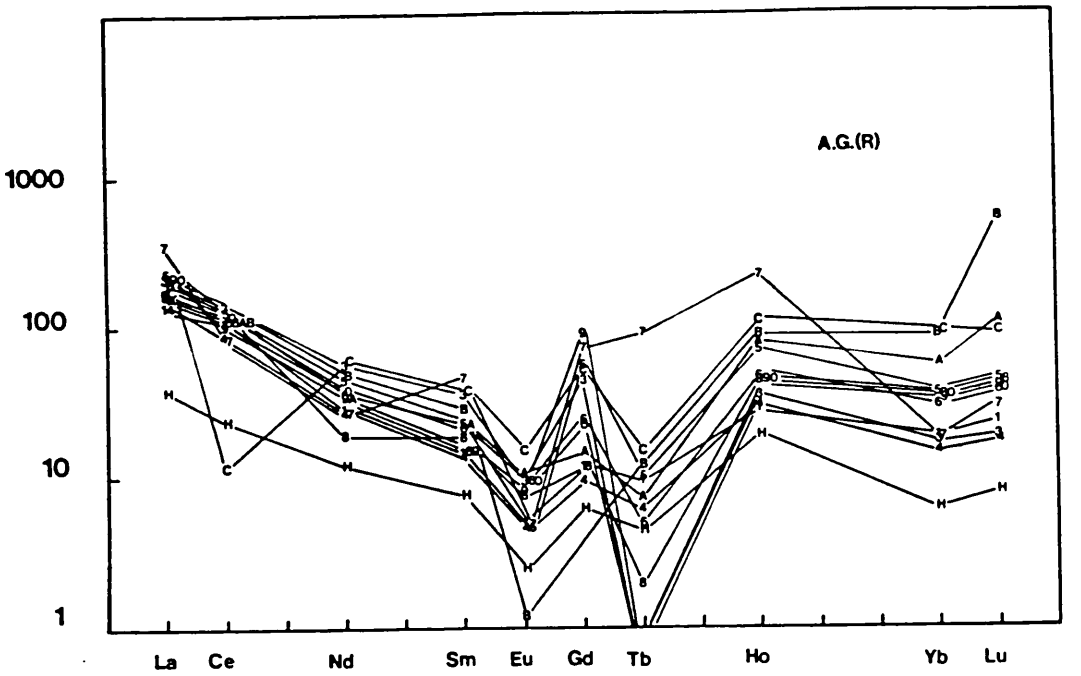
A.G.(R)
1000
100
10
1
La
Ce
Nd
Sm
Eu
Gd
Tb
Ho
Yb
Lu

(g)

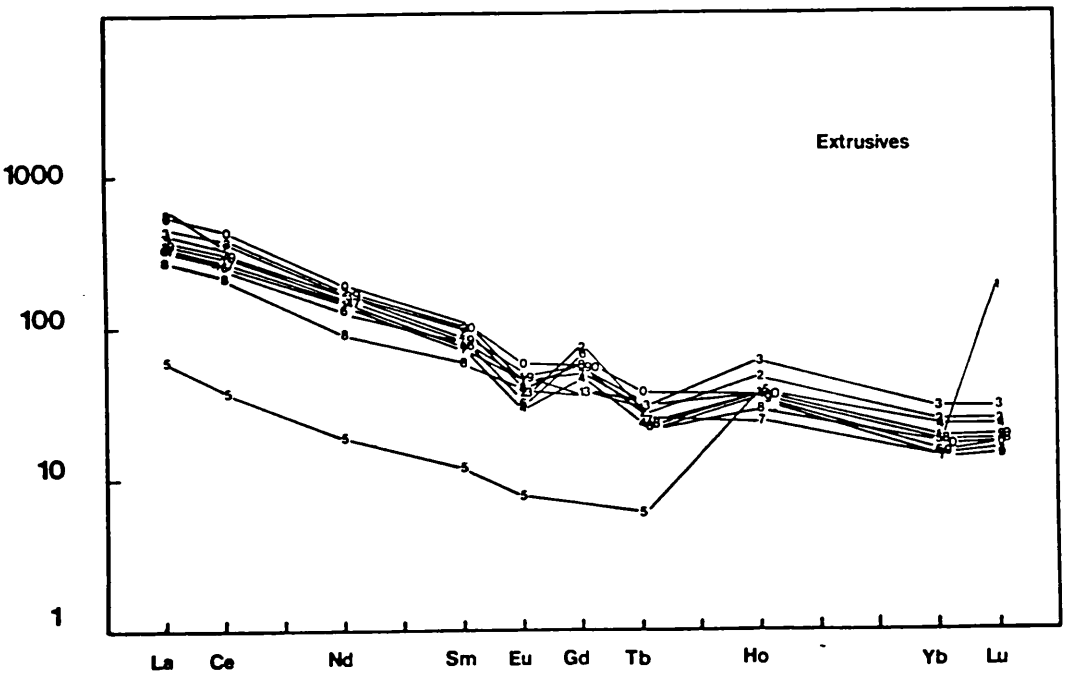
Extrusives
1000
100
10
1
La
Ce
Nd
Sm
Eu
Gd
Tb
Ho
Yb
Lu

the average of ten ordinary chondrites (Nakamura 1974) in Figure 6.5a, and with the average monzodiorite composition in Figure 6.5b. In addition, individual rare earth element distribution patterns for all the principal rock-types are illustrated in Figure 6.6 (a to g).

The rare earth element evolution of intermediate to granitic rocks in the Hurdal area may be summarised as follows. Early evolution, from monzodiorite to alkali feldspar syenite, is characterised by moderate enrichments in all REE and the development of a weak negative Eu anomaly. Subsequent evolution, from alkali feldspar syenite through to alkali feldspar granite, is characterised by progressive depletions in LREE (group II b above) and to a lesser extent Tb and Gd, together with continued, but moderate, enrichments in HREE (Ho, Yb and Lu). Light REE depletion is accompanied by the development of a significant negative Eu anomaly (Figure 6.5). Consideration of individual REE distribution patterns (Figure 6.6), however, indicates considerable overlap exists between the principal rock-types. A similar conclusion was reached on the basis of major element geochemistry in Section 5.4. The behaviour of LREE in particular is highly variable.

As stated in Section 2.5.5, development of a large negative Eu anomaly may be explained in terms of fractionation of feldspar, under conditions of moderate to low oxygen fugacity (high Eu^{2+}/Eu^{3+} ratio). Progressive depletions in LREE and enrichments in HREE, however, are difficult to explain in terms of fractionation of the principal rock-forming minerals, since these minerals generally exclude LREE (Section 2.5.5; Irving 1978). The rare earth element evolution of felsic rocks in the Hurdal area would therefore appear to have been controlled by the presence of a minor mineral phase which preferentially incorporates LREE. Such a mineral might be represented by apatite, zircon or sphene (Section 6.3), or by a rare-earth mineral such as monazite. The fact, however, that apatite was largely fractionated out

by the alkali feldspar syenite stage of evolution (Table 5.1) indicates that this mineral was not responsible for LREE depletion. Sphene also is unlikely to have had much influence on REE evolution, since this mineral is only an important accessory phase in the alkali feldspar syenite, where it occurs as a reaction product of ilmenite (Section 3.3.3). Similarly, zircon is only an important accessory mineral in the alkali feldspar granite and is therefore too late in the crystallisation sequence to have had much influence on REE distributions. No exotic rare earth minerals have been identified in the Hurdal area.

Experimental evidence (Irving 1978) and measurements of phenocryst/matrix relationships in high-silica rhyolites (Mahood and Hildreth 1983) indicate that the crystal/liquid distribution coefficients for trace elements in many of the rock-forming minerals are strongly compositionally (and temperature) dependent. Particularly in high-silica magmas, the distribution coefficients, K_D, for REE, as well as for certain high field strength elements such as Zr and Hf, in orthopyroxene, clinopyroxene, biotite and Fe-Ti oxides may be considerably greater than one. These changes are believed to reflect a decrease in the availability of octahedral coordination sites in the melt, affecting LREE to a greater extent than HREE due to their larger ionic radii. As such they would appear to reflect a reduction in the proportion of modifier cations in the melt (Mg, Fe and Ca; Section 5.5.1), and a consequent increase in the degree of silicate polymerisation (Mysen and Virgo 1980b). This is indicated by the low ratio of non-bridging oxygens to tetrahedral coordination sites in high silica magmas (NBO/T; Mahood and Hildreth 1983).

The large variations in LREE distributions observed within the quartz syenite and alkali feldspar granite (Figure 6.6 d to f) are best explained in terms of variations in the degree of silicate polymerisation. An increase in the degree of

silicate polymerisation in the melt, due to a reduction in the proportion of modifier cations present, results in a decrease in the availability of octahedral coordination sites and increased partitioning of LREE (but not HREE) into mafic mineral phases. The presence of biotite and magnetite, in particular, in the interstices of the quartz syenite and alkali feldspar granite would therefore appear to have effectively controlled the LREE evolution of these rocks. Late-stage enrichments in HREE, however, are likely to have been the result of volatile complexing, the smaller ionic radii of Ho, Yb and Lu favouring complex formation with fluoride and/or carbonate ligands (Section 6.5; Balashov and Krigman 1975).

6.4.4 Trace element distributions in the manganogranitoids

The average major-plus-trace element compositions of four samples of manganogranitoid, from the Steinbratebekken and Hegga river localities (Section 4.3), are compared with the average monzodiorite composition in Figure 6.7a, and with the average alkali feldspar granite (Brennhaugen) in Figure 6.7b. The average hygromagmatophile and rare earth element distributions have already been presented in Figures 6.4 and 6.5, respectively.

Consideration of Figures 6.7a and 6.7b clearly indicates that the manganogranitoids represent the most highly evolved rock-type in the Hurdal area, showing the largest enrichments in group I and group III elements. The only exceptions are Li and Rb, both of which are strongly depleted. Group II elements, on the other hand, show a marked change in their distribution patterns, displaying systematic enrichments relative to the alkali feldspar granite. The only exception is Ce which is strongly depleted in the manganogranitoids (see also Figures 6.5, 6.6e and 6.6f). The major elements Mg, Ca, Fe and Ti, but not P, show similar enrichments (by an order of magnitude).

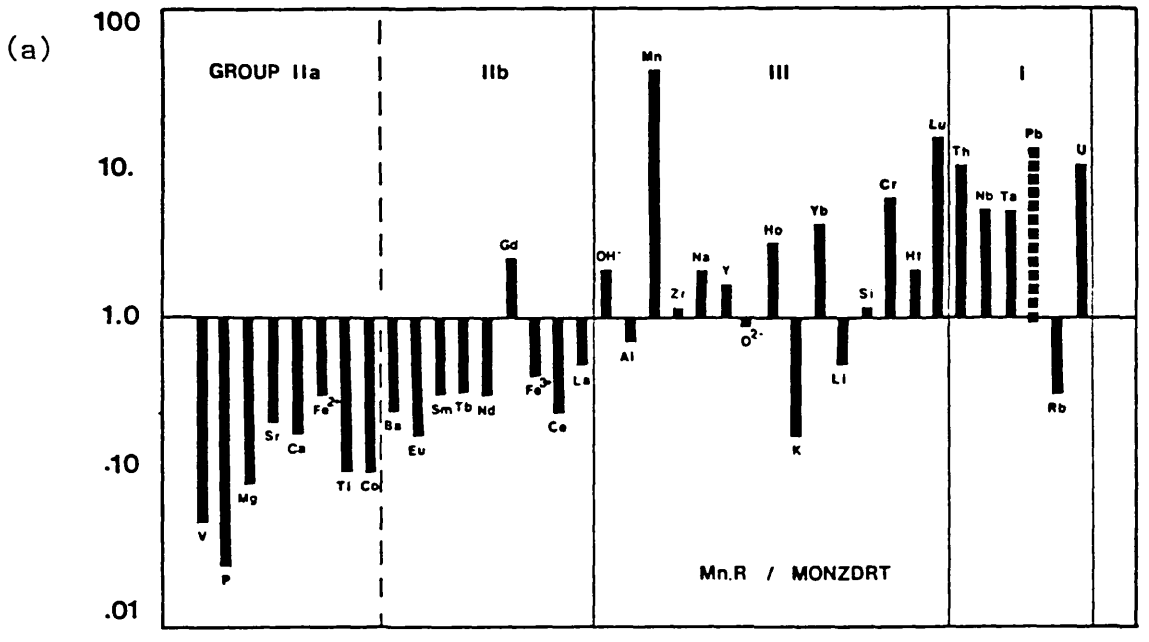

FIGURE 6.7. Trace element distributions in the manganogranitoids (Mn.R), normalised to: (a) The average Monzodiorite composition; and (b) The average Alkali feldspar granite.

The most striking feature of these rocks, however, is the massive increase in Mn concentration, by nearly two orders of magnitude. This is accompanied by substantial enrichments in Na, Al, Zn and F contents, and by depletions in K and Si. These changes are reflected in the mineralogy by the occurrence of rhodonite and/or pyroxmangite as the principal ferromagnesian and Ca-bearing phase, by a predominance of albite over orthoclase, and by the absence of quartz (Section 4.3). Sphalerite and fluorite are important accessory minerals. An increase in the proportion of albite in the rock is reflected in the major element geochemistry by an increase in the ratio of Na to total alkalies (Na/Na+K = .96 $\pm$.Ø2; Table 5.1), while the agpaitic index (Na+K/Al) remains constant at 1.ØØ $\pm$.Ø1 (Figure 5.7a). This indicates a one for one substitution of Na for K. A corresponding increase in the F contents of these rocks (Figure 5.7b), and a strong correlation between the elements of group IIIa and Mn and F (above) strongly suggests that the manganogranitoids are the end-products of late-stage magmatic and/or metasomatic processes involving the build-up of magmatic fluorine and the formation of alkali fluoride, in particular Na-fluoride, complexes (Section 5.5.2). Extreme partitioning of F towards the melt in peralkaline magmas has been demonstrated experimentally by Kogarko and Krigman (1973).

A granitic dyke (HA4D) is observed to cut the manganogranitoids at the Hegga river locality (Figure 4.4). The composition of this dyke is unusual, being depleted in all REE (Figure 6.6f) together with all group IIIb and group I elements with the exception of Rb (Table 6.2). In addition, zones of silicified granite in which most of the Na has been leached out, are observed in close proximity to the manganese-rich rocks in both the Brennhaugen and Rustadkampen granites (samples WW11 and W36A; Section 5.4). The significance of these rock-types will be discussed in relationship to the origin of the manganogranitoids in a

later section (8.5.2).

6.5 Trace element evolution

The trace element evolution of felsic rocks in the Hurdal area to a large extent reflects changes in the proportions of the constituent mineral phases, thereby continually modifying the bulk distribution coefficient for each element. Particularly during the early stages of evolution, fractionation of clinopyroxene and plagioclase has the effect of depleting the magma in elements with high crystal/liquid distribution coefficients for these minerals, in particular V, Co and Sr (but not Eu^{2+}). At the same time fractionation of apatite and ilmenite depletes the magma in P and Ti. The rate at which these elements are depleted (compare Figures 6.1a and 6.1b with Figures 6.8 a to c) strongly suggests fractional crystallisation processes. Vanadium in particular is reduced to a minimum (below detection limits).

Continued fractionation involving plagioclase and alkali feldspar, or ternary feldspar, has the effect of depleting the magma even further in Sr, together with Ba and Eu. Depletions in LREE might also be the result of feldspar fractionation, but would require unusually high K_D's for these elements. More probably, LREE depletion is the result of incorporation of these elements into late interstitial phases such as biotite and magnetite, the unusually high crystal/liquid distribution coefficients for these minerals reflecting increased silicate polymerisation (Section 6.4.3).

Only elements belonging to group I, and to a lesser extent group IIIb, are strongly excluded from the constituent mineral phases, and are therefore concentrated in the residual liquid during fractionation. These are the elements with bulk distribution coefficients closest to zero. But even these elements are not entirely incompatible, Nb and Ta for instance being incorporated into columbite, Zr and Hf into

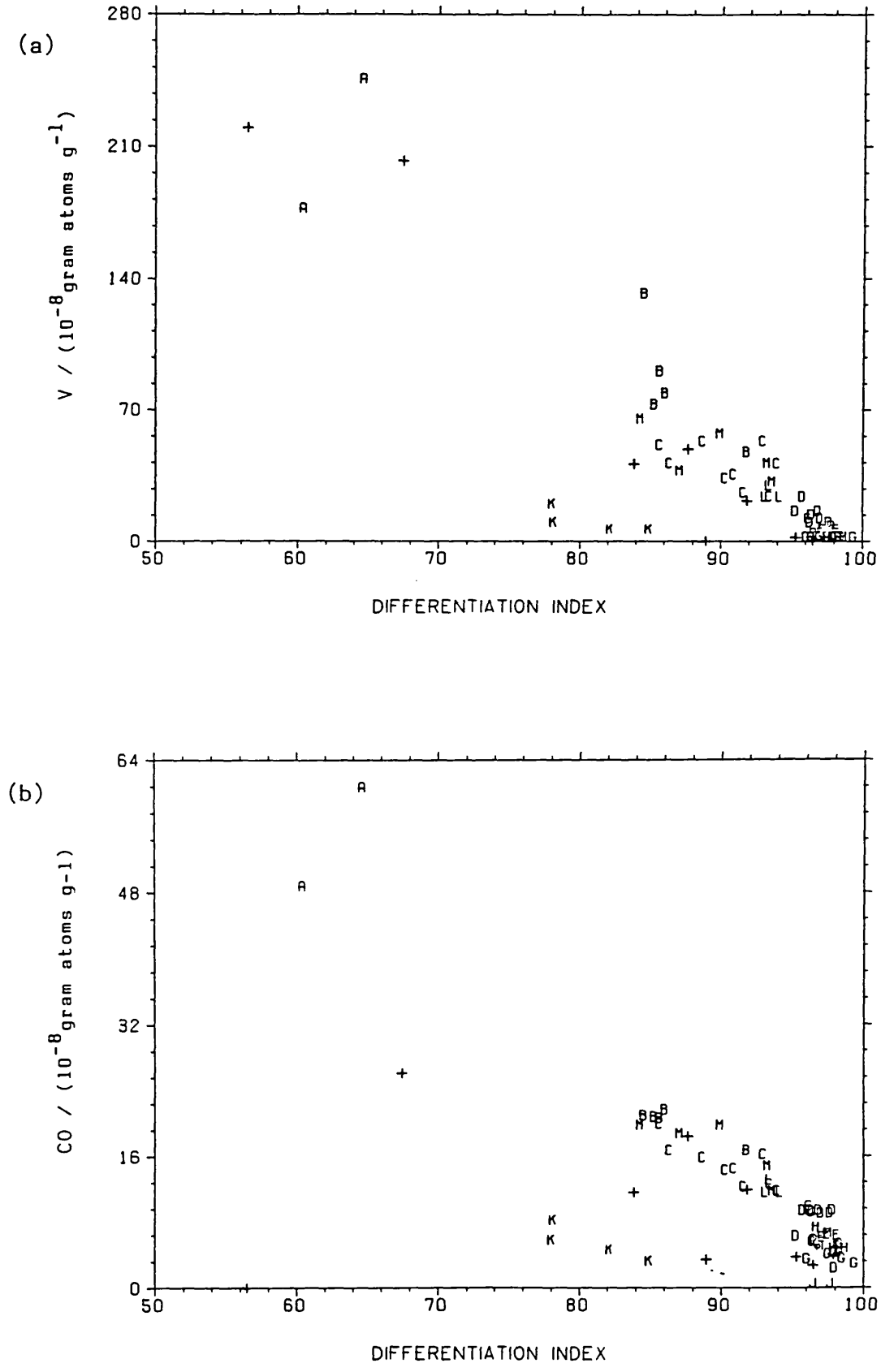

FIGURE 6.8. Scatter plots of Differentiation Index (cation %) versus: (a) V; (b) Co; and (c) Sr (10^{-8} gram atoms g^{-1}). Symbols as in Figure 6.4.

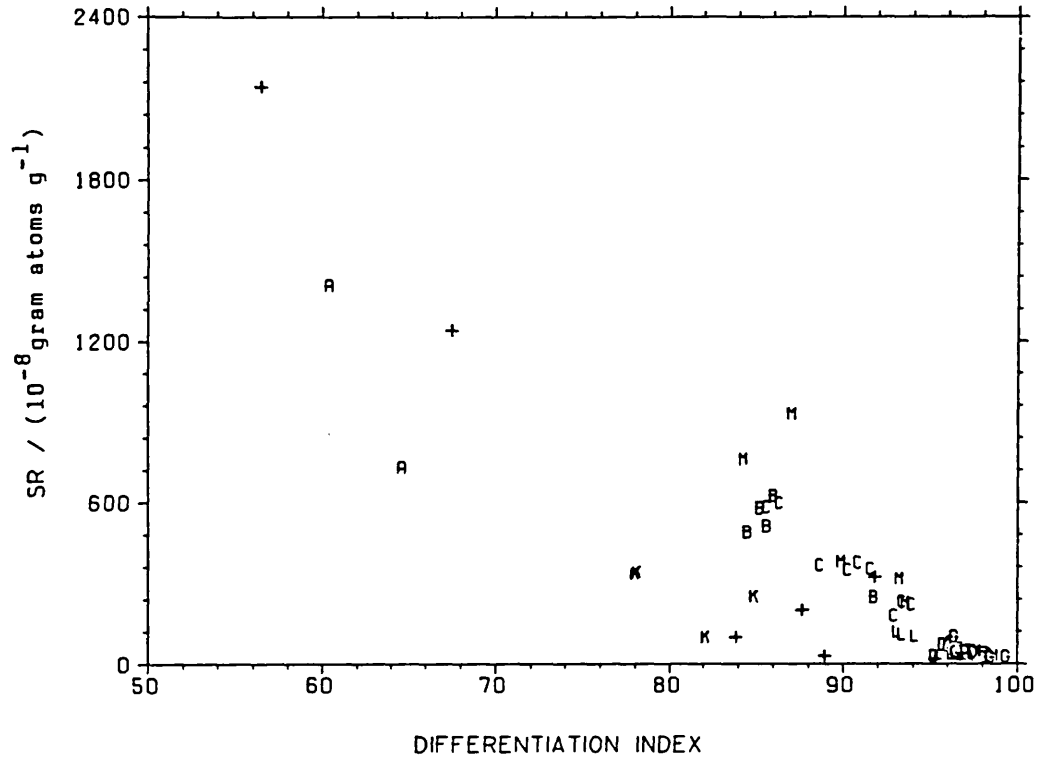

FIGURE 6.8c.

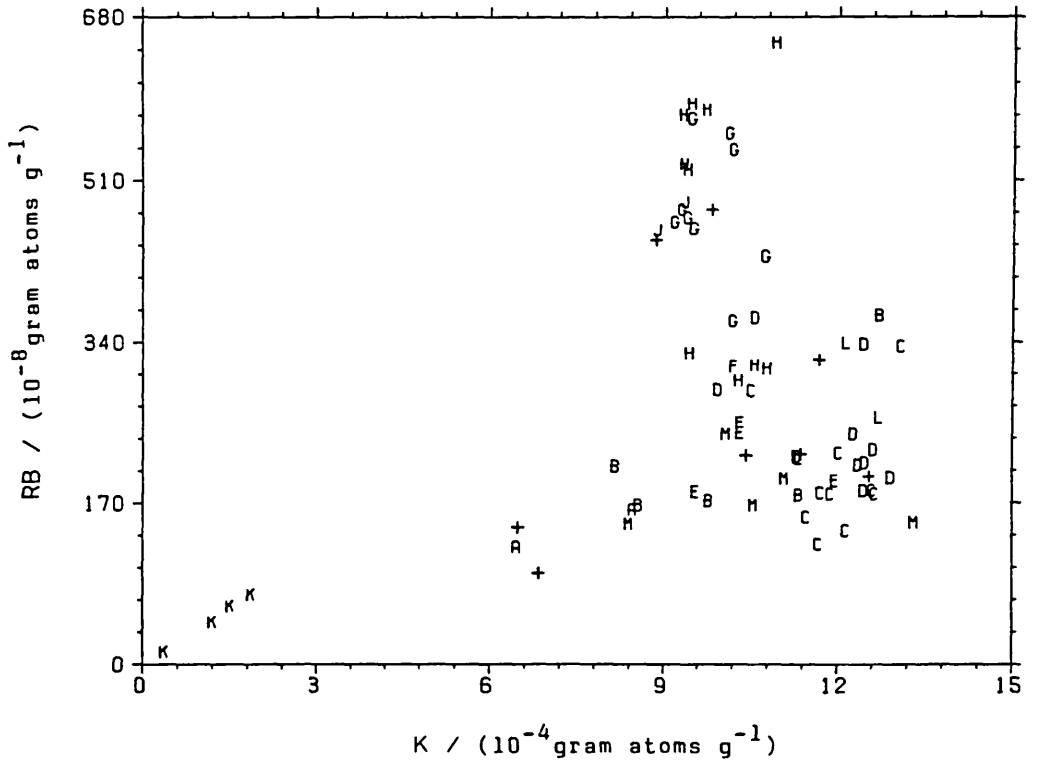

FIGURE 6.9. Scatter plot (gram atoms g^{-1}) of K vs. Rb. Symbols as in Figure 6.4.

zircon. However many of these elements, particularly those with high field strengths (Zr, Nb, Hf, Ta, Th and U; Section 6.3), actually show strong affinities towards the melt.

The behaviour of Rb is particularly interesting. This element has a similar electronegativity, ionization potential and to a lesser extent ionic radius to K (148 pm as opposed to 133 pm). It should therefore behave similarly during evolution (Taylor 1965, Shaw 1968). This probably is the case for the early stages of evolution in the Hurdal area (Figure 6.9). The later stages of evolution, however, are marked by antithetic behaviour of K and Rb. Rubidium therefore is evidently not controlled by alkali feldspar fractionation, except in the sense that it is excluded from this mineral, but must be excluded from all minerals equally. Strong depletions in both K and Rb in the manganogranitoids (Section 6.4.4), however, indicate that these elements behave similarly in the most evolved rocks, being excluded presumably for reasons of large ionic radii (Section 5.5.2).

Rubidium is an example of an element which is excluded from all mineral phases ($K_D < 1$) and does not show a strong chemical affinity towards the melt. It may therefore be regarded as a truely incompatible trace element ($D \approx Ø$) and may be used to estimate the melt fraction remaining after fractional crystallisation processes ($F = C_Ø/C_1$; Section 6.3). In the case of the alkali feldspar granite this is approximately 29 $\pm$ 4 percent.

The behaviour of group III elements is the most variable and the hardest to explain. To a certain extent these elements, in particular HREE, show overlapping behaviour with group I, having bulk distribution coefficients less than one. The fact, however, that they show both enrichments and depletions within individual rock units, notably within the alkali feldspar granite (Section 6.4), indicates that their evolution must have been influenced by late-stage magmatic

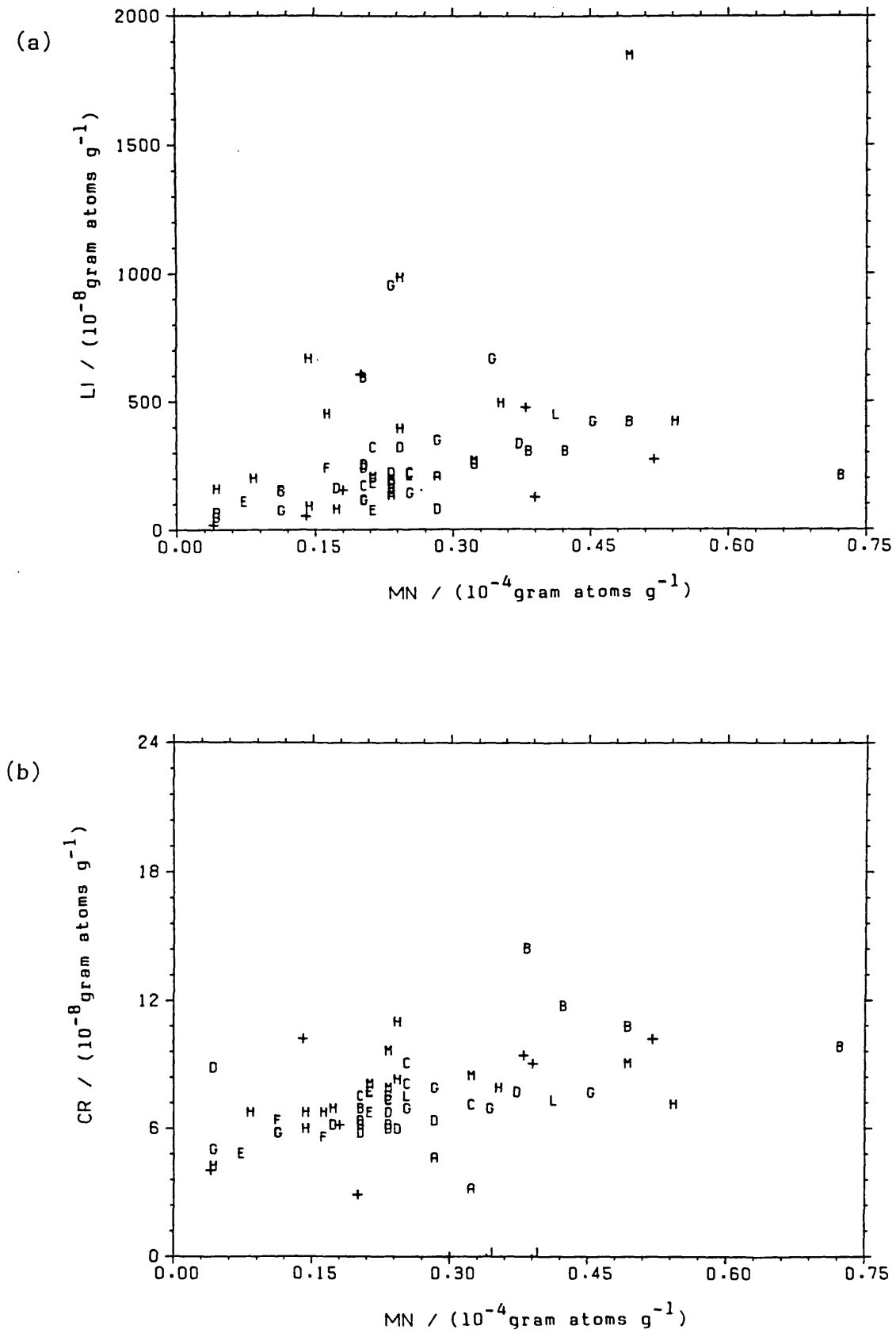

FIGURE 6.1Ø. Scatter plots (gram atoms g^{-1}) of: (a) Mn vs. Li; (b) Mn vs. Cr; (c) Mn vs. Zn; (d) Li vs. F^-; (e) Cr vs. F^-; and (f) Zn vs. F^-. Symbols as in Figure 6.4.

(c)

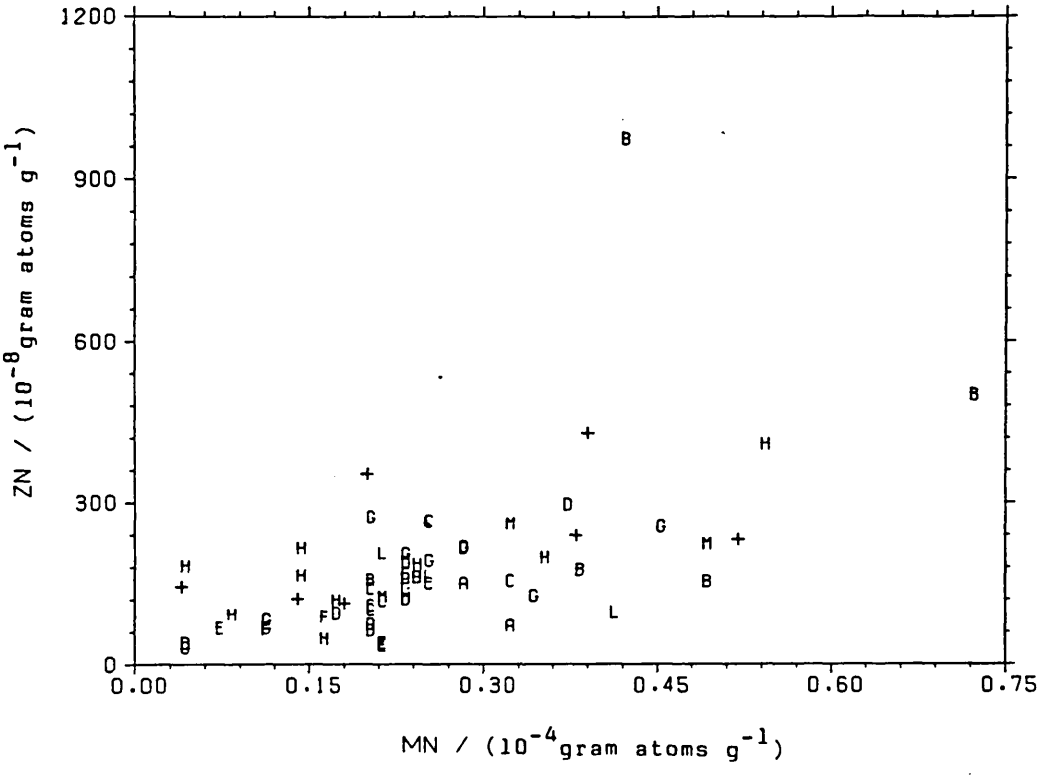
1200
900
600
300
0
0.00
0.15
0.30
0.45
0.60
0.75
ZN / (10^{-8}gram atoms g^{-1})
MN / (10^{-4}gram atoms g^{-1})

(d)

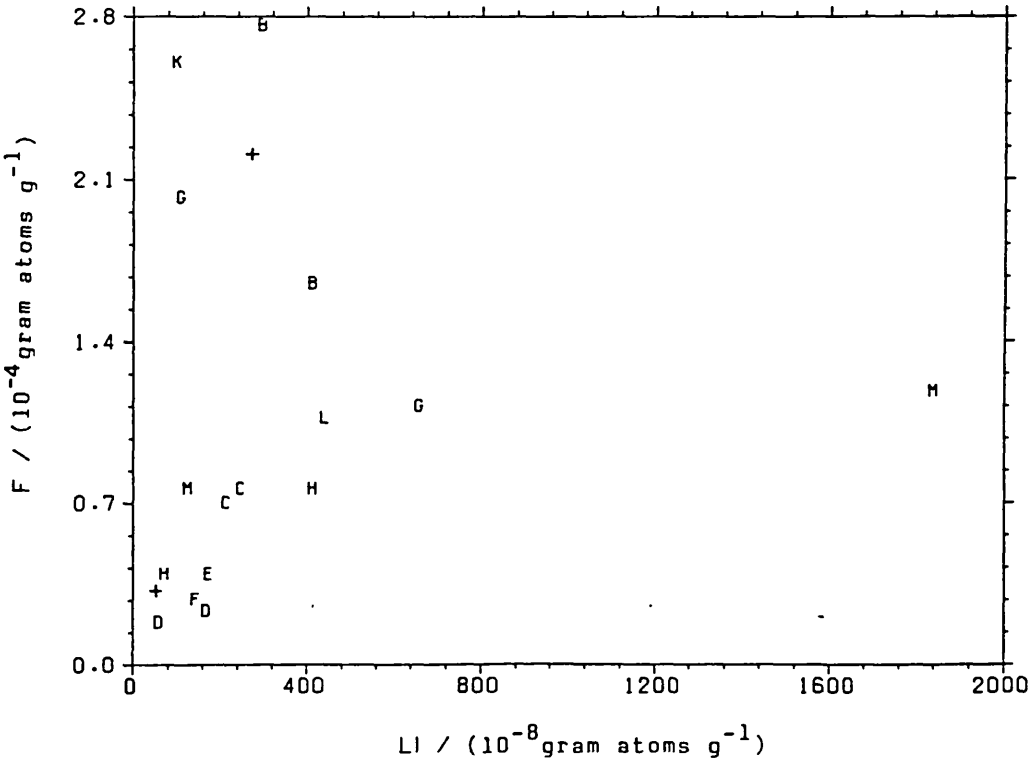
2.8
2.1
1.4
0.7
0.0
0
400
800
1200
1600
2000
F / (10^{-4}gram atoms g^{-1})
LI / (10^{-8}gram atoms g^{-1})

(e)

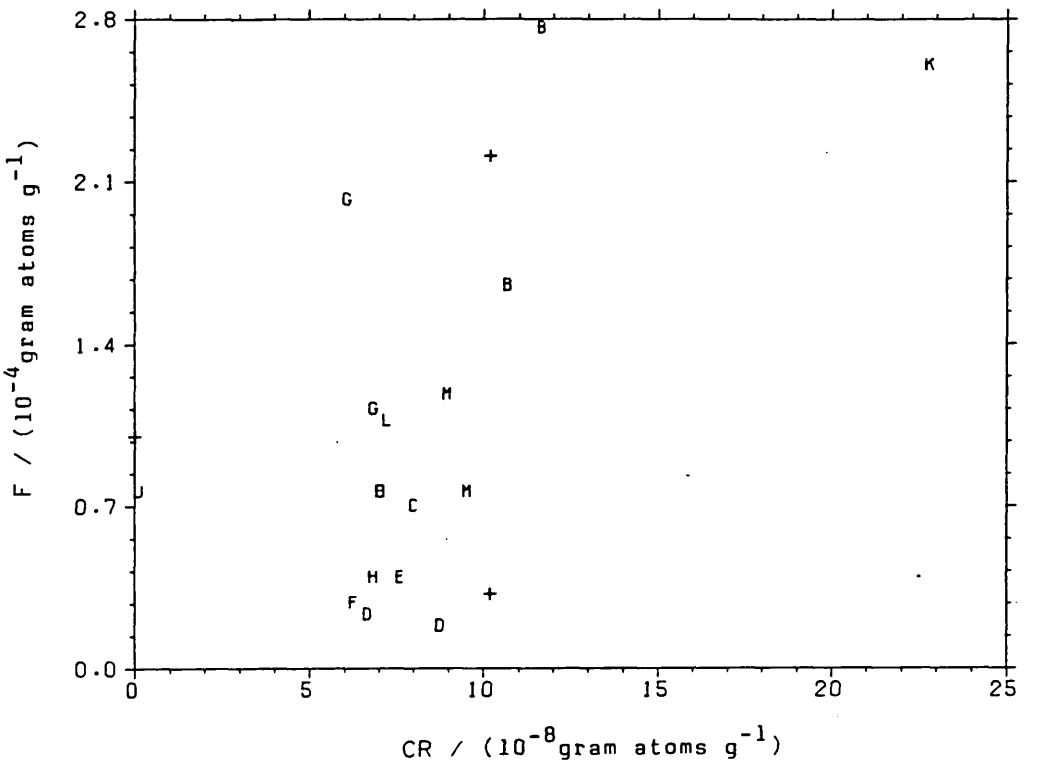
2.8
2.1
1.4
0.7
0.0
0
5
10
15
20
25
F / (10^{-4}gram atoms g^{-1})
CR / (10^{-8}gram atoms g^{-1})
B
K
G
B
M
G L
J
B
C
M
H E
F D
D

(f)

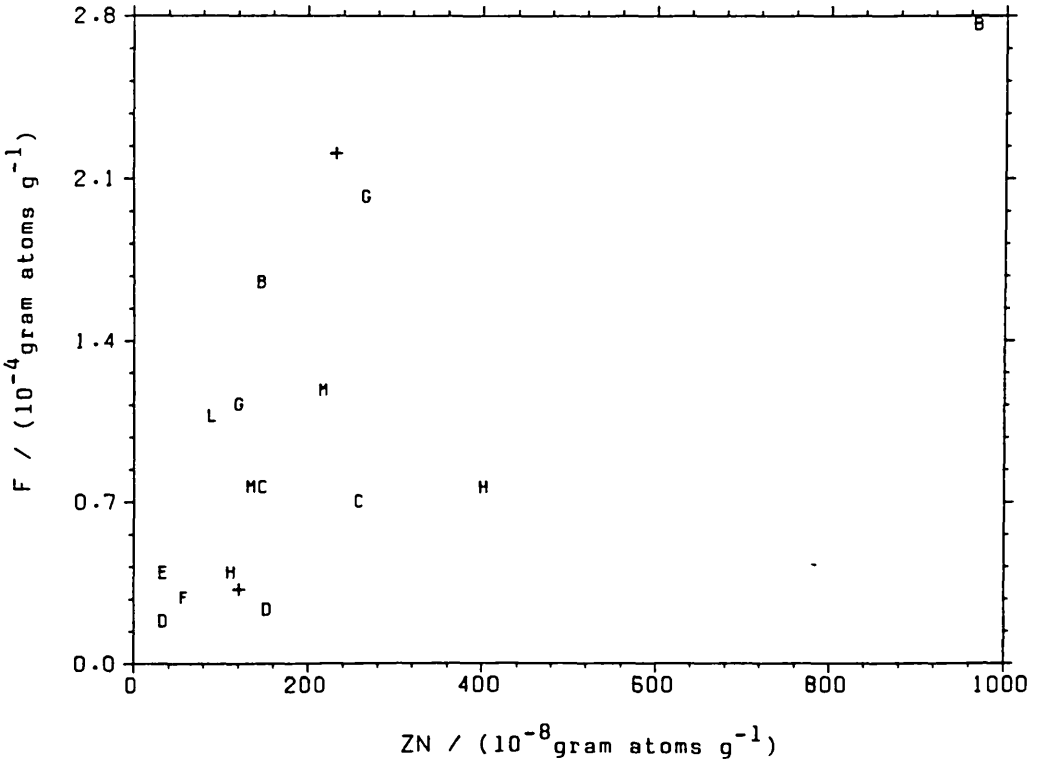
2.8
2.1
1.4
0.7
0.0
0
200
400
600
800
1000
F / (10^{-4}gram atoms g^{-1})
ZN / (10^{-8}gram atoms g^{-1})
B
G
B
M
L G
MC
C
H
E
H
F
D
D

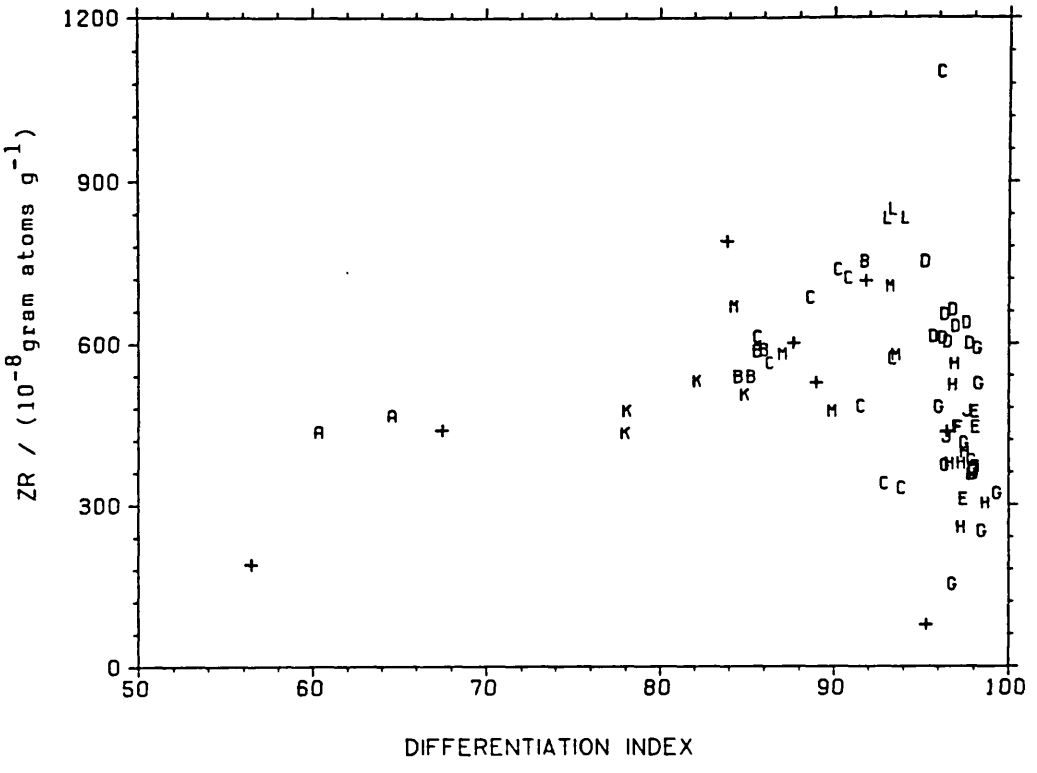

FIGURE 6.11. Scatter plot of Differentiation Index (cation %) vs. Zr (10^{-8} gram atoms g^{-1}). Symbols as in Figure 6.4.

and/or metasomatic processes inducing redistribution of these elements. Elements belonging to group IIIa (Li, Cr, Cu and Zn) show strong correlations with Mn and F (Figure 6.9 a to f). Their concentration in the melt must therefore be related to build-up of magmatic fluorine and, in particular, to the formation of fluoride complexes incorporating these elements (Section 5.5.2). In comparison, elements belonging to group IIIb, in particular Y and HREE, show only moderate to weak correlations with Mn and F, and are probably more closely related to Na in the melt. Similarity in ionic radii between HREE, in particular Yb, and Na^+ (95 pm) supports this contention (cf. Hildreth 1981). The fact, however, that Na is likely to form complexes with F, provides a continuum in the behaviour of group III elements.

Zirconium and Hf, in comparison, appear to show no clear relationships with either F or alkali contents. This is surprising, since the solubility of Zr, and by inference Hf, is believed to be a function of alkalinity, showing an almost linear dependence upon agpaitic index in peralkaline melts (Na+K/Al > 1; Watson 1979). Presence of alkalies in excess of aluminium (and Fe^{3+}) is believed to promote the formation of alkali-zirconosilicate complexes, considerably increasing the solubility of Zr in the melt. In the Hurdal area, however, the concentrations of Zr and Hf in the melt increase to a maximum in the alkali feldspar syenite, but then drop off rapidly in the quartz syenite and alkali feldspar granite (Figure 6.11). Clearly, competition to form bonds with alkalies in the melt renders alkali-zirconosilicate complexes unstable, causing zircon to precipitate out. Zircon is only an important accessory mineral phase in the alkali feldspar granite (Section 3.3.5).

6.5.1 Trace element evidence regarding magma genesis

Consideration of the distribution of compatible trace elements (Group IIa, above) has been used to infer that the

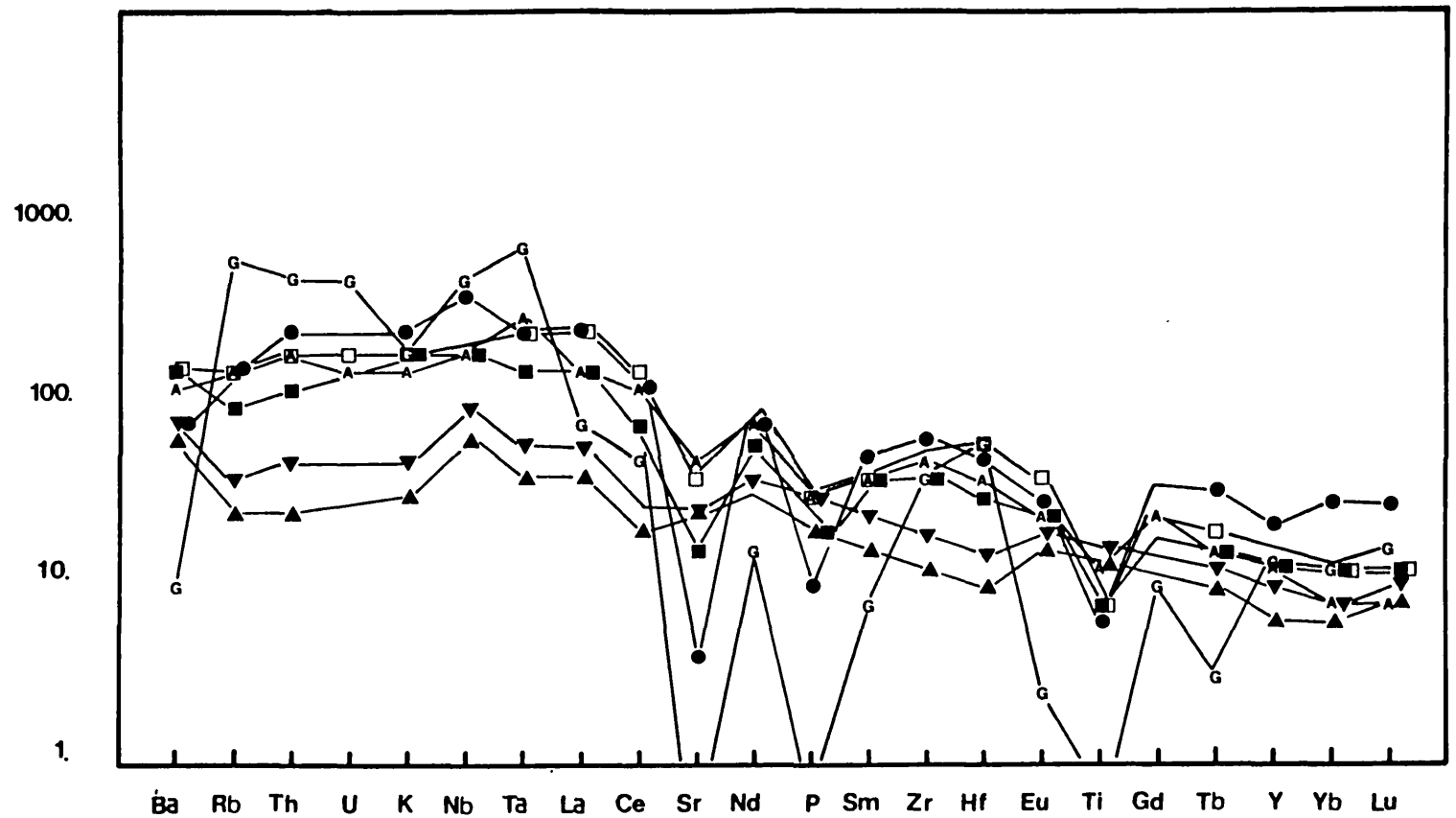

FIGURE 6.12. Comparison between the distributions of hygromagmatophile elements in the Oslo and Kenya rifts. Symbols: A = Monzodiorite, G = Alkali feldspar granite (Brennhaugen), Hurdal area; □ = Average of 24 Larvikites from the Larvik ring complex (Neumann 1980); ▲ = basalt, ▼ = ferrobasalt, ■ = benmoreite, ● = trachyte, Kenya (Baker et al. 1977).

intermediate to granitic rocks in the Hurdal area were formed as a result of fractional crystallisation; in the case of the alkali feldspar granite by 71 percent fractionation of a monzodioritic parent. More elaborate attempts to model the trace element evolution of this suite of rocks have not been considered, since the dividing line between fractional crystallisation and partial melting processes is clearly very thin, depending on the types of model used (fractional melting, batch melting, Rayleigh crystallisation, incremental equilibrium crystallisation, open or closed system fractionation, and so on; Section 6.3).

It has been concluded that the felsic rocks in the Hurdal area were derived from more mafic precursors essentially by fractionation of clinopyroxene, plagioclase and alkali feldspar (Section 5.5). The question is whether the intermediate magmas from which they evolved were derived from alkali basaltic or tholeiitic sources. Similarity in the hygromagmatophile element distributions between the monzodiorites from the Hurdal area and the larvikites from the southern part of the Region (Section 6.4.2) might be used to infer alkali basaltic lines of evolution, since the larvikites would appear to have evolved from an alkali basaltic parent (Section 2.5.2). The absence, however, of similar geochemical data from rocks of proven tholeiitic affinity, makes this assumption hard to prove. The fact that intermediate rocks from the Gregory rift, Kenya (Baker et al. 1977), of suspected tholeiitic affinity (Figure 2.7), also tend to have similar hygromagmatophile element distributions (Figure 6.12), indicates a convergence of magma compositions during low pressure fractionation. The only significant difference between rocks of tholeiitic and alkali basaltic affinity is the presence of a significant negative Sr anomaly (but not Eu^{2+}) in the former, indicating more extensive plagioclase fractionation.

Trace elements with comparably low bulk distribution

coefficients ($D \approx 0$) should behave similarly during evolution (Section 6.3). The ratios of these elements, in particular Y/Tb, Zr/Hf and Nb/Ta, and to a lesser extent Zr/Nb, Zr/Y and Th/U (Table 6.3), should therefore remain more or less constant during fractionation and should reflect similar ratios in their source regions (assuming equilibrium processes). Consideration of the distribution of these elements in the more evolved rocks in the Hurdal area (Section 6.4), however, indicates that caution has to be taken when using elements from group III (Tb, Y, Zr and Hf), since these elements are not always entirely incompatible and may be strongly influenced by late-stage magmatic processes such as volatile complexing and changes in melt structure. Trace element ratios for all the principal rock-types in the Hurdal area are presented in Table 6.4.

Comparison between Tables 6.3 and 6.4 indicates that the least evolved rock-types in the Hurdal area (monzodiorite, biotite syenite and alkali feldspar syenite) have comparable Y/Tb and Zr/Hf ratios to chondritic abundances and to magmatic products from both oceanic and continental rift settings (mid ocean ridges, Iceland and Kenya). It is therefore reasonable to assume that these rocks were derived from parental material ultimately of upper mantle provenance. The more evolved rocks in the Hurdal area, however, have substantially higher Y/Tb ratios and lower Zr/Hf ratios (Figures 6.13a and 6.13b). These differences might be used to imply a different source for the more evolved granitic rocks in the area. The fact, however, that individual rock-types, in particular the quartz syenite, show considerable scatter in Y/Tb and Zr/Hf ratios, combined with the fact that none of these elements are behaving truely incompatibly (Section 6.4), indicates that this is unlikely to be the case. The higher Y/Tb ratio observed in the more evolved rocks reflect the contrast in behaviour of Tb and Y in magmas which are already depleted in Tb. In comparison, the lower Zr/Hf ratios observed in the alkali feldspar granite reflect fractionation

TABLE 6.4: TRACE ELEMENT RATIOS, HURDAL AREA

	Y/Tb	Zr/Hf	Nb/Ta	Zr/Nb	Zr/Y	Th/U
Monzdrt	65.9± 1.6	73.9± 4.5	17.4± .1	4.0± .0	8.2± .3	4.8±1.1
B.S.	62.6± 6.3	68.0± 9.0	16.0± 1.1	4.2± .6	9.2± 1.4	8.1±4.5
A.S.	66.2±13.6	69.6± 8.7	16.2± 1.3	3.8± .8	7.9± 1.3	8.1±3.5
Q.S.	119.7±71.8	63.9±10.4	19.1± 2.9	2.9± .9	7.9± 2.1	8.4±3.0
U.M.	53.0±24.4	57.7±11.0	16.6± 3.9	2.7± .7	14.2±11.8	6.0±4.6
F.P.mG	223.8±130.	49.2± 3.1	20.6± .8	1.8± .1	9.1± .3	7.5± .0
A.G.(B)	306.2±73.7	36.3± 3.9	17.0± 3.5	1.4± .5	11.1±11.3	4.2±2.9
A.G.(R)	416.3±441.	41.9± 8.0	18.7± 1.8	1.2± .3	6.2± 1.8	3.3±1.5
Ap.mG	406.6±121.	36.4± 1.4	17.7± 1.1	1.1± .1	5.8± .3	3.5± .5
Mn.R	299.6±41.4	38.7±11.1	16.6± 3.7	1.1± .4	5.9± 2.1	5.6±7.1
Trach-1	94.6± 8.7	75.0± 7.1	18.5± 1.6	4.3± .1	11.3± .9	6.8± .8
Trach-2	76.3±18.9	80.4± 9.2	18.4± 1.8	4.4± .8	10.3± 2.0	5.5± .6
Trachand	65.4	62.7	4.3	4.8	12.4	1.7
Rhyolite	165.0	38.8	19.9	1.5	17.6	.9
Dolerite	55.5	112.2	23.6	3.1	4.4	10.1
W18AB	63.3	87.8	21.5	5.4	7.2	3.8
W36A	96.7	87.8	20.0	6.2	13.0	4.4
HA4D	276.9	56.6	19.1	1.5	2.1	2.4

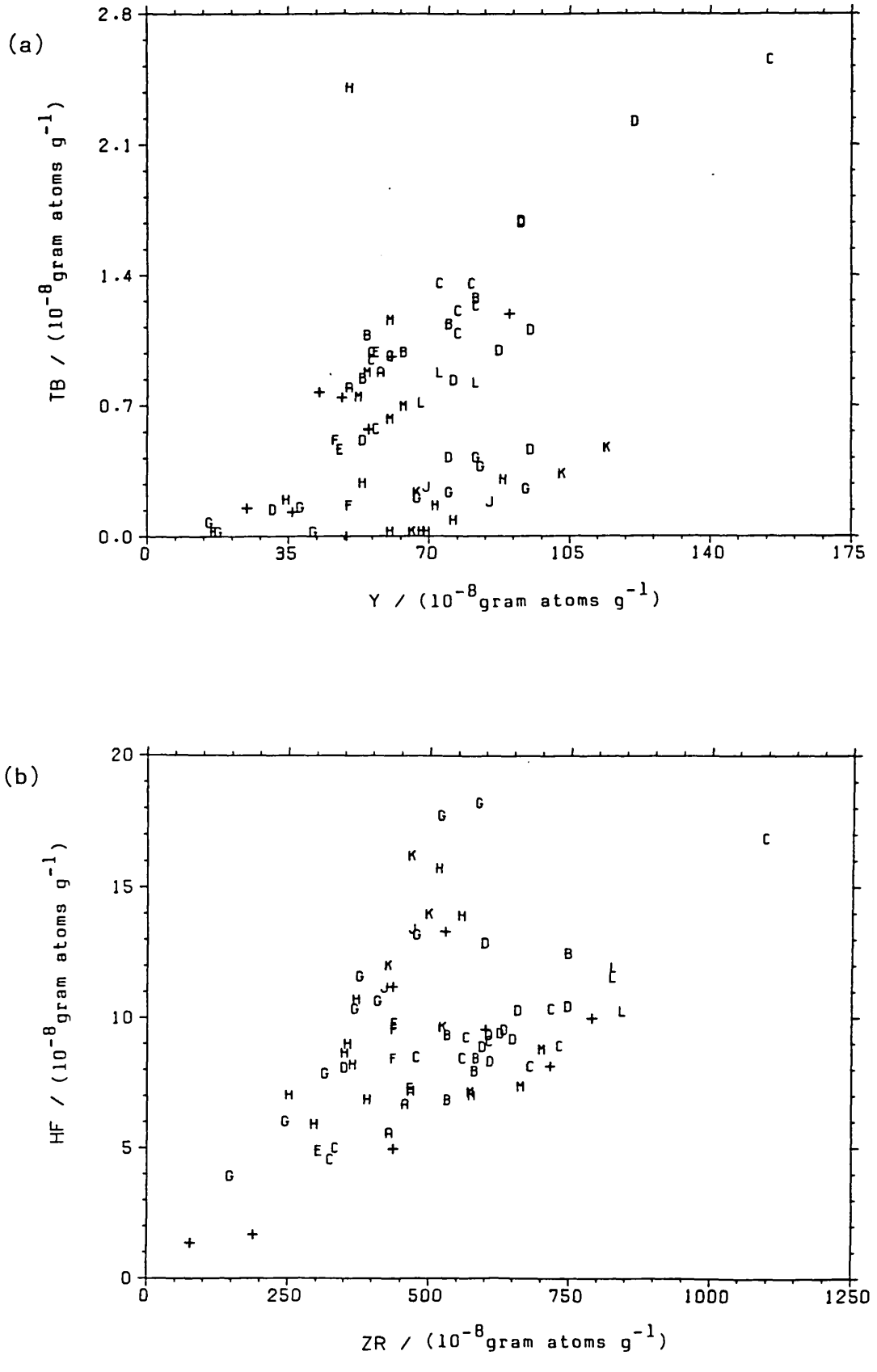

FIGURE 6.13. Scatter plots (10^{-8} gram atoms g^{-1}) of: (a) Y vs. Tb; (b) Zr vs. Hf; (c) Nb vs. Ta; and (d) Zr vs. Nb. Symbols as in Figure 6.4.

(c)

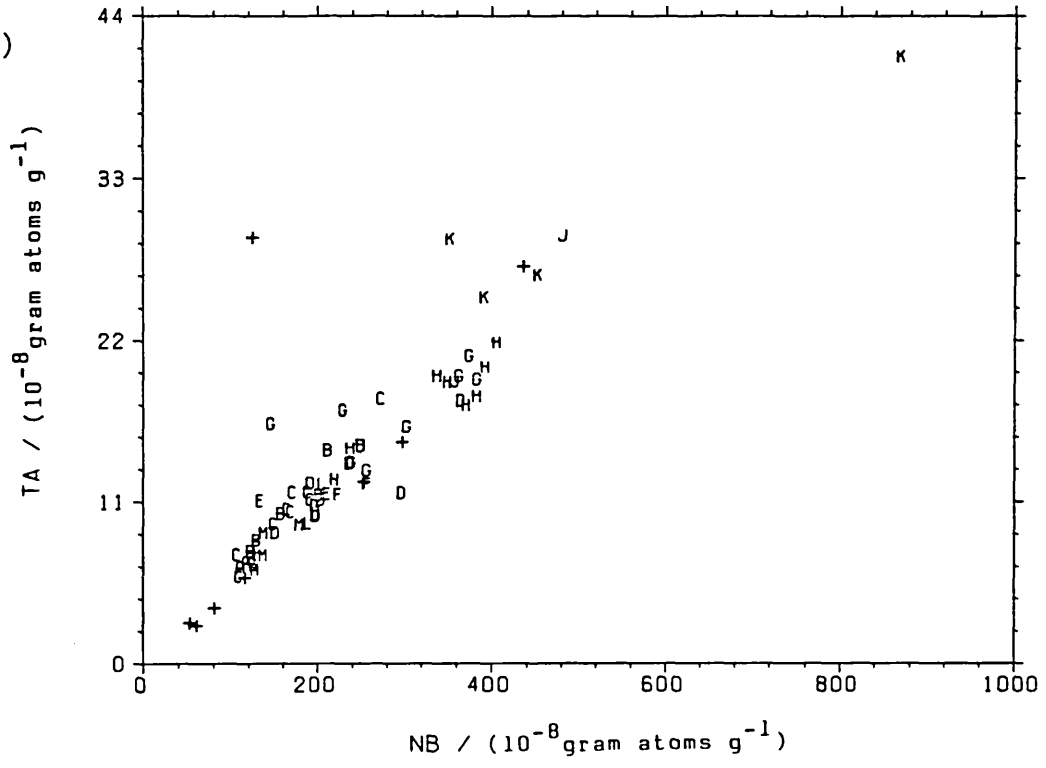
TA / (10^{-8}gram atoms g^{-1})
NB / (10^{-8}gram atoms g^{-1})
0
11
22
33
44
0
200
400
600
800
1000

(d)

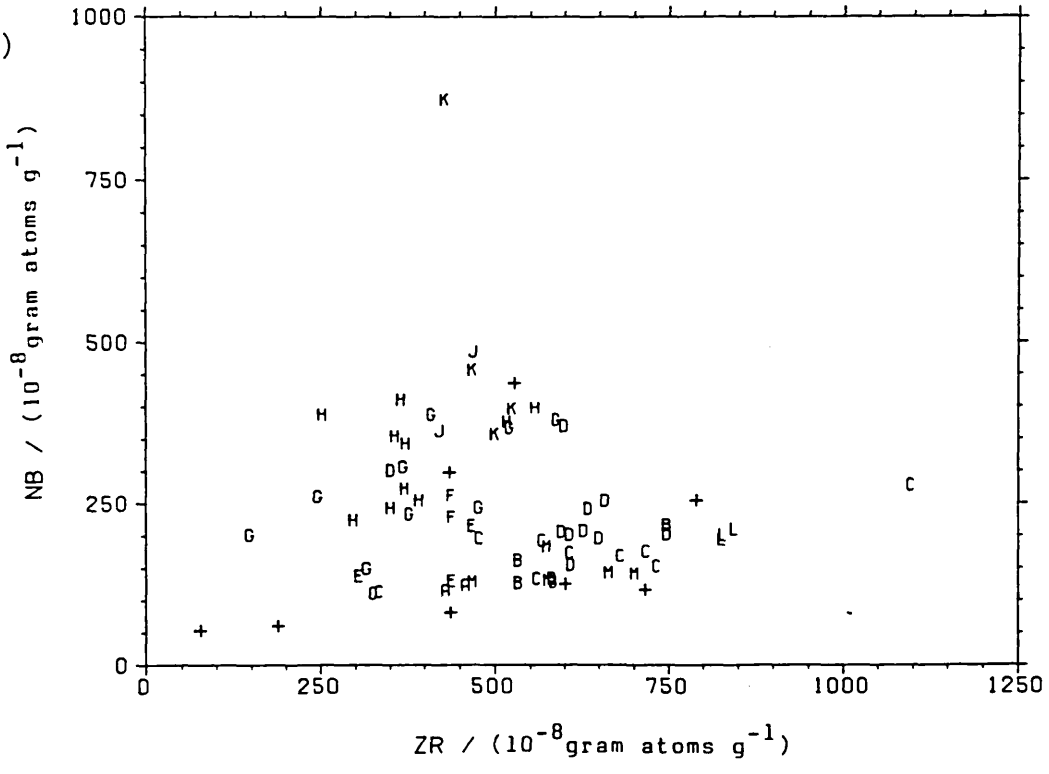
NB / (10^{-8}gram atoms g^{-1})
ZR / (10^{-8}gram atoms g^{-1})
0
250
500
750
1000
0
250
500
750
1000
1250

of zircon of more or less constant composition (Zr/Hf 22.5; Figure 6.13b).

Consideration of Table 6.4 and Figure 6.13c indicates that the ratio of Nb to Ta remains more or less constant throughout evolution from monzodiorite to granite, lieing in the range 17 - 21. These ratios are considerably lower than those observed within oceanic basalts and related rocks, implying a source region enriched in Ta relative to Nb.

Consideration of Table 6.4 and Figure 6.13d indicates that the least evolved rock-types in the Hurdal area have Zr/Nb ratios in the range 3.7 - 4.2. These values are similar to those observed within pyroxene basalts and plagioclase - pyroxene basalts from the Vestfold lava plateau (Section 2.5.5), strongly suggesting an alkali basaltic source for these rocks. The more evolved rocks in the Hurdal area, however, have much lower Zr/Nb ratios, reflecting the contrast in behaviour of Zr and Nb in the more evolved magmas.

Finally, Zr/Y and Th/U ratios show considerable scatter. Particularly in the more evolved magmas Zr and Y behave quite differently, Zr being precipitated out in the form of zircon, Y showing a strong affinity towards the melt. Thorium and uranium, on the other hand, would appear to be affected by late stage magmatic processes (due to their large ionic charge).

6.5.2 Behaviour of the ore-metals

The ore-metals Cu and Zn show a strong dependence upon the concentrations of Mn and F in the melt (Section 6.4). Build-up of magmatic F during evolution would appear to have lead to the formation of complexes incorporating these elements (as in the case of Li and Cr, above). Migration of these complexes within the melt, particularly in the apical

zones of granitic intrusions (Section 4.3), is believed to have lead to the concentration of Cu and Zn. Consideration of the absolute abundances of Cu and Zn (Tables 6.1 and 6.2), however, indicates that Zn is concentrated to a much greater extent than Cu by these processes. The behaviour of Zn and Mn is clearly similar to that predicted for aqueous chloride solutions (Holland 1972).

The concentrations of Mo and Ag in the melt would not appear to be directly related to F activity. The ability of ore-metals to form complexes with F would therefore appear to decrease in the order: Zn > Cu > Mo > Ag. By analogy with experimental systems (for instance Manning and Henderson 1984; Khitarov et al. 1982), Copper and Ag are probably more closely related to chlorine activity in the melt, whereas Mo is likely to show a closer relationship to carbonate concentration.

CHAPTER 7

FLUID INCLUSION STUDIES

7.1 Introduction

A combination of field, petrological and geochemical studies (Chapters 4 to 6) has revealed that mineralisation in the Hurdal area was very closely related to magmatic evolution within the rift. Large increases in the concentrations of Mn and Zn during the evolution of the biotite syenite and alkali feldspar granite would appear to have been directly related to the concentration of F in the evolved magmas (Sections 5.5.2 and 6.5). Strong correlations between F and Mn and Zn, and to a lesser extent with Li, Cr and Cu (Section 6.4), in the whole-rock compositions suggest strong partioning of F towards the melt phase. Whether ore-precipitation was connected directly to the melt phase or to the development of a coexisting hydrothermal phase is however difficult to resolve.

In order to assess the ore-forming potential of hydrothermal solutions in equilibrium with plutonic rocks in the Hurdal area it is necessary to reconstruct the hydrothermal evolution of the rocks in question. A study of fluid inclusion populations has therefore been undertaken with this objective in mind. For reasons of convenience, however, only fluid inclusions in quartz have been studied; although fluid inclusions have also been observed in feldspar, sphalerite and fluorite.

The samples for this study include granitic quartz and vug quartz from the contact zones of the quartz syenite in the Nordgardshogda - Styggberget area (Figure 7.1), and the alkali feldspar granite in the Brennhaugen granite massif (Figure 7.2). In addition, five samples of biotite syenite from the Nordgardshogda area and several granitic samples from the Hegga manganese occurrence have been studied.

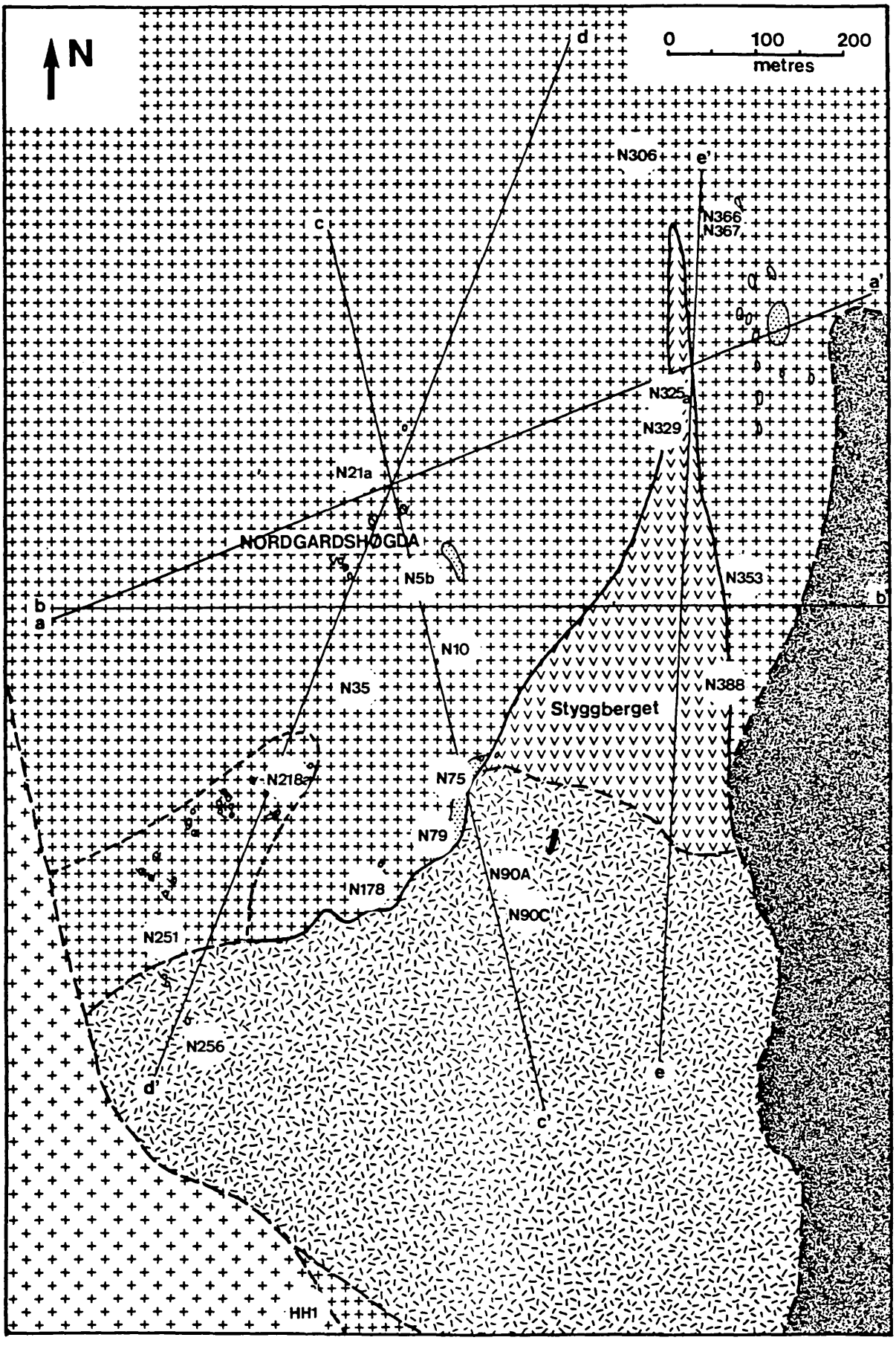

FIGURE 7.1. Sample locality map for the fluid inclusion studies, Nordgardshogda - Styggberget area.

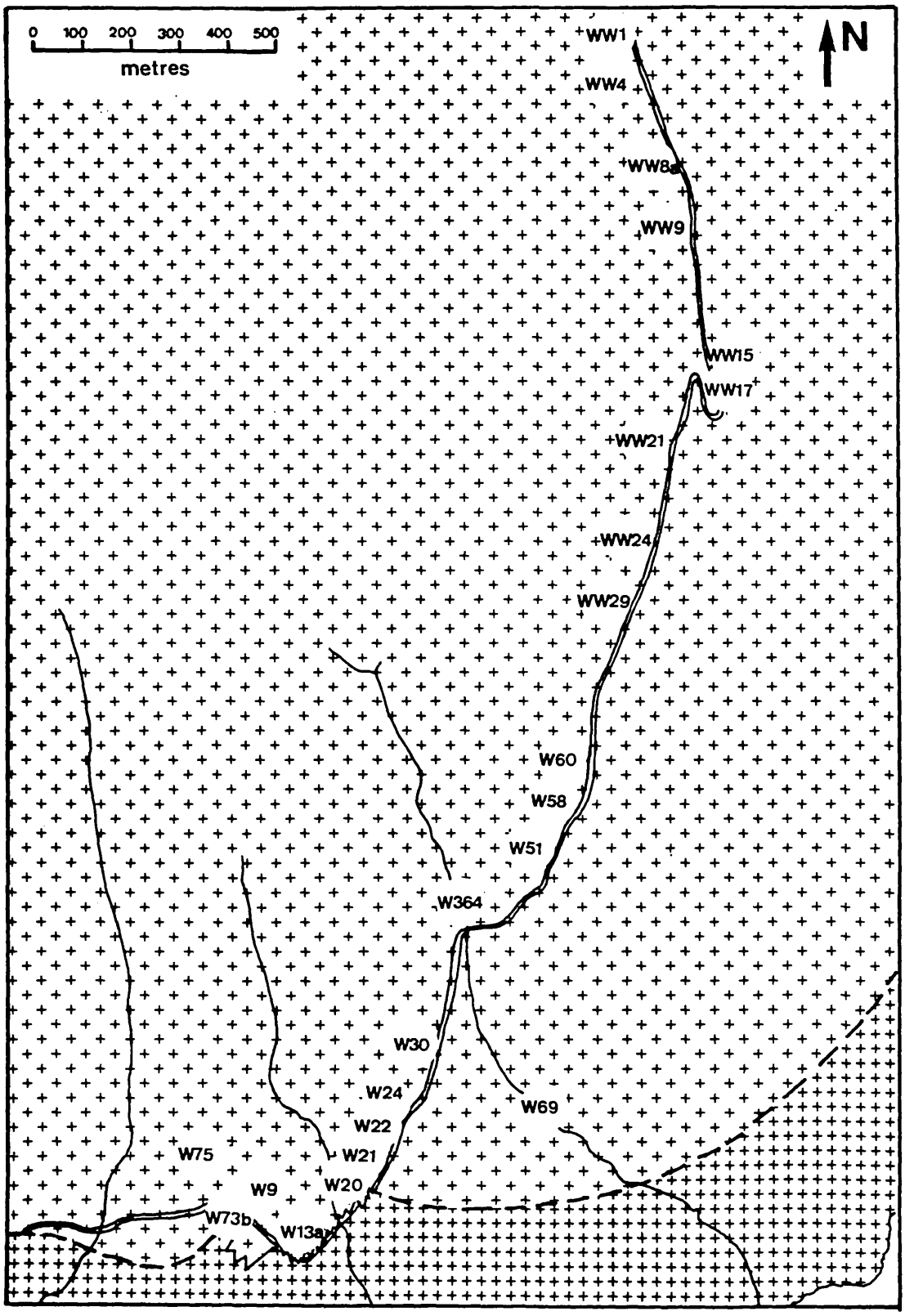

FIGURE 7.2. Sample locality map for the fluid inclusion studies, Brennhaugen area.

The study of fluid inclusions has involved the following procedures: A. Fluid inclusion petrography; B. Microthermometric studies of fluid inclusions in quartz; and C. Chemical analysis of the fluid inclusions by the Decrepitation - inductively coupled plasma spectrometry (D-ICP) method (Thompson et al. 1980).

7.2 Fluid inclusion petrography

Polished wafers from the following rock-types have been examined for fluid inclusions: Altered biotite syenite, quartz syenite, uneven microgranite, feldspar porphyritic microgranite and alkali feldspar granite. In addition, samples of vug quartz from the contact zones of the quartz syenite and alkali feldspar granite have been investigated.

The results of the petrographic examination of 49 samples are listed in Table 7.1. Fluid inclusions are classified according to the number of phases present and their relative proportions. No attempt has been made to classify them according to their origin, except in obvious cases.

7.2.1 Biotite syenite

The biotite syenite in the Nordgardshogda area is a quartz-poor rock, seldom containing greater than 2 percent quartz (Section 3.3.2). The latter tends to be inclusion poor (Table 7.1). In comparison, quartz - pyrite (? quartz syenite) veinlets in altered biotite syenite contain two phase liquid - gas inclusions with a 70 to 90 % degree of filling by volume (D.F. = volume of liquid/volume of inclusion). All inclusions appear to be secondary and range in size between less than 1 μm and 4 μm.

7.2.2 Quartz syenite

TABLE 7.1: FLUID INCLUSION PETROGRAPHY

SAMPLE	SAMPLE TYPE	L	G	L+G		L+G		L+CO$_2$+G		L+S+G		L+S$_1$+S$_2$+G		L+S$_1$+S$_2$+O+G	TOTAL ABUNDANCE
N90A25	B.S.	-	-	-		r sec		-		-		-		-	r
N90A31	B.S.	-	-	-		-		-		-		-		-	n
N90A14	Qtz vn in B.S.	r sec	r sec	p		p		vr		vr		-		-	p
N90A27	Qtz vn in B.S.	c sec	-	c	sec/pr	c sec		-		r		-		-	c
N90A28	Qtz vn in B.S.	p	-	r		p		-		-		vr		-	r
N7	Q.S.	-	-	p	sec	p sec		r		vr		-		-	p
N10	Q.S.	r	-	p	sec	-		-		-		-		-	p
N21A	Q.S.	-	-	p	sec	-		p		-		-		-	c
N35	Q.S.	p	-	p	sec	p		vr		-		-		-	p
N178	Q.S.	r sec	-	p	(sec)	p sec		r		-		-		-	p
N306	Q.S.	p	-	c	(sec)	c sec		-		-		-		-	c
N325A	Q.S.	-	-	c	(sec)	c sec		p		-		-		r	c
N388	Q.S.	-	-	c		p sec		c		-		-		-	c
N218A	U.M.	p sec	-	c	pr	p sec		-		-		-		-	c
N251,6	U.M.	p sec/l	c sec/e	p	sec/l	-		-		-		-		-	c
N366	F.P.mG	p sec	-	c	pr/sec	p sec		-		-		p		-	c
N75	Qtz vg in Q.S.	-	-	vc		c sec		c		c		c		p	vc
N79	Qtz vg in Q.S.	-	-	c	pr/e	vc pr/l		c	sec	c		-		-	vc
N218A	Qtz vg in Q.S.	p	-	vc	pr	c sec		p	pr	-		-		-	vc
N251,7	Qtz vg in Q.S.	c sec	-	c	pr/sec	c sec		c	pr/sec	-		-		-	vc
N251,9	Qtz vg in Q.S.	-	p (sec)	vc	pr/sec	c sec		r		p	sec	-		-	vc
N329	Qtz vg in Q.S.	-	-	vc	pr	c sec		r		c		c		vc	pr vc
N329B	Qtz vg in Q.S.	-	-	vc	pr	c sec		r		-		-		p	pr vc
N353	Qtz vg in Q.S.	-	-	vc	pr	c sec		c	pr	-		-		-	vc
N367	Qtz vg in Q.S.	-	-	vc	pr	vc		c		p	pr	-		p	pr vc
W13A	A.G.	p	-	p		p		-		-		-		-	r
W24	A.G.	p	r	-		vc		p		-		-		-	c
W30	A.G.	c H_2O/CO_2	c	c		c		p		p		c		vr	vc
W364	A.G.	-	-	-		p sec		-		-		c		p	p
W51	A.G.	-	p sec	c		c		r		-		-		vr	p
W58	A.G.	vc	r	-		c		r		-		-		-	p
W60	A.G.	c CO_2	-	r		-		-		vr		-		-	p
WW4	Qtz vg in A.G.	c sec	-	c		vc		p		r		p		-	vc
WW8A	Qtz vg in A.G.	c sec	-	vc		-		-		-		p		-	c
WW17	Qtz vg in A.G.	c	-	c		vc		r		-		-		-	c
W9	Qtz vg in A.G.	r	-	vc		vc		r		-		-		-	vc
W20	Qtz vg in A.G.	-	-	c		p		c		-		-		-	p
W21C	Qtz vg in A.G.	-	-	-		c		vc		r		r		-	vc
W223	Qtz vg in A.G.	-	-	c		c		vc		-		-		p	vc
W22D	Qtz vg in A.G.	r sec	-	-		r sec		c		-		vc		c	c
W24V	Qtz vn in A.G.	p	r	-		-		vc		p	bir	-		-	c
W69	Qtz vg in A.G.	c	-	p		c		-		-		-		-	p
W73B	Qtz vg in A.G.	-	-	-		c		vc		-		-		-	vc
W75	Qtz vg in A.G.	-	-	p		vc sec		c		-		-		-	c
HA11	Mn.R	-	-	-		-		-		-		-		-	vr
HA12	Mn.R	-	-	-		-		-		-		-		-	vr
HB5	A.G./Mn.R	-	p	pr+dm?	-			p	pr	-		p		p	pr p
HC8	Mn.R	-	-	p	sec	-		-		-		-		-	r
H8	Mn.R	-	p sec	-		p		p	sec	-		-		-	p

vc = very common, c = common, p = present, r = rare, vr = very rare, n = none.
pr = primary, sec = secondary, e = early, l = late, dm = daughter mineral, bir = birefringent daughter mineral, vn = vein, vg = vug.

The quartz syenite in the Nordgardshogda area is characterised by the presence of two phase liquid-rich inclusions with a 70 to 90 % degree of filling. The inclusions are generally small (5 to 10 μm) and are usually oriented along fractures (i.e. secondary). Many of the larger inclusions contain a rim of liquid CO_2 around the bubble. This suggests that some of the smaller, apparently two phase inclusions may also contain CO_2, having failed to nucleate a separate CO_2 phase upon cooling. Inclusions with daughter minerals are generally absent; although most samples contain a noticeable number of inclusions with captive solid phases (possibly biotite). The overall fluid inclusion abundance in the quartz syenite is moderate and is noticeably lower than that in the alkali feldspar granite (Table 7.1).

7.2.3 Uneven microgranite

The contact facies of the quartz syenite is relatively enriched in two phase liquid-rich inclusions. Secondary two phase and one phase inclusions are common. Quartz vugs associated with the uneven microgranite tend to have much higher and more variable fluid inclusion contents (Section 7.2.6).

7.2.4 Feldspar porphyritic microgranite

The feldspar porphyritic microgranite (sample N366; Table 7.1) contains abundant, small (<5 μm), randomly distributed inclusions of various types (varying degree of filling and ratio of phases). As such it would appear to have crystallised in the presence of more than one hydrothermal fluid.

7.2.5 Alkali feldspar granite

The alkali feldspar granite contains numerous, small (5 to 15 um), regularly shaped inclusions of probable primary origin.

Late, secondary inclusions tend to be larger and more irregular. The presence in some samples (W3Ø, W364; Table 7.1) of a large number of inclusions with at least two, and frequently three daughter minerals, occasionally including an opaque phase, suggests that the quartz crystallised in the presence of a highly saline hydrothermal fluid of magmatic origin (hydrothermal quartz, below).

Two distinct types of quartz may be identified in the alkali feldspar granite: (a) melt quartz; and (b) hydrothermal quartz. Melt quartz is believed to have precipitated from a silicate melt prior to the exsolution of the hydrous phase. Thus, the only primary inclusions found in melt quartz are melt or solid inclusions. Aqueous and carbon dioxide inclusions are exclusively secondary. Hydrothermal quartz, in comparison, is believed to have precipitated directly from an aqueous or aqueous - CO_2 mixed fluid, either during or after exsolution of the aqueous phase from the melt. Thus primary aqueous and carbon dioxide inclusions may be present.

Fluid inclusions with an obvious liquid CO_2 phase are common. Many of the two phase liquid-gas inclusions possess a thin layer of liquid CO_2 around the bubble. However, most of the CO_2 is likely to be present in the gas phase at room temperature.

Gas-rich and irregular monophase inclusions are fracture controlled and demonstrably secondary. They indicate that low density and low temperature fluids passed through the rock after the crystallisation of the quartz.

Amongst the daughter minerals the largest is normally halite. The second in size is either an anisotropic rod-shaped mineral or sylvite (KCl). A very small (<1 μm) transparent daughter mineral present in a number of two phase inclusions is either halite or nahcolite (Chryssoulis, pers. comm.; $NaHCO_3$, Rankin and Le Bas 1974). Samples W13A and W51 are

noteworthy in that they lack daughter minerals. Captive crystals of rutile may be present in some of the samples (W51 and W3Ø).

A fluid inclusion assemblage believed to be indicative of boiling has been observed in sample HB5 from the Hegga river locality (Figure 4.4). The presence of both gas-rich and liquid-rich inclusions homogenising at the same temperature is believed to be indicative of boiling (Roedder 1979). The fact that the inclusions with the higher degree of filling often contain a small halite crystal indicates the high salinity of the boiling fluid. Such a fluid may have been important in the genesis of manganese-rich rocks in the area (see Section 8.5).

7.2.6 Quartz vugs

Quartz vugs, 1Ø to 2Ø cm in dimension and filled mainly with hydrothermal quartz, are observed in the contact zones of both the quartz syenite in the Nordgardshogda - Styggberget area and the alkali feldspar granite in the Brennhaugen granite massif. In addition, cavities containing quartz and sometimes amphibole are occasionally observed away from the contacts of the Brennhaugen granite (samples WW4, WW8A, WW17 and W69; Figure 7.2). These cavities are best described as miarolytic cavities.

Consideration of Table 7.1 indicates that the quartz vugs may be subdivided into two groups on the basis of the presence of absence of liquid CO_2-bearing inclusions. Quartz vugs in which CO_2-bearing inclusions are rare or absent are particularly common away from the contacts of the Brennhaugen granite (as above). In comparison, quartz vugs in which CO_2-bearing inclusions are abundant are common in the contact zones of both the quartz syenite and the alkali feldspar granite. These relationships suggest the presence of a CO_2 enriched carapace in both the Nordgardshogda and Brennhaugen

intrusions (by analogy with the general model proposed by Burnham 1979b). The principal difference between the quartz from these two areas is that inclusions in the former tend to be more saline and less CO_2 enriched.

Fluid inclusions in the quartz vugs vary in size between 1 um and greater than 40 um, and it is often possible to distinguish more than one fluid inclusion population on the basis of size. The shape of fluid inclusions is also variable, ranging between regular or negative crystals and highly irregular secondary inclusions (with a high degree of filling). A well documented phenomenon in which the number of phases present is directly related to fluid inclusion size is frequently observed (Roedder 1971). Thus, the larger inclusions in a given group tend to have a greater number of phases (i.e. liquid CO_2 and daughter minerals). The presence within individual samples of separate groups of inclusions with different but internally consistent ratios of phases is believed to be indicative of trapping of several discrete homogenous hydrothermal fluids, as opposed to trapping of a single heterogeneous fluid (Roedder 1979).

Two types of fluid inclusion are worthy of separate mention: (i) Gas-rich inclusions (D.F. 30 % by volume) with a halite daughter mineral (<5% of the total inclusion volume); and (ii) liquid CO_2 - aqueous four phase inclusions with a small transparent daughter mineral, presumably halite. The presence of low density, high salinity fluids (type i) is believed to be indicative of high pressures and temperatures (Sourirayan and Kennedy 1962, Chryssoulis 1983a). The presence of high salinity CO_2-bearing fluids (type ii) is probably also indicative of high pressures, the solubility of CO_2 in H_2O decreasing with increasing salinity and decreasing pressure (Takenouchi and Kennedy 1965 a and b).

A non-magnetic, grey, opaque daughter mineral has been observed both in highly saline inclusions (visual estimate of

salinity 40 wt % equ. NaCl) with a halite and anisotropic daughter mineral (e.g. sample N329) and in liquid CO_2-bearing inclusions (e.g. N367) from the Nordgardshogda area. The opaque mineral is hexagonal in outline and is tentatively identified as molybdenite (hematite would be red). The presence of this opaque phase indicates that the hydrothermal fluids released from the quartz syenite during its consolidation were enriched in metallic elements (i.e. Mo). The high salinity and CO_2-bearing nature of these inclusions strongly suggest a magmatic origin for the hydrothermal fluids.

Hematite daughter minerals have been observed within secondary two phase liquid-gas inclusions in sample WW4 from the Brennhaugen area. The presence of these daughter minerals presumably reflects the passage of low temperature Fe-rich fluids through the rocks. Such fluids may have been responsible for the observed reddening of alkali feldspar granite in the area.

7.3 Microthermometry

Microthermometric studies of fluid inclusions in granitic and vug quartz were made using a LINKAM TH600 freezing - heating stage mounted on a petrological microscope. The measurements recorded were calibrated for instrumental error following the procedure outlined by Chryssoulis (1983a); with an estimated precision of less than 0.5°C for freezing runs and 1°C for heating runs.

The fluid inclusions were first frozen in order to study their melting behaviour and to estimate their salinities. They were then heated up in order to record their homogenisation temperatures. The latter are believed to give a minimum estimate of trapping temperature (Roedder 1979). Following this procedure minimises the possibility of recording erroneous values due to stresses caused by heating

(Roedder and Skinner 1968).

Microthermometric measurements were complicated by two factors: Firstly, by the small size of the inclusions to be studied, which was generally less than 10 um (Section 7.2); and secondly, by the presence of carbon dioxide within many of the inclusions. The presence of CO_2 was indicated in the most obvious cases by the occurrence of an annular ring of liquid around the bubble of aqueous two phase inclusions, and/or by the formation of the clathrate compound CO_2 hydrate upon freezing (CO_2 . 5.75 H_2O; Collins 1979). However, the relatively small proportions of liquid CO_2 present, and the similarity in refractive indices between CO_2 hydrate and aqueous solutions, render these phenomena optically unresolvable in the smaller inclusions. It is possible that all the inclusions contain some CO_2. However, failure to nucleate a separate liquid CO_2 phase upon cooling and the generally small size of the inclusions prevent its detection in many cases.

During the cooling cycle of the freezing studies, all inclusions containing an obvious CO_2 phase recorded two distinct freezings: Formation of CO_2 clathrate in the temperature range -30°C to -40°C; and formation of ice at temperatures below -40°C. Formation of ice in all inclusions required supercooling, due to metastability. During the warming cycle, ice melted first in the temperature range -23°C to 0°C. Decomposition of the CO_2 clathrate occurred at higher temperatures, in the range -6°C to +16°C.

During the heating cycle, all inclusions homogenised in the temperature range 110°C to 420°C. Partial homogenisation of CO^2-bearing inclusions, to the vapour phase, occurred at temperatures close to the critical temperature for pure CO_2 at 31.2°C, indicating densities of less than .468 g cm^{-3} (Hollister 1981).

7.3.1 Theoretical considerations

The salinity of aqueous two phase inclusions may be estimated from the depression of fusion point of ice, T_F ice, the temperature at which the last ice crystal melts on warming. The latter is directly related to the concentration of dissolved salts, which is generally expressed in terms of equivalent weight percent NaCl. This is because Na^+ is usually the predominant cation in hydrothermal fluids (Roedder 1979). The maximum salinity which may be measured by this method is that of a pure NaCl brine at approximately 24 wt % equ. NaCl. In comparison, the salinity of inclusions containing a halite daughter mineral may be estimated from the temperature of dissolution of the daughter mineral, since this corresponds to the saturated solution temperature for the fluid concerned (Sourirayan and Kennedy 1962).

During cooling of CO_2-bearing fluid inclusions, the clathrate compound CO_2 hydrate freezes out prior to the freezing of the remaining aqueous solution. Formation of the clathrate compound involves removal of H_2O from the aqueous solution, the amount of CO_2 hydrate formed being directly proportional to the amount of CO_2 in the aqueous solution at the temperature of clathration, and not to the total CO_2 content of the inclusion (Collins 1979). Since the solubility of CO_2 in the aqueous solution increases with decreasing temperature, the amount of clathrate formed will depend on the degree of supercooling required to induce clathration. Dissolved salts such as NaCl and KCl will be excluded from the growing crystals and concentrated in the remaining aqueous solution. It is this solution which freezes to form the ice on further cooling.

During warming of the CO_2-bearing fluid inclusions, the ice melts prior to the decomposition of the clathrate compound. Estimates of salinity based upon the depression of fusion point of ice will therefore be too high (by as much as 50%;

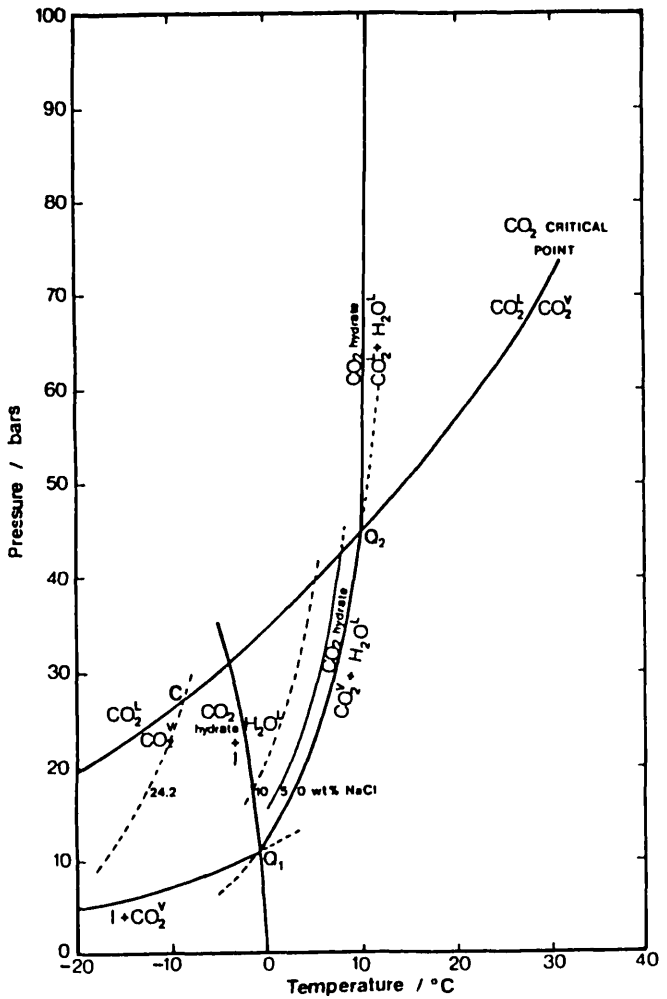

(a)

(b)

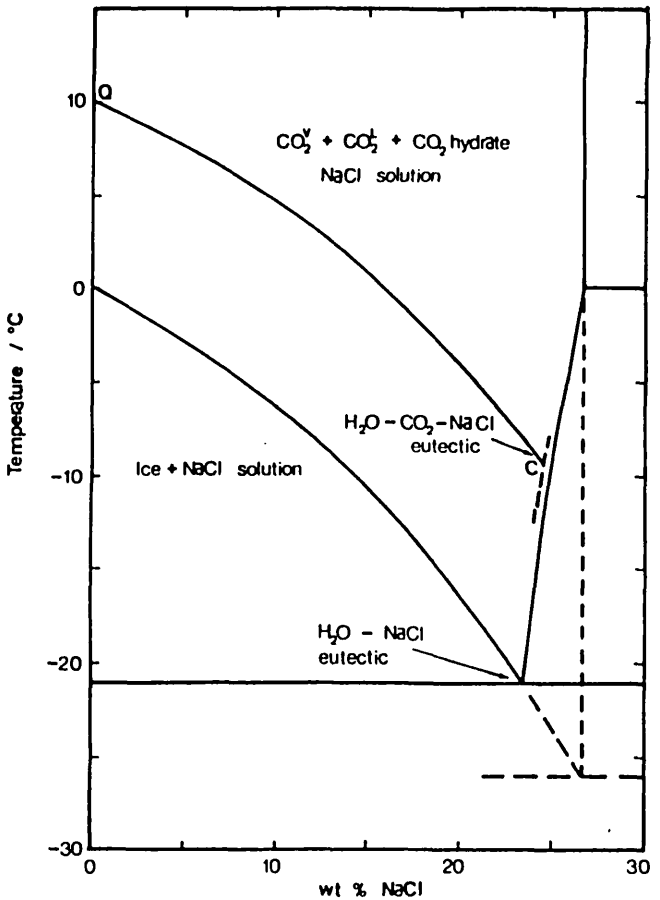

FIGURE 7.3. The system: CO_2 - H_2O - NaCl (after Collins 1979, Burruss 1981): (a) CO_2 - H_2O; the dashed lines indicate the shift to lower temperatures of the decomposition of CO_2 hydrate in equilibrium with 5 mass %, 10 mass %, and saturated NaCl solutions. (b) Depression of the temperature of CO_2 hydrate by NaCl in the presence of CO_2 liquid and CO_2 gas; the effect of NaCl upon the temperature of fusion of ice, T_F ice, is shown for comparison.

Collins 1979). Phase relationships in the system CO_2 - H_2O - NaCl, however, indicate that a more accurate estimate of salinity may be obtained from the temperature of decomposition of CO_2 hydrate, T_F clathrate, provided that both liquid and vapour CO_2 are present at this temperature (Figures 7.3a and 7.3b; Collins 1979). In this case, the phase changes observed upon heating are described by the univariant curve CO_2 in Figure 7.3a. This is compared to the curve for the depression of T_F ice in Figure 7.3b. If, however, liquid CO_2 is not present at the temperature of decomposition, then the phase relationships are described by the divariant surface Q_1Q_2 in Figure 7.3a. In this case, it is very difficult to estimate both CO_2 and NaCl concentrations from the cryometric studies.

Estimates of salinity obtained from T_F clathrate are further complicated by the presence of other compounds in addition to CO_2 within the inclusions. Presence in particular of CH_4 has the effect of counteracting the depression of T_F clathrate by NaCl. Decomposition of the gas hydrate at temperatures above 10°C is believed to be indicative of the presence of other gases such as CH_4 in the inclusions (Collins 1979, ref. cit. Touret 1977).

7.3.2 Discussion of the results

Salinities of both aqueous two phase and CO_2-bearing inclusions were estimated from the depression of fusion point of ice, T_F ice. The temperature of decomposition of CO_2 clathrate could not be used, since liquid CO_2 was seldom present at the temperature of decomposition. The fact that T_F clathrate sometimes occurred at temperatures greater than 10°C indicates the presence of other gases in addition to CO_2 within the inclusions. The estimated salinities for CO_2-bearing inclusions are therefore at best a first approximation. No attempt has been made to estimate the CO_2 contents of these inclusions.

The estimated salinities of hydrothermal solutions in equilibrium with quartz from both the quartz syenite and alkali feldspar granite and from miarolytic cavities within these rock-types are illustrated in the form of histograms in Figure 7.4. The same values are plotted against homogenisation temperature, TH, in Figure 7.5. When plotted in this manner, it is apparent that several of the samples investigated contain more than one generation of fluid inclusions. These may indicate trapping of a single fluid at different stages in its evolution, or the presence of more than one hydrothermal fluid.

Thus, the fluid inclusions in quartz from the quartz syenite, sample N1Ø, cluster into two groups: A group of high temperature, moderately saline inclusions; and a group of moderate to low temperature inclusions of low salinity. Similarly, fluid inclusions within miarolytic quartz from the contact zones of the quartz syenite, sample N251.9, cluster into two groups: A group of high temperature, moderately saline inclusions; and a group of high temperature inclusions of low salinity. In comparison, fluid inclusions in quartz from the alkali feldspar granite, sample W24, define three groups: A group of high temperature CO_2-bearing inclusions of moderate salinity; a group of moderate temperature, moderately saline inclusions; and a group of low temperature inclusions of varying salinity. The latter are interpreted as a boiling fluid inclusion assemblage. The fluid inclusions in sample W58 define a similar low temperature, boiling trend. In contrast, fluid inclusions from sample W51 show an almost linear increase in salinity with homogenistion temperature. This might also be interpreted as a boiling assemblage. The fact, however, that these inclusions homogenise to the liquid phase by dissolution of the halite daughter mineral suggests that they are not representative of a boiling condensate, but of a hypersaline aqueous phase exsolving from the silicate melt (saturated NaCl or magmatic trend; Chryssoulis 1983a).

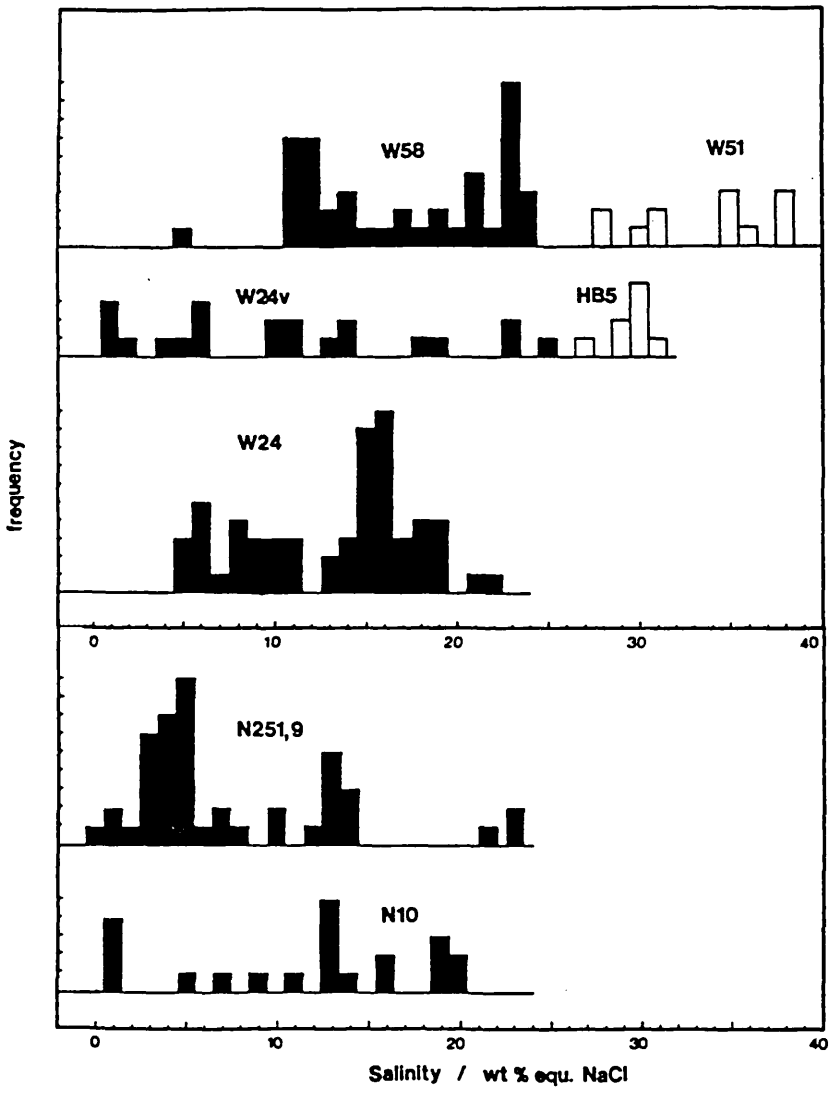

FIGURE 7.4. Histogram of salinities (wt % equ. NaCl), granitic and vug quartz from the Hurdal area.

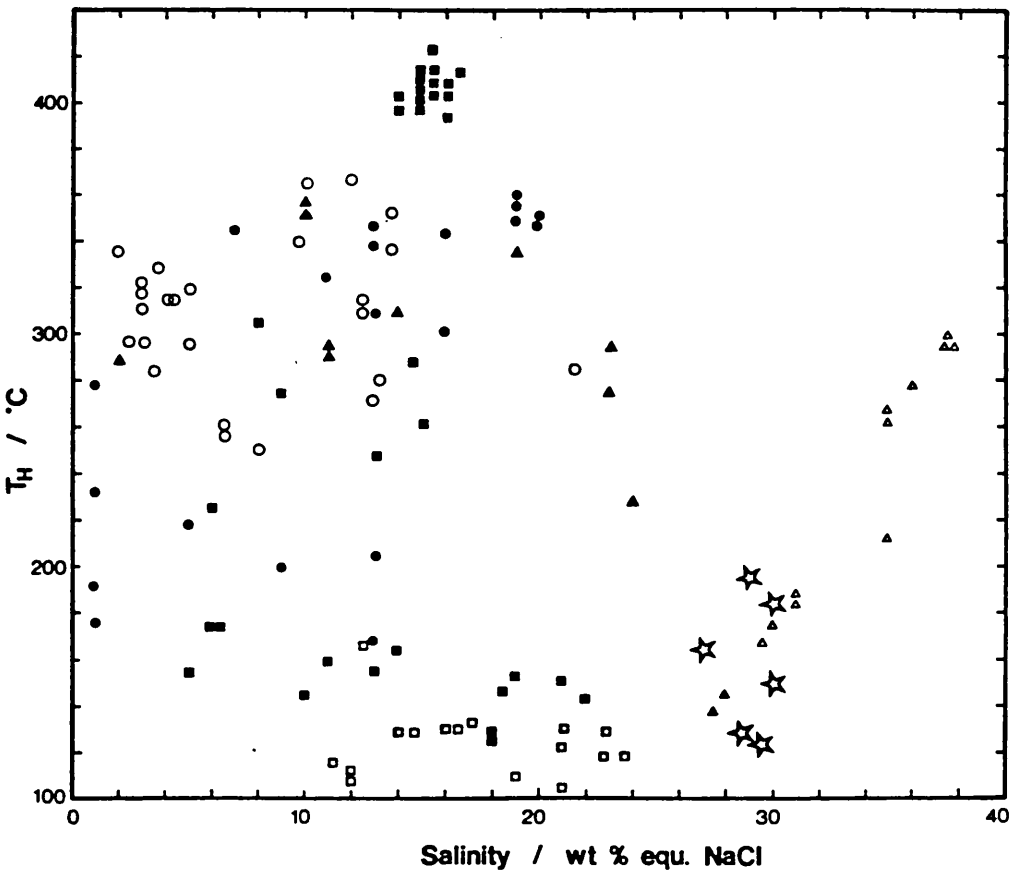

FIGURE 7.5. Scatter plot of salinity (wt % equ. NaCl) vs. T_H (^oC). Symbols: ● = N1Ø; o = N251,6, vug; ■ = W24; ▲ = W24, vein; □ = W58; △ = W51, ☆ = HB5.

Finally, sample HB5 from the Hegga river locality contains a boiling fluid inclusion assemblage of high salinity (Section 7.2.5).

The samples investigated in this study give an indication of the types of hydrothermal fluid which may have exsolved from the silicate melt at different stages in its evolution. In particular, they indicate the importance of saline hydrothermal fluids in the evolution of the granitic rocks, and that boiling of hydrothermal fluids was a common phenomenon. In addition, they verify the existence of high temperature CO_2-bearing fluids of primary magmatic origin. The number of measurements recorded, however, is insufficient to provide a more detailed assessment of the volumes of fluid concerned and of their relative importance in the evolution of the granite.

7.4 Chemical analyses of the fluid inclusions

Fluid inclusions in granitic quartz from the Hurdal area were analysed by the Decrepitation - inductively coupled plasma emission spectrometry method, D-ICP, following the procedure outlined by Thompson et al. (1980) and Alderton et al. (1982). This method provides a qualitative to semi-quantitative assessment of the bulk composition of the fluids concerned. However, only the inclusions which decrepitate upon heating may be analysed by this technique. For a more detailed appraisal of this technique and of the errors inherent in the method, see Chryssoulis (1983a).

7.4.1 Sample preparation

The samples of granitic quartz selected for this study were first crushed and then sieved in order to obtain a uniform grainsize. In the case of the quartz syenite, this was 0.5 to 0.8 mm. All other samples were selected from the size range 0.8 to 1.0 mm. Unwanted grains of feldspar and ferromagnesian

minerals were removed with the aid of a magnetic separator, and then by hand under a binocular stereoscope. Between Ø.5 and 1.Ø g of sample was selected in this way. The quartz separates were then treated in concentrated 1N hydrochloric acid for a period cf 24 hours. Finally, the samples were rinsed in deionised water, and dried.

7.4.2 Method

The pure mineral separates were placed in sealed pyrex containers connected to the ICP by PVC tubing. The containers were then heated in an electrical furnace at temperatures of 6ØØ $\pm$ 3Ø^{o}C for a period of 55 seconds with a pre-flush period of 15 seconds. The temperature was maintained constant at this level in order to allow all the fluid inclusions to decrepitate, at the same time minimising the effects of sublimation (see Chryssoulis and Wilkinson 1983). By this means the fluids were released into the plasma as a dispersion of fine droplets, carried by an argon flow. The fluids were analysed with the aid of an ARL 34ØØØC vacuum emission spectrophotometer equipped with channels for the simultaneous measurement of 36 elements. Blank samples were run at regular intervals.

7.4.3 Calibration

The response of the ICP for a given element, in millivolts, is proportional to the intensity of light emitted by the plasma, of characteristic wavelength for that element. This in turn is proportional to the mass of the element which enters the plasma. The sensitivity of the plasma for different elements, however, varies by several orders of magnitude. Alderton et al. (1982) have overcome this problem by using the standard calibration for solutions, in which the sensitivity of each element, S_x, expressed in mV/(μg g^{-1}), is determined by passing a solution of known concentration through the plasma (Appendix A5, Table A3). In this manner, the raw data may be converted into apparent concentration by

dividing through by the sensitivities for each element. The transformed data, expressed in equivalent parts per million (equ. ppm, Appendix A5), are not however true concentrations, since the volumes of fluid concerned are unknown (Chryssoulis 1983a).

A more meaningful transformation of the data can be achieved by dividing through by the sensitivity of each element relative to that of sodium, S_x/S_{Na}, since Na is known to be an important component of the fluid inclusions. This gives an estimate of the relative mass proportions of each element, expressed in millivolts. This may then be converted into relative atomic proportions by dividing through by the ratio of atomic weights of the particular element to Na, again expressed in millivolts.

7.4.4 Discussion of the results

Average chemical analyses of fluid inclusions in quartz from both the quartz syenite and alkali fedlspar granite, and from quartz vugs within these two rock-types are presented in Table 7.2. In addition, the average of four samples of fluorite from the biotite syenite in the Nordgardshogda area, and one sample of quartz from a vein within the biotite syenite are presented.

The results are expressed in the form of relative atomic proportions mV^{-1} per gram of sample, corrected for background. The intensity of the background has been calculated from the blank samples and subtracted from the raw data, following the procedure outlined in Appendix A5. A statistical comparison between the intensities of the blank samples and of the raw sample data, using standard F and t tests (White et al. 1979), has enabled a distinction to be made between elements which are at or above background levels and elements which can not be discriminated from the background. Twelve elements have been selected in this way:

Lithium, Be, Na, Si, S, K, Ca, Ti, Mn, Fe, Zn and Sr. Of these elements, Si is an important constituent of the host mineral; titanium is of minor importance and is close to background levels; and Ca and Sr are only important constituents in fluorite. In addition, the sulphur analyses should be considered with caution, since S sublimes at temperatures below 600°C (Chryssoulis 1983a). The effects of contamination upon the analyses have not been considered. The very pure nature of the quartz separates suggests that contamination should have been negligeble (Chryssoulis 1983b). The precision of this method, obtained from replicate quartz separates, is presented for each element in Appendix A5, and is seldom better than 30% (2σ; Table A4).

When compared with fluid inclusions from granitic quartz, the fluid inclusions in miarolytic quartz from the quartz syenite show on average higher proportions of Mn, Zn, Na, K, Li, Ca and S, and lower concentrations of Fe (Table 7.2). In contrast, the fluid inclusions from miarolytic quartz from the alkali feldspar granite show similar contents of Zn, Mn and K, and lower contents of Na, Fe, Be, Ca and S when compared with fluid inclusions in granitic quartz from the same rock-type. The principal difference between fluid inclusions in granitic quartz from the quartz syenite and alkali feldspar granite is the presence of higher proportions of Mn, Be, Na, K, Li and S in the granite. Sample N90A27 from the Nordgardshogda area is similar in terms of chemistry to the most Fe-enriched fluid inclusions in the quartz syenite from the same area (Figure 7.1).

Figure 7.6 indicates that the ratio of Na to K in the fluid inclusions remains constant throughout evolution, at approximately 10 to 1. This is in fact the proportion in which these elements enter the plasma. However, the predominance of halite over sylvite within the saline inclusions suggest that a ratio of 10 to 1 for these fluids is reasonable. Only in the quartz syenite do the fluid

TABLE 7.2: STATISTICAL ANALYSIS OF FLUID INCLUSION DATA (Rel. at. props./mV)

SAMPLE TYPE:	Q.S.		Q.S. vug		A.G.		A.G. vug	
NUMBER OF SAMPLES:	10		7		12		12	
ELEMENTS:	$\bar{x}$	σ_{n-1}	$\bar{x}$	σ_{n-1}	$\bar{x}$	σ_{n-1}	$\bar{x}$	σ_{n-1}
Zn	.13	.15	.69	.59	.16	.11	.26	.18
Sr	.03	.03	.03	.03	.03	.03	.03	.02
Mn	.22	.30	2.37	1.93	1.05	1.07	.94	.97
Fe	.70	.71	.26	.22	.72	.28	.29	.25
S	221.52	269.36	395.49	315.86	264.53	112.54	129.70	51.72
Si	55.97	28.49	55.77	33.35	48.19	21.97	144.79	121.26
Na	59.63	24.96	272.16	102.13	244.83	164.41	208.93	138.01
Be	.05	.07	.02	.03	.47	.40	.16	.13
Ca	.23	.48	7.21	19.06	.50	1.08	.28	.44
Li	1.94	2.25	7.89	5.55	2.81	1.76	3.69	1.66
Ti	.46	.57	.05	.05	.23	.17	.21	.19
K	12.49	12.42	34.75	15.26	25.19	15.45	26.39	11.68

SAMPLE:	N90A27	HH1	FLUORITE	
NUMBER OF SAMPLES:	1	1	4	
ELEMENTS:			$\bar{x}$	σ_{n-1}
Zn	.19	.04	.03	.04
Sr	.07	.02	.29	.09
Mn	.83	.02	.89	.42
Fe	1.71	.28	.93	.22
S	4749.09	519.29	326.43	138.19
Si	54.74	36.58	7.84	3.63
Na	138.05	19.06	15.61	12.06
Be	.07	.03	0.00	.00
Ca	.97	.01	786.26	190.57
Li	1.35	1.13	.13	.18
Ti	.19	.23	.18	.18
K	12.88	5.94	1.05	1.48

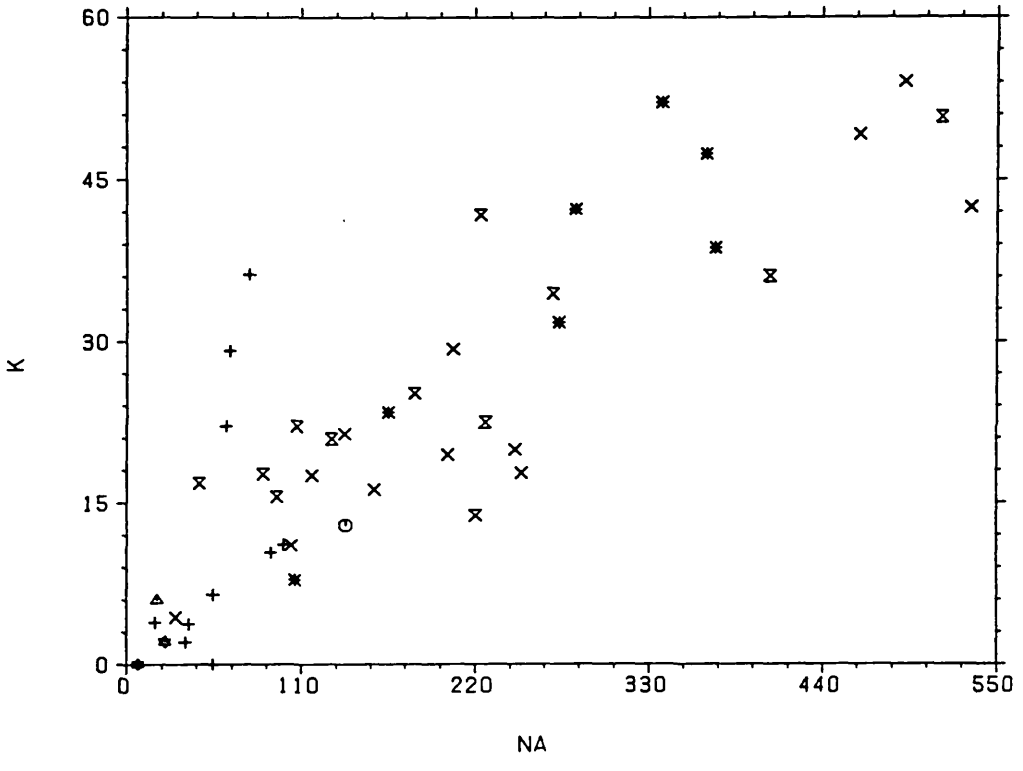

FIGURE 7.6. Scatter plot (rel. at. props / mV) of Na vs. K. Symbols: + = Quartz syenite; * = Quartz syenite, vugs; x = Alkali feldspar granite; x = Alkali feldspar granite, vugs; o = N90A27; △ = HH1; ✿ = Fluorite.

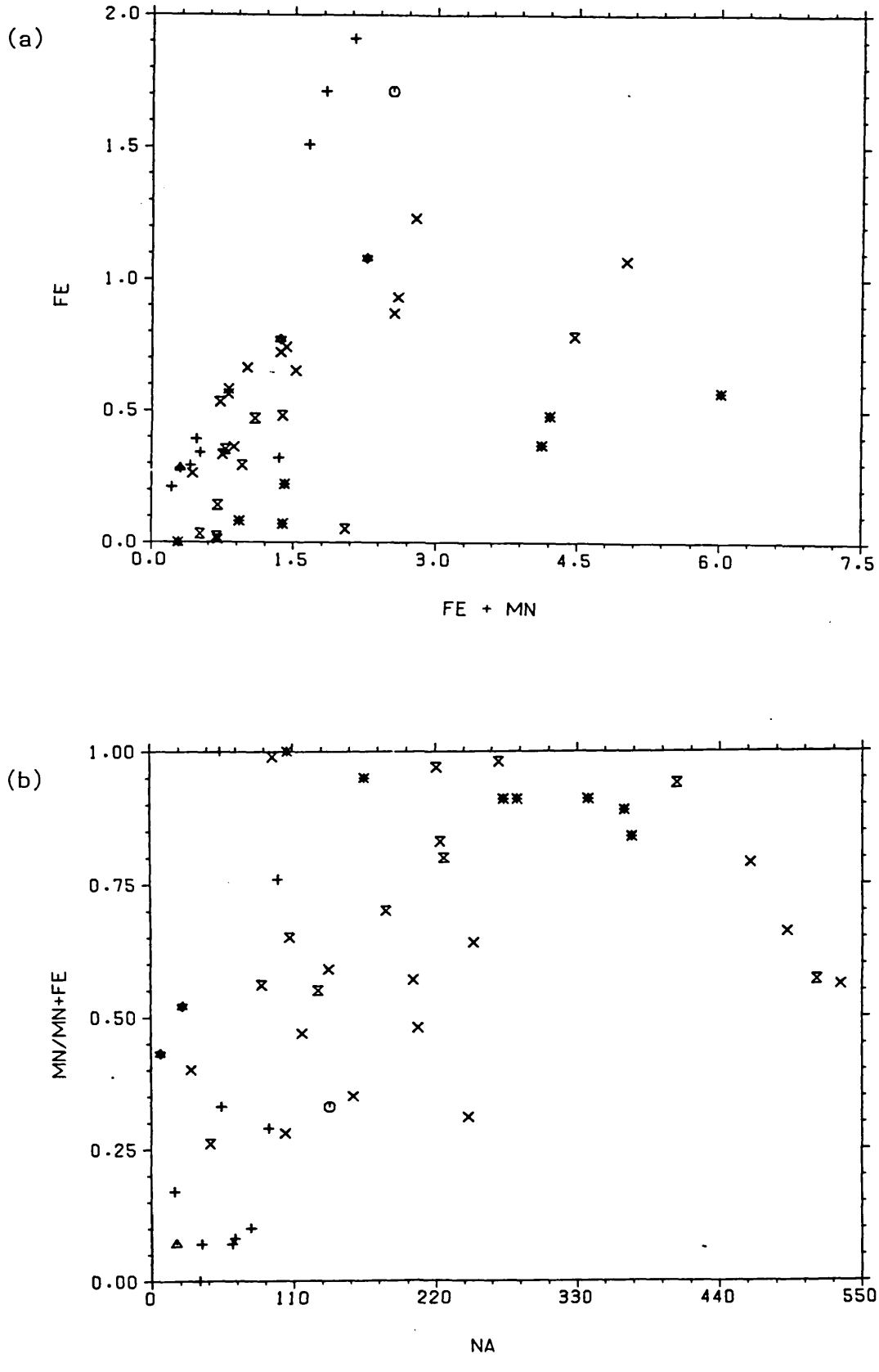

FIGURE 7.7. Scatter plot (rel. at. props / mV) of: (a) Fe+Mn vs. Fe; and (b) Na vs. Mn/Mn+Fe. Symbols as in Figure 7.6.

inclusions deviate from this general trend, having Na/K ratios approaching 2 to 1.

Figures 7.7a and 7.7b indicate the contrasting compositions of fluid inclusions from the different types of quartz. Fluid inclusions in granitic quartz from the quartz syenite have a high ratio of Fe/Fe+Mn, at approximately .8 (Figure 7.7a). In contrast, fluid inclusions from miarolytic quartz from the same rock-type have much lower Fe/Fe+Mn ratios, at approximately .1, indicating a strong preference for Mn in these fluids. Fluid inclusions in granitic and miarolytic quartz from the alkali feldspar granite also show trends towards Mn enrichment with increasing Fe content.

Manganese enrichment in the fluid inclusions is in general accompanied by enrichment in alkalies and Zn. However, the influence of Zn and Li in the inclusions is much greater in miarolytic quartz from the quartz syenite. The relationship between the Mn and Na contents of the inclusions is illustrated in Figure 7.7b. This diagram suggests a general increase in the Mn contents of the inclusions with increasing salinity.

7.5 Hydrothermal evolution

The presence of fluid inclusions within granitic quartz from the Hurdal area confirms the existence of hydrothermal fluids in the evolution of these rocks. The fact that many of these inclusions are evidently of primary nature suggests that the fluids are of magmatic origin, exsolved directly from the silicate melt. A general increase in the size and abundance of fluid inclusions, from biotite syenite through to alkali feldspar granite (Table 7.1), indicates an increase in the volumetric importance of these fluids during evolution.

The biotite syenite and quartz syenite contain only secondary fluid inclusions (Section 7.2). In comparison, the alkali

feldspar granite and quartz vugs contain both primary and secondary inclusions, many of which contain a discrete CO_2 phase. The importance of CO_2 within the inclusions increases from syenite to granite, suggesting that the melt became saturated with respect to carbon dioxide after the aqueous phase. The distribution of CO_2-bearing inclusions within quartz vugs from the Brennhaugen granite and from the quartz syenite in the Nordgardshogda area suggests the presence of a CO_2 enriched carapace in both these intrusions (Section 7.2.6). Migration of CO_2 within the silicate melt has presumably resulted in an outer zone saturated with respect to CO_2.

A combination of petrographic and microthermometric studies has revealed that boiling of hydrothermal solutions was a common phenomenon in the Hurdal area, particularly in the alkali feldspar granite (Sections 7.2 and 7.3). Boiling of hydrothermal fluids may be identified by the coexistence of both gas-rich and liquid-rich inclusions homogenising at the same temperature, or by rapid increases in salinity with homogenisation temperature (Figure 7.5). Boiling may have lead to ore-deposition in certain cases. For instance, the presence of boiling hydrothermal fluids within sample W24 from the Brennhaugen granite may have been responsible for the precipitation of molybdenite within this rock.

The ore-forming potential of hydrothermal fluids in equilibrium with granitic quartz is indicated by the presence of opaque daughter minerals within many of the inclusions (Section 7.2). In particular, the presence of a non-magnetic daughter mineral of hexagonal outline, tentatively identified as molybdenite (Section 7.2.6), within fluid inclusions in miarolytic quartz from the contact zones of the quartz syenite in the Nordgardshogda area suggests that these fluids may have been responsible for molybdenite $\pm$ pyrite mineralisation in the area (Section 4.3.1). The mineralising potential of these fluids is also indicated by their chemical

compositions, which reveal significant amounts of Mn, Zn and S within the inclusions. In comparison, fluid inclusions, from the alkali feldspar granite tend to be enriched in alkalies, Mn and Be (Section 7.4). These fluids, therefore, may have been responsible for manganese enrichment in the area.

Finally, the ratio of Na to K in the fluid inclusions remains more or less constant throughout evolution from syenite to granite. The strong preference for Na as opposed to K in the fluids is presumably a consequence of sub-solidus changes occurring within the rocks. It explains the widespread occurrence of bleaching within the granite and the presence of zones of silicification from which most of the Na has been leached (Section 5.4). In addition, it explains the absence of potassic alteration in the Hurdal area (Lagache and Weisbrod 1977, Burnham 1979b).

CHAPTER EIGHT

MAGMATIC AND HYDROTHERMAL EVOLUTION

8.1 Introduction

In this final chapter, an attempt will be made to bring together some of the ideas which have been introduced in the previous seven chapters, and to unite them into a theory for the origin and evolution of felsic igneous rocks in the Hurdal area. Particular emphasis will be placed upon the magmatic evolution, and upon the roles of F and CO_2 in the genesis of the peralkaline rocks. In addition, the origin of the Mn-silicate bearing, albite-rich rocks will be discussed in detail.

Four interrelated aspects of the evolution will be considered:

I. Magmatic evolution, concerning the effects of pressure, temperature and mineral chemistry upon the composition and structure of the silicate melt;

II. Mineralogical evolution, concerning changes in the nature and composition of the mineral phases and the development of granitic textures;

III. Hydrothermal evolution, concerning the nature, composition and ore-forming potential of hydrothermal fluids exsolved from the melt during its evolution; and

IV. Mineralisation and alteration, concerning the processes of concentration and precipitation of ore-metals.

8.2 Magmatic evolution

The compositional path along which a magma evolves, from the point of its generation in the source region to its consolidation in the crust, is a function of several processes, the most important of which are: Partial melting in the source region to produce the primary magma; partial crystallisation on ascent through the crust, which modifies

the primary composition; and contamination of the magma due to interaction with the country rocks through which it has to rise. In addition, processes of convection and diffusion may lead to the development of compositional gradients within the magma.

The degree to which any of these processes predominates during magmatic evolution depends upon a large number of factors, many of which are mutually related. The composition of the primary magma depends to a large extent upon the composition of the source rocks and the degree of partial melting involved. The latter is a function of the depth and pressure of melting, the ambient temperature regime, and the availability of volatiles such as H_2O and CO_2 in the source region. The extent to which the primary composition is modified by processes of fractional crystallisation or contamination depends upon the initial energy and composition of the magma, its density and viscosity, and the orientation of the regional stress field. These factors control the rate at which the magma rises through the crust. Thus high energy, low viscosity magmas erupted quickly to the surface may still retain their primary composition. Magmas of this type rise adiabatically, with only minor heat loss to their surrounding wall-rocks, and are therefore maintained in a molten state at temperatures above their liquidus. In comparison, low energy, high viscosity magmas erupted slowly to the surface, dissipate heat to their wall-rocks and remain for longer periods at temperatures close to or below their liquidus. Magmas of this type may be subjected to considerable modifications, and are unlikely to reflect their primary composition.

The extent to which contamination occurs is not only dependent upon the composition and thermal energy of the magma, but also upon the composition of the wall-rocks and the ratio of surface area of wall-rock to the volume of melt. The latter depends upon the mechanisms of intrusion. The

magma may be emplaced by forceful diapirism, by more passive stoping or zone melting, or by permitted dyke injection. The largest ratio of surface area of wall-rock to the volume of melt is provided by a stoping model. However, the effects of contamination are believed to become negligible, once the size of the stoped blocks exceeds a critical radius (Marsh 1982). In the case of stoped blocks of mafic composition this is approximately 3 metres. For granitic rocks, however, the critical radius may be as much as 30 metres.

The relative contributions of partial melting and fractional crystallisation in magma genesis are difficult to assess, since these processes in effect represent opposite extremes of a single process, that of crystal fractionation. This is because the nature and composition of mineral phases which occur on or near the liquidus of the melt correspond to those on the solidus of the material being melted (Section 2.5.1). This assumes equilibrium conditions. Thus equilibrium partial melting may be regarded as the opposite of equilibrium crystallisation (Figure 2.5a). Similarly, the effects of contamination are hard to assess, unless the assimilated material is of contrasting composition to the melt.

In the following sections, it will be pertinent to refer to a process of crystal fractionation, and then to assess which of the above processes was the predominant mechanism.

8.2.1 Effects of crystal fractionation upon magma composition

The intermediate to granitic rocks exposed in the Hurdal area are compatible with an origin by fractionation of intermediate magmas, essentially by separation of clinopyroxene, plagioclase and alkali feldspar (Figure 8.1, Section 5.5). Removal of these minerals has the effect of depleting the melt in elements with high crystal/liquid distribution coefficients for these minerals, $K_D > 1$; at the same time enriching the melt in elements with low

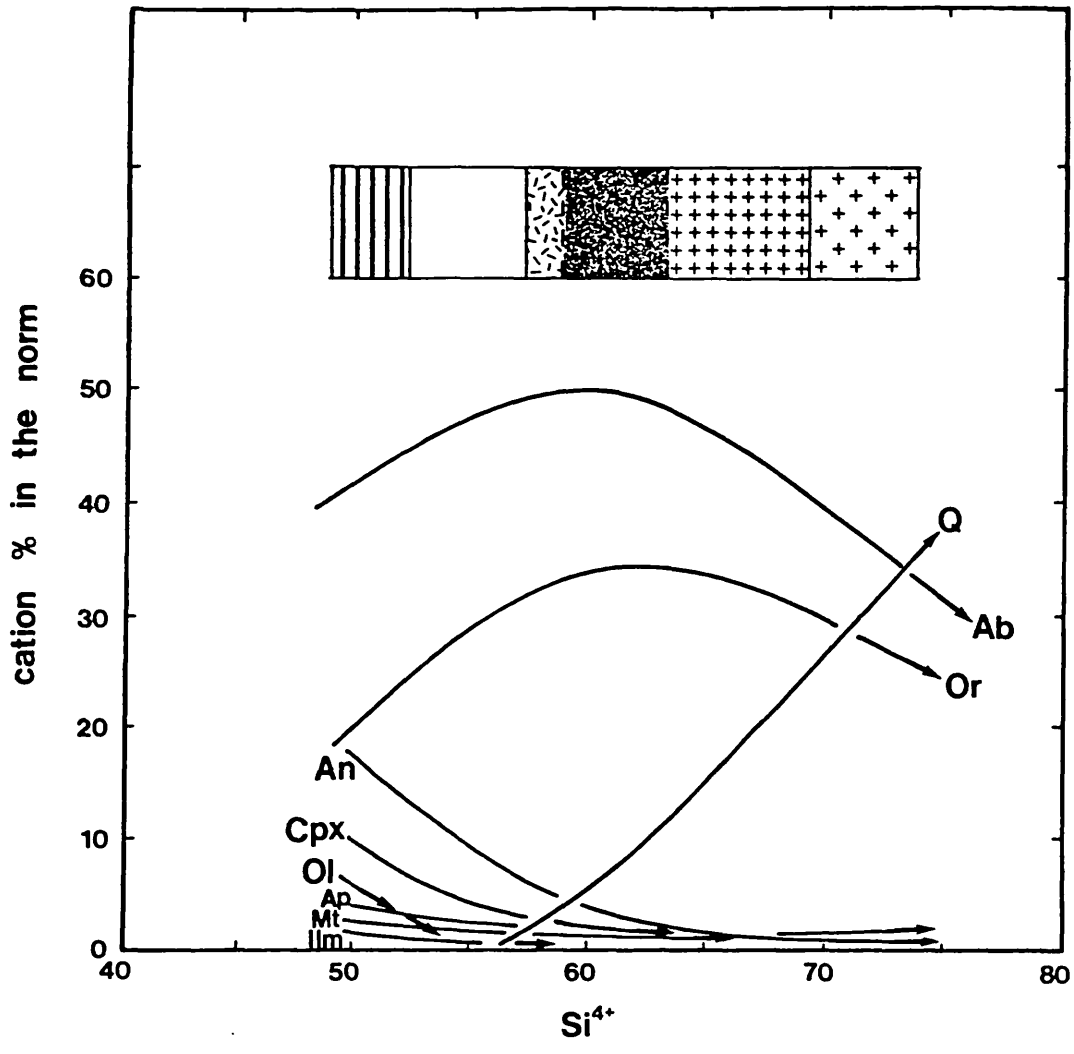

FIGURE 8.1. Summary of fractionation trends in the Hurdal area. Symbols as in Figure 3.1.

distribution coefficients, $K_D < 1$. This has the effect of continually modifying the bulk distribution coefficient, D, for each element (Section 6.5).

Thus, in the early stages of evolution in the Hurdal area, corresponding to the compositional interval between monzodiorite and biotite syenite, separation of clinopyroxene and plagioclase, of initial composition An_{50} - An_{30}, has the effect of depleting the melt in Ca, Mg and Fe^{2+}, together with V, Co and Sr (elements belonging to group IIa, Section 6.4). At the same time, separation of apatite and ilmenite depletes the melt in P and Ti. Removal of these minerals effectively enriches the melt in Na, K and Si, the Na content of the melt increasing to a maximum, at approximately 12 cation %, during the biotite syenite stage of evolution (Figure 8.1). In addition, all elements belonging to group IIb, group III and group I show moderate enrichments (Section 6.4, Figure 6.2a).

The subsequent stages of evolution in the Hurdal area, corresponding to compositions in the range biotite syenite - quartz syenite, may be explained in terms of separation of plagioclase of increasingly sodic composition, accompanied by alkali feldspar of more or less constant composition, Ab_{60} - Ab_{50}. At the same time, the proportion of ferromagnesian minerals decreases to a minimum. Removal of these minerals has the effect of depleting the melt even further in elements belonging to group IIa, together with Ba, Eu and LREE (Group IIb, Section 6.4, Figure 6.2 b and c). Removal of these minerals also has the effect of enriching the melt in K and Si, the K content of the melt reaching a maximum, at approximately 7.3 cation %, during the alkali feldspar syenite stage of evolution (Figure 8.1). In addition, all elements belonging to group III and group I continue to be enriched.

The reversal in the behaviour of LREE in these rocks is

believed to be the result of partitioning of these elements into accessory mineral phases such as biotite and magnetite. The unusually high crystal/liquid distribution coefficients inferred for these minerals reflect the increasing degree of polymerisation of the silicate melt (Section 6.4.3). Accessory minerals such as apatite, zircon and sphene are believed to have had little or no influence upon the REE evolution of these rocks.

Europium may also have been incorporated into biotite and magnetite. However, the reversal in the behaviour of europium might also reflect an increase in the redox ratio Eu^{2+}/Eu^{3+} in the melt, suggesting a change to conditions of lower oxygen fugacity. This is supported by a general decrease in the ratio of $Fe^{3+}/Fe^{3+}+Fe^{2+}$ in the more evolved, granitic end-members (Figure 5.8c). Preferential partitioning of Eu^{2+} into feldspar would result in a reduction in the concentration of this element in the melt during evolution.

The final stages of evolution in the Hurdal area, responsible for compositions in the range quartz syenite - alkali feldspar granite, may be explained essentially in terms of separation of alkali feldspar, fractionation of plagioclase having removed the magma from the compositional field in which two feldspars crystallise. Separation of alkali feldspar has the effect of enriching the residual melt in Si, which increases to a maximum at approximately 73 cation % in the alkali feldspar granite. At this point, alkali feldspar is joined on the liquidus by quartz. Continued separation of alkali feldspar and quartz in constant proportions has no further effect upon the composition of the melt in terms of its principal components (see Section 5.3).

This stage in the evolution is accompanied by the most variable behaviour of elements belonging to group III, these elements showing both enrichments and depletions within individual rock units (Section 6.4). Lithium, Cr, Cu and Zn

show strong to moderate correlations with Mn and F (Figure 6.9) and are probably partitioned into biotite. The latter contains up to 1.6 Mn ions and 2.4 F ions per formula unit (Section 3.5.1). In comparison, HREE, Y, Zr and Hf show only moderate to weak correlations with Mn and F. Heavy REE and Y may also be partitioned into biotite. However, Zr and Hf are incorporated into zircon. This stage in the evolution involves a considerable reduction in the solubility of Zr in the melt, causing zircon to precipitate out (Section 6.5, Figure 6.11). Meanwhile, the concentrations of elements belonging to group I (Rb, Nb, Ta, Pb, Th and U; Section 6.4) continue to rise (Figure 6.2 d and e); and elements belonging to group II show their largest depletions.

Fractionation involving a combination of clinopyroxene, plagioclase and alkali feldspar also has significant effects upon the composition of the melt in terms of its volatile constituents. Separation of these minerals has the effect of enriching the melt in H_2O, F and CO_2. However, enrichment of the melt in these components tends to be counterbalanced by incorporation of H_2O and F into hydrous mineral phases and, at specific stages in the magmatic evolution, by exsolution of a discrete hydrothermal phase. The H_2O content of the melt in particular is always buffered by a certain amount of biotite and/or amphibole crystallisation. In comparison, the concentration of F in the melt increases to a maximum during the biotite syenite stage of evolution. This is indicated by the high ratio of F to OH^- in both the whole-rock compositions and the hydrous mineral phases (Sections 3.5.1 and 5.4). The F content of the melt drops off rapidly during the alkali feldspar syenite and quartz syenite stages of evolution, only to build up again in the alkali feldspar granite. Carbonate minerals, in comparison, are not important constituents of any of the plutonic rocks. Carbon dioxide, therefore, tends to be concentrated in the melt throughout evolution, until a stage is reached where the melt becomes saturated with respect to CO_2 and a separate CO_2-bearing

aqueous phase is exsolved. This occurs during the evolution of the alkali feldspar granite (Section 7.5).

8.2.2 Effects of magma composition upon silicate melt structure

Evolution from monzodiorite to alkali feldspar granite involves both a considerable increase in the concentration of SiO_2 in the melt, and significant reductions in the proportions of potential modifier cations such as Fe^{2+}, Mg and Ca. In addition, the ratio of potential charge-balancing cations such as Na, K and Ca, to aluminium increases to approximately unity (Section 5.5.2.1). Evolution from monzodiorite to granite is therefore accompanied by a considerable increase in the proportion of tetrahedrally coordinated cations in the melt. At the same time, the proportion of octahedrally coordinated cations decreases to a minimum. In the absence of dissolved volatiles, the most evolved granitic magmas should therefore be highly polymerised, and viscous.

The large increase in the ratio of tetrahedral to octahedral coordination sites in the melt (decrease in NBO/T, Section 5.5.2.1) is likely to have a significant effect upon the partitioning behaviour of trace elements. In particular, a decrease in the availability of octrahedral coordination sites in the melt is likely to prohibit the incorporation of divalent cations such as V, Co, Sr, Ba and Eu^{2+}. These elements generally substitute for Mg, Ca and Fe^{2+} in both the structure of the melt and the crystalline mineral phases. Thus, while minerals incorporating these elements have largely been removed from the melt by the quartz syenite stage of evolution, the concentrations of these elements in the melt continue to decrease during the evolution of the alkali feldspar granite.

The reduction in the proportion of octahedral coordination

sites in the melt is also likely to have significant effects upon the partitioning behaviour of rare earth elements, affecting LREE to a greater extent than HREE due to their larger ionic radii (Section 6.4.3; Mysen and Virgo 1980b). Exclusion of LREE from the structure of the melt is likely to be accompanied by increased partitioning of these elements into accessory mineral phases such as biotite and magnetite. It is this effect which is believed to be responsible for the systematic depletions in LREE observed within the more evolved granitic rocks.

The large increase in polymerisation conjectured for the silicate melt during its evolution is to a certain extent counter-balanced by the effects of dissolved volatile components such as H_2O, CO_2 and F (Section 5.5.1). Particularly within the contact zones of the individual intrusions, build-up of dissolved volatiles is likely to have important effects both on the structure of the melt and on the partitioning behaviour of certain elements. The presence within the melt of even small amounts of H_2O is likely to disrupt the three-dimensional network, thereby causing substantial reductions in both silicate polymerisation and magma viscosity. Water reacts with both bridging and non-bridging oxygens in the melt to form Si-OH bonds, and with modifier cations to form M(OH) and $M(OH)_2$ complexes (Section 5.5.1, Mysen et al. 1980b). In comparison, fluorine and carbon dioxide would appear only to react with modifier cations and not with silicon (Kogarko and Krigman 1973, Mysen and Virgo 1980a).

The importance of F as a complexing agent within the melt is indicated by the strong correlations, in the whole-rock analyses, of this element with Mn and Zn, and to a lesser extent with Cu, Li and Cr (Section 6.5). Two types of reaction would appear to be important (Section 5.5.2). Firstly, fluorine reacts with modifier cations in the melt to form MF and MF_2 complexes. Secondly, fluorine reacts with

alkalies in their charge-balancing role with Al^{3+} to form M_3AlF_6 complexes. The first type of reaction leads to an increase in the concentration of bridging oxygens in the melt and is therefore accompanied by an increase in the degree of silicate polymerisation. In contrast, the second type of reaction is accompanied by expulsion of Al^{3+} from tetrahedral coordination, with a consequent reduction in the degree of polymerisation. This has the effect of increasing the number of octahedral coordination sites in the melt and may be accompanied by enrichment in the melt of elements belonging to group II (Section 6.4).

Reaction between F and network modifying cations results in the formation of ccmplexes of the type NaK, KF and CaF_2 (Section 5.5.2). Strong correlations in the whole-rock analyses between Mn and F, together with Li, Cr, Cu and Zn (Section 6.4), however, suggest that F also forms complexes with these elements. Saturation of the melt with respect to fluorine, at approximately Ø.5 wt% in melts of alkali feldspar granite composition (Kovalenko 1973), leads to the precipitation of fluorite. Reactions of this type are not accompanied by any significant enrichment in Na relative to K, indicating that these elements are incorporated into MF complexes to a similar extent (Figure 5.7b).

In comparison, reaction between F and alkalies in their role of stabilising Al^{3+} in tetrahedral coordination results in the formation of complexes of the type AlF_6^{3-}, with a combination of monovalent and divalent cations in the charge balancing role (e.g. $NaMnAlF_6$; Section 5.5.2). At the same time Al^{3+} is released into octahedral coordination. This type of reaction would appear only to be of importance in magmas saturated with respect to F, such as the biotite syenite and manganogranitoids, and would appear to be promoted by hydrolysis. Consideration of the distribution of trace elements in the manganogranitoids indicates that, in addition to Na and Mn, Zn is also enriched in these rocks (Section

6.4.4). Lithium, K and Rb, on the other hand, are strongly depleted. It is therefore reasonable to assume that Zn is also incorporated into alumino-fluoride complexes (i.e. $NaZnAlF_6$). The large ionic radii and low ionization potentials of K and Rb, and the small ionic size of Li, however, would appear to preclude the possibility of complex formation with these elements. Reactions of this type are therefore accompanied by considerable enrichments in Na relative to K (Figure 5.7b).

Late stage enrichments in HREE may also be attributed to complex formation. However, these elements show only moderate to weak correlations with F, suggesting that F was not the main complexing agent in this case. The presence within the evolved magmas of significant volumes of CO_2 suggests that carbonate complexes might have been responsible. This is supported by experimental evidence (Balashov and Krigman 1975), which indicates a general decrease in the affinity of volatile elements for REE in the order: $CO_3^{2-} > F^- > O^{2-} > OH^- > Cl^-$.

8.2.3 Effects of phase equilibria upon mineral/liquid evolution

The intermediate to granitic rocks in the Hurdal area define a single evolutionary series in which separation of clinopyroxene and plagioclase is accompanied and later superceded by removal of alkali feldspar. These are the minerals which appear on or just below the liquidus of the melt, as it responds to changes in pressure and temperature on ascent through the crust. Removal of these minerals has the effect of driving the composition of the residual liquid towards progressively more siliceous compositions.

The early stages of evolution in the Hurdal area may be modelled with reference to synthetic systems such as diopside - forsterite - anorthite, the compositions of intermediate

rocks plotting close to the diopside - anorthite join (Presnall et al. 1978). Phase relationships in this system indicate that the primary field of crystallisation of anorthite expands at the expense of the diopside field with decreasing pressure. Thus, the high ratio of plagioclase to clinopyroxene in the monzodiorites (Figure 8.1) is probably the result of low pressure fractionation.

The later stages of evolution in the Hurdal area may be modelled with reference to phase relationships in the synthetic system $NaAlSi_3O_8$ - $KAlSi_3O_8$ - SiO_2 - X, where X equals other components present in minor amounts in the system (Section 5.5). Compositions of plutonic and associated extrusive rocks plot along a curved path developing out of the Ab-Or join at Ab_{70} and culminating close to the minimum at 1 kbar under water-saturated conditions (Figure 5.4). The position of this fractionation curve does not, however, coincide with the thermal valley in the system under the same pressure conditions, but lies to the K-rich side of this curve. The reasons for this are complex. Firstly, the prerequisite in the synthetic system that pressure is constant does not hold for the natural system. P_{TOTAL} and P_{FLUID} are both variables, P_{FLUID} representing some finite fraction of the total pressure at liquidus temperatures. Secondly, liquidus phase relationships in the natural system are modified by the presence of additional components in the system, in particular H_2O, F and CO_2, but also CaO, MgO and FeO (X, above; Section 5.5).

8.2.4 Origin of peralkaline magmas in the Hurdal area

The magmatic evolution of alkaline to mildly peralkaline igneous rocks in the Hurdal area is satisfactorily explained in terms of fractionation of intermediate magmas corresponding in composition to monzodiorite (kjelsasite; Section 2.3.2). Development of the peralkaline condition in these rocks is essentially the result of plagioclase

separation (Figure 5.1Ø). Separation of clinopyroxene and alkali feldspar has little or no effect upon agpaitic index (Section 5.5). The orthoclase effect of Bailey and Schairer (1964) has not been operative in this system. Enrichments in Na relative to K in the biotite syenite and manganogranitoids are attributed to increased F activity in the melt (Section 8.2.2.).

8.2.4.1 Source rocks

Consideration of the distribution of incompatible trace elements within the felsic rocks from the Hurdal area indicates that the least evolved rock-types have comparable Y/Tb and Zr/Hf ratios to chondritic abundances and to magmatic products from both oceanic and continental rift settings (Section 6.5.2). These relationships confirm the existence of a considerable mantle component within these rocks. In addition, the least evolved rock-types from the Hurdal area have similar Zr/Nb ratios to the pyroxene basalts and plagioclase-pyroxene basalts from the Vestfold lava plateau, strongly suggesting alkali basaltic lines of evolution. The stable, but low ratios of Nb/Ta, however, indicate that the felsic rocks were derived from a source region enriched in Ta relative to Nb.

8.2.4.2 Mechanisms of fractionation

A combination of field, petrological and geochemical evidence has been used to suggest that the more evolved granitic rocks in the Hurdal area were derived from their intermediate precursors by processes of fractional crystallisation (Sections 3.5 and 6.5). The possibility that they may have been formed by remelting of intermediate rocks in the crust has been discounted on the basis of textural evidence. The intermediate magmas from which the main plutonic series evolved may have been derived directly from an alkali basaltic parent by fractional crystallisation. Alternatively,

they may have been formed by remelting of compositionally similar rocks already emplaced in the crust. On the basis of the available evidence, however, these two possibilities are extremely difficult to distinguish.

Consideration of the relative densities of likely phenocryst phases such as clinopyroxene (ρ = 2.96 - 3.52 g cm^{-3}; Deer et al. 1977), plagioclase (ρ = 2.63 g cm^{-3}) and alkali feldspar (ρ = 2.55 - 2.63 g cm^{-3}) and the calculated densities of anhydrous magmas at 1000°C and 1 kbar (ρ = 2.57 - 2.33 g cm^{-3}, Table 5.2) indicates that there is no objection on density grounds to the hypothesis that the felsic rocks in the Hurdal area evolved from their more mafic precursors by fractional crystallisation. Consideration of the likely viscosities of anhydrous magmas (Section 5.5.2.1) and the small size and proportions of phenocyrsts present (Section 3.3), however, suggests that fractionation by crystal settling in large crustal reservoirs is an unlikely mechanism (see, for comparison, Kushiro 1980). The fact that the principal minerals controlling evolution also coincide with those on the liquidus of the melt suggests that fractionation occurred as a result of cooling of the magma on ascent through the crust.

The low densities of anhydrous magmas when compared with the average density of the Precambrian craton (ρ = 2.74 g cm^{-3}; Ramberg 1976) support a model in which the felsic magmas rose buoyantly through the crust (Neumann 1980). Because the maximum confining stress was oriented vertically, and the intermediate and minimum stresses were similar in magnitude, and not vastly different as they had been previously in the tectonic cycle, the rate of ascent was slow. Under these conditions, conversion of thermal energy to work and dissipation of heat to the wall-rocks would have lead to the development of a zone within the melt in which the temperature dropped below the liquidus. This caused the first minerals to crystallise. Under conditions of more rapid

ascent, these minerals would have been resorbed or prevented from forming, due to a combination of adiabatic decompression and latent heat of crystallisation. However, because the rate of ascent was slow and because the thermal budget was constrained, these minerals were prevented from re-equilibrating with the melt. As a result, the composition of the melt began to evolve away from its parental composition.

Crystallisation in this manner would have lead to the development of an enhanced density contrast between the crystals and the melt. However, because of the high viscosity of the silicate melt, the crystals were prevented from settling. This situation would have been maintained in a state of metastability until the density contrast became too great. At this point, depending on the relative position of crystallisation with respect to the wall-rocks, either the crystals would sink through the melt, or the melt would rise up through the crystals. In either case, the crystals would be left behind in accordance with their proportions on the liquidus, immersed in interstitial liquid. In this way, the magma rose upwards in a series of pulses, creating as it did so a large composite batholith.

At various stages in its evolution, the melt was caused to vent to the surface, producing a variety of trachyandesitic and trachytic lava flows. However, as crystallisation progressed and as a large proportion of the heat was dissipated, the energy of the magma became insufficient to initiate subaerial eruption. As a result, the more evolved granitic magmas vented to the surface less frequently; thus explaining the scarcity of rhyolitic lava flows at the graben surface (Section 3.3.6). In this environment, the magmas were forced to differentiate in situ, closed system differentiation leading to the development of a variety of unusual mineral deposits (Chapter 4).

According to this model, some contamination of the magma must have occurred. However, because the composition of the country rocks was in many cases similar to that of the melt, and because the country rocks were partially insulated from the melt by crystallisation in the wall-rock zone, the effects of contamination were minimised. This is clearly demonstrated by the uniform nature of the mineral reaction series (Figure 8.1). The Na and K contents of the melt would appear to have been buffered by the high contents of these elements in the assimilated material (cf. Watson 1982).

In summary, the more evolved granitic rocks in the Hurdal area evolved from their intermediate precursors by fractionation of clinopyroxene, plagioclase and alkali feldspar. The favoured mechanism is by incremental crystallisation on ascent through the crust, in which full equilibrium between the minerals and the melt was not maintained, and the minerals were removed in accordance with their proportions on the liquidus.

8.2.4.3 Mechanisms of emplacement

Intrusive relationships in the Hurdal area indicate that the more evolved granitic magmas were emplaced by forceful mechanisms (Section 3.5.). The widespread occurrence, in the Nordgardshogda - Styggberget and Brennhaugen areas, of sharp, cross-cutting intrusive relationships with frequent signs of brecciation is believed to be indicative of forceful mechanisms of emplacement. In the Nordgardshogda area, arching and subsequent fracturing and dilation of the wall-rocks has been attributed to magmatic pressures in the apical zone of the intrusion.

The existence, however, of several areas of volcanic rock without any apparent basement indicates that the principal mechanism of intrusion had to be by piecemeal stoping. A combination of forceful and permitted intrusion is believed

to be consistent with the proposed model of magmatic evolution discussed in the previous section.

8.3 Mineralogical aspects of evolution

Evolution from monzodiorite to granite involves changes, not only in the composition of the melt, but also in the nature and composition of the mineral phases, and the proportions in which they occur. To a large extent, these changes are the response of the cooling magma to changes in the prevailing conditions of temperature, pressure and volatile activity on ascent through the crust. Thus, clinopyroxene and plagioclase are gradually replaced in the mineralogy by alkali feldspar and quartz (Figure 8.1).

Changes in the proportions of the mineral phases, their respective positions in the crystallisation sequence, and the fluid regime in which they are grown, also have significant effects upon the nature of the mineral aggregates that are formed (Section 3.5.1). Thus, during the early stages of evolution in the Hurdal area, quartz is restricted to late, interstitial positions and is grown in an environment under-saturated with respect to H_2O. Under these conditions, the growth rate of alkali feldspar is significantly greater than that of quartz, and hypidiomorphic granular intergrowths are formed (Swanson 1977). It is only in the final stages of evolution that quartz joins alkali feldspar on the liquidus. In this case, quartz appears early in the crystallisation sequence and is grown in the presence of a CO_2-bearing aqueous phase. Under these conditions, the growth rates of alkali feldspar and quartz are similar, resulting in impeded growth of alkali feldspar and the development of xenomorphic granular intergrowths.

Modifications to the fluid regime also have significant effects upon changes occurring within the granitic rocks after they have solidified (Section 3.5.1). These changes

concern, in particular, the degree of ordering of the feldspar structure. Thus, while the average composition of alkali feldspar remains fairly constant throughout evolution from syenite to granite, the compositions of albite and orthoclase domains become progressively more sodic and potassic respectively. These effects are partly the result of exsolution at lower temperatures on the alkali feldspar solvus, and partly due to increased mobility of magmatic fluids at sub-solidus temperatures. At the same time, the degree of coarsening of perthitic textures and the degree of irregularity of grain boundaries increase considerably.

Evolution from monzodiorite to alkali feldspar granite also involves progressive changes in the nature and compositions of the ferromagnesian minerals. These changes reflect modifications to the bulk chemistry of the system and to the fluid regime (Section 3.5.1). Thus, the compositions of amphiboles and biotites become progressively more siliceous and sodic during evolution. These effects are partly attributed to the increasing Si content of the melt, but also to the increased activity of F (Kogarko and Krigman 1973). Build-up of F in the biotite syenite and alkali feldspar granite is accompanied by increased partitioning of this element into the hydrous minerals. At the same time, the concentration of Mn also increases. This demonstrates the ability of the structural units in the melt to influence those that appear on cooling in the crystalline phases (Burnham 1979a).

8.4 Hydrothermal evolution

At specific stages in the evolution of felsic magmas in the Hurdal area, build up of dissolved volatiles such as H_2O, CO_2, F, and Cl may have lead to the saturation of the melt with respect to one or more of these components. Depending on the composition of the melt and the prevailing conditions of temperature and pressure, the volatile constituents would be

partitioned either into mineral phases incorporating these components, or into a separate vapour phase (Burnham 1979b). Thus, H_2O, F and Cl may have been partitioned into biotite and amphibole, F into fluorite, and CO_2 into carbonate minerals.

The scarcity of carbonate minerals in the plutonic rocks suggests that CO_2 was retained in the melt throughout evolution, until a stage was reached where the melt became saturated with respect to CO_2 and a separate CO_2-bearing aqueous phase was exsolved (Section 8.2.1). In comparison, F was partitioned into a variety of minerals including biotite, amphibole and fluorite. This explains the ability of the F determinations in the whole-rock analyses to give such a good indication of the behaviour of this element in the melt, and confirms that F was partitioned strongly in favour of the melt. In contrast, H_2O was partitioned both into amphiboles and biotites and into a separate aqueous phase. The behaviour of Cl is likely to have been similar to that of water. In general, a decline in the importance of ferromagnesian components in the system was accompanied by an increase in the importance of aqueous fluids in the evolution of these rocks.

Saturation of the melt with respect to volatiles occurred at successivly earlier stages in the crystallisation sequence of the melt during its evolution. Thus, during the earlier stages of evolution in the Hurdal area, exsolution of the vapour phase occurred after the crystallisation of quartz. The biotite syenite and quartz syenite therefore contain only melt quartz (Section 7.2.5). During the later stages of evolution, however, exsolution of the vapour phase occurred much earlier in the crystallisation sequence, accompanying the crystallisation of quartz. As a result, the alkali feldspar granite and miarolytic cavities in the contact zones of both the quartz syenite and the alkali feldspar granite contain mostly hydrothermal quartz, grown in the presence of

a discrete hydrothermal phase. This striking change in the conditions of crystallisation of quartz is partly the result of an increase in the volumetric importance of hydrothermal fluids in the system. More important, it is the result of CO_2 saturation of the system (Section 5.5.1, Holloway 1976). Saturation of the melt with respect to CO_2 has lead to the development of an aqueous CO_2-bearing phase at liquidus temperatures.

Evidence that exsolution of the vapour phase from the alkali feldspar granite occurred during the crystallisation of quartz is provided by the presence of boiling fluid inclusion assemblages within the quartz. Boiling of hydrothermal fluids has lead to the development of extremely saline fluids in many cases, and may have been accompanied by ore-deposition. The presence of boiling hydrothermal solutions within sample W24 from the Brennhaugen granite may have been responsible for the precipitation of molybdenite within this rock.

The ore-forming potential of hydrothermal fluids released from the melt during its evolution is indicated by the presence of opaque daughter minerals within many of the fluids, now preserved in the form of inclusions in quartz (Section 7.5). In particular, the presence of an opaque daughter mineral, tentatively identified as molybdenite, within fluid inclusions in miarolytic quartz from the contact zones of the quartz syenite in the Nordgardshogda area suggests that these fluids may have been responsible for molybdenite $\pm$ pyrite mineralisation in the area. The mineralising potential of these fluids is also indicated by their chemical compositions, which reveal significant amounts of Mn, Zn and S within the inclusions. In comparison, fluid inclusions from the alkali feldspar granite tend to be enriched in alkalies, Mn and Be. These fluids, therefore, could have been responsible for Mn mineralisation in the area.

Finally, the ratio of Na to K in the hydrothermal fluids remains fairly constant throughout their evolution, at approximately 1Ø to 1. The strong preference for Na as opposed to K in the fluids explains the widespread occurrence of bleaching within the granite. It also explains the presence of zones of silicification in which most of the Na has been leached out, and the absence of significant potassic alteration in the Hurdal area.

8.5 Mineralisation and alteration

At two specific stages in the evolution of felsic magmas in the Hurdal area, specialisation of the magma lead to the concentration and precipitation of ore-metals. Thus, during the evolution of the biotite syenite, closed system differentiation of the magma lead to the formation of a residual melt fraction enriched in Mo, Fe^{2+} and Zn (Section 4.3.1). Similarly, during the evolution of the alkali feldspar granite, late-stage magmatic and/or metasomatic processes lead to the concentration of Mn and Zn, and to a lesser extent Fe^{2+} and Pb (Sections 4.3.2 and 4.3.3). In both cases, the concentrations of Mn and Zn in the evolved magmas would appear to have been directly related to the concentration of F dissolved in the melt. This has been clearly demonstrated by the studies of major and trace element geochemistry (Chapters 5 and 6).

In a previous section (8.2.2), it has been suggested that enrichment in the melt of Mn and Zn may have been related to the formation of fluoride complexes incorporating these elements. In particular, release of Al from tetrahedral coordination, possibly during hydrolysis, is believed to have lead to the formation of complexes of the type ALF_6^{3-}, with a combination of monovalent and divalent cations in the charge-balancing role (e.g. $NaMnAlF_6$ and $NaZnAlF_6$). A preference for Na as opposed to K within these complexes is believed to have been responsible for the large increase in

the ratio of Na/Na+K observed within the biotite syenite and manganogranitoids (Figure 5.7b).

Mineralisation may have been related directly to the melt phase or to the development of a separate fluid phase. In the case of the manganogranitoids, direct precipitation of albite and rhodonite from a silicate melt would require that processes of silicate liquid immiscibility be responsible (Section 4.3.3.1). In comparison, precipitation of ore-minerals from a coexisting fluid phase could have occurred either from a SiO_2-poor, F-rich melt or vapour, or from a SiO_2-poor, F-poor, Cl-rich aqueous solution. Separation of F-saturated melts of granitic composition into coexisting silicate and fluoride melts has been demonstrated experimentally by Glyuk and Anfilogov (1973) and Anfilogov et al. (1973). The existence of aqueous, hydrothermal solutions of appropriate composition has, however been revealed by the fluid inclusion studies (Sections 7.4 and 7.5).

8.5.1 Origin of Mo - Fe - Zn mineral deposits

Molybdenite - pyrite - sphalerite mineralisation in the Hurdal area is generally located within the apical, endo-contact position of the biotite syenite, where it intrudes compositionally similar extrusive rocks. The most notable occurrence is in the Nordgardshogda - Styggberget area (Section 4.3.1); although similar deposits have also been observed in the Rustad and Svartjern areas.

Mineralisation is believed to have been the result of late-stage magmatic processes operating within the biotite syenite (Section 4.3.1.1). Migration of volatile elements and alumino-fluoride complexes incorporating Mo, Fe^{2+} and Zn towards the apical zones of the biotite syenite is believed to have lead to the formation of a residual melt fraction enriched in these components. Whether mineralisation was related directly to this residual melt fraction or to a

separate fluid phase is, however, uncertain. In theory, two possibilities should be considered: I. Mineralisation was related to the exsolution of a F-rich melt or vapour; and II. Mineralisation was related to the exsolution of a Cl-rich, aqueous solution.

I. Saturation of the melt with respect to F may have lead to the exsolution of a F-rich fluid phase. Partitioning of ore-metals and S into this fluid phase would have preceded ore-deposition. Evidence suggesting that fluids of this type existed in the Nordgardshogda - Styggberget area is provided by the common occurrence of thin, discontinuous veinlets of fluorite + quartz $\pm$ muscovite $\pm$ pyrite, both within the mineralised rocks and within the adjoining wall-rocks. In addition, the presence within the mineralised rocks of significant amounts of fluorite suggests that the ore-minerals were precipitated from a fluid phase saturated with respect to fluorine.

II. Saturation of the melt with respect to H_2O may have lead to the exsolution of a Cl-rich, aqueous solution. The presence of aqueous fluid inclusions containing significant amounts of Fe, Mn and Zn within miarolytic quartz from the contact zones of the quartz syenite in the Nordgardshogda - Styggberget area suggests that these fluids could have been responsible for mineralisation (Section 7.5). The fact, however, that the bulk of the mineralisation occurred prior to the intrusion of the quartz syenite indicates that this is unlikely to have been the case. These fluids could only have been responsible for the weak mineralisation associated with the quartz syenite in its contact zones.

In conclusion, it is suggested that the precipitation of ore-minerals in the Nordgardshogda - Styggberget area occurred from a F-rich melt or fluid phase of magmatic origin. Aqueous hydrothermal solutions are believed to have been of secondary importance. This is supported by the

limited lateral and vertical extent of hydrothermal alteration, and by the fact that silicification and simple recrystallisation are the predominant types of alteration in the wall-rock zone. In addition, the fact that pyrite is the only ore-mineral to occur in the wall-rock zone suggests that S was the only element to have been introduced in significant quantities from the biotite syenite.

8.5.2 Origin of the manganogranitoids

Manganese - Zn - (Fe) - (Pb) mineralisation in the Hurdal area is exclusively associated with albitised facies of the alkali feldspar granite in the contact zones of the Brennhaugen and Rustadkampen granites. Manganese silicate-bearing, albite-rich rocks with a distinct granitic texture are observed at the Hegga river locality (Section 4.3.3), at Steinmyrveien (Section 4.3.2), and at Steinbratebekken (Figure 4.1).

Manganese enrichment is believed to have been the product of late-stage, magmatic processes operating within the alkali feldspar granite (Section 4.3.3.1). As in the case of the biotite syenite, these processes are believed to have involved the formation of alumino-fluoride complexes, and the migration of these complexes towards the contact zones of the intrusion. It is not certain, however, whether mineralisation was related directly to the melt phase or to the generation of a separate fluid phase. In the case of the manganogranitoids, three possibilities should be considered: I. Mineralisation was related to the exsolution of an albite-rich silicate melt; II. Mineralisation was related to the exsolution of a SiO_2-poor, F-rich melt or vapour; and III. Mineralisation was related to the exsolution of a Cl-rich, CO_2-bearing, aqueous solution. An origin by contamination of granitic magma is not supported by the geological evidence (Section 4.3.3.1).

I. Under extreme conditions, an increase in the degree of ordering of oxygen species in the melt may have lead to the formation of two coexisting silicate liquids, one rich in non-bridging oxygens and metal cations, the other in silicon and bridging oxygens (Section 5.5.1). A preference for F and octahedrally coordinated Al to enter the melt fraction with the lower degree of polymerisation would have favoured strong partitioning of Mn, Zn and Na into the less siliceous melt. Under these conditions, precipitation of albite, rhodonite and sphalerite could have occurred directly from a low silica melt corresponding in composition to the manganogranitoids.

Phase relationships in synthetic systems, such as K_2O - Al_2O_3 - FeO - Fe_2O_3 - SiO_2 (Naslund 1977, Freestone 1978, Roedder 1978, 1983, Visser and Koster van Groos 1979 a, b and c, Biggar 1983, Freestone and Powell 1983) and Na_2O - Al_2O_3 - FeO - Fe_2O_3 - SiO_2 (Naslund 1977), indicate the existence of a significant field of liquid immiscibility within the range of composition of some natural magmas. Particularly under conditions of high oxygen fugacity, the compositional field in which two liquids occur is large enough to incorporate some Fe-rich basalts and peralkaline granites. The effect of increasing oxygen fugacity is to shift the equilibrium between bridging, free and non-bridging oxygens in favour of free and bridging oxygens. This has the effect of producing a volume of melt with an inherently higher degree of network ordering, and is accompanied by an expansion of the two liquid field to a wider range of compositions (Naslund 1977, Hess 1980).

In theory, addition of F to the systems described above might be expected to have a similar effect to that of increasing oxygen fugacity. This is because F reacts only with modifier cations in the melt and not with Si (Section 5.5.1). It thereby has the effect of increasing the concentration of bridging oxygens in the melt. Segregation of the melt into F-rich and F-poor melt fractions should, therefore, be

accompanied by an increase in the degree of network ordering and could, under extreme conditions, lead to liquid immiscibility in the system.

Under the volatile-free conditions of the experiments described above, both Na and K are partitioned into the more polymerised melt, providing local charge balance to tetrahedrally coordinated Al. Under the influence of F, however, some alkalies must also be partitioned into the less polymerised melt. Assuming alumino-fluoride complexes are formed, Mn, Zn and Na should all be partitioned into the less polymerised melt. The smaller ionic radius and more electronegative nature of Na would appear to favour strong partitioning of Na into the less siliceous melt.

The larger proportion of octahedral coordination sites in the less polymerised melt should favour the incorporation of divalent cations such as Fe^{2+}, Mg, Ca, Ba, Sr and Eu^{2+}, together with the trivalent REE and certain highly charged cations such as P and Ti (Watson 1976, Ryerson and Hess 1978). These elements should therefore be enriched in the less siliceous melt. Consideration of the distribution of trace elements in the manganogranitoids indicates that these elements are, in general, enriched when compared with the average composition of the alkali feldspar granite (Figure 6.7b). The only exception is phosphorous. This element should be strongly enriched in the manganogranitoids, but shows no change. There are two possible reasons for this. Either phosphate complexes were unstable, or the manganogranitoids were not formed as a result of silicate liquid immiscibility.

Enrichment of trace elements in the less polymerised melt must be accompanied by depletion of the same trace elements in the more polymerised melt. Depending on the relative volumes of the two melt fractions, it should therefore be possible to identify the more polymerised melt on the basis of its trace element distributions. At the Hegga river

locality, the dyke HA4D is depleted in all REE, together with all elements belonging to group IIIb and group I with the exception of Rb (Section 6.4.4). This dyke could, therefore, represent the complementary high SiO_2 melt to a low SiO_2 melt fraction corresponding in composition to the manganogranitoids.

II. Saturation of the melt with respect to F may have lead to the exsolution of a SiO_2-poor, F-rich fluid phase. Partitioning of Mn, Zn and Na into this fluid phase would have preceded the precipitation of albite, rhodonite and sphalerite by metasomatic exchange reactions. In many respects, this possibility is similar to the one described above, with the exception that Si is not partitioned into the fluid phase.

III. Saturation of the melt with respect to H_2O may have lead to the exsolution of a saline, aqueous solution. The fact that the melt would also have been saturated with respect to CO_2 suggests that carbon dioxide would also have entered the fluid phase. Partitioning of Na, Mn and Zn into this hydrothermal fluid would have preceded the precipitation of albite, rhodonite and sphalerite by metasomatic exchange reactions (as above). The presence of aqueous, CO_2-bearing fluid inclusions containing significant amounts of Na, Mn and Be within granitic quartz from the alkali feldspar granite suggests that these fluids could have been responsible for mineralisation (Section 7.5). This is supported by the presence within the granite in the vicinity of the manganogranitoids of saline fluid inclusion assemblages believed to be indicative of boiling (sample HB5, Section 7.3).

8.5.2.1 Discussion

Metasomatism of granitic material by a Mn and Na enriched residual fluid of magmatic origin is believed to be

consistent with the textural evidence (Section 4.3.3.1). The tendency for rhodonite to occur in the form of fine-grained aggregates in the interstices between albite grains is believed to be indicative of an origin by replacement, suggesting that rhodonite may have replaced quartz in the granitic texture. In addition, the predominance of albite over orthoclase suggests that alkali exchange reactions between a Na enriched fluid and alkali feldspar may have lead to the replacement of orthoclase by albite. Similar processes have been conjectured for the replacement of quartz by pyroxene and orthoclase by albite characteristic of fenite metasomatism (Rubie 1982, Rubie and Gunter 1983).

Additional evidence supporting an origin by metasomatic replacement is provided by the existence of zones of silicified granite in the vicinity of the manganogranitoids (Section 4.3.3). Leaching of Na and reddening of these rocks is believed to have been the result of the passage of low temperature, Fe-rich fluids through the granite (Section 7.2.6). The observed dependence of these zones upon the orientation of joint surfaces confirms that silicification occurred under sub-solidus conditions.

In order to assess the changes in composition which occur during metasomatism, it is necessary to take into account changes in volume of the system (Gresens 1967). Thus, during reactions of the type: Rock A ⇌ Rock B, the gains or losses of an element, ΔX_n, may be related to the concentration of that element in the unaltered starting material by an equation of the form (Gresens 1967):

$$\Delta X = 100\ (f_V\ (\rho_B/\rho_A)\ x_{n,B} - x_{n,A})$$

where $x_{n,A}$ and $x_{n,B}$ are the mass fractions of the element in rocks A and B; ρ_A and ρ_B are the densities of rock A and rock B; and f_V is the ratio of their volumes. The volume factor, f_V, is unknown.

The results of mass-balance calculations for the conversion

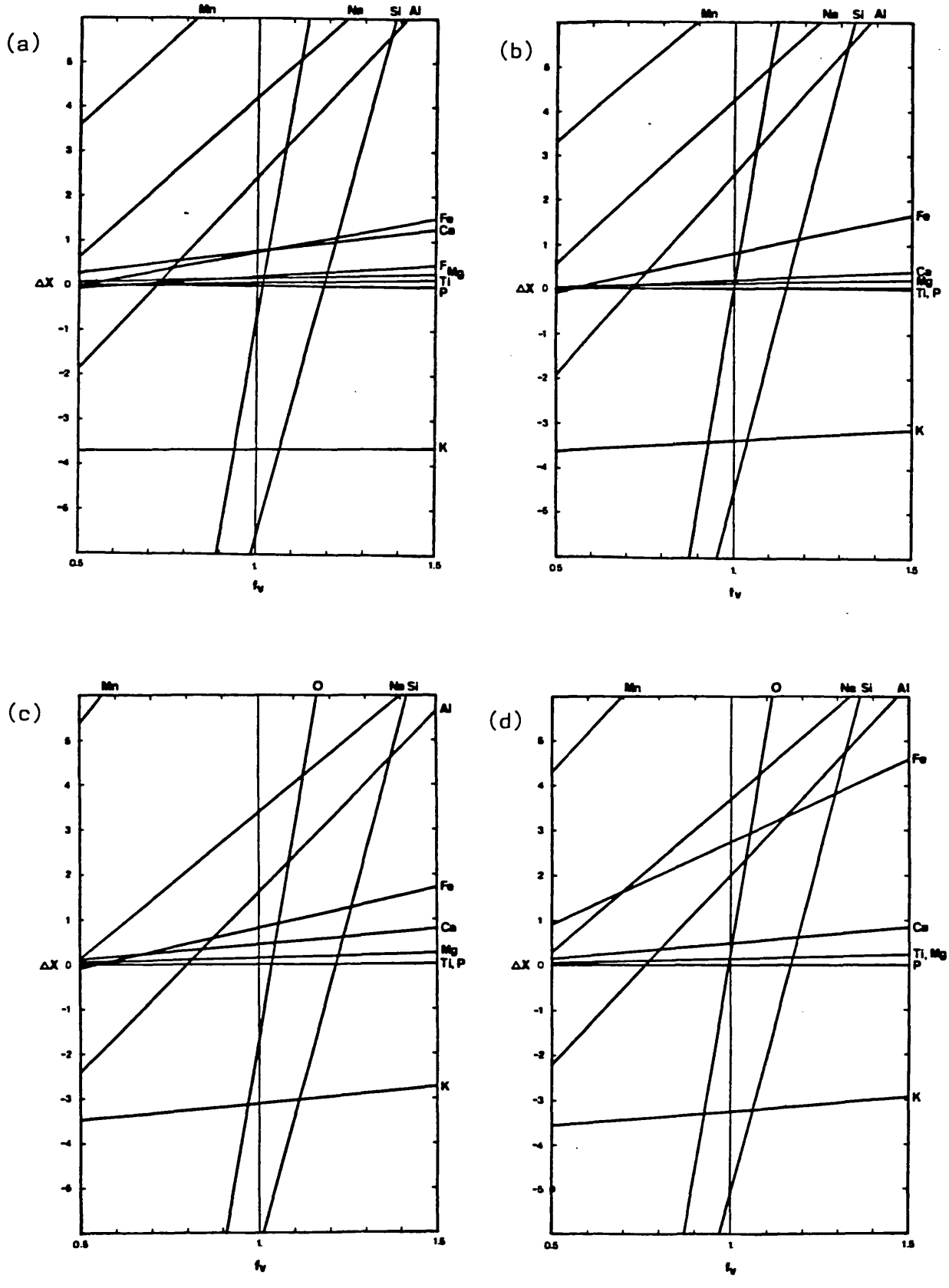

FIGURE 8.2. Plots of f_v versus .X (Wt %) for the conversion of alkali feldspar granite into manganogranitoid: (a) A.G.(B) - W362; (b) A.G.(R) - HC3; (c) A.G.(R) - HC7; and (d) A.G.(R) - HC1Ø.

of alkali feldspar granite into manganogranitoid are illustrated in Figure 8.2 a to d, for different values of f_V. The main conclusion that may be drawn from these diagrams is that Al was mobile. In order for Al to have been immobile, it would have required a 20 to 30 % reduction of volume during metasomatism. This is believed to be inconsistent with the textural evidence which suggests a volume for volume substitution (see, for comparison, Rubie 1982). It may be significant that, with a volume factor close to 1, the concentration of oxygen in the system remains unchanged.

The conclusion that Al was an important constituent of the fluids suggests that fluorine-rich liquids may have been responsible, since Al forms bonds with F more readily than with hydroxyl (Section 5.5.1, Mysen et al. 1980b, Manning et al. 1980, Manning 1981). The absence of Al as an important constituent of the fluid inclusions in granitic quartz provides indirect support to this hypothesis (Section 7.4). Whether Si was an important constituent of these fluids remains, however, uncertain.

In conclusion, it is suggested that the manganogranitoids were formed as a result of the exsolution of a fluorine-rich melt or fluid phase of magmatic origin. Partitioning of Na, Mn, Zn and Al into this fluid phase preceded the precipitation of albite, rhodonite and sphalerite by metasomatic exchange reactions. The lower degree of polymerisation of this low-SiO_2 fluid also favoured the incorporation of divalent cations such as Mg, Fe^{2+} and Ca, together with the trivalent REE and certain highly charged cations such as Zr and Hf, but not P.

8.6 Synopsis

The intermediate to granitic rocks in the Hurdal area are compatible with an origin by fractionation of intermediate magmas, essentially by separation of clinopyroxene,

plagioclase and alkali feldspar. The favoured mechanism is by incremental crystallisation on rising bouyantly through the crust, in which full equilibrium between the minerals and the melt was not maintained and the crystals were removed in accordance with their proportions on the liquidus. In this fashion, the magma rose upwards in a series of pulses creating as it did so a large composite batholith.

At various stages in its evolution, the melt was caused to vent to the surface, producing a variety of trachyandesitic and trachytic lava flows. However, as crystallisation progressed and as a large proportion of the thermal energy was dissipated, the energy of the magma became insufficient to initiate subaerial eruption. Under these conditions, the magma was forced to differentiate in situ, closed system differentiation leading to a variety of unusual mineral deposits.

8.7 Proposals for further work

Research on the Hurdal area is far from complete. The following are suggestions for further work:

(I) Determination of the distributions of trace elements in the principal mineral phases, preferably on mineral separates and by the same techniques as were used for the whole-rock analyses.

(II) Strontium and Nd isotope studies of the principal rock-types to determine the mutual age relationships of the intrusive rocks, and to assess the effects of contamination.

(III) More detailed studies of the fluid inclusions; and

(IV) Detailed studies of the mineral parageneses in the Nordgardshogda - Styggberget area.

REFERENCES

ALDERTON D.H.M., THOMPSON M., RANKIN A.H. and CHRYSSOULIS S. (1982): Developments of the ICP - linked decrepitation technique for the analysis of fluid inclusions in quartz. Chemical Geology, 37, 203-213.

ANFILOGOV V.N., GLYUK D.S. and TRUFANOVA L.G. (1973): Phase relations in interaction between granite and sodium fluoride at water vapor pressure of 1000 kg/cm^2. Geochemistry International, 10, 24-29.

BAILEY D.K. (1974): Experimental petrology relating to oversaturated peralkaline volcanics: A review. Bulletin Volcanologique, 38, 637-652.

BAILEY D.K. and SCHAIRER J.F. (1964): Feldspar-liquid equilibria in peralkaline liquids - The orthoclase effect. American Journal of Science, 262, 1198-1206.

BAILEY J.C. (1977): Fluorine in granitic rocks and melts: A review. Chemical Geology, 19, 1-42.

BAKER B.H. and WOHLENBERG H. (1971): Structure and evolution of the Kenya rift valley. Nature, 229, 538-542.

BAKER B.H., GOLES G.G., LEEMAN W.P. and LIDSTROM M.M. (1977): Geochemistry and petrogenesis of a basalt - benmoreite - trachyte suite from the southern part of the Gregory Rift, Kenya. Contributions to Mineralogy and Petrology, 64, 303-332.

BAKER B.H., MOHR P.A. and WILLIAMS L.A.J. (1972): Geology of the Eastern Rift System of Africa. Geological Society of America, special paper 136.

BALASHOV Y.A. and KRIGMAN L.D. (1975): The effects of

alkalinity and volatiles on rare-earth separation in magmatic systems. Geokhimiya, 12, 1885-1890.

BANKS R.J. and BEAMISH D. (1979): Melting in the crust and upper mantle beneath the Kenya Rift: Evidence from geomagnetic deep sounding experiments. Quarterly Journal of the Geological Society of London, 136, 225-233.

BARTH T.F.W. (1944): Studies on the igneous rock complex of the Oslo Region. II. Systematic petrography of the plutonic rocks. Skr. Norske Vidensk.-Akad i Oslo, I. Mat.-naturv. Kl. 1944, no. 9.

BARTH T.F.W. (1954): Studies on the igneous rock complex of the Oslo Region. XIV. Provenance of the Oslo magmas. Skr. Norske Vidensk.-Akad i Oslo, I. Mat.-naturv. Kl. 1954, no. 4, 20 pp.

BARTH T.F.W. and BRUUN B. (1945): Studies on the igneous rock complex of the Oslo Region. IV. Fluorine in the Oslo petrographic province. Skr. Norske Vidensk.-Akad i Oslo, I. Mat.-naturv. Kl. 1945, no. 8, 6-12.

BECKINSALE R.D., PANKHURST R.J., SKELHORN R.R. and WALSH J.N. (1978): Geochemistry and petrogenesis of the early Tertiary lava pile of the isle of Mull, Scotland. Contributions to Mineralogy and Petrology, 66, 415-427.

BIGGAR G.M. (1983): A re-assesssment of phase equilibria involving liquids in the system K_2O - Al_2O_3 - FeO - SiO_2. Contributions to Mineralogy and Petrology, 82, 274-283.

BLACK R. and GIROD M. (1970): Late palaeozoic to recent igneous activity in West Africa and its relationship to basement structure. In CLIFFORD T.N. and GASS I.G. (Eds.): African magmatism and tectonics. Edinburgh, Oliver and Boyd, 185-206.

BODKIN J.B. (1977): Determination of fluorine in silicates by use of an ion-selective electrode following fusion with lithium metaborate. The Analyst, 102, 409-413.

BOTTINGA Y. and WEILL D.F. (1970): Densities of liquid silicate systems calculated from the partial molar volumes of oxide components. American Journal of Science, 269, 169-182.

BOUGAULT H., JORON J.L. and TREUIL M. (1980): The primordial chondritic nature and large-scale heterogeneities in the mantle: Evidence from high and low partition coefficient elements in oceanic basalts. Philosophical Transactions of the Royal Society of London, A297, 203-213.

BOWDEN P. (1966): Zirconium in younger granites of northern Nigeria. Geochimica et Cosmochimica Acta, 30, 985-993.

BOWDEN P. (1982): Magmatic evolution and mineralisation in the Nigerian Younger Granite Province. In EVANS A.M. (Ed.): Metallization associated with acid magmatism. John Wiley and sons Ltd., 51-61.

BOWDEN P. and JONES J.A. (1974): Mineralization in the younger granite province of northern Nigeria. In STEMBROK M. (Ed.): Metallization associated with acid magmatism, 3, 179-190. Ustredni ustav geologicky, Praha.

BOWDEN P. and TURNER D.C. (1974): Peralkaline and associated ring complexes in the Nigeria - Niger province, West Africa. In SORENSEN H. (Ed.): The alkaline rocks. Wiley and sons Ltd., 330-351.

BOWDEN P. and WHITLEY J.E. (1974): Rare earth patterns in peralkaline and associated granites. Lithos, 7, 15-21.

BOWDEN P., BENNETT J.N., WHITLEY J.E. and MOYES A.B. (1977):

Rare earths in Nigerian mesozoic granites and related rocks. In AHRENS L.H. (Ed.): Origin and distribution of the elements. Proceedings of the second symposium; Paris 1970, 479-491.

BOWEN N.L. (1945): Phase equilibria bearing on origin and differentiation of alkaline rocks. American Journal of Science, Daly volume 243-A, 75-89.

BROCH O.A. (1964): Age determination of Norwegian minerals up to March 1964. Norges geologiske undersokelse, 228, 84-113.

BROWN G.C. and HENNESSY J. (1978): The initiation and thermal diversity of granite magmatism. Philosophical Transactions of the Royal Society of London, A288, 631-643.

BROWN G.C., THORPE R.S. and WEBB P.C. (1984): The geochemical characteristics of granitoids in contrasting arcs and comments on magma sources. Quarterly Journal of the Geological Society of London, 141.

BROGGER W.C. (1933): Essexitrekkens erupsjoner. Norges geologiske undersokelse, 138, 103pp.

BULTITUDE R.J. and GREEN D.H. (1968): Experimental study at high pressures on the origin of olivine nephelinite and olivine melilite nephelinite magmas. Earth and Planetary Science Letters, 3, 325-337.

BULTITUDE R.J. and GREEN D.H. (1971): Experimental study of crystal liquid relationships at high pressures in olivine nephelinite and basanite compositions. Journal of Petrology, 12, 121-147.

BURKE K. and DEWEY J.F. (1973): Plume-generated triple junctions: Key indicators in applying plate tectonics to old rocks. Journal of Geology, 81, 406-433.

BURNHAM W.C. (1979a): The importance of volatile constituents. In YODER H.S. (Ed.): The evolution of the igneous rocks. Fiftieth anniversary perspectives. Princeton University Press, Princeton, New Jersey, 439-482.

BURNHAM W.C. (1979b): Magmas and hydrothermal fluids. In BARNES H.L. (Ed.): Geochemistry of hydrothermal ore deposits. Second edition. John Wiley and sons LTd., 71-133.

CARMICHAEL I.S.E. and MACKENZIE W.S. (1963): Feldspar - liquid equilibria in pantellerites: An experimental study. American Journal of Science, 261, 382-396.

CARMICHAEL I.S.E., TURNER F.J. and VERHOOGEN J. (1974): Igneous petrology. McGraw-HIll Book Company, 739pp.

CHAPPELL B.W. and WHITE A.J.R. (1974): Two contrasting granite types. Pacific Geology, 8, 173-174.

CHAUVEL C. and JAHN B.M. (1984): Nd-Sr isotope and REE geochemistry of alkali basalts from the Massif Central, France. Geochimica et Cosmochimic Acta, 48, 93-11Ø.

CHRYSSOULIS S.L. (1983a): Development of fluid inclusion techniques and their application to mineral exploration, with reference to selected Mexican deposits. Unpublished Ph.D. thesis, University of London.

CHRYSSOULIS S.L. (1983b): Study of the effects of feldspar and mica contamination upon the analyses of fluid inclusions by the Decrepitation - ICP method. Chemical Geology, 4Ø, 323-335.

CHRYSSOULIS S.L. and WILKINSON N. (1983): High silver content of fluid inclusions in quartz from Guadalcazar Granite, San Luis Potosi, Mexico: A contribution to ore-genesis theory.

Economic Geology, 78, 302-318.

CLARK K.F. (1972): Stockwork molybdenum deposits in the Western Cordillera of North America. Economic Geology, 67, 731-758.

CLAQUE D.A. and FREY F.A. (1982): Petrology and trace element geochemistry of the Honolulu volcanics, Oahu: Implications for the oceanic mantle below Hawaii. Journal of Petrology, 23, 447-504.

COLLINS P.L.F. (1979): Gas hydrates in CO_2-bearing fluid inclusions and the use of freezing data for the estimation of salinity. Economic Geology, 74, 1435-1444.

COLLINS W.J., BEAMS S.D., WHITE A.J.R. and CHAPPELL B.W. (1982): Nature and origin of A-type granites with particular reference to southeastern Australia. Contributions to Mineralogy and Petrology, 80, 189-200.

COX K.G., BELL J.D. and PANKHURST R.J. (1979): Trace elements in igneous processes. The interpretation of igneous rocks. George Allen and Unwin, London/Boston/Sydney.

CZAMANSKE G.K. (1965): Petrologic aspects of the Finnmarka igneous complex, Oslo area, Norway. Journal of Geology, 73, 293-322.

CZAMANSKE G.K. and MIHALIK P. (1972): Oxidation during magmatic differentiation, Finnmarka complex, Oslo, Norway. Part I: The opaque oxides. Journal of Petrology, 13, 493-509.

CZAMANSKE G.K. and WONES D.R. (1973): Oxidation during magmatic differentiation, Finnmarka complex, Oslo, Norway. Part II: The mafic silicates. Journal of Petrology, 14, 349-380.

DEER W.A., HOWIE R.A. and ZUSSMAN J. (1977): An introduction to the rock forming minerals. Tenth impression. Longman Group Limited, London, 528pp.

DIETRICH R.V. and HEIER K.S. (1967): Differentiation of Qtz - bearing syenite (Nordmarkite) and riebeckite - arfvedsonite granite (Ekerite) of the Oslo series. Geochimica et Cosmochimica Acta, 31, 275-280.

DIETRICH R.V., HEIER K.S. and TAYLOR S.R. (1965): Studies on the igneous rock complex of the Oslo Region. XX. Petrology and geochemistry of ekerite. Skr. Norske Vidensk.-Akad. i Oslo, I. Mat.-naturv. Kl., NY Serie 19, 1-31.

DONS J.A. (1977): Diabase from Styg, 219 m.y. Nytt fra Oslofeltgruppen 4, 1972, 29-31 (printed in 1977).

DONS J.A. (1978): Terminolgy and history of investigations. In DONS J.A. and LARSEN B.T. (Eds.): The Oslo palaeorift: A review and guide to excursions. Norges geologiske undersokelse, 337, 9-16.

DONS J.A. and LARSEN B.T. (1978): The Oslo palaeorift: A review and guide to excursions. Norges geologiske undersokelse, 337, 199pp.

DRAKE M.J. and WEILL D.F. (1975): Partition of SR, Ba, Ca, Y, Eu^{2+}, Eu^{3+}, and other REE between plagioclase feldspar and magmatic liquid: An experimental study. Geochimica et Cosmochimica Acta, 32, 1057-1086.

FAIRHEAD J.D. (1976): The structure of the lithosphere beneath the Eastern Rift, East Africa, deduced from gravity studies. Tectonophysics, 30, 269-298.

FALVEY D.A. (1974): Development of continental margins in plate tectonic theory. A.P.E.A. Journal 1974, 14.

FEIGENSON M.D., HOFFMAN A.W. and SPERA F.J. (1983): Case studies on the origin of basalt. II. Transition from tholeiitic to alkalic volcanism on Kohala volcano, Hawaii. Contributions to Mineralogy and Petrology, 84, 390-405.

FERRARA G. and TREUIL M. (1974): Petrological implications of trace element and Sr isotope distributions in basalt - pantellerite series. Bulletin Volcanologique, 38, 548-574.

FINSTAD K.G. (1972): En undersokelse av utvalgte edelmetaller og sjeldne jordatselementer i noen norske, hovesakelig basiske og ultrabasiske begarter. Unpublished thesis, Univerisity of Oslo, 113pp.

FOURCADE S. and ALLEGRE C.J. (1981): Trace elements in granite genesis: A case study. The calc-alkaline plutonic association from the Queriqut complex (Pyrennees, France). Contributions to Mineralogy and Petrology, 76, 177-195.

FREESTONE I.C. (1978): Liquid immiscibility in alkali-rich magmas. Chemical Geology, 23, 115-123.

FREESTONE I.C. and POWELL R. (1983): The low temperature field of liquid immiscibility in the system K_2O - Al_2O_3 - FeO - SiO_2 with special reference to the join fayalite - leucite - silica. Contributions to Mineralogy and Petrology, 82, 291-299.

GAUT A. (1981): Field relations and petrography of the Biotite Granites of the Oslo Region. Norges geologiske undersokelse, 367, 39-64.

GEYTI A. and SCHONWANDT H.K. (1979): Bordvika - A possible porphyry molybdenum occurrence within the Oslo Rift, Norway. Economic Geology, 74, 1211-1220.

GIRDLER R.W. (1977): Comparison of the East African Rift System and the Permian Oslo Rift. In RAMBERG I.B. and NEUMANN E.-R. (Eds.): Tectonics and geophysics of continental rifts. Proceedings of the NATO Advanced Study Institute. D. Reidel Publishing Company, Dordrecht, Holland ; Boston, USA, 329-324.

GLYUK D.S. and ANFILOGOV V.N. (1973): Phase equilibria in the system Granite - H_2O - HF at a pressure of 1000 kg/cm^2. Geochemistry International, 10, 321-325.

GOLES G.G. (1977): Instrumental methods of neutron activation analysis. In ZUSSMAN J. (Ed.): Physical methods in determinative mineralogy. Second edition. Academic Press, London; New York; San Francisco.

GREEN D.H. (1973a): Conditions of melting of basanite magma from garnet peridotite. Earth and Planetary Science Letters, 17, 456-465.

GREEN D.H. (1973b): Experimental melting studies on model upper mantle compositions at high pressure under both water-saturated and water under-saturated conditions. Earth and Planetary Science Letters, 19, 37-53.

GRESENS R.L. (1967): Composition - volume relationships of metasomatism. Chemical Geology, 2, 47-65.

GROMET L.P. and SILVER L.T. (1983): Rare earth element distributions among minerals in a granodiorite and their petrogenetic implications. Geochimica et Cosmochimica Acta, 47, 925-939.

HAMILTON D.L. and MACKENZIE W.S. (1965): Phase - equilibrium studies in the system $NaAlSiO_4$ (nepheline) - $KAlSiO_4$ (kalsilite) - SiO_2 - H_2O. Mineralogical Magazine, 34, 214-231.

HANSON G.N. (1978): The application of trace elements to the petrogenesis of igneous rocks of granitic composition. Earth and Planetary Science Letters, 38, 26-43.

HATCH F.H., WELLS A.K. and WELLS M.K. (1975): Petrology of the igneous rocks. Thirteenth edition, third impression. Thomas Murby and Company, London, 551pp.

HAWTHORNE F.C. (1981): Crystal chemistry of amphiboles. In VERBLEN D.R. (Ed.): Amphiboles and other hydrous pyriboles - mineralogy. Mineralogical Society of America, Reviews in Mineralogy, 9A, 1-1Ø2.

HEIER K.S. and COMPSTON W. (1969): Rb - Sr isotopic studies of the plutonic rocks of the Oslo Region. Lithos, 2, 133-145.

HELZ R.T. (1976): Phase relations of basalts in their melting ranges at P_{H2O} = 5 kbar. Part II. Melt compositions. Journal of Petrology, 17, 139-193.

HENDERSON P. (198Ø): Rare earth element partition between sphene, apatite and other coexisting minerals of the Kangerolugssuag intrusion, E. Greenland. Contributions to Mineralogy and Petrology, 42, 81-85.

HENNINGSMOEN G. (1978): Sedimentary rocks associated with the lava series. In DONS J.A. and LARSEN B.T. (Eds.): The Oslo palaeorift: A review and guide to excursions. Norges geologiske undersokelse, 337, 17-24.

HESS P.C. (198Ø): Polymerization model for silicate melts. In HARGRAVES R.B. (Ed.): Physics of magmatic processes. Princeton University Press, Princeton, New Jersey, 3-48.

HESS P.C. and WOOD M.I. (1982): Aluminium coordination in metaluminous and peralkaline silicate melts. Contributions to

Mineralogy and Petrology, 81, 103-112.

HILDRETH W. (1981): Gradients in silicic magma chambers: Implications for lithospheric magmatism. Journal of Geophysical Research, 86, 10153-10192.

HOLLAND D.H. (1972): Granites, solutions, and base metal deposits. Economic Geology, 67, 281-301.

HOLLISTER L.S. (1981): Information intrinsically available from fluid inclusions. Chapter 1 in: Short course in fluid inclusions, applications to petrology. Mineralogical Association of Canada, 1-13.

HOLLOWAY J.R. (1976): Fluids in the evolution of granitic magmas: Consequences of finite CO_2 solubility. Bulletin of the Geological Society of America, 87, 1513-1518.

HUSEBYE E.S. and RAMBERG I.B. (1978): Geophysical invetigations. In DONS J.A. and LARSEN B.T. (Eds.): The Oslo palaeorift: A review and guide to excursions. Norges geologiske undersokelse, 337, 41-54.

IHLEN P.M. (1977): Ore deposits in the north-eastern part of the Oslo Region and in the adjacent Precambrian areas. In NEUMANN E.-R. and RAMBERG I.B. (Eds.): Petrology and geochemistry of continental rifts. Proceedings of the NATO Advanced Study Institute. D. Reidel Publishing Company; Dordrecht, Holland; Boston, USA, 277-288.

IHLEN P.M. (1985): Skarn deposits within the lower palaeozoic rocks of the Oslo Rift, Norway. I: Geology, paragenesis and regional zoning of iron ore deposits in the Skreia area. In preparation.

IHLEN P.M. and RASMUSSEN E. (1981): Geologisk kartlegging av intrusive bergarter i Hurdals omradet, sommeren 1981.

Internal report, Norsk Hydro A/S.

IHLEN P.M. and VOKES F.M. (1978a): Metallogeny. In DONS J.A. and LARSEN B.T. (Eds.): The Oslo palaeorift: A review and guide to excursions. Norges geologiske undersokelse, 337, 75-90.

IHLEN P.M. and VOKES F.M. (1978b): Metallogeny associated with the Oslo rifting. In DONS J.A. and LARSEN B.T. (Eds.): The Oslo palaeorift: A review and guide to excursions. Norges geologiske undersokelse, 337, 125-142.

IHLEN P.M., TRONNES R. and VOKES F.M. (1982): Mineralisation, wall rock alteration and zonation of ore deposits associated with the Drammen Granite in the Oslo Region, Norway. In EVANS A.M. (Ed.): Metallization associated with acid magmatism. John Wiley and sons Ltd., 111-136.

ILLIES J.H. (197Ø): Graben tectonics and relation to crust - mantle interaction. In ILLIES J.H. and MUELLER St. (Eds.): Graben problems. Schweizerbart, Stuttgart, 4-27.

IRVING A.J. (1978): A review of experimental studies of crystal/liquid trace element partitioning. Geochimica et Cosmochimica Acta, 42, 743-77Ø.

KAY R.W. and GAST P.W. (1973): The rare earth content and origin of alkali-rich basalts. Journal of Geology, 81, 653-682.

KHITAROV N.I., MALININ S.P., LEBELEY Ye. B. and Shibayeva N.P. (1982): The distribution of Sn, Cu, Pb and Mo between a fluid phase and a silicate melt of granitic composition at high temperatures and pressures. Geochemistry International, 18, 123-136.

KING B.C. (197Ø): Vulcanicity and rift tectonics in East

Africa. In CLIFFORD T.N. and GASS I.G. (Eds.): African magmatism and tectonics. Edinburgh, Oliver and Boyd, 263-283.

KING B.C. and CHAPMAN G.R. (1972): Volcanism of the Kenya Rift Valley. Philosophical Transactions of the Royal Society of London, A271, 185-208.

KINSMAN D.J.J. (1976): Rift valley basins and sedimentary history of trailing continental margins. In FISCHER A.G. and JUDSON S. (Eds.): Petroleum and global tectonics. Princeton University Press, Princeton, New Jersey.

KOGARKO L.N. and KRIGMAN L.D. (1973): Structural position of fluorine in silicate melts (according to melting curves). Geochemistry International, 10, 34-40.

KOVALENKO V.I. (1973): Distribution of fluorine in a topaz-bearing quartz keratophyre dike (ongonite) and solubility of fluorine in granitic melts. Geochemistry International, 10, 41-49.

LAGACHE M. and WEISBROD A. (1977): The system: Two alkali feldspars - KCl - NaCl - H_2O at moderate to high temperatures and pressures. Contributions to Mineralogy and Petrology, 62, 77-101.

LARSEN B.T. (1975): Petrological, geochemical and volcanological features of the volcanic rocks in the Permian Oslo palaeorift zone. A preliminary note (abstract). In Rifting problems, Symposium on rift zones of the Earth. Irkutsk.

LARSEN B.T. (1978): Krokskogen lava area. In DONS J.A. and LARSEN B.T. (Eds.): The Oslo palaeorift: a review and guide to excursions. Norges geologiske undersokelse, 337, 143-162.

LAUER H.V., Jr. (1977): Effect of glass composition on major

element redox equilibria: Fe^{2+}/Fe^{3+}. Phys. Chem. Glasses, 18, 49-52.

LEAKE B.E. (1978): Nomenclature of amphiboles. Canadian Mineralogist, 16, 501-520.

LONG J.V.P. (1977): Electron probe microanalysis. In ZUSSMAN J. (Ed.): Physical methods of determinative mineralogy. Second edition. Academic Press: London, New York, San Francisco.

LOWELL J.D. and GUILBERT J.M. (1970): Lateral and vertical alteration - mineralisation zoning in porphyry ore deposits. Economic Geology, 65, 373-408.

MACDONALD R. (1974): Nomenclature and petrochemistry of the peralkaline oversaturated extrusive rocks. Bulletin Volcanologique, 38, 498-516.

MACDONALD R. (1975): Petrochemistry of the early Carboniferous (Dinantian) lavas of Scotland. Scottish Journal of Geology, 11, 269-314.

MACDONALD R. (1980): Trace element evidence for mantle heterogeneity beneath the Scottish Midland Valley in the Carboniferous and Permian. Philosophical Transactions of the Royal Society of London, A297, 245-257.

MAHOOD G. and HILDRETH W. (1983): Large partition coefficients for trace elements in high-silica rhyolites. Geochimica et Cosmochimica Acta, 47, 11-30.

MANNING D.A.C. (1981): The effect of fluorine on liquidus phase relationships in the system Qz - Ab - Or with excess water at 1 kbar. Contributions to Mineralogy and Petrology, 76, 206-215.

MANNING D.A.C. and HENDERSON P. (1984): The behaviour of tungsten in granitic melt - vapour systems. Contributions to Mineralogy and Petrology, 86, 286-293.

MANNING D.A.C., HAMILTON D.L., HENDERSON C.M.B. and DEMPSEY M.J. (1980): The probable occurrence of interstitial Al in hydrous, F-bearing and F-free aluminosilicate melts. Contributions to Mineralogy and Petrology, 75, 257-262.

MARSH B.D. (1982): On the mechanics of igneous diapirism, stoping and zone melting. American Journal of Science, 282, 808-855.

MARSH N.G., SAUNDERS A.D., TARNEY J. and DICK H.J.B. (1980): Geochemistry of basalts from the Shikokv and Dailo Basins, Deep Sea Drilling Project Leg 58. In DE KRIES KLEIN G. and KOBAYASHI K. (Eds.): Initial Report Deep Sea Drilling project,58, 805-842. US Government Printing Office, Washington.

MARTINSEN M., OLESEN O. and TRONNES R. (1979): Feltarbeidsrapport fra geologisk kartlegging i Rustad - Oyangen omradet (Hurdal og Gran Kommune). Internal report. Norsk Hydro A/S.

McCARTHY T.S. and HASTY R.A. (1976): Trace element distribution patterns and their relationship to the crystallisation of granitic melts. Geochimica et Cosmochimica Acta, 40, 1351-1358.

McCONNEL R.B. (1972): Geological development of the Rift System of East Africa. Bulletin of the Geological Society of America, 83, 2549-2572.

MEHNERT K.R. (1968): Migmatites and the origin of granitic rocks. Elsevier, Amsterdam, 393pp.

MOLLER P. and MUECKE G.K. (1984): Significance of Eu anomalies in silicate melts and crystal melt equilibria: A re-evaluation. Contributions to Mineralogy and Petrology, 87, 242-250.

MUTSCHLER F.E., WRIGHT E.G., LUDINGTON S. and ABBOTT J.T. (1981): Granite molybdenite systems. Economic Geology, 76, 874-897.

MYSEN B.O. (1976): The role of volatiles in silicate melts: Solubility of carbon dioxide and water in feldspar, pyroxene and feldspathoid melts to 30 kbar and 1626°C. American Journal of Science, 276, 969-996.

MYSEN B.O. and VIRGO D. (1980a): Solubility mechanisms of carbon dioxide in silicate melts: A raman spectroscopic study. American Mineralogist, 65, 885-899.

MYSEN B.O. and VIRGO D. (1980b): Trace element partitioning and melt structure: An experimental study at 1 atmosphere pressure. Geochimica et Cosmochimica Acta, 44, 1917-1930.

MYSEN B.O., SEFERT F. and VIRGO D. (1980a): Structure and redox equilibria of iron-bearing silicate melts. American Mineralogist, 65, 867-884.

MYSEN B.O., VIRGO D., HARRISON W.J. and SCARFE C.M. (1980b): Solubility mechanisms of H_2O in silicate melts at high pressures and temperatures: A raman spectroscopic study. American Mineralogist, 65, 900-914.

MYSEN B.O., VIRGO D. and SCARFE C.M. (1980c): Relations between the anionic structure and viscosity of silicate melts: A raman spectroscopic study. American Mineralogist, 65, 690-710.

MYSEN B.O., VIRGO D. and KUSHIRO I. (1981): The structural

role of aluminium in silicate melts - A Raman spectroscopic study at 1 atmosphere. American Mineralogist, 66, 678-701.

NAKAMURA N. (1974): Determination of REE, Ba, Fe, Mg, Na and K in carbonaceous and ordinary chondrites. Geochimica et Cosmochimica Acta, 38, 757-775.

NASLUND H.R. (1977): Liquid immiscibility in the system $KAlSi_3O_8$ - $NaAlSi_3O_8$ - FeO - Fe_2O_3 - SiO_2 and its application to natural magmas. Carnegie Institute Washington Yearbook, 75, 592-597.

NEUMANN E.-R. (1976): Compositional relations among pyroxenes, amphiboles and other mafic phases in the Oslo Region plutonic rocks, Lithos, 9, 85-109.

NEUMANN E.-R. (1977): Petrogenesis of the Larvik ring-complex in the Permian Oslo Rift, Norway. In NEUMANN E.-R. and RAMBERG I.B. (Eds.): Petrology and geochemistry of continental rifts. Proceedings of the NATO Advanced Study Institute. D. Reidel Publishing Company; Dordrecht, Holland; Boston, USA, 231-236.

NEUMANN E.-R. (1978): Petrology of the plutonic rocks. In DONS J.A. and LARSEN B.T. (Eds.): The Oslo palaeorift: A review and guide to excursions. Norges geologiske undersokelse, 337, 25-34.

NEUMANN E.-R. (1980): Petrogenesis of the Oslo Region larvikites and associated rocks. Journal of Petrology, 21, 499-531.

NEUMANN E.-R. and RAMBERG I.B. (1977a): Palaeorifts - concluding remarks. In RAMBERG I.B. and NEUMANN E.-R. (Eds.): Tectonics and geophysics of continental rifts. Proceedings of the NATO Advanced Study Institute. D. Reidel Publishing Company; Dordrecht, Holland; Boston, USA, 409-423.

NEUMANN E.-R. and RAMBERG I.B. (1977): Petrology and geochemistry of continental rifts. Proceedings of the NATO Advanced Study Institute. D. Reidel Publishing Company; Dordrecht, Holland; Boston, USA, 296pp.

NEUMANN E.-R., BRUNFELT A.D. and FINSTAD K.G. (1977): Rare earth elements in some igneous rocks in the Oslo Rift, Norway. Lithos, 10, 311-319.

NEUMANN H. (1960): Apparent age of Norwegian minerals and rocks. Norsk geologisk Tidsskrift, 40, 173-191.

NORRY M.J., TRUCKLE P.H., LIPPARD E.J., HAWKESWORTH C.J., WEAVER D. and MARRINER G.F. (1980): Isotopic and trace element evidence from lavas, bearing on mantle heterogeneity beneath Kenya. Philosophical Transactions of the Royal Society of London, A297, 259-271.

NYSTUEN J.P. (1975a): Studies on the igneous rock complex of the Oslo Region. XXV. Diatremes and volcanic rocks in the Hurdal area, Oslo Region. Skr. Norske Vidensk.-Akad. i Oslo, I. Mat.-naturv. Kl., Ny Serie 33, 39pp.

NYSTUEN J.P. (1975b): Plutonic and subvolcanic intrusions in the Hurdal area, Oslo Region. Norges geologiske undersokelse, 317, 1-21.

OFTEDAHL C. (1946): Studies on the igneous rock complex of the Oslo Region. VI. On akerites, felsites and rhomb - porphyries. Skr. Norske Vidensk.-Akad. i Oslo, I. Mat.-naturv. Kl. 1946, no. 1, 51pp.

OFTEDAHL C. (1948): Studies on the igneous rock complex of the Oslo Region. IX. The feldspars. Skr. Norske Vidensk.-Akad. i Oslo, I. Mat.-naturv. Kl. 1948, no. 3, 71pp.

OFTEDAHL C. (1952): Studies on the igneous rock complex of the Oslo Region. XII. The lavas. Skr. Norske Vidensk.-Akad. i Oslo, I. Mat.-naturv. Kl. 1952, no. 3, 64pp.

OFTEDAHL C. (1953): Studies on the igneous rock complex of the Oslo Region. XIII. The cauldrons. Skr. Norske Vidensk.-Akad. i Oslo, I. Mat.-naturv. Kl. 1953, no. 3, 108pp.

OFTEDAHL C. (1957a): Studies on the igneous rock complex of the Oslo Region. XVI. On ignimbrite and related rocks. Skr. Norske Vidensk.-Akad. i Oslo, I. Mat.-naturv. Kl. 1957, no. 4, 21pp.

OFTEDAHL C. (1957b): Studies on the igneous rock complex of the Oslo Region. XV. Origin of composite dikes. Skr. Norske Vidensk.-Akad. i Oslo, I. Mat.-naturv. Kl. 1957, no. 2, 17pp.

oftedahl 1950

OFTEDAHL C. (1977): Origin of the magmas of the Vestfold lava plateau. In NEUMANN E.-R. and RAMBERG I.B. (Eds.): Petrology and geochemistry of continental rifts. Proceedings of the NATO Advanced Study Institute. D. Reidel Publishing Company; Dordrecht, Holland; Boston, USA, 193-208.

O'HARA M.J. (1965): Primary magmas and the origin of basalt. Scottish Journal of Geology, 1, 19-40.

O'HARA M.J. (1968): The bearing of phase equilibria studies on synthetic and natural systems on the origin and evolution of basic and ultrabasic rocks. Earth Science Reviews, 4, 69-133.

OLERUD S. and SANDSTAD J.S. (1984): Geology of the Skrukkelia molybdenite deposit, northwestern margin of the Oslo Graben, Norway. Norges geologiske undersokelse, 387, 1-20.

O'NIONS R.K. and HEIER K.S. (1972): A reconnaissance Rb - Sr

geochronological study of the Kongsberg area, South Norway. Norsk geologisk Tidsskift, 52, 143-150.

O'NIONS R.K., MORTON R.D. and BAADSGAARD H. (1969): Potassium argon ages from the Bamble sector of the Fennoscandian Shield in South Norway. Norsk geologisk Tidsskrift, 49, 171-190.

PALME H. and RAMMENSEE W. (1981): The cosmic abundance of molybdenum. Earth and Planetary Science Letters, 55, 356-362.

PARSONS I. (1978): Feldspars and fluids in cooling plutons. Mineralogical Magazine, 42, 1-17.

PETERSEN J.S. (1977a): Structure of the larvikite - lardalite complex, Oslo Region, Norway, and its evolution. Geologische Rundschau, 67, 330-342.

PETERSEN J.S. (1977b): Composite plutonic ring-complex: A structural characteristic of rift-zone plutonism. In NEUMANN E.-R. and RAMBERG I.B. (Eds.): Petrology and geochemistry of continental rifts. Proceedings of the NATO Advanced Study Institute. D. Reidel Publishing Company; Dordrecht, Holland; Boston, USA, 217-229.

PRESNALL D.C., DIXON S.A., DIXON J.R., O'DONNELL T.H., BRENNER N.L., SCHROCK R.L. and DYCUS D.W. (1978): Liquidus phase relations on the join diopside - forsterite - anorthite from 1 atm to 20 kbar: Their bearing on the generation and crystallisation of basaltic magma. Contributions to Mineralogy and Petrology, 66, 203-220.

PRIEM H.N.A., VERSCHURE R.H., VERDURMEN E.A.Th., HEBEDA E.H. and BOELIRIJK H.A.I.M. (1970): Isotopic evidences on the age of the Trysil porphyries and granites in the eastern Hedmark, Norway. Norges geologiske undersokelse, 266, 263-276.

RAADE G. (1973): Distribution of radioactive elements in the

plutonic rocks of the Oslo Region. Unpublished thesis, University of Oslo, 162pp.

RAADE G. (1977): Distribution of Th, U, K in the plutonic rocks of the Oslo Region, Norway. In NEUMANN E.-R. and RAMBERG I.B. (Eds.): Petrology and geochemistry of continental rifts. Proceedings of the NATO Advanced Study Institute. D. Reidel Publishing Company; Dordrecht, Holland; Boston, USA, 185-192.

RAMBERG I.B. (1976): Gravity interpretation of the Oslo Graben and associated igneous rocks. Norges geologiske undersokelse, 325, 194pp.

RAMBERG I.B. and LARSEN B.T. (1978): Tectonomagmatic evolution. In DONS J.A. and LARSEN B.T. (Eds.): The Oslo palaeorift: A review and guide to excursions. Norges geologiske undersokelse, 337, 55-74.

RAMBERG I.B. and NEUMANN E.-R. (1977): Tectonics and geophysics of continental rifts. Proceedings of the NATO Advanced Study Institute. D. Reidel Publishing Company; Dordrecht, Holland: Boston, USA, 444pp.

RAMBERG I.B. and SPJELDNAES N. (1977): The tectonic history of the Oslo Region. In RAMBERG I.B. and NEUMANN E.-R. (Eds.): Tectonics and geophysics of continental rifts. Proceedings of the NATO Advanced Study Institute. D. Reidel Publishing Company; Dordrecht, Holland; Boston, USA, 167-194.

RANKIN A.H. and LE BAS M.J. (1974): Nahcolite ($NaHCO_3$) in inclusions in apatites from some East African ijolites and carbonatites. Mineralogical Magazine, 39, 564-570.

RASMUSSEN E. (1982): En petrologisk og geokjemisk undersokelse av Permiske Suprakrustale og intrusive bergarter nord for Oyangen, nordlige Oslo felt. Unpublished thesis,

University of Oslo.

RINGWOOD A.E. (1975): Composition and petrology of the Earth's mantle. McGraw-Hill Book Company, 618pp.

ROEDDER E. (1971): Metastability in fluid inclusions. Soc. Min. Geol. Japan, special issue 3, 327-334.

ROEDDER E. (1978): Silicate liquid immiscibility in magmas and in the system K_2O - FeO - Al_2O_3 - SiO_2: An example of serendipity. In Geochimica et Cosmochimica Acta, 42, 1597-1617.

ROEDDER E. (1979): Fluid inclusions as samples of ore fluids. In BARNES H.L. (Ed.): Geochemistry of hydrothermal ore deposits. Second edition. John Wiley and sons Ltd., 684-737.

ROEDDER E. (1983): Discussion of "A re-assessment of phase equilibria involving two liquids in the system K_2O - Al_2O_3 - FeO - SiO_2", by G.M. Biggar. Contributions to Mineralogy and Petrology, 82, 284-290.

ROEDDER E. and SKINNER B.J. (1968): Experimental evidence that fluid inclusions do not leak. Economic Geology, 63, 715-724.

RUBIE D.C. (1982): Mass transfer and volume change during alkali metasomatism at Kisingiri, Western Kenya. Lithos, 15, 99-109.

RUBIE D.C. and GUNTER W.D. (1983): The role of speciation in alkaline igneous fluids during fenite metasomatism. Contributions to Mineralogy and Petrology, 82, 165-175.

RYERSON F.J. and HESS P.C. (1978): Implications of liquid - liquid distribution coefficients to mineral - liquid partitioning. Ceochimica et Cosmochimica Acta, 42, 921-932.

SAETHER E. (1946): Studies on the igneous rock complex of the Oslo Region. VII. The area of lavas and sediments in Nittedal. Skr. Norske Vidensk.-Akad. i Oslo, I. Mat.-naturv. Kl. 1946, no. 6, 34pp.

SAETHER E. (1947): Studies on the igneous rock complex of the Oslo Region. VIII. The dykes in the Cambro-Silurian lowland of Baerum. Skr. Norske Vidensk.-Akad. i Oslo, I. Mat.-naturv. Kl. 1947, no. 3, 60pp.

SAETHER E. (1962): Studies on the igneous rock complex of the Oslo Region. XVIII. General investigation of the igneous rocks in the area north of Oslo. Skr. Norske Vidensk.-Akad. i Oslo, I. Mat.-naturv. Kl., Ny Serie no. 1, 184pp.

SEGALSTAD T.V. (1975): Cauldron subsidences, ring-structures, and major faults in the Skien district, Norway. Norsk geologisk Tidsskrift, 55, 321-333.

SEGALSTAD T.V. (1977): Petrology of the Skien basaltic rocks and the early basaltic (Bl) volcanicity of the Permian Oslo Rift. In NEUMANN E.-R. and RAMBERG I.B. (Eds.): Petrology and geochemistry of continental rifts. Proceedings of the NATO Advanced Study Institute. D. Reidel Publishing Company; Dordrecht, Holland; Boston, USA, 209-210.

SEGALSTAD T.V. (1979): Petrology of the Skien basaltic rocks, southwestern Oslo Region, Norway. Lithos, 12, 221-239.

SHAW D.M. (1968): A review of K - Rb fractionation trends by covariance analysis. Geochimica et Cosmochimica Acta, 32, 573-601.

SHIMIZU N. and ARCULUS R.J. (1975): Rare earth element concentrations in a suite of basanitoids and alkali olivine basalts from Grenada, Lesser Antilles. Contributions to

Mineralogy and Petrology, 50, 231-240.

SILLITOE R.H. (1973): The tops and bottoms of porphyry copper deposits. Economic Geology, 64, 755-777.

SMITH R.L. and BAILEY R.A. (1968): Resurgent cauldrons. Memoirs of the Geological Society of America, 116, 613-662.

SOURIRAYAN S. and KENNEDY G.C. (1962): The system H_2O - NaCl at elevated temperature and pressure. American Journal of Science, 260, 115-141.

SPANGSBERG JENSEN I. (1982): En geologisk undersokelse af det centrale granitkompleks i Glitrevann kalderen, Oslo feltet. Unpublished thesis, University of Arhus, Denmark.

SPJELDNAES N. (1972): Er Brumundsanstenen Triassick? Abstract, X^{th} Nordic geologic winter meeting, Oslo, January 6, 1972.

STRECKEISEN A. (1976): To each plutonic rock its proper name. Earth Science Reviews, 12, 1-33.

SUN S.S. (1982): Chemical composition and origin of the Earth's primitive mantle. Geochimica et Cosmochimica Acta, 46, 179-192.

SUNDVOLL B. (1977): Rb / Sr - Relationships in the Oslo igneous rocks. In NEUMANN E.-R. and RAMBERG I.B. (Eds.): Petrology and geochemistry of continental rifts. Proceedings of the NATO Advanced Study Institute. D. Reidel Publishing Company; Dordrecht, Holland; Boston, USA, 181-192.

SUNDVOLL B. (1978): Isotope- and trace-element chemistry, geochronology. In DONS J.A. and LARSEN B.T. (Eds.): The Oslo palaeorift: A review and guide to excursions. Norges geologiske undersokelse, 337, 35-40.

SWANSON S.E. (1977): Relation of nucleation and growth rate to the development of granitic textures. American Mineralogist, 62, 966-978.

TAKENOUCHI S. and KENNEDY G.C. (1965a): The binary system H_2O - CO_2 at high temperatures and pressures. American Journal of Science, 262, 1055-1074.

TAKENOUCHI S. and KENNEDY G.C. (1965b): The solubility of carbon dioxide in NaCl solutions at high temperatures and pressures. American Journal of Science, 263, 445-454.

TAYLOR R.P., STRONG D.F. and FRYER B.J. (1981): Volatile control of contrasting trace element distributions in peralkaline granitic and volcanic rocks. Contributions to Mineralogy and Petrology, 77, 267-271.

TAYLOR R.P., STRONG D.F. and KEAN B.F. (1980): The Topsails igneous complex: Silurian - Devonian peralkaline magmatism in western Newfoundland. Canadian Journal of the Earth Sciences, 17, 425-439.

TAYLOR S.R. (1965): The application of trace element data to problems in petrology. Physics and Chemistry of the Earth, 6, 133-201.

THOMPSON M. and WALSH J.N. (1983): A handbook of inductively coupled plasma spectrometry. Blackie and Son Ltd., Bishopbriggs, Glasgow.

THOMPSON M., RANKIN A.H., WALTON S.J., HALLS C. and FOO B.N. (1980): The analysis of fluid inclusion decrepitates by inductively - coupled plasma atomic emission spectroscopy: An exploratory study. Chemical Geology, 30, 121-133.

THOMPSON R.N. (1982): Magmatism of the British Tertiary

Volcanic Province. Scottish Journal of Geology, 18, 49-107.

THOMPSON R.N. and MACKENZIE W.S. (1967): Feldspar - liquid equilibria in peralkaline acid liquids: An experimental study. American Journal of Science, 265, 714-734.

TOMKEIEFF S.J. (1937): Petrochemistry of the Scottish Carboniferous - Permian igneous rocks. Bulletin Volcanologique, Series II., 1, 59-87.

TOURET J. (1977): The significance of fluid inclusions in metamorphic rocks. In FRASER D.G. (Ed.): Thermodynamics in geology. D. Reidel Publishing Company; Dordrecht, Holland, 203-227.

TRONNES R.G. (1980): Bergartstyper, intrusjonsforhold og hydrotermale omvandlinger og mineraliseringer, Rustad - Oyangen omradet, Hurdal. Internal report, Norsk Hydro A/S.

TRONNES R.G. (1982): Granitic intrusions and associated late to post-magmatic Mn - Zn - Pb mineralisations west of Hurdalssjoen, Oslo Region, South Norway. Unpublished manuscript.

TURNER D.C. and BOWDEN P. (1979) : The Ningi - Burra complex, Nigeria: Dissected calderas and migrating magmatic centres. Quarterly Journal of the Geological Society of London, 136, 105-119.

TUTTLE O.F. and BOWEN N.L. (1958): Origin of granite in the light of experimental studies in the system $NaAlSi_3O_8$ - $KAlSi_3O_8$ - SiO_2 - H_2O. Geolical Society of America Memoir 74.

VISSER W. and KOSTER VAN GROOS A.F. (1979a): Phase relations in the system K_2O - FeO - Al_2O_3 - SiO_2 at 1 atmosphere with special emphasis on low temperature liquid immiscibility. American Journal of Science, 279, 70-91.

VISSER W. and KOSTER VAN GROOS A.F. (1979b): Effects of P_2O_5 and TiO_2 on liquid - liquid equilibria in the system K_2O - FeO - Al_2O_3 - SiO_2. American Journal of Science, 279, 970-989.

VISSER W. and KOSTER VAN GROOS A.F. (1979c): Effect of pressure on liquid immiscibility in the system K_2O - FeO - Al_2O_3 - SiO_2 - P_2O_5. American Journal of Science, 279 1160-1175.

VOKES F.M. (1973): Metallogeny possibly related to continental break-up in southwest Scandinavia. In TARLING D.H. and RUNCORN S.K. (Eds.): Implications of continental drift to earth sciences, I, NATO Advanced Study Institute, April 1972. Academic Press, London - New York, 573-579.

VOKES F.M. and GALE G.M. (1976): Metallogeny relatable to global tectonics in southern Scandinavia. Geological Association of Canada, special paper 14, 413-441.

VOKES F.M. and IHLEN P.M. (1980): The southern Scandinavian region. In BAUMANN L. (Ed.): Mineral parageneses of the European Variscan zone. Proceedings of the IAGOD Paragenetic commission, 1977. Freit. Forsch., Hefte C354, 19-31.

WALLACE S.R., MUNCASTER N.K., JONSON D.C., MACKENZIE W.B., BOOKSTROM A.A. and SURFACE V.E. (1968): Multiple intrusion and mineralisation at Climax, Colorado. In Ore Deposits. U.S. Am. Inst. Min. Met. Pet. Eng., New York, 29, 605-640.

WATSON E.B. (1976): Two - liquid partition coefficients: Experimental data and geochemical implications. Contributions to Mineralogy and Petrology, 56, 115-134.

WATSON E.B. (1979): Zircon saturation in felsic liquids: Experimental results and applications to trace element

geochemistry. Contributions to Mineralogy and Petrology, 70, 407-419.

WATSON E.B. (1982): Basalt contamination by continental crust: Some experiments and models. Contributions to Mineralogy and Petrology, 80, 73-87.

WEIGAND P.W. (1975): Studies on the igneous rock complex of the Oslo Region. XXIV. Geochemistry of the Oslo basaltic rocks. Skr. Norske Vidensk.-Akad. i Oslo, I. Mat.-naturv. Kl. 1975, 37pp.

WESTRA G. and KEITH S.B. (1981): Classification and genesis of Stockwork molybdenum deposits. Economic Geology, 76, 844-873.

WHIPPLE E.R. (1974): A study of Wilson's determination of ferrous iron in silicates. Chemical Geology, 14, 223-238.

WHITE A.J.R. and CHAPPLE B.W. (1977): Ultrametamorphism and granitoid genesis. Tectonophysics, 43, 7-22.

WHITE J., YEATS A. and SKIPWORTH G. (1979): Tables for statisticians. 3rd edition. Stanley Thomas (publishers) Ltd., 70pp.

WILLIAMS L.A.J. (1970): The volcanics of the Gregory rift valley, East Africa. Bulletin Volcanologique, 34, 439-465.

WILLIAMS L.A.J. (1972): The Kenya rift volcanics: A note on volumes and chemical composition. In GIRDLER R.W. (Ed.): East African Rifts. Tectonophysics, 15, 83-96.

WINKLER H.G.F. (1976): Petrogenesis of metamorphic rocks. Fourth edition. New York: Springer-Verlag.

WOOD D.A., JORON J.L. and TREUIL M. (1979a): A reappraisal of

the use of trace elements to classify and discriminate between magma series erupted in different tectonic settings. Earth and Planetary Science Letters, 45, 326-336.

WOOD D.A., JORON J.L. and TREUIL M. (1979b): Elemental and Sr isotope variations in basic lavas from iceland and the surrounding ocean floor. The nature of mantle source inhomogeneities. Contributions to Mineralogy and Petrology, 70, 319-339.

WOODCOCK J.R. and HOLLISTER V.F. (1978): Porphyry molybdenite deposits of the North American Cordillera. Min. Sci. Engng., 10, 3-18.

WYBORN D., CHAPPELL B.W. and JOHNSTON R.M. (1981): Three S-type volcanic suites from the Lachland fold belt, Southeast Australia. Journal of Geophysical Research, 86, no. B11, 10335-10348.

WYLLIE P.J. (1979): Magmas and volatile components. American Mineralogist, 64, 469-500.

WYLLIE P.J., HUANG W-L, STERN C.R. and MAALOE S. (1976): Granitic magmas: Possible and impossible sources, water contents, and crystallization sequences. Canadian Journal of the Earth Sciences, 13, 1007-1019.

YODER H.S. and TILLEY C.E. (1962): Origin of basalt magmas: An experimental study of natural and synthetic rock systems. Journal of Petrology, 3, 342-532.

APPENDIX A1

ACCURACY AND PRECISION

The accuracy and precision for each element are summarised in Table A1. Estimates of accuracy are obtained from the difference between the expected values and the determined values in the standards, expressed as a percentage. Estimates of the precision are presented in the form of the mean deviation in the replicate samples (2σ), and as a percentage of the mean composition ($200\sigma/\bar{x}$). This is believed to give a conservative estimate of the precision of the methods used.

TABLE A1: SUMMARY OF ACCURACY AND PRECISION

	Method	Standards	Max. error %	Mean Comp.	n	2σ	%
SiO_2	XRF			69.27	74	.362	.52
TiO_2	XRF			.52	74	.006	1.15
Al_2O_3	XRF			14.45	74	.098	.68
Fe_2O_3	XRF			2.78	74	.020	.72
FeO	Col.			2.71	15	.055	2.03
MnO	XRF			.72	74	.006	.83
MgO	XRF			.56	74	.012	2.14
CaO	XRF			1.05	74	.008	.76
Na_2O	XRF			4.95	74	.072	1.45
K_2O	XRF			4.68	74	.028	.60
P_2O_5	XRF			.12	74	.004	3.33
	LOI			.91	8	.032	3.52
F	SIE	GSP-1	-22.16	.29	3	.006	1.98
Li	ICP	HRM1, HRM2	+2.53	17.81	30	.826	4.64
Be	ICP	HRM1, HRM2	-17.50	6.40	29	.200	3.13
V	XRF			23.00	30	.000	0.
V	ICP	HRM1, HRM2	+1.82	10.93	3	.536	4.90
Cr	ICP	HRM1, HRM2	-10.50	4.05	30	.688	16.99
Co	ICP	HRM1, HRM2	+4.21	4.08	30	.530	12.99
Ni	XRF			1.75	3	.500	28.57
Ni	ICP	HRM1, HRM2	+7.40	2.50	30	.756	30.24
Cu	ICP	HRM1, HRM2	+7.25	4.75	30	1.094	23.03
Zn	ICP	HRM1, HRM2	-8.18	300.3	30	23.6	7.86
Rb	XRF			220.7	3	4.66	2.11
Rb	ICP	HRM1, HRM2	+8.47	290.7	29	17.9	6.17
Sr	XRF			215.8	3	1.66	.77
Sr	ICP	HRM1, HRM2	+6.02	93.38	30	4.42	4.74
Y	XRF			55.83	3	.340	.61
Zr	XRF			531.7	3	8.00	1.50
Nb	XRF			170.9	3	3.66	2.14
Mo	ICP	HRM1, HRM2	+59.38	24.85	22	3.80	15.29
Ag	ICP	HRM1, HRM2	+25.45	1.28	30	.596	46.56
Cd	ICP	HRM1, HRM2	+12.14	1.21	18	.286	23.64
Ba	XRF			691.0	3	2.66	.38
Ba	ICP	HRM1, HRM2	-20.62	252.2	30	11.4	4.54
La	INAA	GSP-1	+1.57	92.20	14	4.52	4.90
Ce	INAA	GSP-1	+19.04	185.0	14	30.7	16.60
Nd	INAA	GSP-1	+4.26	60.07	14	6.70	11.15
Sm	INAA	GSP-1	-4.06	10.97	14	.600	5.47
Eu	INAA	GSP-1	-25.00	2.13	14	.200	9.39
Gd	INAA	GSP-1	-2.00	16.71	14	10.1	60.68
Tb	INAA	GSP-1	+7.69	1.21	14	.180	14.88
Ho	INAA	GSP-1	-	2.73	14	.540	19.78
Tm	INAA	GSP-1	-	.09	14	.180	200.0
Yb	INAA	GSP-1	-33.33	4.81	14	.280	5.82
Lu	INAA	GSP-1	-21.74	.86	14	.200	23.26
Hf	INAA	GSP-1	-1.89	16.50	14	2.32	14.06
Ta	INAA	GSP-1	+44.00	22.08	14	1.72	7.79
W	INAA	GSP-1	-	15.85	14	25.8	162.8
Pb	ICP	HRM1, HRM2	-8.50	94.77	29	8.46	8.93
Th	XRF			34.00	3	2.00	5.88
Th	INAA	GSP-1	+28.85	56.11	14	12.5	22.22
U	INAA	GSP-1	-3.06	8.54	14	.620	7.26

APPENDIX A2

CALCULATION OF NORMATIVE MINERALOGIES

The normative mineralogies presented in this thesis have been calculated according to a procedure of progressive silicification of the minerals. The steps involved are essentially the same as those described by Cox et al. (1979), only the sequence is different. The sequence of the steps has been modified in order to produce a form of the calculation more suitable for computation, at the same time minimising the number of steps involved.

The calculation is divided essentially into three parts: A, B and C. In part A of the calculation, the elements, expressed in cation %, are distributed between the principal silica undersaturated minerals: Apatite (Ap), ilmenite (Ilm), kalsilite (Ks), nepheline (Ne), anorthite (An), perovskite (Pv), acmite (Ac), sodium metasilicate (Ns), magnetite (Mt), clinopyroxene (Cpx), and olivine (Ol). In part B of the calculation, the amount of Si^{4+} left over from part A is redistributed to convert kalsilite into leucite (Lc), leucite into orthoclase (Or), nepheline into albite (Ab), perovskite into sphene (Sph), and olivine into orthopyroxene (Opx). In part C of the calculation, the amount of Si^{4+} left over from the preceding stages is used up to make quartz (Q), Fe^{3+} to make hematite (He), Ti^{4+} to make rutile (Rt), and Al^{3+} to make corundum (C). In addition, the Mg, Fe, and Mn end-members of olivine, orthopyroxene, clinopyroxene, magnetite and ilmenite are calculated. Thus, olivine is converted into forsterite (Fo) and fayalite (Fa), orthopyroxene into enstatite (En) and ferrosilite (Fs), clinopyroxene into diopside (Di), hedenbergite (Hd) and johannsenite (Js), magnetite into magnetite and jacobsite (Jc), and ilmenite into ilmenite and pyrophanite (Pn). Finally the proportions of each mineral are calculated. The results, expressed in cation %, describe the arrangement of 100 atoms in terms of the principal anhydrous rock forming

minerals.

The sequence of the steps is as follows:

A. The Fe^{2+} and Mn^{2+} components are added together, and the ratio of $Fe^{2+}/Fe^{2+}+Mn^{2+}$ is calculated.

A1. IF P^{5+} is in excess of zero, combine 5 n atoms of Ca^{2+} with 3 n atoms of P^{5+} to make n molecules of Ap, $Ca_5P_3(OH,F,Cl)$.

A2. IF Ti^{4+} is in excess of zero, combine n atoms of Fe^{2+} + Mn^{2+} with n atoms of P^{5+} to make n molecules of Ilm, $(Fe^{2+},Mn)TiO_3$.

A3. IF K^+ is in excess of zero, combine n atoms of Si^{4+} and n atoms of Al^{3+} with n atoms of K^+ to make n molecules of Ks, $KAlSiO_4$.

A4. IF AL^{3+} is in excess of zero, combine n atoms of Si^{4+} and n atoms of Al^{3+} with n atoms of Na^+ to make n molecules of Ne, $NaAlSiO_4$.

A5. IF Al^{3+} is in excess of zero, combine 2 n atoms of Si^{4+} and 2 n atoms of Al^{3+} with n atoms of Ca^{2+} to make n molecules of An, $CaAL_2Si_2O_8$.

A6. IF Ti^{4+} and Ca^{2+} are in excess of zero, combine n atoms of Ca^{2+} with n atoms of Ti^{4+} to make n molecules of Pv, $CaTiO_3$.

A7. IF Na^+ is in excess of zero, combine 2 n atoms of Si^{4+} and n atoms of Fe^{3+} with n atoms of Na^+ to make n molecules of Ac, $NaFe^{3+}Si_2O_6$.

A8. IF Na^+ is in excess of zero, combine n atoms of Si^{4+} with 2 n atoms of Na^+ to make n molecules of Ns, Na_2SiO_3.

A9. IF Fe^{3+} is in excess of zero, combine n atoms of Fe^{2+} + Mn^{2+} with 2 n atoms of Fe^{3+} to make n molecules of Mt, $Fe^{3+}_2(Fe^{2+},Mn)O_4$.

At this stage, the Fe^{2+} + Mn^{2+} and Mg^{2+} components are added together, and the ratio of $Mg^{2+}/Mg^{2+}+Fe^{2+}+Mn^{2+}$ is calculated.

A1Ø. IF Ca^{2+} is in excess of zero, combine 2 n atoms of Si^{4+} and n atoms of Mg^{2+} + Fe^{2+} + Mn^{2+} with n atoms of Ca^{2+} to make n molecules of Cpx, $Ca(Mg,Fe^{2+},Mn)Si_2O_6$.

A11. IF Ca^{2+} is in excess of zero, combine n atoms of Si^{4+} with n atoms of Ca^{2+} to make n molecules of Wo, CaSiO3.

A12. IF Mg^{2+} + Fe^{2+} + Mn^{2+} is in excess of zero, combine n atoms of Si^{4+} with 2 n atoms of Mg^{2+} + Fe^{2+} + Mn^{2+} to make n atoms of Ol, $(Mg,Fe^{2+},Mn)_2SiO_4$.

At this stage, a record of the amounts of the Si^{4+}, Ks, Ne, anf Ol may be taken. These may be multiplied by the number of cations in each mineral to produce Q', Ks', Ne' and Ol', respectively. These are the proportions of quartz, kalsilite, nepheline and olivine, prior to silicification of the minerals.

B. IF Si^{4+} is less than zero, go to part C.

B1. IF Si^{4+} is in excess of zero, add n atoms of Si^{4+} to n molecules of Ks to make n molecules of Lc, $KAlSiO_4$.

B2. IF Si^{4+} is in excess of zero, add n atoms of Si^{4+} to n molecules of Lc to make n molecules of Or, $KAlSi_3O_8$.

B3. IF Si^{4+} is in excess of zero, add 2 n atoms of Si^{4+} to n molecules of Ne to make n molecules of ab, $NaAlSi_3O_8$.

B4. IF Si^{4+} is in excess of zero, add n atoms of Si^{4+} to n molecules of Pv to make n molecules of Sph, $CaTiSiO_4(O,OH,F)$.

B5. IF Si^{4+} is in excess of zero, add n atoms of Si^{4+} to n molecules of Ol to make Ø.5 n molecules of Opx, $(MgFe^{2+}Mn)SiO_3$.

C1. IF Si^{4+} is in excess of zero, make n molecules of Q, SiO_2.

C2. IF Fe^{3+} is in excess of zero, make n molecules of He, $Fe^{3+}{}_2O_3$.

C3. IF Ti^{4+} is in excess of zero, make n molecules of Rt, TiO_2.

C4. IF Al^{3+} is in excess of zero, make n molecules of C, Al_2O_3.

C5. Multiply Ol by $Mg^{2+}/Mg^{2+}+Fe^{2+}+Mn^{2+}$ to make Fo, Mg_2SiO_4.

C6. Multiply Ol by $(1 - Mg^{2+}/Mg^{2+}+Fe^{2+}+Mn^{2+})$ to make Fa, $(Fe^{2+},Mn)_2SiO_4$.

C7. Multiply Opx by $Mg^{2+}/Mg^{2+}+Fe^{2+}+Mn^{2+}$ to make En, $MgSiO_3$.

C8. Multiply Opx by $(1 - Mg^{2+}/Mg^{2+}+Fe^{2+}+Mn^{2+})$ to make Fs, $(Fe^{2+},Mn)SiO_3$.

C9. Multiply Cpx by $Mg^{2+}/Mg^{2+}+Fe^{2+}+Mn^{2+}$ to make Di, $CaMgSi_2O_6$.

C10. Multiply Cpx by $(1 - Mg^{2+}/Mg^{2+}+Fe^{2+}+Mn^{2+})$ to make Hd, $Ca(Fe^{2+},Mn)Si_2O_6$.

C11. Multiply Hd by $(1 - Fe^{2+}/Fe^{2+}+Mn^{2+})$ to make Js, $CaMnSi_2O_6$.

C12. Multiply Hd by $Fe^{2+}/Fe^{2+}+Mn^{2+}$ to make Hd, $CaFe^{2+}Si_2O_6$.

C13. Multiply Mt by $(1 - Fe^{2+}/Fe^{2+}+Mn^{2+})$ to make Jc, $Fe^{3+}_2MnO_3$.

C14. Multiply Mt by $Fe^{2+}/Fe^{2+}+Mn^{2+}$ to make Mt, $Fe^{3+}_2Fe^{2+}O_3$.

C15. Multiply Ilm by $(1 - Fe^{2+}/Fe^{2+}+Mn^{2+})$ to make Pn, $MnTiO_3$.

C16. Multiply Ilm by $Fe^{2+}/Fe^{2+}+Mn^{2+}$ to make Ilm, $Fe^{2+}TiO_3$.

At this stage, the number of molecules of each mineral, n, may be converted into mass proportions by multiplying by the formula weight of the mineral concerned. Alternatively, the number of molecules of each mineral may be converted into cation % by multiplying by the number of cations in the formula unit.

APPENDIX A3

CHONDRITIC AND PRIMORDIAL MANTLE ABUNDANCES

Estimated primordial mantle abundances (Sun 1982, Wood et al. 1979b) are compared with chondritic abundances (Nakamura 1974, Sun 1982, Palme and Rammensee 1981) in Table A2. The primordial abundances of the LREE have been estimated from twice the chondritic values, as suggested by Sun (1982).

TABLE A2: CHONDRITIC AND PRIMORDIAL MANTLE ABUNDANCES

	C-1 Chondrites	Primordial Mantle
MAJOR ELEMENTS (Wt % oxide):		
SiO_2	21.82	42.95
TiO_2	.0734	.217
Al_2O_3	1.607	4.309
FeO*	21.99	8.359
MnO	.2195	.142
MgO	15.34	37.97
CaO	1.301	3.498
Na_2O	.6160	.390
K_2O	.0578	.028
P_2O_5	.1787	.021
F	.0059	.0026
Cl	.069	.003
S	5.830	.675
TRACE ELEMENTS ($\mu g\ g^{-1}$):		
Li	1.570	1.40
V	42.	87.
Cr	2430.	3000.
Co	480.	110.
Ni	9900.	2000.
Cu	110.	30.
Zn	300.	56.
Rb	1.8	.86
Sr	11.8	23.
Y	2.	4.87
Zr	6.84	11.
Nb	.35	.62
Mo	.915	-
Ag	.18	7.5
Cd	.64	-
Ba	6.9	7.56
Hf	.2	.35
Ta	.02	.043
W	.089	.021
Pb	.058	.0032
Th	.042	.096
U	.013	.027
RARE EARTH ELEMENTS:		
La	.329	.71
Ce	.865	1.9
Pr	.135	-
Nd	.63	1.29
Pm	-	-
Sm	.203	.385
Eu	.077	(.154)
Gd	.276	(.552)
Tb	.052	.099
Dy	.343	(.69)
Ho	.078	(.156)
Er	.225	(.45)
Tm	.034	(.068)
Yb	.220	(.44)
Lu	.0339	(.068)

APPENDIX A4

CORRECTION OF INA ANALYSES FOR VARIATIONS IN IRRADIATION FLUX

The INA analyses have been corrected for variations in irradiation flux according to the positions of the samples within the reactor. The largest corrections were applied for the samples located furthest away from the core of the reactor.

A correction factor for each element was calculated from the concentrations of the elements in the standards placed at opposite ends of the sample holders:

$$X = St_m / (St_b + n(St_t - St_b) / (N + 1))$$

where St_m, St_t and St_b are the mean constant, and constants for the standards at the top and bottom of the sample holder, respectively (output from the computer); n is the position of the sample in the sample holder (n = 1,N); and N is the number of samples between standards in the sample holder.

APPENDIX A5

D-ICP DETERMINATIONS

The output from the D-ICP, in raw mV, was corrected for background by the following procedure. The intensity of the background for each element was calculated from the intensity of the element in the blank samples at time, t_i:

$$I_i = I_\emptyset + t_i \, (I_n - I_\emptyset) \, / \, (t_n - t_\emptyset)$$

where I_i is the intensity of the background at time t_i; $I_\emptyset$ is the intensity of the blank sample at time $t_\emptyset$; and I_n is the intensity of the blank sample at time t_n; and where $t_\emptyset$ is less than t_i is less than t_n.

The calculated intensity of the element in the background was then subtracted from the intensity of the element in the sample:

$$X = X_i - I_i$$

where X and X_i are the corrected and uncorrected values of the intensity at time t_i, respectively. This procedure was followed for all 36 elements.

The corrected values were then converted into equivalent parts per million (equ. ppm), relative mass proportions (rel. mass props. / mV), and relative atomic proportions (rel. at. props. / mv), as required:

$$\text{equ. ppm} = X \, / \, S_x$$

$$\text{rel. mass props / mV} = X \cdot S_{Na} \, / \, S_x$$

$$\text{rel. at. props / mV} = X \cdot S_{Na} \, / \, S_x \cdot w_{Na} \, / \, w_x$$

where S_{Na} and w_{Na} are the sensitivity and atomic mass of sodium; and S_x and w_x are the sensitivity and atomic mass of an element, x, in the sample. The sensitivities for each element are listed in Table A3. Estimates of the precision of the method are summarised in Table A4, expressed in relative atomic proportions per gram of sample.

TABLE A3: SENSITIVITIES FOR THE ELEMENTS IN THE STANDARD SOLUTIONS / mV $(\mu g\ g^{-1})^{-1}$

Se	10.47	Zn	128.1	Sr	857.8	Sb	10.37	Pb	86.90	Bi	8.360
Cd	660.7	Ba	678.2	Ni	144.3	B	422.3	Mn	29.19	Fe	7.526
P	78.77	S	27.64	Mg	6.963	Mo	912.6	Sn	136.9	Si	84.56
As	41.72	Na	30.00	Al	8.784	V	395.2	Be	8400.	Ca	5.721
Te	60.95	Cu	253.9	Ag	1222.	Li	330.1	Ti	11.30	Co	91.84
Zr	887.8	Hg	116.8	K	52.99	Rb	24.66	La	213.0	Cr	396.8

TABLE A4: SUMMARY OF PRECISION IN THE D-ICP METHOD / Rel. at. props. mV^{-1}

	Mean Comp.	2σ	n	%
Zn	.097	.048	21	24.74
Sr	.033	.022	21	66.67
Mn	.607	.134	21	22.08
Fe	.385	.212	21	55.06
S	271.3	195.9	21	72.21
Si	47.96	17.80	21	37.11
Na	112.4	34.17	21	30.40
Be	.161	.058	21	36.02
Ca	43.13	5.104	21	11.83
Li	1.513	.838	21	55.39
Ti	.130	.146	21	112.3
K	12.53	4.918	21	39.25